TRANSACTIONS
OF THE ASME
Series E

Journal of APPLIED MECHANICS

June 1959

DYNAMICS • VIBRATIONS • ELASTICITY • LUBRICATION AND WEAR
RHEOLOGY • FRACTURES • STRUCTURES • HYDRAULICS • AERODYNAMICS
INTERNAL FLOW • MECHANICAL PROPERTIES OF METALS • THERMODYNAMICS
TURBULENCE • HEAT TRANSFER • COMPUTING DEVICES AND METHODS
BOUNDARY LAYERS • AEROELASTICITY • EXPERIMENTAL STRESS ANALYSIS

Published Quarterly by
THE AMERICAN SOCIETY OF MECHANICAL ENGINEERS

TRANSACTIONS
OF THE ASME
Series E

EDITORIAL DEPARTMENT

Editor, J. J. JAKLITSCH, JR.
Editor Emeritus, GEORGE A. STETSON
Consulting Editor, LEO BLODGETT
Art Editor, HENRY BALFOUR
Production, MILDA E. WILBUR

APPLIED MECHANICS DIVISION

Chairman, W. PRAGER
Secretary, P. S. BATDORF
Technical Editor, R. C. DRUCKER
Technical Editor, J. KESTIN
Acting Technical Editor, P. F. MAEDER
Honorary Editor, JOHN M. LESSELLS

OFFICERS OF THE ASME

President, C. B. WARREN
Secretary, C. B. SCHMIDT, II
Treasurer, E. J. KATES
Assistant Treasurer, H. J. BAUER

PUBLICATIONS COMMITTEE

Chairman, JOHN de S. COUTINHO
B. G. A. SKROTZKI
HOWARD N. BLACKMON
R. D. MINDLIN
MARTIN SOLAND

Junior Representatives
A. T. WUSKA
A. E. GOLDSTEIN

REGIONAL ADVISORY BOARD

Region I, ROY L. PARSELL
Region II, GLENN R. FRYLING
Region III, F. J. HEINZE
Region IV, FRANCIS C. SMITH
Region V, H. M. GATHER
Region VI, C. R. EARLE
Region VII, M. POPOVICH
Region VIII, LIBEN MELANDER

Published quarterly by The American Society of Mechanical Engineers. Publication office at 20th and Northampton Streets, Easton, Pa. The editorial department is located at the headquarters of the Society, 29 West Thirty-Ninth Street, New York 18, N.Y. Cable address, "Mechaneer," New York. Price $3.00 a copy, $10.00 annually; to members, $1.50 a copy, $5.00 annually. Add 50 cents for postage to all countries outside the United States, Canada, and Pan American Union. Changes of address must be received at Society headquarters seven weeks before they are to be effective on the mailing list. Please send old as well as new address. ... By-Law: The Society shall not be responsible for statements or opinions advanced in papers or ... printed in its publications (B13, Par. 4). ... Second-class mail privileges authorized at Easton, Penna. This publication is authorized to be mailed at the special rates of postage prescribed by Section 132.122. ... © Copyrighted, 1959, by The American Society of Mechanical Engineers. Reprints from this publication may be made on condition that full credit be given the Transactions of the ASME, Series E — Journal of Applied Mechanics, and the author, and that date of publication be stated.

TRANSACTIONS OF THE ASME
is indexed by the Engineering Index, Inc.

Journal of APPLIED MECHANICS

VOLUME 26 • SERIES E • NUMBER 2
June 1959

CONTENTS

TECHNICAL PAPERS

161 **Effect of a Nonisothermal Free Stream on Boundary-Layer Heat Transfer**
E. M. Sparrow and J. L. Gregg

166 **Visual Studies of the Wall Layers in the Turbulent Boundary Layer**
S. J. Kline and P. W. Runstadler

171 **Unsteady Laminar Boundary Layers Over an Arbitrary Cylinder**
Kwang-Tzu Yang

179 **On Journal Bearings of Finite Length With Variable Viscosity**
L. N. Tao

184 **Analysis of Complex Kinematic Chains With Influence Coefficients**
J. Modrey

189 **A Theory of Oil Whip**
Yukio Hori

199 **On Critical Speeds of a Shaft Supported by a Ball Bearing**
Toshio Yamamoto

205 **Root-Locus Analysis of Structural Coupling in Control Systems**
R. H. Cannon, Jr.

210 **Normal Vibrations of Uniform Plate Carrying Any Number of Finite Masses**
W. F. Stokey and C. F. Zorowski

217 **Transients in Simple Undamped Oscillators Under Inertial Disturbances**
Antongiulio Dornig

224 **On Laterally Loaded Semicircular Plate With Clamped Edges**
W. H. Jurney

227 **Direct Determination of Stresses in Plane Elasticity Problems**
P. S. Theocaris

235 **Stresses in a Stretched Slab Having a Spherical Cavity**
Chih-Bing Ling

241 **Influence Coefficients for Edge-Loaded Short, Thin, Conical Frustums**
J. H. Baltrukonis

246 **Upper and Lower Bounds for Special Eigenvalues**
F. C. Appl and C. F. Zorowski

251 **Analysis of a Compression Test of a Model of a Granular Medium**
C. W. Thurston and H. Deresiewicz

259 **A Reassessment of Deformation Theories of Plasticity**
Bernard Budiansky

265 **Collapse Loads of Rings and Flanges Under Uniform Twisting Moment**
Burton Paul

271 **Creep of Thick-Walled Tubes Under Internal Pressure**
F. P. J. Rimrott

276 **Strain-Hardening Solutions to Plate Problems**
Nicholas Perrone and P. G. Hodge, Jr.

285 **Determination of Creep Deflection of a Rivet in Double Shear**
Joseph Marin

CONTENTS

DESIGN DATA AND METHODS

290 The Frequency of Vibration of Rectangular Isotropic Plates, *H. J. Fletcher*

BRIEF NOTES

291 Large Deflections of a Clamped Elliptical Plate, *W. A. Nash and I. D. Cooley*

293 Thermal Stress at Spherical Cavities, *A. L. Florence and J. N. Goodier*

294 Deflection of a Thick Ring in Diametral Compression, *Alexander Blake*

296 The Biot-Willis Coefficients for a Sandstone, *I. Fatt*

297 Circular Plates on Elastic Foundation, *G. D. Galletly*

298 Frequencies of Vibration of Stiffened Plates, *R. L. Thorkildsen and W. H. Hoppmann, II*

300 Design of a π Network for Heat-Flow Analog, *D. G. Stephenson and G. O. Starke*

301 Stress Distribution in a Square Tube, *M. A. Sadowsky and E. E. Zwicky, Jr.*

DISCUSSION

303 Discussion of previously published papers by *R. H. Cannon, Jr.; C. G. Van Niekerk; M. Hetényi and P. H. McDonald, Jr.; K. A. Foss; N. J. Huffington, Jr., and W. H. Hoppmann, II; T. J. Harvey; H. Tramposch and G. Gerard; C. E. Crede; C. J. Ancker, Jr., and J. N. Goodier; H. Poritsky and F. A. Fend; K. L. Johnson; J. H. Haywood and L. B. Wilson*

BOOK REVIEWS

317 Elasticity and Plasticity

317 Thermal Turbomachines

317 Random Vibration

318 Kinematical Analysis of Mechanisms

318 Hohere Technische Mechanik

TRANSACTIONS OF THE ASME Series D

Journal of BASIC ENGINEERING

Vol. 81 • Series D • No. 2

CONTENTS FOR JUNE, 1959

101 Elastic and Damping Properties of Cylindrical Journal Bearings, by B. Sternlicht. (58—Lub-3)

109 Axial, Relative Motion of a Circular Step Bearing, by L. Licht. (58—LUB-1)

118 Friction and Wear of Metals to 1000 C, by E. P. Kingsbury and E. Rabinowicz. (58—Lub-6)

123 Friction Factors for Turbulent Flow in Curved Pipes, by H. Itō. (58—SA-14)

135 Characteristics of a Self-Lubricated Stepped Thrust Pad of Infinite Width With Compressible Lubricant, by K. C. Kochi. (58—A-194)

147 Direct Measurement of Net Positive Suction Head, by R. B. Jacobs, K. B. Martin, and R. J. Hardy. (58—A-38)

153 Transitional Phenomena in Ultrasonic Shock Waves Emitted by Cavitation on Hydrofoils, by F. Numachi. (58—A-117)

167 Cavitation and NPSH Requirements of Various Liquids, by Victor Salemann. (58—A-82)

181 The Unsteady Wake Interaction in Turbomachinery and Its Effect on Cavitation, by Hsuan Yeh and J. J. Eisenhuth. (58—A-114)

193 Thermal-Stress Ratchet Mechanism in Pressure Vessels, by D. R. Miller. (58—A-129)

197 Refractory Metal Facings for Protection of Metal Surfaces Subjected to Repeated High-Temperature Pulses, by Aaron Cohen and Edward Homer. (58—A-188)

203 The Failure of Structural Metals Subjected to Strain-Cycling Conditions, by R. W. Swindeman and D. A. Douglas. (58—A-198)

213 Evaluation of Material Wear and Self-Welding in Sodium-Cooled Reactor Systems, by R. B. Jerman, R. C. Williams, and D. O. Leeser.

226 Irradiation of Haynes-25 and Inconel-X Compression Springs in High-Temperature High-Pressure Water, by R. L. Mehan. (58—A-94)

233 Energy Losses of Balls Rolling on Plates, by R. C. Drutowski. (58—A-190)

239 On the Effect of Lubricant Inertia in the Theory of Hydrodynamic Lubrication, by A. A. Milne. (58—A-195)

245 Surface Finish and Clearance Effects on Journal-Bearing Load Capacity and Friction, by F. W. Ocvirk and G. B. DuBois. (58—A-134)

254 Statistical Optimization of Regulators Employing a Binary Error Criterion, by J. H. Milsum. (58—A-71)

263 An Introduction to the Time-Modulated Acceleration Switching Electrohydraulic Servomechanism, by S. A. Murtaugh, Jr. (58—A-159)

272 Discussion on previously published paper by B. Sternlicht and R. C. Elwell.

TRANSACTIONS OF THE ASME Series A

Journal of
ENGINEERING FOR POWER
Volume 81 • Series A • Number 2

CONTENTS FOR APRIL, 1959

111 The Control System of a 225,000-Kw Double-Automatic Extraction Steam Turbine and Related Reducing Stations, by M. A. Eggenberger and P. G. Ipsen. (58—SA-36)
123 Design of 321-Mw Cross-Compound Steam Turbine—River Rouge Unit No. 3, by C. D. Wilson. (58—SA-22)
133 Five Years' Experience on the Consolidated Edison System With Protection of Turbine Generators and Boilers by Automatic Tripping, by W. C. Beattie, H. A. Bauman, J. M. Driscoll, P. T. Onderdonk, and R. L. Webb. (58—Pwr-8)
142 A Simplified Regenerator Theory, by W. F. Schalkwijk. (58—A-135)
151 Development of a Smooth Running, Double-Spool, Gas-Turbine Rotor System, by J. R. Schnittger. (58—A-197)
161 M-252 Alloy for Heavy-Duty Gas-Turbine Buckets, by G. R. Fusner and D. L. Newhouse. (58—A-191)
177 The Calibration of Thermocouples by Freezing-Point Baths and Empirical Equations, by R. P. Benedict. (58—A-175)
189 Theoretical Stresses Near a Circular Opening in a Flat Plate, Reinforced With a Cylindrical Outlet, by E. O. Waters. (58—A-171)
201 Effect of Steam-Turbine Reheat on Speed-Governor Performance, by Charles Concordia. (58—A-36)
208 Load Capacity Tests on Tapered-Land and Pivoted-Shoe Thrust Bearings for Large Steam-Turbine Application, by R. E. Brandon and H. C. Bahr. (58—A-172)

TRANSACTIONS OF THE ASME Series B

Journal of
ENGINEERING FOR INDUSTRY
Volume 81 • Series B • Number 2

CONTENTS FOR MAY, 1959

95 The Strength of Thick-Walled Cylinders, by B. Crossland, S. M. Jorgensen, and J. A. Bones. (58—Pet-20)
115 Steady-State Creep Analysis of the Weight Loadings of Furnace Tubes on Multiple Supports, by J. L. Jacobowitz and C. K. Mader. (58—Pet-14)
126 How to Replace Gears by Mechanisms (Linkages), by Kurt Hain and Gerhard Marx. (58—SA-33)
131 The Effect of a Lead Additive on the Machinability of Alloy Steels, by Norman Zlatin and J. V. Gould. (58—SA-53)
139 Controlled Contact Cutting Tools, by B. T. Chao and K. J. Trigger. (58—SA-42)
152 A Study of the Effects of Tool Flank Wear on Tool Chip Interface Temperature, by D. R. Olberts. (58—SA-41)
159 Synthesis of Path-Generating Mechanisms by Means of a Programmed Digital Computer, by Ferdinand Freudenstein and G. N. Sandor. (58—A-85)
169 Synthesis of the Four-Bar Linkage to Match Prescribed Velocity Ratios, by Philip Barkan and E. J. Tuohy. (58—A-115)
178 High-Range Plasticity of Metals Beyond Normal Work-Hardening, by E. V. Crane and W. S. Wagner (58—A-132)
183 Self-Excited Vibrations in Metal Cutting, by N. H. Cook. (58—A-189)

TRANSACTIONS OF THE ASME Series C

Journal of
HEAT TRANSFER
Vol. 81 • Series C • No. 2

CONTENTS FOR MAY, 1959

95 Heat and Mass Transfer From a Rotating Disk, by F. Kreith, J. H. Taylor, and J. P. Chong.
106 Numerical and Machine Solutions of Transient Heat-Conduction Problems Involving Melting or Freezing, Part I, by W. D. Murray and Fred Landis. (58—HT-16)
113 A Theory of Rotating Condensation, by E. M. Sparrow and J. L. Gregg. (58—A-70)
121 Laminar Heat Transfer in Rectangular Channels, by L. S. Han. (58—A-124)
129 Heat Transfer to Water in Thin Rectangular Channels, by S. Levy, R. A. Fuller, and R. O. Niemi. (58—A-127)
144 Combined Geometric and Network Analog Computer for Transient Heat Flow, by Victor Paschkis. (58—A-69)
151 Heat Transfer From an Annular Fin of Constant Thickness, by H. H. Keller and E. V. Somers. (58—A-116)
157 A Variational Method for Fully Developed Laminar Heat Transfer in Ducts, by E. M. Sparrow and R. Siegel. (58—A-92)
168 The Effect of Surface Roughness on the Convection Heat-Transfer Coefficient for Fully Developed Turbulent Flow in Ducts With Uniform Heat Flux, by R. T. Lancet. (58—A-122)

E. M. SPARROW

Aeronautical Research Scientist,
NASA Lewis Research Center,
Cleveland, Ohio.
Assoc. Mem. ASME

J. L. GREGG

Aeronautical Research Scientist,
NASA Lewis Research Center,
Assoc. Mem. ASME

The Effect of a Nonisothermal Free Stream on Boundary-Layer Heat Transfer

An analysis is made for laminar forced-convection heat transfer from a flat plate to a nonisothermal free stream. An exact solution of the boundary-layer energy equation is found for the situation of linearly varying free-stream temperature. Numerical calculations are carried out for Prandtl numbers in the range $0.01 \leqslant Pr \leqslant 50$. Results are presented for the change in heat transfer due to the variation in free-stream temperature. This effect decreases with increasing Prandtl number.

Introduction

THE Pohlhausen analysis[1] for the thermal boundary layer on a flat plate aligned parallel to a uniform free-stream flow is one of the classical solutions of forced-convection heat transfer. A particular property of Pohlhausen's solution, and of all subsequent boundary-layer heat-transfer analyses, is that the temperature of the approaching free-stream flow is assumed to be uniform. In terms of the co-ordinates of Fig. 1, this assumption requires that for $x < 0$, the free-stream temperature T_∞ does not depend upon y.

The present study is concerned with the more general situation in which the temperature of the approaching stream may be nonuniform. We are able to find exact boundary-layer solutions for this problem. Numerical calculations have been carried out for Prandtl numbers of 0.01, 0.1, 0.7, 1.0, 10, and 50. Heat-transfer results are presented.

The analysis is carried out for laminar flow over an isothermal surface. The free-stream velocity is taken as uniform. For simplicity of presentation, viscous dissipation and property variations are omitted in the main body of the analysis, but they will be included in a later section.

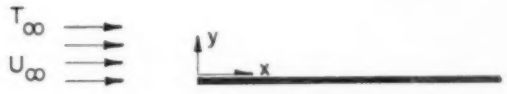

Fig. 1 Co-ordinates

In this first attack on the problem, we consider the case where the temperature of the approaching fluid varies in a linear fashion with y, that is,

$$T_\infty = T_0 + \lambda y, \quad x \leqslant 0 \tag{1}$$

where T_0 and λ are constants. Since the heat transfer from the plate is affected only by free-stream temperature variations which interact with the boundary layer, Equation (1) need only be an accurate description of T_∞ for values of y extending to slightly beyond the boundary-layer thickness.

Analysis

The Energy Equation and Its Boundary Conditions. The differential equation expressing conservation of energy for steady, laminar, nondissipative flow in a boundary layer is

$$u\frac{\partial T}{\partial x} + v\frac{\partial T}{\partial y} = \alpha\frac{\partial^2 T}{\partial y^2} \tag{2}$$

The boundary conditions for the temperature are assigned as

$$T(x, 0) = T_w \tag{2a}$$

$$T(x, y) \to T_\infty \quad \text{as} \quad y\sqrt{\text{Re}} \to \infty \tag{2b}$$

[1] "Der Wärmeaustausch zwischen festen körpern und Flüssigkeiten mit kleiner Reibung und kleiner Wärmeleitung," *Zeitschrift für angewandte Mathematik und Mechanik*, vol. 1, 1921, p. 115. See also reference, footnote 4, pp. 265–270.

Contributed by the Applied Mechanics Division and presented at the Annual Meeting, New York, N. Y., November 30–December 5, 1958, of THE AMERICAN SOCIETY OF MECHANICAL ENGINEERS.

Discussion of this paper should be addressed to the Secretary, ASME, 29 West 39th Street, New York, N. Y., and will be accepted until July 10, 1959, for publication at a later date. Discussion received after the closing date will be returned.

NOTE: Statements and opinions advanced in papers are to be understood as individual expressions of their authors and not those of the Society. Manuscript received by ASME Applied Mechanics Division, February 10, 1958. Paper No. 58—A-42.

Nomenclature

c_p = specific heat at constant pressure
F = Blasius function
k = thermal conductivity
L = plate length
Pr = Prandtl number, $c_p\mu/k = \nu/\alpha$
q = local heat-transfer rate per unit area
q_0 = value of q for uniform $T_w = T_0$
Q = over-all heat-transfer rate, $\int_0^L q\,dx$
Q_0 = value of Q for uniform $T_w = T_0$
T = static temperature
U_∞ = free-stream velocity, a constant
u = velocity component in x-direction
v = velocity component in y-direction
x = co-ordinate measuring distance along plate from leading edge
y = co-ordinate measuring distance normal to plate
α = thermal diffusivity, $k/\rho c_p$
δ^* = displacement thickness of boundary layer
η = dimensionless independent variable, $\frac{y}{2}\left(\frac{U_\infty}{\nu x}\right)^{1/2}$
θ = dimensionless temperature, $(T - T_0)/(T_w - T_0)$
$\theta_1, \theta_2, \theta_3$ = functions of η
λ = free-stream temperature gradient
μ = absolute viscosity
ν = kinematic viscosity
ξ = dimensionless independent variable, $\frac{2\lambda}{T_w - T_0}\left(\frac{\nu x}{U_\infty}\right)^{1/}$
ρ = density
Φ = function of η satisfying Equations (20a) and (20b)

Subscripts

w = wall conditions
∞ = free-stream conditions

where T_w is a constant. It is known from experience that conditions of the type (2*b*) are satisfied to a high degree of accuracy within a short distance from the surface. So, practically speaking, infinity is not very far away.

An approach to the solution of Equation (2) cannot be made without a prior knowledge of the velocity distribution in the boundary layer. An analysis for the velocity boundary layer for incompressible flow over a flat plate was first made by Blasius in 1908. So, the required velocity information is available from his work, although it was necessary to recompute his results to greater accuracy for the purposes of this analysis.

Aside from the numerical results for the velocity components u and v appearing in Equation (2), there is another important property of the velocity boundary-layer solution which enters our temperature problem; namely, that there is a transverse flow of fluid from the boundary layer to the free stream given by

$$\frac{v_\infty}{U_\infty} = 0.86039 \ldots \left(\frac{\nu}{U_\infty x}\right)^{1/2} \tag{3a}$$

This transverse flow affects the free-stream temperature distribution. It is found that the distribution of T_∞ which satisfies the free-stream energy equation[2] as well as Equation (1) is

$$T_\infty = T_0 + \lambda(y - \delta^*), \quad x > 0 \tag{4}$$

where δ^* is the displacement thickness given by

$$\frac{\delta^*}{x} = 1.7208 \ldots \left(\frac{\nu}{U_\infty x}\right)^{1/2} \tag{3b}$$

Equation (4) is to be used in conjunction with the boundary condition (2*b*).

Solution of the Energy Equation. Now, we proceed with a solution of Equation (2). Rather than work in the x,y-co-ordinate system, it is more fruitful to introduce new independent variables η and ξ by the definitions

$$\eta \equiv \frac{y}{2}\left(\frac{U_\infty}{x\nu}\right)^{1/2}, \qquad \xi \equiv \frac{2\lambda}{T_w - T_0}\left(\frac{\nu x}{U_\infty}\right)^{1/2} \tag{5}$$

η is seen to be the Blasius variable, while ξ is essentially a stretching of the x-co-ordinate which also includes the free-stream temperature gradient λ.

For the velocities u and v, we may substitute the boundary-layer variables. So,

$$\frac{u}{U_\infty} = \frac{1}{2}F', \qquad v = -\frac{1}{2}\left(\frac{\nu U_\infty}{x}\right)^{1/2}[F - \eta F'] \tag{6}$$

where F is the well-known Blasius function which obeys the following differential equation

$$F''' + FF'' = 0, \quad F(0) = F'(0) = 0, \quad F'(\infty) = 2$$

The primes represent differentiation with respect to η. Finally, a dimensionless temperature variable θ is defined by the relation

$$\theta \equiv \frac{T - T_0}{T_w - T_0}, \qquad T_w \neq T_0 \tag{7}$$

Under the transformation given by Equations (5), (6), and (7) the energy Equation (2) becomes

$$\frac{\partial^2\theta}{\partial\eta^2} + \Pr\left[F\frac{\partial\theta}{\partial\eta} - \xi F'\frac{\partial\theta}{\partial\xi}\right] = 0 \tag{8}$$

where the symbol Pr represents the Prandtl number. Next, the boundary conditions (2*a*) and (2*b*) are transformed. Taking account of Equation (4) for T_∞, it is found that

$$\theta(\xi, 0) = 1 \tag{8a}$$

$$\theta(\xi, \eta) \to \xi(\eta - 0.86039 \ldots) \quad \text{or} \quad \partial\theta/\partial\eta \to \xi \quad \text{as} \quad \eta \to \infty \tag{8b}$$

Inspection of the boundary conditions suggests that best advantage is taken of the linearity of Equation (8) by writing

$$\theta(\xi, \eta) = \theta_1(\eta) + \xi\theta_2(\eta) \tag{9}$$

By substituting back into Equations (8), (8*a*), and (8*b*), it is found that θ_1 and θ_2 must satisfy

$$\theta_1'' + \Pr F\theta_1' = 0, \qquad \theta_1(0) = 1, \qquad \theta_1(\infty) = 0 \tag{10}$$

$$\theta_2'' + \Pr[F\theta_2' - F'\theta_2] = 0, \qquad \theta_2(0) = 0, \ \theta_2'(\infty) = 1$$

$$\text{or} \quad \theta_2(\infty) = \eta - 0.86039 \tag{11}$$

Equation (10) for θ_1 coincides precisely with the governing equation for the boundary-layer temperature distribution corresponding to a uniform free-stream temperature. So, the effects of the nonuniform free-stream temperature on boundary-layer heat transfer will be found from the solutions of Equation (11).

Solutions of Equations (10) and (11) have been obtained for Prandtl numbers of 0.01, 0.1, 0.7, 1.0, 10, and 50 using the numerical methods of Gregg[3] in conjunction with IBM 650 electronic calculating equipment. The numerical method, five-point forward integration, requires that both the function and its derivative be specified at the starting point of the calculation for a second-order equation. In terms of our present problem, it is necessary that the pairs $[\theta_1(0), \theta_1'(0)]$, $[\theta_2(0), \theta_2'(0)]$ be specified. As is seen from the boundary conditions of Equations (10) and (11), the derivatives $\theta_1'(0)$ and $\theta_2'(0)$ are not known. So, the computational problem reduces to a systematic search for the appropriate values of these derivatives which lead to solutions of Equations (10) and (11), respectively, satisfying the condition $\theta_1(\infty) = 0$ and $\theta_2'(\infty) = 1$. The values of $\theta_1'(0)$ and $\theta_2'(0)$ thus obtained are listed in Table 1. For Pr = 0.7, 1.0, and 10, where previous work for the uniform free-stream temperature situation is available, excellent agreement is found between our $\theta_1'(0)$ values and those of past solutions.

Table 1 Temperature derivatives for 0.01 ≤ Pr ≤ 50

Pr	$\theta_1'(0)$	$\theta_2'(0)$	$\theta_2'(0)/\theta_1'(0)$
0.01	−0.103	0.873	−8.46
0.1	−0.281	0.699	−2.49
0.7	−0.585	0.495	−0.846
1.0	−0.664	0.457	−0.688
10	−1.46	0.246	−0.169
50	−2.49	0.15	−0.060

Results

Heat Transfer. The most important result of practical interest is the heat transfer. The local rate of heat transfer from the surface to the fluid may be calculated using Fourier's law

$$q = -k\left[\frac{\partial T}{\partial y}\right]_{y=0}$$

In terms of the variables of Equations (5), (7), and (9), the expression for q becomes

[2] It is to be remembered that $(\mathrm{Re\ Pr})^{-1}$ is required to be much less than 1 according to boundary-layer assumptions.

[3] J. L. Gregg, "A General Purpose IBM 653 Routine for the Solution of Simultaneous Ordinary Differential Equations," IBM 650 Scientific Computation Seminar, Endicott, N. Y., October, 1957.

$$q = -\frac{k}{2}(T_w - T_0)\left(\frac{U_\infty}{x\nu}\right)^{1/2}\left(\frac{\partial\theta}{\partial\eta}\right)_{\eta=0}$$

$$= -\frac{k}{2}(T_w - T_0)\left(\frac{U_\infty}{x\nu}\right)^{1/2}[\theta_1'(0) + \xi\theta_2'(0)] \quad (12)$$

where $\theta_1'(0)$ is an abbreviation for $[d\theta_1/d\eta]_{\eta=0}$, etc.

The result for the case of uniform free-stream temperature is obtained as a special case of Equation (12). By setting $\xi = 0$ (i.e., $\lambda = 0$), we find the local heat transfer q_0 corresponding to a uniform free-stream temperature $T_\infty = T_0$ to be

$$q_0 = -\frac{k}{2}(T_w - T_0)\left(\frac{U_\infty}{x\nu}\right)^{1/2}\theta_1'(0) \quad (13)$$

Using the information of Table 1, Equation (13) has been plotted in Fig. 2.

The important relationship showing the change in boundary-layer heat transfer due to nonuniform free-stream temperature is provided by combining Equations (12) and (13). So,

$$\frac{q}{q_0} = 1 + \xi\left[\frac{\theta_2'(0)}{\theta_1'(0)}\right] \quad (14)$$

Equation (14) may be evaluated from the values of Table 1. Fig. 3 shows a plot of q/q_0 for values of ξ between 0 and 1. It is immediately seen from the figure that the heat transfer to low Prandtl-number fluids is much more affected by nonuniformities in T_∞ than it is for high Prandtl-number fluids. This finding is made plausible by noting that the thickness of the thermal boundary layer increases with decreasing Prandtl number. So, for the same free-stream temperature gradient (i.e., same λ), the thermal boundary layer is aware of a greater change of free-stream temperature as Prandtl number decreases.

It is worth while to examine the conditions under which the nonuniformity in T_∞ may be neglected in computing local heat-transfer rates. Our goal is to find a quantitative criterion for determining when the heat-transfer relationship for uniform free-stream temperature [Equation (13) or Fig. 2] will yield sufficiently accurate results for the situation of nonuniform free-stream temperature. Suppose we decide that an accuracy of 5 per cent should be adequate for the great majority of heat-transfer applications. Then Fig. 4 distinguishes the conditions under which nonuniformities in ambient temperature may be ignored in the local heat-transfer computation. As a simple illustration, consider a flat plate in air (Pr = 0.7) on which the Reynolds number, $U_\infty x/\nu$, is 10^5 at $x = 1$ ft. The temperature difference $(T_w - T_0)$ is 100 deg F. For these circumstances, it is found that free-stream temperature gradients up to 77 deg F per in. will have negligible effect on the heat transfer.

For some purposes, the over-all rate heat transfer Q for a length of plate between $x = 0$ and $x = L$ may be desired. For a unit width of plate, Q is found from

$$Q = \int_0^L q\,dx$$

After integrating Equation (12) and rearranging the result, we find

$$Q/Q_0 = 1 + 0.5\xi\left[\frac{\theta_2'(\theta)}{\theta_1'(0)}\right] \quad (15)$$

where Q_0, the over-all heat transfer corresponding to $T_\infty = T_0$, is given by

$$Q_0 = -k(T_w - T_0)\left(\frac{UL}{\nu}\right)^{1/2}\theta_1'(0) \quad (16)$$

Although Fig. 3 was constructed for the local heat transfer, it may be applied with only minor reinterpretation to the average heat transfer. For a given ξ and Pr, the corresponding result for $[1 - Q/Q_0]$ is found by halving the value read from the ordinate of Fig. 3. So, the over-all heat transfer from $x = 0$ to $x = L$ is less

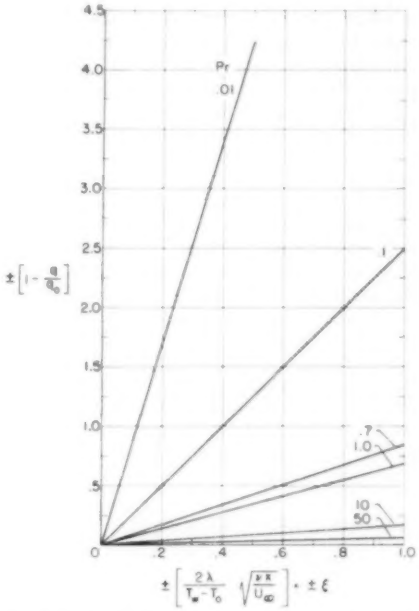

Fig. 3 Effect of nonisothermal free stream on heat transfer

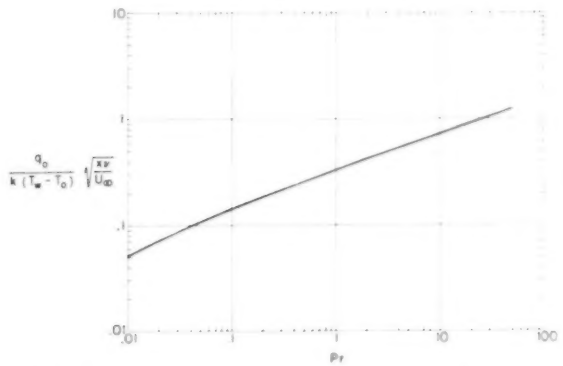

Fig. 2 Heat-transfer results for isothermal free stream, $T_\infty = T_0$

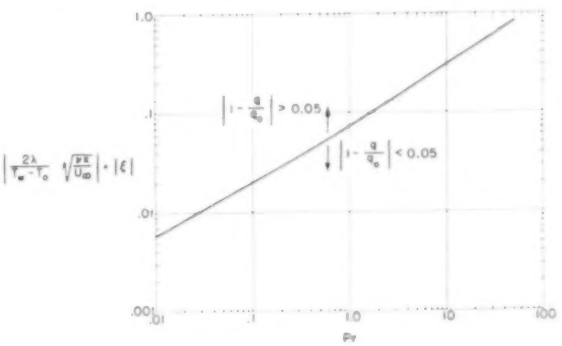

Fig. 4 Values of ξ corresponding to a 5 per cent change in heat transfer

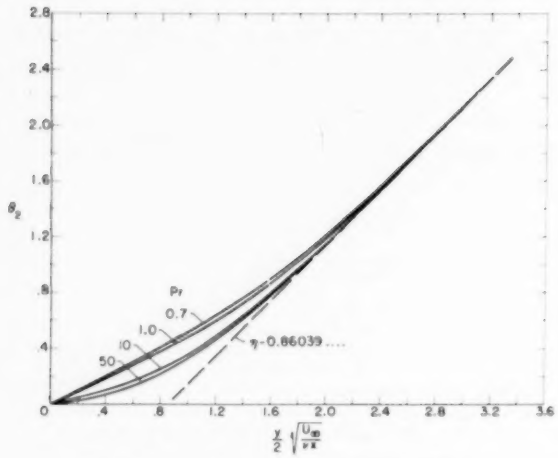

Fig. 5(a) Distribution of θ_2 across boundary layer

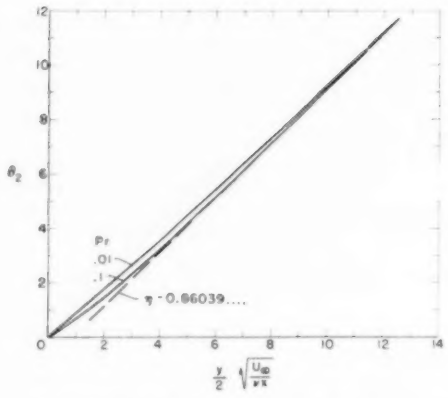

Fig. 5(b) Distribution of θ_2 across boundary layer

affected by nonuniform T_∞ than is the local heat transfer at $x = L$, as might have been expected since boundary-layer thickness increases with increasing x.

Temperature Profiles. The temperature distribution across the boundary layer also may be of some interest. According to Equation (9), the dimensionless temperature θ is found by combining θ_1 and θ_2. It has been noted already that θ_1 coincides with the temperature solution corresponding to uniform T_∞. Representations of the θ_1 distribution appear in many places in the literature for a wide Prandtl-number range, e.g., Schlichting[4] (Fig. 14.7), and there is no need for repetition here. The variation of θ_2 across the boundary layer has been plotted in Figs. 5(a) and (b). The first of these graphs shows the curves for the higher Prandtl numbers, while the second shows the lower Prandtl-number curves. Included in the figures is a dashed line which represents the θ_2 distribution in the free stream. It is seen that the boundary-layer profiles asymptotically approached this limiting line from above. The trends with Prandtl number are identical to previous findings in laminar boundary-layer theory; namely, that the limiting free-stream values are approached more and more rapidly as Prandtl number increases.

Viscous Dissipation; Variable Properties

Viscous Dissipation. The inclusion of viscous dissipation adds the term

$$\left(\frac{\mu}{\rho c_p}\right)\left(\frac{\partial u}{\partial y}\right)^2$$

to the right side of the energy Equation (2). Taking account of this additional term, the energy equation is transformed in the same manner as before, giving

$$\frac{\partial^2\theta}{\partial\eta^2} + \Pr\left[F\frac{\partial\theta}{\partial\eta} - \xi F'\frac{\partial\theta}{\partial\xi} + \frac{U_\infty^2}{4c_p(T_w - T_0)}(F'')^2\right] = 0 \quad (17)$$

This now replaces Equation (8) as the governing equation for θ. The boundary conditions (8a) and (8b) are unchanged. As a consequence of the linearity of the problem, θ can be written as the following sum

$$\theta(\xi, \eta) = \theta_1(\eta) + \xi\theta_2(\eta) + \frac{U_\infty^2}{2c_p(T_w - T_0)}\theta_3(\eta) \quad (18)$$

The functions θ_1 and θ_2 obey Equations (10) and (11) as before, while θ_3 must satisfy

$$\theta_3'' + \Pr\left[F\theta_3' + \frac{(F'')^2}{2}\right] = 0 \quad (19a)$$

$$\theta_3(0) = \theta_3(\infty) = 0 \quad (19b)$$

The solution of Equations (19a) and (19b) is facilitated by first considering an auxiliary problem, namely,

$$\Phi'' + \Pr\left[F\Phi' + \frac{(F'')^2}{2}\right] = 0 \quad (20a)$$

$$\Phi'(0) = 0, \qquad \Phi(\infty) = 0 \quad (20b)$$

Equations (20a) and (20b) describe the so-called thermometer problem, which has been studied in detail by Eckert and Drewitz as well as by Pohlhausen. Their results are reported in some detail by Schlichting[4] pp. 266–267).

We now propose a solution of θ_3 in terms of known functions as follows:[5]

$$\theta_3(\eta) = \Phi(\eta) - \Phi(0)\theta_1(\eta) \quad (21)$$

That this is in fact a solution of (19a) is easily verified by direct substitution, taking account of Equations (10) and (20a). The boundary conditions (19b) are also satisfied.

Assuming that θ_3 is known, we proceed to evaluate the local heat transfer q according to Fourier's law. In terms of the variables of the analysis, the expression for q is

$$q = -\frac{k}{2}(T_w - T_0)\left(\frac{U_\infty}{x\nu}\right)^{1/2}\left[\theta_1'(0) + \xi\theta_2'(0) + \frac{U_\infty^2}{2c_p(T_w - T_0)}\theta_3'(0)\right] \quad (22)$$

Noticing that $\theta_3'(0) = -\Phi(0)\theta_1'(0)$, Equation (22) becomes

$$q = -\frac{k}{2}(T_w - T_0)\left(\frac{U_\infty}{x\nu}\right)^{1/2}\theta_1'(0)\left[1 + \xi\frac{\theta_2'(0)}{\theta_1'(0)} - \frac{U_\infty^2}{2c_p(T_w - T_0)}\Phi(0)\right] \quad (22a)$$

[4] H. Schlichting, "Boundary Layer Theory" (translated by Dr. J. Kestin), McGraw-Hill Book Company, Inc., New York, N. Y., 1955.

[5] This solution has been used in the following reference: S. Ostrach, "Compressible Laminar Boundary Layer and Heat Transfer for Unsteady Motions of a Flat Plate," NACA TN 3569, 1955.

Values of $\Phi(0)$ are given on the ordinate of Schlichting's Fig. 14.8,[4] while $\theta_1'(0)$ and $\theta_2'(0)$ are given in Table 1.

For the situation of uniform free-stream temperature ($\xi = 0$), the heat transfer q_0 is

$$q_0 = -\frac{k}{2}(T_w - T_0)\left(\frac{U_\infty}{x\nu}\right)^{1/2}\theta_1'(0)\left[1 - \frac{U_\infty^2}{2c_p(T_w - T_0)}\Phi(0)\right] \quad (23)$$

Finally, by combining Equations (22*a*) and (23), we are able to relate the change in heat transfer with the nonuniform free-stream temperature.

$$q/q_0 = 1 + \xi\left[\frac{[\theta_2'(0)/\theta_1'(0)]}{1 - \Phi(0)\dfrac{U_\infty^2}{2c_p(T_w - T_0)}}\right] \quad (24)$$

Although Fig. 3 was constructed for the nondissipative case, it can be applied to the dissipative situation represented by Equation (24) with only minor modification. Entering Fig. 3 with a given ξ and Pr, the value of $[1 - q/q_0]$ for the dissipative case is found by dividing the ordinate by

$$\left[1 - \Phi(0)\frac{U_\infty^2}{2c_p(T_w - T_0)}\right]$$

Inasmuch as $\Phi(0) > 0$, the effect of including viscous dissipation is to increase the effect of nonuniform T_∞ when $T_w > T_0$, and to diminish the effect when $T_w < T_0$.

Variable Properties. The analysis which has been presented for the constant-property situation may be extended without essential modification to the variable-property situation which is characterized by

$$\rho\mu = \text{const}, \qquad \rho k = \text{const}, \qquad c_p = \text{const} \quad (25)$$

By using Howarth's transformation

$$Y = \int_0^y (\rho/\rho_0)dy$$

and replacing y by Y in Equation (5) defining η, the formulation of the solution remains as before. Practically speaking, the property variations of Equation (25) may serve as reasonable approximations only for gases.

Concluding Remarks

We have shown that the problem of forced-convection heat transfer to a linearly nonisothermal free stream gives rise to an exact solution of the boundary-layer energy equation. The change in heat transfer due to the variation in T_∞ has been computed. This effect is found to diminish with increasing Prandtl number, suggesting that the high-Prandtl-number fluids may be excluded from further study.

S. J. KLINE

Associate Professor,
Department of Mechanical Engineering,
Stanford University, Calif.
Mem. ASME

P. W. RUNSTADLER

Research Assistant,
Department of Mechanical Engineering,
Stanford University,
Calif.

Some Preliminary Results of Visual Studies of the Flow Model of the Wall Layers of the Turbulent Boundary Layer[1]

Preliminary studies of the flow model in the wall layers of the turbulent boundary layer are presented. Results are summarized for investigations of positive pressure gradients, zero and negative pressure gradients, readjusting zones, and the later stages of transition. In all cases, the special visual methods developed for these studies show a definite three-dimensional vortex-flow model. The presently available details of this model are described, a possible interpretation of the physics of the turbulent boundary layer is given, and some of the many implications of the flow model are discussed.

RECENT investigations of the performance and flow models in subsonic diffusers by the authors and co-workers at Stanford University [1–5][2] have shown the existence of several phenomena that cannot be explained in terms of the classical two-dimensional picture of the turbulent shear layer. In order to explain these phenomena a series of visual studies of the wall layers, that is, the flow very near the wall, has been instituted and is continuing. While these data are at present only qualitative in nature, they are believed to be of sufficient importance to justify publication as preliminary results. These results are given below and are followed by a brief discussion of some of their possible implications together with some corroborating evidence for the interpretations suggested from the results of other workers.

Flow-Visualization Techniques

In order to study the wall layers, two special flow-visualization techniques have been devised. These both consist of the injection of a line of dye in a two-dimensional fashion across the entire flow on a wall. In the first method, this is accomplished by use of a 6-in-long, 0.010-in-diam hypodermic needle attached to a standard medical syringe. In the second method, the dye is injected through a 0.003-in. slot in the wall made by cutting and shimming a single sheet of lucite to minimize the disturbances introduced. In both cases a strong downstream angle of injection is maintained to avoid any spurious upstream flows, and the dye is injected as uniformly as possible across the flow. It is to be emphasized that in the case of the turbulent boundary layer these techniques show a portion of the flow that cannot be seen with ordinary dye-injection methods; this has been verified repeatedly by simultaneous use of both methods.

Visual Studies

Visual studies of this type have now been carried out in four types of flows: (*a*) Adverse pressure-gradient flows in straight-walled diffusers with divergence angles varying from zero to that where large stalls commence; (*b*) channels with zero and slightly favorable pressure gradients; (*c*) readjusting zones in which a boundary layer generated in a favorable pressure gradient moves past a point of minimum pressure into a diffuser; (*d*) transition from laminar to turbulent flow in an adverse pressure gradient. All these observations have been made in a two-dimensional water channel with a water depth of 4 in. and a free-stream velocity of 0.2–0.6 fps. Varying inlet conditions, various types of dye, two injection methods, and several channels have been employed by a number of observers; apparently consistent results have been obtained.

When dye is introduced very near the wall in a turbulent boundary layer it is found that the wall layers are not two-dimensional, as has long been believed, but instead they consist of a repeated three-dimensional pattern. The details of this pattern are not defined completely and are still under study, but the following has been observed. The pattern or flow model appears to consist of an array of "islands of hesitation"[3] and longitudinal vortexes which impart a wispy appearance to the flow; these are interspaced with areas of faster moving fluid. The islands of hesitation appear as long stretched filaments in the direction of flow which move downstream more slowly than the surrounding fluid. The vortexes apparently originate as a breakdown or roll-up along the edges of the islands of hesitation. The primary orientation of the vortex elements is longitudinal,[4] that is, in the flow direction, but each vortex stands at a slight angle to the wall so that its distance from the wall increases as it moves downstream. After the vortex element reaches a certain critical

[1] This work has been supported in the past under the financial sponsorship of the National Advisory Committee for Aeronautics and the Small Aircraft Engine Department of the General Electric Company. Current work is continuing under the sponsorship of the United States Air Force Office of Scientific Research and Development Command, under contract No. AF 49 (638)-295, and also under National Science Foundation Grant G5223. Reproduction in whole or in part is permitted for any purpose of the United States Government.

[2] Numbers in brackets designate References at end of paper.

Contributed by the Applied Mechanics Division and presented at the Annual Meeting, New York, N. Y., November 30–December 5, 1958, of THE AMERICAN SOCIETY OF MECHANICAL ENGINEERS.

Discussion of this paper should be addressed to the Secretary, ASME, 29 West 39th Street, New York, N. Y., and will be accepted until July 10, 1959, for publication at a later date. Discussion received after the closing date will be returned.

NOTE: Statements and opinions advanced in papers are to be understood as individual expressions of their authors and not those of the Society. Manuscript received by ASME Applied Mechanics Division, February 19, 1958. Paper No. 58—A-64.

[3] This very appropriate term, "island of hesitation," is believed to have originated with the work of T. Theodorsen and J. Weske who have observed apparently similar patterns in the later stages of transition in a zero pressure gradient.

[4] The use of word "longitudinal" here refers only to the observed primary orientation of the vortexes, and should not be construed as necessarily implying a connection to a Görtler type.

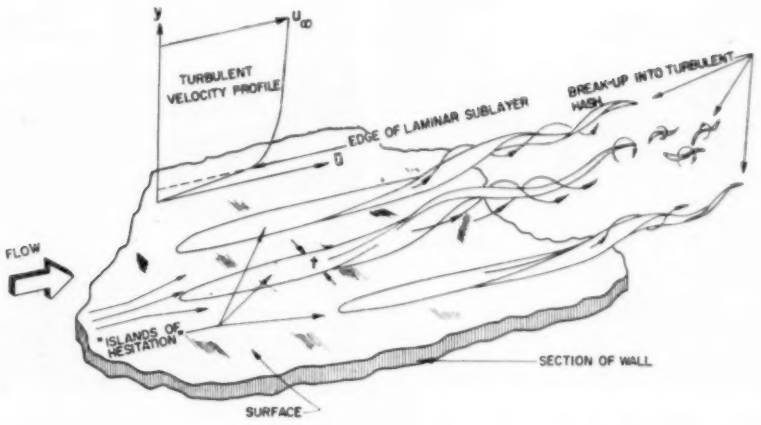

Fig. 1 Diagrammatic sketch of flow model in wall layers of fully developed turbulent boundary layer

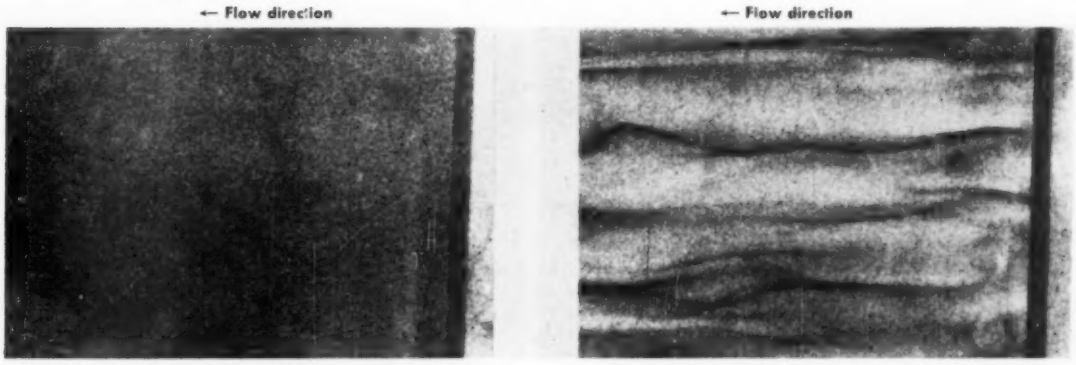

(a) Laminar boundary layer 6-ft slightly convergent inlet channel **(b) Turbulent boundary layer 6-ft straight inlet channel**

Fig. 2 Wall-slot dye method. Free-stream velocity = 0.4 fps; 0-deg plane wall channel; throat width = 3 in.

distance from the wall, which cannot be given quantitatively at present, it breaks up into a typical turbulent hash by a process which is too rapid for the eye to follow. A sketch of those details which have been observed is given in Fig. 1.

When these same visualization methods are applied to the laminar boundary layer, the expected two-dimensional flow is found in the wall layers. A comparison of the laminar and turbulent cases is shown in Figs. 2(*a*) and (*b*). It should be noted that the dye is injected two-dimensionally at the wall and that the wispy appearance in the turbulent case is created purely by the flow itself. Similar results have been obtained in all tests to date; that is, in every case where the normal Reynolds visualization test shows turbulent flow farther from the wall, the island of hesitation and vortex pattern have been found in the wall layers; but in every case where the flow is laminar farther from the wall, a smooth two-dimensional flow is found in the wall layers.

As noted in the foregoing, four cases have been studied qualitatively, and elements of what appear to be at least very similar flow patterns have been seen in all four cases. However, certain differences between the various cases also have been noted. The major element of similarity appears to be the island and vortex pattern sketched in Fig. 1. A brief discussion of the further features of each case now follows.

Adverse Pressure Gradient. In the case of turbulent boundary layers in an adverse pressure gradient, Fig. 3(*a*), the size of the island and vortex pattern is strongly dependent on the magnitude of the adverse pressure gradient. The transverse size increases rapidly with increased adverse pressure gradient. In the cases studied, the transverse spacing t, Fig. 1, increases from perhaps $^1/_{16}$ in. or less at zero pressure gradient to $^1/_2$ in. or more near the inception of large stalls. As the size increases the characteristic breakup frequency appears to decrease. In adverse pressure gradients the patterns are quite unsteady; that is, the island and vortex patterns move as a function of time. This unsteadiness becomes more pronounced as the adverse pressure gradient is increased.

At the same time that the transverse size of the island and vortex pattern increases, the length of each island decreases; that is, the vortex system stands at a larger angle to the wall, and hence breaks up a shorter distance downstream from its point of origin even though the thickness of the wall layer increases rapidly in an adverse pressure gradient. This apparently implies that the number of vortex breakups, and hence the losses, are sharply increased, although this point has not yet been verified quantitatively.

The changes in geometry and frequency of occurrence just described for the adverse-pressure-gradient case seem to be in agreement with the known over-all physical facts. They are in agreement with the fluctuation measurements in a 7.5-deg conical diffuser reported by Robertson and Calehuff [13]. They also probably are the explanation for the surprisingly small

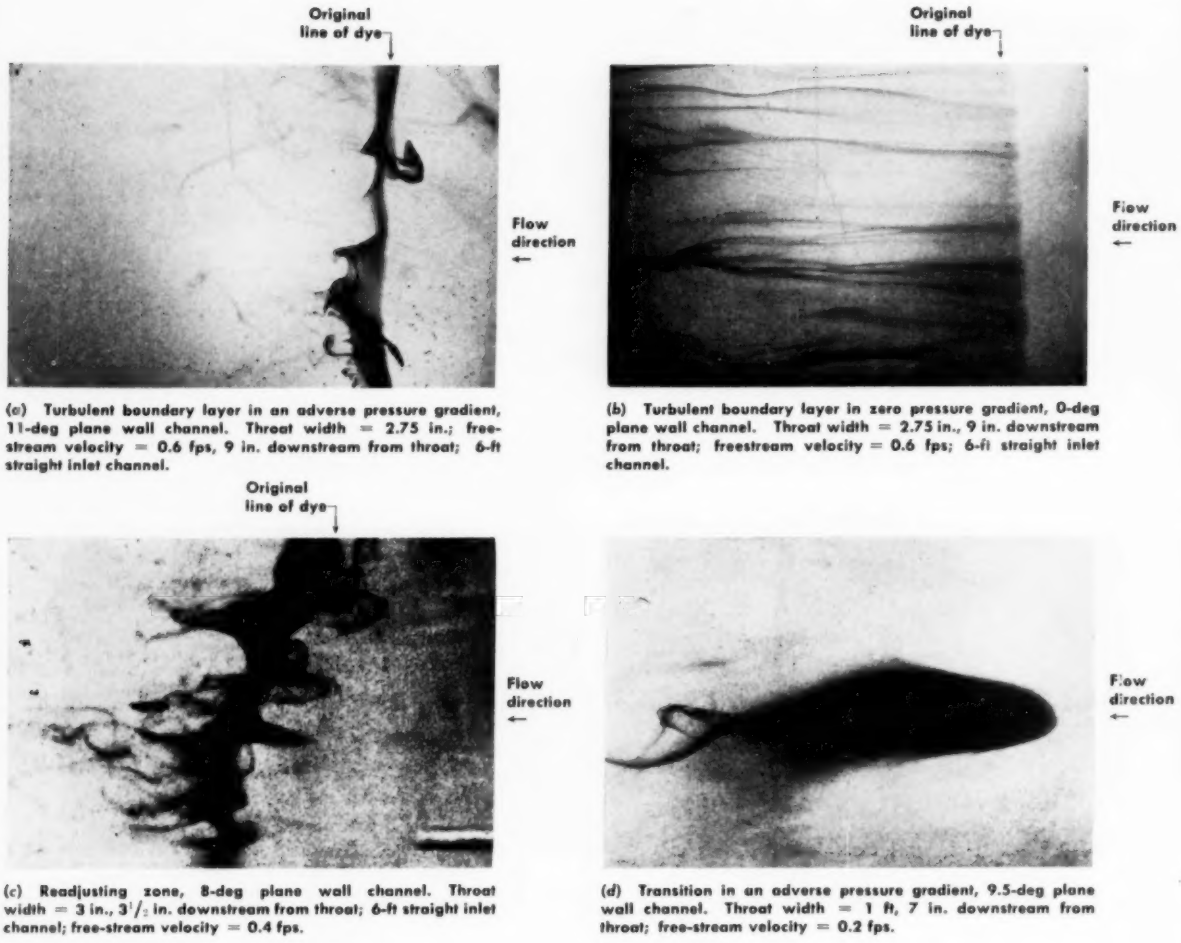

(a) Turbulent boundary layer in an adverse pressure gradient, 11-deg plane wall channel. Throat width = 2.75 in.; free-stream velocity = 0.6 fps, 9 in. downstream from throat; 6-ft straight inlet channel.

(b) Turbulent boundary layer in zero pressure gradient, 0-deg plane wall channel. Throat width = 2.75 in., 9 in. downstream from throat; freestream velocity = 0.6 fps; 6-ft straight inlet channel.

(c) Readjusting zone, 8-deg plane wall channel. Throat width = 3 in., $3^1/_2$ in. downstream from throat; 6-ft straight inlet channel; free-stream velocity = 0.4 fps.

(d) Transition in an adverse pressure gradient, 9.5-deg plane wall channel. Throat width = 1 ft, 7 in. downstream from throat; free-stream velocity = 0.2 fps.

Fig. 3 Needle trace dye method (scale $^3/_4$ in. = 1 in.)

effect of "history" on boundary-layer performance and stall reported by Robertson and Holl [15] and Kline [16].

When an adverse pressure gradient is applied, the islands of hesitation already present are naturally slowed still further by the pressure forces, and a relatively small adverse pressure gradient is thus sufficient to create streaks of fluid very near the wall that actually move a short distance in the upstream direction. Each such streak appears to correspond to an island of hesitation, and terminates by leaving the wall; it is then caught up by the higher speed fluid, and swept back downstream. It is these streaks that were reported in references [3] and [5] and called small transitory stall. Thus the present observations are fully in accord with and provide an explanation for the earlier observations on stall inception. This explanation is not a final answer since it raises the yet more fundamental question, "Why does this particular pattern of islands and vortexes occur in the wall layers of the turbulent boundary layer in the first place?"

Zero and Slightly Favorable Pressure Gradients. In fully turbulent boundary layers in zero and favorable pressure gradients, Fig. 3(*b*), the island and vortex pattern also moves as a function of time, but appears much smaller in transverse dimension with a higher characteristic frequency than in the case of adverse pressure gradients. The size and frequencies of the motion in favorable pressure gradients are such that they are difficult to observe with the eye even at the low velocities employed, and further studies are definitely needed. It appears that increased Reynolds number, owing to increased velocity, causes the size of the pattern to diminish and the frequency to increase, but the range of data thus far available is very limited.

Readjusting Zones. In readjusting zones, Fig. 3(*c*), the pattern appears to be about the same size as in moderately large adverse pressure gradients and is also very unsteady. Frequently, the dimension *l*, Fig. 1, is $^1/_2$ in. or more in size, and very strong unsteady elements have been observed in all cases studied.

Transition. In the case of transition in an adverse pressure gradient, Fig. 3(*d*), the pattern appears to be largest in size and is often relatively steady. In some cases, the width of the island of hesitation is as much as 3 in., and the island may stay in one location for an indefinitely long period provided flow conditions upstream are constant and free from large disturbances. The islands also occur singly as well as in an array in this case. It has been suggested by Mr. P. S. Klebanoff that the bubble or

island shown in Fig. 3(*d*) probably occurs in the later stages of transition in the adverse pressure gradient, that is, downstream from the well-known Tollmien Schlichting two-dimensional wave amplification range. The authors now tend to concur in this belief, but adequate substantiation is lacking.

A Possible Physical Interpretation of Observed Flow Model

Possible Interpretation. The foregoing states what has been observed in various cases in the layers of fluid very near the wall by direct visual observations. The following remarks suggest a possible interpretation of these results. It is the authors' belief that an appropriate interpretation of the physics of the turbulent boundary layer may be as follows: The model that creates the large-scale eddies near the wall is composed of an array of islands of hesitation and vortexes of the type shown in Fig. 1. This model is formed by an instability that probably first occurs in the later stages of transition and then repeats itself in time and space over the entire downstream wall. This instability is formed in the layers normally called the sublayer and buffer layer. The vortexes so generated move out from the wall as they go downstream and subsequently break up into the characteristic fluctuating motion of the outer portions of the turbulent shear layer. Thus at any given location the fluctuation components of the outer portion of the layer would be the downstream wake of the vortexes generated near the wall farther upstream.

This picture implies a continual transport of fluid between the wall layers and the outer fully turbulent portion of the flow. Apparently it is this continual transport of fluid which makes normal dye injection ineffective in showing the flow very near the wall and has thus made the flow patterns so difficult to unravel.

Some Supporting Evidence of Other Observers. In addition to the visual evidence just cited there is also now available a very considerable body of evidence attributable to other workers which tends to substantiate the viewpoint suggested in the foregoing. Some of this is now cited.

Townsend [9] has deduced from the fluctuation measurements that a pattern very close to that actually observed and reported in the foregoing should exist in the wall layers. In particular, Townsend remarks that a typical eddy of finite length should exist with a structure elongated in the flow direction and that return flow from the eddy should occur normal to the wall. All of these observations are confirmed by the present visual studies.

Many sets of measurements of the fluctuation scale and intensity in a turbulent shear layer are now available; the most careful and complete are perhaps those due to Laufer [6, 7] and Shigemitsu [14]. All of these measurements show that the largest fluctuations in absolute magnitude occur very near the wall in contradiction to older assumptions based on the concept of damping by the wall. They are thus very much in agreement with the present view although a theoretical study showing that the precise correlations obtained agree with the present model is not available.

Einstein and Li [8] showed that an autocorrelated pressure fluctuation does exist at the wall in the turbulent shear layer. By measurement of the frequency of this fluctuation with special pressure pickups they were able to make a prediction of the mean velocity profile in the laminar sublayer and buffer layer. This prediction is in far better agreement with the best available measurements of velocity profile than any other known to the authors.

Mr. R. Sherrer and J. Lundell of the Ames Laboratory of the NACA also have made measurements of similar fluctuations at low supersonic Mach numbers. Their results, although still unpublished, are also consistent with those of the present work. It is thus likely that the patterns found are not limited to low Reynolds and Mach numbers.

Coles [10] and Clauser [11], as well as a great many previous workers, have developed expressions for the velocity profile and shear coefficients of the turbulent boundary layer. These results show that wall shear and velocity profile can be correlated by a surprisingly small number of parameters provided the free-stream turbulence is not very high. Thus a certain relatively simple type of similarity is strongly suggested. These results also show a primary dependence of velocity profile on the shear action at the wall. Both of these results, which are *a priori* unexpected in view of the complex nature of turbulent fluctuations, suggest some type of underlying single flow model which is closely related to the action at the wall. They thus also tend to support the present view rather than a view in which one visualizes an evenly distributed sublayer which is dragged along by the action of fluctuations impressed from the outer layers of fluid.

None of the foregoing results answers the fundamental question raised concerning why the observed pattern exists. It is likely that at least part of the explanation lies in the action of vortex stretching advanced by Hama [12] in connection with the later stages of transition. However, further work on this question, on the interaction between the wall layers and the outer portion of the flow, and also on quantitative results relating the observations recorded to the usual types of mean and fluctuation measurements is definitely needed. Work on these matters is continuing, and the authors will welcome direct communication on further evidence or opinion bearing on this subject.

Conclusions

All of the presently available evidence appears to be in keeping with a picture of the turbulent shear layer as generated by a repeated instability of the wall layers occurring over the entire wall in a turbulent boundary layer. The instability appears to take the form of a longitudinal vortex island-of-hesitation pattern that breaks up in the region near the edge of the viscous sublayer. This picture of the flow is actually verified by direct visual studies and provides an explanation of a number of previously observed but unexplained phenomena. The total evidence now available argues strongly against the older picture of a two-dimensional sublayer which is dragged along by fluctuations impressed from the outer portion of the boundary layer.

The results now available also suggest that further detailed quantitative studies of this vortex model may hopefully form the proper basis for a rational theory of the turbulent boundary layer.

References

1 C. A. Moore and S. J. Kline, "Some Effects of Vanes and of Turbulence on Two-Dimensional Wide-Angle Subsonic Diffusers," Final Report on NACA Contract NAw-6317 and Progress Report on NACA Contract NAw-6404, Department of Mechanical Engineering, Stanford University, 1955; to be published as NACA TN-4080.

2 D. Cochran and S. J. Kline, "The Use of Short Flat Vanes for Producing Efficient Wide-Angle Two-Dimensional Subsonic Diffusers," Final Report on NACA Contract NAw-6404 and Progress Report PD-3 on NACA Contract NAw-6500, Department of Mechanical Engineering, Stanford University, 1957; to be published as NACA TN 4309.

3 S. J. Kline, "Some New Mechanisms and Conceptions of Stall Including the Behavior of Vaned and Unvaned Diffusers," Progress Report MD-1 on NACA Contract NAw-6500, Department of Mechanical Engineering, Stanford University, 1957.

4 S. J. Kline, C. A. Moore, and D. L. Cochran, "Wide-Angle Diffusers of High Performance and Diffuser Flow Mechanisms," Readers' Forum, *Journal of the Aeronautical Sciences*, vol. 24, 1957, pp. 469–470.

5 S. J. Kline, "Some New Conceptions on the Mechanism of Stall in Turbulent Boundary Layers," Readers' Forum, *Journal of the Aeronautical Sciences*, vol. 24, 1957, pp. 470–471.

6 J. Laufer, "Investigation of Turbulent Flow in a Two-Dimensional Channel," NACA Report 1053, 1951.

7 J. Laufer, "The Structure of Turbulence in Fully Developed Pipe Flow," NACA Report 1174, 1954.

8 H. A. Einstein and H. Li, "Shear Transmission from a Turbulent Flow to Its Viscous Boundary Sub-Layer," 1955 Heat Transfer and Fluid Mechanics Institute, XIII.

9 A. A. Townsend, "The Structure of Turbulent Shear Flow," Cambridge University Press, 1956, pp. 206–212.

10 D. Coles, "Remarks on the Equilibrium Turbulent Boundary Layer," *Journal of the Aeronautical Sciences*, vol. 24, 1957, pp. 495–506.

11 F. H. Clauser, "Turbulent Boundary Layers in Adverse Pressure Gradients," *Journal of the Aeronautical Sciences*, vol. 21, 1954, pp. 91–108.

12 F. R. Hama, "Three-Dimensional Vortex Pattern Behind a Circular Cylinder," Readers' Forum, *Journal of the Aeronautical Sciences*, vol. 24, 1957, p. 156 (and underlying unpublished reports).

13 J. M. Robertson and G. L. Calehuff, "Turbulence in a Diffuser Boundary Layer," *Journal of the Hydraulics Division, Proc. ASCE*, Proc. Paper 1393, vol. 83, No. HY-5, Oct., 1957.

14 Y. Shigemitsu, "Experimental Studies on Laminar Sub-Layer in Turbulent Boundary Layer Involving Separation," *Journal of the Physical Society of Japan*, vol. 12, 1957, pp. 183–190.

15 J. M. Robertson and J. W. Holl, "Effect of Adverse Pressure Gradients on Turbulent Boundary Layers in Axisymmetric Conduits," JOURNAL OF APPLIED MECHANICS, vol. 24, TRANS. ASME, vol. 79, 1957, pp. 191–196.

16 S. J. Kline, "On the Nature of Stall," ASME Paper No. 58—A-170.

Unsteady Laminar Boundary Layers Over an Arbitrary Cylinder With Heat Transfer in an Incompressible Flow

KWANG-TZU YANG

Assistant Professor,
Department of Mechanical Engineering,
University of Notre Dame,
Notre Dame, Ind.
Assoc. Mem. ASME

A method is presented for calculating the development of momentum and thermal laminar boundary layers on a heated cylinder of arbitrary shape when the cylinder moves in an incompressible fluid at rest with an unsteady velocity. This analysis is based on solutions to the unsteady momentum and energy-integral equations in conjunction with a set of universal functions, derived from exact solutions to the boundary-layer equations for a specific unsteady problem. These universal functions are given in tabulated form. Those associated with the energy-integral equation are calculated with a Prandtl number of 0.7. The reliability and limitation of these functions are indicated and discussed in the light of several simple problems of which solutions are available. A detailed calculation procedure for the general unsteady problem is given and then followed by a numerical example.

THE study on laminar boundary layers in unsteady flows has recently attracted wider attention, primarily due to the growing realization of their importance in applications. However, because of the complication as a result of introducing the time variable into the analysis of laminar boundary-layer equations, practical solutions to these equations, exact or approximate, are rather difficult to obtain. Consequently, like some of the well-known classical solutions, most of the recent investigations on unsteady laminar-boundary layer problems have been restricted to either bodies of simple shapes, or specific time variations of the velocity in the undisturbed flow, or both For compressible flow, Moore [1][1] considered the unsteady motion of a heat-insulated semi-infinite plate and derived first-order deviations of some boundary-layer characteristics from their respective quasi-steady values, and his analysis was later extended to the case of an isothermal flat plate [2], thus yielding unsteady heat-transfer characteristics at the plate surface. For incompressible-flow cases, results have been more fruitful. Lighthill [3] studied skin-friction and heat-transfer behaviors on the surface of a cylinder oscillating in the direction of an oncoming steady flow by means of an integral procedure. Using a series expansion, Cheng and Elliott [4] succeeded in obtaining a solution to the problem of a semi-infinite plate moving with an arbitrary time-dependent velocity in a stagnant fluid. For the immediate vicinity of the forward stagnation point of a blunt-nosed cylinder, Rott [5] obtained an exact solution to the Navier-Stokes equa-

Contributed by the Applied Mechanics Division and presented at the Annual Meeting, November 30–December 5, 1958, New York, N. Y., of THE AMERICAN SOCIETY OF MECHANICAL ENGINEERS.

Discussion of this paper should be addressed to the Secretary, ASME, 29 West 39th Street, New York, N. Y., and will be accepted until July 10, 1959, for publication at a later date. Discussion received after the closing date will be returned

NOTE: Statements and opinions advanced in papers are to be understood as individual expressions of their authors and not those of the Society. Manuscript received by ASME Applied Mechanics Division, February 26, 1958. Paper No 58—A-49.

[1] Numbers in brackets designate References at end of paper.

Nomenclature

$A \equiv \left(\frac{4}{\xi^*}\right)\left(\frac{\partial u_\infty^*}{\partial x^*}\right)$

a = thermal diffusivity of fluid

$B \equiv \left(\frac{1}{\xi^{*2}}\right)\left(\frac{\partial \xi^*}{\partial t^*}\right)$

b = parameter in Lagrange's method for momentum-field calculations

$C \equiv \left(\frac{u_\infty^*}{\xi^{*2}}\right)\left(\frac{\partial \xi^*}{\partial x^*}\right)$

$c_f \equiv \frac{\tau_w}{\frac{1}{2}\rho u_0^2}$ = local skin-friction coefficient

$D \equiv \left(\frac{\partial u_\infty^*}{\partial x^*}\right)$

F_1, F_2, F_3, F_4, F_5 = universal functions of K

$G \equiv \Delta_1/\Delta_2$

g = arbitrary dimensionless function of t^*

$H \equiv \delta_1/\delta_2$

h = local coefficient of heat transfer

$K \equiv Z\xi$

k = thermal conductivity of fluid

L = a characteristic length of cylinder

M = quantity defined in Equation (24)

$\mathbf{N} = hL/k$ = Nusselt number

$P \equiv x^*/(u_\infty^* t^*)$

$\mathbf{R} \equiv Lu_0/\nu$ = Reynolds number

S = quantity defined in Equation (24)

T = temperature

t = time

$t^* \equiv u_0 t/L$ = a dimensionless time

t_s^* = a certain definite value of t^*

u, v = velocity components in the x and y- directions, respectively

u_0 = a constant reference velocity

$u^* \equiv u/u_0$

$W \equiv \Delta_2^2/\nu$

$W^* \equiv W\frac{u_0}{L}$

x = distance on cylinder surface measured from forward stagnation point or from leading edge

(Continued on next page)

tions of motion when the stagnation point itself is in motion over the surface. Moore [6] in a recent work utilized a similar analysis as that used in his compressible-flow problem to investigate unsteady boundary-layer characteristics for flow over wedges. Very recently, the author [7] solved exactly the laminar boundary-layer equations for an incompressible stagnation flow over a heated blunt-nosed body, which moves with a velocity inversely proportional to a linear function of time.

A general unsteady laminar boundary-layer problem in an incompressible flow is to consider the development of boundary layers on the surface of a heated cylinder of arbitrary shape, moving in a stagnant fluid with a velocity varying arbitrarily with time. The only method of solution available in the literature for this general problem seems to be that of Schuh [8], who, however, only considered the momentum field. In his analysis, the unsteady momentum-integral equation was utilized together with universal functions derived directly from different steady-flow velocity profiles. Since Schuh apparently was only interested in demonstrating the accuracy of his analysis by way of comparison with some available results of certain elementary unsteady problems, no calculation procedure for the general problem was indicated.

The purpose of this paper is to present a method of calculation to this general unsteady laminar boundary-layer problem including heat transfer. The analysis, which is a modification and extension of Schuh's procedure, also utilizes the unsteady momentum and energy-integral equations together with, however, an entirely different set of universal functions derived from unsteady velocity and temperature profiles. The relative merits of applying these different sets of universal functions will be indicated and discussed in the light of known solutions available in the literature for certain simpler problems. Also shown will be a complete, but still reasonably simple, calculation procedure for the general problem, based on solutions to the momentum and energy-integral equations by means of Lagrange's method. Finally, the calculation procedure is to be demonstrated by a numerical example for the case of a circular cylinder moving from rest with a constant acceleration, and the results for the momentum field compared with the well-known series solution.

Integral Equations and Universal Functions

In dealing with unsteady incompressible-flow problems with a cylinder moving in a stagnant fluid, it is customary, for reason of simplicity in analysis, to fix space co-ordinates on the cylinder surface, instead of in space. The equivalence between the problems using these two co-ordinate systems is exact, as long as the flow is incompressible. Thus we may now consider an equivalent problem of an incompressible fluid, flowing with an arbitrarily unsteady velocity over a stationary and heated cylinder of arbitrary shape. Under the conditions that Prandtl's boundary-layer assumptions are valid in this case and property values are constant, the development of momentum and thermal boundary layers are described by the following well-known equations:

Momentum equation

$$\frac{\partial u}{\partial t} + u\frac{\partial u}{\partial x} + v\frac{\partial u}{\partial y} = \frac{\partial u_\infty}{\partial t} + u_\infty\frac{\partial u_\infty}{\partial x} + \nu\frac{\partial^2 u}{\partial y^2} \tag{1}$$

Continuity equation

$$\frac{\partial u}{\partial x} + \frac{\partial v}{\partial y} = 0 \tag{2}$$

Energy equation

$$\frac{\partial T}{\partial t} + u\frac{\partial T}{\partial x} + v\frac{\partial T}{\partial y} = a\frac{\partial^2 T}{\partial y^2} \tag{3}$$

Initial conditions generally depend on specific problems, while the appropriate boundary conditions may be written as

$$y = 0 \qquad u = v = 0 \qquad T = T_w(x, t)$$

$$y \to \infty \qquad u \to u_\infty(x, t) \qquad T \to T_\infty$$

The present problem is restricted, however, only to the case where the cylinder surface is maintained at a uniform temperature.

The present method of solution resembles to a certain extent that of the well-known Holstein and Bohlen modification of the original Karman-Pohlhausen integral procedure for treating steady laminar boundary-layer problems. The momentum and energy-integral equations, which may be derived readily from Equations (1), (2), and (3), assume the following dimensionless forms, respectively:

$$\frac{\delta_2^2}{\nu}\frac{H}{u_\infty}\frac{\partial u_\infty}{\partial t} + \frac{\delta_2}{\nu}\frac{\partial(H\delta_2)}{\partial t} + u_\infty\frac{\delta_2}{\nu}\frac{\partial\delta_2}{\partial x} + (2 + H)\frac{\delta_2^2}{\nu}\frac{\partial u_\infty}{\partial x} = \frac{\tau_w\delta_2}{\mu u_\infty} \tag{4}$$

Nomenclature

$x^* \equiv x/L$

x_i^* = a certain definite value of x^*

y = distance normal to cylinder surface measured from surface

$Z \equiv \delta_2^2/\nu$

$Z^* \equiv Z\dfrac{u_0}{L}$

α = a dimensionless parameter for hyperbolic time-variation flow

β = parameter in Lagrange's method for energy-field calculations

Δ = a thermal boundary-layer thickness

$\Delta_1 \equiv \displaystyle\int_0^\Delta \theta dy$

$\Delta_2 \equiv \displaystyle\int_0^\Delta \frac{u}{u_\infty}\theta dy$

δ = a momentum boundary-layer thickness

$\delta_1 \equiv \displaystyle\int_0^\delta \left(1 - \frac{u}{u_\infty}\right) dy$

$\delta_2 \equiv \displaystyle\int_0^\delta \frac{u}{u_\infty}\left(1 - \frac{u}{u_\infty}\right) dy$

$\delta_2^* \equiv \delta_2\left(\dfrac{u_\infty}{\nu x}\right)^{1/2}$

$\theta \equiv (T - T_\infty)/(T_w - T_\infty)$

μ = dynamic viscosity of fluid

ν = kinematic viscosity of fluid

$\xi \equiv \dfrac{\partial u_\infty}{\partial x} + \dfrac{1}{u_\infty}\dfrac{\partial u_\infty}{\partial t}$

$\xi^* \equiv \xi\dfrac{L}{u_0}$

ρ = density of fluid

σ = Prandtl number

τ = shear stress

ϕ = a dimensionless function of x^*

Subscripts

0 = conditions at $t = 0$

w = wall conditions

∞ = conditions at outer edge of boundary layer

Superscript

$'$ = derivatives with respect to independent variable

$$\frac{\Delta_2}{\nu}\frac{\partial(G\Delta_2)}{\partial t} + \frac{\Delta_2}{\nu}\frac{\partial(u_\infty\Delta_2)}{\partial x} = -\frac{\Delta_2}{\sigma}\left(\frac{\partial\theta}{\partial y}\right)_w \tag{5}$$

where θ is the Pohlhausen variable defined by $(T - T_w)/(T_w - T_\infty)$. If now we assume that unsteady velocity and temperature profiles on an arbitrary cylinder all belong to a single-parameter family of curves and boundary-layer characteristics such as H, G, $\tau_w\delta_2/\mu u_\infty$, and $\Delta_2(\partial\theta/\partial y)_w$ are universal functions of this parameter.[2] Equations (4) and (5) are reducible to such forms that solutions are possible. Let this parameter be

$$K = Z\xi \tag{6}$$

where

$$Z = \frac{\delta_2^2}{\nu} \qquad \xi = \frac{\partial u_\infty}{\partial x} + \frac{1}{u_\infty}\frac{\partial u_\infty}{\partial t}$$

Equations (4) and (5) then become, respectively:

$$u_\infty^*\frac{\partial K}{\partial x^*} + F_1\frac{\partial K}{\partial t^*} = \xi^*[F_3 + K(C - A + HB)] \tag{7}$$

$$u_\infty^*\frac{\partial W^*}{\partial x^*} + G\frac{\partial W^*}{\partial t^*} = \frac{F_5}{\sigma} - 2W^*\left(F_4\frac{\partial K}{\partial t^*} + D\right) \tag{8}$$

where H, G, F_1, F_3, F_4, and F_5 are all universal functions of K with

$$F_1 = H + 2K\frac{dH}{dK} \qquad F_3 = 2F_2 - 2KH$$

$$F_2 = \frac{\tau_w\delta_2}{\mu u_\infty} \qquad F_4 = \frac{dG}{dK}$$

$$F_5 = -2\Delta_2\left(\frac{\partial\theta}{\partial y}\right)_w$$

and

$$A = \frac{4}{\xi^*}\frac{\partial u_\infty^*}{\partial x^*} \qquad B = \frac{1}{\xi^{*2}}\frac{\partial\xi^*}{\partial t^*}$$

$$C = \frac{u_\infty^*}{\xi^{*2}}\frac{\partial\xi^*}{\partial x^*} \qquad D = \frac{\partial u_\infty^*}{\partial x^*}$$

Further, the asterisk refers to dimensionless quantities defined in the Nomenclature. Note that Equation (7) is similar to that used by Schuh [8].

In a specific problem, Equations (7) and (8) may be solved when K and W^* are known functions of x^* at a certain instant t^*. If the cylinder under consideration moves steadily first, and then changes to an unsteady velocity, functions K and W^* may be calculated from the steady-flow theory for the instant the velocity of the cylinder changes from steady conditions. These functions may then serve as initial conditions for the unsteady problem. On the other hand, when the cylinder moves from rest with an unsteady velocity, W^* is obviously zero for any x^* at $t^* = 0$. However, as both Z^* and $1/\xi^*$ also vanish at $t^* = 0$, the initial value of K must be determined from a limiting procedure as follows: For an incompressible flow, the dimensionless free-stream velocity distribution, without losing any generality, may be written as

$$u_\infty^* = \phi(x^*)g(t^*) \tag{9}$$

where $\phi(x^*)$ physically represents the steady-flow free-stream velocity distribution on the same cylinder, while $g(t^*)$ indicates the unsteadiness in the velocity of the undisturbed flow. Based on Equation (9), the initial value of K for any x^* becomes

$$K_0 = \lim_{t^*\to 0}\frac{Z^*(\phi' g^2 + g')}{g} = \left[Z^*\left(\frac{g''}{g'}\right) + \frac{\partial Z^*}{\partial t^*}\right]_0 = \left(\frac{\partial Z^*}{\partial t^*}\right)_0 \tag{10}$$

provided that $g'(0)$ is not zero. Equation (7), when substituted with Equation (10) and evaluated at $t^* = 0$, then assumes the following form:

$$3K_0H(K_0) = 2F_3(K_0) \tag{11}$$

from which K_0 may be uniquely determined, once the universal functions are known. This limiting procedure can be extended to cases such as $g(0) = g'(0) = 0$, $g''(0) \neq 0$[3]; $g(0) = g'(0) = g''(0) = 0$, $g'''(0) \neq 0$, etc.

Universal functions associated with Equations (7) and (8) are now considered. As pointed out previously, the author [7] has obtained exact solutions to Equations (1), (2), and (3) for the special case of a "hyperbolic time-variation" flow over the forward stagnation point of a heated cylinder with a free-stream velocity distribution given by

$$u_\infty^* = \frac{x^*}{1 - \alpha t^*} \tag{12}$$

where α is a flow parameter, of which positive values indicate acceleration, while negative values imply deceleration. Unsteady laminar boundary-layer characteristics have been reported in [7] for a range of α from -3.0 to $+1.0$,[4] and this range has recently been extended to $\alpha = +1.6$. Since it is known in steady-flow cases that the growths of both momentum and thermal laminar boundary layers along an arbitrary cylinder are rather small except in the immediate neighborhood of the separation point, it is therefore reasonable to expect that those unsteady boundary-layer characteristics from the afore-mentioned exact solutions could be used with good accuracy to yield appropriate universal functions for the general unsteady problem, especially when the acceleration or deceleration in the undisturbed flow is large. Consequently, it is only necessary now to establish a unique relationship between the parameter K of our present problem and the parameter of the exact solutions. According to the exact solutions and the definition of K in Equation (6), it may be shown readily that this relationship is

$$K = \delta_2^{*2}(1 + \alpha) \tag{13}$$

where δ_2^*, a dimensionless momentum thickness, is a pure function of α as calculated from the exact solutions. On the basis of Equation (13), universal functions H, G, F_1, F_2, F_3, F_4, and F_5 have been calculated for a range of K from -0.1323 corresponding to separation up to $+0.21$ and are shown in Table 1. It should be pointed out, however, that the values of these functions at $K = -0.1323$ are extrapolated.

Schuh [8] in his study has proposed the use of two different sets of universal functions based on different velocity profiles for steady flow, one being the fourth-degree polynomial of Pohlhausen for $K < 0$, and the other the Hartree wedge-flow velocity profiles for $K > 0$. An inherent weak point of these universal functions is obviously in their composite structure, since in the general case where an arbitrary cylinder is considered, the value of K always varies in its full range. Furthermore, the accuracy of these universal functions has to be limited when the unsteadiness in the flow velocity becomes large, since in this case, steady-

[2] Even though the Prandtl number σ is actually another parameter, it may be treated simply as a constant for the entire problem.

[3] For this case, it may be shown readily that $K_0 = 2(\partial Z^*/\partial t^*)_0$.

[4] Separation occurs at $\alpha = -3.175$.

Table 1 Universal functions for unsteady laminar boundary layers in an incompressible flow

K	H	G $\sigma = 0.7$	F_1	F_2	F_3	F_4 $\sigma = 0.7$	F_5 $\sigma = 0.7$
0.210	2.040	1.221	1.448	0.468	0.082	−4.241	0.756
0.200	2.054	1.262	1.554	0.462	0.101	−4.044	0.774
0.190	2.066	1.301	1.611	0.454	0.121	−3.894	0.785
0.180	2.080	1.338	1.639	0.446	0.142	−3.777	0.787
0.170	2.092	1.376	1.662	0.438	0.163	−3.682	0.784
0.160	2.105	1.412	1.686	0.428	0.184	−3.601	0.779
0.150	2.119	1.449	1.710	0.420	0.206	−3.536	0.771
0.140	2.132	1.483	1.737	0.411	0.226	−3.495	0.761
0.130	2.147	1.520	1.764	0.402	0.247	−3.468	0.751
0.1215	2.159	1.549	1.788	0.394	0.264	−3.453	0.743
0.120	2.161	1.554	1.793	0.392	0.268	−3.452	0.741
0.110	2.176	1.588	1.823	0.384	0.289	−3.462	0.730
0.100	2.192	1.620	1.855	0.374	0.310	−3.485	0.719
0.090	2.210	1.656	1.892	0.365	0.331	−3.524	0.708
0.080	2.228	1.692	1.932	0.354	0.353	−3.571	0.696
0.070	2.247	1.728	1.977	0.344	0.375	−3.631	0.685
0.060	2.266	1.764	2.025	0.334	0.397	−3.720	0.673
0.050	2.289	1.803	2.076	0.324	0.419	−3.836	0.662
0.040	2.309	1.842	2.131	0.313	0.441	−3.954	0.650
0.030	2.332	1.882	2.191	0.302	0.463	−4.089	0.638
0.020	2.356	1.925	2.256	0.291	0.486	−4.240	0.626
0.010	2.381	1.969	2.328	0.279	0.509	−4.409	0.613
0	2.408	2.013	2.410	0.266	0.532	−4.607	0.601
−0.010	2.438	2.059	2.500	0.253	0.556	−4.870	0.589
−0.020	2.471	2.108	2.606	0.240	0.580	−5.209	0.576
−0.030	2.506	2.162	2.726	0.226	0.604	−5.590	0.563
−0.040	2.544	2.220	2.864	0.212	0.628	−6.026	0.550
−0.050	2.586	2.283	3.040	0.196	0.653	−6.558	0.534
−0.055	2.609	2.318	3.125	0.189	0.665	−6.870	0.528
−0.060	2.631	2.353	3.220	0.181	0.677	−7.210	0.521
−0.065	2.655	2.390	3.325	0.173	0.691	−7.600	0.513
−0.070	2.682	2.429	3.450	0.164	0.704	−8.050	0.506
−0.075	2.710	2.469	3.570	0.156	0.718	−8.600	0.498
−0.080	2.738	2.515	3.735	0.146	0.732	−9.100	0.489
−0.085	2.770	2.562	3.920	0.137	0.746	−9.850	0.480
−0.090	2.806	2.613	4.140	0.128	0.760	−10.60	0.471
−0.095	2.843	2.668	4.400	0.117	0.775	−11.55	0.461
−0.100	2.883	2.726	4.725	0.106	0.789	−12.70	0.451
−0.105	2.935	2.790	5.050	0.094	0.803	−14.30	0.440
−0.110	2.990	2.864	5.620	0.081	0.819	−16.35	0.429
−0.115	3.053	2.951	6.320	0.066	0.836	−19.40	0.417
−0.120	3.132	3.063	7.390	0.052	0.854	−25.80	0.404
−0.125	3.235	3.230	9.300	0.032	0.873	−37.60	0.388
−0.130	3.388	3.440	12.50	0.008	0.893	−58.10	0.356
−0.1323	3.470	3.550	15.10	0	0.905	−71.30	0.336

flow velocity profiles are not expected to describe appropriately the corresponding unsteady profiles.

In order to demonstrate the accuracy and limitation of the universal functions in Table 1, several simple unsteady problems are considered in the following paragraphs. Whenever possible, results from other available exact or approximate solutions to the same problem are utilized for comparison.

When the velocity along an infinitely long flat plate, which is initially at rest, undergoes a stepwise change, an unsteady momentum boundary layer develops on the plate surface. The exact solution to this classical problem is well known. Equation (4), when applied to this case reduces to

$$\frac{\delta_1}{\nu}\frac{d\delta_1}{dt} = F_2(0)H(0) \tag{14}$$

since K is identically zero. Solution to Equation (14) is elementary and assumes the form $\delta_1/(\nu t)^{1/2} = 1.132$, according to functions listed in Table 1. This constant compares with 1.128 from the exact solution, 1.068 from Hartree's profiles, and 1.095 from Pohlhausen's fourth-degree velocity polynomial. Physically, this problem represents a case of large acceleration, and therefore it is not surprising that the universal functions in Table 1 yield very accurate results, especially when compared with those based on steady-flow velocity profiles. Incidentally, Schuh [8] also has applied universal functions based on Pohlhausen's profiles to an energy (kinetic)-integral equation,[5] and obtained for the same problem a result of $\delta_1/(\nu t)^{1/2} = 1.132$, which is the same as that from using the momentum-integral equation with functions in Table 1. However, this kinetic-energy-integral equation is of no practical interest, since it is too complicated for practical application in the general unsteady problem.

Another classical unsteady problem, of which there is an exact solution, also deals with an infinitely long flat plate, which, however, moves from rest with a constant acceleration. For this case, Equation (4) reduces to

$$\frac{\delta_1}{\nu u_\infty}\frac{d(u_\infty\delta_1)}{dt} = HF_2 \tag{15}$$

and K becomes a constant K_0, since $K = \delta_2^2/\nu t$. A solution to Equation (15) may be written as

$$\delta_1^2/\nu t = \frac{2}{3}H(K_0)F_2(K_0)$$

which, together with

$$K_0 = \delta_2^2/\nu t = (1/H^2)(\delta_1^2/\nu t)$$

yields an equation identical to Equation (11), from which K_0 is

[5] This equation is obtained by multiplying Equation (1) by u and then integrating across the boundary layer.

Table 2 Unsteady local skin-friction and heat-transfer characteristics for a semi-infinite plate moving from rest with a constant acceleration

	$c_f\mathbf{R}^{1/2}u_\infty^{*-3/2}x^{*-1/2}$				$\mathbf{NR}^{-1/2}x^{*1/2}u_\infty^{*-1/2}$	
P	Present solution	Hartree's profiles	Moore [1]	Cheng and Elliott [4]	Present solution $\sigma = 0.7$	Ostrach [2] $\sigma = 0.72$
0	0.729	0.664	0.664	0.664	0.325	0.296
0.1	0.905	0.889	0.834	0.840	0.335	0.294
0.2	1.065	1.094	1.003	1.034	0.346	0.292
0.3	1.240	1.276	1.173	1.236	0.246	0.290
0.4	1.432	1.474	1.343	1.427	0.284	0.288
0.5	1.601	1.648	1.512	1.596	0.317	0.286
0.6	1.754	1.805	1.682	1.748	0.347	0.284
0.7	1.894	1.949	1.852	1.888	0.375	0.282
0.8	2.025	2.084	2.021	2.019	0.401	0.280
0.9	2.148	2.210	2.191	2.141	0.426	0.278
1.0	2.264	2.330	2.361	2.257	0.449	0.275

determined as $+0.1215$ from values in Table 1. Therefore the final solution to this problem is $\delta_1/(\nu t)^{1/2} = 0.753$, which is compared with 0.7512 from the exact solution, and 0.776 from Hartree's profiles. It is seen that universal functions proposed in the present paper again yield results in closer agreement with the exact solution.

In the case of a semi-infinite plate moving with a constant acceleration from rest, the solution is not too simple. With $\xi^* = 1/t^*$, $C = 0$, $A = 0$, $B = -1$, Equation (7) reduces to

$$u_\infty^* \frac{\partial K}{\partial x^*} + F_1 \frac{\partial K}{\partial t^*} = \frac{F_2 - KH}{t^*} \tag{16}$$

If we assume that in this problem K is only a function of a new independent variable P, defined as $P = x^*/u_\infty^* t^*$, Equation (16) may be reduced to a total differential equation:

$$\frac{dK}{dP} = \frac{F_2 - kH}{1 - 2PF_1} = \frac{2F_2 - 3KH}{1 - 2PF_1} \tag{17}$$

Owing to the presence of the leading edge, there are two boundary conditions to be satisfied. At the leading edge, the boundary-layer thickness remains zero at any t^*, i.e., $K(0) = 0$. In addition, at $t^* = 0$, the boundary-layer thickness is zero over the entire length of the plate, i.e., $K(\infty) = +0.1215$ according to Equation (11). Since only one condition is required to solve Equation (17), the complete solution may be considered as consisting of two parts. The solution to Equation (17) with the boundary condition $K(0) = 0$ has been obtained by the method of isoclines up to a P-value of 0.279, at which $K = 0.1215$. For the range $0.279 \leq P \lesssim \infty$, the condition $K(\infty) = +0.1215$ is valid and the solution is simply $K(P) = +0.1215$. From this complete solution, local skin-friction coefficient may then be calculated according to the relations

$$c_f\mathbf{R}^{1/2}u_\infty^{*-3/2}x^{*-1/2} = \begin{cases} 2F_2\sqrt{(P/K)} & 0 \leq P \leq 0.279 \\ 2.264\sqrt{P} & 0.279 \leq P \leq \infty \end{cases}$$

Table 2 shows a comparison of this result for different values of P with that of other available methods of solution to the same problem. The values calculated from Cheng and Elliott's analysis [4] are probably the most accurate, as their solution is based on a series expansion for small values of P and an exact solution for large P-values. Moore's solution [1] is only valid when flow is nearly quasi-steady; i.e., P is close to zero. Results based on Hartree's profiles do enjoy certain advantage over the present method for very small values of P. However, as P increases, this advantage diminishes quickly and the present solution becomes much more accurate. Obviously, this is due to the steady-flow nature of Hartree's profiles.

A similar analysis has been carried out for the temperature field of this same problem, and the heat-transfer coefficients thus calculated may be compared with that of Ostrach's study [2], which again deals only with nearly quasi-steady conditions. This comparison is also shown in Table 2. The discontinuity in the present solution arises from the two different boundary conditions associated with the transformed energy equation. It is surprising to note that, for P-values close to zero, the rate of change of local Nusselt numbers from the present solution with respect to P is different from that in Ostrach's results, even though the magnitudes still agree satisfactorily. Owing to the nature of these two solutions, Ostrach's results have to be taken as more accurate, at least in this region. However, the present solution again tends to be more reliable as P becomes large.

The integral equations, together with universal functions in Table 1, are expected to yield very accurate results for a stagnation flow with large unsteadiness. This may be demonstrated by considering the flow to the immediate neighborhood of the forward stagnation point of a blunt-nosed cylinder, undergoing a stepwise velocity change from rest. For this case, Equation (7) reduces to

$$\frac{dK}{dt^*} = \frac{F_2 - 4K}{F_1} \tag{18}$$

which, together with the condition $K(0) = 0$, may be integrated easily. Skin-friction coefficients, calculated from the result of Equation (18), are shown in Table 3 together with corresponding values from the classical series solution. Agreement at small values of t^* is excellent, and as t^* increases, the present result becomes much more accurate and approaches the steady-flow value asymptotically.

As already pointed out, the present solution tends to be less accurate in the immediate vicinity of the separation point, even when the unsteadiness in flow velocity is large. An explanation is that in this region, the boundary-layer thickens so rapidly that the velocity profiles at the vicinity of the forward stagnation point with the same unsteadiness in the free-stream velocity do not describe adequately those near the separation point. The extent of this inaccuracy may be seen in an example of predicting the instant at which the flow at the rearward stagnation point of a cylinder first separates from the cylinder surface, when the

Table 3 Skin-friction coefficients at forward stagnation point of a cylinder moving from rest with a stepwise velocity change

	$c_f\mathbf{R}^{1/2}u_\infty^{*-1}$	
t^*	Present solution	Series solution
0	∞	∞
0.1	4.091	4.077
0.2	3.246	3.242
0.3	2.921	2.941
0.4	2.759	2.800
0.5	2.661	2.732
1.0	2.500	2.735
∞	2.465	∞

cylinder undergoes a stepwise velocity change from rest. Equation (18) is still applicable, except that now the integration is performed from $K = 0$ to $K = -0.1323$. The result thus calculated shows that the first separation occurs at $t^* = 0.587$, compared to 0.639 from the series solution and 0.623 from the Pohlhausen profiles. Even though the exact quantity is not known, the value 0.639, however, is probably the most accurate. It is surprising that Pohlhausen's profiles predict the separation point rather accurately in the unsteady case, while it is well known that in the steady-flow case they fail to do so almost completely.

In view of the foregoing comparisons, it may be concluded that the unsteady integral equations, together with universal functions proposed in this paper are capable of yielding very accurate results in unsteady laminar boundary-layer problems, especially when the unsteadiness in the free-stream velocity is large. The only limitation seems to be that the present solution is not able to predict separation point too closely. However, for this purpose alone the present set of universal functions can always be replaced by that based on Pohlhausen's velocity polynomial. Other practical advantages of the universal functions in Table 1 over those based on steady-flow velocity profiles as calculated by Schuh [8] are that no discontinuity exists in any of the functions for the entire range of K, that the K-range extends to higher positive value so that unsteady problems dealing with very large acceleration also may be handled, and that unsteady heat-transfer characteristics for $\sigma = 0.7$ on an isothermal surface may be determined at the same time.

Solutions to Integral Equations and Calculation Procedure

Since Equations (7) and (8) are two linear first-order partial differential equations, they may be solved by the well-known Lagrange method. Equation (7), which is independent of Equation (8), is first considered. The characteristic equations may now be written as

$$\frac{dx^*}{dt^*} = \frac{{u_\infty}^*}{F_1} \tag{19}$$

$$\frac{dK}{dt^*} = \frac{\xi^*}{F_1}\left[F_2 + K(C - A + HB)\right] \tag{20}$$

which must be integrated simultaneously along the same characteristic. Equation (19) has a general solution in the form of $x^* = x^*(b, t^*)$, where b is an arbitrary constant of integration, which defines the characteristic curve. On the basis of this solution, Equation (20) then becomes a total differential equation, which, together with the initial condition $K(x^*, 0)$ or $K_0(x^*)$, may be solved, resulting in $K = K(b, t^*)$. By eliminating b from $K = K(b, t^*)$ and $x^* = x^*(b, t^*)$, we obtain the desired solution $K = K(x^*, t^*)$. A calculation procedure may now be described.

Without loss of generality, the constant b may be considered as the value of x^* at $t^* = 0$. With an arbitrarily chosen value of b, Equations (19) and (20) are then integrated according to

$$\int_b^{x^*} \frac{dx^*}{\phi(x^*)} = \int_0^{t^*} \frac{g(t^*)}{F_1}\,dt^* \tag{21}$$

$$K - K_0(b) = \int_0^{t^*} \frac{\xi^*}{F_1}\left[F_2 + K(C - A + HB)\right]dt^* \tag{22}$$

The procedure of numerical calculation obviously involves cut and trial. If the time interval is taken small enough, the simple trapezium rule may be used for all stepwise integrations without introducing appreciable inaccuracy. For any value of t^*, or t_i^*, a K-value is first assumed. This leads to a value for F_1, based on which Equation (21) may be integrated, resulting in x_i^*. For the same values of K, x_i^*, and t_i^*, the integrand in Equation (22) is next calculated, and then one further step of integration yields K, which is to be checked with the value originally assumed. When more accurate results are desirable, any integration step can be carried out by the usual Simpson rule. The only difference in the procedure is that now a pair of K-values at two adjacent values of t^* has to be assumed. This cut-and-trial procedure is then repeated for increasing values of t^* until either K reaches -0.1323 or a prescribed t^* is attained, depending primarily on the b-value chosen.

The result thus calculated represent $K = K[x^*(b, t^*), t^*]$. Similar calculations are then made for other different values of b until a prescribed portion of the cylinder surface is covered. Finally, plotting up all the results for various b-values yields the solution $K = K(x^*, t^*)$.

The calculation procedure of the solution to the energy integral equation is even simpler. It is based on the following set of equations derived from the characteristic equations of Equation (8):

$$\int_\beta^{x^*} \frac{dx^*}{\phi(x^*)} = \int_0^{t^*} \frac{g(t^*)}{G}\,dt^* \tag{23}$$

$$W^* = e^{-\int_0^{t^*} M dt^*}\left[{W_0}^*(\beta) + \int_0^{t^*} S e^{\int_0^{t^*} M dt^*}\,dt^*\right] \tag{24}$$

where

$$M = \frac{2}{G}\left(F_4\frac{\partial K}{\partial t^*} + D\right) \qquad S = \frac{F_5}{\sigma G}$$

and β is another constant of integration similar to b for the momentum field. Since now G is a known function of K, Equation (23) becomes independent of Equation (24), and hence may be solved first by a procedure similar to that of solving Equation (21), resulting in $x^* = x^*(\beta, t^*)$. It is then substituted in Equation (24), yielding $W^* = W^*[x^*(\beta, t^*), t^*]$. Again these calculations are repeated for different β-values until it covers a desired portion on the cylinder surface. A final plot of all the results thus obtained represents the complete solution $W^* = W^*(x^*, t^*)$.

Finally, unsteady skin-friction and heat-transfer characteristics may be calculated, respectively, from the following equations:

$$c_f \mathbf{R}^{1/2} = \frac{2F_2{u_\infty}^*}{(K/\xi^*)^{1/2}} \tag{25}$$

$$\mathbf{N}\mathbf{R}^{-1/2} = \frac{F_5}{2(W^*)^{1/2}} \tag{26}$$

A Numerical Example

In order to demonstrate the calculation procedure described in the foregoing, a complete numerical example has been calculated for the case of a uniformly heated circular cylinder, moving from rest with a constant acceleration in a stagnant field of air. The reason for choosing this problem is that, at least for the momentum field, the results from the present calculation may be compared directly with that from the classical series solution, which is known to be accurate for short time elapses. For simplification, the free-steam velocity distribution in the present problem is assumed to be given by

$${u_\infty}^* = 2t^* \sin 2x^* \tag{27}$$

with $\phi(x^*) = 2 \sin 2x^*$ and $g(t^*) = t^*$. For any b or β, $K_0(b)$ and ${W_0}^*(\beta)$ now have constant values of $+0.1215$ and zero, respectively.

Calculations have been made for the following b and β-values:

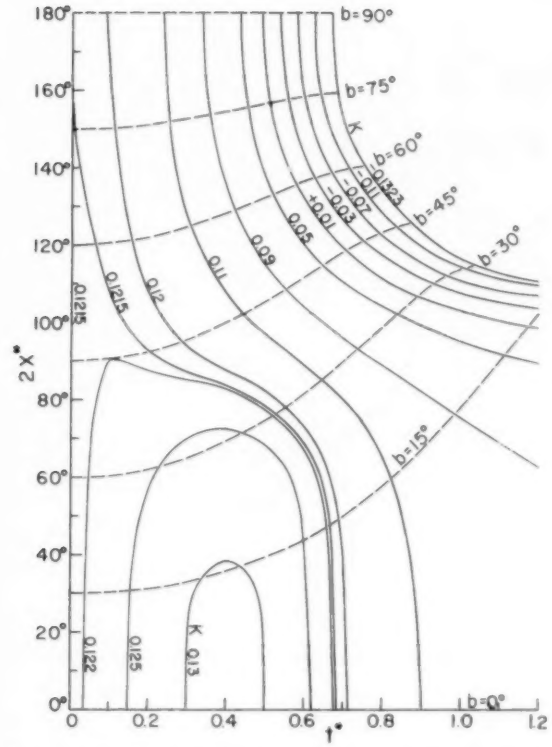

Fig. 1 Solutions to equations (21) and (22) for the numerical example

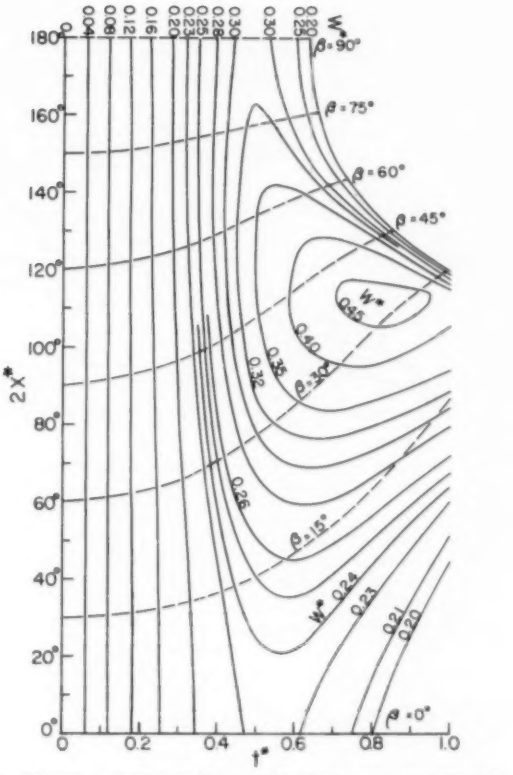

Fig. 2 Solutions to equations (23) and (24) for the numerical example

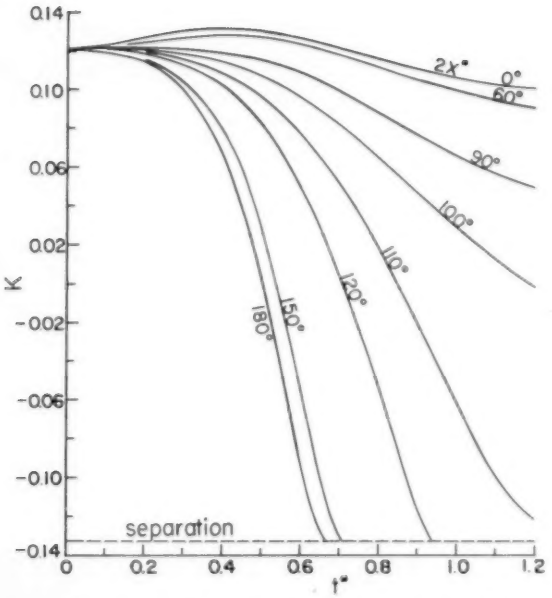

Fig. 3 Development of momentum boundary layer on circular cylinder

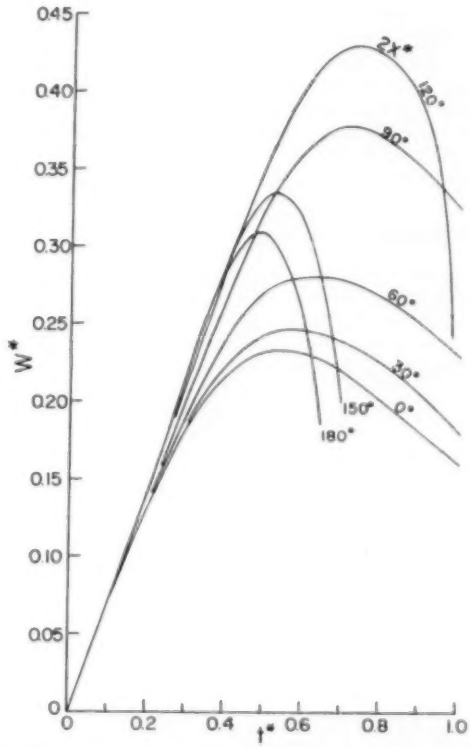

Fig. 4 Development of thermal boundary layer on circular cylinder

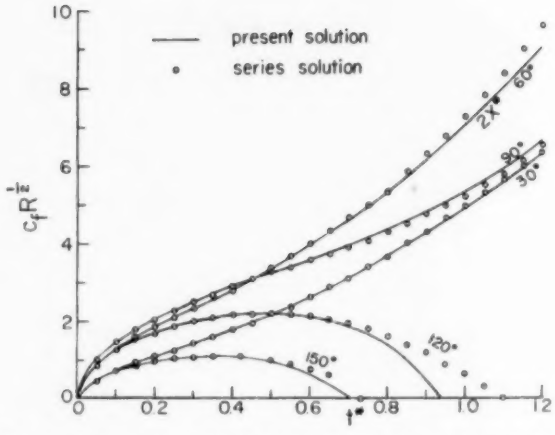

Fig. 5 Unsteady local skin-friction coefficients on circular cylinder

0°, 15°, 30°, 45°, 60°, 75°, 90°, where 0° correspond to the forward stagnation point and 90° the rearward stagnation point. Fig. 1 shows the result for the momentum field, and Fig. 2 that of the energy field. Simple cross plots may then be made to yield the desired solution; namely, $K = K(x^*, t^*)$ and $W^* = W^*(x^*, t^*)$, which are shown, respectively, in Figs. 3 and 4.

Finally, unsteady skin-friction and heat-transfer characteristics for this problem are calculated from Equations (25) and (26). These final results are shown in Figs. 5 and 6.

Also indicated in Fig. 5 are the same characteristics from the classical series solution. In the region of small t^*-values, the agreement is excellent, indicating the reliability of the present solution. It may be of interest to know that separation first occurs at the rearward stagnation point at $t^* = 0.675$, compared to 0.721 from the same series solution.

Because of its simplicity, the present analysis may be extended to other unsteady laminar boundary-layer problems, such as problems involving suction or blowing, large temperature differences or compressible flow. Work along these lines is progressing satisfactorily here at the University of Notre Dame, and results will be published at a future date.

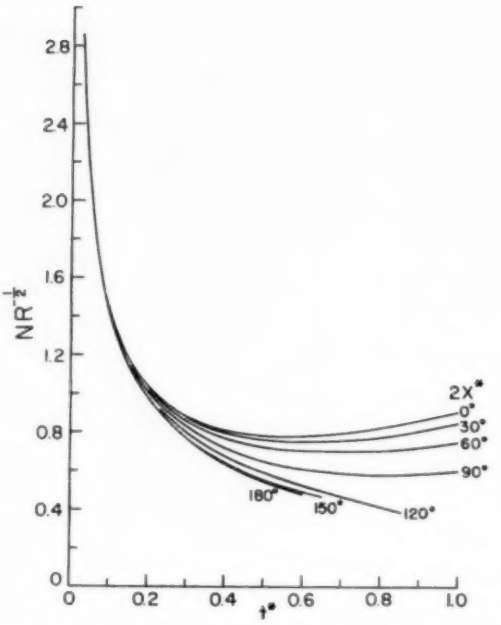

Fig. 6 Unsteady heat-transfer characteristics on circular cylinder

Acknowledgment

The present study is a part of a research program on unsteady laminar boundary layers with heat transfer sponsored by the National Science Foundation under Contract NSF G-2772 with the University of Notre Dame. Their financial assistance is hereby gratefully acknowledged.

References

1 F. K. Moore, "Unsteady Laminar Boundary-Layer Flow," NACA TN 2471, 1951.

2 S. Ostrach, "Compressible Laminar Boundary Layer and Heat Transfer for Unsteady Motions of a Flat Plate," NACA TN 3569, 1955.

3 M. J. Lighthill, "The Response of Laminar Skin Friction and Heat Transfer to Fluctuations in the Stream Velocity," *Proceedings of the Royal Society*, London, England, series A, vol. 224, 1954, pp. 1–23.

4 S. I. Cheng and D. Elliott, "The Unsteady Laminar Boundary Layer on a Flat Plate," preprints of Papers, Heat Transfer and Fluid Mechanics Institute, Stanford University, Stanford, Calif., 1956, pp. 221–238.

5 N. Rott, "Unsteady Viscous Flow in the Vicinity of a Stagnation Point," *Quarterly of Applied Mathematics*, vol. 13, January, 1956 pp. 444–451.

6 F. K. Moore, "The Unsteady Laminar Boundary Layer of a Wedge and a Related Three-Dimensional Problem," Preprints of Papers, Heat Transfer and Fluid Mechanics Institute, California Institute of Technology, Pasadena, Calif., 1956, pp. 99–117.

7 K-T. Yang, "Unsteady Laminar Boundary Layers in an Incompressible Stagnation Flow," JOURNAL OF APPLIED MECHANICS, vol. 25, TRANS. ASME, vol. 80, 1958, pp. 421–427.

8 H. Schuh, "Calculation of Unsteady Boundary Layers in Two-Dimensional Laminar Flow," *Zeitschrift für Flugwissenschaften*, vol. 1 1953 pp. 122–131.

On Journal Bearings of Finite Length With Variable Viscosity

L. N. TAO
Assistant Professor of Mechanics, Illinois Institute of Technology, Technology Center, Chicago, Ill. Assoc. Mem. ASME

An exact solution of the Reynolds equation for journal bearings of finite length with viscosity as a function of pressure is found. The analytical solution is expressed in terms of Heun functions. The load capacity and the attitude angle are derived. It is found that the load vector, in general, is not perpendicular to the line of journal and bearing centers as shown in the constant-viscosity case.

SINCE the establishment of the governing equation of hydrodynamic lubrication some 70 years ago by Reynolds [1],[1] numerous works on the solutions of the equation have been published. For a plane rectangular slider bearing, which is equivalent to lubricant flow between two nonparallel surfaces in relative motion, solutions for both infinite and finite widths have been obtained. Michell [2] and Muskat, et al. [3], gave their solutions for a finite-width bearing in terms of Bessel functions. In the case of a journal bearing, which is equivalent to lubricant flow between two eccentric cylinders in relative motion, Sommerfeld [4] showed that for an infinitely long bearing the Reynolds equation becomes an ordinary differential equation. The solution of the problem is obtainable in closed form by direct integrations. For a journal bearing of finite length an exact solution only recently has been established [5]. It is shown that with constant viscosity the solution of a finite journal bearing may be expressed in terms of some comparatively unknown functions, the Heun functions. Also the locus of the journal center (relative position of journal and bearing centers) is found to be always perpendicular to the load vector. This does not quite agree with experimental test results, although the solution is exact in the mathematical sense.

In the present paper the study is extended to problems with variable viscosity (as a function of pressure). The pressure distribution in the journal bearing is established. The load capacity and the attitude angle (angle between the load vector and line of centers) are then derived. The lower and upper bounds of the load capacity also are given.

Reynolds Equation

The Reynolds equation of hydrodynamic lubrication was derived based on the fact that the film thickness of the lubricant between the surfaces is small in comparison with other dimensions of physical interest. This leads to the conclusion that the contribution to the pressure gradient may be averaged over the thickness of the film. Mathematically, this gives the relation that the velocity vector $\bar{q}$ in the film due to the pressure gradients is

$$\bar{q} = \left(\frac{h^2}{12\mu}\right)\nabla p \tag{1}$$

where $\bar{q}$ and the fluid pressure p are to be averaged over the film thickness h, and μ is the viscosity of the lubricant. Also the dragging and pumping effect due to the relative motion U of the surfaces is $Uh/2$. Applying the continuity equation to the lubricant film, we then immediately get

$$\nabla\cdot\left(\frac{h^3}{12\mu}\nabla p\right) = \frac{U}{2}\frac{\partial h}{\partial x} \tag{2}$$

where x is taken in the direction of rotation.

Now let x and z be the co-ordinates along the circumferential and axial directions of the bearing, Fig 1. The film thickness h may then be written as

$$h = c(1 + \eta\cos\theta) \text{ and } \eta = \frac{e}{c} \tag{3}$$

where r, c, e, and η are the radius, radial clearance, eccentricity, and eccentricity ratio of the bearing, respectively. Introducing dimensionless quantities

$$\theta = \frac{x}{r} \quad \text{and} \quad Z = \frac{z}{r} \tag{4}$$

the Reynolds equation for journal bearing becomes

$$\frac{\partial}{\partial\theta}\left[\frac{(1+\eta\cos\theta)^3}{\mu}\frac{\partial p}{\partial\theta}\right] + \frac{\partial}{\partial Z}\left[\frac{(1+\eta\cos\theta)^3}{\mu}\frac{\partial p}{\partial Z}\right] = \frac{6Ur}{c^2}(-\eta\sin\theta) \tag{5}$$

subject to the boundary conditions

$$p(-\pi, Z) = p(\pi, Z) \tag{6a}$$

$$\frac{\partial p(-\pi, Z)}{\partial\theta} = \frac{\partial p(\pi, Z)}{\partial\theta} \tag{6b}$$

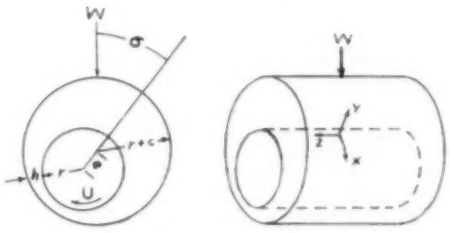

Fig. 1 Journal-bearing configuration

[1] Numbers in brackets designate References at end of paper.

Contributed by the Applied Mechanics Division and presented at the Annual Meeting, November 30–December 5, 1958, New York, N. Y., of THE AMERICAN SOCIETY OF MECHANICAL ENGINEERS.

Discussion of this paper should be addressed to the Secretary, ASME, 29 West 39th Street, New York, N. Y., and will be accepted until July 10 1959, for publication at a later date. Discussion received after the closing date will be returned.

NOTE: Statements and opinions advanced in papers are to be understood as individual expressions of their authors and not those of the Society. Manuscript received by ASME Applied Mechanics Division, April 21, 1958. Paper No. 58—A-75.

$$p(\theta, -L/2) = 0 \tag{6c}$$

$$p(\theta, L/2) = 0 \tag{6d}$$

where $L = l/2r$ and l is the length of the bearing. The first two conditions (6a) and (6b) insure the continuity of the pressure and its first derivative along the circumferential direction, while the last two conditions (6c) and (6d) state that the pressure at the free ends is atmospheric.

Since μ is a function of p, in order to remove the nonlinearity of the equation, we introduce

$$\Omega = \mu_0 \int_0^p \frac{dp}{\mu} \tag{7}$$

where μ_0 is a reference viscosity, the value at $p = 0$. To facilitate the necessary information for integration, the widely used expression between μ and p is employed,

$$\mu = \mu_0 e^{bp} \tag{8}$$

This expression also has been used in the study of slider-bearing lubrication by Charnes and Saibel [11]. Though this expression is empirically determined, it does have a theoretical interpretation in the study of kinetics of liquid [6]. Hence Equation (7) becomes

$$\Omega = \frac{1}{b}(1 - e^{-bp})$$

or

$$p = -\frac{1}{b}\log(1 - b\Omega) \tag{9}$$

Since e^{-bp} is always positive, this implies that $b\Omega$ is always less than unity. Particularly, for positive p, $b\Omega$ is in the range between 0 and 1.

To remove the nonhomogeneous term in the equation,

$$\frac{\partial}{\partial\theta}\left[(1 + \eta\cos\theta)^3 \frac{\partial\Omega}{\partial\theta}\right] + \frac{\partial}{\partial Z}\left[(1 + \eta\cos\theta)^3 \frac{\partial\Omega}{\partial Z}\right] = -\frac{6\mu_0 U r\eta}{c^2}\sin\theta \tag{10}$$

we write

$$\Omega(\theta, Z) = \zeta(\theta, Z) + \xi(\theta) \tag{11}$$

where $\xi(\theta)$ satisfies the equation of the infinitely long journal bearing, i.e.,

$$\frac{d}{d\theta}\left[(1 + \eta\cos\theta)^3 \frac{d\xi}{d\theta}\right] + \frac{6\mu_0 U r\eta}{c^2}\sin\theta = 0 \tag{12}$$

and boundary conditions

$$\xi(-\pi) = \xi(\pi)$$

and (13)

$$\frac{d\xi(-\pi)}{d\theta} = \frac{d\xi(\pi)}{d\theta}$$

The solution of Equation (10) with the given boundary conditions is [4]

$$\xi(\theta) = \frac{6\mu_0 U r\eta}{c^2(2 + \eta^2)} \frac{(2 + \eta\cos\theta)\sin\theta}{(1 + \eta\cos\theta)^2} \tag{14}$$

$\zeta(\theta, Z)$ must satisfy

$$\frac{\partial}{\partial\theta}\left[(1 + \eta\cos\theta)^3 \frac{\partial\zeta}{\partial\theta}\right] + \frac{\partial}{\partial Z}\left[(1 + \eta\cos\theta)^3 \frac{\partial\zeta}{\partial Z}\right] = 0 \tag{15}$$

and boundary conditions

$$\zeta(-\pi, Z) = \zeta(\pi, Z) \tag{16a}$$

$$\frac{\partial\zeta(-\pi, Z)}{\partial\theta} = \frac{\partial\zeta(\pi, Z)}{\partial\theta} \tag{16b}$$

$$\zeta(\theta, -L/2) = -\xi(\theta) \tag{16c}$$

$$\zeta(\theta, L/2) = -\xi(\theta) \tag{16d}$$

Separation of variables

$$\zeta(\theta, Z) = \phi(\theta)\psi(Z) \tag{17}$$

gives

$$\frac{d^2\phi}{d\theta^2} - \frac{3\eta\sin\theta}{1 + \eta\cos\theta}\frac{d\phi}{d\theta} + \lambda\phi = 0 \tag{18}$$

$$\frac{d^2\psi}{dZ^2} - \lambda\psi = 0 \tag{19}$$

From Sturm-Liouville theory [7] it can be shown that Equation (18) with the given boundary conditions has a set of real, nonnegative eigenvalues λ_i.

The solutions of Equation (19) are then

$$\lambda_i \neq 0 \qquad \psi_i = A_i\cosh\sqrt{\lambda_i}\,Z + B_i\sinh\sqrt{\lambda_i}\,Z$$
$$\lambda_i = 0 \qquad \psi_0 = A_0 + B_0 Z \tag{20}$$

The solutions of Equation (18) may be found by the substitution of

$$u = \sin^2(\theta/2) \tag{21}$$

Equation (18) then becomes

$$u(u-1)\left(u - \frac{1+\eta}{2\eta}\right)\frac{d^2\phi}{du^2} + \left[4u^2 - \left(4 + \frac{1}{2\eta}\right)u + \frac{1+\eta}{4\eta}\right]\frac{d\phi}{du} - \lambda\left(u - \frac{1+\eta}{2\eta}\right)\phi = 0 \tag{22}$$

This is known as Heun's equation.

Writing Heun's equation in standard form [8, 9], we have

$$z(z-1)(z-a)\frac{d^2y}{dz^2} + \{(\alpha+\beta+1)z^2 - [\alpha+\beta+1 - \delta + a(\gamma+\delta)]z + a\gamma\}\frac{dy}{dz} + \alpha\beta(z-q)\,y = 0 \tag{23}$$

where a, q, α, β, γ, and δ are arbitrary constants. With regular singularities of the equation at 0, 1, a, and ∞, and exponents 0 and $1 - \gamma$ at $z = 0$, the solutions for noninteger γ are

$$y = F(a, q;\ \alpha, \beta, \gamma, \delta;\ z) \tag{24a}$$

and

$$y = z^{1-\gamma}F(a, q_1;\ \alpha - \gamma + 1, \beta - \gamma + 1, 2 - \gamma, \delta;\ z) \tag{24b}$$

with

$$q_1 = \frac{\alpha\beta q + (1-\gamma)[(\alpha+\beta) + \delta(a-1) + (1-\gamma)]}{(\alpha - \gamma + 1)(\beta - \gamma + 1)}$$

where $F(a, q;\ \alpha, \beta, \gamma, \delta;\ z)$ is the Heun function,

$$F(a, q;\ \alpha, \beta, \gamma, \delta;\ z) = 1 + \sum_1^\infty c_n z^n \tag{25}$$

with recurrence relations

$$
\begin{aligned}
&a\gamma c_1 = \alpha\beta q \\
&2a^2\gamma(\gamma+1)c_2 = (\alpha\beta q)^2 + [(\alpha+\beta+1-\delta) \\
&\qquad + (\gamma+\delta)a]\alpha\beta q - a\gamma\alpha\beta
\end{aligned}
\Bigg\} \quad (26)
$$

and

$$
\begin{aligned}
&a(n+1)(\gamma+n)c_{n+1} = [(\alpha+\beta+n-\delta)n \\
&\qquad + an(\gamma+\delta+n-1) \\
&+ \alpha\beta q]c_n - [(n-1)(\alpha+\beta+n-1) + \alpha\beta]c_{n-1}
\end{aligned}
$$

The convergence of the Heun function may be established by the use of continued fractions. It can be shown [5] that the Heun function is convergent for all $|z| < |a|$ if $|a| > 1$.

Pressure Distribution

Comparing Equations (22) and (23) we get

$$
a = \frac{1+\eta}{2\eta}, \qquad q = \frac{1+\eta}{2\eta}, \qquad \alpha, \beta = \frac{1}{2}\,[3 \pm (9+4\lambda)^{1/2}],
$$

$$
\gamma = \frac{1}{2}, \qquad \delta = \frac{1}{2}
$$

For hydrodynamic lubrication,[2] $\eta < 1$ or $a > 1$, this indicates that the Heun function of the problem is convergent for all θ.

The general solution of Equation (15) is therefore

$$
\zeta(\theta, Z) = \phi_0\psi_0 + \sum_{i=1}^{\infty} (A_i \cosh \sqrt{\lambda_i}\, Z + B_i \sinh \sqrt{\lambda_i}\, Z)(C_iF_i + D_iH_i) \quad (27)
$$

where

$$
\begin{aligned}
F_i &= F\left(\frac{1+\eta}{2\eta}, \frac{1+\eta}{2\eta}; \frac{3+(9+4\lambda_i)^{1/2}}{2}, \frac{3-(9+4\lambda_i)^{1/2}}{2}, \frac{1}{2}, \frac{1}{2}; \sin^2\frac{\theta}{2}\right) \\
H_i &= \sin\frac{\theta}{2}\, F\left(\frac{1+\eta}{2\eta}, q_i; \frac{4+(9+4\lambda_i)^{1/2}}{2}, \frac{4-(9+4\lambda_i)^{1/2}}{2}, \frac{3}{2}, \frac{1}{2}; \sin^2\frac{\theta}{2}\right) \\
q_i &= \left(\frac{7}{4} - \lambda_i\right)^{-1}\left[\frac{3}{2} + \frac{1+\eta}{2\eta}\left(\frac{1}{4} - \lambda_i\right)\right] \\
\psi_0 &= A_0 + B_0 Z \\
\phi_0 &= C_0 + D_0 \int (1+\eta\cos\theta)^{-3}d\theta \\
&= C_0 + D_0\left\{\frac{2+\eta^2}{(1-\eta^2)^{5/2}}\tan^{-1}\left[\left(\frac{1-\eta}{1+\eta}\right)^{1/2}\tan\frac{\theta}{2}\right] - \frac{\eta\sin\theta}{2(1-\eta^2)(1+\eta\cos\theta)^2} - \frac{3\eta\sin\theta}{2(1-\eta^2)^2(1+\eta\cos\theta)}\right\}
\end{aligned}
\quad (28)
$$

and A_i, B_i, C_i, and D_i are constants.

Boundary conditions (16c) and (16d) indicate that ζ is an even function of Z, so

$$
B_0 = B_i = 0
$$

Boundary conditions (16c) and (16d) also show that ζ is an odd function of θ, since $\xi(\theta)$ is an odd function of θ. In addition, F_i and H_i are even and odd functions of θ, respectively. This implies

$$
C_0 = C_i = 0
$$

Boundary conditions (16a) and (16b) require

$$
D_0\int_0^{\pi}(1+\eta\cos\theta)^{-3}d\theta = 0 \text{ and } D_iH_i(\theta)\Big|_{\theta=\pi} = 0
$$

Since $\int_0^{\pi}(1+\eta\cos\theta)^{-3}d\theta \neq 0$ and $D_i \neq 0$, therefore

$$
D_0 = 0 \text{ and } H_i(\pi) = 0.
$$

Now if we absorb D_i into A_i, we get

$$
\Omega(\theta, Z) = \bar{\Pi}(\theta) + \sum_{i=1}^{\infty} A_i \cosh\sqrt{\lambda_i}\, Z\, H_i(\lambda_i;\ \theta) \quad (29)
$$

where

$$
\bar{\Pi}(\theta) = \xi(\theta) = \frac{6\mu_0 U r\eta}{c^2(2+\eta^2)}\,\frac{(2+\eta\cos\theta)\sin\theta}{(1+\eta\cos\theta)^2}
$$

and λ_i are the roots of

$$
F\left(\frac{1+\eta}{2\eta}, q_i; \frac{4+(9+4\lambda)^{1/2}}{2}, \frac{4-(9+4\lambda)^{1/2}}{2}, \frac{3}{2}, \frac{1}{2};\ 1\right) = 0 \quad (30)
$$

Also $H_i(\theta)$ are orthogonal with respect to the weight function

$$
w(\theta) = (1+\eta\cos\theta)^2 \quad (31)
$$

over the interval $(-\pi, \pi)$, that is

$$
\int_{-\pi}^{\pi} w(\theta)H_i(\theta)H_j(\theta)d\theta = 0 \qquad \text{for } i \neq j \quad (32)
$$

Multiplying Equation (29) at $Z = L/2$ by $w(\theta)H_i(\theta)$ and integrating over the interval $(-\pi, \pi)$, we get

$$
A_i = -\frac{\int_{-\pi}^{\pi} w(\theta)\bar{\Pi}(\theta)H_i(\theta)d\theta}{\cosh(\sqrt{\lambda_i}L/2)\int_{-\pi}^{\pi} w(\theta)H_i^2(\theta)d\theta} \quad (33)
$$

Hence the pressure distribution in the journal bearing is

$$
\begin{aligned}
p &= -\frac{1}{b}\log(1-b\Omega) \\
&= -\frac{1}{b}\log\left\{1 - b\left[\bar{\Pi}(\theta) + \sum_{i=1}^{\infty} A_i\cosh\sqrt{\lambda_i}\, Z\, H_i(\lambda_i;\ \theta)\right]\right\}
\end{aligned}
\quad (34)
$$

Bearing Characteristics

As mentioned, one of the objectives of the present study is to investigate the attitude angle of the bearing in the case of variable viscosity. In this section the bearing characteristics, the load capacity, and attitude angle will be discussed. Other bearing characteristics, such as the coefficient of friction, oil flow, and so on, are not to be derived. If necessary, they may be obtained readily by the integrations of pressure distribution.

Relating the load capacity W of the bearing to the pressure distribution, W is resolved into two components along and perpendicular to the line of centers,

[2] When $\eta = 1$, there is a direct contact of journal and bearing surfaces. This does not constitute a problem of hydrodynamic lubrication.

$$
\begin{aligned}
W_1 = W\cos\sigma &= -\int_{-L/2}^{L/2}\int_{-\pi}^{\pi} pr^2\cos\theta\, d\theta\, dZ \\
&= \frac{r^2}{b}\int_{-L/2}^{L/2}\int_{-\pi}^{\pi}\log(1-b\Omega)\cos\theta\, d\theta\, dZ \\
W_2 = W\sin\sigma &= \int_{-L/2}^{L/2}\int_{-\pi}^{\pi} pr^2\sin\theta\, d\theta\, dZ \\
&= -\frac{r^2}{b}\int_{-L/2}^{L/2}\int_{-\pi}^{\pi}\log(1-b\Omega)\sin\theta\, d\theta\, dZ
\end{aligned}
\tag{35}
$$

and the load capacity W is

$$
W = (W_1^2 + W_2^2)^{1/2} \tag{36}
$$

The attitude angle σ is immediately obtained by

$$
\sigma = \tan^{-1}(W_2/W_1) \tag{37}
$$

By virtue of the complexities of the expression for pressure distribution, without any numerical or graphical evaluations, it is difficult to obtain quantitative statements of these bearing characteristics. However, in establishing the lower and upper bounds of the load capacity, some necessary information in question may be revealed.

As shown in the Appendix, we find

$$
\begin{aligned}
&0 \le W_1 \le \frac{r^2 L}{b}\log\frac{1}{1-b^2\Omega_m^2} \\
&\text{and} \\
&\frac{12\pi\mu_0 U\eta L r^2}{c^2(2+\eta^2)(1-\eta^2)^{1/2}} + \sum_{i=1}^{\infty}\frac{2A_i}{\sqrt{\lambda_i}}\sinh\left(\sqrt{\lambda_i}\,L/2\right) \\
&\qquad r^2\int_0^1 H_i(\lambda_i;\, u)du \le W_2 \le \frac{2r^2 L}{b}\log(1+b\Omega_m)
\end{aligned}
\tag{38}
$$

where Ω_m denotes the maximum value of Ω. The equalities in these two expressions are valid only when $b\Omega$ is identically zero or constant in the given interval. Also the lower bounds are the corresponding solutions for constant viscosity [5].

For $b\Omega \equiv$ const they are problems of either constant viscosity ($b = 0$) or constant pressure ($\eta = 0$). Ignoring these trivial cases, both components of load capacity are nonzero. This implies that the line of centers, in general, is not perpendicular to the load vector as shown in the constant-viscosity case. This agrees with experimental fact.

References

1 O. Reynolds, "On the Theory of Lubrication and Its Application to Mr. Bearchamp Tower's Experiments," *Philosophical Transactions of the Royal Society of London*, series A, vol. 177, 1886, pp. 157–234.

2 A. G. M. Michell, "The Lubrication of Plane Surfaces," *Zeitschrift für Mathematik und Physik*, band 52, 1905, pp. 123–137.

3 M. Muskat, F. Morgan, and M. W. Meres, "The Lubrication of Plane Sliders of Finite Width," *Journal of Applied Physics*, vol. 11, 1940, pp. 208–219.

4 A. Sommerfeld, "Zur Hydrodynamischen Theorie der Schmiermittel Reibung," *Zeitschrift für Mathematik und Physik*, band 50, 1904, pp. 97–153.

5 L. N. Tao, "General Solution of Reynolds Equation for a Journal Bearing of Finite Width," to be published in *Quarterly of Applied Mathematics*.

6 S. Glasstone, K. Laidler, and H. Eyring, "The Theory of Rate Processes," McGraw-Hill Book Company, Inc., New York, N. Y., 1941, pp. 506–510.

7 E. L. Ince, "Ordinary Differential Equations," Dover Publications, New York, N. Y., 1944, chapter 10.

8 E. T. Whittaker and G. N. Watson, "A Course of Modern Analysis," fourth edition, Cambridge University Press, London, England, 1952, pp. 576–577.

9 A. Erdelyi, editor, "Higher Transcendental Functions, vol. III," McGraw-Hill Book Company, Inc., New York, N. Y., 1955, pp. 57–62.

10 G. H. Hardy, J. E. Littlewood, and G. Pólya, "Inequalities," Cambridge University Press, London, England, 1934, pp. 150–152.

11 A. Charnes and E. Saibel, "On the Solution of the Reynolds Equation for Slider-Bearing Lubrication—II, The Viscosity, a Function of the Pressure," TRANS. ASME, vol. 75, 1955, pp. 269–272.

APPENDIX

Lower and Upper Bounds of Load Capacity

The components of load capacity of the journal bearing are

$$
\begin{aligned}
W_1 &= \frac{r^2}{b}\int_{-L/2}^{L/2}\int_{-\pi}^{\pi}\log(1-b\Omega)\cos\theta\, d\theta\, dZ \\
W_2 &= -\frac{r^2}{b}\int_{-L/2}^{L/2}\int_{-\pi}^{\pi}\log(1-b\Omega)\sin\theta\, d\theta\, dZ
\end{aligned}
\tag{39}
$$

Write

$$
\begin{aligned}
I_1 &= \frac{1}{b}\int_{-\pi}^{\pi}\log(1-b\Omega)\cos\theta\, d\theta \\
I_2 &= -\frac{1}{b}\int_{-\pi}^{\pi}\log(1-b\Omega)\sin\theta\, d\theta
\end{aligned}
\tag{40}
$$

With Ω an odd function of θ, we get

$$
I_1 = \frac{1}{b}\int_0^{\pi}\log(1-b^2\Omega^2)\cos\theta\, d\theta \tag{41}
$$

A substitution of $\pi - \theta$ for θ over the interval $(\pi/2, \pi)$ gives

$$
I_1 = \frac{1}{b}\int_0^{\pi/2}\log\frac{1-b^2\Omega^2(\theta)}{1-b^2\Omega^2(\pi-\theta)}\cos\theta\, d\theta \tag{42}
$$

Since $\Omega(\theta) \le \Omega(\pi - \theta)$ in $(0, \pi/2)$,

$$
\log\frac{1-b^2\Omega^2(\theta)}{1-b^2\Omega^2(\pi-\theta)} \ge 0 \tag{43}
$$

With both

$$
\log\frac{1-b^2\Omega^2(\theta)}{1-b^2\Omega^2(\pi-\theta)}
$$

and $\cos\theta$ of Equation (42) being non-negative,

$$
I_1 \ge 0 \tag{44}
$$

Also Ω is non-negative in $(0, \pi)$,

$$
\begin{aligned}
I_1 &= \frac{1}{b}\int_0^{\pi/2}\log\frac{1-b^2\Omega^2(\theta)}{1-b^2\Omega^2(\pi-\theta)}\cos\theta\, d\theta \\
&\le \frac{1}{b}\int_0^{\pi/2}\log\frac{1}{1-b^2\Omega_m^2}\cos\theta\, d\theta = \frac{1}{b}\log\frac{1}{1-b^2\Omega_m^2}
\end{aligned}
\tag{45}
$$

where Ω_m denotes the maximum value of Ω. These two results (44) and (45) give the lower and upper bounds of I_1. Similarly we may establish those of I_2:

$$
\begin{aligned}
I_2 &= -\frac{1}{b}\int_{-\pi}^{\pi}\log(1-b\Omega)\sin\theta\, d\theta \\
&= \frac{1}{b}\int_0^{\pi}\left(\log\frac{1+b\Omega}{1-b\Omega}\right)\sin\theta\, d\theta
\end{aligned}
\tag{46}
$$

Using the mean value theorem of integrals [10], that is

$$G\left(\frac{\int gf\,dx}{\int g\,dx}\right) \leq \frac{\int G(f)g\,dx}{\int g\,dx} \tag{47}$$

where $G(f)$ is a convex function in the given interval and there is equality only when $f \equiv$ const. We let $G(f) = -\log f$, this gives

$$\frac{\int g \log f\,dx}{\int g\,dx} \leq \log\left[\frac{\int fg\,dx}{\int g\,dx}\right] \tag{48}$$

With $f = (1 + b\Omega)/(1 - b\Omega)$ and $g = \sin\theta$, we get

$$I_2 \leq \frac{2}{b}\log\left[\frac{1}{2}\int_0^\pi \frac{1 + b\Omega}{1 - b\Omega}\sin\theta\,d\theta\right] \leq \frac{2}{b}\log(1 + b\Omega_m) \tag{49}$$

The last term is obtained since Ω is non-negative in $(0, \pi)$. Also by expansion

$$I_2 = \frac{1}{b}\int_0^\pi \log\frac{1 + b\Omega}{1 - b\Omega}\sin\theta\,d\theta = \frac{2}{b}\int_0^\pi \left[b\Omega + \frac{1}{3}(b\Omega)^3 + \ldots.\right]\sin\theta\,d\theta$$

$$\geq 2\int_0^\pi \Omega\sin\theta\,d\theta = \frac{12\pi\mu_0 U\eta r}{c^2(2 + \eta^2)(1 - \eta^2)^{1/2}} + \sum_{i=1}^{\infty} A_i \cosh\sqrt{\lambda_i}\,Z\int_0^1 H_i(\lambda_i; u)du \tag{50}$$

Furthermore, it should be mentioned that the equalities in these expressions are true only when $b\Omega$ is identically zero or constant.

Substituting these lower and upper bounds of I_1 and I_2 into Equations (39) and (40), we obtain

$$0 \leq W_1 \leq \frac{r^2L}{b}\log\frac{1}{1 - b^2\Omega_m^2} \tag{51}$$

and

$$\frac{12\pi\mu_0 U\eta r^2 L}{c^2(2 + \eta^2)(1 - \eta^2)^{1/2}} + \sum_{i=1}^{\infty}\frac{2A_i}{\sqrt{\lambda_i}}\sinh(\sqrt{\lambda_i}\,L/2)$$

$$r^2\int_0^1 H_i(\lambda_i; u)du \leq W_2 \leq \frac{2r^2L}{b}\log(1 + b\Omega_m) \tag{52}$$

Analysis of Complex Kinematic Chains With Influence Coefficients

J. MODREY

Professor and Chairman,
Department of Mechanical Engineering,
Union College, Schenectady, N. Y.
Assoc. Mem. ASME

Highly complex kinematic chains such as Fig. 1(c) can be analyzed by the use of simple vector equations involving influence coefficients. The influence-coefficient equations are related to superposition of simple kinematic chains. The technique for determining the necessary influence coefficients is one of sequentially setting all variables but one to zero and relaxing appropriate constraints to maintain mobility. This "zero-relax" process creates a series of mechanisms each simple enough to be solved by a direct process rather than by simultaneous equations. The analysis of the velocities and accelerations for these simpler mechanisms yields the influence coefficients of the related but more highly complex mechanism.

ACCELERATIONS within a simple four-bar linkage may be determined by the solution of a single vector equation. If in a series n links are joined to form a mechanism, $(n - 2)/2$ simultaneous vector equations are required to determine the accelerations of the system. Systems defined by simultaneous equations have been variously called "floating link mechanisms" or "complex mechanisms." Both expressions were inspired by the difficulty encountered in the analysis of such chains. This paper suggests the following descriptive names which imply the quality of mechanism complexity.

(a) First-Order Complexity (FOC). This refers to an arrangement of links whereby the simultaneous equations can be solved in sequence. Fig. 1(*a*) is a kinematic example. Three simultaneous equations define the motion of the eight-link system. On the other hand, the linkage 1-2-3-4 is a self-sufficient chain: its motion is entirely independent of the other links. A complete solution is available for chain 1-2-3-4. This solution may be followed by analysis of 3-5-6-1 with 3 as the driver. Finally, 5-7-8-1 is analyzed as a simple four-bar linkage with 5 as the driver. From this example, we may identify FOC systems as those which may be solved as a series arrangement of simple four-bar linkages.

(b) Second-Order Complexity (SOC). All systems possessing complexity higher than the first cannot be solved directly as described previously. A second-order complex system is an intermediate example though. This refers to a system that misses being an FOC arrangement only because the driver is not located in a self-sufficient four-bar chain. Fig. 1(*b*) is an example of an SOC system. Geometrically it is identical to Fig. 1(*a*), but the analysis is no longer as straightforward because the driver is not located in 1-2-3-4. The most familiar method for handling this system is often referred to as the "trial-and-error method."[1,2] The trial-and-error method is a legitimate graphical technique for

[1] R. Hinkle, "Kinematics of Machines," Prentice-Hall, Inc., New York, N. Y.

[2] J. H. Billings, "Applied Kinematics," D. Van Nostrand Company, Inc., New York, N. Y.

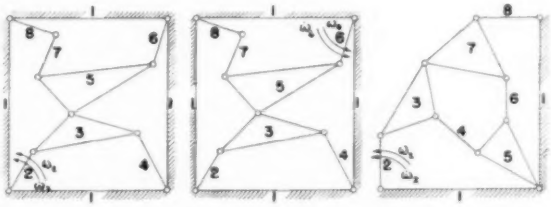

Fig. 1(a) Driver at (2) (F. O. C.) Fig. 1(b) Driver at (6) (S. O. C.) Fig. 1(c) Driver at (2) (H. O. C.)

Fig. 1 Eight-bar linkages of ascending orders of complexity

Contributed by the Applied Mechanics Division and presented at the Annual Meeting, November 30–December 5, 1958, New York, N. Y., of THE AMERICAN SOCIETY OF MECHANICAL ENGINEERS.

Discussion of this paper should be addressed to the Secretary, ASME, 29 West 39th Street, New York, N. Y., and will be accepted until July 10, 1959, for publication at a later date. Discussion received after the closing date will be returned.

NOTE: Statements and opinions advanced in papers are to be understood as individual expressions of their authors and not those of the Society. Manuscript received by ASME Applied Mechanics Division, February 7, 1958. Paper No. 58—A-74.

Nomenclature

$\mathrm{I}\,\mathbf{V}_j$, $\mathrm{II}\,\mathbf{V}_j$ = velocities at poin (j) due to special driving and restraining conditions described as velocity Stages I and II, respectively; example, Fig. 2

$\mathrm{I}\,\dot{\mathbf{V}}_j$, $\mathrm{II}\,\dot{\mathbf{V}}_j$ = accelerations at point (j) due to special driving and restraining conditions described as acceleration Stages I and II, respectively; example, Fig. 3

$\mathrm{III}\,\dot{\mathbf{V}}_j$ = acceleration at point (j) due to special driving and restraining conditions described as acceleration Stage III; example, Fig. 3

$\mathrm{I}\,\omega_i$, $\mathrm{II}\,\omega_i$, $\mathrm{III}\,\omega_i$ = assumed magnitude of angular speed for link i under conditions described as Stages I, II, and III

$\bar{\mu}_{ji}$ = velocity influence coefficient. Influence of angular velocity of link i on velocity of point (j). (L^1, T^0)

$\bar{\gamma}_{ji}$ = tangential acceleration influence coefficient. Influence of angular acceleration of link i on acceleration of point (j). (L^1, T^0). Actually, $\bar{\gamma}_{ji} = \bar{\mu}_{ji}$

$\bar{\beta}_{ji}$ = acceleration influence coefficient. Influence of angular velocity of link i on acceleration of point (j). (L^1, T^0)

NOTE: Bold symbols and barred Greek letters refer to vector quantities. Light symbols refer to scalar quantities.

solving simultaneous vector equations. Recently, a technique strictly directed at SOC systems has been described.[2] This method takes advantage of the fact that an SOC system differs from the FOC case only because of an unfortunate location of the driver. Since the kinematic ratios throughout a chain are independent of the location of the driver, these ratios are determined by analyzing the chain as an FOC system. This is accomplished by the simple expedient of assuming a hypothetical drive in the self-sufficient four-bar chain.

It should be noted at this stage that many systems which may not seem at first to be of FOC or SOC may be converted readily by proper inversion.

(c) Higher-Order Complexity (HOC). This paper concerns itself with HOC systems. These are chains *which cannot be solved in sequence regardless of the choice of drivers*. An example is shown in Fig. 1(*c*). The similarity between Fig. 1(*c*) and Figs. 1(*a*) and 1(*b*) is that all are eight-link chains, but unlike Figs. 1(*a*) and 1(*b*), Fig. 1(*c*) cannot be solved sequentially because no matter what link is chosen as a driver or whatever inversion is attempted there is no self-sufficient bar linkage which may be used for starting the analysis. Goodman's technique[2] is inapplicable. The technique of graphical trial and error is applicable because it accepts the concept of simultaneous solutions. On the other hand, the graphical trial-and-error method while rigorous becomes awkward in HOC systems.

It is proposed here that HOC systems be analyzed by a superposition of motion components of the system. These components may be selected at the analyst's will; hence they most conveniently take the form of a series of FOC systems so chosen as to make the superimposed sum consistent with the known conditions of restraint.

Reducing an HOC System to Several FOC Systems

The major difficulty with HOC systems is that there is no discrete four-bar linkage within the chain. This, of course, militates against the exploitation of the simplicity inherent in FOC systems. To side step this obstacle, the HOC chain is pictured as a sum of two (or more) FOC chains superimposed on each other. To create these FOC chains, consider what must be done with a five-bar linkage involving the driver. If the driven crank of this five-bar linkage is frozen, a convenient four-bar linkage is created. Of course, this operation has added an additional constraint to the system hence some other constraint (preferably another follower crank) in another part of the system must be relaxed. In most cases, this freezing-relaxing operation will create an FOC system.

Analysis of this FOC system while very convenient does not result in motions consistent with the original system. This deviation is most apparent in the observation that one link which should be mobile has been frozen and the direction of the relaxed point is not consistent with the known conditions. A second FOC system must be added to the first. This second system must assume such motions as to provide a corrective for the first FOC system. Since the first system utilized the total qualities of the driver, it is necessary that the second system call for freezing the original driver. In this fashion when the two motions of the driver are added, the result as far as the driver is concerned is accurate. The other corrective action to be taken by the second system is to give back the frozen link its mobility. Once again an FOC system evolves. Meanwhile, the one other crank must remain unconstrained (relaxed). The second system is given such a motion as to correct the relaxed motion of the first. The corrected total motion of the relaxed motion must be:

(*a*) A velocity direction perpendicular to the relaxed crank.

(*b*) An acceleration whose component along the crank line is equal to the known centripetal acceleration at this point.

Technique Using Influence Coefficients

Whenever superposition techniques are applicable, the problem may be alternately solved by the use of influence coefficients. Since each of the FOC components described previously is influencing the total motion of the systems, the introduction of influence coefficients is valid. Furthermore, the use of these coefficients systematizes the process of superposition. The steps outlined and the use of influence coefficients are best described by reference to a specific example such as Fig. 1(*c*).

Since link 2 in Fig. 1(*c*) is the assigned driver, the obvious way to involve 2 in a four-bar linkage is to freeze link 5. Link 8 must be relaxed (removed) to regain mobility for the system. Fig. 2 shows this operation in Stage I. To Stage I we must add Stage II to recreate the original system. In Stage II the assigned driver 2 is frozen and the previously frozen crank 5 becomes a driver. Note that Stage II is once again an FOC system.

The graphical superpositions of Fig. 2 may be expressed analytically as follows:

Velocity Analysis. Before an acceleration analysis is conducted, it is necessary to perform a velocity study.

Using the concept of influence coefficients, the velocity at point (*g*) of the original system is:

$$\mathbf{V}_g = \bar{\mu}_{g2}\omega_2 + \bar{\mu}_{g5}\omega_5 \tag{1}$$

To evaluate influence coefficient $\bar{\mu}_{g2}$ set $\omega_5 = 0$ and find the velocity of (*g*), i.e. ($\mathrm{I}\,\mathbf{V}_g$). Of course, under these conditions ω_2 is the only influencing agent. This condition is graphically depicted as Stage I of Fig. 2. From Stage I

$$\mathrm{I}\,\mathbf{V}_g = \bar{\mu}_{g2}\omega_2 + \bar{\mu}_{g5}\cdot 0; \quad \text{i.e., } \bar{\mu}_{g2} = \frac{\mathrm{I}\,\mathbf{V}_g}{\omega_2} \tag{2}$$

To evaluate $\bar{\mu}_{g5}$ set $\omega_2 = 0$ (i.e., Stage II) and assume any convenient value for $\mathrm{II}\,\omega_5$. Then it follows that:

$$\mathrm{II}\,\mathbf{V}_g = \bar{\mu}_{g2}\cdot 0 + \bar{\mu}_{g5}\,\mathrm{II}\,\omega_5$$

or

$$\bar{\mu}_{g5} = \frac{\mathrm{II}\,\mathbf{V}_g}{\mathrm{II}\,\omega_5} \tag{3}$$

Substituting these influence coefficients into Equation (1):

$$\mathbf{V}_g = \left[\frac{\mathrm{I}\,\mathbf{V}_g}{\omega_2}\right]\omega_2 + \left[\frac{\mathrm{II}\,\mathbf{V}_g}{\mathrm{II}\,\omega_5}\right]\omega_5 \tag{4}$$

In this vector equation there are only two unknown quantities,

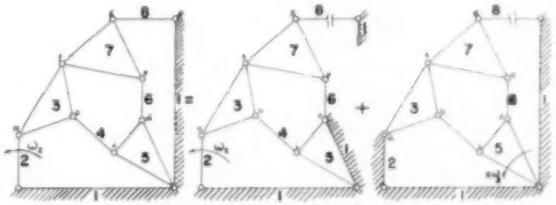

Fig. 2 Original velocity system as a superposition of two simpler systems

[2] T. P. Goodman, "An Indirect Method for Determining Accelerations in Complex Mechanisms," TRANS. ASME, vol. 81, 1958, pp. 1676–1682.

namely, the magnitudes of $\mathbf{V}_g$ and ω_5, and Equation (4) is sufficient for solving for both.

The direct kinematic process of solving for $\mathbf{V}_g$ in Stages I and II also yields velocities at all other points. The corresponding velocity-influence coefficients at any general point (j) can be written as:

$$\bar{\mu}_{j2} = \frac{\text{I}\,\mathbf{V}_j}{\omega_2}; \quad \bar{\mu}_{j5} = \frac{\text{II}\,\mathbf{V}_j}{\text{II}\,\omega_5} \tag{5}$$

The velocity of point (j) in the original system becomes:

$$\mathbf{V}_j = \bar{\mu}_{j2}\omega_2 + \bar{\mu}_{j5}\omega_5 \tag{6}$$

or

$$\mathbf{V}_j = \text{I}\,\mathbf{V}_j + \text{II}\,\mathbf{V}_j\left(\frac{\omega_5}{\text{II}\,\omega_5}\right) \tag{7}$$

Equations (6) and (7) are sufficient for defining $\mathbf{V}_j$ since ω_5 was solved for earlier with equation (4).

Accelerations. The accelerations at point (g) will be influenced by both the angular velocity of the driver and its tangential acceleration. The influence equation becomes:

$$\dot{\mathbf{V}}_g = \bar{\gamma}_{g2}\dot{\omega}_2 + \bar{\gamma}_{g5}\dot{\omega}_5 + \bar{\beta}_{g2}\omega_2^2 \tag{8}$$

Once again to evaluate the coefficients all but one variable in Equation (8) will be set to zero in sequence.

To determine $\bar{\gamma}_{g2}$ set $\omega_2 = 0, \omega_5 = 0, \dot{\omega}_5 = 0$ and solve for $\text{I}\,\dot{\mathbf{V}}_g$. To evaluate $\bar{\gamma}_{g5}$ set $\omega_2 = 0, \dot{\omega}_2 = 0, \omega_5 = 0$ and solve for $\text{II}\,\dot{\mathbf{V}}_g$. For $\bar{\beta}_{g2}$ set $\dot{\omega}_2 = 0, \dot{\omega}_5 = 0$ and solve for $\text{III}\,\dot{\mathbf{V}}_g$. This sequence is graphically illustrated in Stages I, II, and III of Fig. 3. Note that no attempt is made to create an obvious four-bar chain for Stage III. On the other hand, link 5 is "frozen" to the extent that $\dot{\omega}_5$ is set to zero. With the unknown $\dot{\omega}_5$ eliminated, Stage III can be analyzed directly; hence it satisfies the definition of an FOC system.

Comparison of Stages I and II of Fig. 2 and Fig. 3 will reveal that the constraints are precisely alike. The drives in both Fig. 2 and Fig. 3 and all other motions are strictly tangential, hence in the general case:

$$\bar{\gamma}_{j5} = \bar{\mu}_{j5}; \quad \bar{\gamma}_{g2} = \bar{\mu}_{g2}; \quad \bar{\gamma}_{g5} = \bar{\mu}_{g5} \tag{9}$$

In other words, we may substitute for the $\bar{\gamma}$ coefficients the $\bar{\mu}$ coefficients previously evaluated; therefore, Stages I and II of Fig. 3 may be ignored and only Stage III need be evaluated.

Equation (8) may now be simplified to:

$$\dot{\mathbf{V}}_g = \bar{\mu}_{g2}\dot{\omega}_2 + \bar{\mu}_{g5}\dot{\omega}_5 + \bar{\beta}_{g2}\omega_2^2 \tag{10}$$

Applying Equation (10) to Stage III yields:

$$\text{III}\,\dot{\mathbf{V}}_g = \bar{\mu}_{g2}\cdot 0 + \bar{\mu}_{g5}\cdot 0 + \bar{\beta}_{g2}\omega_2^2$$

or

$$\bar{\beta}_{g2} = \frac{\text{III}\,\dot{\mathbf{V}}_g}{\omega_2^2} \tag{11}$$

and at any general point (j):

$$\bar{\beta}_{j2} = \frac{\text{III}\,\dot{\mathbf{V}}_j}{\omega_2^2} \tag{12}$$

Substituting into Equation (10):

$$\dot{\mathbf{V}}_g = \left[\frac{\text{I}\,\mathbf{V}_g}{\omega_2}\right]\dot{\omega}_2 + \left[\frac{\text{II}\,\mathbf{V}_g}{\text{II}\,\omega_5}\right]\dot{\omega}_5 + \text{III}\,\dot{\mathbf{V}}_g \tag{13}$$

There are only two unknown quantities in Equation (13), the magnitudes of the *tangential* acceleration of (g) and $\dot{\omega}_5$. Equation (13) is sufficient for evaluating both quantities. After $\dot{\omega}_5$ is evaluated, the general point (j) can be solved for, i.e.:

$$\dot{\mathbf{V}}_j = \bar{\mu}_{j2}\dot{\omega}_2 + \bar{\mu}_{j5}\dot{\omega}_5 + \bar{\beta}_{j2}\omega_2^2 \tag{14}$$

The chain of Fig. 1(*c*) was analyzed by a superposition of two FOC systems. Most systems will succumb to the treatment described. On rare occasions a system will be encountered so complex that more than one crank will have to be frozen to create FOC components. If m cranks are so frozen, m constraints must be relaxed. This means that m number of velocity equations and m number of acceleration equations will have to be written instead of the single equations (1) and (10). This merely compounds the labor but no new concepts are involved.

Example. Solution of Fig. 1(*c*).

Given: $\omega_2 = 10$ and $\dot{\omega}_2 = 125$. Determine $\mathbf{V}_c$, $\mathbf{V}_g$, $\dot{\omega}_5$.

The conditions described as Stage I yield the velocity polygon of Fig. 4(*a*). Starting with $\omega_2 = 10$ ($\text{I}\,\mathbf{V}_2 = 10$) the construction terminates with the other bold vector $\text{I}\,\mathbf{V}_g$. The vector influence

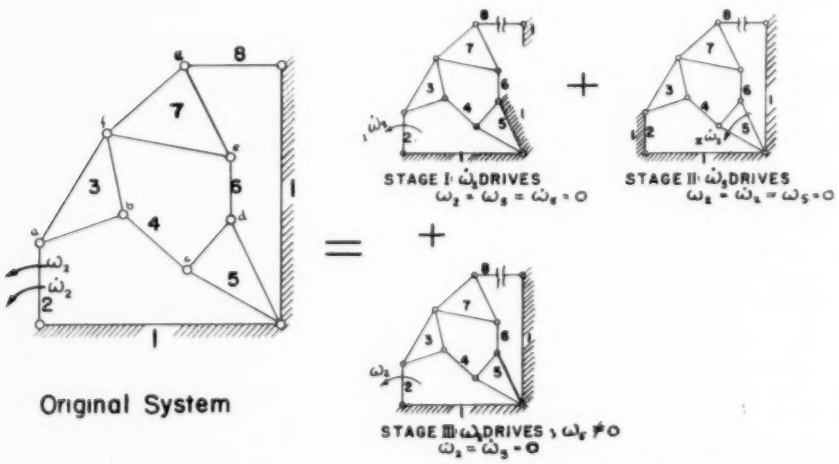
Original System
STAGE I: $\dot{\omega}_2$ DRIVES
$\omega_3 = \omega_5 = \dot{\omega}_6 = 0$
STAGE II: $\dot{\omega}_5$ DRIVES
$\omega_3 = \dot{\omega}_3 = \omega_5 = 0$
STAGE III: $\dot{\omega}_3$ DRIVES, $\omega_5 \neq 0$
$\omega_3 = \dot{\omega}_3 = 0$

Fig. 3 Original acceleration system as a superposition of three simpler systems

Table 1 Quantities from Figs. 4, 5

① Item	② IV	③ IIV	④ $\bar{\mu}_{j2}$	⑤ $\bar{\mu}_{j5}$	⑥ $\bar{\mu}_{j5}\omega_5$	⑦ V_j	⑧ V_j^2	⑨ R	⑩ $\frac{V_j^2}{R}$	⑪ $\mathrm{III}\dot{V}_j$	⑫ $\bar{\beta}_{j2}$	⑬ V_j
a/o	10	0	1	0	0	10	100.0	1.0	100.0	100	1	150
b/a	+ 8.60	+2.7	9.86	0.35	+1.67	10.27	105.5	1.1	96.0	105	1.05	
c/o	0	10.0	0	1.30	6.20	6.20	38.5	1.3	30.0	30	0.30	
c/b	+10.8	−8.5	1.08	−1.10	−5.27	5.53	30.5	1.1	27.8	187	1.87	
e/d	+1.80	+12.5	0.18	+1.63	+7.75	9.55	91.0	0.8	113.5	117	1.17	
f/e	+6.5	−2.6	0.65	−0.338	−1.61	4.89	24.0	1.5	16.0	110	1.10	
g/o	4.0	6.0	0.40	0.780	3.72	4.7	22.1	1.2	18.4	216	2.16	335

Fig. 4(*a*) Fig. 4(*b*) ② + $\omega_2$③ + $\mathrm{II}\omega_s$ ③ + ⑥ ⑧^2 Fig. 3 ⑤ + ⑨ Fig. 5(*a*) ⑪ + ω_2^2

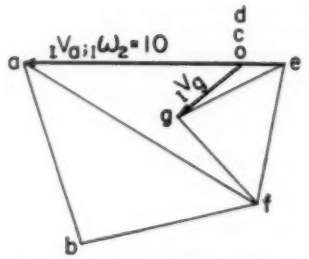

FIG-4a STAGE I Analysis $V_c=0$

Divide vectors by $_{\mathrm{I}}\omega_2$ to get μ_{j_2}

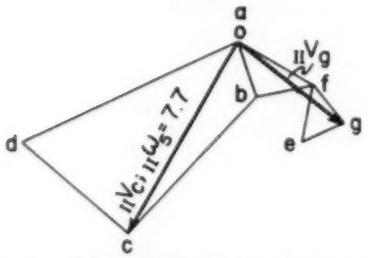

FIG 4b STAGE II Analysis $V_0=0$

Divide vectors by $_{\mathrm{II}}\omega_5$ to get μ_{j_5}

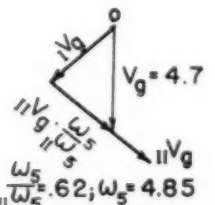

FIG 4c Solution of eq. I

Fig. 4 Velocity polygons for stages I, II, and Equation (1)

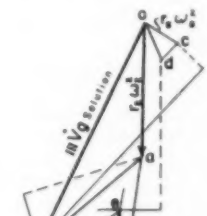

FIG 5a STAGE III Analysis ($\dot{\omega}_2=\dot{\omega}_5=0$)

Divide vectors by ω_2^2 to get β_{j_2}

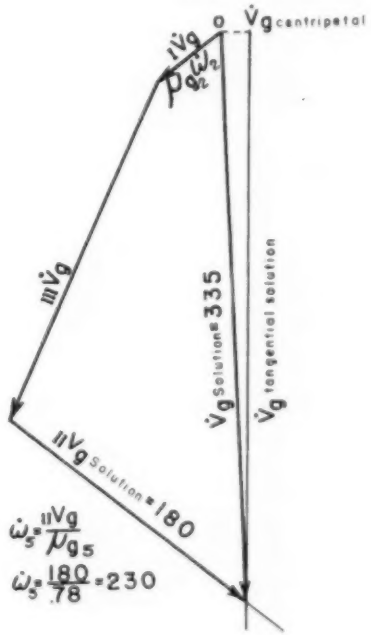

FIG 5b Solution of eq. 10

Fig. 5 Acceleration polygons for stage III and Equation (10)

coefficients $\bar{\mu}_{j2}$ are evaluated by dividing the appropriate vectors of Fig. 4(*a*) by the scalar ω_2.

The conditions of Stage II yield the velocity polygon of Fig. 4(*b*). Starting with an assumed vector $\text{II}\,\mathbf{V}_c = 10$ ($\text{II}\,\omega_3 = 7.7$) the construction is terminated with the bold vector $\text{II}\,\mathbf{V}_g$. Applying Equation (4) enables us to evaluate the true magnitude ω_3. Fig. 4(*c*) is the solution of Equation (4).

Columns 1 through 6 of Table 1 record the magnitudes of the vectors from Fig. 4. Columns 7 through 10 are used to compute the centripetal acceleration of significant points in the system. With these data the acceleration polygon based on the known restrictions of Stage III is laid out as in Fig. 5(*a*). Starting with the vectors $\text{III}\,\mathbf{\dot{V}}_a$ and $\text{III}\,\mathbf{\dot{V}}_c$ and setting $\dot{\omega}_2 = \dot{\omega}_3 = 0$, we arrive at the acceleration of point *g*, $\text{III}\,\mathbf{V}_g$. Dividing the vectors of Fig. 5(*a*) by the scalar ω_2^2 yields the vector influence coefficients $\bar{\beta}_{j2}$ (columns 12 and 13).

The final step in the solution is to solve Equation (10). Vector $\bar{\mu}_{g2}\dot{\omega}_2$ of Equation (10) has a magnitude of $0.40 \times 125 = 50$ with the direction of $\text{I}\,\mathbf{V}_g$ (Fig. 4*a*). Vector $\bar{\beta}_{g2}\omega_2^2$ has a magnitude of $2.16 \times 100 = 216$. Only the direction of vector $\bar{\mu}_{g3}\dot{\omega}_3$ is known because the scalar $\dot{\omega}_3$ remains to be found. The centripetal acceleration component of $\mathbf{\dot{V}}_g$ is known but the magnitude of the tangential component is unknown. Fig. 5(*b*) is the vector polygon representing Equation (10). The two unknown magnitudes are resolved by the intersection of the known direction lines. The completed polygon not only yields complete data on $\mathbf{\dot{V}}_g$ but also for $\text{II}\,\mathbf{\dot{V}}_g = \bar{\mu}_g\,\dot{\omega}_3$. The value of $\dot{\omega}_3$ is computed to be 230.

Conclusions

HOC systems can be reduced to a superposition of several FOC systems. The velocity analysis of most HOC mechanisms will require the use of only two FOC systems (described here as Stage I and II). The acceleration analysis in most cases will require only one more FOC system (described here as Stage III). Let ω_D and $\dot{\omega}_D$ refer to the angular velocity and acceleration of the driver crank *D*, and ω_F and $\dot{\omega}_F$ refer to the angular velocity and acceleration of one of the driven cranks *F*. The velocity and accelerations of any point (*j*) in the system can be expressed in terms of influence coefficients as

$$\mathbf{V}_j = \bar{\mu}_{jD}\omega_D + \bar{\mu}_{jF}\omega_F \tag{15}$$

and

$$\mathbf{\dot{V}}_j = \bar{\mu}_{jD}\dot{\omega}_D + \bar{\mu}_{jF}\dot{\omega}_F + \bar{\beta}_{jD}\omega_D^2 \tag{16}$$

where

$$\bar{\mu}_{jD} = \frac{\text{I}\,\mathbf{V}_j}{\omega_D};\quad \bar{\mu}_{jF} = \frac{\text{II}\,\mathbf{V}_j}{\text{II}\,\omega_F};\quad \bar{\beta}_{jD} = \frac{\text{III}\,\mathbf{\dot{V}}_j}{\omega_D^2} \tag{17}$$

Prefixes I, II, and III refer to the original system modified to the following driving conditions:

I Link *D* drives at ω_D but link *F* frozen; i.e., $\omega_F = 0$. (Used to evaluate $\bar{\mu}_{jD}$.)

II Link *F* drives at ω_F but link *D* frozen; i.e., $\omega_D = 0$. (Used to evaluate $\bar{\mu}_{jF}$.)

III Links *D* and *F* driven at the known speeds ω_D and ω_F, but $\dot{\omega}_D$ and $\dot{\omega}_F$ set to zero. (Used to evaluate $\bar{\beta}_{jD}$.)

To permit the modifications in the foregoing, one link of the original system must be relaxed. The magnitudes of ω_F and $\dot{\omega}_F$ are determined by solving Equations (15) and (16) with the relaxed point substituting for the general point (*j*).

In addition to simplifying the solution of highly complex systems the concept of superposition with influence coefficients serves as yet another tool for the synthesis of mechanisms. If the influence of components can be separated from the performance of the whole, the synthesis of mechanisms by variation becomes more feasible.

YUKIO HORI

Assistant Professor,
Department of Mechanical Engineering,
University of Tokyo,
Bunkyo-ku, Tokyo, Japan

A Theory of Oil Whip

Oil whip was investigated theoretically and experimentally. In the paper it is shown that the inherent instability of the rotor in previous theories can be avoided by assuming zero pressure in place of negative pressure in the oil film and that the "inertia effect" in occurrences of oil whip can be understood by distinguishing small vibrations and large vibrations of the rotor. It is also shown that oil whip of higher order and the effect of oil viscosity on amplitude of oil whip give possible causes of some peculiar phenomena.

OIL WHIP is a self-excited lateral vibration of a shaft rotating in fluid-film bearings. In high-speed machines, it is sometimes so violent that the bearings or even the machine itself may be damaged. Therefore, oil whip has attracted many investigators since it was first reported by Newkirk and Taylor in 1925, especially in recent years as speeds of rotating machines have increased tremendously. It seems, however, that no satisfactory explanation has been given yet.

Newkirk and Taylor [1][1] reported in the first paper a violent whip of shafts which was due to the action of the oil film in the bearing. They found that the whip started at a speed twice the critical and persisted at speeds higher than that. They gave a qualitative theory for this phenomenon, but it could not explain the persistence of the whip at higher speeds. Robertson [2] made a calculation under certain assumptions and reached the conclusion that the rotor is inherently unstable at all speeds of rotation. Poritsky [3] showed, by introducing an additional radial force to the oil-film force, that the instability occurs only at speeds exceeding twice the first critical speed which, however, might decrease even to zero depending upon the oil-film condition. On the other hand, Newkirk and Lewis [5, 6] reported experimental cases in which the rotating speed reached five or six times the critical before the instability developed. This also was observed by the author.

Pinkus [8] reported that in a number of experiments a phenomenon that might be called an inertia effect in whip was observed and that in some cases the stable and unstable states of shafts were separated by a region of transient whip. These also were observed by the author.

Newkirk and Taylor [1] reported that some shafts running smoothly could be led to a violent whip by only a shock, but Pinkus [8] did not observe such a case.

Newkirk and Taylor [1, 6] reported also that whipping of the shaft continued with increasing violence at all speeds higher than twice the critical. But the author observed in some cases that the amplitudes of whipping decreased as the speed of rotation increased. Pinkus [7, 8] found even more complicated examples in which the whipping disappeared once and resumed again.

The effect of oil viscosity (or oil temperature) gives the most problematic subject. It has been reported by many investigators [5] that hotter oil gives greater range of stable operation, but Pinkus' experiments [8] showed the opposite. According to the same paper [8], some investigators reported that either cold or hot oil had a stabilizing effect on oil whip.

Thus the matter is very complicated and controversial. The author intends to give a comprehensive theory which explains these facts consistently.

In the present paper, oil whip will be treated as a problem of dynamical stability of a rotor (concentrated mass) supported by an elastic shaft rotating in fluid-film bearings. In calculating the pressure distribution in the oil film, the pressure in the unshaded area of Fig. 1 will be assumed to be zero.

Nomenclature in Stability Chart

r = radius of bearing
b = width of bearing
δ = radial clearance of bearing
κ = eccentricity ratio
F = transverse load upon journal
m = effective mass of rotor observed from journal
μ = coefficient of viscosity of lubricant
ω = angular velocity of rotation of rotor
ω_1 = angular velocity of first critical speed of rotor
ω_n = angular velocity of nth critical speed of rotor

Oil-Film Force on Journal

In most previous papers on oil whip, the pressure distribution in the oil film is calculated under the assumption that the bearing clearance is completely filled with lubricant and the pressure distribution is completely two-dimensional. Then, the oil pressure in the unshaded region of Fig. 1 is theoretically negative, and we arrive at the conclusion that the shaft is always unstable. This, however, is not true.

As many experiments show, the oil pressure in the unshaded region is not negative but almost zero. This is evident from the evaporation of the lubricant, from the segregation of gases in the lubricant and from the possible axial air flow from both ends of the bearing, provided that the oil inlet pressure is not very high. Considering these facts, we make the assumption that the pressure in the unshaded region is zero and the pressure in the other region remains two dimensional.

Therefore, our assumptions including the usual Reynolds assumptions will be:

(*a*) The oil film is thin enough and the effect of its curvature may be neglected.

(*b*) There is no pressure change across the film thickness.

[1] Numbers in brackets designate References at end of paper.

For presentation at the Summer Conference of the Applied Mechanics Division, Troy, N. Y., June 18–20, 1959, of THE AMERICAN SOCIETY OF MECHANICAL ENGINEERS.

Discussion of this paper should be addressed to the Secretary, ASME, 29 West 39th Street, New York, N. Y., and will be accepted until July 20, 1959, for publication at a later date. Discussion received after the closing date will be returned.

NOTE: Statements and opinions advanced in papers are to be understood as individual expressions of their authors and not those of the Society. Manuscript received by ASME Applied Mechanics Division, February 17, 1958. Paper No. 59—APM-2.

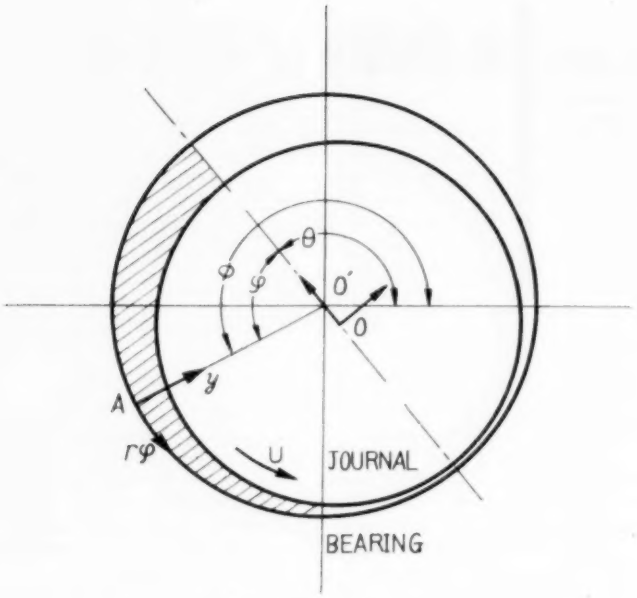

Fig. 1 Oil film in bearing

(*c*) The inertia force of the oil may be neglected.
(*d*) The oil pressure in the unshaded region in Fig. 1 is zero.
(*e*) The pressure distribution is two dimensional.

Now, we take the co-ordinates ($r\varphi$, y), the angle ϕ, and the other symbols as in Fig. 1. According to the theory of hydrodynamics, we have

$$\frac{1}{r}\frac{\partial p}{\partial \varphi} = \mu \frac{\partial^2 u}{\partial y^2} \tag{1}$$

where p and u are the oil pressure and oil velocity, respectively, at a certain point A. μ is the coefficient of viscosity of the oil.

Integrating equation (1) under the boundary conditions:

$$\begin{aligned} u &= 0, && y = 0 \\ u &= U = r\omega, && y = h, \quad h = \text{film thickness} \end{aligned} \tag{2}$$

we get the velocity of the oil flow u. Integrating the velocity u again across the thickness of the oil film, we get the rate of the oil flow Q at the point A:

$$Q = \int_0^h u dy \tag{3}$$

On the other hand, when the journal is moving, there should be the relation (4) between the film thickness and the rate of flow of the oil:

$$\frac{1}{r}\frac{\partial Q}{\partial \phi} + \frac{\partial h}{\partial t} = 0 \tag{4}$$

From these equations and

$$h = \delta(1 + \kappa \cos \varphi) \tag{5}$$

we get the pressure distribution $p(\varphi)$.

Integrating $p(\varphi) \cos \varphi$ and $p(\varphi) \sin \varphi$ from $\varphi = 0$ to $\varphi = \pi$, we get two components of the oil reaction upon the journal, one of which F_x is parallel to the displacement of the journal center and the other F_y is perpendicular to the former:

$$F_x = -6\mu \left(\frac{r}{\delta}\right)^2 rb \left[\frac{2\dot{\kappa}^2(\omega - 2\dot{\theta})}{(2 + \kappa^2)(1 - \kappa^2)} + \frac{2\dot{\kappa}}{(1 - \kappa^2)^{3/2}}\left(\frac{\pi}{2} - \frac{8}{\pi(2 + \kappa^2)}\right)\right] \tag{6}$$

$$F_y = 6\mu \left(\frac{r}{\delta}\right)^2 rb \left[\frac{\pi\kappa(\omega - 2\dot{\theta})}{(2 + \kappa^2)(1 - \kappa^2)^{1/2}} + \frac{4\kappa\dot{\kappa}}{(2 + \kappa^2)(1 - \kappa^2)}\right] \tag{7}$$

where b and r are the width and the radius of the bearing, respectively.

Statical Equilibrium Points of Journal Center

It is easy to find the equilibrium points by equating the transverse load F upon the journal and static parts of the oil reaction (6, 7). If we denote its components by F_{x0} and F_{y0}, we have

$$F^2 = F_{x0}^2 + F_{y0}^2 \tag{8}$$

or

$$F_a = \frac{\kappa^2[\pi^2 - (\pi^2 - 4)\kappa^2]^{1/2}}{(2 + \kappa^2)(1 - \kappa^2)} \tag{9}$$

where

$$F_a = F/6\mu \left(\frac{r}{\delta}\right)^2 rb\omega$$

If we find the value of κ corresponding to F_a by (9), we can calculate the value of angle θ, taken as in Fig. 2, by the following relationship:

$$\tan \theta = \frac{F_{y0}}{F_{x0}} = \frac{\pi(1 - \kappa^2)^{1/2}}{2\kappa} \tag{10}$$

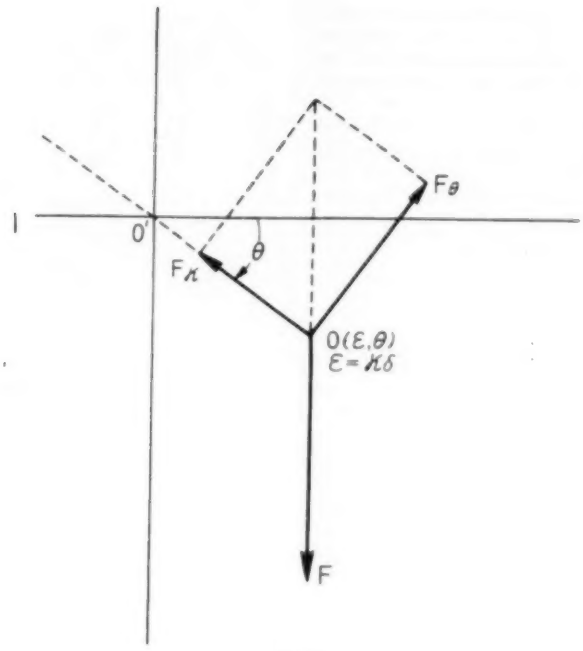

Fig. 2

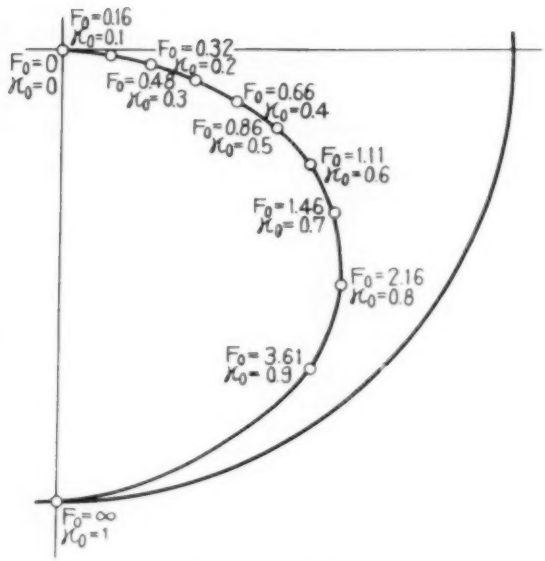

Fig. 3 Journal locus

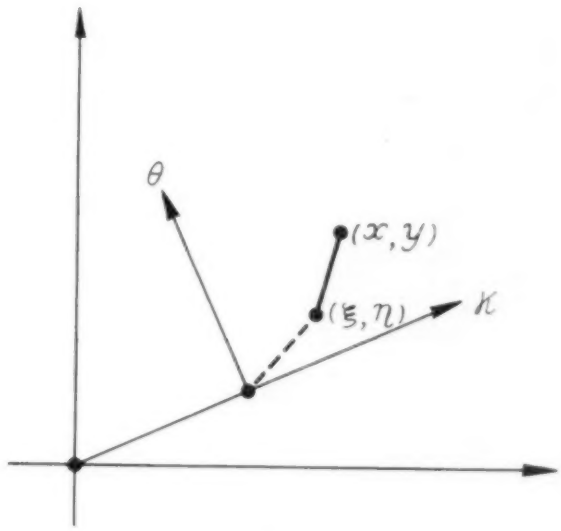

Fig. 4

This gives the locus of the equilibrium points of the journal center. The locus is depicted in Fig. 3, where we see that the journal center floats up along a semicircle with increase in speed of the journal. We denote the equilibrium points of the journal by (κ_0, θ_0). In cases of vertical shafts, the equilibrium points of the shafts are at the bearing center.

Stability of Rotors

In discussing stability of a rotor, we divide its vibrations into two parts, i.e., small vibrations and large vibrations, which frequently have been mixed up. By doing this, we shall be able to remove one of the confusions in the theory of oil whip.

Small vibrations mean such vibrations of the rotor that the amplitude of the journal is sufficiently small compared with its eccentricity from the bearing center. Large vibrations mean such vibrations that its shaft bends considerably. In this case, the amplitude of the journal cannot be small.

Stability for Small Vibrations. In this section, at first, we shall derive the equation of motion of a rotor and linearize it and investigate the stability of the rotor by means of Hurwitz criteria.

For simplicity, we shall not take statical deflection of the shaft into account. We assume that the alignment of the two bearings is perfect and everything is dynamically symmetrical about the plane normal to the shaft at its mid-point, and that the mass of the shaft may be neglected.

We take rectangular co-ordinates with the origin at the equilibrium point of the journal center as in Fig. 4, and denote coordinates of the rotor center and journal center by (x, y) and (ξ, η), respectively. Then, the equation of motion of the rotor will be

$$\left.\begin{aligned} m\ddot{x} + k(x - \xi) + mg \sin\theta &= 0 \\ m\ddot{y} + k(y - \eta) + mg \cos\theta_i &= 0 \\ k(x - \xi) + F_x - \frac{\eta}{\delta\kappa} F_\theta &= 0 \\ k(y - \eta) + F_\theta + \frac{\eta}{\delta\kappa} F_x &= 0 \end{aligned}\right\} \tag{11}$$

where k is the elastic constant of the shaft and F_x and F_θ are the oil reaction given by (6) and (7).

Considering small vibrations of the rotor at the equilibrium point, we replace κ by $\kappa_0 + \kappa$, $(\kappa \ll \kappa_0)$. If the new κ is small enough and $\kappa^2, \kappa^3, \ldots$ are negligible compared with κ_0, we can rewrite equation (11) in the following linear form (variation equation):

$$\left.\begin{aligned} &a_1 \frac{F}{k\omega\delta}\dddot{x} + \left[a_2 \frac{F}{k\delta} + 1\right]\ddot{x} + a_1 \frac{F}{m\omega\delta}\dot{x} + a_2 \frac{F}{m\delta} x \\ &\quad - a_3 \frac{F}{k\omega\delta}\dddot{y} + a_4 \frac{F}{k\delta}\ddot{y} - a_3 \frac{F}{m\omega\delta}\dot{y} + a_4 \frac{F}{m\delta} y = 0 \\ &a_3 \frac{F}{k\omega\delta}\dddot{x} + b_2 \frac{F}{k\delta}\ddot{x} + a_3 \frac{F}{m\omega\delta}\dot{x} + b_2 \frac{F}{m\delta} x \\ &\quad - 2a_4 \frac{F}{k\omega\delta}\dddot{y} - \left[\frac{a_3}{2}\frac{F}{k\delta} + 1\right]\ddot{y} - 2a_4 \frac{F}{m\omega\delta}\dot{y} \\ &\quad - \frac{a_3}{2}\frac{F}{m\delta} y = 0 \end{aligned}\right\} \tag{12}$$

where $a_1, a_2, \ldots, b_2, \ldots$ are constants determined by the eccentricity of the journal κ_0 alone. The characteristic equation of (12) is

$$A_0 s^6 + A_1 s^5 + A_2 s^4 + A_3 s^3 + A_4 s^2 + A_5 s + A_6 = 0 \tag{13}$$

where $A_0, A_1, A_2, \ldots$ are constants determined by the running conditions of the shaft. Applying Hurwitz criteria to (13), we get the following simultaneous inequalities for stable running of the rotor:

$$\left.\begin{aligned} &A_0, A_1, A_2, \ldots A_6 > 0 \quad (14a) \\ &\begin{vmatrix} A_1 A_3 A_5 \\ A_0 A_2 A_4 A_6 \\ A_1 A_3 A_5 \\ A_0 A_2 A_4 A_6 \\ A_1 A_3 A_5 \end{vmatrix} > 0 \quad (14b) \\ &\begin{vmatrix} A_1 A_3 A_5 \\ A_0 A_2 A_4 \\ A_1 A_3 \end{vmatrix} > 0 \quad (14c) \end{aligned}\right\} \tag{14}$$

It will be seen that (14a) is always satisfied and (14b) can be rewritten in the following form:

$$\frac{1}{\omega^2}\left(\frac{F}{m\delta}\right) > K_1(\kappa_0)\left[K_2(\kappa_0) + \frac{1}{\omega_1^2}\left(\frac{F}{m\delta}\right)\right] \tag{15}$$

(See nomenclature after the introduction.)

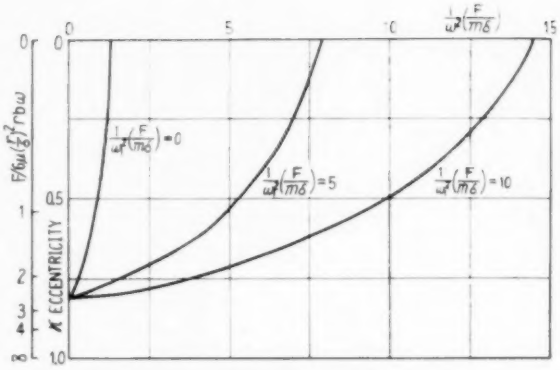

Fig. 5 Stability chart

And if we rewrite (14c) in the same way, it will be seen that the condition (14c) is weaker than (14b); i.e., whenever (14b) is satisfied, (14c) is always satisfied. Therefore we can discuss the stability by (15) alone.

Since $K_1(\kappa_0)$, $K_2(\kappa_0)$ are functions of κ_0 alone, we can express the condition (15) graphically on a plane with two axes κ_0 and $(1/\omega^2)$ $(F/m\delta)$, see Fig. 5. Expression $(1/\omega_1^2)$ $(F/m\delta)$ is a parameter relating to the critical speed of the shaft. We call this diagram a stability chart. The right-hand side and the left-hand side of each curve correspond to the stable and the unstable running of the shaft, respectively.

The stability chart shows that the shaft is always stable if the displacement of the journal center from the bearing center is more than approximately 80 per cent of the radial clearance of the bearing, or if the vertical displacement of the journal center from its lowest position is less than 50 per cent of the clearance, Fig. 3. Therefore, large eccentricity will be favorable for stable running. This agrees with practical experiences. (For further details, see Appendix.)

Stability for Large Vibrations. Next, we shall consider conditions for occurrences of such large vibrations of the rotor that its shaft bends considerably. In this case, the journal centers inevitably rotate around the bearing center and the dynamical situation is entirely different from that in the previous section.

When the rotor is whirling with large amplitudes, as is easily seen from Fig. 6, the journal contacts with the edge of the bearing and the center points of the journal run along circular loci surrounding the center line of the bearing, as in Fig. 7(b). (Therefore we cannot assume that $\kappa \ll \kappa_0$ as before.) And if the oil force is not very large, the frequency of the circular motion will be approximately equal to the natural frequency of the rotor. There-

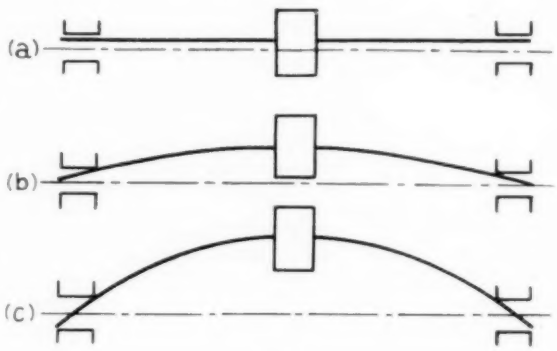

Fig. 6

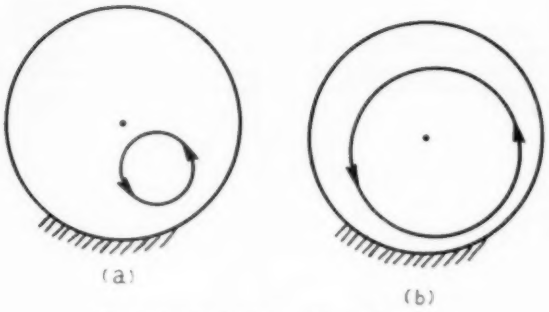

Fig. 7 Small vibrations and large vibrations

fore the system consisting of the rotor, the shaft, and the journal may be simplified to that of Fig. 8 in which a rotating cylinder is connected to the center of the bearing with a spring of such stiffness that the natural frequency of the cylinder is equal to that of the rotor in question and rotates around the center. Let us discuss motions of the cylinder.

If we consider nearly stationary whirling, then $\dot{\kappa} \fallingdotseq 0$ in (7) and F_θ will be given by the following expression:

$$F_\theta = K\left(\frac{\omega}{2} - \dot{\theta}\right)\kappa, \quad K = 12\mu\left(\frac{r}{\delta}\right)^2 rb\,\frac{\pi\kappa}{(2+\kappa^2)(1-\kappa^2)^{1/2}} \tag{16}$$

Then the equation of motion of the cylinder will be

$$\frac{d^2Z}{dt^2} + K'\left(\dot{\theta} - \frac{\omega}{2}\right)iZ + \omega_1{}^2Z = 0, \quad K' = \frac{K}{m} \tag{17}$$

where

$$Z = (\delta\kappa)e^{i\theta}$$

θ = angular displacement
$\dot{\theta}$ = whirling speed
ω_1 = circular frequency of natural vibration of rotor

It is easily seen that this differential equation has a stationary solution:

$$Z = Ae^{i\omega_1 t}, \quad \omega = 2\dot{\theta} = 2\omega_1 \tag{18}$$

and when $\omega \gtrless 2\omega_1$ the vibration will diverge or converge, respectively [9].

Therefore, we arrive at the conclusion that such a large vibration of the rotor can continue to exist only when the speed of rotation of the shaft is higher than twice its critical speed.

Occurrence of Oil Whip

Combining the conclusions in the previous sections, we get a comprehensive explanation of the occurrences of oil whip. As an example, we take a shaft of

$$\frac{1}{\omega_1{}^2}\left(\frac{F}{m\delta}\right) = 10$$

the stability chart of which is shown in Fig. 9. Two vertical broken lines, right and left, show the critical and twice the critical speed of the shaft, respectively.

Shaft With Light Load. If we increase the speed of rotation of a shaft with light load from 0 to ∞, a point showing its running condition moves along a dotted curve a_1a_2, for instance, in Fig. 9 in the direction of the arrow and the rotor becomes unstable at the point A, where the speed can be even less than the critical speed. In this case, the shaft is usually compelled by the oil force to whirl around the bearing center at the speed of one half the speed of rotation as easily seen from (7). However, as large vibration cannot exist at this speed, the shaft is almost straight and the vibration might not be recognized by the naked eye.

When the speed reaches the critical speed, a large vibration due to resonance occurs. Beyond the critical speed, however, the amplitude will decrease again, because large self-excited vibration still cannot exist at this speed.

When the speed reaches twice the critical speed, the whirling speed of the shaft coincides with the critical speed and large vibration occurs. The amplitude no longer will decrease even if the speed is increased further, because beyond this speed the large vibration can exist self-excitingly. The frequency of the vibration is, roughly speaking, independent of the speed of the shaft and equal to the natural frequency (or critical speed) of the shaft. This is the so-called oil whip. Sometimes, the mild whirl before the large vibration is also called oil whip.

Fig. 10(a) shows the changes of the amplitude and the frequency of this case as functions of the speed of rotation.

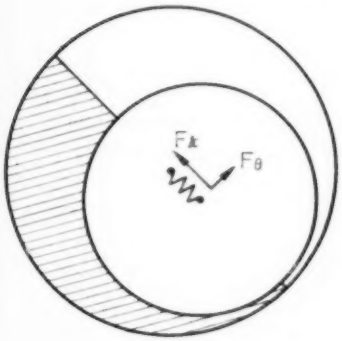

Fig. 8 Simplified model for large vibrations

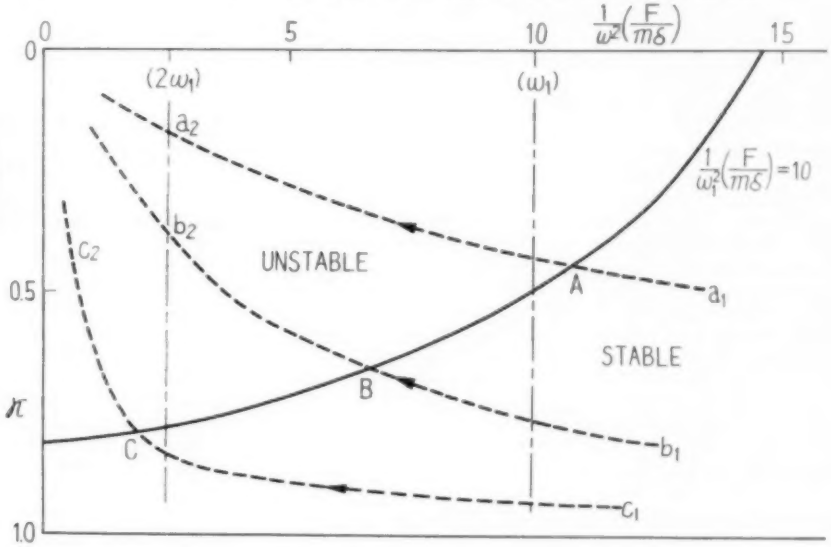

Fig. 9 Stability chart ▶

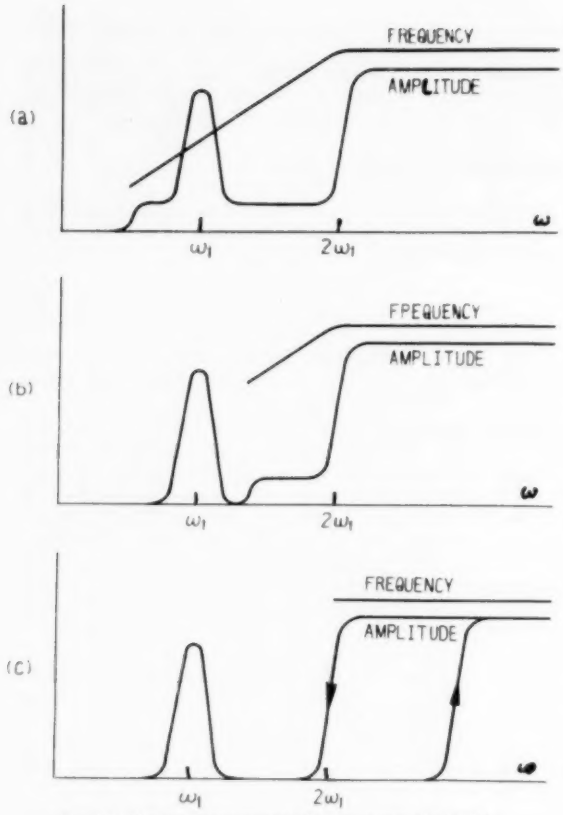

Fig. 10 Various appearances of occurrences of oil whip

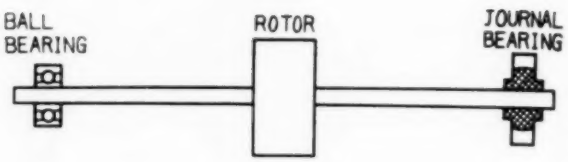

Fig. 11

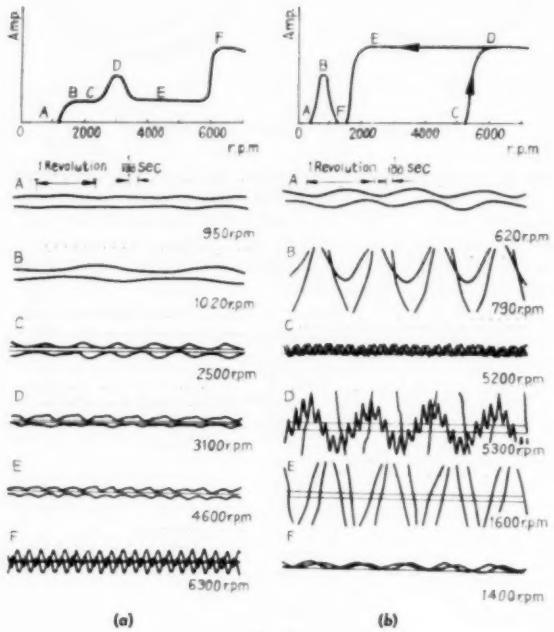

Fig. 12

Shaft With Heavy Load. This case corresponds to the curve c_1c_2 in Fig. 9. In this case, vibration does not occur even if the speed of the shaft reaches twice the critical speed because the rotor is still stable and there is no stimulation. When the rotating speed reaches the point C, the rotor becomes unstable and, if once the journal center rotates around the bearing center, such motion grows rapidly and large vibration starts. This is the oil whip.

If the large vibration once starts, it continues self-excitingly at all speeds higher than twice the critical speed. Therefore, even if the rotating speed is decreased, the large vibration will not disappear until the speed reaches twice the critical speed.

This is shown in Fig. 10(*c*).

Shaft With Medium Load. This is a case between the two preceding cases, and is shown in Fig. 10(*b*) which corresponds to the curve b_1b_2 in Fig. 9.

Experiments. Our experimental apparatus consists of a rotor with a slender shaft supported by a fluid-film bearing at one end and by a ball bearing at the other, as shown in Fig. 11. The shaft is driven by a variable-speed motor through a cloth belt and a rubber coupling. The recording system consists of a photographic recording drum, a light source, and a pair of mirrors, for horizontal and vertical direction, attached on vibrating metal strips which are in contact with the shaft. Three weights, three shafts, and nine bearings are provided.

Figs. 12(*a*) and (*b*) are the photographic records of two series of experiments which correspond to shafts with a light rotor and a heavy rotor, respectively.

In Fig. 12(*a*) (light rotor):

At B the shaft becomes unstable and begins to whirl at the speed of one half of the rotating speed of the shaft;

At D (critical speed) a large vibration caused by resonance, occurs. D shows the superposition of the whirl and the resonance vibration.

At E the amplitude decreases again.

At F (twice the critical speed) violent oil whip occurs.

In Fig. 12(*b*) (heavy rotor):

At B the resonance vibration occurs.

At C (far beyond twice the critical speed) suddenly oil whip occurs.

At E (twice the critical speed) the oil whip continues down to this point.

At F the oil whip disappears.

Changes of Amplitude of Oil Whip

The amplitude of vibration of a shaft caused by oil whip is always very large when the speed of the shaft is equal to or a little higher than twice the critical speed. But under certain conditions, it might decrease as the speed of the shaft increases beyond twice the critical, and sometimes not. In this section, we consider changes of amplitudes of oil whip.

Effects of Oil Force. The problem of determining the amplitude of a rotor may be considered as a problem of forced vibration of the rotor caused by two external oscillatory stimulations; i.e., the rotation of the shaft and the whirling of the journal. But, here, we shall discuss the effect of whirling only, because we are now interested in the behavior of the shaft at speeds more than twice the critical.

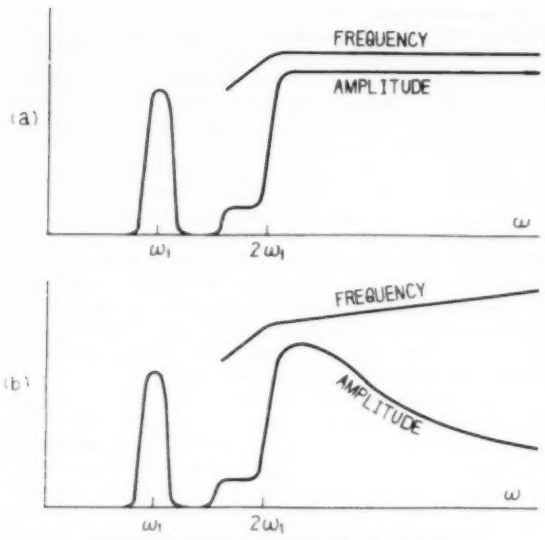

Fig. 13 Changes of amplitude due to oil force

As stated before, the whirling speed of the shaft is usually almost equal to its natural frequency and so the amplitude of whirling is large. Strictly speaking, however, if the oil force is large and the rotating speed is also large, the shaft will be driven by the oil force and whirling speed of the shaft will become larger than the natural frequency [9]. If we take equation (17) again for simplicity, the approximate whirling speed will be

$$\theta = \frac{\omega_1}{\sqrt{2}}\left[\left[\left\{\left(\frac{K'}{2\omega_1}\right)^2 - 1\right\}^2 + \left(\frac{K'}{2\omega_1}\right)^2\left(\frac{\omega}{\omega_1}\right)^2\right]^{1/2} - \left\{\left(\frac{K'}{2\omega_1}\right)^2 - 1\right\}\right]^{1/2}$$

$$= \omega_1 \qquad \text{if} \quad \frac{K'}{2\omega_1} = 0$$

$$= \left(\frac{\omega_1\omega}{2}\right)^{1/2} \quad \text{if} \quad \frac{K'}{2\omega_1} = 1$$

$$= \frac{\omega}{2} \qquad \text{if} \quad \frac{K'}{2\omega_1} = \infty$$

where K' is the oil-force coefficient, ω is angular velocity of rotation of the shaft, and ω_1 is angular velocity of natural vibration of the shaft.

Therefore the higher the rotating speed is, the higher the whirling speed will be. The larger the oil force is, the more rapidly the whirling speed increases. Now the amplitude of the journal is limited by the bearing clearance. Therefore if the oil force is large, the amplitude of the rotor should decrease as the rotating speed increases, Fig. 13(*b*), but, if the oil force is small, the whirling speed remains constant and the amplitude does not decrease, Fig. 13(*a*).

An experimental example is shown in Fig. 14. The bearing used in case (*a*) is shorter than that in case (*b*)—the ratio of the length is 2.5—in other words, the oil force in case (*b*) is larger than that in case (*a*). In both cases the same shaft was used. In case (*b*), the whirling speed of the shaft increases with the increase of rotating speed and the amplitude decreases, while it does not in case (*a*).

Thus it is possible to decrease the amplitude of the oil whip by using a longer bearing or more viscous lubricant if the rotor is operated at speeds much higher than twice the critical speed.

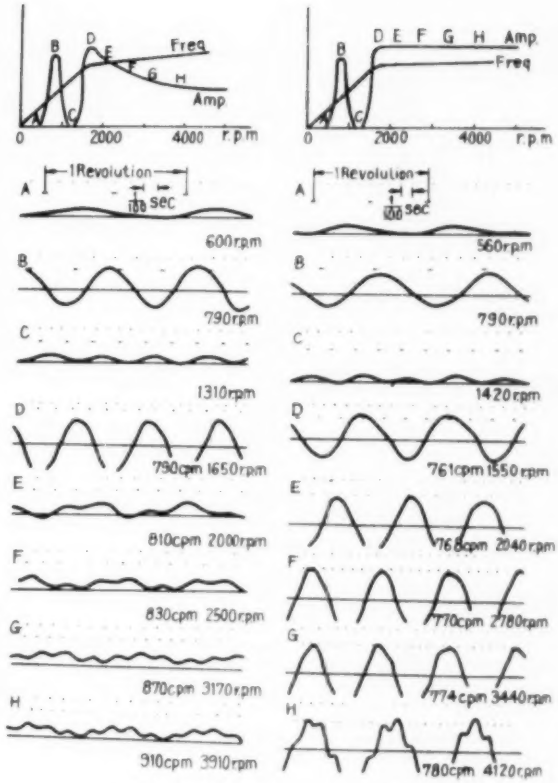

Fig. 14

Occurrences of Resonance Vibration and Oil Whip of Higher Order. In the preceding section, we found that if the oil force is large (or if K' is large) the amplitude of the oil whip decreases as the speed of the shaft increases. Even in such cases, the amplitude can resume again when the speed reaches a higher critical speed or twice a higher critical speed.

(*a*) **Resonance Vibration of Higher Order.** When the speed of the shaft coincides with the higher critical speed the usual resonant vibration occurs. But it would be recognizable only when oil whip is not violent.

(*b*) **Oil Whip of Higher Order.** In the section, Stability for Large Vibrations, we considered only the lowest critical speed; but the same arguments hold for the higher critical speeds, too. For example, if the speed of the shaft is twice the second critical or more, a large vibration of the second critical frequency can exist, although it might be damped out by the same reason as in the preceding section, with further increase of the speed of rotation. The same phenomena can occur successively as the speed of the shaft increases passing several higher critical speeds. These might be called oil whips of higher order. But if the effect of oil force is not large enough the whips of higher order will not be recognizable, because the previous oil whip will not disappear, Fig. 15(*a*). If the oil force is large, the amplitude of whip will decrease before the oil whip of the next order starts and the whip of higher order can be noticed. The amplitude changes in such cases would look like Fig. 15(*b*).

In actual cases, the resonant vibration and the oil whip of higher order will appear together in complicated forms.

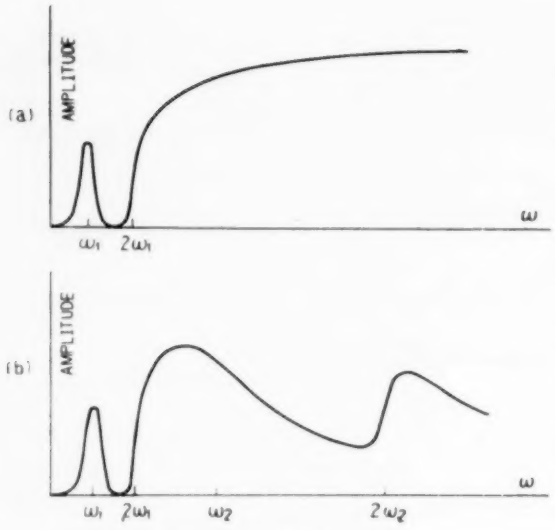

Fig. 15 Oil whip of higher order

Discussion

We have considered some fundamentals of oil whip. Using these considerations as bases, the author will try to interpret some of the contradictions mentioned in the introduction and in other papers.

Oil-Whip Starting Speeds. A shaft becomes unstable when its operating condition enters the left side of each curve in Fig. 5 or Fig. 9. Therefore, the rotor can be stable at any speed if the journal eccentricity is large enough. Newkirk and Lewis [5] reported that the range of stable operation reached five times the critical speed or more. This ratio, at least theoretically, can be infinitely large.

In the case of a heavy rotor (c_1c_2 in Fig. 9), if the oil force is not large enough to raise the shaft up to the bearing center when the rotor enters the unstable region, the journal cannot go around the bearing center and the large vibration does not commence until the oil force, i.e., the speed of the shaft, becomes large enough. Therefore, the rotor will vibrate with small amplitude but hesitate to get into violent whip. This might be the causes for the difficulties of determining the whirl-impending speed in the cases of large eccentricity reported by Newkirk and Lewis [5]. When the rotor is not very heavy, the hesitation will not be observed

Again in the case of a heavy rotor (c_1c_2 in Fig. 9), there is a kind of hysteresis in changes of amplitude as in Fig. 10(c). This would give an explanation for the inertia effect (resistance to whip when the shaft is stable and unwillingness to pull out of whip once it starts) and the region of transient whip (region where the shaft would alternately become stable and unstable) in Pinkus' sense [8].

If the rotor is light, it can become unstable even before the speed of rotation reaches the first critical speed.

Effect of a Blow. Newkirk [1] and Newkirk and Lewis [5] found cases in which a stable shaft could be brought into a violent whipping with a sudden blow, but Pinkus [8] did not.

Newkirk's case might correspond to the transient region of the c_1c_2 in Fig 9 or Fig. 10(c). In this case, if the blow is strong enough to make the journal center jump up to the bearing center, it suddenly grows into a violent oil whip. It seems that in Pinkus' case, either the blow was not strong enough or the rotor was not heavy enough.

Changes of Amplitude. Newkirk [1, 5, 6] reported that oil whip continued with increasing violence and there seemed no stable range above twice the critical speed. But actually, owing to the oil force, the frequency more or less increases and consequently the amplitude decreases as the speed of shaft increases. This was confirmed by the author's experiment. In Newkirk's case, the oil force must have been too small.

In the same paper [5], however, Newkirk and Lewis reported another case which seems, to the author, to be a typical case of large oil force. They observed the half running speed-frequency whirl with running speed well over twice the critical speed. This means the oil force was extremely large and the motion of the journal was under strong control of the oil action. Furthermore, they added that the disturbances were easily damped out and did not build up resonant vibration of the shaft except when the running speed was twice the critical speed. This is exactly the case stated in the section, Effects of Oil Force.

Pinkus [7, 8] reported very complicated experimental examples and set forth the theory that whenever a speed is reached corresponding to a higher critical of the shaft or other resonance of the system, whip tends to be damped out and the resonant vibration prevails, although whip returns as soon as this region is passed. But he mentioned some exceptions, that is, in some cases the amplitude decreased before the resonant region was reached and in some cases the whip could not be damped out at all.

The author would like to paraphrase Pinkus' theory as that, whenever a speed is reached corresponding to a higher critical of the shaft or twice a higher critical (including other resonance of the system), an oil whip or a resonant vibration of higher order will occur, although they can be noticed only when the previous whip has been damped out beforehand by large oil force (sections under Changes of Amplitude of Oil Whip).

Effect of Viscosity (or Temperature) of Lubricant. Viscosity of lubricant has caused considerable confusion. Newkirk and Lewis [5] reported that warming the oil increased the range of stable operation. But Pinkus [7, 8] reported that he constantly observed the opposite. In his experiment, some of the bearings which whipped at high inlet oil temperature had a narrow whipping range at intermediate temperature and did not whip at all at low temperature. Even when whip occurred, the violence of the vibration was less for the lower temperature.

These two were reported as a contradiction. It seems, however, that they are just seeming inconsistencies. As easily seen from the stability chart, lower viscosity gives greater stability for small vibration. Therefore, low viscosity is effective in preventing the occurrence of oil whip and Newkirk and Lewis were correct. On the other hand, as discussed in the section, Effects of Oil Force, high viscosity is effective in depressing the oil whip after it once develops. Therefore, Pinkus was also correct. Pinkus' experiment just mentioned is really a beautiful example of the case of the section, Effects of Oil Force.

Conclusion

The author investigated oil whip theoretically and experimentally and tried to explain various peculiar, seemingly inconsistent phenomena of oil whip as mentioned in the introduction.

We could explain "inertia effect" by distinguishing small vibrations and large vibrations of oil whip.

We found that it is possible to stabilize a rotor by increasing the eccentricity of the journal from the bearing center (by using a shorter bearing, by using less viscous lubricant, and so on) and also it is possible to decrease the amplitude of oil whip by making the oil force larger (by using a longer bearing, by using more viscous lubricant and so on), if the rotor is operated at the speeds considerably higher than twice the critical speed. It is interesting to see that these two are the reverse of one other.

A vertical shaft, which we have not discussed yet, is just a special case of our general theory. It may be considered to be the case of very light shafts, or the case of $F = 0$. Therefore a vertical shaft will be unstable at all speeds, as easily seen from the stability chart, and oil whip will always start when the speed of rotation reaches twice the critical speed. It should be noted, however, that usually there are some damping forces, for example, due to thrust bearings, in cases of vertical shafts. These damping forces might reduce or eliminate oil whip.

The whirling in vertical Francis water turbines mentioned in reference [11] could be understood as a kind of oil whip. In this case, water in the annular passage plays the role of oil in journal bearings. The fact that the whirling occurred only at loads greater than half the rated horsepower could also be understood because when the water pressure is high the assumption (d) in the section, Oil-Film Force on Journal, does not hold and the instability becomes larger.

Acknowledgment

Finally, the author thanks Profs. T. Yoshizawa, S. Fujii, and T. Okazaki at the University of Tokyo, Japan, and Prof. S. H. Crandall at Massachusetts Institute of Technology, for their valuable discussions and constant aid in the preparation of the paper. He also thanks the Hitachi, Ltd. (Kawasaki Plant), Japan, which made the experimental apparatus for the author.

References

1 B. L. Newkirk and H. D. Taylor. "Shaft Whipping Due to Oil Action in Journal Bearing," *General Electric Review*, August, 1925 pp. 559–568.

2 D. Robertson, "Whirling of a Journal in a Sleeve Bearing," *Philosophical Magazine*, series 7, vol. 15 January, 1933, pp. 113–130.

3 H. Poritsky, "Contribution to the Theory of Oil Whip," TRANS. ASME, vol. 75, 1953, pp. 1153–1161.

4 B. L. Newkirk and L. P. Grobel, "Oil-Film Whirl—A Non-Whirling Bearing," TRANS. ASME, vol. 56, 1934, pp. 607–615.

5 B. L. Newkirk and J. F. Lewis, "Oil Film Whirl—An Investigation of Disturbances Due to Oil Films in Journal Bearings," TRANS. ASME, vol. 78, 1956, pp. 21–27.

6 B. L. Newkirk, "Varieties of Shaft Disturbances Due to Fluid Films in Journal Bearings," TRANS. ASME, vol. 78, 1956, pp. 985–988.

7 O. Pinkus, "Note on Oil Whip," JOURNAL OF APPLIED MECHANICS, vol. 20, TRANS. ASME, vol. 75, 1953, pp. 450–451.

8 O. Pinkus, "Experimental Investigation of Resonant Whip," TRANS. ASME, vol. 78, 1956, pp. 975–983.

9 S. Fujii, "The Roles of Resistances in the Vibration of a Shaft," *The Japan National Congress for Applied Mechanics*, vol. 1, 1951, pp. 599–603.

10 G. S. A. Shawki, "Whirling of a Journal Bearing," *Engineering*, February, 1955, pp. 243–246.

11 J. P. Den Hartog, "Mechanical Vibrations," McGraw-Hill Book Company, Inc., New York, N. Y., 1956 p. 321.

APPENDIX

The coefficients $a_1, a_2, \ldots, b_2, \ldots$ in equation (12) are as follows:

$$a_1 = \frac{2(2+\kappa_0^2)}{\kappa_0(1-\kappa_0^2)^{1/2}[\pi^2-(\pi^2-4)\kappa_0^2]^{1/2}}\left\{\frac{\pi}{2} - \frac{8}{\pi(2+\kappa_0^2)}\right\}$$

$$a_2 = \frac{4\kappa_0}{[\pi^2-(\pi^2-4)\kappa_0^2]^{1/2}}\left(\frac{1}{\kappa_0} + \frac{\kappa_0}{1-\kappa_0^2} - \frac{\kappa_0}{2+\kappa_0^2}\right)$$

$$a_3 = \frac{4}{[\pi^2-(\pi^2-4)\kappa_0^2]^{1/2}}, \quad a_4 = \frac{\pi(1-\kappa_0^2)^{1/2}}{\kappa_0[\pi^2-(\pi^2-4)\kappa_0^2]^{1/2}}$$

$$b_2 = \frac{\pi(1-\kappa_0^2)^{1/2}}{[\pi^2-(\pi^2-4)\kappa_0^2]^{1/2}}\left(\frac{1}{\kappa_0} + \frac{\kappa_0}{1-\kappa_0^2} - \frac{2\kappa_0}{2+\kappa_0^2}\right)$$

$$b_1 = a_2, \quad b_2 = 2a_4, \quad b_4 = \frac{1}{2}\,a_3$$

The coefficients $A_0, A_1, A_2, \ldots$ in equation (13) are as follows:

$$A_0 = (2a_1a_4 - a_3^2)\frac{1}{\omega^2\omega_1^4}\left(\frac{F}{m\delta}\right)^2 \equiv B_0\frac{1}{\omega^2\omega_1^4}\left(\frac{F}{m\delta}\right)^2$$

$$A_1 = \left(\frac{1}{2}\,a_1a_3 + 2a_2a_4 + a_3a_4 - a_3b_2\right)\frac{1}{\omega\omega_1^4}\left(\frac{F}{m\delta}\right)^2 + (a_3 + 3a_4)\frac{1}{\omega\omega_1^2}\left(\frac{F}{m\delta}\right)$$

$$\equiv B_1\frac{1}{\omega\omega_1^4}\left(\frac{F}{m\delta}\right)^2 + B_1'\frac{1}{\omega\omega_1^2}\left(\frac{F}{m\delta}\right)$$

$$A_2 = (4a_1a_4 - 2a_3^2)\frac{1}{\omega^2\omega_1^2}\left(\frac{F}{m\delta}\right)^2 + \left(\frac{1}{2}\,a_3a_3 + a_4b_2\right)\frac{1}{\omega_1^4}\left(\frac{F}{m\delta}\right)^2 + \left(a_2 + \frac{1}{2}\,a_3\right)\frac{1}{\omega_1^2}\left(\frac{F}{m\delta}\right) + 1$$

$$\equiv B_2\frac{1}{\omega^2\omega_1^2}\left(\frac{F}{m\delta}\right)^2 + B_2'\frac{1}{\omega_1^4}\left(\frac{F}{m\delta}\right)^2 + B_2''\frac{1}{\omega_1^2}\left(\frac{F}{m\delta}\right) + 1$$

$$A_3 = (a_1a_3 + 4a_2a_4 + 2a_3a_4 - 2a_3b_2)\frac{1}{\omega\omega_1^2}\left(\frac{F}{m\delta}\right)^2 + (a_1 + 2a_4)\frac{1}{\omega}\left(\frac{F}{m\delta}\right)$$

$$\equiv B_3\frac{1}{\omega\omega_1^2}\left(\frac{F}{m\delta}\right)^2 + B_3'\frac{1}{\omega}\left(\frac{F}{m\delta}\right)$$

$$A_4 = (a_3a_3 + 2a_4b_2)\frac{1}{\omega_1^2}\left(\frac{F}{m\delta}\right)^2 + (2a_1a_4 - a_3^2)\frac{1}{\omega^2}\left(\frac{F}{m\delta}\right)^2 + \left(a_2 + \frac{1}{2}\,a_3\right)\left(\frac{F}{m\delta}\right)$$

$$\equiv B_4\frac{1}{\omega_1^2}\left(\frac{F}{m\delta}\right)^2 + B_4'\frac{1}{\omega^2}\left(\frac{F}{m\delta}\right)^2 + B_4''\left(\frac{F}{m\delta}\right)$$

$$A_5 = \left(\frac{1}{2}\,a_1a_3 + 2a_2a_4 + a_3a_4 - a_3b_2\right)\frac{1}{\omega}\left(\frac{F}{m\delta}\right)^2$$

$$\equiv B_5\frac{1}{\omega}\left(\frac{F}{m\delta}\right)^2$$

$$A_6 = \left(\frac{1}{2}\,a_3a_3 + a_4b_2\right)\left(\frac{F}{m\delta}\right)^2 \equiv B_6\left(\frac{F}{m\delta}\right)^2$$

$B_1, B_1', \ldots$ etc. are all functions of $a_1, a_2, \ldots$ and consequently functions of κ_0 alone. There are the following relations between them:

$$B_2 = 2B_0, \quad B_3 = 2B_1, \quad B_3' = B_1', \quad B_4 = 2B_2'$$

$$B_4' = B_0, \quad B_4'' = B_2'', \quad B_5 = B_1, \quad B_6 = B_2'$$

$K_1(\kappa_0), K_2(\kappa_0)$ in equation (15) are as follows:

$$K_1 = \frac{B_1^2 - B_1B_1'B_2'' + B_1'^2B_2'}{B_0B_1'^2}, \quad K_2 = \frac{B_1'}{B_1}$$

Let us consider the meaning of equation (15). At first, we consider the case of a rotor supported by a rigid shaft. Then, as $\omega_1 = \infty$, A_0 and A_1 become zero and equation (13) will be re-

duced to a biquadratic equation with simpler coefficients. In this case, the circular frequency ω_l of self-excited vibration of the rotor at the moment when the rotor starts to vibrate will be given by vibration theory as follows:

$$\frac{1}{\omega_l^2} = \frac{A_3}{A_4} = \frac{B_1'}{B_1}\left(\frac{m\delta}{F}\right) = K_2(\kappa_0)\left(\frac{m\delta}{F}\right)$$

Using this result, we can rewrite (15) in the following form:

$$\frac{1}{\omega^2} > K_1(\kappa_0)\left[\frac{1}{\omega_l^2} + \frac{1}{\omega_1^2}\right]$$

In this expression, the interior of the brackets is equal to the inverse square of the circular frequency of the natural vibration of the rotor (or the critical speed) supported by the elastic shaft and oil film which are considered to be two springs connected in series.

On Critical Speeds of a Shaft Supported by a Ball Bearing

TOSHIO YAMAMOTO

Professor-Doctor,
Department of Engineering,
Nagoya University,
Furo-cho, Chikusa-ku, Nagoya, Japan

The author points out that two kinds of critical speeds induced by a slight difference in the diameter of balls in a ball bearing appear in a rotating shaft supported by ball bearings. These two critical speeds have peculiar modes of vibrations which are determined by dimensions of ball bearings; one of them is motion of forward precession, the other is backward precession. The paper describes the cause of these critical speeds and the behavior of those vibrations.

An optical record of lateral vibrations of a rotating vertical shaft is made in the x and y-directions, Fig. 1. The shaft mounts one disk and is supported by self-aligning double-row ball bearings, the inner diameter of which is 0.394 in. In our experiment, we use shafts (length $\fallingdotseq$ 20 in., diameter $\fallingdotseq$ 0.45 in.) and disks (diameter = 14 $\sim$ 20 in., weight = 14 $\sim$ 17 lb) which are placed in different positions on the shafts.

Critical Speeds of $\left[+\frac{1}{2.65}\omega\right]$

Vibrations at Critical Speed. The following expressions are used to represent the mode of vibration. Notation $[+m\omega]$ is given to the motion which has a whirling speed of elastic curve of the shaft of m times the rotating speed of the shaft ω. Here the positive sign $+$ represents a whirling motion of forward precession in which the direction of whirl is the same as the direction of rotation of the shaft. In $[-n\omega]$ the negative sign, on the other hand, means a backward precession in which the whirl is in a reversed direction. Hence $[-n\omega]$ represents a whirling motion of backward precession with whirling speed $n\omega$.

Experimentally, the critical speed

$$\left[+\frac{1}{2.65}\omega\right]$$

which is denoted by the notation ω_a, appears at a considerably higher speed than the major critical speed ω_c. Although location of critical speed ω_a varies according to change of dimensions of disk and shaft, and position of disk a:b, Fig. 1, the value of $+1/2.65$ $(=\alpha_1)$ is universally constant in all cases in which various kinds of disks and shafts are used. This fact suggests that critical speed ω_a is not caused by the disks and shafts themselves.

Vibratory waves of vibration of

$$[\alpha_1\omega] = \left[+\frac{1}{2.65}\omega\right]$$

on oscillographic paper are given in Fig. 2 where vertical white lines are rotating marks recorded by a small piece of paper P, Fig. 1, at each revolution of shaft. By comparing vibratory waves in both the x and y-directions, we can determine the forward or backward precession.

Obviously, by the shape of waves in Fig. 2, we can see that motion at this critical speed can be represented by

$$x = A\cos\omega t + B\cos\alpha_1\omega t, \quad y = A\sin\omega t + B\sin\alpha_1\omega t \quad (1)$$

viz., that this motion is composed of two vibrations the circular frequencies of which are, respectively, ω and $\alpha_1\omega$. When self-aligning double-row ball bearings of 0.394-in. diam are used, the values of α_1 is about $+1/2.65$, and because α_1 takes a positive value, the locus of the shaft center is epitrochoid. An example of such a locus obtained from recorded vibratory waves is given in

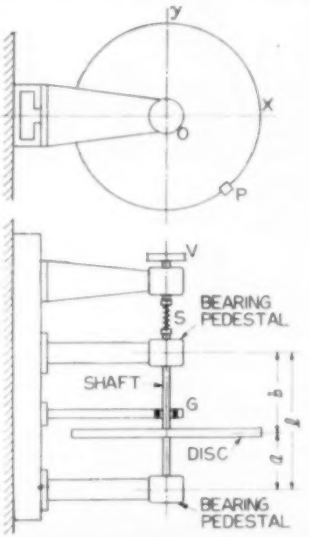

Fig. 1 Experimental apparatus

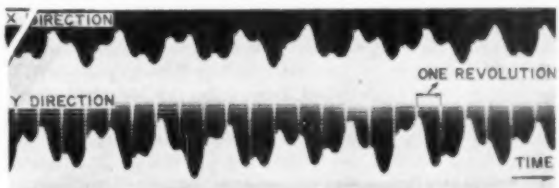

Fig. 2 Vibratory waves of vibration $\left[+\frac{1}{2.65}\omega\right] = [\alpha_1\omega]$

For presentation at the Summer Conference of the Applied Mechanics Division, Troy, N. Y., June 18–20, 1959, of The American Society of Mechanical Engineers.

Discussion of this paper should be addressed to the Secretary, ASME, 29 West 39th Street, New York, N. Y., and will be accepted until July 20, 1959, for publication at a later date. Discussion received after the closing date will be returned.

Note: Statements and opinions advanced in papers are to be understood as individual expressions of their authors and not those of the Society. Manuscript received by ASME Applied Mechanics Division, October 22, 1957. Paper No. 59—APM-12.

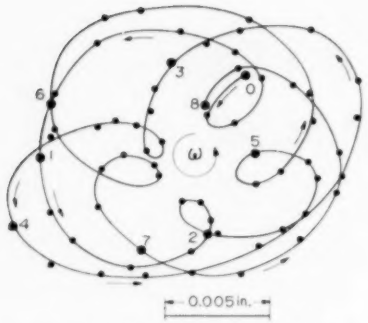

Fig. 3 Path of whirling motion in vibration $[\alpha_1\omega]$

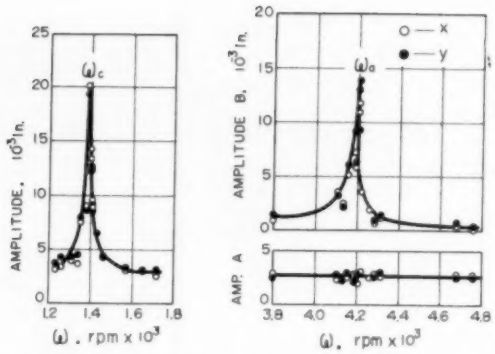

Fig. 4 Resonance curve at critical speeds ω_c and ω_a. Disk : diam = 19.00 in., thickness = 0.250 in., weight = 17.21 lb; shaft : length = 19.99 in., diam = 0.462 in.; position of disk a:b = 2.56 : 7.44 ≒ 1 : 3

Fig. 3, where the interval between one double circular mark to the next means one revolution of the shaft, and the curve shown there is the locus during the time interval of 8 revolutions of shaft. In the neighborhood of this critical speed ω_a, the amplitude A in (1) is unchanged and B alone builds up and forms the peak of critical speed ω_a. In Fig. 4, separating amplitudes A and B by analyzing vibratory waves, A and B are plotted against rotating speed ω. For comparison, the peak of the major critical speed ω_c is additionally shown.

Cause of Occurrence of the Critical Speed. As a general rule, the ball motion is carried out under conditions in which the rolling contact between ball and inner and outer rings is kept.[1] Therefore, precessional motion of balls (motion of ball center around the center of inner ring) can be determined as follows:

$$\frac{\omega}{\omega_1} = 2 + 2\,\frac{d}{D}, \qquad (2)$$

where ω_1 is the angular velocity of the precessional motion of balls, d is diameter of balls, and D is outer diameter of inner rings. For the self-aligning double-row ball bearings used in the experiments, the value ω/ω_1 given by experiments is plotted against ω between 100 ~ 4000 rpm in Fig. 5. Here the value ω/ω_1 is almost constant, and is independent of ω and of magnitudes of amplitude of vibrations. The mean value of ω/ω_1 is 2.647. Since D = 0.5795 in. and d = 0.1879 in. for ball bearings used in the experiments, then inserting these values into (2) we have ω/ω_1 = 2.6485 which coincides with the value obtained by experiments.

Now we should note that the value of α_1 in (1) obtained by analyzing shapes of vibratory waves agrees with ω_1/ω; i.e.,

$$\alpha_1 = \omega_1/\omega, \quad \omega_1 = \alpha_1\omega, \qquad (3)$$

Consequently we note that vibrations in the critical speed ω_a have the same frequency as the precessional revolution of balls ω_1.

However accurate the inner and outer ring may be, if there should be any difference in diameters of the balls, the center line of the journal of the shaft would not coincide accurately with the bearing center line. When one comparatively large ball is inserted into the bearing, the inner ring is displaced by this larger ball and is forced off center toward the opposite side of the bearing along the diameter in which the larger ball lies. If a ball smaller than the others be inserted in the bearing, the inner ring would be forced toward the smaller ball and the opposite side of the bearing would be forced off center along the diameter toward the smaller ball. Therefore, owing to this small deviation of e_0 at the ball bearing, the center of the disk is also deviated from the bearing center line, as shown in Fig. 6. This small deviation

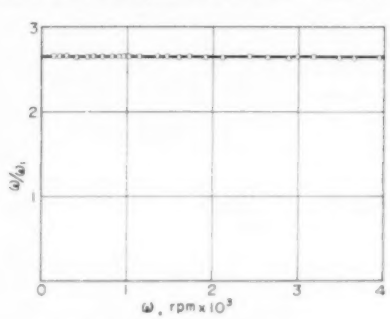

Fig. 5 ω/ω_1 — ω curves

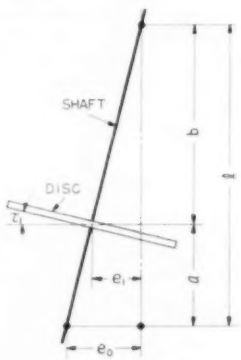

Fig. 6 e_1 and τ_1

e_1 is decided according to e_0 and a:b, and the direction of e_1 rotates with the same velocity as the precessional rotating speed of balls ω_1. Under such a condition, the disturbing force having frequency ω_1 is applied to the disk and the forced vibration of $[\omega_1] = [\alpha_1\omega]$ is induced; thus the critical speed ω_a of $[\alpha_1\omega]$ appears.

Amplitudes of vibrations $[\alpha_1\omega]$ clearly increase as magnitudes of e_1 and τ_1, Fig. 6, increase. The arrangement of balls used in the experiments is shown in Fig. 7. This self-aligning double-row ball bearing contains 18 balls, 9 balls each in one row. For instance, supposing that two of the balls are somewhat larger than the others and that these two balls are inserted in symmetrical positions 1 and 5′, Fig. 7, both e_1 and τ_1 are very small. On the other hand, supposing that two larger balls are put side by side as 1 and 1′, then e_1 and τ_1 become larger. Furthermore, when the

[1] T. Sasaki, "On the Planetary Motion of the Roller in the Roller Bearing—Part I," *Transactions of The Japan Society of Mechanical Engineers*, vol. 8, 1932, p. 64.

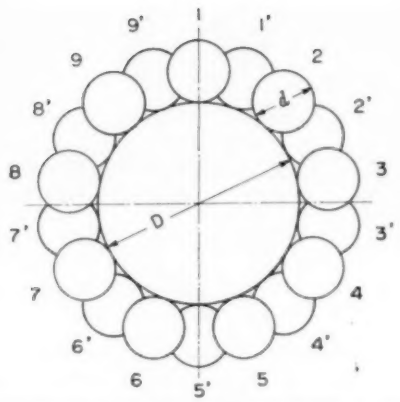

Fig. 7 Arrangement of balls in self-aligning double-row ball bearing

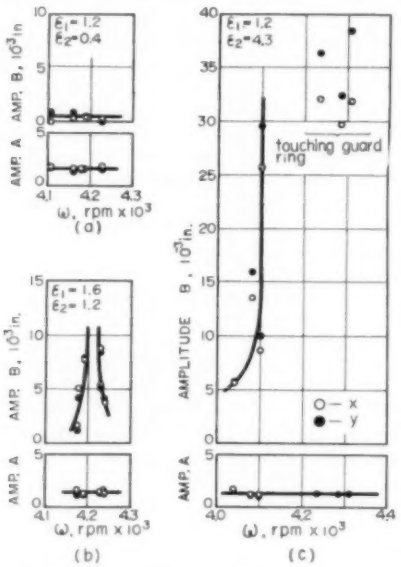

Fig. 8 Effects of difference in diameter of balls. ε_1, ε_2 = difference in diameter of ball in upper and lower ball bearings in 10^{-4} in., respectively; disk and shaft used in experiments shown in Fig. 8 are same as those in Fig. 4. Position of disk = a:b ≒ 1:3.

disk is not mounted at the middle point of the shaft but is one-sided toward either the upper or lower bearing pedestal, i.e., $a \neq b$, the bearing nearer the disk exerts more influence upon e_1 and τ_1 and the bearing further away exerts less.

It can be seen by experiments shown in Fig. 8, how amplitudes vary with different ball diameters. Because the position of the disk is 1:3, the influence of the ball bearing in the lower pedestal is three times greater than that in the upper pedestal in this figure. Commercial ball bearings purchased on the market are used in experiments shown in Fig. 8(a, b). In Fig. 8(c), the difference in diameters of balls in the lower bearing is artificially enlarged. In Fig. 8(c), two balls of 0.18783 in. with diameters larger by 0.00043 in. than those of the other balls are inserted side by side into a ball bearing with balls of 0.18740 in., as shown in 1 and 1′, in Fig. 7. Amplitudes of the peak ω_a increase greatly and build up so large that the shaft touches the guard ring G, Fig. 1, placed to check the increase of deflections of the shaft. Results of numerous experiments show that, when ball bearings

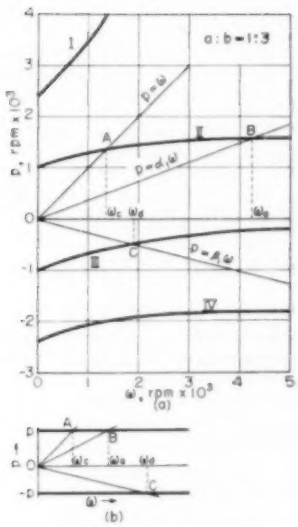

Fig. 9 p — ω diagrams

on the market are used, the critical speed ω_a almost always appears irrespective of the magnitudes of amplitudes cases in which it does not appear are the few exceptions.

Location of the Critical Speed ω_a. The frequency equation of the system is[2]

$$\{(\alpha - m_1 p^2)(\delta - Ip^2 - I_p\omega p) - \gamma^2\} \{(\alpha - mp^2)(\delta - Ip^2 + I_p\omega p) - \gamma^2\} = 0, \quad (4)$$

where m is mass of disk, α, γ, and δ are spring constants of shaft, I is moment of inertia about diameter, I_p is polar moment of inertia of disk, and p is natural frequency. In Fig. 9(a), $p - \omega$ curves I, II III, and IV are given. Since the critical speed ω_a takes place when ω_1 ($= \alpha_1\omega$) coincides with one of the natural frequencies, ω_a is found by obtaining the intersecting point where the straight line $p = \alpha_1\omega$ crosses curves of p. Because $I_p > I$, the critical speeds ω_c and ω_a are unique. When the disk is located at the middle of the shaft, i.e., $a = b$, p is constant, and the $p - \omega$-curve becomes as shown in Fig. 9(b), hence $\omega_a/\omega_c = 1/\alpha_1$. For a disk not so located ($a \neq b$), the relation $\omega_a/\omega_c > 1/\alpha_1$ always holds good and the critical speed ω_a shifts to higher speed accordingly as the disk moves away from the middle point of the shaft, as indicated in Table 1 obtained by experiments.

Table 1 Critical speeds ω_a

Location of disk $a:b$	1:1	1:2.33	1:3
ω_a/ω_c	2.665	2.860	3.036

Critical Speeds of $\left[-\frac{1}{4.1}\omega\right]$

Relation Between Stiffness of Shaft and Difference in Diameters of Balls. In ball bearings, a radial clearance is usually provided against a rise of temperature during operation. If there should be a difference in ball diameters, this radial clearance would be smaller or it might disappear entirely, or interference between balls and inner and outer rings may occur in the position where the larger ball is inserted. Consequently, when the stiffness of shaft is considered together with ball bearings, we can say that the stiffness increases at the position where the large ball is inserted be-

[2] T. Yamamoto, "On the Critical Speeds of a Shaft," Memoirs of the Faculty of Engineering, Nagoya University, vol. 6, 1954, p. 116.

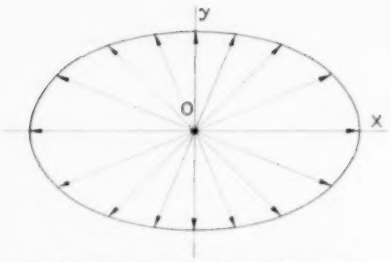

Fig. 10 Vectors representing spring forces

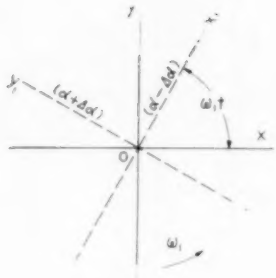

Fig. 11

cause the shaft is supported more tightly there and, further, the shaft is never equally stiff in all directions. Obviously this nonuniformity of stiffness rotates with ω_1. Therefore the difference in ball diameters causes the shaft to have the directional nonuniformity of stiffness rotating with ω_1. Although the existence of radial clearance induces the nonlinear spring force, we consider that the spring force has an approximately linear character because the radial clearance is very small.

Now we consider Fig. 10, which is obtained by connecting the tops of vectors which represent the stiffness in all directions. We assume this figure to be symmetrical with respect to the origin O and the direction of maximum stiffness to be at right angles to the direction of minimum stiffness, as shown in Fig. 10. In Fig. 11, let the center of ball bearing be point O, and $O - x_1y_1$ be a rotating rectangular co-ordinate system revolving with ω_1. Then let us assume that the minimum and maximum spring constants $\alpha - \Delta\alpha$, $\gamma - \Delta\gamma$, $\delta - \Delta\delta$ and $\alpha + \Delta\alpha$, $\gamma + \Delta\gamma$, $\delta + \Delta\delta$ lie, respectively, in the directions ox_1 and oy_1. Calculating spring forces in the x and y-directions, we have differential equations of motion

$$\left.\begin{aligned}
&m\ddot{x} + \alpha x + \gamma\theta_x - \Delta\alpha(y \sin 2\omega_1 t + x \cos 2\omega_1 t) \\
&\quad - \Delta\gamma(\theta_y \sin 2\omega_1 t + \theta_x \cos 2\omega_1 t) = me\omega^2 \cos \omega t, \\
&m\ddot{y} + \alpha y + \gamma\theta_y - \Delta\alpha(x \sin 2\omega_1 t - y \cos 2\omega_1 t) \\
&\quad - \Delta\gamma(\theta_x \sin 2\omega_1 t - \theta_y \cos 2\omega_1 t) = me\omega^2 \sin \omega t, \\
&I\ddot{\theta}_x + I_p\omega\dot{\theta}_y + \gamma x + \delta\theta_x - \Delta\gamma(y \sin 2\omega_1 t + x \cos 2\omega_1 t) \\
&\quad - \Delta\delta(\theta_y \sin 2\omega_1 t + \theta_x \cos 2\omega_1 t) = 0, \\
&I\ddot{\theta}_y - I_p\omega\dot{\theta}_x + \gamma y + \delta\theta_y - \Delta\gamma(x \sin 2\omega_1 t - y \cos 2\omega_1 t) \\
&\quad - \Delta\delta(\theta_x \sin 2\omega_1 t - \theta_y \cos 2\omega_1 t) = 0,
\end{aligned}\right\} \quad (5)$$

where θ_x, θ_y are components of inclination angle of disk and e is an eccentricity of disk. Assuming the higher powers of $\Delta\alpha$, and so on, to be negligible, the solution of (5) can be written

$$\left.\begin{aligned}
x &= A_1 \cos \omega t + \frac{(\Delta\alpha A_1 + \Delta\gamma B_1)[\delta + (2\omega_1 - \omega)\{I_p\omega - I(2\omega_1 - \omega)\}] - \gamma(\Delta\gamma A_1 + \Delta\alpha B_1)}{\{\alpha - m(2\omega_1 - \omega)^2\}[\delta + (2\omega_1 - \omega)\{I_p\omega - I(2\omega_1 - \omega)\}] - \gamma^2} \cos(2\omega_1 - \omega)t, \\
\theta_x &= B_1 \cos \omega t + \frac{(\Delta\gamma A_1 + \Delta\delta B_1)\{\alpha - m(2\omega_1 - \omega)^2\} - \gamma(\Delta\alpha A_1 + \Delta\gamma B_1)}{\{\alpha - m(2\omega_1 - \omega)^2\}[\delta + (2\omega_1 - \omega)\{I_p\omega - I(2\omega_1 - \omega)\}] - \gamma^2} \cos(2\omega_1 - \omega)t
\end{aligned}\right\} \quad (6)$$

where

$$\left.\begin{aligned}
A_1 &= \frac{me\omega^2\{\delta + (I_p - I)\omega^2\}}{(\alpha - m\omega^2)\{\delta + (I_p - I)\omega^2\} - \gamma^2}, \\
B_1 &= \frac{-me\omega^2\gamma}{(\alpha - m\omega^2)\{\delta + (I_p - I)\omega^2\} - \gamma^2}
\end{aligned}\right\} \quad (7)$$

By putting sin in place of cos in (6) the solutions for y and θ_y are obtained. The first term on the right-hand side of (6) gives the common forced vibration induced by e, and the second term represents vibration $[2\omega_1 - \omega]$.

If Fig. 10 should become more irregular, the terms of sin $n\omega_1 t$ and cos $n\omega_1 t$ (n is any integer) may also be included in (5), and the vibrations $[n\omega_1 \pm \omega]$ may appear. But it would seem that the figure could resemble an ellipse, as shown in Fig. 10, regardless of the order of arrangement of balls. For instance, if there were three balls of equal diameter larger than the others and they were arranged equally in a bearing at angular intervals of 120 deg, at first glance it would seem that Fig. 10 resembles a triangle. As a matter of fact, it is more like a circle and this can be clearly understood when we consider that the shaft having three keyways at equal intervals of 120 deg has the same stiffness in all directions.[3] Therefore Fig. 10 is more like a circle.

Not considering the magnitudes of the differences in stiffness $\Delta\alpha$, and so on, when two larger balls are inserted, the figure also may resemble an ellipse no matter how the balls are inserted, either side by side as 1 and 1′, at right angles as 1 and 3, or at 180 deg as 1 and 5′, Fig. 7. Consequently, in many cases the figure resembles an ellipse which fact is also suggested by the further fact that the stiffness of a shaft with any cross section can be represented by an inertia ellipse. Actually, the experiments carried out under various conditions hardly ever furnished vibrations of mode of $[n\omega_1 \pm \omega]$.

Although at first glance it is expected that vibrations $[2\omega_1 \pm \omega]$ can be induced by periodic fluctuation of stiffness with period $2\pi/2\omega_1$,[4] only vibration $[2\omega_1 - \omega]$ takes place for the reason that equations of motion take such forms as indicated in (5).

Behavior of Vibrations and Shape of Vibratory Waves. Now putting

$$2\omega_1 - \omega = \beta_1\omega, \quad (8)$$

we obtain the following relation

$$\beta_1 = 2\alpha_1 - 1, \quad (9)$$

because $\omega_1 = \alpha_1\omega$. The value α_1 is always smaller than 1/2, hence β_1 takes a negative value and vibrations $[\beta_1\omega] = [2\omega_1 - \omega]$ become backward precession. For a self-aligning double-row ball bearing with 0.394 in. bore, α_1 is equal to about +1/2.65, hence β_1 approximates −1/4.1, and vibrations take the following forms:

$$\left.\begin{aligned}
x &= A \cos \omega t + B \cos \beta_1\omega t = A \cos \omega t + B \cos \frac{1}{4.1}\omega t, \\
y &= A \sin \omega t + B \sin \beta_1\omega t = A \sin \omega t - B \sin \frac{1}{4.1}\omega t,
\end{aligned}\right\} \quad (10)$$

Only amplitude B builds up and forms the peak of critical speed

[3] J. P. Den Hartog, "Mechanical Vibrations," fourth edition, McGraw-Hill Book Company, Inc., New York, N. Y., 1956, p. 339.

[4] O. Föppl, "Kritische Drehzahlen rasch umlaufender Welle," *Zeitschrift des Vereines Deutscher Ingenieure*, Band 63, 1919, p. 886.

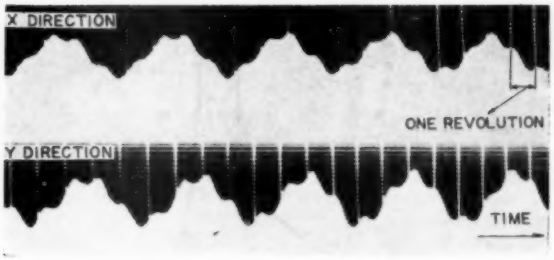

Fig. 12 Vibratory waves of vibration $\left[-\frac{1}{4.1}\,\omega\right] = [\beta_1\omega]$

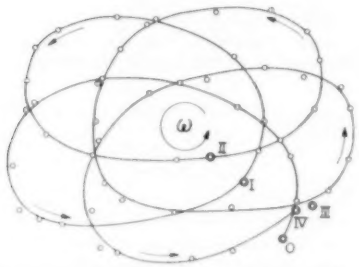

Fig. 13 Path of whirling motion in vibration $[\beta_1\omega]$

ω_d where vibration $[\beta_1\omega]$ increases. An example of vibratory waves is given in Fig. 12. Since β_1 is negative, the locus of the disk center becomes hypotrochoid, as is shown in Fig. 13, where the interval between one double-circular mark and the next means one revolution of shaft.

Results of Experiments. As we see in (6), amplitudes of vibration $[2\omega_1 - \omega]$ increase with increase of eccentricity e. Figs. 14(b) and (c) make this fact experimentally plain. The disk in Fig. 14(c) has a larger eccentricity than that in Fig. 14(b), all other conditions in both cases being the same. Amplitude B of vibrations $[\beta_1\omega]$ in Fig. 14(c) builds up larger than that in Fig. 14(b).

The substantial cause of $\Delta\alpha$, and so on, is the difference itself in diameters of balls, although the magnitudes of $\Delta\alpha$, and so on, may also be affected by radial clearance and by the order of arrangement of balls; therefore, generally speaking, it may be expected that $\Delta\alpha$, and so forth, increases with the greater differences in diameters of balls. In Fig. 14(b), the difference in diameters of balls is larger than that in Fig. 14(a); with larger differences in diameter, amplitude B is larger.

Clearly the magnitude of directional nonuniformity of stiffness $\Delta\alpha$, and so on, is influenced not only by the difference in ball diameters but also by the order of arrangement of balls. The influence of the order of arrangement of balls is clarified in Fig. 15 where the difference in diameters of balls in the lower ball bearing is artificially enlarged. In Fig. 15(a) two larger balls are inserted side by side, and in Fig. 15(b), they are put at 180 deg; viz., in positions 1 and 5′ in Fig. 7. It is evident that Fig. 15(b) has amplitudes larger than those of Fig. 15(a).

An experiment in which considerably large amplitudes appear is given in Fig. 16. In ball bearing used in Fig. 16(a), although balls are inserted at random, amplitudes are considerably larger than those in other experiments because of the larger difference in ball diameters. In the ball bearing used in Fig. 16(b), balls are arranged symmetrically as shown in Fig. 17; viz., the larger balls are inserted in positions directly opposite each other and the smaller ones also directly opposite at right angles to the larger. In this case, the peak of the critical speed ω_d builds up

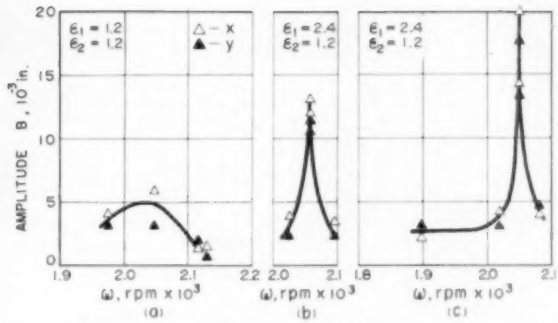

Fig. 14 Peak at ω_d (effects of difference in ball diameters and eccentricity e). ϵ_1, ϵ_2 = difference in diameter of ball in upper and lower ball bearing in 10^{-4} in., respectively. Disk: diam = 19.00 in., thickness = 0.250 in., weight = 17.21 lb; shaft: length = 20.01 in., diam = 0.468 in.; position of disk a:b = 3:7.

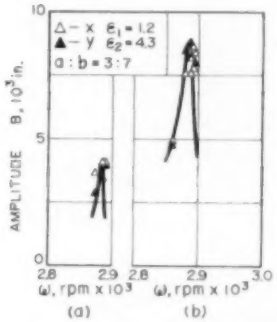

Fig. 15 Effects of the order of arrangement of balls. Disk: diam = 14.20 in., thickness = 0.559 in., weight = 16.15 lb; shaft: length = 19.95 in., diam = 0.472 in.; ϵ_1, ϵ_2 . . . . . 10^{-4} in.

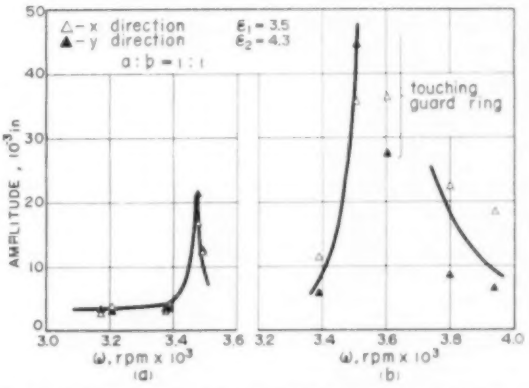

Fig. 16 Considerable peak at ω_d. Disk: diam = 19.00 in., thickness = 0.250 in., weight = 17.21 lb; shaft: length = 19.92 in., diam. = 0.439 in.; ϵ_1, ϵ_2 . . . . 10^{-4} in.

considerably so as to make the shaft strike the guard ring violently.

Location of Critical Speed. In Fig. 9, the abscissa of point c, on which the straight line $p = \beta_1\omega$ cuts curve III, gives the critical speed ω_d. As we see in Fig. 9(a), a straight line $p = \beta_1\omega$ cannot only cut curve III but can cut curve IV also; then two critical speeds ω_d can appear. In the simple case $a = b$, the critical speed ω_d is unique and is equal to $|p/\beta_1|$ as shown in Fig. 9(b).

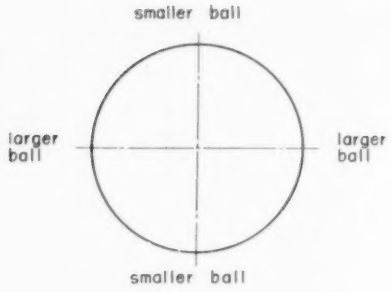

Fig. 17

The more nearly the disk is mounted to the end of the shaft, the more nearly the critical speed ω_d approaches the major critical speed ω_c, and consequently ω_d is not always larger than ω_c. This is in direct contrast to the fact that ω_a is always larger than ω_c. In fact, in $a:b = 1:4$, the peak of the critical speed ω_d appears near the major critical speed ω_c as shown in Fig. 18.

To summarize, the vibrations of $[\beta_1\omega]$ of backward precession occur because of the difference in stiffness rotating with ω_1, and the differences in stiffness are produced by the differences in diameter of balls. Amplitudes of these vibrations are influenced by magnitudes of differences in diameters and the order of arrangement of balls. Critical speed ω_d nearly always appears when ball bearings on the market are used.

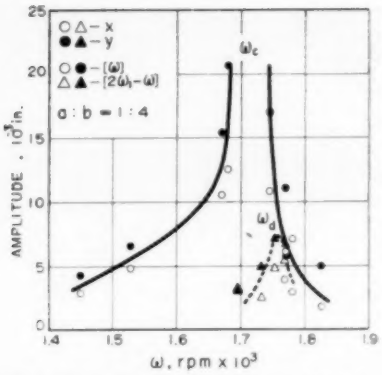

Fig. 18 Disk: diam = 19.00 in., thickness = 0.250 in., weight = 17.21 lb; shaft: length = 19.98 in., diam = 0.462 in.

Vibrations $[\alpha_1\omega]$ and $[\beta_1\omega]$ necessarily come into question for the shaft at high speed.

Acknowledgment

The author acknowledges his debt to the late Dr. Y. Shimoyama for guidance and valuable advice and especially for his instruction over a long period of time. Thanks go to Mr. A. Tsujii and Mr. H. Todoroki for their assistance in these experiments.

Root-Locus Analysis of Structural Coupling in Control Systems[1]

R. H. CANNON, JR.

Associate Professor
of Mechanical Engineering,
Massachusetts Institute of Technology,
Cambridge, Mass.

When a feedback system is devised to control a mechanical member that is structurally limber, unstable ("self-excited") vibrations may be encountered at approximately a natural frequency of the structural member. Cures are generally easy to effect once the phenomena are understood. Two interesting cases are described: ground vibrations of an airplane control system due to a limber fuselage, and vibrations of a stable platform system due to limberness in the platform structure. The investigations are carried out using the root-locus technique, which provides a plot of system characteristics as explicit functions of control strength. In the case of the stable platform, the analysis is found to be more reliable than physical intuition.

A MOST common type of control system consists of a mechanical element being positioned by a "feedback" device. Sometimes the element is structurally limber. In such cases it may be found that if the "gain" of the feedback is made too large unstable vibrations ensue at approximately the natural frequency of the mechanical element. Such cases are additional examples of the classic "self-excited vibrations"[2] (along with airplane wing flutter, galloping transmission lines, and hunting steam-engine governors).

When several degrees of freedom are present the dynamic relations describing a control system may lead to a "characteristic equation" of fourth order or higher. The classical procedure for predicting the behavior of the system in terms of its parameters is to interpret the characteristic equation by the method of Routh,[3] which yields relations between parameters just at the point of neutral stability. This method is very effective for determining the stable limit in third and fourth-order systems. For fifth order and above it becomes quite involved.

In cases, such as feedback systems, where the characteristics of each of the elements appear explicitly in the over-all characteristic equation, the newer "root-locus" technique[4] usually leads to rapid solution of higher-order systems. Moreover, the system characteristics are given explicitly for *all* values of the control parameter.

The method is demonstrated in the following for two interesting examples.[5] The first involves troubles which can arise when an autopilot is installed in a limber aircraft in such a way that structural flexibility becomes inertially coupled into the control system to produce unstable airframe vibrations.

The second problem concerns determining where to mount instruments on a stable platform so as to avoid unstable vibrations due to flexibility of the platform structure.

Control Coupling in a Limber Aircraft

One type of unstable vibration that can occur when the structure of an airplane is limber has been well known for some time. It is called "flutter" and is produced by a steady stream of air over a wing or other flexible aerodynamic surface.

When an automatic control system is installed in a limber aircraft, another type of unstable vibration can result, even in the absence of aerodynamic forces: the fuselage flexibility can become inertially coupled into the control system to produce unstable vibrations even when the craft is sitting on the ground. Once they occur, such phenomena are usually easy to correct; but a *priori* prediction of them is highly desirable.

For demonstration, consider a special-purpose control system that was developed for an interceptor aircraft.[6] Need for the special control arose because rapid maneuvering of the airplane was found to produce uncomfortable accelerations at the cockpit. Since an automatic control system was already present for positioning the rudder, it was proposed to measure the unwanted airplane motion and to produce—via the rudder "servo"—an aerodynamic force to oppose it. Specifically, an accelerometer was to be located at the cockpit which would call for rudder deflections in the proper direction to nullify its signals, and thus give the pilot a more comfortable ride.

Control Requirements. Since the topic under discussion is the structural coupling problem, rather than the aerodynamic design study, the results of the latter will merely be stated. Briefly, it was found from a rigid-body analysis of the airplane dynamics, Fig. 1, that good "side force alleviation" could be obtained by arranging the rudder servo to produce a starboard rudder position in response to port acceleration, the gain of this control loop being about 60 deg of rudder per g of lateral acceleration.

To investigate the structural coupling problem we must first

---

[1] Presented as a sequel to an earlier paper by R. H. Cannon, Jr., "Vibration Analysis by the Root-Locus Method," Third U. S. National Congress of Applied Mechanics, ASME, 1958, pp. 95–100.

[2] J. P. Den Hartog, "Mechanical Vibrations," McGraw-Hill Book Co., Inc., New York, N. Y., 1956, chap. 7.

[3] Ibid., and M. F. Gardner and J. L. Barnes, "Transients in Linear Systems," John Wiley and Sons, Inc., New York, N. Y., 1954, p. 197.

[4] The root-locus method is explained by its inventor, Walter R. Evans, in "Control-System Dynamics," McGraw-Hill Electrical and Electronic Series, McGraw-Hill Book Co., Inc., New York, N. Y., 1954. Use of the method in vibration problems is described in reference, footnote 1.

Contributed by the Applied Mechanics Division and presented at the Annual Meeting, New York, N. Y., November 30–December 5, 1958, of THE AMERICAN SOCIETY OF MECHANICAL ENGINEERS.

Discussion of this paper should be addressed to the Secretary, ASME, 29 West 39th Street, New York, N. Y., and will be accepted until July 10, 1959, for publication at a later date. Discussion received after the closing date will be returned.

NOTE: Statements and opinions advanced in papers are to be understood as individual expressions of their authors and not those of the Society. Manuscript received by ASME Applied Mechanics Division, February 26, 1958. Paper No. 58—A-65.

[5] The examples are based on work done at Autonetics, a Division of North American Aviation, Inc., Downey, Calif.

[6] The inertial coupling problem is encountered even more frequently in missile control systems, with both aerodynamic and rocket-engine steering.

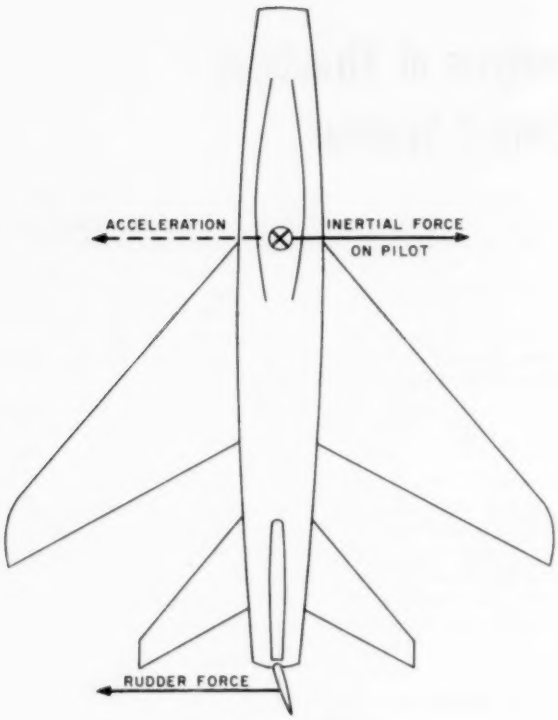

Fig. 1 Airplane

establish the differential equations relating rudder motion and fuselage vibration. We must also make an assumption about the dynamic response of the rudder servo system. Then we can calculate what the dynamic characteristics of the over-all system will be when the rudder servo is installed in the fuselage and is controlled by an accelerometer attached to the fuselage. These steps will now be taken in turn.

Structural Dynamics of the Fuselage. The limber fuselage, vibrating in its first bending mode, behaves as a simple second-order system. This can be shown, for example, by applying the Lagrangian technique using, as a generalized co-ordinate, the magnitude of first bending mode. Alternatively, the form of the fuselage dynamics can be deduced with less elegant mathematics using the model of Fig. 2(*a*), where, for simplicity of calculation, the mass of the fuselage has been lumped in three equal masses, $M/3$. The fuselage is shown in its first bending mode, wherein the central mass moves a distance $2x$ in one direction and the other two masses move a distance x in the other direction (so that the center of gravity remains stationary). If the mass of the rudder, m, is very small compared to M, the rigid-body rotation of the fuselage can be neglected and the bending can be calculated by considering—from symmetry—that the center of the fuselage is the "built-in" end of a cantilever beam. In the absence of aerodynamic effects (e.g., with the vehicle on the ground) the forces and moments on the cantilever are purely inertial as shown in Fig. 2(*b*). Then from the usual cantilever-beam formulas, the deflection of the fuselage will be

$$3x = -\left[\frac{M}{3}\,\ddot{x} + mr\ddot{\delta}\right]\frac{l^3}{3EI} - m\rho^2\ddot{\delta}\,\frac{l^2}{2EI} \qquad (1)$$

in which r is the distance from the hinge to the center of gravity of the rudder, and ρ is the radius of gyration of the rudder. Grouping terms, and letting

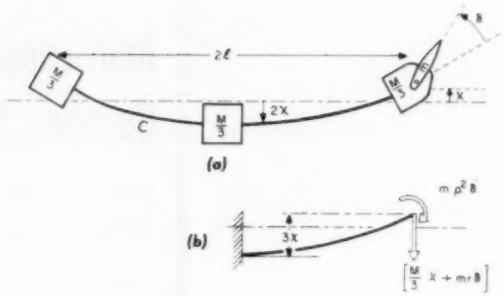

Fig. 2 Model of limber airplane

$$\omega_0^2 = \frac{27EI}{Ml^3}$$

(the natural frequency of the first bending mode of the fuselage). (1) becomes

$$\ddot{x} + \omega_0^2 x = -\frac{m}{M/3}\left[r + \left(\frac{3}{2}\,\frac{\rho}{l}\right)\rho\right]\ddot{\delta}$$

Actually, there will be some structural damping in the fuselage. Let this be represented by the usual symbol, ζ:

$$\ddot{x} + 2\zeta\omega_0\dot{x} + \omega_0^2 x = -\frac{m}{M/3}\left[r + \left(\frac{3}{2}\,\frac{\rho}{l}\right)\rho\right]\ddot{\delta} \qquad (2)$$

This equation may be put in "operational" form—for easier combination with the expressions for other elements of the system—by assuming that motion δ will be of the form $\delta = \Delta e^{st}$, and "guessing" that the solution of (2) will have the form $x = Xe^{st}$. Substituting these expressions into (2) leads to

$$(s^2 + 2\zeta\omega_0 s + \omega_0^2)X = -\frac{m}{M/3}\left[r + \left(\frac{3}{2}\,\frac{\rho^2}{l}\right)\right]s^2\Delta \qquad (3)$$

which also can be written in the form of a "transfer function":

$$\frac{X}{\Delta} = \frac{-\dfrac{m}{M/3}\left[r + \left(\dfrac{3}{2}\,\dfrac{\rho}{l}\right)\rho\right]s^2}{s^2 + 2\zeta\omega_0 s + \omega_0^2} \qquad (4)$$

Setting $\Delta = 0$ in (3) leads to the characteristic equation of the fuselage structure

$$(s^2 + 2\zeta\omega_0 s + \omega_0^2) = (s + \sigma + j\omega)(s + \sigma - j\omega) = 0,$$

the roots of which—$s = -\sigma - j\omega$, $s = -\sigma + j\omega$—are the characteristics of natural transient vibrations of the fuselage; that is, ω is the natural frequency and σ the damping constant. These are shown in a standard complex-plane plot in Fig. 3.

Rudder Servo Dynamics. The rudder-positioning servo is generally a "second-order" system, also; that is, the differential equation relating input signal δ_d, to actual rudder position, δ, has the form

$$I\ddot{\delta} + C\dot{\delta} + K\delta = K\delta_d$$

in which the "spring" force K is furnished by a "feedback loop." With

$$\omega_{0r} = (K/I)^{1/2}, \quad \zeta_r = \frac{C}{2(KI)^{1/2}}:$$

$$\ddot{\delta} + 2\zeta_r\omega_{0r}\dot{\delta} + \omega_{0r}^2\delta = \omega_{0r}^2\delta_d$$

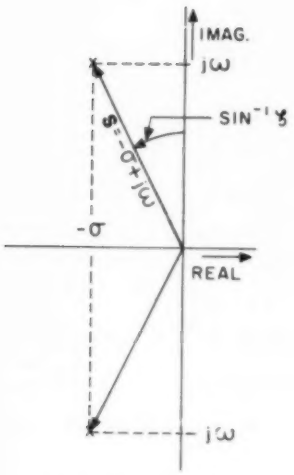

Fig. 3 The complex plane

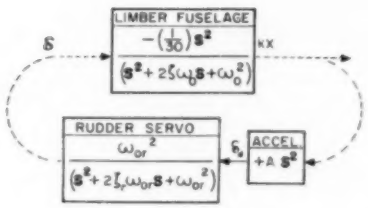

Fig. 4 Rudder-control system

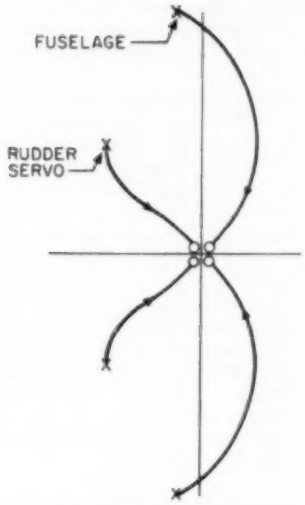

Fig. 5 Stability of rudder-control system

Again, guessing that $\delta_d = \Delta_d e^{st}$, a transfer function is obtained for the rudder servo:

$$\frac{\Delta}{\Delta_d} = \frac{\omega_{0r}^2}{s^2 + 2\zeta_r\omega_{0r}s + \omega_{0r}^2} \tag{5}$$

Complete System. The complete "side-force alleviation loop" is shown in Fig. 4. The rigid-body acceleration of the aircraft is sensed by the accelerometer. The accelerometer signal, amplified by the amount A, is sent into the rudder servo which produces a proportional rudder deflection δ, according to the dynamics of (5). But in addition to sensing rigid-body motions, the accelerometer senses some portion, kx—depending upon its location—of the bending of the fuselage. Typically, if the accelerometer is placed at cockpit location C in Fig. 2(*a*), the transfer function from rudder deflection δ to accelerometer displacement kx has the same form as (4), the sign being negative and the combined constant being of the order of 1/30 in/rad. This transfer function is inserted at the proper place in Fig. 4.

The characteristic equation for the complete system of Fig. 4 is then

$$\left[(s^2 + 2\zeta\omega_0 s + \omega_0^2)(s^2 + 2\zeta_r\omega_{0r}s + \omega_{0r}^2) + \frac{A}{30}\omega_{0r}^2 s^4\right] = 0 \tag{6}$[7]

[7] This result can be obtained, alternatively, by considering the individual differential equations in the classical form:

Structure: $\ddot{x} + 2\zeta\omega_0\dot{x} + \omega_0^2 x = -\dfrac{m}{M/3}\left[r + \left(\dfrac{3}{2}\dfrac{\rho}{l}\right)\rho\right]\ddot{\delta}$

Rudder servo: $\ddot{\delta} + 2\zeta_r\omega_{0r}\dot{\delta} + \omega_{0r}^2\delta = \omega_{0r}^2\delta_d$

Controller: $\delta_d = kA\ddot{x}$,

and guessing that the solution is $x = Xe^{st}$, $\delta = \Delta e^{st}$, $\delta_d = \Delta_d e^{st}$. This then leads to a set of simultaneous equations:

$$(s^2 + 2\zeta\omega_0 s + \omega_0^2)X + \frac{m}{M/3}\left[r + \left(\frac{3}{2}\frac{\rho}{l}\right)\rho\right]s^2\Delta = 0$$

$$(s^2 + 2\zeta_r\omega_{0r}s + \omega_{0r}^2)\Delta - \omega_{0r}^2\Delta_d = 0$$

$$ks^2AX - \Delta_d = 0$$

from which Δ and Δ_d can be eliminated to give (6).

Equation (6) is the "characteristic equation" of the system of Fig. 4: The values of s which satisfy it constitute the characteristics of its transient motions, each imaginary part giving the frequency, and the corresponding real part the rate of decay of one motion.

Root-Locus Plot. The roots of (6) can be obtained quickly from a root-locus plot. The equation is first put in the form

$$\frac{30}{\omega_{0r}^2}\frac{(s + \sigma \pm j\omega)(s + \sigma_r \pm j\omega_r)}{s^4} = -A \tag{7}$$

in which $(s + \sigma \pm j\omega)$ is understood to mean $(s + \sigma + j\omega)(s + \sigma - j\omega)$. Next, the (complex) values of s which make the left-hand side of (7) zero are plotted as × in a complex plane, Fig. 5. These values are $s = -\sigma - j\omega$, $s = -\sigma + j\omega$, and $s = -\sigma_r - j\omega_r$, $s = -\sigma_r + j\omega_r$. These are, of course, the individual dynamic characteristics ("poles") of the limber fuselage, Fig. 3, and of the rudder system, and would be well known. The values of s which make the left-hand side of (7) infinite are also plotted in Fig. 5, as O. These consist of four terms, each of which is $s = 0$. They are the "zeros" of the open-loop system.

The next step is to construct the loci of all values of s for which the net "phase angle" of the left-hand side of (7) is 180 deg. (This is to match the − sign on the right-hand side.) Finally, a value of A is assigned for each point of interest on the loci [to match the magnitude of the right-hand side of (7)]. The values of s so obtained are the roots of the characteristic equation—(6) or (7).

The loci of the roots of (7) are plotted in Fig. 5. (With a little practice such loci can be found very quickly by trial and error. Details of locus sketching are given in an earlier paper.[1] Several short cuts further speed the process.[4])

Interpretation of the Plot. The loci of Fig. 5 are seen to terminate at the × and O. Points × correspond, of course, to the case $A = 0$, wherein the system characteristics are simply the characteristics of the individual elements, because there is zero feedback. As A is increased from zero the corresponding points in Fig. 5 progress along the loci in the direction of the arrows.

A point of great interest is, of course, the value of A for which the locus crosses the imaginary axis, for this is the point of neutral dynamic stability. (It is this single value of A that is given by the method of Routh.)

For the actual system this value of A was found to be much too low to give effective side-force control. Fuselage vibrations would ensue at nearly the fuselage bending frequency if this system were used.

The simplest solution to the structural coupling problem in this case is to move the accelerometer to a more favorable location. For example, if the accelerometer could be put exactly at a vibrational node, Fig. 2, then no coupling would take place ($k = 0$ in Fig. 4). If this point is inaccessible or is not precisely known, the next best thing is to move the accelerometer to a point in the nose of the airplane, forward of the node, where the fuselage vibration will be interpreted by the accelerometer as a starboard (rather than port) rigid-body acceleration of the fuselage. This changes the sign of the accelerometer transfer function from (+) to (−) in Fig. 4 and causes the loci of Fig. 5 to move in a more stable direction, thus permitting the desired magnitude of control gain A.

In the actual system with the accelerometer in the nose, the control gain A was set at about 60 deg of rudder per g of lateral acceleration, which resulted in much improved lateral acceleration characteristics at the cockpit with no structural coupling or other unfavorable effects.

Structural Coupling in Platform Stabilization System

A stable platform is an apparatus used to maintain reference angles, in inertial space, for such systems as inertial autonavigators.[8] In some systems gimballing is made more compact—as represented in Fig. 6—by arranging the platform in two parts, connected by a "post" which serves as the "inner gimbal." Fundamentally, the system for controlling the spatial attitude of the platform consists of an angular-motion sensor to detect platform rotation and a torquer to apply corrective coercion.

Suppose, for illustrative purposes, that a "position" gyro is the sensor and that an electric motor is used for applying corrective torques. The control equation then would be, basically: $T = -A\phi_1$, where ϕ_1 is the rotation of the upper table (which is sensed by the gyro), T is the corrective torque applied by the motor, and A is the control "gain." As a practical matter, it is necessary to include in the control loop a network for supplying "dynamic lead," so that a more realistic control equation would be:

$$T = -A\frac{(\tau s + 1)}{\alpha\left(\frac{\tau}{\alpha}s + 1\right)}\phi_1 \tag{8}$$

in which α is larger than 1.

The azimuth post has some limberness to it, K, so that the dynamic equations of the platform itself are obtained by summing the torques on the upper and lower tables, respectively:

$$\begin{aligned}(I_1s^2 + Cs + K)\phi_1 - (Cs + K)\phi_2 &= 0\\ -(Cs + K)\phi_1 + (I_2s^2 + Cs + K)\phi_2 &= T\end{aligned} \tag{9}$$

For the control arrangement shown, the transfer function of interest is that relating rotation ϕ_1 to applied torque T:

$$\frac{\phi_1}{T} = \frac{(Cs + K)}{(I_1s^2 + Cs + K)(I_2s^2 + Cs + K) - (Cs + K)^2}$$

the denominator of which is, as usual, the characteristic equation of the platform. This particular denominator can be factored explicitly by simple algebraic cancellation to give:

$$\frac{\phi_1}{T} = \frac{\frac{C}{I_1I_2}\left(s + \frac{K}{C}\right)}{s^2(s + \sigma \pm j\omega)} \tag{10}$$

[8] R. H. Cannon, Jr., and D. P. Chandler, "Stable Platforms for High-Performance Aircraft," *Aeronautical Engineering Review*, vol. 16, December, 1957.

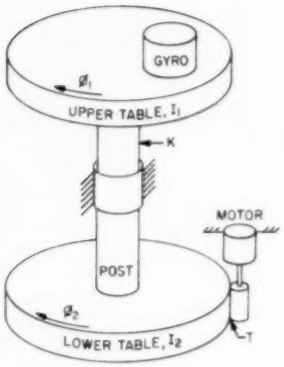

Fig. 6 Stable platform

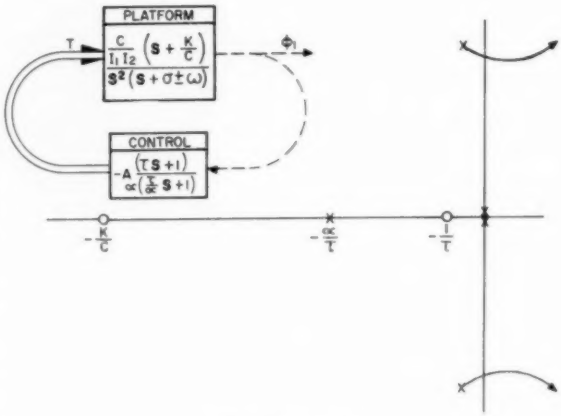

Fig. 7 Platform control

The s^2 term represents the first "natural mode of vibration" in which the entire platform moves as a rigid body. The other vibratory mode consists of contrary rotations of the upper and lower tables, the center of the post being stationary. Typically, if $I_1 = I_2$ the natural frequency of this mode involves half the length of the post:

$$\omega = (2K/I)^{1/2}$$

The control loop can now be drawn as in Fig. 7 where the applied torque T is generated from measured rotation ϕ_1 according to (8), and produces in turn a vibration ϕ_1 in accordance with (10). The characteristic equation for the closed-loop system is

$$\frac{\alpha s^2(s + \sigma \pm j\omega)\left(\frac{\tau}{\alpha}s + 1\right)}{\frac{C}{I_1I_2}\left(s + \frac{K}{C}\right)(\tau s + 1)} = -A$$

Again, the locus of values of s which satisfy the characteristic equation is plotted, for increasing A, in Fig. 7. As with the limber fuselage problem, the platform control system goes unstable for an intolerably low value of control gain A. The situation is remedied in practice by moving the torquer from the lower to the upper table in Fig. 6. This causes torque T to appear in the first of equations (9) instead of the second and results in a transfer function:

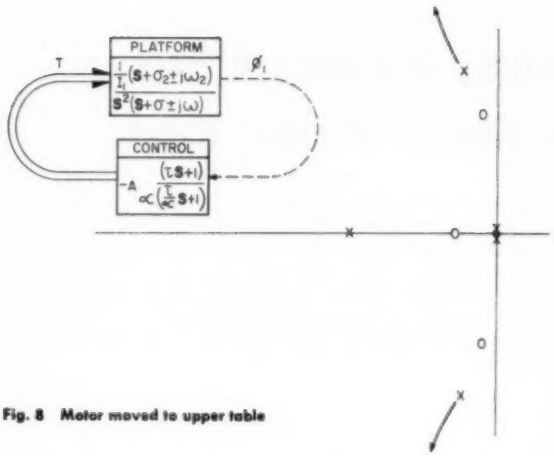

Fig. 8 Motor moved to upper table

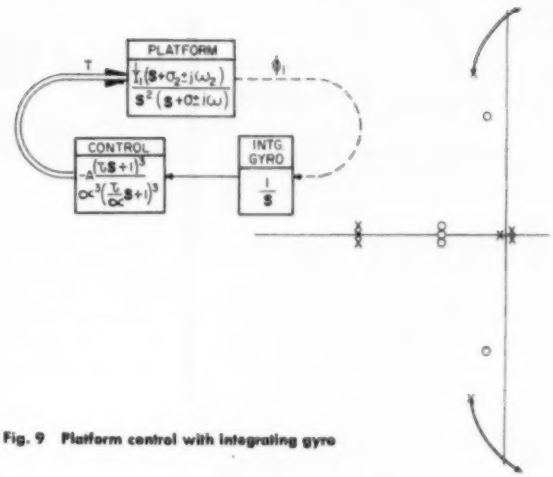

Fig. 9 Platform control with integrating gyro

$$\frac{\phi_1}{T} = \frac{\dfrac{1}{I_1}(s + \sigma_2 \pm j\omega_2)}{s^2(s + \sigma \pm j\omega)} \tag{11}$$

instead of (10). When this transfer function is inserted in the control block diagram, Fig. 8, the characteristic equation then becomes:

$$I_1\alpha \frac{s^3(s + \sigma \pm j\omega)\left(\dfrac{\tau}{\alpha}s + 1\right)}{(s + \sigma_2 \pm j\omega_2)(\tau s + 1)} = -A,$$

and the locus is plotted in Fig. 8, where no instability of the vibrational mode occurs even when control gain A becomes very large.

As a matter of interest, the frequency ω_2, in the numerator term of the platform transfer function of Fig. 8, involves the lower table vibrating on the entire post K, and is therefore only 0.707 as much as frequency ω of the combined vibration. This is indicated by the relative location of the complex × and O in Fig. 8.

Fallibility of Intuition. It might be argued on an intuitive basis that the system of Fig. 6 would always be more stable with the motor on the same table as the gyro. In order to cast some doubt on the intuitive process, consider the control system in Fig. 9, in which the position gyro has been replaced by a position-integrating gyro; i.e., one whose output is proportional to the integral of the upper table motion ϕ_1. The platform transfer function in Fig. 9 is for the motor on the same table as the gyro, expression (11).

More "lead"

$$\frac{(\tau s + 1)^3}{\alpha^3\left(\dfrac{\tau}{\alpha}s + 1\right)^3}$$

has been added to the controller to offset the additional lag of the gyro. The characteristic equation for the closed-loop system is now:

$$I_1\alpha^3 \frac{s^3(s + \sigma \pm j\omega)\left(\dfrac{\tau}{\alpha}s + 1\right)^3}{(s + \sigma_2 \pm j\omega_2)(\tau s + 1)^3} = -A$$

which leads to the root-locus plot shown in Fig. 9. The system becomes unstable for a relatively low control gain A. The indicated remedy in this case would be to try deliberately putting the motor on the lower table with the gyro still on the upper table. This particular problem came up in a recent platform development and was solved by that very measure, the correctness of which had been indicated by a root-locus analysis similar to Fig. 9.

Conclusions

The two cases treated in the foregoing are typical of control-system stability problems, which commonly involve several dynamic elements coupled together in a simple manner. It is seen that each dynamic characteristic (root) of the complete system is associated with the characteristic (pole) of one of the elements, the former differing from the latter—in frequency and damping—to a degree depending upon the strength of the control feedback. Structural elements usually have such light inherent damping that special precaution must be exercised to insure that the system roots move away from the elemental poles in a direction of increasing (rather than decreasing) damping. In the particular problems discussed this was accomplished by appropriate location of the sensing element of the control system with respect to the bending mode of the structural element.

The root-locus technique is found to be well suited to analyzing this type of problem. It presents explicitly a picture of the way in which the system roots change—with respect to the poles of the elements—as the control gain is increased. Not only the existence of stability or instability, but the actual degree of damping can be read directly, and the effect of altering system parameters can be seen at once.

W. F. STOKEY

Associate Professor,
Department of Mechanical Engineering,
Carnegie Institute of Technology,
Pittsburgh, Pa.
Assoc. Mem. ASME

C. F. ZOROWSKI

Assistant Professor,
Department of Mechanical Engineering,
Carnegie Institute of Technology.
Assoc. Mem. ASME

Normal Vibrations of a Uniform Plate Carrying Any Number of Finite Masses[1]

A general method is presented for determining approximately the natural frequencies of the normal vibrations of a uniform plate carrying any number of finite masses. Its application depends on knowing the frequencies and natural modes of vibration of the unloaded plate and the physical characteristics of the mass loadings. A numerical example is presented in detail in which this method is applied to a simply supported plate carrying two masses. Results also are included of experimentally measured frequencies for this configuration and several additional cases along with the frequencies computed using this method for comparison.

Introduction

THE problem of determining the natural frequencies of oscillation of a continuous elastic structural element restricted in its free movement by some type of intermediate constraint finds particular interest in the field of vibration isolation. The vibrations of elastic beams subjected to a great variety of constraints, intermediate to the end supports, has been treated in considerable detail by Lee and Saibel [1, 2].[2] This paper presents an adaptation of the solution of the problem of the vibrations of a uniform plate with point constraints, which was reported by Winston F. Lee in his doctoral thesis [3]. The solution has been extended to the vibrations of a uniform flat plate constrained by any number of finite masses rigidly attached to it, taking into account the effects of both their translational and rotational inertias. The application of this method depends on a knowledge of the natural frequencies and modes of oscillation of the unconstrained plate. In many cases these either will be known exactly or can be approximated sufficiently well, which makes the method useful in treating plates with many combinations of edge supports.

Theory

The differential equation for small free vibrations of a homo-

[1] The research underlying this paper was supported in part by a U. S. Air Force contract from the Rome Air Development Center with Carnegie Institute of Technology.

[2] Numbers in brackets designate References at end of paper.

Contributed by the Applied Mechanics Division and presented at the Annual Meeting, New York, N. Y., November 30–December 5, 1958, of THE AMERICAN SOCIETY OF MECHANICAL ENGINEERS.

Discussion of this paper should be addressed to the Secretary, ASME, 29 West 39th Street, New York, N. Y., and will be accepted until July 10, 1959, for publication at a later date. Discussion received after the closing date will be returned.

NOTE: Statements and opinions advanced in papers are to be understood as individual expressions of their authors and not those of the Society. Manuscript received by ASME Applied Mechanics Division, November 21, 1957. Paper No. 58—A-28.

Nomenclature

w = time and space-dependent normal deflection of plate, in.

$W(x, y)$ = space-dependent normal deflection of plate, in.

x, y = rectangular co-ordinates in plane of plate, in.

a, b = length and width of plate, in.

h = plate thickness, in.

μ = Poisson's ratio for plate material

E = modulus of elasticity, psi

$D = \frac{Eh^3}{12(1-\mu^2)}$ = flexural rigidity of plate, in-lb

ρ = mass density of plate per unit area, lb sec²/cu in.

$\phi_{rs}(x, y)$ = value of eigenfunction of the $r$sth mode of the unloaded plate at position x, y (in/lb sec²)$^{1/2}$

ω_{rs} = natural circular frequency of $r$sth mode of unloaded plate, radians per sec

ω = natural circular frequency of loaded plate, radians per sec

t = time, sec

a_{rs} = shape coefficients associated with w(in. lb sec²)$^{1/2}$

$\bar{a}_{rs}$ = time-dependent shape coefficient (in. lb sec²)$^{1/2}$

U = total strain energy of bending in plate, in-lb

T = total kinetic energy of plate, in-lb

X, Y = rectangular co-ordinates passing through center of gravity of mass and parallel to x, y co-ordinates, in.

Z = axis perpendicular to plane of plate, in.

M = total mass of a body attached to plate, lb sec²/in.

I_X, I_Y = mass moment of inertia of a mass about X and Y-axes of that mass, lb sec² in.

V_X, V_Y, V_Z = components of linear velocity of the center of gravity of any mass, ips

α, β = rotation of mass with respect to Z-axis, radians

c = perpendicular distance from plate to center of gravity of mass, in.

I_x, I_y = mass moment of inertia about the x and y-axes at base of mass, lb sec² in.

$R_v, \Phi_{rs}^u, \Phi_{rs}^v$ = inertia and eigenfunction forms defined in Equation (22)

δ_{uv} = Kronecker delta

Subscripts and Superscripts

i, j, k, m = refer to a given mass

x, y = represent first partial derivatives with respect to x and y separately

geneous flat plate of uniform thickness with no constraints other than at the boundaries is given by

$$D\nabla^4 w + \rho\ddot{w} = 0 \tag{1}$$

The deflection w in any natural mode may be expressed in the form

$$w = W(x, y) \sin \omega t \tag{2}$$

where $W(x, y)$ must satisfy the equation

$$D\nabla^4 W - \rho\omega^2 W = 0 \tag{3}$$

The solution to Equation (3), subject to the usual natural boundary conditions for a plate, is a complete set of eigenfunctions (normal modes of oscillation) $\phi_{rs}(x, y)$ and eigenvalues (natural circular frequencies) ω_{rs}. These eigenfunctions will be orthonormal, satisfying the relations

$$\begin{gathered} \iint_A \rho\phi_{rs}^2 dxdy = 1 \\ \iint_A \rho\phi_{rs}\phi_{r's'}dxdy = 0 \quad rs \neq r's' \end{gathered} \tag{4}$$

Now consider a plate on which are mounted a number of finite masses. In free vibration the total energy of the system at any time is composed of the kinetic and potential energies of all its parts. In this analysis the only potential energy considered will be the strain energy of bending of the plate. This can be expressed in terms of the deflection of the plate by the relation

$$U = \frac{D}{2} \iint_A \left\{ \left(\frac{\partial^2 w}{\partial x^2} \right)^2 + \left(\frac{\partial^2 w}{\partial y^2} \right)^2 + 2\mu \frac{\partial^2 w}{\partial x^2} \frac{\partial^2 w}{\partial y^2} + 2(1 - \mu) \left(\frac{\partial^2 w}{\partial x \partial y} \right)^2 \right\} dxdy \tag{5}$$

Since the eigenfunctions for the unloaded plate form a complete set, the deflection of the loaded plate in a natural mode can be expressed in terms of these known functions in the form

$$w = \sum_{r=1}^{\infty} \sum_{s=1}^{\infty} a_{rs}\phi_{rs}(x, y) \sin \omega t \tag{6}$$

Substituting any one term of (6) into Equation (5) yields the potential energy associated with a particular ϕ_{rs}

$$U_{rs} = \frac{D}{2} a_{rs}^2 \sin^2 \omega t \iint_A \left\{ \left(\frac{\partial^2 \phi_{rs}}{\partial x^2} \right)^2 + \left(\frac{\partial^2 \phi_{rs}}{\partial y^2} \right)^2 + 2\mu \frac{\partial^2 \phi_{rs}}{\partial x^2} \frac{\partial^2 \phi_{rs}}{\partial y^2} + 2(1 - \mu) \left(\frac{\partial^2 \phi_{rs}}{\partial x \partial y} \right)^2 \right\} dxdy \tag{7}$$

Integrating the expression on the right side of (7) twice by parts and making use of the natural boundary conditions for the plate results in the following simplification. (See Appendix for details of the integration.)

$$U_{rs} = \frac{D}{2} a_{rs}^2 \sin^2 \omega t \iint_A \phi_{rs}\nabla^4 \phi_{rs} dxdy \tag{8}$$

Since the eigenfunctions ϕ_{rs} satisfy Equation (3) then

$$D\nabla^4 \phi_{rs} = \rho\omega_{rs}^2 \phi_{rs} \tag{9}$$

Substituting (9) into (8) and making use of Equation (4) gives

$$U_{rs} = \frac{1}{2} \bar{a}_{rs}^2 \omega_{rs}^2 \tag{10}$$

where

$$\bar{a}_{rs} = a_{rs} \sin \omega t.$$

The total potential energy is obtained by summing Equation (10) with respect to r and s:

$$U = \frac{1}{2} \sum_{r=1}^{\infty} \sum_{s=1}^{\infty} \bar{a}_{rs}^2 \omega_{rs}^2 \tag{11}$$

The kinetic energy of the system will be expressed in two parts; i.e., the kinetic energy of the plate and the kinetic energy of the finite masses attached to the plate. Mathematically the kinetic energy of the plate may be expressed by

$$T = \frac{\rho}{2} \left\{ \frac{\partial}{\partial t} \iint_A w \, dxdy \right\}^2 \tag{12}$$

Using w as given in Equation (6), performing the indicated operations, and making use of Equation (4) the kinetic energy of the plate is reduced to

$$T = \frac{1}{2} \sum_{r=1}^{\infty} \sum_{s=1}^{\infty} \dot{\bar{a}}_{rs}^2 \tag{13}$$

where

$$\dot{\bar{a}}_{rs} = \frac{\partial \bar{a}_{rs}}{\partial t}$$

For small vibrations the kinetic energy of a cylindrically shaped mass attached to the plate is given by the product of one half its mass and the square of the plate velocity at the point of attachment plus the sum of the products of half its moment of inertia about its base and the square of the angular velocity of the plate in two perpendicular directions at the point of attachment. Referring to Fig. 1 with the X and Y-axes drawn through the center of gravity of the mass, its kinetic energy assuming no rotation about the Z-axis is given by

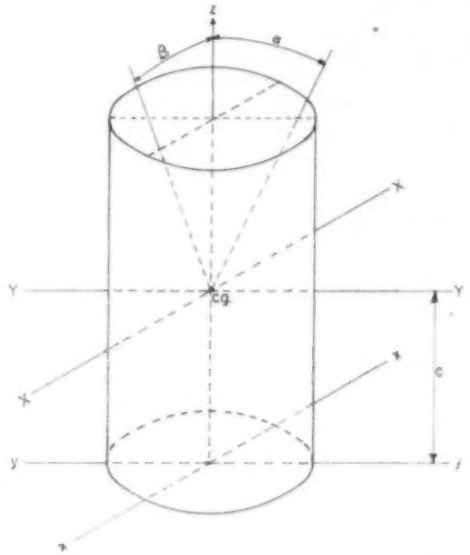

Fig. 1 Axis orientation for cylindrical body

$$T = \frac{1}{2} M \{V_X^2 + V_Y^2 + V_Z^2\} + \frac{I_X}{2}\left(\frac{\partial \alpha}{\partial t}\right)^2 + \frac{I_Y}{2}\left(\frac{\partial \beta}{\partial t}\right)^2 \quad (14)$$

For small deflections the following expressions may be considered true:

$$V_Z = \frac{\partial w}{\partial t} \qquad \alpha \cong \frac{\partial w}{\partial y} \qquad \beta \cong \frac{\partial w}{\partial x}$$

$$V_X \cong c\frac{\partial \beta}{\partial t} = c\frac{\partial}{\partial t}\left(\frac{\partial w}{\partial x}\right)$$

$$V_Y \cong c\frac{\partial \alpha}{\partial t} = c\frac{\partial}{\partial t}\left(\frac{\partial w}{\partial y}\right)$$

Making use of the foregoing expressions, Equation (14) can be written in the form

$$T = \frac{1}{2} M\left(\frac{\partial w}{\partial t}\right)^2 + \frac{1}{2} I_x\left\{\frac{\partial}{\partial t}\left(\frac{\partial w}{\partial y}\right)\right\}^2 + \frac{1}{2} I_y\left\{\frac{\partial}{\partial t}\left(\frac{\partial w}{\partial x}\right)\right\}^2 \quad (15)$$

where

$$I_x = I_X + Mc^2, \quad I_y = I_Y + Mc^2$$

For masses not having a cylindrical shape, Equation (15) is still a satisfactory approximation for the kinetic energy in most cases. Making use of Equation (6) the three terms of Equation (15) for the ith mass on the plate become

$$\left.\begin{aligned} T_{ii} &= \frac{M_i}{2}\left\{\sum_{r=1}^{\infty}\sum_{s=1}^{\infty} \dot{a}_{rs}\phi_{rs}(x_i, y_i)\right\}^2 \\ T_{iy} &= \frac{I_{iy}}{2}\left\{\sum_{r=1}^{\infty}\sum_{s=1}^{\infty} \dot{a}_{rs}\phi_{rs}^x(x_i, y_i)\right\}^2 \\ T_{ix} &= \frac{I_{ix}}{2}\left\{\sum_{r=1}^{\infty}\sum_{s=1}^{\infty} \dot{a}_{rs}\phi_{rs}^y(x_i, y_i)\right\}^2 \end{aligned}\right\} \quad (16)$$

The sum of expressions (16) then represents the total kinetic energy of the ith mass.

Assuming a conservative system, the equation of motion governing the plate and attached masses can be obtained from the previously developed kinetic and potential-energy expressions by making use of Lagrange's equation in the following form:

$$\frac{d}{dt}\left(\frac{\partial T}{\partial \dot{q}}\right) - \left(\frac{\partial T}{\partial q}\right) + \frac{\partial U}{\partial q} = 0 \quad (17)$$

It is convenient in this application to choose the generalized coordinates q to be equal to a_{rs}.

Substituting the potential energy of the plate given by Equation (11) and the total kinetic energy of the system given by the sum of Equations (13) and (16) into Equation (17), the equations of motion of the system consisting of a plate to which are attached n finite masses become

$$\ddot{a}_{rs} + \sum_{i=1}^{n}\left\{M_i\phi_{rs}(x_i, y_i)\sum_{r=1}^{\infty}\sum_{s=1}^{\infty}\ddot{a}_{rs}\phi_{rs}(x_i, y_i) + I_{iy}\phi_{rs}^x(x_i, y_i)\sum_{r=1}^{\infty}\sum_{s=1}^{\infty}\ddot{a}_{rs}\phi_{rs}^x(x_i, y_i) + I_{ix}\phi_{rs}^y(x_i, y_i)\sum_{r=1}^{\infty}\sum_{s=1}^{\infty}\ddot{a}_{rs}\phi_{rs}^y(x_i, y_i)\right\} + a_{rs}\omega_{rs}^2 = 0 \quad (18)$$

Equation (18) is now solved for a_{rs} by first substituting for $\ddot{a}_{rs}$ and a_{rs}, and then dividing through by sin ωt, making use of the relations

$$\left.\begin{aligned} W(x_i, y_i) &= \sum_{r=1}^{\infty}\sum_{s=1}^{\infty} a_{rs}\phi_{rs}(x_i, y_i) \\ W(x_i, y_i) &= \sum_{r=1}^{\infty}\sum_{s=1}^{\infty} a_{rs}\phi_{rs}^x(x_i, y_i) \\ W(x_i, y_i) &= \sum_{r=1}^{\infty}\sum_{s=1}^{\infty} a_{rs}\phi_{rs}^y(x_i, y_i) \end{aligned}\right\} \quad (19)$$

$$a_{rs} = \frac{\omega^2}{\omega_{rs}^2 - \omega^2}\sum_{i=1}^{n}\{M_i\phi_{rs}(x_i, y_i)W(x_i, y_i) + I_{iy}\phi_{rs}^x(x_i, y_i)W^x(x_i, y_i) + I_{ix}\phi_{rs}^y(x_i, y_i)W^y(x_i, y_i)\} \quad (20)$$

Consider now both sides of Equations (20) multiplied by $\phi(x_j, y_j)$, $\phi^x(x_j, y_j)$, and $\phi^y(x_j, y_j)$ successively and summed on r and s. Performing this operation and making use of relations (19) yields the following three sets of equations:

$$\left.\begin{aligned} W(x_j, y_j) &= \omega^2\sum_{i=1}^{n}\left\{M_i\sum_{r=1}^{\infty}\sum_{s=1}^{\infty}\frac{\phi_{rs}(x_i, y_i)\phi_{rs}(x_j, y_j)}{\omega_{rs}^2 - \omega^2}W(x_i, y_i) + I_{iy}\sum_{r=1}^{\infty}\sum_{s=1}^{\infty}\frac{\phi_{rs}^x(x_i, y_i)\phi_{rs}(x_i, y_i)}{\omega_{rs}^2 - \omega^2}W^x(x_i, y_i) + I_{ix}\sum_{r=1}^{\infty}\sum_{s=1}^{\infty}\frac{\phi_{rs}^y(x_i, y_i)\phi_{rs}(x_j, y_j)}{\omega_{rs}^2 - \omega^2}W^y(x_i, y_i)\right\} \\ W^x(x_j, y_j) &= \omega^2\sum_{i=1}^{n}\left\{M_i\sum_{r=1}^{\infty}\sum_{s=1}^{\infty}\frac{\phi_{rs}(x_i, y_i)\phi_{rs}^x(x_j, y_j)}{\omega_{rs}^2 - \omega^2}W(x_i, y_i) + I_{iy}\sum_{r=1}^{\infty}\sum_{s=1}^{\infty}\frac{\phi_{rs}^x(x_i, y_i)\phi_{rs}^x(x_j, y_j)}{\omega_{rs}^2 - \omega^2}W^x(x_i, y_i) + I_{ix}\sum_{r=1}^{\infty}\sum_{s=1}^{\infty}\frac{\phi_{rs}^y(x_i, y_i)\phi_{rs}^x(x_j, y_j)}{\omega_{rs}^2 - \omega^2}W^y(x_i, y_i)\right\} \\ W^y(x_j, y_j) &= \omega^2\sum_{i=1}^{n}\left\{M_i\sum_{r=1}^{\infty}\sum_{s=1}^{\infty}\frac{\phi_{rs}(x_i, y_i)\phi_{rs}^y(x_j, y_j)}{\omega_{rs}^2 - \omega^2}W(x_i, y_i) + I_{iy}\sum_{r=1}^{\infty}\sum_{s=1}^{\infty}\frac{\phi_{rs}^x(x_i, y_i)\phi_{rs}^y(x_j, y_j)}{\omega_{rs}^2 - \omega^2}W^x(x_i, y_i) + I_{ix}\sum_{r=1}^{\infty}\sum_{s=1}^{\infty}\frac{\phi_{rs}^y(x_i, y_i)\phi_{rs}^y(x_j, y_j)}{\omega_{rs}^2 - \omega^2}W^y(x_i, y_i)\right\} \end{aligned}\right\} \quad (21)$$

Equations (21) represent a system of $3n$ homogeneous linear equations in the $3n$ unknowns $W(x_jy_j)$, $W^x(x_jy_j)$, and $W^y(x_jy_j)$. The condition for the existence of a nontrivial solution requires that the determinant of the coefficients of the unknowns of the system be zero. This determinant is the frequency equation of the system.

For convenience let the following notation be adopted: u will

represent the number of the row of the determinant and v the number of the column.

$$\left.\begin{aligned}
\Phi_{rs}{}^{u}(x_k, y_k) &= \phi_{rs}(x_k, y_k) && \text{for } u = 3k-2\\
&= \phi_{rs}{}^{x}(x_k, y_k) && \text{for } u = 3k-1\\
&= \phi_{rs}{}^{y}(x_k, y_k) && \text{for } u = 3k\\
& && k = 1, 2, 3 \ldots . n\\
\Phi_{rs}{}^{v}(x_m y_m) &= \phi_{rs}(x_m, y_m) && \text{for } v = 3m-2\\
&= \phi_{rs}{}^{x}(x_m, y_m) && \text{for } v = 3m-1\\
&= \phi_{rs}{}^{y}(x_m, y_m) && \text{for } v = 3m\\
& && m = 1, 2, 3, \ldots . n\\
R_v &= M_i && \text{for } v = 3i-2\\
&= I_{ix} && \text{for } v = 3i-1\\
&= I_{iy} && \text{for } v = 3i\\
& && i = 1, 2, 3, \ldots n
\end{aligned}\right\} \quad (22)$$

In terms of the notation of (22) the determinant of the system of Equations (21) can be written in the form

$$\left| \omega^2 R_v \sum_{r=1}^{\infty} \sum_{s=1}^{\infty} \frac{\Phi_{rs}{}^{u}(x_k, y_k)\Phi_{rs}{}^{v}(x_m, y_m)}{\omega_{rs}{}^2 - \omega^2} - \delta_{uv} \right| = 0 \quad (23)$$

The solution of Equation (23) will yield n roots for ω corresponding to the frequencies of the first n natural modes of vibration of the plate with attached finite masses.

General Application

Even with the eigenfunctions ϕ_{rs} known for a particular problem the solution of Equation (23) for the natural circular frequencies ω presents two difficulties; i.e., the evaluation of a double infinite sum involving the unknown ω, and the solution of a $3n$th order equation in ω.[2] The first difficulty is eliminated by approximating the doubly infinite sum by a finite number of terms. Experimental verification of the method has indicated that usually only the first four eigenfunctions need be considered in determining the fundamental frequency of the constrained plate. The second difficulty is alleviated by making use of the matrix iteration method introduced by Duncan and Collar [4] for the solution of the frequency determinant. In applying this procedure it is found convenient first to multiply the frequency equation (23) by $(\omega_{11}/\omega)^2$, the ratio of the fundamental natural frequency of the unconstrained plate to that of the constrained plate. The matrix for which the roots must be found will then be given by

$$\left[R_v \sum_{r=1}^{n} \sum_{s=1}^{n} \frac{\Phi_{rs}{}^{u}(x_k, y_k)\Phi_{rs}{}^{v}(x_m, y_m)}{\left(\frac{\omega_{rs}}{\omega_{11}}\right)^2 - \frac{1}{\lambda}} \right] \quad (24)$$

and the roots will be of the form

$$\lambda = \left(\frac{\omega_{11}}{\omega}\right)^2$$

It is to be noted that the matrix itself (24) contains the unknown ω. In practice, an approximate value for ω must be assumed and the root of the resulting matrix found. If the computed value of ω is the same as the assumed value, the correct root has been determined. If the two values are different, a new value must be assumed and the root recalculated. However, changing the value of the assumed ω has a relatively small effect on the solution of the matrix so that even if a slight difference exists between the computed and assumed values, the computed result will be very close to the correct root.

A first approximation to the fundamental frequency which in many cases is sufficiently accurate to be used in setting up the characteristic matrix (24) for finding the correct fundamental frequency can be obtained from the following expression:

$$\lambda = 1 + \sum_{i=1}^{n} \{M_i[\phi_{11}(x_i, y_i)]^2 + I_{ix}[\phi_{11}{}^{x}(x_i, y_i)]^2 + I_{ix}[\phi_{11}{}^{y}(x_i, y_i)]^2\} \quad (25)$$

Equation (25) is the root obtained from Equation (23) for the fundamental frequency when only the first eigenfunction in the double infinite sum is used and the same approximations are used as in obtaining Dunkerley's formula [5].[3] The formation and iteration of the matrix of Equation (24) is a process that can be readily programmed for a digital computer. This permits an accurate solution to the problem to be obtained very quickly and with little effort on the part of the analyst. To carry out the solution by hand is, of course, more laborious, but not impractical. The calculated frequencies presented in the next two sections were obtained using an IBM 650 to form and iterate the characteristic matrices.

Numerical Example

The method is now applied in detail to the problem of determining the fundamental frequency of a simply supported rectangular plate carrying two cylindrical masses attached to the plate at locations B and D as shown in Fig. 2. The physical properties of the plate and the constraints are listed in the following table. An experimental setup of this system was used to check the calculated frequency.

Plate	Constraints
$a = 20$ in.	$M_B = 7.15 \times 10^{-3}$ lb sec^2/in
$b = 20$ in.	$I_{Bx} = 21 \times 10^{-3}$ lb sec^2 in.
$h = 0.091$ in.	$I_{By} = 21 \times 10^{-3}$ lb sec^2 in.
$\mu = 0.33$	$M_D = 7 \times 10^{-3}$ lb sec^2/in.
$E = 10.15 \times 10^6$ psi	$I_{Dx} = 20 \times 10^{-3}$ lb sec^2 in.
$\rho = 2.34 \times 10^{-4}$ lb sec^2/in.^{4}	$I_{Dy} = 20 \times 10^{-3}$ lb sec^2 in.

For a simply supported rectangular plate the normalized eigenfunctions are

$$\phi_{rs} = \frac{2}{(\rho ab)^{1/2}} \sin \frac{r\pi x}{a} \sin \frac{s\pi y}{b} \quad (26)$$

and the corresponding eigenvalues are given by

$$\omega_{rs}{}^2 = \frac{D}{\rho} \pi^4 \left(\frac{r^2}{a^2} + \frac{s^2}{b^2}\right)^2 \quad (27)$$

From Equation (26) the first four eigenfunction values corresponding to the locations of the two masses are presented in Table 1.

Table 1 Eigenfunction values

$\phi_{rs} \backslash rs$	11	12	21	22
$\phi(D)$	14.65	20.70	0	0
$\phi^x(D)$	0	0	−4.58	−6.48
$\phi^y(D)$	2.29	0	0	0
$\phi(B)$	14.65	0	20.70	0
$\phi^x(B)$	2.29	0	0	0
$\phi^y(B)$	0	−4.58	0	−6.48

[3] A mathematical demonstration of the approximation involved in Dunkerley's formula is due to Hahn (1918) and is referred to in [5].

The eigenvalues corresponding to these four eigenfunctions are obtained from Equation (27)

$$\omega_{11} = 271, \quad \omega_{21} = 687, \quad \omega_{12} = 687, \quad \omega_{22} = 1083$$

Using Equation (25), λ is found to be 4.26. This will give a high value for ω since the poorer the approximation to the correct shape of the plate the higher the calculated frequency will be. To compensate for this a value of 5.26 is assumed as a first trial for λ. With this value the characteristic matrix, (24), becomes

$$\begin{bmatrix} 2.35 & 0 & 0.83 & 1.91 & 0.87 & -0.33 \\ 0 & 0.12 & 0 & -0.11 & 0 & 0.06 \\ 0.29 & 0 & 0.13 & 0.30 & 0.14 & 0 \\ 1.85 & -0.31 & 0.83 & 2.42 & 0.87 & 0 \\ 0.29 & 0 & 0.13 & 0.30 & 0.14 & 0 \\ -0.11 & 0.05 & 0 & 0 & 0 & 0.13 \end{bmatrix}$$

Iteration of this matrix yields a root for λ of 4.51. This being considerably lower than the assumed value, several additional trials are made. The results follow:

Trial	λ Assumed	λ Computed
1	5.26	4.51
2	4.76	4.61
3	4.54	4.66

By linear interpolation λ is found to be 4.63. The computed natural frequency of the system is then 20 cycles per sec. This compares favorably with the experimentally determined frequency of 18 cps given in Table 4.

Experimental Results

A series of experiments was conducted on simply supported rectangular plates with masses attached to them in numerous positions to check the analytical results obtained from (24) and (25). Tests were performed on two aluminum plates, 20 in. × 20 in. and 20 in. × 10 in., with an average thickness of 0.091 in. These plates were supported on knife edges milled from one edge of a section of angle iron, the other edge being firmly attached to a steel table. Since it was impractical to make the plate perfectly flat and its own weight was not sufficient to keep it in contact with the knife edges at all points it was impossible to determine experimentally the natural frequencies of the unconstrained plate. However, the addition of a mass of about 2 lb at the center of the plate did prove sufficient to keep the plate in complete contact with the knife edges while undergoing small oscillations. These oscillations were excited by lightly striking the masses in the direction transverse to the plate. The frequencies of the oscillations were measured by an arrangement in which the movement of the plate produced an alternating voltage whose frequency was compared to a standard source.

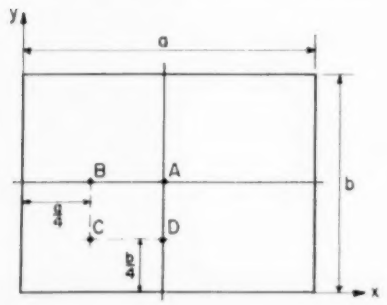

Fig. 2 Mass locations on test plate

Three distinct sets of tests were conducted. The first consisted of the addition of a single mass, varying from 2 to 12 lb, to the center of each plate, location A in Fig. 2. In the second set a cylindrical mass weighing about 2¾ lb was placed at positions away from the center of the plate, locations B, C, and D. In the third set a second mass was added similar to that used in set 2 and the masses were placed at the locations indicated in Table 4.

The results of the tests carried out on the 20-in. × 20-in. plate are presented in Tables 2, 3, and 4 along with the computed values of the frequency obtained from Equations (25) and (24). Only the first four eigenfunctions were considered in the application of matrix (24). The results of the tests on the 20-in. × 10-in. plate are not presented here but were found to be comparable to those obtained for the 20-in. × 20-in. plate.

Table 2

Location	Weight, lb	Meas. f, cps	Eq. (25), cps	Eq. (24), cps
A	2	23.4	24.1	23.5
A	4	17.5	18.5	18.0
A	6	15.0	15.6	15.1
A	8	13.2	13.8	13.2
A	10	12.0	12.4	11.9
A	12	11.0	11.5	11.0

Table 3

Location	Weight, lb	I, lb in. sec²	Meas. freq, cps	Eq. (25), cps	Eq. (24), cps
B, D	2.75	0.021	26.0	26.6	25.1
C	2.75	0.021	28.5	30.9	28.7

Table 4

Location	Weight, lb	I, lb in. sec²	Meas. freq, cps	Eq. (25), cps	Eq. (24), cps
A	2.70	0.020	15.5	18.2	17.9
B	2.75	0.021			
D	2.70	0.020	18.0	20.7	20.1
B	2.75	0.021			

Discussion

Comparison of the measured and computed frequencies in Table 2 indicates a very close agreement between the two calculated frequencies and the measured values. This good agreement probably results from the fact that, with the plate constrained by only a single mass at its center, its shape, while oscillating, is very much like that of the fundamental mode of the unconstrained plate. This would account for the closeness of the simplified solution and small change in the computed value even when three additional eigenfunctions are considered, Equation (24). It is to be noted that in all cases the more accurately computed frequency is the lower of the two calculated values and the closer to the measured value indicating a better approximation to the exact shape.

An investigation of the computed results presented in Table 3 again shows the more accurate solution to give a lower frequency with a greater difference now appearing between the two calculated values. This is to be expected with the mass away from the center, since contributions from the higher eigenfunctions will be required to obtain a better approximation to the oscillating shape of the constrained plate. The poorer agreement of the more accurate solution with the measured value in the first case in Table

3 probably can be attributed to difficulties in experimental measurements. These will be discussed separately.

In Table 4 the calculated results once again agree more closely. This is probably due to the added mass at the center of the plate which again brings into dominance the fundamental mode of the unconstrained plate. The more accurate solutions are still lower indicating a better approximation to the exact shape. These values do not agree as well, however, with the measured frequencies as in Tables 2 and 3. Nowhere, in any of the tests, is the best computed frequency in error with the measured value by more than 15½ per cent.

The differences which do exist between the computed and measured frequencies are in part due to difficulties encountered in the experimental setup. In order to support the plates on the knife edges properly, it was necessary to make them slightly larger than the nominal size. This itself would tend to lower the measured frequency. An additional factor to be considered is that the attached masses were not supported at a point as assumed in the theory but actually cover a finite area. This introduces an additional constraint which would further change the frequency. This effect becomes more pronounced when the mass is located away from the center of the plate and away from the point of maximum amplitude where a second mass may be located as the case is in Table 4. Of course, the measurement of the frequency itself will also involve some error. Variations in frequency of as much as 2 cycles were obtained from different tests of the same configuration. All things considered the agreement between the measured values and the computed frequencies using the approximate method of analysis as presented appears quite good.

Acknowledgment

Several graduate students participated in the setting up and operation of the equipment used in obtaining the experimental results. Frederic C. Appl, Ronald C. Kurtz, and George Hutchinson made notable contributions to this portion of the work.

References

1 E. Saibel, "Vibration Frequencies of Continuous Beams," *Journal of the Aeronautical Sciences*, vol. 11, 1944, pp. 88–90.

2 W. F. Z. Lee and E. Saibel, "Free Vibrations of Constrained Beams," JOURNAL OF APPLIED MECHANICS, vol. 19, TRANS. ASME, vol. 74, 1952, pp. 471–477.

3 W. F. Z. Lee, "Free and Forced Vibrations of Constrained Beams and Plates," Doctor of Science Thesis in Mechanical Engineering, Carnegie Institute of Technology, Pittsburgh, Pa., 1952.

4 W. J. Duncan and A. R. Collar, "A Method for the Solution of Oscillation Problems by Matrices," *Philosophical Magazine*, S7, vol. 17, May, 1934, pp. 866–909.

5 A. Stodola, "Steam and Gas Turbines," McGraw-Hill Book Co., Inc., New York, N. Y., vol. II, 1927, pp. 1110–1112.

APPENDIX

The reduction of Equation (7) to the form given in (8) is accomplished by integrating each term on the right side of (7) by parts twice. Consider the first term integrated once with respect to x

$$\iint_A \left(\frac{\partial^2\phi}{\partial x^2}\right)^2 dxdy = \int_0^b \left[\frac{\partial^3\phi_{rs}}{\partial x^2}\frac{\partial\phi_{rs}}{\partial x}\right]_0^a dy - \iint_A \frac{\partial\phi_{rs}}{\partial x}\frac{\partial^3\phi_{rs}}{\partial x^3}\,dxdy \quad (28)$$

Now integrating the second term on the right side of (28) again with respect to x gives

$$\iint_A \left(\frac{\partial^2\phi_{rs}}{\partial x^2}\right)^2 dxdy = \int_0^b \left[\frac{\partial^3\phi_{rs}}{\partial x^3}\frac{\partial\phi_{rs}}{\partial x}\right]_0^a dy - \int_0^b \left[\frac{\partial^3\phi_{rs}}{\partial x^3}\phi_{rs}\right]_0^a dy + \iint_A \phi_{rs}\frac{\partial^4\phi_{rs}}{\partial x^4}\,dxdy \quad (29)$$

In a similar manner the second term of Equation (7) can be integrated by parts twice with respect to y to give

$$\iint_A \left(\frac{\partial^2\phi_{rs}}{\partial y^2}\right)^2 dxdy = \int_0^a \left[\frac{\partial^3\phi_{rs}}{\partial y^2}\frac{\partial\phi_{rs}}{\partial y}\right]_0^b dx - \int_0^a \left[\frac{\partial^3\phi_{rs}}{\partial y^3}\phi_{rs}\right]_0^b dx + \iint_A \phi_{rs}\frac{\partial^4\phi_{rs}}{\partial y^4}\,dxdy \quad (30)$$

The third term of Equation (7) is separated into two parts and each is integrated twice by parts, one with respect to x, the other with respect to y:

$$2\mu\iint_A \frac{\partial^2\phi_{rs}}{\partial x^2}\frac{\partial^2\phi_{rs}}{\partial y^2}\,dxdy = \mu\int_0^b \left[\frac{\partial^3\phi_{rs}}{\partial y^2}\frac{\partial\phi_{rs}}{\partial x}\right]_0^a dy - \mu\int_0^b \left[\frac{\partial^3\phi_{rs}}{\partial x\partial y^2}\phi_{rs}\right]_0^a dy + \mu\int_0^a \left[\frac{\partial^3\phi_{rs}}{\partial x^2}\frac{\partial\phi_{rs}}{\partial y}\right]_0^b dx - \mu\int_0^a \left[\frac{\partial^3\phi_{rs}}{\partial y\partial x^2}\phi_{rs}\right]_0^b dx + 2\mu\iint_A \phi_{rs}\frac{\partial^4\phi_{rs}}{\partial x^2\partial y^2}\,dxdy \quad (31)$$

The last term of (7) is treated in a similar manner except that one part is integrated first with respect to x and then with respect to y, and the procedure is reversed for the remaining part.

$$2(1-\mu)\iint_A \left(\frac{\partial^2\phi_{rs}}{\partial x\partial y}\right)^2 dxdy = (1-\mu)\int_0^b \left[\frac{\partial^3\phi_{rs}}{\partial x\partial y}\frac{\partial\phi_{rs}}{\partial y}\right]_0^a dy - (1-\mu)\int_0^b \left[\frac{\partial^3\phi_{rs}}{\partial x\partial y^2}\phi_{rs}\right]_0^a dy + (1-\mu)\int_0^a \left[\frac{\partial^3\phi_{rs}}{\partial x\partial y}\frac{\partial\phi_{rs}}{\partial x}\right]_0^b dx - (1-\mu)\int_0^a \left[\frac{\partial^3\phi_{rs}}{\partial y\partial x^2}\phi_{rs}\right]_0^b dx + 2(1-\mu)\iint_A \phi_{rs}\frac{\partial^4\phi_{rs}}{\partial x^2\partial y^2}\,dxdy \quad (32)$$

Consider the first term of the right side of (32). Since

$$\frac{\partial}{\partial y}\left\{\phi_{rs}\frac{\partial^2\phi_{rs}}{\partial x\partial y}\right\} = \frac{\partial\phi_{rs}}{\partial y}\frac{\partial^2\phi_{rs}}{\partial x\partial y} + \phi_{rs}\frac{\partial^3\phi_{rs}}{\partial x\partial y^2}$$

then this term can be expressed in the form

$$\int_0^b \left[\frac{\partial^3\phi_{rs}}{\partial x\partial y}\frac{\partial\phi_{rs}}{\partial y}\right]_0^a dy = -\int_0^b \left[\frac{\partial^3\phi_{rs}}{\partial x\partial y^2}\phi_{rs}\right]_0^a dy + \left\{\phi_{rs}\frac{\partial^2\phi_{rs}}{\partial x\partial y}\right\}_{\substack{x=a,\ y=b\\ x=0,\ y=0}} - \left\{\phi_{rs}\frac{\partial^2\phi_{rs}}{\partial x\partial y}\right\}_{\substack{x=a,\ y=0\\ x=0,\ y=b}} \quad (33)$$

The last two terms of (33) are zero, however, provided the edges are simply supported, clamped, or free. Similarly, the third term on the right of (32) becomes

$$\int_0^a \left[\frac{\partial^3 \phi_{rs}}{\partial x \partial y} \frac{\partial \phi_{rs}}{\partial x}\right]_0^b dx = -\int_0^a \left[\frac{\partial^3 \phi_{rs}}{\partial y \partial x^2} \phi_{rs}\right]_0^b dx \quad (34)$$

Combining Equations (28) through (34) now gives

$$\iint_A \left\{\left(\frac{\partial^2 \phi_{rs}}{\partial x^2}\right)^2 + \left(\frac{\partial^2 \phi_{rs}}{\partial y^2}\right)^2 + 2\mu \frac{\partial^2 \phi_{rs}}{\partial x^2} \frac{\partial^2 \phi_{rs}}{\partial y^2} + 2(1-\mu)\left(\frac{\partial^2 \phi_{rs}}{\partial x \partial y}\right)^2\right\} dxdy = \iint_A \phi_{rs} \nabla^4 \phi_{rs} dxdy$$

$$+ \int_0^a \left\{\frac{\partial \phi_{rs}}{\partial y}\left[\frac{\partial^2 \phi_{rs}}{\partial y^2} + \mu \frac{\partial^2 \phi_{rs}}{\partial x^2}\right]\right\}_0^b dx + \int_0^b \left\{\frac{\partial \phi_{rs}}{\partial x}\left[\frac{\partial^2 \phi_{rs}}{\partial x^2} + \mu \frac{\partial^2 \phi_{rs}}{\partial y^2}\right]\right\}_0^a dy - \int_0^b \left\{\phi_{rs}\left[\frac{\partial^2 \phi_{rs}}{\partial x^2} + (2-\mu) \frac{\partial^3 \phi_{rs}}{\partial x \partial y^2}\right]\right\}_0^a dy - \int_0^a \left\{\phi_{rs}\left[\frac{\partial^3 \phi_{rs}}{\partial y^3} + (2-\mu) \frac{\partial^3 \phi_{rs}}{\partial y \partial x^2}\right]\right\}_0^b dx \quad (35)$$

All the line integrals in Equation (35) will be zero, reducing it to the form of Equation (8) providing all edges of the plate are either simply supported, clamped, or free or any combinations of these natural boundary conditions.

Transients in Simple Undamped Oscillators Under Inertial Disturbances

ANTONGIULIO DORNIG

Assistant Professor,
Institute of Applied Mechanics
and Machine Design,
Polytechnic of Milan,
Milan, Italy

Single-degree-of-freedom systems acted upon inertial forces are often found in technical applications. In this paper we shall study the transients in the vibrations of the system due to a change in speed in the machine in which the inertial forces are generated. We shall state the problem in the most general case, and then study the starting and the stopping with constant acceleration. After giving the exact solution of the problem we shall derive very simple approximate formulas for the determination of the maximum amplitude reached in these transients.

Introduction

It is well known that frequently technical vibratory nuisances are caused by inertial disturbances. Rotating masses eccentrically mounted are typical instances of such disturbances.

When a machine is in its normal working condition, the vibrations are stationary, or they may be, with a fair degree of approximation, classified as such; in this case the analysis does not present any particular difficulty

Transients, on the other hand, are of a more complex nature.

An analysis of the transients occurring when a machine changes its speed may be an interesting technical point, especially when the machine is being started or coming to rest.

It may happen that, during these transients, the frequency of the inertial disturbance is passing through the resonance of the system.

The most typical and frequent example is given by a machine supported by springs in order to obtain a vibration isolation from its support. We know that in this case the natural frequency of the suspended system must be much lower than the disturbing frequency corresponding to the normal speed of the machine. It is then inevitable that, both in being started and coming to rest, the disturbing frequency becomes, at a given instant, equal to the natural frequency of the vibrating system. It is clear that when this happens the amplitude of the vibration may increase sensibly.

In this paper we shall deal with inertial disturbances exciting an undamped single-degree-of-freedom system. It is a problem which presents some similarity to the one which has been studied by Pöschl [1][1] and still more completely by Lewis [2]. The work of the latter is partially related by Klotter [3].

These authors have studied the problem of single-degree-of-freedom undamped systems (Lewis also has studied the damped systems) excited by a force:

$$F(t) = f_0 \sin \varphi(t),$$

f_0 being a constant and $\varphi(t) = \lambda t^2$.

On the contrary with inertial disturbances, also when the effect of tangential accelerations is not taken into account, the exciting force will be

$$F(t) = f(t) \sin \varphi(t),$$

i.e., still sinusoidal in the argument $\varphi(t)$, but of amplitude variable with the time.

Formulation of Problem

Let us refer to the case schematically illustrated in Fig. 1: A rigid body of mass M is supported by the massless linear spring k and free to move only in the x-direction. This body is excited by the inertial forces caused by an eccentric mass m rotating around an axis at a distance r.

Let $\varphi = \varphi(t)$ and $\varphi(0) = 0$.

The differential equation of motion is

$$M\ddot{x} + kx = F(t) = rm[\dot{\varphi}^2 \sin(\varphi + \varphi_0) - \ddot{\varphi} \cos(\varphi + \varphi_0)]$$

Contributed by the Applied Mechanics Division and presented at the Annual Meeting, November 30–December 5, 1958, New York, N. Y., of The American Society of Mechanical Engineers.

Discussion of this paper should be addressed to the Secretary, ASME, 29 West 39th Street, New York, N. Y., and will be accepted until July 10, 1959, for publication at a later date. Discussion received after the closing date will be returned.

Note: Statements and opinions advanced in papers are to be understood as individual expressions of their authors and not those of the Society. Manuscript received by ASME Applied Mechanics Division, March 24, 1958. Paper No. 58—A-58.

[1] Numbers in brackets designate References at end of paper.

Nomenclature

M = mass of vibrating system
k = linear stiffness of spring
m = eccentrically rotating mass
r = eccentricity of mass m
x = co-ordinate of vibrating system
u = component in x-direction of relative displacement of mass m with respect to M
$F(t)$ = exciting force
ω_0 = steady-state angular velocity of machine before transient
2λ = angular acceleration or deceleration of machine
$A(t)$ = indicial admittance of vibrating system
$C(z)$, $S(z)$ = Fresnel's integrals
$e = mr/M$
$\Omega = (k/M)^{1/2}$
$\xi(t) = x/e$ = dimensionless co-ordinate
$\xi_s(t)$ = dimensionless co-ordinate of envelope of $\xi(t)$
$\eta = (2\lambda t - \omega_0)/\Omega$ = "dimensionless time" in deceleration transient
$\eta = 2\lambda t/\Omega$ = dimensionless time in acceleration transient
$\rho = \Omega/(2\pi\lambda)^{1/2}$ = dimensionless characteristic parameter
$\Phi(\eta) = \xi_s(\eta)/(\pi/2)\rho$
$\psi_0 = (\omega_0^2/4\lambda) + \varphi_0$

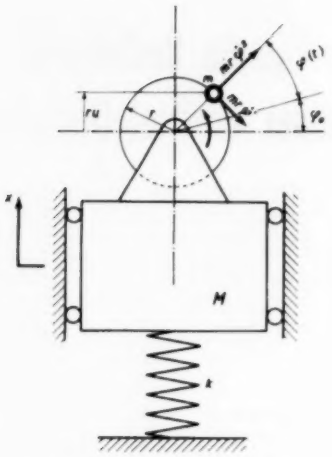

Fig. 1 Simple oscillator excited by an eccentric rotating mass

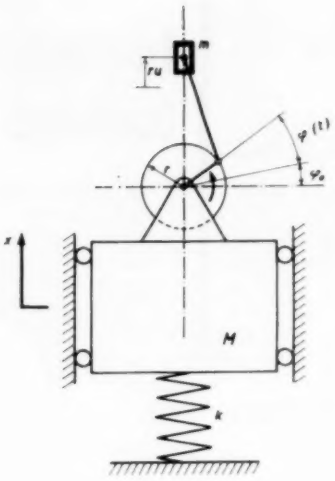

Fig. 2 Simple oscillator excited by reciprocating motion of a mass

It is important to observe that the force $F(t)$ is connected with the component ru in the x-direction of the displacement of m relative to M by the following relation:

$$F(t) = -mr\ddot{u} \tag{1}$$

in which

$$u = \sin(\varphi + \varphi_0) \tag{2}$$

Consequently the equation of motion will be

$$M\ddot{x} + kx = -mr\ddot{u} \tag{3}$$

It is important to note that we have referred to the case of Fig. 1 just in order to give a concrete example. We may always reach a similar conclusion also when we consider a more general case in which the inertial disturbances are caused by the relative motion of one or more masses with respect to M, when the components in x-direction of the relative displacements may be represented by a series of sines.

In fact, if the exciting force, as we may see in Fig. 2, is caused by the reciprocating motion of a mass m concentrated on the slider of a slider-crank mechanism, the equation of motion of the vibrating system is once again (3), in which, however,

$$u = \sin(\varphi + \varphi_0) + h_1 \sin 2(\varphi + \varphi_1) + h_2 \sin 4(\varphi + \varphi_2) + \dots .$$

Since the effects may be superimposed, the problem is identical to the previous one.

Let us suppose that for $t < 0$ the machine is running in a steady state and that, starting from $t = 0$, its motion becomes variable; it will be

for $t < 0$ $\qquad \varphi = \omega_0 t$

for $t > 0$ $\qquad \varphi = \varphi(t)$

for $t < 0$ the exciting force is

$$F(t) = mr\omega_0^2 \sin(\omega_0 t + \varphi_0)$$

If we suppose that this force has been acting for a long time, the vibration may be considered in a steady state and it will be expressed by the well-known relation

$$x = -e \frac{\sin(\omega_0 t + \varphi_0)}{1 - \left(\frac{\Omega}{\omega_0}\right)^2}$$

where $e = mr/M$.

At the time $t = 0$, the displacement and the velocity of the system are

$$x(0) = -e \frac{\sin \varphi_0}{1 - \left(\frac{\Omega}{\omega_0}\right)^2} \qquad \dot{x}(0) = -e \frac{\omega_0 \cos \varphi_0}{1 - \left(\frac{\Omega}{\omega_0}\right)^2} \tag{4}$$

Equations (4) represent also the initial conditions of the system when the speed of the machine becomes variable.

For $t > 0$ the equation of motion is given by equation (3), the general integral of which is as follows:

$$x = C_1 \cos \Omega t + C_2 \sin \Omega t + \bar{x} \tag{5}$$

where C_1 and C_2 are constants, which are to be determined by the initial conditions, and $\bar{x}$ is a particular integral.

If we indicate by $A(t)$ the indicial admittance of the vibrating system, this integral may be determined easily by means of Duhamel's formula:

$$\bar{x} = F(0)A(t) + \int_0^t \frac{dF(\tau)}{d\tau} A(t - \tau)d\tau$$

By means of three consecutive integrations by parts this expression, taking into account equation (1), becomes

$$\bar{x} = -mr \left\{ \dot{u}(t)A(0) + \dot{u}(t)\dot{A}(0) - \dot{u}(0)\dot{A}(t) + u(t)\ddot{A}(0) - u(0)\ddot{A}(t) + \int_0^t u(\tau)\dddot{A}(t - \tau)d\tau \right\}$$

Since

$$A(t) = \frac{1}{k}(1 - \cos \Omega t) \qquad A(0) = 0$$

$$\dot{A}(t) = \frac{1}{M\Omega} \sin \Omega t \qquad \dot{A}(0) = 0$$

$$\ddot{A}(t) = \frac{1}{M} \cos \Omega t \qquad \ddot{A}(0) = \frac{1}{M}$$

$$\dddot{A}(t) = -\frac{\Omega}{M} \sin \Omega t$$

$$C_1 = -e \frac{\sin \varphi_0}{1 - \left(\frac{\Omega}{\omega_0}\right)^2} \qquad C_2 = -e \frac{\omega_0}{\Omega} \frac{\cos \varphi_0}{1 - \left(\frac{\Omega}{\omega_0}\right)^2}$$

the equation of motion, referred to the dimensionless co-ordinate $\xi(t) = x(t)/c$ is

$$\xi(t) = -\frac{1}{1-\left(\frac{\Omega}{\omega_0}\right)^2}\left[\sin\varphi_0\cos\Omega t + \frac{\omega_0}{\Omega}\cos\varphi_0\sin\Omega t\right] + \dot{u}(0)\frac{\sin\Omega t}{\Omega} - u(t) + u(0)\cos\Omega t + \Omega\int_0^t u(\tau)\sin\Omega(t-\tau)d\tau \quad (6)$$

It is to be noted that the dimensionless co-ordinate ξ represents the generic amplitude of the vibration referred to the amplitude e at steady state when the disturbing frequency is very great with respect to the natural frequency of the vibrating system.

Motion With Constant Acceleration

Let us consider the case in which for $t > 0$, the machine rotates with constant angular acceleration 2λ; we shall then have

$$\varphi(t) = \lambda t^2 + \omega_0 t \quad (7a)$$

Since

$$\varphi(0) = 0 \quad \text{and} \quad \dot{\varphi}(0) = \omega_0$$

it follows that

$$u(0) = \sin\varphi_0 \qquad \dot{u}(0) = \omega_0\cos\varphi_0$$

Equation (6) then becomes

$$\xi(t) = \frac{1}{1-\left(\frac{\omega_0}{\Omega}\right)^2}\left[\sin\varphi_0\cos\Omega t + \frac{\omega_0}{\Omega}\cos\varphi_0\sin\Omega t\right] - \sin(\lambda t^2 + \omega_0 t + \varphi_0) + I' \quad (8a)$$

where we put

$$I' = \Omega\int_0^t \sin(\lambda\tau^2 + \omega_0\tau + \varphi_0)\sin\Omega(t-\tau)d\tau = \frac{\Omega}{2}\int_0^t \cos[\lambda\tau^2 + (\omega_0+\Omega)\tau + (\varphi_0 - \Omega t)]d\tau - \frac{\Omega}{2}\int_0^t \cos[\lambda\tau^2 + (\omega_0-\Omega)\tau + (\varphi_0 + \Omega t)]d\tau$$

Introducing Fresnel's integrals $C(z)$ and $S(z)$ defined as

$$C(z) = \int_0^z \cos\frac{\pi}{2}\zeta^2 d\zeta$$

$$S(z) = \int_0^z \sin\frac{\pi}{2}\zeta^2 d\zeta$$

we can easily obtain

$$\int \cos(l\tau^2 + n\tau + p)d\tau = \int \cos\left[l\left(\tau + \frac{n}{2l}\right)^2 + \left(p - \frac{n^2}{4l}\right)\right]d\tau = \left(\frac{\pi}{2l}\right)^{1/2}\cos\left(p - \frac{n^2}{4l}\right)C\left[\left(\frac{2l}{\pi}\right)^{1/2}\left(\tau + \frac{n}{2l}\right)\right] - \left(\frac{\pi}{2l}\right)^{1/2}\sin\left(p - \frac{n^2}{4l}\right)S\left[\left(\frac{2l}{\pi}\right)^{1/2}\left(\tau + \frac{n}{2l}\right)\right]$$

Integral I' then becomes

$$I' = \left(\frac{\pi\Omega^2}{8\lambda}\right)^{1/2}\left\{\cos\left[\Omega t + \frac{(\omega_0+\Omega)^2}{4\lambda} - \varphi_0\right][C(a') - C(a_0')] + \sin\left[\Omega t + \frac{(\omega_0+\Omega)^2}{4\lambda} - \varphi_0\right][S(a') - S(a_0')] - \cos\left[\Omega t - \frac{(\omega_0-\Omega)^2}{4\lambda} + \varphi_0\right][C(b') - C(b_0')] + \sin\left[\Omega t - \frac{(\omega_0-\Omega)^2}{4\lambda} + \varphi_0\right][S(b') - S(b_0')]\right\} \quad (9a)$$

where

$$\left.\begin{aligned} a' &= \left(\frac{2}{\pi\lambda}\right)^{1/2}\left[\lambda t + \frac{\omega_0+\Omega}{2}\right] \\ b' &= \left(\frac{2}{\pi\lambda}\right)^{1/2}\left[\lambda t + \frac{\omega_0-\Omega}{2}\right] \\ a_0' &= \left(\frac{2}{\pi\lambda}\right)^{1/2}\left(\frac{\omega_0+\Omega}{2}\right) \\ b_0' &= \left(\frac{2}{\pi\lambda}\right)^{1/2}\left(\frac{\omega_0-\Omega}{2}\right) \end{aligned}\right\} \quad (10a)$$

Motion With Constant Deceleration

Let the constant angular deceleration be 2λ. We have

$$\varphi(t) = -\lambda t^2 + \omega_0 t \quad (7b)$$

The equation of motion then becomes

$$\xi(t) = \frac{1}{1-\left(\frac{\omega_0}{\Omega}\right)^2}\left[\sin\varphi_0\cos\Omega t + \frac{\omega_0}{\Omega}\cos\varphi_0\sin\Omega t\right] - \sin(-\lambda t^2 + \omega_0 t + \varphi_0) + I'' \quad (8b)$$

I'' is obtained from equation (9a), by substituting $-\lambda$ for λ.

If we remember that $C(iz) = iC(z)$ and $S(iz) = -iS(z)$ and that $C(-z) = -C(z)$ and $S(-z) = -S(z)$, we can easily obtain the following expression:

$$I'' = \left(\frac{\pi\Omega^2}{8\lambda}\right)^{1/2}\left\{\cos\left[\Omega t - \frac{(\omega_0+\Omega)^2}{4\lambda} - \varphi_0\right][C(a'') + C(a_0'')] - \sin\left[\Omega t - \frac{(\omega_0+\Omega)^2}{4\lambda} - \varphi_0\right][S(a'') + S(a_0'')] - \cos\left[\Omega t + \frac{(\omega_0-\Omega)^2}{4\lambda} + \varphi_0\right][C(b'') + C(b_0'')] - \sin\left[\Omega t + \frac{(\omega_0-\Omega)^2}{4\lambda} + \varphi_0\right][S(b'') + S(b_0'')]\right\} \quad (9b)$$

where

$$
\left.
\begin{aligned}
a'' &= \left(\frac{2}{\pi\lambda}\right)^{1/3}\left(\lambda t - \frac{\omega_0 + \Omega}{2}\right) \\
b'' &= \left(\frac{2}{\pi\lambda}\right)^{1/3}\left(\lambda t - \frac{\omega_0 - \Omega}{2}\right) \\
a_0'' &= a_0' = \left(\frac{2}{\pi\lambda}\right)^{1/3}\left(\frac{\omega_0 + \Omega}{2}\right) \\
b_0'' &= b_0' = \left(\frac{2}{\pi\lambda}\right)^{1/3}\left(\frac{\omega_0 - \Omega}{2}\right)
\end{aligned}
\right\} \qquad (10b)
$$

Acceleration Transient

Let us suppose that the machine is started from rest with a constant acceleration 2λ. The equation of motion, during the acceleration, is given by (8*a*), where we must set $\omega_0 = 0$.

Let us call

$$t_0 = \frac{\Omega}{2\lambda}$$

the time taken by the machine to reach the angular velocity Ω equal to the natural frequency of the vibrating system.

Let us introduce the dimensionless ratio

$$\eta = \frac{t}{t_0} = \frac{2\lambda t}{\Omega}$$

that becomes equal to 1 when the instantaneous angular velocity $\dot{\varphi} = 2\lambda t$ is equal to the natural frequency Ω.

Let us also put

$$\rho = \frac{\Omega}{(2\pi\lambda)^{1/3}}$$

Introducing in Equation (8*a*) these dimensionless ratios, the equation of motion during acceleration becomes

$$\xi'(\eta) = \frac{\pi}{2}\rho[L' \sin\varphi_0 + N' \cos\varphi_0] \qquad (11a)$$

where

$$
\begin{aligned}
L' = {} & \{C[\rho(\eta+1)] - C[\rho]\} \sin \pi\rho^2\left(\eta + \frac{1}{2}\right) \\
& - \{S[\rho(\eta+1)] - S[\rho]\} \cos \pi\rho^2\left(\eta + \frac{1}{2}\right) \\
& + \{C[\rho(\eta-1)] + C[\rho]\} \sin \pi\rho^2\left(\eta - \frac{1}{2}\right) \\
& + \{S[\rho(\eta-1)] + S[\rho]\} \cos \pi\rho^2\left(\eta - \frac{1}{2}\right) \\
& + \frac{2}{\pi\rho}\left[\cos \pi\rho^2\eta - \cos\frac{\pi}{2}\rho^2\eta^2\right] \qquad (12a)
\end{aligned}
$$

$$
\begin{aligned}
N' = {} & \{C[\rho(\eta+1)] - C[\rho]\} \cos \pi\rho^2\left(\eta + \frac{1}{2}\right) \\
& + \{S[\rho(\eta+1)] - S[\rho]\} \sin \pi\rho^2\left(\eta + \frac{1}{2}\right) \\
& - \{C[\rho(\eta-1)] + C[\rho]\} \cos \pi\rho^2\left(\eta - \frac{1}{2}\right) \\
& + \{S[\rho(\eta-1)] + S[\rho]\} \sin \pi\rho^2\left(\eta - \frac{1}{2}\right) \\
& - \frac{2}{\pi\rho}\sin\frac{\pi}{2}\rho^2\eta^2 \qquad (13a)
\end{aligned}
$$

In Fig. 3, for $\rho = 5$ and $\varphi_0 = \pi/2$, line (*a*) represents the inertial disturbance $F(\eta)$ and (*b*) the response $\xi(\eta)$ to this disturbance, obtained by means of equation (11*a*).

For the same ρ, a given curve corresponds to each value of the initial phase angle φ_0. The envelope $\xi_i(\eta)$ of the family of curves $\xi(\eta, \varphi_0)$ is easily obtained by eliminating the angle φ_0 from (11*a*) and from

$$\frac{\pi}{2}\rho[L' \cos\varphi_0 - N' \sin\varphi_0] = 0$$

which is obtained by derivation of (11*a*) with respect to φ_0.

Thus we have

$$\xi_i'(\eta) = \frac{\pi}{2}\rho\Phi'(\eta) \qquad (14a)$$

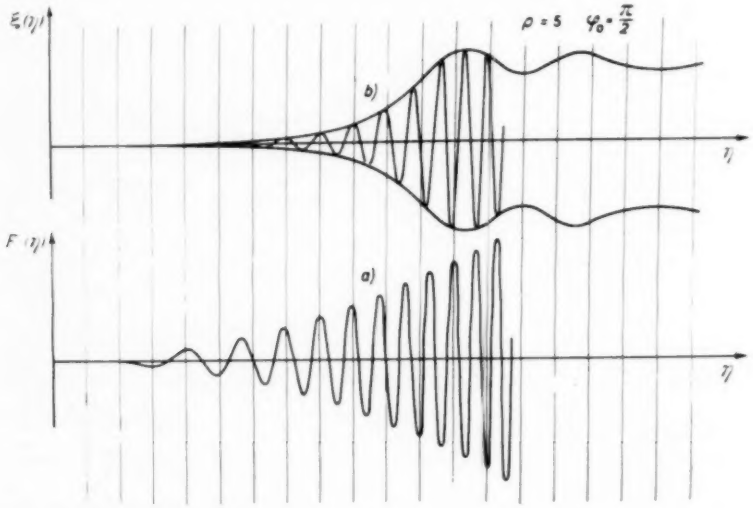

Fig. 3 Starting from rest: $\rho = 5$, $\varphi_0 = \pi/2$. (a) Exciting force, (b) vibration of the oscillator.

being

$$\Phi'(\eta) = (L'^2 + N'^2)^{1/2}$$

In Fig. 4 we have drawn the envelopes $\xi_s'(\eta)$, obtained by means of (14*a*), for four different values of ρ. The maximum amplitude of vibration is reached at time η greater than 1 and is therefore lagging behind the resonance point ($\eta = 1$).

The maximum value of the amplitude is

$$[\xi_s'(\eta)]_{max} = \frac{\pi}{2}\rho[\Phi'(\eta)]_{max}$$

In Fig. 5, for values of ρ between 5 and 12.5, we have drawn a few diagrams that represent the function $\Phi'(\eta)$ obtained by tabulating the expressions (12*a*) and (13*a*). Fresnel's integrals $C(z)$ and $S(z)$ are tabulated in [4].

We can observe that, within this range of ρ, the maximum values that Φ' can assume vary little, with a linear law, between 1.68 for $\rho = 5$ and 1.65 for $\rho = 12.5$.

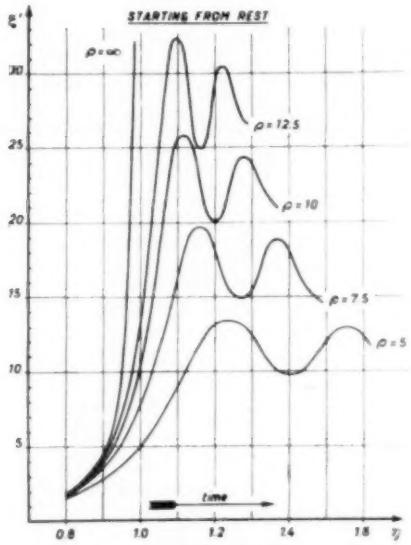

Fig. 4 Envelope of vibration during start from rest

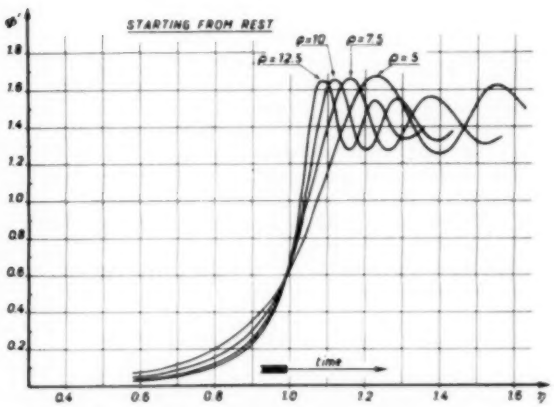

Fig. 5 Behavior of function $\Phi'(\eta)$ during start from rest

Therefore we can conclude that, at least in the range of values of greater technical interest, the maximum amplitude of vibration is, with a good approximation, proportional to ρ. Therefore during the acceleration, we may put

$$[\xi_s'(\eta)]_{max} = 2.615\rho = 3.7\frac{f_r}{\sqrt{\alpha}}$$

where f_r is the resonant frequency (in cps) of the vibrating system and α the angular acceleration of the machine in rounds per sec^2.

Deceleration Transient

Let us suppose that, before we begin to reduce its speed, i.e., for $t < 0$, the machine rotates in a steady state with a constant angular velocity ω_0.

Starting from the time $t = 0$ let us suppose that the machine reduces its speed with a constant angular deceleration equal to 2λ. The equation of the vibrations is then given by Equation (8*b*).

Let us call t_f the stopping time of the machine:

$$t_f = \frac{\omega_0}{2\lambda}$$

Let us define the dimensionless variable η by means of the ratio

$$\eta = \frac{t - t_f}{t_0} = \frac{2\lambda t - \omega_0}{\Omega}$$

Evidently η is still proportional to the time t and takes the value -1 when the instantaneous angular velocity coincides with the resonance, and the value 0 at the time corresponding to the full rest.

Let us define the new parameter:

$$\psi_0 = \frac{\omega_0^2}{4\lambda} + \varphi_0$$

function of the initial conditions for the deceleration transient and of the deceleration 2λ.

As a function of the new variable η, the equation of motion becomes

$$\xi(\eta) = \frac{1}{1 - \left(\frac{\omega_0}{\Omega}\right)^2}\left[\sin\varphi_0 \cos\pi\rho^2\left(\eta + \frac{\omega_0}{\Omega}\right) + \frac{\omega_0}{\Omega}\cos\varphi_0 \sin\pi\rho^2\left(\eta + \frac{\omega_0}{\Omega}\right)\right] + \sin\left(\frac{\pi}{2}\rho^2\eta^2 - \psi_0\right) + I'' \quad (8c)$$

The I'' takes the following expression:

$$I'' = \frac{\pi\rho}{2}\left\{\cos\left[\pi\rho^2\left(\eta - \frac{1}{2}\right) - \psi_0\right][C(a'') + C(a_0'')] - \sin\left[\pi\rho^2\left(\eta - \frac{1}{2}\right) - \psi_0\right][S(a'') + S(a_0'')] - \cos\left[\pi\rho^2\left(\eta + \frac{1}{2}\right) + \psi_0\right][C(b'') + C(b_0'')] - \sin\left[\pi\rho^2\left(\eta + \frac{1}{2}\right) + \psi_0\right][S(b'') + S(b_0'')]\right\} \quad (9c)$$

where

$$\left.\begin{aligned} a'' &= \rho\,(\eta - 1) \\ b'' &= \rho\,(\eta + 1) \\ a_0'' &= \rho\left(\frac{\omega_0}{\Omega} + 1\right) \\ b_0'' &= \rho\left(\frac{\omega_0}{\Omega} - 1\right) \end{aligned}\right\} \qquad (10c)$$

In the technical applications, and particularly in the case of machines elastically supported in order to obtain a vibration isolation, one often makes sure that the working speed is much larger than the natural frequency of the vibrating system.

In this case the ratio ω_0/Ω is great in comparison to unity; it is then clear that in equation (8c) we can neglect the first term of the second member since this, near the resonance, i.e., in the zone of greatest interest to us, takes values great in comparison to unity.

Separating then the terms $\sin\psi_0$ and $\cos\psi_0$ and observing that, for values of z great with respect to unity, Fresnel's functions $C(z)$ and $S(z)$ approach the limit 1/2, equation (8c) becomes

$$\xi''(\eta) = \frac{\pi\rho}{2}\,[L''\sin\psi_0 + N''\cos\psi_0] \qquad (11b)$$

where

$$\begin{aligned} L'' = {} & \left\{\frac{1}{2} + C[\rho(\eta-1)]\right\}\sin\pi\rho^2\left(\eta - \frac{1}{2}\right) \\ & + \left\{\frac{1}{2} + S[\rho(\eta-1)]\right\}\cos\pi\rho^2\left(\eta - \frac{1}{2}\right) \\ & + \left\{\frac{1}{2} + C[\rho(\eta+1)]\right\}\sin\pi\rho^2\left(\eta + \frac{1}{2}\right) \\ & - \left\{\frac{1}{2} + S[\rho(\eta+1)]\right\}\cos\pi\rho^2\left(\eta + \frac{1}{2}\right) \\ & - \frac{2}{\pi\rho}\cos\frac{\pi}{2}\,\rho^2\eta^2 \end{aligned} \qquad (12b)$$

$$\begin{aligned} N'' = {} & \left\{\frac{1}{2} + C[\rho(\eta-1)]\right\}\cos\pi\rho^2\left(\eta - \frac{1}{2}\right) \\ & - \left\{\frac{1}{2} + S[\rho(\eta-1)]\right\}\sin\pi\rho^2\left(\eta - \frac{1}{2}\right) \\ & - \left\{\frac{1}{2} + C[\rho(\eta+1)]\right\}\cos\pi\rho^2\left(\eta + \frac{1}{2}\right) \\ & - \left\{\frac{1}{2} + S[\rho(\eta+1)]\right\}\sin\pi\rho^2\left(\eta + \frac{1}{2}\right) \\ & + \frac{2}{\pi\rho}\sin\frac{\pi}{2}\,\rho^2\eta^2 \end{aligned} \qquad (13b)$$

Following the same procedure used in the case of acceleration, we can deduce the equation of the envelope of the family of curves that are obtained from (11b) by varying the parameter ψ_0.

We get

$$\xi_i''(\eta) = \frac{\pi}{2}\,\rho\Phi''(\eta) \qquad (14b)$$

being

$$\Phi''(\eta) = (L''^2 + N''^2)^{1/2}$$

In Fig. 6, for the same values of ρ, we have drawn the envelopes obtained by means of equation (14b). Also in this case we may see that the maximum amplitude of the vibration is lagging behind the resonance point.

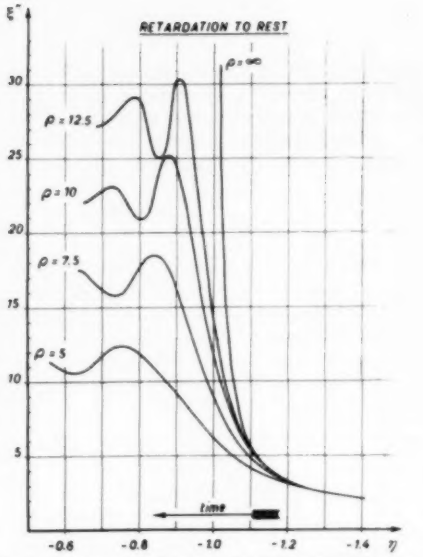

Fig. 6 Envelope of vibration during retardation to rest

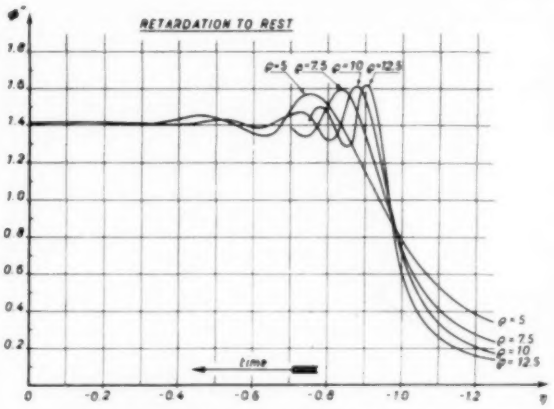

Fig. 7 Behavior of function $\Phi''(\eta)$ during retardation to rest

In Fig. 7 we have drawn the corresponding curves $\Phi''(\eta)$. We can observe that, as in the case of acceleration, the maximum values taken by this function Φ'', in the assumed range of the parameter ρ, vary little and go from the value 1.57 for $\rho = 5$, to the value 1.62 for $\rho = 12.5$. The average values of $[\Phi''(\eta)]_{max}$ may be taken equal to 1.595.

With a good approximation, for the technical application, we may then assume

$$[\xi_i''(\eta)]_{max} = 2.505\rho = 3.54\,\frac{f_r}{\sqrt{\alpha}}$$

where, as usual, f_r is the resonant frequency of the vibrating system in cps and α the angular deceleration of the machine in rounds per sec^2.

References

1 Th. Pöschl, "Das Anlaufen eines einfaches Schwingers," *Ingenieur-Archiv*, IV bd, 1933, p. 98.

2 F. M. Lewis, "Vibration During Acceleration Through a Critical Speed," JOURNAL OF APPLIED MECHANICS, TRANS. ASME, vol. 54, 1932, APM-54-24.

3 K. Klotter, "Einführung in die Technische Schwingungslehre," Springer-Verlag, Berlin, vol. 1, 1951, p. 382.

4 E. Jahnke and F. Emde, "Tables of Functions," Teubner-Verlag, Leipzig, 1938, p. 34.

5 W. Zeller, "Näherungsverfahren zur Bestimmung der beim Durchfahren der Resonanz auftretenden Höchstamplitude," MTZ, Jahrg. 10, 1949, p. 11.

6 F. Söchting, "Berechnung mechanischer Schwingungen," Springer-Verlag, Wien, 1951, p. 45.

7 G. D. McCann and R. R. Bennett, "Vibration of Multifrequency Systems During Acceleration Through Critical Speeds," JOURNAL OF APPLIED MECHANICS, vol. 16, TRANS. ASME, vol. 71 1949, p. 375.

Displacements and Stresses of a Laterally Loaded Semicircular Plate With Clamped Edges

W. H. JURNEY

Associate Professor,
Department of Mathematics,
Colorado School of Mines,
Golden, Colo.

A solution is obtained for the case of the clamped semicircular plate of constant thickness, subjected to a uniformly distributed normal load. The method employed is superposition of solutions for a circular plate with fixed edges. The technique involved could be extended to study more general types of loading of the clamped semicircular plate. Results are based on the assumption that the Kirchhoff, or small deflection, theory applies.

THE work in this paper arose in connection with the design of a large reinforced-concrete floor slab. The lack of a solution for a semicircular plate under the required conditions led to the present investigation. Computed stresses for the slab are given as an application of the theory. The notation for stresses and displacements is the same as that of Timoshenko[1] (except that θ replaces t, i.e., $M_{r\theta} = M_{rt}$, and so on). Fig. 1 shows the polar co-ordinate system used in relation to a circular plate sustaining a concentrated normal load at any point of the plate. Polar co-ordinates (r, θ) are for the point at which displacement, and so on, is to be computed.

Clamped Circular Plate Loaded Along a Diameter

The fundamental solution used as a starting point is the displacement of a circular plate loaded as in Fig. 1 and was solved in a series form by Clebsch,[2] also by Michell,[3] in finite form. The latter solution in polar co-ordinates is

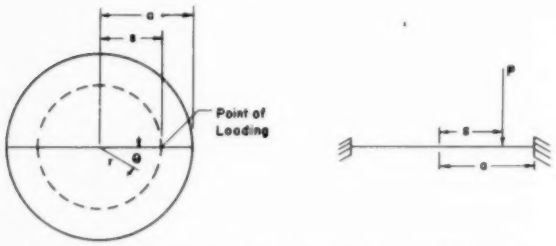

Fig. 1 Plan and cross section of a circular plate sustaining a concentrated load P

$$\frac{16\pi D w_1}{P} = R \log\left(\frac{a^2R}{S}\right) + \frac{(a^2 - r^2)(a^2 - s^2)}{a^2} \qquad (1)$$

where

$$R = r^2 - 2rs\cos\theta + s^2$$
$$S = a^4 - 2rsa^2\cos\theta + r^2s^2$$

The next step is to obtain the displacement w_2 of a circular plate loaded along the diameter $\theta = 0$ by an arbitrary load $f(s)$(force/-unit length), s as in Fig. 1. This is accomplished by replacing P in equation (1) by $f(s)ds$ and integrating the result with respect to s from $-a$ to $+a$ giving

$$16\pi D w_2 = \int_{-a}^{+a} \left\{ R \log\frac{(a^2R)}{S} + \frac{(a^2 - r^2)(a^2 - s^2)}{a^2} \right\} f(s)ds \qquad (2)$$

Stresses corresponding to displacements w_1 or w_2 can be computed as in the reference cited.[4] For the stresses corresponding to w_1, the following forms are convenient:

$$\frac{16\pi D\nabla^2 w_1}{P} = 4\log\left(\frac{a^2R}{S}\right) + 4\frac{(a^2 - s^2)(a^4 - r^2s^2)}{a^2S} = \frac{-16\pi}{P(1-\mu)}(M_r + M_\theta)$$

$$\frac{16\pi D}{P}\left(\frac{1}{r}\frac{\partial w}{\partial r} + \frac{1}{r^2}\frac{\partial^2 w}{\partial\theta^2}\right) = 2\,\mathrm{Log}\left(\frac{a^2R}{S}\right) + \frac{2s^2(a^2 - s^2)(a^2 - r^2)}{a^2S} + \frac{4s^2\sin^2\theta\,(a^2 - s^2)^2(a^2 - r^2)^2}{RS^2} = \frac{-16\pi}{P(1+\mu)}(M_\theta - \mu M_r) \qquad (3)$$

$$\frac{16\pi D}{P}\frac{\partial}{\partial r}\left(\frac{1}{r}\frac{\partial w}{\partial\theta}\right) = \frac{4s\sin\theta}{RS^2}(a^2 - s^2)^2(a^2 - r^2)[r(a^2 + s^2) - s\cos\theta(a^2 + r^2)] = \frac{16\pi M_{r\theta}}{(1-\mu)P}$$

$$\frac{-16\pi D}{P}\frac{1}{r}\frac{\partial\nabla^2 w}{\partial\theta} = 8s\sin\theta\,(a^2 - s^2)\left[\frac{a^2 - r^2}{RS} - \frac{(a^4 - r^2s^2)}{S^2}\right] = \frac{-16\pi Q_\theta}{P}$$

[1] S. Timoshenko, "Theory of Plates and Shells," McGraw-Hill Book Company, Inc., New York and London, 1940.

[2] Ibid., p. 266.

[3] J. H. Michell, "The Flexure of a Circular Plate," Proceedings of the London Mathematical Society, vol. 34, 1903, p. 225.

For presentation at the Summer Conference of the Applied Mechanics Division, Troy, N. Y., June 18–20, 1959, of THE AMERICAN SOCIETY OF MECHANICAL ENGINEERS.

Discussion of this paper should be addressed to the Secretary, ASME, 29 West 39th Street, New York, N. Y., and will be accepted until July 20, 1959, for publication at a later date. Discussion received after the closing date will be returned.

NOTE: Statements and opinions advanced in papers are to be understood as individual expressions of their authors and not those of the Society. Manuscript received by ASME Applied Mechanics Division, September 6, 1955; final draft received September 12, 1958. Paper No. 59—APM-3.

[4] Loc. cit.,[1] p. 259.

$$\frac{-16\pi D}{P}\frac{\partial\nabla^2 w}{\partial\theta} = 8(a^2 - s^2)\left[r(a^2 + s^2) - \frac{s\cos\theta(a^2 + r^2) - Rs\cos\theta}{RS} - \frac{2a^2rs^2\sin^2\theta}{S^2}\right] = \frac{-16\pi Q_r}{P}$$

Another solution used, due to Poisson,[5] is that for a circular plate subjected to uniform lateral pressure and clamped at the circular edge. Denoting the deflection in the direction of the pressure q by w_3, the expression for this quantity is

$$w_3 = \frac{q}{64D}(a^2 - r^2)^2 \tag{4}$$

The stresses associated and computed by use of (3) are

$$M_r = \frac{q}{16}[(a^2 - 3r^2) + \mu(a^2 - r^2)]$$

$$M_\theta = \frac{q}{16}[a^2 - r^2 + \mu(a^2 - 3r^2)]$$

$$M_{r\theta} \equiv 0 \tag{5}$$

$$Q_r = -\frac{qr}{2}$$

$$Q_\theta \equiv 0$$

Positive M_r and M_θ are such as to produce compression in top elements of plate where displacement is positive downward.

Uniformly Loaded Semicircular Plate With Fixed Edges

It is now desired to determine the distributed load $f(s)$ along a diameter which will produce the same displacement at every point of the diameter as that due to uniformly distributed pressure over the entire plate so that the two applied oppositely will result in the given diameter being fixed. This is accomplished by equating the displacement of equation (2), for $\theta = 0$, to the displacement w_3 of equation (4);

$$\frac{q}{64D}(a^2 - r^2)^2 = \frac{1}{16\pi D}\int_{-a}^{+a}\left\{(r^2 - 2rs + s^2)\log\left[\frac{a^2r^2 - 2rs + s^2)}{a^4 - 2rsa^2 + r^2s^2}\right] + \frac{(a^2 - r^2)(a^2 - s^2)}{a^2}\right\}f(s)ds \tag{6}$$

[5] Loc. cit., p. 58.

or letting $r = a\rho$ and $s = a\lambda$

$$(1 - \rho^2)^2 = \frac{4}{\pi aq}\int_{-1}^{+1}\left[(\rho - \lambda)^2\log\left(\frac{\rho - \lambda}{1 - \rho\lambda}\right)^2 + (1 - \rho^2)(1 - \lambda^2)\right]f(a\lambda)d\lambda \tag{7}$$

It is convenient to let

$$\frac{4f(a\lambda)}{\pi aq} = g(\lambda)$$

then

$$(1 - \rho^2)^2 = \int_{-1}^{+1}\left[(\rho - \lambda)^2\log\left(\frac{\rho - \lambda}{1 - \rho\lambda}\right)^2 + (1 - \rho^2)(1 - \lambda^2)\right]g(\lambda)d\lambda \tag{8}$$

is the integral equation for the determination of the required loading. All attempts to solve (8) in finite form or by a suitable series were unsuccessful. Apparently some new transcendental function is involved. A definite integral solution was obtained which seems to be of no value from a computational viewpoint.

Since no satisfactory solution of the integral equation in closed form could be obtained, an approximate solution was found as follows:

Equation (8) was replaced by a system of linear equations according to the trapezoidal rule of integration. Successive division of the interval of integration into 8 and 16 intervals was used for the purpose of checking accuracy. The system of equations in each case was solved for the function $g(\lambda)$-values at the division points of the interval of integration. The results are given in Table 1.

Stresses for the semicircular plate were approximated as follows:

1 $g(\lambda)$ was taken as $1.25(1 - \lambda^2)$. Indications, from differences and $g(\lambda)$-values, are that three-figure accuracy is obtained in this replacement.

2 In the stress relations (3) P was replaced by $f(s)ds$ and the results integrated from $-a$ to $+a$ with respect to s; i.e., from -1 to $+1$ with respect to λ (s replaced by $a\lambda$).

Forms for computing stress components are given in Tables 2, 3, 4, 5, and 6.

Table 1 Approximate values for the function g(λ)

λ	0	0.125	0.25	0.375	0.500	0.625	0.750	0.875	1.00
$g(\lambda)$	1.266	1.249	1.197	1.108	0.978	0.797	0.554	0.218	0.00

Table 2 Moments due to loading f(s) for θ = 0 deg

ρ	0.00	0.25	0.50	0.75	1.00
$\frac{-16(M_r + M_\theta)}{(1 + \mu)a^2q}$	−3.111	−2.815	−1.722	−0.102	+2.000
$\frac{-32(M_\theta - \mu M_r)}{(1 - \mu^2)a^2q}$	−4.254	−3.922	−2.972	−1.539	0.000

Table 3 Moments due to loading f(s) for θ = 90 deg

ρ	0.00	0.25	0.50	0.75	1.00
$\frac{-16(M_r + M_\theta)}{(1 + \mu)a^2q}$	−3.111	−1.465	−0.350	+0.474	+1.042
$\frac{-32(M_\theta - \mu M_r)}{(1 - \mu^2)a^2q}$	−2.000	−1.722	−1.205	−0.559	0.000

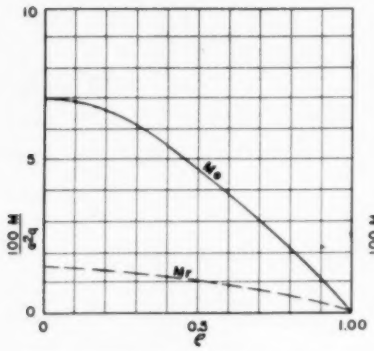

Fig. 2 Moments M_r and M_θ for $\theta = 0$ deg

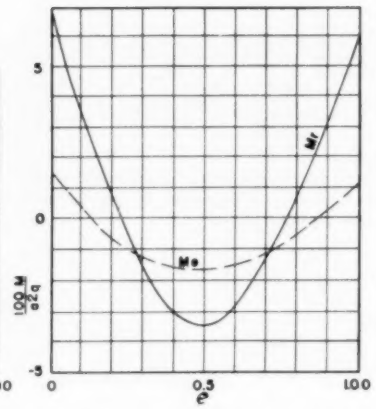

Fig. 3 Moments M_r and M_θ for $\theta = 90$ deg

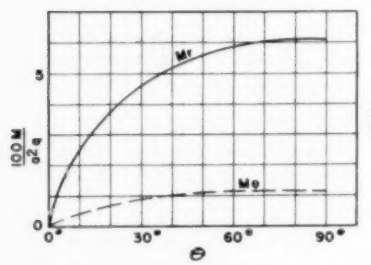

Fig. 4 Moments M_r and M_θ for $\rho = 1$

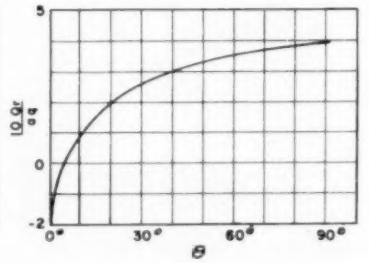

Fig. 5 Shear Q_r for $\rho = 1$

Table 4 Moments due to loading $f(s)$ for $\rho = 1$

θ, deg	0	30	60	90
$\frac{-16(M_r + M_\theta)}{(1+\mu)a^2q}$	+2.000	+1.406	+1.120	+1.042
$\frac{-32(M_\theta - \mu M_r)}{(1-\mu^2)a^2q}$	0.000	0.000	0.000	0.000

Table 5 Shear Q_r for loading $f(s)$ for $\rho = 1$

θ, deg	0	30	60	90
$\frac{Q_r}{aq}$	−0.625	−0.206	−0.135	−0.120

Table 6 Moments due to loading q (q positive down)

ρ	0.000	0.25	0.50	0.75	1.00
$\frac{-16M_r}{a^2q}$	$1+\mu$	$\frac{13+15\mu}{16}$	$\frac{1+3\mu}{4}$	$\frac{-11+7\mu}{16}$	−2.000
$\frac{-16M_\theta}{a^2q}$	$1+\mu$	$\frac{15+13\mu}{16}$	$\frac{3+\mu}{4}$	$\frac{7-11\mu}{16}$	-2μ

An Application

As has been stated, the present semicircular plate problem arose in connection with the design of a floor slab. The walls of the structure involved were conceived as transmitting the load supported by the floor slab in such a way as to fix the slab at its boundary. An upward hydrostatic load q was to act on the bottom of the slab. For this example the following data were assumed:

a = 24 ft
h = thickness of plate = 7.5 ft
μ = Poisson's ratio = 0.2
E = Young's modulus = 3,000,000 psi
q = 9068 psf

The stress components for loading $f(s)$ along a diameter and those for loading q (uniform pressure) were combined to give the stress components for the semicircular plate with fixed edges under uniform pressure. The results are given in Figs. 2, 3, 4, and 5.

The remaining stress components on the boundary of the semicircular plate and for $\theta = 90$ for the most part vanish; i.e., if

$\theta = 0: M_{r\theta} \equiv Q_\theta \equiv 0$
$\theta = 90: M_{r\theta} = 0$
$\rho = 1: M_{r\theta} = 0$

That the results are reasonably accurate is indicated by the following features:

1 The circular plate as a whole is in vertical load equilibrium.
2 The semicircular plate part is in vertical load equilibrium.
3 Moments at a fixed boundary behave properly.

Each of these hold to the order of accuracy indicated earlier. By item 3 is meant that M_2 is a moment across a fixed boundary, and M_1 is a moment in a perpendicular direction; then

$$M_1 = \mu M_2$$

Direct Determination of Stresses in Plane Elasticity Problems Based on the Properties of Isostatics[1]

PERICLES S. THEOCARIS

Visiting Research Associate,
Illinois Institute of Technology,
Chicago, Ill.
Mem. ASME

An experimental method is developed for the calculation of stresses in plane elasticity problems. The method consists substantially in determining a function of the complex variable representing the field of isostatics. This function has a convenient form so that the boundary conditions can be expressed by simple relations. From the isostatics, which are traced experimentally, the differential parameter of first order h can be calculated all over the field. The components of stresses are expressed by relations depending on boundary conditions and the parameter h. The method is applied to two particular problems of plane elasticity and a comparison of the results obtained by this method and by analytic methods is provided.

In this paper a new method is set forth for the determination of stresses in plane elasticity fields. The method consists in determining a function $\zeta(z)$ of the complex variable $z = (x + iy)$ representing the field of the isostatics. For the choice of this function the boundary conditions of the examined field are used, so that the relations expressing these conditions are simple and can be deduced easily from the foregoing function.

The directions of isostatics are known at every point of a free boundary and of boundaries subjected to purely normal loads. Furthermore, in the most common cases of loadings the isostatics neighboring a boundary along which shear stresses are present can be accepted as coincident with this boundary for all practical purposes. Thus all the boundaries can be divided into two groups each of them belonging to one type of isostatics. This determination of isostatics along the boundaries makes it possible to establish the function $\zeta(z)$.

The representation of the field of isostatics by a function of the complex variable $z = (x + iy)$ enables the correlation of this field with analogous physical fields defined by the same function of the complex variable. We use, among other analogous fields, the electric potential field in a thin and homogeneous conducting plate for the tracing of isostatics. This choice is made because of the simplicity of the experimental conditions and the great accuracy obtained by using the electrical analogy. The graphited-paper method, as it has been already developed [10],[2] provides an easy means for this purpose. In this case only a small number of electrodes is necessary for the tracing of one of two families of isostatics and, furthermore, this simplifies the experimental procedure. The tracing of isostatics allows the determination of the value of differential parameter of first order h at every point in the field. The equations expressing the stresses have been transformed to a form depending only on the boundary conditions of the problem, the differential parameter of first order h and the semi-sum of stresses σ. On the other hand, the function σ is expressed in terms of the same parameter h and the boundary conditions and, therefore, it can be determined by integration over the field. From this function σ the function $\zeta(z)$ can be found and the stress components can be deduced easily.

[1] The major part of this paper, in particular the experimental work, was carried out at the Athens National Technical University during the academic year 1956–1957.

Contributed by the Applied Mechanics Division and presented at the Annual Meeting, New York, N. Y., November 30–December 5, 1958, of THE AMERICAN SOCIETY OF MECHANICAL ENGINEERS.

Discussion of this paper should be addressed to the Secretary, ASME, 29 West 39th Street, New York, N. Y., and will be accepted until July 10, 1959, for publication at a later date. Discussion received after the closing date will be returned.

NOTE: Statements and opinions advanced in papers are to be understood as individual expressions of their authors and not those of the Society. Manuscript received by ASME Applied Mechanics Division, January 17, 1958. Paper No. 58—A-43.

[2] Numbers in brackets designate References at end of paper.

Nomenclature

$\zeta(z)$ = an analytic function of the complex variable $z = (x + iy)$

h = differential parameter of first order at an isometric network of curves $\xi = \xi(x, y) =$ const and $\eta = \eta(x, y) =$ const

ds_ξ, ds_η = elementary arcs contained between curves $\xi(x, y) =$ const and $\eta(x, y) =$ const, respectively

σ_ξ, σ_η = values of principal stresses

σ_x, σ_y, τ_{xy} = components of stresses in Cartesian co-ordinates

$2\sigma = (\sigma_\xi + \sigma_\eta)$ = sum of principal stresses

$2\tau = (\sigma_\xi - \sigma_\eta)$ = difference of principal stresses

$H = -\tau/h^2$

H_x, H_y = partial derivatives of H in a system of Cartesian co-ordinates

μ = an analytic function expressed by equation:

$$\mu = \mu(x, y) = -[a + bx + cy + d(x^2 + y^2)]$$

φ = electric potential of a plane potential field in a system of curvilinear co-ordinates $s = s(x, y)$ and $n = n(x, y)$

ψ = conjugate function of φ in the same field

$\frac{dI}{dS}$ = density of current in the same field

γ = conductivity of medium in the same field

The method is applied to two illustrative examples concerning well-known problems of plane elasticity. The results obtained are compared with the results derived from existing analytical solutions in order to illustrate the accuracy of the method.

Finally, it should be mentioned that the domain of application of the properties of physical fields defined by the function $\zeta(z)$ to the fields of isostatics is limited and it cannot contain, in general, all the problems of plane elasticity. This is based on the fact that the field of isostatics, related to a given problem is not susceptible *a priori* to representation by a function $\zeta(z)$. But in these cases it is possible to obtain experimentally, by a judicious choice of the function $\zeta(z)$, an approximate solution of the problem and the approximation can be calculated to any desired degree of accuracy.

Therefore we can determine real practical solutions which are defined by a finite number of terms containing only elementary functions. The numerical calculus for the solution of different problems of plane elasticity by this method is relatively simple in comparison with the classical methods based on the knowledge of the Airy stress function or the complex function $[(\lambda + 2\mu)\Delta + i2\mu\omega]$ [1]. Furthermore, the approximation obtained by this method is sufficiently good from a practical standpoint and the results obtained are shown to be in good agreement with the theoretical or other experimental solutions.

Theoretical Study of Equations of Plane Elasticity

We consider a system of Cartesian co-ordinates x, y and a system of orthogonal curvilinear co-ordinates $\xi = \xi(x, y)$ and $\eta = \eta(x, y)$ related to the first system, Fig. 1. Moreover, we suppose that the two families of curves $\xi = \text{const}$ and $\eta = \text{const}$ belong to an isometric network of curves, that is, that their differential parameters of first order h and h_1 are equal [6, 9]. These parameters are given by the relations [9]

$$h^2 = h_1^2 = \left(\frac{\partial \xi}{\partial x}\right)^2 + \left(\frac{\partial \xi}{\partial y}\right)^2 = \left(\frac{\partial \eta}{\partial x}\right)^2 + \left(\frac{\partial \eta}{\partial y}\right)^2 \quad (1)$$

The Lamé-Maxwell equations of equilibrium in curvilinear co-ordinates can be written as follows [1, 9]:

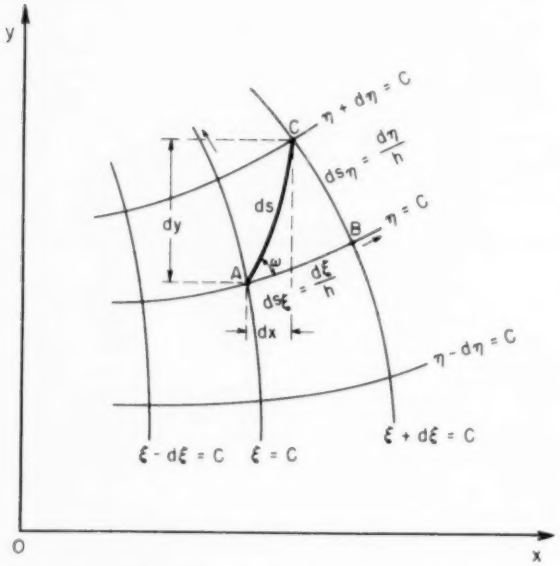

Fig. 1 Differential elements in an isometric co-ordinate system

$$\frac{\partial \sigma_\xi}{\partial \xi} - \frac{\sigma_\xi - \sigma_\eta}{h}\frac{\partial h}{\partial \xi} = 0$$
$$\frac{\partial \sigma_\eta}{\partial \eta} + \frac{\sigma_\xi - \sigma_\eta}{h}\frac{\partial h}{\partial \eta} = 0 \quad (2)$$

If we call

$$2\sigma = (\sigma_\xi + \sigma_\eta)$$
$$2\tau = (\sigma_\xi - \sigma_\eta) \quad (3)$$

then

$$\sigma_\xi = (\sigma + \tau)$$
$$\sigma_\eta = (\sigma - \tau) \quad (3a)$$

and Equations (2) become

$$\frac{\partial(\sigma + \tau)}{\partial \xi} - \frac{2\tau}{h}\frac{\partial h}{\partial \xi} = 0$$
$$\frac{\partial(\sigma - \tau)}{\partial \eta} + \frac{2\tau}{h}\frac{\partial h}{\partial \eta} = 0 \quad (4)$$

or

$$\frac{\partial \sigma}{\partial \xi} = -\frac{\partial \tau}{\partial \xi} + \frac{2\tau}{h}\frac{\partial h}{\partial \xi}$$
$$\frac{\partial \sigma}{\partial \eta} = \frac{\partial \tau}{\partial \eta} - \frac{2\tau}{h}\frac{\partial h}{\partial \eta} \quad (5)$$

By dividing both parts by h^2 we obtain

$$\frac{1}{h^2}\frac{\partial \sigma}{\partial \xi} = -\frac{1}{h^2}\frac{\partial \tau}{\partial \xi} + \frac{2\tau}{h^3}\frac{\partial h}{\partial \xi}$$
$$\frac{1}{h^2}\frac{\partial \sigma}{\partial \eta} = \frac{1}{h^2}\frac{\partial \tau}{\partial \eta} - \frac{2\tau}{h^3}\frac{\partial h}{\partial \eta} \quad (6)$$

The second parts of these equations are the derivatives of the term τ/h^2 with respect to co-ordinates ξ and η, respectively. Thus we have the relations [4]

$$\frac{\partial \sigma}{\partial \xi} = -h^2\frac{\partial}{\partial \xi}\left(\frac{\tau}{h^2}\right), \quad \frac{\partial \sigma}{\partial \eta} = h^2\frac{\partial}{\partial \eta}\left(\frac{\tau}{h^2}\right) \quad (7)$$

But we have also that [6, 7]

$$ds_\xi = \frac{d\xi}{h}, \quad ds_\eta = \frac{d\eta}{h} \quad (7a)$$

where ds_ξ and ds_η are the elementary arcs along the curves $\eta = \text{const}$ and $\xi = \text{const}$, respectively. Then the relations (7) become

$$\frac{\partial \sigma}{\partial \xi} = -h\frac{\partial}{\partial s_\xi}\left(\frac{\tau}{h^2}\right), \quad \frac{\partial \sigma}{\partial \eta} = h\frac{\partial}{\partial s_\eta}\left(\frac{\tau}{h^2}\right) \quad (8)$$

If we call

$$H = -\frac{\tau}{h^2} \quad (9)$$

then relations (8) become

$$\frac{\partial \sigma}{\partial \xi} = h\frac{\partial H}{\partial s_\xi}, \quad \frac{\partial \sigma}{\partial \eta} = -h\frac{\partial H}{\partial s_\eta}$$

We represent now with h_x and h_y the components of h in a system of Cartesian co-ordinates and H_x and H_y the partial derivatives of H in the same system. Then we have

$$\frac{\partial \sigma}{\partial \xi} = H_x h_x + H_y h_y \quad (10)$$

$$\frac{\partial \sigma}{\partial \eta} = H_x h_y - H_y h_x \qquad (10)$$
(Cont.)

On the other hand, the function $\sigma = (\sigma_\xi + \sigma_\eta)/2$ is a harmonic function of the complex variable

$$\xi(x, y) + i\eta(x, y) = \zeta(x + iy) \equiv \zeta(z)$$

Thus we have that its derivative

$$\left(\frac{\partial \sigma}{\partial \xi} - i\,\frac{\partial \sigma}{\partial \eta}\right)$$

is also a function of the same complex variable. Herewith

$$f(z) = \frac{\partial \sigma}{\partial \xi} - i\,\frac{\partial \sigma}{\partial \eta} \qquad (11)$$

If in this equation we replace the values of $\partial\sigma/\partial\xi$ and $\partial\sigma/\partial\eta$ with those given in Equations (10) we obtain

$$f(z) = (H_x h_x + H_y h_y) - i(H_x h_y - H_y h_x)$$

or

$$f(z) = (H_x + iH_y)(h_x - ih_y) \qquad (11a)$$

But we have also that

$$\frac{\partial \zeta}{\partial z} = (h_x - ih_y)$$

Thus

$$f(z) = (H_x + iH_y)\,\frac{\partial \zeta}{\partial z} \qquad (12)$$

From Equation (12) it becomes evident that the function $(H_x + iH_y)$ must also be a harmonic function of the complex variable $z = (x + iy)$ and, according to the Cauchy-Riemann conditions, we have

$$\frac{\partial H_x}{\partial x} = \frac{\partial H_y}{\partial y} \quad \text{and} \quad \frac{\partial H_x}{\partial y} = -\frac{\partial H_y}{\partial x} \qquad (13)$$

From the second of the above relations we deduce that

$$\frac{\partial H_x}{\partial y} = -\frac{\partial H_y}{\partial x} = 0 \qquad (14)$$

From relations (13) and (14) and also by taking into account the relation (9), it can be proved that the shear stresses are equal to zero along any curve of the isometric network of orthogonal curves $\xi(x, y) = \text{const}$ and $\eta(x, y) = \text{const}$. *These curves, therefore, represent the isostatics.*

Now we can express the function H as follows:

$$H = \mu(x, y)$$

where $\mu(x, y)$ is an analytic function given by the equation

$$\mu = \mu(x, y) = -[a + bx + cy + d(x^2 + y^2)] \qquad (15)$$

where a, b, c, and d are independent arbitrary constants, the last three of which must not be simultaneously equal to zero.

The difference of principal stresses 2τ can be expressed by

$$2\tau = -2\mu h^2 = 2(a + bx + cy + dr^2)\left|\frac{\partial \zeta}{\partial z}\right|^2 \qquad (16)$$

Since the function σ is harmonic, it can be the real component of a complex function $S = S(x + iy)$ in the Cartesian co-ordinates (x, y) or $S = S(\xi + i\eta)$ in the isometric co-ordinates (ξ, η). Thus the relation (11) can be written

$$f(z) = \frac{\partial S}{\partial \zeta} = \frac{\partial S}{\partial z}\,\frac{\partial z}{\partial \zeta} \qquad (17)$$

or

$$\sigma = R\cdot\left\{\int_{z_0}^{z} f(z)\,\frac{\partial \zeta}{\partial z}\,dz + p\right\} \qquad (18)$$

where $R\cdot$ represents the real part of the function $\int_{z_0}^{z} f(z)\,\frac{d\zeta}{dz}\,dz$ and p is the constant of the integration. Taking into account Equation (12), Equation (18) can be written as follows:

$$\sigma = R\cdot\left\{\int_{z_0}^{z} (H_x + iH_y)\left(\frac{\partial \zeta}{\partial z}\right)^2 dz + p\right\} \qquad (19)$$

But from Equation (15) we have, by taking the complex derivative of H in the x, y-system,

$$H_x + iH_y = -[b + ic + 2dz]$$

Herewith, Equation (19) becomes

$$\sigma = -R\cdot\left\{\int_{z_0}^{z} (2dz + b + ic)\left(\frac{d\zeta}{dz}\right)^2 dz + p\right\} \qquad (20)$$

From Equations (3*a*) and (16) we can easily deduce that the principal stresses σ_ξ and σ_η along the isostatics $\eta = \text{const}$ and $\xi = \text{const}$ can be expressed by

$$\begin{aligned} \sigma_\xi &= (\sigma - h^2\mu) \\ \sigma_\eta &= (\sigma + h^2\mu) \end{aligned} \qquad (21)$$

where the values of σ and μ are taken from Equations (20) and (15), respectively.

Equation (20) can be written also in the form of a derivative

$$\frac{\partial \sigma}{\partial z} = -\left\{(2dz + b + ic)\left(\frac{\partial \zeta}{\partial z}\right)^2\right\} \qquad (22)$$

and from Equations (7) we also have

$$\begin{aligned} \frac{\partial \sigma}{\partial \xi} &= h^2\,\frac{\partial \mu}{\partial \xi} \\ \frac{\partial \sigma}{\partial \eta} &= -h^2\,\frac{\partial \mu}{\partial \eta} \end{aligned} \qquad (23)$$

We now express the stresses in Cartesian co-ordinates. We have that

$$\tau_{xy} = \tau \sin 2(\xi, x)$$

$$(\sigma_x - \sigma_y) = \frac{2\tau_{xy}}{\tan 2(\xi, x)}$$

and

$$\sin 2(\xi, x) = \frac{2}{h^2}\,\frac{\partial \xi}{\partial x}\,\frac{\partial \xi}{\partial y}$$

$$\tan 2(\xi, x) = \frac{2\,\dfrac{\partial \xi}{\partial x}\,\dfrac{\partial \xi}{\partial y}}{\left(\dfrac{\partial \xi}{\partial x}\right)^2 - \left(\dfrac{\partial \xi}{\partial y}\right)^2}$$

Then

$$\begin{aligned} (\sigma_x - \sigma_y) &= -2\mu\left[\left(\frac{\partial \xi}{\partial x}\right)^2 - \left(\frac{\partial \xi}{\partial y}\right)^2\right] \\ \tau_{xy} &= -2\mu\,\frac{\partial \xi}{\partial x}\,\frac{\partial \xi}{\partial y} \end{aligned} \qquad (24)$$

From these equations one can deduce that

$$\sigma_x = \left\{\sigma - \mu\left[\left(\frac{\partial\xi}{\partial x}\right)^2 - \left(\frac{\partial\xi}{\partial y}\right)^2\right]\right\}$$

$$\sigma_y = \left\{\sigma + \mu\left[\left(\frac{\partial\xi}{\partial x}\right)^2 - \left(\frac{\partial\xi}{\partial y}\right)^2\right]\right\} \qquad (25)$$

$$\tau_{xy} = -2\mu\,\frac{\partial\xi}{\partial x}\,\frac{\partial\xi}{\partial y}$$

where

$$\mu = \mu(x, y) = -[a + bx + cy + d(x^2 + y^2)]$$

By taking the function

$$G(z) = \frac{\partial\xi}{\partial y} - i\,\frac{\partial\xi}{\partial x} = -ih(z)$$

one obtains

$$G^2(z) = -h^2(z) = \left(\frac{\partial\xi}{\partial y}\right)^2 - \left(\frac{\partial\xi}{\partial x}\right)^2 - 2i\left(\frac{\partial\xi}{\partial x}\right)\left(\frac{\partial\xi}{\partial y}\right)$$

which is also an analytic function. We can express the relations given in Equations (25) in terms of the function $[-h^2(z)]$ so that we have

$$\sigma_x = \sigma + \mu R\cdot[-h^2(z)]$$

$$\sigma_y = \sigma - \mu R\cdot[-h^2(z)] \qquad (26)$$

$$\tau_{xy} = 2\mu I\cdot[-h^2(z)]$$

where $R\cdot$ and $I\cdot$ represent the real and imaginary parts of the function $[-h^2(z)]$, respectively.

The components of the stresses expressed in Equations (21) or (25) contain five arbitrary constants a, b, c, d, and p. The constants b, c, d are geometric constants. A variation of constant d means a change of the unit of measure. Variation of the geometric constants b, c means a parallel displacement of the system of curves which does not alter the geometric relationship of isostatics. Letting the constant p equal zero corresponds to a superposition on the principal system of stresses of a secondary system characterized by the stresses:

$$\sigma_x = \pm p, \quad \sigma_y = \pm p, \quad \tau_{xy} = 0$$

which alters neither the form nor the geometric relationship of the isostatics.

If we place the constant a equal to zero, the harmonic system of stresses

$$\sigma_x = -aR\cdot[h^2(z)] \quad \sigma_y = +aR\cdot[h^2(z)] \quad \tau_{xy} = -aI\cdot[h^2(z)]$$

is superimposed on the principal one without changing the form and the geometric relationship of the isostatics.

The constants b, c, d cannot be simultaneously equal to zero. In the case where $b = c = d = 0$ the function σ becomes a constant, as it can be easily found from relation given as Equation (20), and the stresses σ_x, σ_y, τ_{xy} are reduced to the following:

$$\sigma_x = a\left[\left(\frac{\partial\xi}{\partial x}\right)^2 - \left(\frac{\partial\xi}{\partial y}\right)^2\right] + \sigma$$

$$\sigma_y = 2\sigma - \sigma_x$$

$$\tau_{xy} = 2a\,\frac{\partial\xi}{\partial x}\,\frac{\partial\xi}{\partial y}$$

It has already been shown that the curves $\zeta(z)$ can always represent families of isostatics in plane elasticity problems. The inverse property is not always valid. This means that there exist some fields of isostatics not represented by families of curves $\zeta(z)$.

We can express generally the stresses in a plane field by the relations [5]:

$$\sigma_x = -r^2R\cdot[(F(z)] + R\cdot\left[\int_{z_0}^{z} zF(z)dz + p\right] - R\cdot[N(z)]$$

$$\sigma_y = r^2R\cdot[F(z)] + R\cdot\left[\int_{z_0}^{z} zF(z)dz + p\right] + R\cdot[N(z)]$$

$$\tau_{xy} = r^2I\cdot[F(z)] + I\cdot[N(z)] \qquad (27)$$

where the functions $F(z)$ and $N(z)$ are two arbitrary analytic functions.

This field of stresses can be considered as a superposition of two plane fields of stresses of which one corresponds only to the function $F(z)$ and the other only to the function $N(z)$. Each of the two fields alone can be represented by a field of isostatics. We can choose for the two fields as complex functions of the differential parameter of first order h the following:

$$h_1(z) = i[F(z)]^{1/3} \qquad h_2(z) = i[N(z)]^{1/3}$$

Because of the quadratic form of these relations we cannot generally represent the principal field of stresses as a superposition of these two analytic fields.

The necessary and sufficient condition for the principal plane field of stresses to be represented by an isometric network of isostatics is that, between the functions $F(z)$ and $N(z)$, the following relation is valid:

$$N(z) = \frac{z^2(b - ic + 2az)}{(2dz + b + ic)}\,F(z) \qquad (28)$$

where the constants b, c, d correspond to function $F(z)$.

We try now to express an easy criterion for the validity of this condition [7, 8]. It has already been found that along isostatics

$$h = \frac{d\xi}{ds_\xi} = \frac{d\eta}{ds_\eta} \qquad (29)$$

Equation (29) means that the differential parameter of first order is inversely proportional to the corresponding distances between isostatics.

Along free boundaries where $\eta = \text{const}$ the principal stress σ_η vanishes. Thus from the first of the Equations (2), we have

$$\frac{\partial\sigma_\xi}{\partial\xi} - \frac{\sigma_\xi}{h}\,\frac{\partial h}{\partial\xi} = 0 \qquad (30)$$

or, dividing Equation (30) by h, we obtain

$$\frac{1}{h}\,\frac{\partial\sigma_\xi}{\partial\xi} - \frac{\sigma_\xi}{h^2}\,\frac{\partial h}{\partial\xi} = 0$$

which can be written as follows:

$$\frac{\partial}{\partial\xi}\left(\frac{\sigma_\xi}{h}\right) = 0 \qquad (31)$$

Equation (31) gives

$$\frac{\sigma_\xi}{h} = \lambda$$

where λ is a constant and

$$\sigma_\xi = \lambda h \qquad (32)$$

Thus along free boundaries the only existing stress is proportional to the differential parameter of first order h.

On the other hand, we have from Equation (16)

$$(\sigma_\xi - \sigma_\eta) = 2\tau = -2h^2(a + bx + cy + dr^2)$$

and, along free boundaries where η = const,

$$\sigma_\xi = 2h^2\mu \tag{33}$$

From Equations (32) and (33)

$$h = \frac{\lambda}{2\mu}$$

and

$$\sigma_\xi = \frac{\alpha}{2\mu} \tag{34}$$

where α is a new constant.

If the existing stress along a free boundary of a plane elastic field fulfills this condition given by Equation (34), then the network of isostatics of this field can be represented by an isometric network of curves (z) = const and also this condition is sufficient.

Every random selection of the five afore-mentioned constants on which the stresses depend generally yields two different solutions to the problem, one of which is the solution of isostatics. By a proper choice of the harmonic function $\zeta(z)$ and its five constants, which can be determined from the particular shape and form and the boundary conditions of a given problem, we can find a solution approaching the exact solution to any desired degree by using the general formulas given by Equations (20), (21), and (25), provided that the values of the parameter h can be calculated or measured throughout the field of the problem.

Application of Properties of Isostatics to Experimental Determination of Stresses

The orthogonal curves $\zeta(z)$ = const previously defined can represent a number of characteristic families of curves in different physical fields which are analogous among themselves.

We set forth, among others, two important analogous fields, i.e., the field of isostatics in plates elastically deformed in their plane and the electric potential field in a thin and homogeneous conducting sheet. The analogy existing between these two fields has already been examined in a previous paper [10], and it has been found that

$$\left|\frac{d\bar{I}}{ds}\right| = \gamma \left|\frac{d\varphi}{dn}\right| = \gamma\left[\left(\frac{\partial\varphi}{\partial x}\right)^2 + \left(\frac{\partial\varphi}{\partial y}\right)^2\right]^{1/2} = \gamma h \tag{35}$$

where $d\bar{I}/ds$ is the density of current, γ the conductivity of the medium, φ the potential of the electric field, and h the differential parameter of first order of isostatics.

On the other hand, it is also known that

$$h = \left|\frac{\partial\zeta(z)}{\partial z}\right| = \frac{\Delta\xi}{\Delta s_\xi} = \frac{\Delta\eta}{\partial s_\eta} \tag{36}$$

and for the analogous electric potential field

$$h' = \frac{\Delta\varphi}{\Delta n} = \frac{\Delta\psi}{\Delta s}$$

where φ and ψ represent the families of equipotentials and flow lines in the corresponding electric field. By always taking the distances $\Delta\xi$ and $\Delta\eta$ or $\Delta\varphi$ and $\Delta\psi$ constant we note that the values of h and h' are inversely proportional to the sides of networks of the curves ξ, η and φ, ψ.

As the two physical systems are analogous, we can obtain the isostatics of a plane elastic field by tracing the equipotentials in the electric field for various values of $\Delta\varphi$ = const. From these equipotentials the value of the parameter h can be determined for points equidistant from two adjacent isostatics according to the relation

$$h = \frac{k}{\Delta s_\eta} \tag{37}$$

where k is a constant and Δs_η is the perpendicular distance between the two equipotentials. For nonequidistant points the value of h is obtained by linear interpolation of the values of the two neighbor equidistant points.

The value of the constant k can be determined by application of the relations (7a) and (37) to a suitable point on an isostatic. As such points we choose the intersections of axes of symmetry in the cases of symmetrical loadings or points situated in those parts of the isostatics parallel to one of the principal axes of the model [10].

The two analogous systems must have identical boundary conditions. The directions of isostatics are generally known at every point of the boundaries of the field. Indeed, it is well known that free boundaries coincide with an isostatic. The same occurs for loaded boundaries with normal loads. For loaded boundaries along which shear stresses are present, these boundaries do not belong to an isostatic. However, in the most common cases of loading, these boundaries are very close to the neighboring isostatics and the two lines can be considered as coincident for all practical purposes. For this reason all the boundaries of a model can be separated into two groups, of which each belongs to one of the two families of isostatics. Along each of these trajectories one of the two parameters ξ and η is constant. Therefore the electric potential, which simulates one of the two parameters ξ and η, must have a constant value on the corresponding parts of the boundaries.

In order to trace one family of isostatics the two extreme isostatics of this family must be determined. If the examined field does not contain isotropic points or if it contains isotropic points on the boundaries, then the parts of the boundaries belonging to each trajectory must be separated. This can be done easily by a proper examination of the shape of the field and of the existing loading. Isotropic points on the boundaries are points of separation of isostatics. These points correspond either to points of transition from one isostatic to its orthogonal, or to isolated points belonging to one type of isostatics surrounded by the two extreme isostatics of the other type [2, 3].

Isotropic points, for which $\sigma_\xi = \sigma_\eta$, can be determined from Equations (21). For these points the following relation is valid.

$$h^2[a + bx + cy + d(x^2 + y^2)] = 0 \tag{38}$$

From this relation we can determine the place of the existing isotropic points all over the field and thus separate the boundaries into two types, each of which belongs to one family of isostatics.

When isotropic points or isotropic lines occur in the interior of the field, and these lines or points determine the extreme isostatics of both families or the transition of isostatics from one family to the other, then these points or lines must be taken into account when tracing the isostatics.

For the construction of isostatics we apply the electrical analogy method using the graphited paper[3] as the conducting surface for the tracing of equipotentials. The technique used for the preparation of models as well as the electrical arrangement for the tracing of equipotentials has been described already in a previous paper [10].

Illustrative Examples

In order to evaluate the method developed in the foregoing, it

[3] Sold under the trade name "Teledeltos"

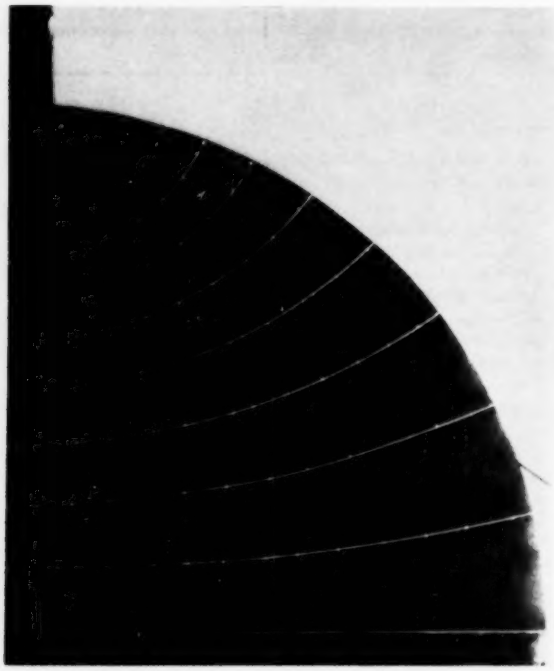

Fig. 2 One of families of isostatics for a disk under diametral compression

will be applied to two different problems. The first is that of a circular disk subjected to diametral compression. Because of the symmetry of the problem, each of the models consists of a quarter of a circle. Fig. 2 shows the one family of isostatics obtained using this method. Next, the principal stresses along the y-axis, perpendicular to the applied loads, are calculated.

For this purpose the y-axis is divided into ten uniform intervals to establish a set of equally spaced points. From the isostatic adjacent to y-axis we determine the parameter h for these ten points.

Consider now the Equations (21), (22), and (25): in the special case of the circular disk subjected to diametral compression the coefficients b and c are equal to zero due to the symmetry of the problem. Thus Equations (23) become:

$$\frac{\partial \sigma}{\partial \xi} = -h^2 \frac{\partial}{\partial \xi}[a + dr^2] = -2dh^2 r \frac{dr}{d\xi}$$
$$\frac{\partial \sigma}{\partial \eta} = h^2 \frac{\partial}{\partial \eta}[a + dr^2] = 2dh^2 r \frac{dr}{d\eta} \tag{39}$$

On the circumferential boundary of the disk we have that $r = R = \text{const}$ and $\sigma_\xi = 0$. Herewith, $\partial\sigma/\partial\xi = 0$ and $\sigma = \text{const}$.

But the parameter h is not constant on this boundary, as it can be easily checked from the variable distance of isostatics along the boundary. Therefore along this boundary we have that $\sigma = 0$ and $a + dr^2 = 0$ for $r = R$. Thence $a = -dR^2$ and the equations of the stresses become

$$\sigma_\xi = -dh^2(R^2 - r^2) + \sigma$$
$$\sigma_\eta = 2\sigma - \sigma_\xi \tag{40}$$
$$\sigma_x = -dh^2(R^2 - r^2)\cos 2\theta + \sigma$$
$$\sigma_y = 2\sigma - \sigma_x \tag{41}$$
$$\tau_{xy} = -dh^2(R^2 - r^2)\sin 2\theta$$

and

$$\frac{\partial \sigma}{\partial z} = -2dz\left(\frac{\partial \xi}{\partial z}\right)^2$$

or

$$\frac{\partial \sigma}{\partial x} = -2dh^2[x\cos 2\theta + y \sin 2\theta]$$
$$\frac{\partial \sigma}{\partial y} = 2dh^2[y\cos 2\theta - x \sin 2\theta] \tag{42}$$

where the angle θ is the angle made by the normal of the curve ξ and the x-axis. With the exception of the constant d, the stresses can be determined in the case where we know the angle θ and the parameter h at every point. The angle θ can be measured easily graphically from the isostatic pattern and the parameter h is inversely proportional to the normal distances of the corresponding curves ξ at the points under study.

The function σ can be calculated by graphical integration by applying the Equations (39).

Along the y-axis of the disk the Equations (40) and (41) become

$$\sigma_x = \sigma_\xi = -d(R^2 - r^2)h^2 + \sigma$$
$$\sigma_y = \sigma_\eta = 2\sigma - \sigma_\xi \tag{43}$$
$$\frac{\partial \sigma}{\partial y} = -2dh^2 y$$

The calculations are arranged in the manner presented in Table 1. The constant d is determined by the fact that the resultant of σ_x stresses along the y-axis must be equal to the applied load P. The stresses calculated by the analytic method are also presented in Table 1. The accuracy of the method can be established by comparing the experimental and analytical results.

Table 1 Values of principal stresses along y-axis

Point	Δs_z	kh	h	h^2	y	h^2y	$\sigma = 2\int h^2 y dy$	$(R^2 - \rho^2)$	$(R^2 - \rho^2)h^2$	σ_ξ/d	σ_η/d	σ_ξ	σ_η	Theoretical values σ_ξ	Theoretical values σ_η
0	3.00	1.672	1.306	1.700	0	0	0.865	1.00	1.700	−2.56	0.84	−6.02	1.98	−6.00	2.00
0.1	3.04	1.650	1.286	1.650	0.1	0.165	0.852	0.99	1.633	−2.49	0.79	−5.86	1.86	−5.85	1.91
0.2	3.10	1.612	1.258	1.585	0.2	0.317	0.807	0.96	1.522	−2.33	0.71	−5.48	1.67	−5.42	1.69
0.3	3.22	1.556	1.210	1.470	0.3	0.441	0.733	0.91	1.339	−2.08	0.60	−4.89	1.41	−4.74	1.38
0.4	3.42	1.462	1.140	1.300	0.4	0.520	0.642	0.84	1.092	−1.74	0.45	−4.09	1.06	−3.93	1.05
0.5	3.66	1.367	1.064	1.132	0.5	0.567	0.532	0.75	0.850	−1.39	0.32	−3.27	0.74	−3.14	0.71
0.6	3.97	1.260	0.983	0.965	0.6	0.578	0.419	0.64	0.618	−1.04	0.20	−2.45	0.47	−2.34	0.43
0.7	4.36	1.145	0.892	0.794	0.7	0.556	0.306	0.51	0.405	−0.71	0.10	−1.67	0.23	−1.62	0.23
0.8	4.77	1.048	0.818	0.664	0.8	0.530	0.198	0.36	0.239	−0.44	0.04	−1.04	0.09	−0.99	0.09
0.9	5.27	0.950	0.741	0.550	0.9	0.493	0.095	0.19	0.105	−0.20	0.01	−0.47	0.02	−0.43	0.02
1.0	5.76	0.870	0.678	0.458	1.0	0.458	0	0	0	0	0	0	0	0	0

NOTE: Values of constants: $k = 0.780$, $d = 0.425$.

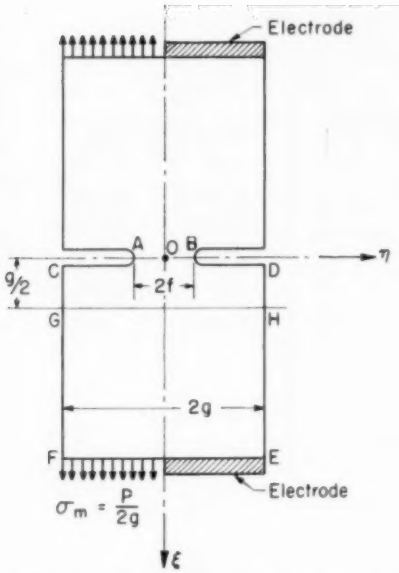

Fig. 3 Sketch showing deeply grooved strip in tension with locations of electrodes in model

As a second illustrative example we calculate the stresses at the longitudinal edges and a transverse section of a strip with deep grooves subjected to an axial load, Fig. 3. The minimum transverse section of the strip is taken equal to one third of its width. The models for tracing the isostatics need only represent half of the strip because of symmetry. The two transverse edges of the strip belong to the one family of isostatics and the longitudinal edges to the other.

Therefore each of these two types of boundary contains the supply electrodes for the tracing of each of the two orthogonal families of isostatics. Fig. 4 shows one family of isostatics. The determination of stresses is accomplished in the following manner: Because of symmetry the terms in y and r^2 of the Equations (20) to (23) are equal to zero; therefore the components of stresses are expressed as follows:

$$\sigma_\xi = h^2(a + bx) + \sigma$$
$$\sigma_\eta = 2\sigma - \sigma_\xi \tag{44}$$

$$\sigma_x = (a + bx)\left[\left(\frac{\partial \xi}{\partial x}\right)^2 - \left(\frac{\partial \xi}{\partial y}\right)^2\right] + \sigma$$
$$\sigma_y = 2\sigma - \sigma_x \tag{45}$$
$$\tau_{xy} = 2(a + bx)\,\frac{\partial \xi}{\partial x}\,\frac{\partial \xi}{\partial y}$$

and

$$\frac{\partial \sigma}{\partial z} = -b\left(\frac{\partial \xi}{\partial z}\right)^2$$

or

$$\frac{\partial \sigma}{\partial x} = -b\left[\left(\frac{\partial \xi}{\partial x}\right)^2 - \left(\frac{\partial \xi}{\partial y}\right)^2\right], \quad \frac{\partial \sigma}{\partial y} = -2b\,\frac{\partial \xi}{\partial x}\,\frac{\partial \xi}{\partial y} \tag{46}$$

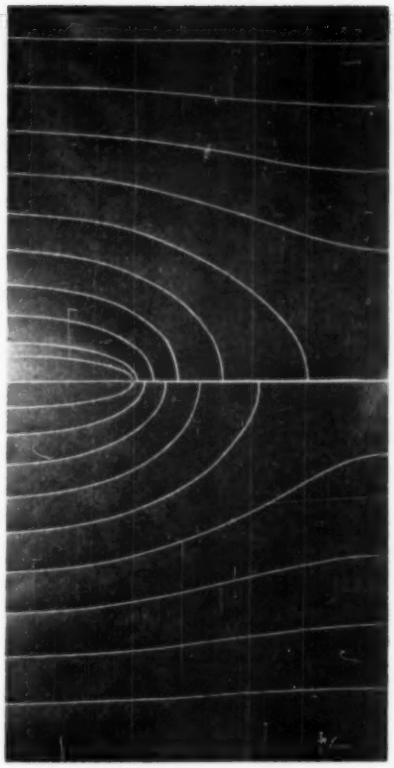

Fig. 4 Family of isostatics for a deeply grooved strip in tension. Isostatics are symmetrical with respect to grooved section. The shown isostatics on two parts of strip are of different parameters in order to avoid crowding of curves.

If, again, θ is the angle of the normal at a point of an isostatic and the ξ-axis we have

$$\left(\frac{\partial \xi}{\partial x}\right)^2 - \left(\frac{\partial \xi}{\partial y}\right)^2 = h^2 \cos 2\theta$$
$$2\,\frac{\partial \xi}{\partial x}\,\frac{\partial \xi}{\partial y} = h^2 \sin 2\theta \tag{47}$$

Along the grooved edges of the strip where $\theta = \pi/2$, we obtain

$$\frac{\partial \sigma}{\partial y} = -bh^2 \sin 2\theta = 0 \tag{48}$$

or $\sigma = \text{const}$. On the other hand, we have for this part of the boundary that the stresses $\sigma_\eta = 0$, or

$$\sigma_\eta = -h^2(a + bx) + \sigma = 0 \tag{49}$$

But, since h is not constant along this part of the boundary (which can be easily proved from the varying distances between the isostatics) it is required that: $a = 0$, $\sigma = 0$, and $\sigma_\xi = 0$ along the grooved parts of the boundary of the strip.

Thus Equations (44) and (45) are reduced to the following:

$$\sigma_\xi = bh^2x + \sigma$$
$$\sigma_\eta = -bh^2x + \sigma \tag{50}$$

$$\sigma_x = bh^2x \cos 2\theta + \sigma$$
$$\sigma_y = -bh^2x \cos 2\theta + \sigma \tag{51}$$
$$\tau_{xy} = bh^2x \sin 2\theta$$

Table 2 Values of semi-sum σ and stress σ_x along longitudinal edges of strip

$x = \frac{\xi}{2g}$	Δs_η	$kh = \frac{1}{2\Delta s_\eta}$	h	h^2	h^2x	$\sigma = \int h^2 dx$	$\frac{1}{b}\sigma_x = (h^2x - \int h^2 dx)$	σ_x	σ_x (theoretical values)
0	—	0	0	0	0	0	0	0	0
0.1	1.122	0.446	0.332	0.110	0.011	0.005	0.006	0.021	0.028
0.2	0.650	0.770	0.574	0.329	0.066	0.025	0.041	0.141	0.282[a]
0.3	0.472	1.061	0.791	0.626	0.188	0.073	0.115	0.398	
0.4	0.421	1.189	0.887	0.788	0.315	0.144	0.171	0.590	
0.5	0.397	1.259	0.938	0.880	0.440	0.228	0.212	0.731	0.745
0.6	0.387	1.291	0.963	0.928	0.557	0.318	0.239	0.825	
0.7	0.380	1.316	0.981	0.962	0.673	0.412	0.261	0.900	
0.8	0.375	1.333	0.993	0.987	0.790	0.510	0.280	0.966	
0.9	0.374	1.339	0.999	0.998	0.898	0.609	0.289	1.000	
1.0	0.373	1.342	1.000	1.000	1.000	0.710	0.290	1.000	0.980

[a] This value corresponds to the point of boundary with $x = 0.25$.
NOTE: Values of constants: $k = 0.745$, $b = 0.290$.

Table 3 Values of stress σ_x along section GH of deeply grooved strip

$y = \frac{\eta}{2g}$	Δs_η	$kh = \frac{1}{2\Delta s_\eta}$	h	h^2	2θ	$\cos 2\theta$	$\sin 2\theta$	$h^2 \cos 2\theta$	$h^2 \sin 2\theta$	$\int h^2 \sin 2\theta dy$	$xh^2 \cos 2\theta$	σ_x	σ_x (theory)
0	0.292	1.710	1.274	1.620	0°	1	0	1.620	0	−0.114	0.405	1.788	1.775
0.1	0.301	1.661	1.238	1.532	16°	0.961	0.276	1.471	0.423	−0.100	0.368	1.614	1.600
0.2	0.333	1.530	1.120	1.257	32°	0.848	0.530	1.064	0.666	−0.041	0.266	1.060	1.200
0.3	0.403	1.241	0.925	0.856	29° 30′	0.870	0.492	0.744	0.420	0.011	0.187	0.608	0.765
0.4	0.500	1.000	0.747	0.558	16° 40′	0.958	0.287	0.535	0.160	0.039	0.134	0.328	0.410
0.5	0.535	0.935	0.696	0.490	0°	1	0	0.490	0	0.045	0.123	0.269	0.282

NOTE: Values of constants: $K = 0.745$, $b = 0.290$.

and

$$\frac{\partial \sigma}{\partial x} = -bh^2 \cos 2\theta$$
$$\frac{\partial \sigma}{\partial y} = bh^2 \sin 2\theta \qquad (52)$$

Along the longitudinal boundary $\overline{DE}$ of the strip we have

$$\frac{\partial \sigma}{\partial x} = -bh^2 \qquad (53)$$

It is already known that the value of σ at the point D is equal to zero. By starting from this point and by graphical integration we can determine from Equation (53) the values of σ along the boundary DE. The value of constant k, necessary to find the values of h, is determined at point E where the value of h must be equal to unity.[4] On the other hand, the value of constant b is determined from the value of the only existing stress σ_x along $\overline{DE}$ which must be equal to the applied tension $\sigma_m = P/2g$. The values of σ as well as those of the stress σ_x along the longitudinal boundaries of the strip, are tabulated in Table 2.

Values of stress σ_x along a transverse section GH at a distance $g/2$ from the y-axis are calculated next. The corresponding values of σ_x and σ at the points G and H are taken from Table 2. The values along this line are tabulated in Table 3. The same table also contains the values of the stress σ_x calculated analytically. The discrepancies presented are rather small and both groups of values are practically identical.

Acknowledgments

The author is indebted to Prof. George M. Petropoulos, Director of the Electrical Measurements and High Voltage Laboratory of Athens National Technical University, for permission to carry out in his laboratory the experimental work contained in this paper. He wishes also to express his appreciation to Dr. August J. Durelli, Professor at the Illinois Institute of Technology, for reading the paper and for his valuable advice.

[4] This results from the Equation (7a).

References

1 A. E. H. Love, "A Treatise on the Mathematical Theory of Elasticity," Cambridge at the University Press, fourth edition, 1934, p. 643.

2 A. Pirard, "La Photo-élasticité," Dunod Editor, Paris, France, first edition, 1947, p. 420.

3 M. M. Frocht, "Photoelasticity," John Wiley & Sons, Inc., New York, N. Y., vol. 1, 1948, pp. 411, 198–213, and 287–322.

4 P. Neményi, "Stromlinien und Hauptspannungstrajectorien," *Zeitschrift für angewandte Mathematik und Mechanik*, Band 13, Heft 5, 1933, pp. 364–366.

5 U. Wegner, "Über du Zusammenhang von Stromungs und Spannungsproblemen." *Ingenieur-Archiv*, Band 5, Heft 6, 1934, pp. 449–469.

6 G. Lamé, "Leçons sur les Coordonnées Curvilignes et leurs Diverses Applications," Mallet-Bachelet, Paris, France, 1859, pp. 18–56.

7 H. Neuber, "Die Randbedingungen der Hauptspannungs-Stromlinien," *Zeitschrift für angewandte Mathematik und Mechanik*, Band 15, Heft 6, 1935, pp. 374–375.

8 A. J. Durelli, "Determination of Stresses on Free Boundaries by Means of Isostatics," Proceedings of the 15th Semi-Annual Eastern Photoelasticity Conference, June, 1942, pp. 32–42.

9 M. Bricas, "La Théorie de l'Elasticité Bi-dimensionnelle," Pyrsos, Athens, 1936, pp. 90–96.

10 P. S. Theocaris, "On an Electrical Analogy Method for the Separation of Principal Stresses Along Stress Trajectories," *Proceedings of the Society for Experimental Stress Analysis*, vol. 14, no. II, 1957, pp. 11–20.

Stresses in a Stretched Slab Having a Spherical Cavity

CHIH-BING LING

Director,
Aeronautical Research Laboratory, Taichung;
Acting Director,
Institute of Mathematics, Academia Sinica,
Taipei, China.

This paper presents an analytic solution for an infinite slab having a symmetrically located spherical cavity when it is stretched by an all-round tension. The required stress function is constructed by combining linearly two sets of periodic biharmonic functions and a biharmonic integral. The sets of biharmonic functions are derived from two fundamental functions specially built up for the purpose. The arbitrary functions involved in the biharmonic integral are first adjusted to satisfy the boundary conditions on the surfaces of the slab by applying the Hankel transform of zero order. Then the stress function is expanded in spherical co-ordinates and the boundary conditions on the surface of the cavity are satisfied by adjusting the coefficients of superposition attached to the sets of biharmonic functions. The resulting system of linear equations is solved by the method of successive approximations. The solution is finally illustrated by numerical examples for two radii of the cavity.

THE stresses in an infinite circular cylinder having a spherical cavity when the cylinder is under torsion at its ends or under tension along its axis have been investigated by the author in two previous papers [1, 2].[1] In the present paper the stresses in a slab of infinite size having a spherical cavity when it is stretched by an all-around tension will be investigated. The cavity is assumed to be located symmetrically between the surfaces of the slab. The theory of symmetrical strain for solids of revolution [3] is used in the analysis.

The required stress function is constructed by combining linearly two sets of periodic biharmonic functions and a biharmonic integral. The boundary conditions on the boundary at infinity are automatically satisfied. The boundary conditions on the surfaces of the slab are satisfied by adjusting the arbitrary functions involved in the biharmonic integral. The stress function is then expanded in spherical co-ordinates and the boundary conditions on the surface of the cavity are satisfied by adjusting the coefficients of superposition attached to the sets of biharmonic functions. The resulting system of linear equations is solved by a method of successive approximations.

The method of solution is first described. Then the solution is illustrated by numerical examples for two radii of the cavity. In particular, the maximum stresses in the slab are computed to show the effect of the nearby boundary on the cavity.

Method of Solution

Denote as usual the cylindrical and spherical co-ordinates of a point by (r, θ, z) and (ρ, ϕ, θ), respectively. They are connected with each other by

$$z = \rho \cos \phi, \quad r = \rho \sin \phi \tag{1}$$

[1] Numbers in brackets designate References at end of paper.

Contributed by the Applied Mechanics Division and presented at the Annual Meeting, November 30–December 5, 1958, New York, N. Y., of THE AMERICAN SOCIETY OF MECHANICAL ENGINEERS.

Discussion of this paper should be addressed to the Secretary, ASME, 29 West 39th Street, New York, N. Y., and will be accepted until July 10, 1959, for publication at a later date. Discussion received after the closing date will be returned.

NOTE: Statements and opinions advanced in papers are to be understood as individual expressions of their authors and not those of the Society. Manuscript received by ASME Applied Mechanics Division, January 30, 1958. Paper No. 58—A-45.

For convenience, r, z, and ρ henceforth will be regarded as dimensionless quantities referring to a typical length a.

Consider an infinite slab of thickness $2a$ having a spherical cavity of radius λa located symmetrically between the surfaces of the slab. Let the origin of the co-ordinates be at the center of the cavity and the z-axis normal to the surfaces of the slab. The surfaces of the slab are thus represented by $z = \pm 1$ and the surface of the cavity by $\rho = \lambda$. In the absence of the cavity, a uniform all-around tension of T per unit area acting in the plane of the slab would be given by a *basic* stress function.

$$\chi_0 = \frac{Ta^2}{6(1+\nu)} \{2(2-\nu)z^3 - 3(1-\nu)zr^2\} \tag{2}$$

where ν is Poisson's ratio. The method of satisfying the boundary conditions when the cavity is present is to construct an *auxiliary* stress function χ_1 by using suitable biharmonic functions such that it gives no traction on the surfaces of the slab and at the same time gives no stress on the boundary at infinity. This is added to χ_0 so that the required stress function is given by

$$\chi = \chi_0 + \chi_1 \tag{3}$$

The remaining boundary conditions on the surface of the cavity are satisfied by adjusting the coefficients of superposition attached to the biharmonic functions. The biharmonic functions have singularities at the origin.

The Auxiliary Stress Function

The auxiliary stress function will be constructed by combining linearly two sets of periodic biharmonic functions which are derived by differentiation from two fundamental functions U_0 and V_0 to be defined below. The function U_0 and V_0 have a series of singularities along the z-axis.

First, consider a function U_0 defined as follows:

$$U_0 = -\frac{1}{2} \log \left\{ \frac{1+\mu}{1-\mu} \prod_{p=1}^{\infty} \frac{(1+\mu_p)(1+\mu_{-p})}{(1-\mu_p)(1-\mu_{-p})} \exp\left(-\frac{2z}{p}\right) \right\}, \tag{4}$$

where $\mu = \dfrac{z}{\rho} = \cos \phi, \quad \mu_p = \dfrac{z-2p}{(\rho^2 - 4p\rho\mu + 4p^2)^{1/2}}$ (5)

It can be shown readily that the function satisfies the harmonic

equation $\nabla^2 U_0 = 0$, where ∇^2 stands for the Laplace operator

$$\frac{\partial^2}{\partial r^2} + \frac{1}{r}\frac{\partial}{\partial r} + \frac{\partial^2}{\partial z^2} \quad \text{or} \quad \frac{1}{\rho^2}\frac{\partial}{\partial \rho}\left(\rho^2 \frac{\partial}{\partial \rho}\right) + \frac{1}{\rho^2}\frac{\partial}{\partial \mu}\left\{(1-\mu^2)\frac{\partial}{\partial \mu}\right\} \quad (6)$$

Again, the function possesses logarithmic singularities along the z axis at the points $z = 0, \pm 2, \pm 4, \ldots$, and in fact, represents a series of *centers of radial tension* along the z axis at these points. The exponential factor $\exp(-2z/p)$ is introduced to render the function convergent.

Define a set of harmonic functions U_s by

$$U_s = \frac{(-1)^s}{(s-1)!}\frac{\partial^s U_0}{\partial z^s} \quad (7)$$

each of which is periodic in z of period 2 and has singularities along the z axis at the points $z = 0, \pm 2, \pm 4, \ldots$. The functions U_{2s}, save U_0, vanish identically on the planes $z = \pm 1, \pm 3, \pm 5, \ldots$.

The preceding definition gives, when $s = 1$,

$$U_1 = \frac{1}{\rho} + \sum_{p=1}^{\infty}\left\{\frac{1}{(\rho^2 - 4p\rho\mu + 4p^2)^{1/2}} + \frac{1}{(\rho^2 + 4p\rho\mu + 4p^2)^{1/2}} - \frac{1}{p}\right\} \quad (8)$$

which may be expanded near the origin in the form

$$U_1 = \frac{1}{\rho} + \sum_{n=1}^{\infty}\frac{\omega_{2n+1}}{2^{2n}}\rho^{2n}P_{2n}(\mu), \quad (9)$$

where P_n is the Legendre function of the first kind of order n and

$$\omega_n = 1 + \frac{1}{2^n} + \frac{1}{3^n} + \frac{1}{4^n} + \ldots. \quad (10)$$

With the aid of the relations [4]

$$\frac{\partial}{\partial z}\{\rho^n P_n(\mu)\} = n\rho^{n-1}P_{n-1}(\mu), \qquad \frac{\partial}{\partial z}\left\{\frac{P_n(\mu)}{\rho^{n+1}}\right\} = -(n+1)\frac{P_{n+1}(\mu)}{\rho^{n+2}}, \quad (11)$$

the subsequent functions take the following forms for $s \geq 1$,

$$U_{2s} = \frac{P_{2s-1}(\mu)}{\rho^{2s}} - \sum_{n=0}^{\infty}{}^{2n+1}\alpha_{2s}\rho^{2n+1}P_{2n+1}(\mu),$$
$$U_{2s+1} = \frac{P_{2s}(\mu)}{\rho^{2s+1}} + \sum_{n=0}^{\infty}{}^{2n}\alpha_{2s+1}\rho^{2n}P_{2n}(\mu) \quad (12)$$

where

$${}^{n}\alpha_s = \binom{n+s-1}{s-1}\frac{\omega_{n+s}}{2^{n+s-1}} \quad (13)$$

For uniformity in notation, the two initial functions may be rewritten as follows:

$$U_0 = -\frac{1}{2}\log\frac{1+\mu}{1-\mu} - \sum_{n=1}^{\infty}{}^{2n+1}\alpha_0\rho^{2n+1}P_{2n+1}(\mu),$$
$$U_1 = \frac{1}{\rho} + \sum_{n=1}^{\infty}{}^{2n}\alpha_1\rho^{2n}P_{2n}(\mu) \quad (14)$$

where, in particular,

$${}^{n}\alpha_0 = \frac{\omega_n}{n2^{n-1}} \quad (15)$$

It is noted that the expansion of U_0 can be obtained readily from that of U_1 by integration with respect to z.

Next consider a function V_0 defined as follows:

$$V_0 = \mu + \sum_{p=1}^{\infty}(\mu_p + \mu_{-p}) = \frac{z}{\rho} + \sum_{p=1}^{\infty}\left\{\frac{z-2p}{(\rho^2 - 4p\rho\mu + 4p^2)^{1/2}} + \frac{z+2p}{(\rho^2 + 4p\rho\mu + 4p^2)^{1/2}}\right\} \quad (16)$$

This function can be shown to satisfy the biharmonic equation $\nabla^4 V_0 = 0$.

Define a set of biharmonic functions V_s by

$$V_s = (-1)^s\frac{2s+1}{(s+1)!}\frac{\partial^s V_0}{\partial z^s} \quad (17)$$

each of which is also periodic in z of period 2 and has singularities long the z-axis at the points $z = 0, \pm 2, \pm 4, \ldots$. The functions V_{2s} for $s \geq 1$ vanish identically on the planes $z = \pm 1, \pm 3, \pm 5, \ldots$, while V_0 becomes a constant on each such plane, which is different on a different plane.

The function V_0 may be expanded near the origin in the form:

$$V_0 = P_1(\mu) + \sum_{n=1}^{\infty}{}^{2n+1}\beta_0\rho^{2n+1}\{P_{2n-1}(\mu) - P_{2n+1}(\mu)\}, \quad (18)$$

and the subsequent functions in the forms:

$$V_{2s} = \frac{1}{\rho^{2s}}\{P_{2s+1}(\mu) - P_{2s-1}(\mu)\} + \sum_{n=1}^{\infty}{}^{2n+1}\beta_{2s}\rho^{2n+1}\{P_{2n-1}(\mu) - P_{2n+1}(\mu)\}, \quad (19)$$

$$V_{2s+1} = \frac{1}{\rho^{2s+1}}\{P_{2s+2}(\mu) - P_{2s}(\mu)\} - \sum_{n=1}^{\infty}{}^{2n}\beta_{2s+1}\rho^{2n}\{P_{2n-2}(\mu) - P_{2s}(\mu)\}$$

where

$${}^{n}\beta_s = \frac{2s+1}{2n-1}\binom{n+s-1}{s+1}\frac{\omega_{n+s}}{2^{n+s-1}} \quad (20)$$

It will be seen later that the two sets of biharmonic functions U_{2s} and V_{2s} thus defined give no tangential stress on the surfaces of the slab in question. This will simplify considerably the subsequent analysis.

Now, construct the required auxiliary stress function as follows:

$$\chi_1 = Ta^3\sum_{s=0}^{\infty}(A_{2s}U_{2s} + B_{2s}V_{2s}) + Ta^3\int_0^{\infty}\{\psi_1(k)\sinh kz + \psi_2(k)z\cosh kz\}J_0(kr)\,dk \quad (21)$$

where A_{2s} and B_{2s} are coefficients of superposition; the factor Ta^3 being introduced to render the coefficients dimensionless. J_n are the Bessel functions of the first kind of order n and ψ_n are arbitrary functions. The function thus constructed satisfies the biharmonic equation. The integral is added to annul the tractions on the surfaces of the slab derived from the preceding series of functions. The function is odd in z or μ as required by symmetry. Besides, it satisfies the conditions of single-valuedness of stresses and displacements throughout the slab.

With the aid of the relation

$$\nabla^2 V_s = -2(2s+1)U_{s+2} \tag{22}$$

the following normal and tangential stresses on the surfaces $z = \pm 1$ are derived:

$$\begin{aligned}
\sigma_z &= \frac{1}{a^3}\left[\frac{\partial}{\partial z}\left\{(2-\nu)\nabla^2 - \frac{\partial^2}{\partial z^2}\right\}\chi_1\right]_{z=\pm 1} \\
&= T\left[2A_0U_2 + \sum_{s=1}^{\infty} 2s(2s+1)(2s+2)A_{2s}U_{2s+2}\right. \\
&\quad + \sum_{s=0}^{\infty}(2s+2)(4s+1)B_{2s}\left\{2(2-\nu)U_{2s+2}\right. \\
&\quad \left.\left. + \frac{(2s+3)(2s+4)}{4s+7}V_{2s+2}\right\}\right]_{z=\pm 1} \\
&\quad - T\int_0^{\infty} e^{\mp k}\{\psi_1(k)k\cosh k + \psi_2(k)[k\sinh k \\
&\quad - (1-2\nu)\cosh k]\}J_0(kr)dk \\
\tau_{rz} &= \frac{1}{a^3}\left[\frac{\partial}{\partial r}\left\{(1-\nu)\nabla^2 - \frac{\partial^2}{\partial z^2}\right\}\chi_1\right]_{z=\pm 1} \\
&= \pm T\int_0^{\infty} k^2\{\psi_1(k)k\sinh k + \psi_2(k)(k\cosh k \\
&\quad + 2\nu\sinh k)\}J_1(kr)dk
\end{aligned} \tag{23}$$

The latter vanishes identically for all values of r provided that

$$\psi_1(k)k\sinh k + \psi_2(k)(k\cosh k + 2\nu\sinh k) = 0 \tag{24}$$

Again, the former vanishes identically for all values of r provided that by the Hankel transform of order zero [5],

$$\begin{aligned}
&\psi_1(k)k\cosh k - \psi_2(k)[k\sinh k - (1-2\nu)\cosh k] \\
&\quad = \frac{1}{k}\int_0^{\infty}\left[2A_0U_2 + \sum_{s=1}^{\infty}2s(2s+1)(2s+2)A_{2s}U_{2s+2}\right. \\
&\qquad - \sum_{s=0}^{\infty}(2s+2)(4s+1)B_{2s}\left\{2(2-\nu)U_{2s+2}\right. \\
&\qquad \left.\left. + \frac{(2s+3)(2s+4)}{4s+7}V_{2s+2}\right\}\right]_{z=\pm 1} rJ_0(kr)dr
\end{aligned} \tag{25}$$

In view of the relations

$$\begin{aligned}
\int_0^{\infty} U_{2s+2}rJ_0(kr)dr &= -\frac{1}{(2s+2)!}\frac{\partial^{2s+1}}{\partial z^{2s+1}}\int_0^{\infty} U_2rJ_0(kr)dr \\
\int_0^{\infty} V_{2s+2}rJ_0(kr)dr &= -\frac{4s+7}{(2s+4)!}\frac{\partial^{2s+3}}{\partial z^{2s+3}}\int_0^{\infty} V_0rJ_0(kr)dr
\end{aligned} \tag{26}$$

the integrals can now be evaluated by using the expression of U_2 derived from Equation (8) and that of V_0 given in Equation (16). With the aid of the following integrals of the Hankel type [6] valid for $k > 0$ and $t > 0$,

$$\int_0^{\infty}\frac{rJ_0(kr)dr}{(t^2+r^2)^{1/2}} = \frac{e^{-kt}}{k}, \quad \int_0^{\infty}\frac{rJ_0(kr)dr}{(t^2+r^2)^{3/2}} = \frac{e^{-kt}}{t} \tag{27}$$

we find

$$\int_0^{\infty}[U_{2s+2}]_{z=\pm 1}rJ_0(kr)dr = \frac{k^{2s+1}}{(2s+2)!\sinh k}$$

$$\int_0^{\infty}[V_{2s+2}]_{z=\pm 1}rJ_0(kr)dr = \frac{(4s+7)k^{2s+1}}{(2s+4)!\sinh k}(k\coth k - 2s - 3) \tag{28}$$

Consequently, we solve from Equations (24) and (25),

$$\psi_1(k) = -(2\nu + k\coth k)\psi_2(k)/k,$$

$$\begin{aligned}
\psi_2(k) = -\frac{2}{\sinh 2k + 2k}&\left\{A_0 + \sum_{s=1}^{\infty}\frac{A_{2s}k^{2s}}{(2s-1)!}\right. \\
&\left. - \sum_{s=0}^{\infty}\frac{(4s+1)B_{2s}k^{2s}}{(2s+1)!}(2s+1+2\nu-k\coth k)\right\}
\end{aligned} \tag{29}$$

which are the conditions of zero tractions derived from the auxiliary stress function χ_1 on the surfaces $z = \pm 1$.

However, since A_{2s} and B_{2s} are coefficients independent of k, it appears that the integral in Equation (21) with the values of ψ_1 and ψ_2 given by Equations (29) becomes divergent at the lower limit, for the integrand of the integral becomes of the order $0(k^{-1})$ as k tends to zero. Nevertheless, the divergence can be removed by subtracting a term $\{A_0 + (1-2\nu)B_0\}\nu ze^{-k}/k$ from the integrand. The resulting integrand then vanishes as k tends to zero and the new integral is now convergent. This modification is permissible for it does not affect the stresses in the slab as well as the convergence at the upper limit.

It is readily seen that the auxiliary stress function χ_1 thus obtained gives no stress on the boundary at infinity.

Boundary Conditions on Surface of the Cavity

To adjust the boundary conditions on the surface of the cavity it is necessary to expand the stress function χ in spherical coordinates valid near the origin. The expansion of χ_0 is simple. The series in χ_1 can be expanded by using Equations (12), (14), (18), and (19), while the integral in χ_1 can be expanded by using the following relations [7]:

$$\begin{aligned}
J_0(kr)\sinh kz &= \sum_{n=0}^{\infty}\frac{(k\rho)^{2n+1}}{(2n+1)!}P_{2n+1}(\mu), \\
J_0(kr)kz\cosh kz &= \sum_{n=0}^{\infty}\frac{1}{(2n)!}\left\{\frac{2n+1}{4n+1}\right. \\
&\quad \left. + \frac{k^2\rho^2}{(2n+1)(4n+5)}\right\}(k\rho)^{2n+1}P_{2n+1}(\mu)
\end{aligned} \tag{30}$$

The resulting expansion is expressed in the following condensed form:

$$\begin{aligned}
\chi &= \chi_0 + \chi_1 \\
&= \frac{Ta^3\rho^3}{15(1+\nu)}\{3P_1(\mu) + (7-5\nu)P_3(\mu)\} \\
&\quad - \frac{1}{2}Ta^3A_0\log\frac{1+\mu}{1-\mu} + Ta^3\sum_{n=0}^{\infty}\left\{A_{2n+2} - \frac{B_{2n+2} + B_{2n}\rho^2}{\rho^{2n+2}}\right. \\
&\quad \left. + (C_{2n} + D_{2n+2}\rho^2)\rho^{2n+1}\right\}P_{2n+1}(\mu)
\end{aligned} \tag{31}$$

where, for $n \geq 1$,

$$\begin{aligned}
C_{2n} &= -\sum_{s=0}^{\infty}({}_{2n+1}\alpha_{2s}A_{2s} + {}_{2n+1}\beta_{2s}B_{2s}) \\
&\quad + \frac{1}{(2n)!}\int_0^{\infty}\left\{\frac{k}{2n+1}\psi_1(k) + \frac{2n+1}{4n+1}\psi_2(k)\right\}k^{2n}dk \\
D_{2n} &= \sum_{s=0}^{\infty}{}_{2n+1}\beta_{2s}B_{2s} + \frac{1}{(4n+1)(2n-1)!}\int_0^{\infty}\psi_2(k)k^{2n}dk
\end{aligned} \tag{32}$$

in which ψ_1 and ψ_2 are given by Equations (29). Here the co-

efficient C_0 is not defined. This is immaterial, for it is the coefficient of the trivial term $\rho\mu$ or z.

The stress function gives the following normal and tangential stresses in spherical co-ordinates [8],

$$\sigma_\rho = \frac{1}{a^3}\left\{(2-\nu)\mu\frac{\partial}{\partial\rho} + \frac{\nu(1-\mu^2)}{\rho}\frac{\partial}{\partial\mu}\right\}\nabla^2\chi - \frac{1}{a^3}\frac{\partial^2}{\partial\rho^2}\left(\mu\frac{\partial}{\partial\rho} + \frac{1-\mu^2}{\rho}\frac{\partial}{\partial\mu}\right)\chi$$

$$= \frac{2T}{3}\{1 - P_2(\mu)\} + \frac{2TA_0}{\rho^3} + T\sum_{n=0}^{\infty}\left\{2n(2n+1)(2n+2)\frac{A_{2n} - B_{2n}}{\rho^{2n+3}} + \frac{2(2n+1)(2n+2)(6n-8n\nu+1-2\nu)B_{2n}}{(4n+3)\rho^{2n+3}} + \frac{4n(4n-3)(2n^2+3n-\nu)B_{2n-2}}{(4n-1)\rho^{2n+1}} - 2n(2n-1)(2n+1)C_{2n}\rho^{2n-2} + \frac{4n(4n-2)(3n-4n\nu+1-\nu)}{4n-1}D_{2n}\rho^{2n-2} - \frac{(4n+2)(4n+5)(2n^2-n-1-\nu)}{4n+3}D_{2n+2}\rho^{2n}\right\}P_{2n}(\mu) \quad (33)$$

$$\tau_{\rho\phi} = \frac{(1-\mu^2)^{1/2}}{a^3}\left\{-(1-\nu)\left(\frac{\partial}{\partial\rho} + \frac{\mu}{\rho}\frac{\partial}{\partial\mu}\right)\nabla^2\chi + \frac{\partial}{\partial\rho}\left(\frac{1}{\rho}\frac{\partial}{\partial\mu}\right)\left(\mu\frac{\partial}{\partial\rho} + \frac{1-\mu^2}{\rho}\frac{\partial}{\partial\mu}\right)\chi\right\}$$

$$= \frac{T}{3}(1-\mu^2)^{1/2}P_2'(\mu) + T(1-\mu^2)^{1/2}\sum_{n=1}^{\infty}\left\{2n(2n+2)\frac{A_{2n} - B_{2n}}{\rho^{2n+3}} + \frac{2(2n+2)(6n-8n\nu+1-2\nu)B_{2n}}{(4n+3)\rho^{2n+3}} + \frac{2(4n-3)(2n^2-1+\nu)B_{2n-2}}{(4n-1)\rho^{2n+1}} + (2n-1)(2n+1)C_{2n}\rho^{2n-2} - \frac{2(4n-2)(3n-4n\nu+1-\nu)}{4n-1}D_{2n}\rho^{2n-2} + \frac{(4n+5)(4n^2+4n-1+2\nu)}{4n+3}D_{2n+2}\rho^{2n}\right\}P_{2n}'(\mu) \quad (34)$$

The remaining boundary conditions to be satisfied are that on the surface of the cavity these normal and tangential stresses vanish identically. By inserting $\rho = \lambda$ into Equations (33) and (34), and equating separately the coefficient of each Legendre function or its derivative to zero, a system of linear equations is obtained. The system of equations may be replaced by the following system:

$$A_{2n}' = -\frac{2}{3}\delta_{0,n} - \frac{4}{7-5\nu}\delta_{1,n} - 2n(n+1)(4n-1)C_{2n}' - 2(4n+1)(4n^4+4n^3-n^2-n+1-\nu^2)D_{2n+2}', \quad (n \geq 0) \quad (35)$$

$$B_{2n-2}' = \frac{5}{3(7-5\nu)}\delta_{1,n} + (4n+1)C_{2n}' + (2n-1)(2n+1)(4n+3)D_{2n+2}' \quad (n \geq 1)$$

where $\delta_{mn} = 1$ or 0, according as $m = n$ or $m \neq n$, and

$$A_{2n}' = \frac{2n(2n+2)(A_{2n} - B_{2n})}{\lambda^{2n+3}} + \frac{2(2n+2)(6n-8n\nu+1-2\nu)B_{2n}}{(4n+3)\lambda^{2n+3}}$$

$$B_{2n}' = \frac{2(4n+1)B_{2n}}{(4n+3)\lambda^{2n+3}}$$

$$C_{2n}' = \frac{(2n-1)(2n+1)C_{2n}\lambda^{2n-2}}{4n^2+2n-4n\nu+1-\nu} - \frac{4(2n-1)(3n-4n\nu+1-\nu)D_{2n}\lambda^{2n-2}}{(4n-1)(4n^2+2n-4n\nu+1-\nu)}$$

$$D_{2n+2}' = \frac{(4n+5)D_{2n+2}\lambda^{2n}}{(4n+3)(4n^2+2n-4n\nu+1-\nu)} \quad (36)$$

and in particular,

$$A_0' = \frac{2A_0}{\lambda^3} + \frac{4(1-2\nu)B_0}{3\lambda^3}$$

By Equations (32) and (29), C_{2n}' and D_{2n}' may be expressed in terms of A_{2n}' and B_{2n}' as follows: for $n \geq 1$,

$$C_{2n}' = \sum_{s=0}^{\infty}({}^{2n}\gamma_{2s}A_{2s}' + {}^{2n}\epsilon_{2s}B_{2s}')\lambda^{2n+2s+1}$$
$$D_{2n}' = \sum_{s=0}^{\infty}({}^{2n}\delta_{2s}A_{2s}' + {}^{2n}\sigma_{2s}B_{2s}')\lambda^{2n+2s+1} \quad (37)$$

where

$${}^{2n}\delta_{2s} = -\binom{2n+2s}{2s}\times\frac{2nI_{2n+2s}}{(2s+2)(4n-1)(4n^2-6n-4n\nu+3+3\nu)2^{2n+2s-1}}$$

$${}^{2n}\gamma_{2s} = -\binom{2n+2s}{2s}\frac{2n-1}{(2s+2)(4n^2+2n-4n\nu+1-\nu)2^{2n+2s}}\times\left\{\frac{2(4n^2-4n-1+2\nu)}{4n-1}I_{2n+2s} + \omega_{2n+2s+1} - (2n+2s+1)I_{2n+2s+1}\right\}$$

$${}^{2n}\sigma_{2s} = \binom{2n+2s}{2s+1}\frac{4s+3}{(4n-1)(4n^2-6n-4n\nu+3+3\nu)2^{2n+2s+1}}\times\left\{\frac{2(4s^2+4s-1+2\nu)}{4s+3}I_{2n+2s} + \omega_{2n+2s+1} - (2n+2s+1)I_{2n+2s+1}\right\}$$

$${}^{2n}\epsilon_{2s} = \binom{2n+2s}{2s+1}\frac{(2n-1)(4s+3)}{2n(4n^2+2n-4n\nu+1-\nu)2^{2n+2s}}\times\left\{\frac{(4n^2-4n-1+2\nu)(4s^2+4s-1+2\nu)}{(4n-1)(4s+3)}I_{2n+2s} - \left(\frac{n(2n+3-4\nu)}{4n-1} + \frac{(2s+1)(s-1+2\nu)}{4s+3}\right)\omega_{2n+2s+1} - \left(\frac{4n^2-4n-1+2\nu}{4n-1} + \frac{4s^2+4s-1+2\nu}{4s+3}\right)\times\frac{2n+2s+1}{2}I_{2n+2s+1} + \frac{(2n+2s+1)(2n+2s+2)}{4}K_{2n+2s+2}\right\} \quad (38)$$

The coefficient ω_n is defined by Equation (10) and the remaining coefficients by

$$I_n = \frac{2^n}{n!}\int_0^\infty \frac{k^n dk}{\sinh 2k + 2k}$$

$$L_n = \frac{2^n}{n!}\int_0^\infty \frac{k^n \coth k\, dk}{\sinh 2k + 2k} \tag{39}$$

$$K_n = \frac{2^n}{n!}\int_0^\infty \frac{k^n \coth^2 k\, dk}{\sinh 2k + 2k}$$

each of which tends asymptotically to unity as n tends to infinity.

The system of equations in (35) may be solved by a method of successive approximations as follows: Write, for $n \geq 0$,

$$A_{2n}' = \sum_{p=0}^{\infty} A_{2n}'^{(p)}, \qquad B_{2n}' = \sum_{p=0}^{\infty} B_{2n}'^{(p)} \tag{40}$$

where

$$A_{2n}'^{(0)} = -\frac{2}{3}\delta_{0,n} - \frac{4}{7-5\nu}\delta_{1,n}$$

$$B_{2n}'^{(0)} = \frac{5}{3(7-5\nu)}\delta_{0,n} \tag{41}$$

and for $p \geq 1$,

$$A_{2n}'^{(p)} = -2n(n+1)(4n-1)C_{2n}'^{(p-1)} - 2(4n+1)(4n^4+4n^3-n^2-n+1-\nu^2)D_{2n+2}'^{(p-1)}, \quad (n \geq 0) \tag{42}$$

$$B_{2n-2}'^{(p)} = (4n+1)C_{2n}'^{(p-1)} + (2n-1)(2n+1)(4n+3)D_{2n+2}'^{(p-1)}, \quad (n \geq 1)$$

in which $C_{2n}'^{(p-1)}$ and $D_{2n}'^{(p-1)}$ are computed from $A_{2n}'^{(p-1)}$ and $B_{2n}'^{(p-1)}$ by Equations (37).

Obviously the foregoing method of solving the linear equations is valid as long as the series in Equations (40) are both convergent. From physical considerations alone, it seems likely that there will be convergence if λ is less than unity. The convergence can be established over a considerable range of λ by the method used by Howland [9] and Knight [10]. However, for the sake of brevity, no proof will be shown here and the convergence will only be illustrated by the numerical examples which follow.

Numerical Examples

Numerical examples will be given for the cases $\lambda = 1/2$ and $1/4$. The coefficients in Equations (38) are first computed for a given value of ν. The values of ω_n have been tabulated by Glaisher [11] and those of I_n and L_n by the author in two recent papers [12, 13], one with the collaboration of Nelson. The integral K_n may be evaluated by splitting the integrand into the following and then integrating both sides from zero to infinity:

$$\frac{k^n \coth^2 k}{\sinh 2k + 2k} = \frac{k^n}{\sinh 2k + 2k} + \frac{k^{n-1}}{2\sinh^2 k} - \frac{k^{n-1}\coth k}{\sinh 2k + 2k} \tag{43}$$

This leads to

$$K_n = I_n + 2(\omega_{n-1} - L_{n-1})/n \tag{44}$$

The values thus obtained together with the known values are shown in Table 1. Table 2 shows the values of the coefficients in Equations (38) corresponding to $\nu = 1/4$.

The coefficients A_{2n}', B_{2n}', C_{2n}', and D_{2n}' are then computed by the method of successive approximations for the cases $\lambda = 1/2$ and $1/4$, respectively. The results are shown in Table 3. In the former case, the computation has been carried out up to the fifth approximation. The convergence becomes more rapid when λ is smaller. The coefficients thus found are converted readily to A_{2n}, B_{2n}, C_{2n}, and D_{2n} by Equations (36).

It is now rather straightforward to compute the stress at any point in the slab. The most important, however, is the maximum stress occurring at the poles of the cavity, i.e., at $(\rho, \mu) = (\lambda, \pm 1)$. Since

$$\sigma_\rho + \sigma_\phi + \sigma_\theta = \frac{1+\nu}{a^3}\frac{\partial}{\partial z}\nabla^2\chi, \tag{45}$$

and at the poles

$$\sigma_\rho = 0, \quad \sigma_\phi = \sigma_\theta, \quad P_{2n}(\pm 1) = 1, \tag{46}$$

we find

$$\max \sigma_\phi = \frac{1+\nu}{2a^3}\left[\frac{\partial}{\partial z}\nabla^2\chi\right]_{\lambda,\pm 1}$$

$$= T + (1+\nu)T\sum_{n=0}^{\infty}\left\{\frac{(2n+2)(4n+1)B_{2n}}{\lambda^{2n+3}} + (2n+1)(4n+5)D_{2n+2}\lambda^{2n}\right\}$$

$$= T + (1+\nu)T\sum_{n=0}^{\infty}(4n+3)\left\{(n+1)B_{2n}' + (2n+1)(4n^2+2n-4n\nu+1-\nu)D_{2n+2}'\right\} \tag{47}$$

Table 1 The coefficients

n	I_{2n}	ω_{2n+1}	L_{2n+1}	K_{2n+2}
1	0.767847	1.202057	0.943138	1.012966
2	0.883507	1.036928	0.951644	0.982620
3	0.954192	1.008349	0.979538	0.991327
4	0.984124	1.002008	0.992746	0.996775
5	0.994922	1.000494	0.997654	0.998933
6	0.998460	1.000123	0.999283	0.999669
7	0.999549	1.000031	0.999789	0.999902
8	0.999871	1.000008	0.999939	0.999971
9	0.999964	1.000002	0.999983	0.999992
10	0.999990	1.000000	0.999995	0.999998
11	0.999997	1.000000	0.999999	0.999999
12	0.999999	1.000000	1.000000	1.000000
13	1.000000	1.000000	1.000000	1.000000

Table 2 The coefficients, for $\nu = 1/4$

Coeff.	$2s$	$2n = 2$	$2n = 4$	$2n = 6$	$2n = 8$	$2n = 10$	$2n = 12$
$^{2n}\gamma_{2s}$	0	4.0941×10^{-2}	9.1403×10^{-3}	1.7408×10^{-3}	3.3805×10^{-4}	6.8475×10^{-5}	1.4388×10^{-5}
	2	6.5475×10^{-2}	3.5660×10^{-2}	1.2822×10^{-2}	4.1081×10^{-3}	1.2462×10^{-3}	3.6579×10^{-4}
	4	4.1892×10^{-2}	4.2466×10^{-2}	2.4604×10^{-2}	1.1622×10^{-2}	4.8809×10^{-3}	1.8944×10^{-3}
	6	1.9642×10^{-2}	3.2163×10^{-2}	2.7398×10^{-2}	1.7884×10^{-2}	9.9205×10^{-3}	4.9146×10^{-3}
	8	7.8760×10^{-3}	1.9048×10^{-2}	2.2423×10^{-2}	1.9328×10^{-2}	1.3683×10^{-2}	8.4230×10^{-3}
	10	2.8778×10^{-3}	9.6572×10^{-3}	1.5020×10^{-2}	1.6524×10^{-2}	1.4536×10^{-2}	1.0883×10^{-2}
$^{2n}\delta_{2s}$	0	-1.7063×10^{-1}	-5.4876×10^{-3}	-4.3372×10^{-4}	-5.1579×10^{-5}	-7.4381×10^{-6}	-1.2027×10^{-6}
	2	-1.4725×10^{-1}	-1.1112×10^{-2}	-1.5657×10^{-3}	-2.9331×10^{-4}	-6.1583×10^{-5}	-1.3695×10^{-5}
	4	-6.6263×10^{-2}	-8.9142×10^{-3}	-1.9785×10^{-3}	-5.3965×10^{-4}	-1.5584×10^{-4}	-4.5665×10^{-5}
	6	-2.3920×10^{-2}	-5.0692×10^{-3}	-1.6381×10^{-3}	-6.1453×10^{-4}	-2.3383×10^{-4}	-8.7343×10^{-5}
	8	-7.7728×10^{-3}	-2.3983×10^{-3}	-1.0659×10^{-3}	-5.2691×10^{-4}	-2.5557×10^{-4}	-1.1854×10^{-4}
	10	-2.3835×10^{-3}	-1.0115×10^{-3}	-5.9237×10^{-4}	-3.7326×10^{-4}	-2.2481×10^{-4}	-1.2677×10^{-4}
$^{2n}\epsilon_{2s}$	0	2.7775×10^{-1}	1.0364×10^{-1}	2.8031×10^{-2}	7.1602×10^{-3}	1.8036×10^{-3}	4.5264×10^{-4}
	2	5.2570×10^{-1}	4.9724×10^{-1}	2.5517×10^{-1}	1.0652×10^{-1}	3.9842×10^{-2}	1.3900×10^{-2}
	4	4.2631×10^{-1}	7.6507×10^{-1}	6.3537×10^{-1}	3.9105×10^{-1}	2.0242×10^{-1}	9.3369×10^{-2}
	6	2.4460×10^{-1}	7.1741×10^{-1}	8.7838×10^{-1}	7.4758×10^{-1}	5.1126×10^{-1}	3.0105×10^{-1}
	8	1.1671×10^{-1}	5.0827×10^{-1}	8.6125×10^{-1}	9.6846×10^{-1}	8.4550×10^{-1}	6.1887×10^{-1}
$^{2n}\sigma_{2s}$	0	-6.2777×10^{-1}	-3.7414×10^{-2}	-4.2044×10^{-3}	-6.4943×10^{-4}	-1.1557×10^{-4}	-2.2266×10^{-5}
	2	-7.1091×10^{-1}	-1.0336×10^{-1}	-2.1619×10^{-2}	-5.3943×10^{-3}	-1.4177×10^{-3}	-3.7900×10^{-4}
	4	-4.0595×10^{-1}	-1.1143×10^{-1}	-3.7555×10^{-2}	-1.3777×10^{-2}	-5.0040×10^{-3}	-1.7674×10^{-3}
	6	-1.7708×10^{-1}	-8.0194×10^{-2}	-3.9846×10^{-2}	-2.0200×10^{-2}	-9.6883×10^{-3}	-4.3673×10^{-3}
	8	-6.7942×10^{-2}	-4.6082×10^{-2}	-3.1699×10^{-2}	-2.1225×10^{-2}	-1.2992×10^{-2}	-7.2771×10^{-3}

Table 3 The coefficients, for $\nu = 1/4$

λ	$2n$	A_{2n}'	B_{2n}'	C'_{2n+2}	D_{2n+2}'
1/2	0	-6.5255×10^{-1}	3.1660×10^{-1}	6.1707×10^{-3}	-7.5308×10^{-3}
	2	-7.5612×10^{-1}	4.797×10^{-3}	6.438×10^{-4}	-1.958×10^{-4}
	4	-4.419×10^{-2}	4.405×10^{-4}	4.349×10^{-5}	-6.042×10^{-6}
	6	-8.878×10^{-3}	3.307×10^{-5}	2.684×10^{-6}	-2.379×10^{-7}
	8	-1.161×10^{-3}	2.255×10^{-6}	1.609×10^{-7}	-1.049×10^{-8}
	10	-1.218×10^{-4}	...	...	-4.935×10^{-10}
1/4	0	-6.6478×10^{-1}	2.9374×10^{-1}	8.0454×10^{-4}	-1.0077×10^{-3}
	2	-7.0484×10^{-1}	1.916×10^{-4}	2.227×10^{-5}	-6.693×10^{-6}
	4	-1.783×10^{-2}	4.881×10^{-6}	3.976×10^{-7}	-5.358×10^{-8}
	6	-9.898×10^{-5}	1.027×10^{-7}	6.482×10^{-9}	-5.478×10^{-10}
	8	-3.619×10^{-6}	1.978×10^{-9}	1.025×10^{-10}	-6.272×10^{-12}
	10	-1.073×10^{-7}	...	...	-7.662×10^{-14}

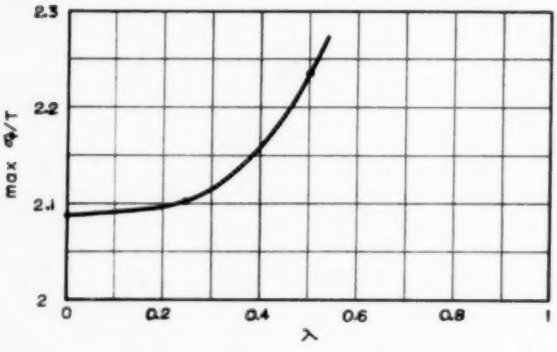

Fig. 1 Maximum stress versus radius of cavity

The following values are obtained:

λ	0,	$\frac{1}{4}$,	$\frac{1}{2}$
$T^{-1}(\max \sigma_\phi)$	2.087,	2.101,	2.232

The value in the limiting case $\lambda = 0$ is the known result of a large solid having a spherical cavity under an all-around tension, that is, $12/(7 - 5\nu)$. The results are also shown graphically in Fig. 1.

References

1 C. B. Ling, "Torsion of Circular Cylinder Having a Spherical Cavity," *Quarterly of Applied Mathematics*, vol. 10, 1952, pp. 149–156.

2 C. B. Ling, "Stresses in a Circular Cylinder Having a Spherical Cavity Under Tension," *Quarterly of Applied Mathematics*, vol. 13, 1956, pp. 381–291.

3 A. E. H. Love, "Mathematical Theory of Elasticity," fourth edition, Dover Publication, New York, N. Y., pp. 274–277.

4 R. C. J. Howland, "Potential Functions With Periodicity in One Coordinate," *Proceedings of Cambridge Philosophical Society*, vol. 30, 1934, pp. 315–326.

5 I. N. Sneddon, "Fourier Transforms," McGraw-Hill Book Company, Inc., New York, N. Y., 1951, p. 6.

6 A. Erdelyi, "Tables of Integral Transforms," vol. 2, McGraw-Hill Book Company, Inc., New York, N. Y., 1954, p. 7.

7 T. M. MacRobert, "Spherical Harmonics," second edition, Methuen, 1947, p. 363.

8 C. B. Ling and K. L. Yang, "On Symmetrical Strain in Solids of Revolution in Spherical Co-ordinates," JOURNAL OF APPLIED MECHANICS, vol. 18, TRANS. ASME, vol. 73, 1951, pp. 367–371. Note that in Equations [32] and [34], p. 370, the factor $(2n^2 + 2n - 3 + \nu)$ should be read as $(2n^2 - 1 + \nu)$.

9 R. C. J. Howland, "Stresses in a Plate Containing an Infinite Row of Holes," *Proceedings of the Royal Society of London*, series A, vol. 148, 1935, pp. 471–491.

10 R. C. Knight, "On the Stresses in a Perforated Strip," *Quarterly Journal of Mathematics*, Oxford Series, vol. 5, 1934, pp. 255–268.

11 J. W. L. Glaisher, "Tables of $1 \pm 2^{-n} + 3^{-n} \pm 4^{-n} +$ etc., and $1 + 3^{-n} + 5^{-n} + 7^{-n} +$ etc., to 32 Places of Decimals," *Quarterly Journal of Mathematics*, vol. 45, 1914, pp. 141–158. The table also appears in "Tables of Higher Mathematical Functions," vol. 2, by H. T. Davis, Principia Press, Bloomington, Ind., 1955.

12 C. B. Ling and C. W. Nelson, "On Evaluation of Howland Integrals," *Annals of Academia Sinica*, Taiwan, China, no. 2, part 2, 1955, pp. 45–50.

13 C. B. Ling, "Tables of Values of 16 Integrals of Algebraic-Hyperbolic Type," *Mathematical Tables and Other Aids to Computation*, vol. 11, no. 59, 1957, pp. 160–166

Influence Coefficients for Edge-Loaded Short, Thin, Conical Frustums

J. H. BALTRUKONIS

Space Technology Laboratories, Inc., Los Angeles, Calif.

An exact solution is obtained in terms of Kelvin functions for axisymmetrically edge-loaded, short, thin, conical frustums. Expressions for the edge-deflectional and rotational influence coefficients are presented in matrix form. Approximate expressions for the influence coefficients are evolved by using one-term asymptotic expansions for the Kelvin functions. It is shown that the range of validity is somewhat larger for this approximate solution than for the solution by Horvay, Linkous, and Born.[1]

Introduction

The history and development of the problem of axisymmetrical deformations of edge-loaded conical shells are not repeated here, having been covered by Taylor and Wenk.[2] These authors calculated the deflectional and rotational influence coefficients resulting from axisymmetrical edge loading at the edges of a frustum of a conical shell. However, their consideration was restricted to long conical elements; i.e., frustums of cones which are long enough so that the edge loadings do not interact. Recently, Horvay, Linkous, and Born[1] presented an approximate solution to the general problem of the short, thin, axisymmetrical shell under axisymmetrical edge loading. This solution was obtained by asymptotic integration of the governing differential equation. By specialization of these results, an approximate solution can be obtained for an edge-loaded conical frustum short enough so that the edge loadings will interact. In the present paper, an exact solution for a conical frustum with interacting edge loadings is obtained by using a general solution in terms of the Kelvin functions. Expressions for the edge deflectional and rotational influence coefficients are presented in matrix form.

From these results, an approximate solution is obtained by using one-term asymptotic expansions for the Kelvin functions. This solution is restricted to thin conical frustums in which the semivertex angle is not close to $\pi/2$. It will be shown, however, that the range of validity is somewhat greater than for the solution by Horvay, Linkous, and Born.

General Equations

The exact general solution for the axisymmetrical deformations of a conical shell was obtained by Watts and Burrows[3] in terms of ber_2, bei_2, ker_2, and kei_2 functions. It was subsequently repeated in a somewhat different form by Taylor and Wenk.[2] Following these results, the stress resultants, stress couples, deformations, and rotations are as follows:

$$Q_y = \frac{\cot \alpha}{y} (C_1 \,\mathrm{ber}_2 \,\xi + C_2 \,\mathrm{bei}_2 \,\xi + C_3 \,\mathrm{ker}_2 \,\xi + C_4 \,\mathrm{kei}_2 \,\xi) \quad (1a)$$

[1] G. Horvay, C. Linkous, and J. S. Born, "Analysis of Short Thin Axisymmetrical Shells Under Axisymmetrical Edge Loading," JOURNAL OF APPLIED MECHANICS, vol. 23, TRANS. ASME, vol. 78, 1956, pp. 68–72.

[2] C. E. Taylor and E. Wenk, Jr., "Analysis of Stresses in the Conical Elements of Shell Structures," Proceedings of the Second U. S. National Congress of Applied Mechanics, ASME, New York, N. Y., 1954, pp. 323–331.

Presented at the West Coast Conference of the Applied Mechanics Division, Los Angeles, Calif., September 8–10, 1958, of THE AMERICAN SOCIETY OF MECHANICAL ENGINEERS. This paper was not preprinted.

Discussion of this paper should be addressed to the Secretary, ASME, 29 West 39th Street, New York, N. Y., and will be accepted until July 10, 1959, for publication at a later date. Discussion received after the closing date will be returned.

NOTE: Statements and opinions advanced in papers are to be understood as individual expressions of their authors and not those of the Society. Manuscript received by ASME Applied Mechanics Division, April 1, 1958.

[3] G. W. Watts and W. R. Burrows, "The Basic Elastic Theory of Vessel Heads Under Internal Pressure," JOURNAL OF APPLIED MECHANICS, vol. 16, TRANS. ASME, vol. 71, 1949, pp. 55–73.

Nomenclature

y = co-ordinate distance from apex of cone
θ = circumferential co-ordinate variable
α = cone semivertex angle
Q_y = shear-stress resultant
H = radial-stress resultant
N_y, N_θ = meridional and circumferential normal stress resultants, respectively
M_y, M_θ = meridional and circumferential bending-stress couples, respectively
δ = radial deflection measured along perpendicular to axis of cone
V = rotation of tangent to meridian
E, ν = elastic modulus and Poisson's ratio of shell material
m^4 = $12(1 - \nu^2)$
h = wall thickness
λ^4 = $m^4/h^2 \tan^2 \alpha$
ξ = $2\lambda \sqrt{y}$
μ = $(\xi_2 - \xi_1)/\sqrt{2}$
C_1, C_2, C_3, C_4 = constants of integration
H_1, H_2 = radial-stress results, externally applied at edges 1 and 2 of the conical shell, respectively
M_1, M_2 = meridional bending-stress couples, externally applied at edges 1 and 2, respectively
$\delta_{h_{ij}}$ = radial-stress deflectional influence coefficient—radial deflection of edge j due to unit radial stress resultant applied at edge i
$\delta_{m_{ij}}$ = bending-stress deflectional influence coefficient—radial deflection of edge j due to unit bending-stress couple applied at edge i
$\alpha_{h_{ij}}$, $\alpha_{m_{ij}}$ = radial and bending-stress rotational influence coefficients, respectively
F_i = generalized load, Equation (3*b*)
$\delta_{f_{ij}}$ = generalized influence coefficient, Equation (5*c*)
$\delta_{f_{ij}}^*$ = dimensionless influence coefficient, Equations (9)

$$H = -\frac{\csc \alpha}{y}\,(C_1\,\mathrm{ber}_2\,\xi + C_2\,\mathrm{bei}_2\,\xi + C_3\,\mathrm{ker}_2\,\xi + C_4\,\mathrm{kei}_2\,\xi) \quad (1b)$$

$$N_y = -\frac{1}{y}\,(C_1\,\mathrm{ber}_2\,\xi + C_2\,\mathrm{bei}_2\,\xi + C_3\,\mathrm{ker}_2\,\xi + C_4\,\mathrm{kei}_2\,\xi) \quad (1c)$$

$$N_\theta = -\frac{1}{2y}\,(C_1\,\xi\,\mathrm{ber}_2'\,\xi + C_2\xi\,\mathrm{bei}_2'\,\xi + C_3\xi\,\mathrm{ker}_2'\,\xi + C_4\xi\,\mathrm{kei}_2'\,\xi) \quad (1d)$$

$$M_y = \frac{h}{2m^2y}\,[C_1(\xi\,\mathrm{bei}_2'\,\xi + 2\nu\,\mathrm{bei}_2\xi) - C_2(\xi\,\mathrm{ber}_2'\,\xi + 2\nu\,\mathrm{ber}_2\,\xi) + C_3(\xi\,\mathrm{kei}_2'\,\xi + 2\nu\,\mathrm{kei}_2\,\xi) - C_4(\xi\,\mathrm{ker}_2'\,\xi + 2\nu\,\mathrm{ker}_2\,\xi)] \quad (1e)$$

$$M_\theta = \frac{h}{2m^2y}\,[C_1(2\,\mathrm{bei}_2\,\xi + \nu\xi\,\mathrm{bei}_2'\,\xi) - C_2(2\,\mathrm{ber}_2\,\xi + \nu\xi\,\mathrm{ber}_2'\,\xi) + C_3(2\,\mathrm{kei}_2\,\xi + \nu\xi\,\mathrm{kei}_2'\,\xi) - C_4(2\,\mathrm{ker}_2\,\xi + \nu\xi\,\mathrm{ker}_2'\xi)] \quad (1f)$$

$$\delta = -\frac{\sin\alpha}{Eh}\left[C_1\left(\frac{\xi}{2}\,\mathrm{ber}_2'\,\xi - \nu\,\mathrm{ber}_2\,\xi\right) + C_2\left(\frac{\xi}{2}\,\mathrm{bei}_2'\,\xi - \nu\,\mathrm{bei}_2\,\xi\right) + C_3\left(\frac{\xi}{2}\,\mathrm{ker}_2'\xi - \nu\,\mathrm{ker}_2\,\xi\right) + C_4\left(\frac{\xi}{2}\,\mathrm{kei}_2'\,\xi - \nu\,\mathrm{kei}_2\,\xi\right)\right] \quad (1g)$$

$$V = -\frac{m^2}{Eh^2}\,(C_1\,\mathrm{bei}_2\,\xi - C_2\,\mathrm{ber}_2\,\xi + C_3\,\mathrm{kei}_2\,\xi - C_4\,\mathrm{ker}_2\,\xi) \quad (1h)$$

where the primes indicate differentiation with respect to ξ. These expressions differ only in notation and sign convention from those of Watts and Burrows, and Taylor and Wenk. The present notations and sign convention, as shown in Fig. 1, are essentially those of Timoshenko.[4]

[4] S. Timoshenko, "Theory of Plates and Shells," McGraw-Hill Book Company, Inc., New York, N. Y., 1940, p. 450.

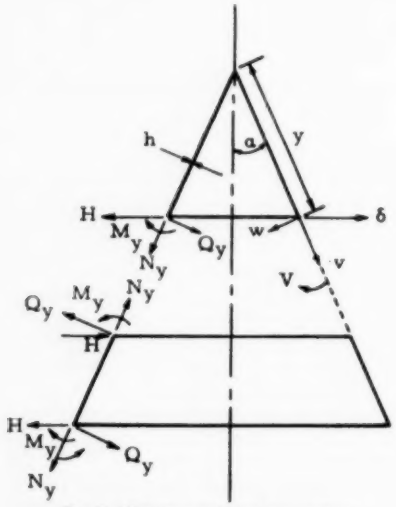

Fig. 1 Notation and sign conventions

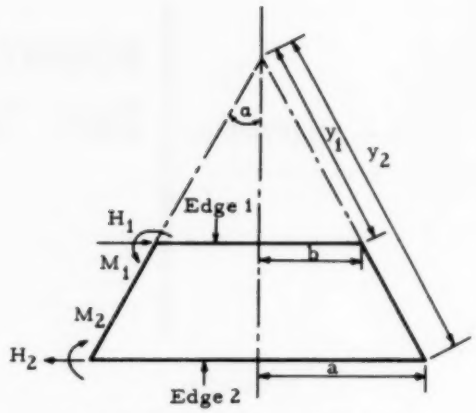

Fig. 2 Edge-loaded, short, conical shell

Influence Coefficients

The problem to be considered is set forth in Fig. 2. It is assumed that the edge loadings will interact so that all four constants in the general solution must be evaluated. The boundary conditions for this purpose are given by

$$H(y_1) = +H_1 \quad (2a)$$

$$H(y_2) = +H_2 \quad (2b)$$

$$M_y(y_1) = +M_1 \quad (2c)$$

$$M_y(y_2) = +M_2 \quad (2d)$$

Substitution from Equations (1b) and (1e) into Equations (2) results in

$$\beta_{ip}C_p = f_{ip}F_p \qquad (i = 1, 2, 3, 4) \quad (3a)$$

where summation is implied over the repeated dummy index p and

$$[F_i] = \begin{bmatrix} H_1 \\ H_2 \\ M_1 \\ M_2 \end{bmatrix} \quad (3b)$$

$$[f_{ij}] = \begin{bmatrix} -\frac{y_1}{\csc\alpha} & 0 & 0 & 0 \\ & -\frac{y_2}{\csc\alpha} & 0 & 0 \\ & & +\frac{2m^2y_1}{h} & 0 \\ & & & +\frac{2m^2y_2}{h} \end{bmatrix} \quad (3c)$$

$$[\beta_{ij}] = \begin{bmatrix} \mathrm{ber}_2\,\xi_1 & \mathrm{bei}_2\,\xi_1 & \mathrm{ker}_2\,\xi_1 & \mathrm{kei}_2\,\xi_1 \\ \mathrm{ber}_2\,\xi_2 & \mathrm{bei}_2\,\xi_2 & \mathrm{ker}_2\,\xi_2 & \mathrm{kei}_2\,\xi_2 \\ (\xi_1\,\mathrm{bei}_2'\,\xi_1 + 2\nu\,\mathrm{bei}_2\,\xi_1) & -(\xi_1\,\mathrm{ber}_2'\,\xi_1 + 2\nu\,\mathrm{ber}_2\,\xi_1) & (\xi_1\,\mathrm{kei}_2'\,\xi_1 + 2\nu\,\mathrm{kei}_2\,\xi_1) & -(\xi_1\,\mathrm{ker}_2'\,\xi_1 + 2\nu\,\mathrm{ker}_2\,\xi_1) \\ (\xi_2\,\mathrm{bei}_2'\,\xi_2 + 2\nu\,\mathrm{bei}_2\,\xi_2) & -(\xi_2\,\mathrm{ber}_2'\,\xi_2 + 2\nu\,\mathrm{ber}_2\,\xi_2) & (\xi_2\,\mathrm{kei}_2'\,\xi_2 + 2\nu\,\mathrm{kei}_2\,\xi_2) & -(\xi_2\,\mathrm{ker}_2'\,\xi_2 + 2\nu\,\mathrm{ker}_2\,\xi_2) \end{bmatrix} \quad (3d)$$

We now solve Equation (3a) to get

$$C_i = \frac{\beta^{qi}}{\beta} f_{qp} F_p \qquad (i = 1, 2, 3, 4) \tag{4}$$

where $\beta = |\beta_{ij}|$ is the determinant of β_{ij} and β^{ij} is the cofactor of β_{ij}; i.e., $(-1)^{i+j}$ times the determinant obtained from the determinant β by striking out the ith row and jth column. Once again, in Equations (4) summation is implied over the dummy indexes p and q. Equations (4) give the values of the constants of integration which satisfy the boundary conditions. Substituting in Equations (1), all necessary quantities are determined.

The edge deflections and rotations may be written in terms of the edge deflectional and rotational influence coefficients, as follows:

$$\delta_i = F_p \delta_{fip} \qquad (i = 1, 2, 3, 4) \tag{5a}$$

where

$$[\delta_i] = \begin{bmatrix} \delta_1 \\ \delta_2 \\ V_1 \\ V_2 \end{bmatrix} \tag{5b}$$

and

$$[\delta_{fij}] = \begin{bmatrix} \delta_{h_{11}} & \delta_{h_{21}} & \delta_{m_{11}} & \delta_{m_{21}} \\ \delta_{h_{12}} & \delta_{h_{22}} & \delta_{m_{12}} & \delta_{m_{22}} \\ \alpha_{h_{11}} & \alpha_{h_{21}} & \alpha_{m_{11}} & \alpha_{m_{21}} \\ \alpha_{h_{12}} & \alpha_{h_{22}} & \alpha_{m_{12}} & \alpha_{m_{22}} \end{bmatrix} \tag{5c}$$

For example, the rotation of edge 1 can be obtained from Equation (5a), as follows:

$$\begin{aligned} \delta_1 &= F_p \delta_{fip} \\ &= F_1 \delta_{f11} + F_2 \delta_{f12} + F_3 \delta_{f13} + F_4 \delta_{f14} \end{aligned} \tag{5d}$$

and, from Equations (3b), (5b), and (5c),

$$V_1 = H_1 \alpha_{h_{11}} + H_2 \alpha_{h_{21}} + M_1 \alpha_{m_{11}} + M_2 \alpha_{m_{21}} \tag{5e}$$

We must now calculate the δ and α in Equations (5c).

From Equations (1g) and (1h) we can write the edge displacements and rotations as follows:

$$\delta_i = C_p \phi_{iq} g_{qp} \tag{6a}$$

where

$$g_{ij} = \begin{bmatrix} \xi_1 \operatorname{ber}_2' \xi_1 & \xi_1 \operatorname{bei}_2' \xi_1 & \xi_1 \operatorname{ker}_2' \xi_1 & \xi_1 \operatorname{kei}_2' \xi_1 \\ -2\nu \operatorname{ber}_2 \xi_1 & -2\nu \operatorname{bei}_2 \xi_1 & -2\nu \operatorname{ker}_2 \xi_1 & -2\nu \operatorname{kei}_2 \xi_1 \\ \xi_2 \operatorname{ber}_2' \xi_2 & \xi_2 \operatorname{bei}_2' \xi_2 & \xi_2 \operatorname{ker}_2' \xi_2 & \xi_2 \operatorname{kei}_2' \xi_2 \\ -2\nu \operatorname{ber}_2 \xi_2 & -2\nu \operatorname{bei}_2 \xi_2 & -2\nu \operatorname{ker}_2 \xi_2 & -2\nu \operatorname{kei}_2 \xi_2 \\ \operatorname{bei}_2 \xi_1 & -\operatorname{ber}_2 \xi_1 & \operatorname{kei}_2 \xi_1 & -\operatorname{ker}_2 \xi_1 \\ \operatorname{bei}_2 \xi_2 & -\operatorname{ber}_2 \xi_2 & \operatorname{kei}_2 \xi_2 & -\operatorname{ker}_2 \xi_2 \end{bmatrix} \tag{6b}$$

$$\phi_{ij} = \begin{bmatrix} -\frac{\sin\alpha}{2Eh} & 0 & 0 & 0 \\ 0 & -\frac{\sin\alpha}{2Eh} & 0 & 0 \\ 0 & 0 & -\frac{m^2}{Eh^2} & 0 \\ 0 & 0 & 0 & -\frac{m^2}{Eh^2} \end{bmatrix} \tag{6c}$$

Substituting from Equation (4) into Equation (6a) results in

$$\delta_i = \frac{\beta^{rp}}{\beta} f_{rs} F_s \phi_{iq} g_{qp} \tag{7}$$

Equating the right-hand sides of Equations (5a) and (7) gives

$$F_p \delta_{fip} = \frac{\beta^{rp}}{\beta} f_{rs} F_s \phi_{iq} g_{qp}$$

and comparing coefficients of like F_i gives

$$\delta_{fij} = \frac{\beta^{rp}}{\beta} f_{rj} \phi_{iq} g_{qp} \tag{8}$$

From this relation the sixteen radial and bending-stress deflectional and rotational influence coefficients can be calculated through the use of Equations (3c), (3d), (5c), (6b), and (6c).

The influence coefficients defined by Equations (8) can be discussed for a specific problem only, since the material constants and shell geometry must be given. In order to establish dimensionless influence coefficients which can be discussed in general, we can nondimensionalize Equations (8) to obtain

$$\delta_{fij}^* = \frac{\beta^{ip}}{\beta} g_{ip} \tag{9a}$$

where δ_{fij}^* are the dimensionless influence coefficients given by

$$\delta_{fij}^* = \begin{bmatrix} \frac{2Eh}{b\sin\alpha}\delta_{h_{11}} & \frac{2Eh}{a\sin\alpha}\delta_{h_{21}} & -\frac{Eh^2}{m^2 b}\delta_{m_{11}} & -\frac{Eh^2}{m^2 a}\delta_{m_{21}} \\ \frac{2Eh}{b\sin\alpha}\delta_{h_{12}} & \frac{2Eh}{a\sin\alpha}\delta_{h_{22}} & -\frac{Eh^2}{m^2 b}\delta_{m_{12}} & -\frac{Eh^2}{m^2 a}\delta_{m_{22}} \\ \frac{Eh^2}{m^2 b}\alpha_{h_{11}} & \frac{Eh^2}{m^2 a}\alpha_{h_{21}} & -\frac{Eh^3}{2m^4 y_1}\alpha_{m_{11}} & -\frac{Eh^3}{2m^4 y_2}\alpha_{m_{21}} \\ \frac{Eh^2}{m^2 b}\alpha_{h_{12}} & \frac{Eh^2}{m^2 a}\alpha_{h_{22}} & -\frac{Eh^3}{2m^4 y_1}\alpha_{m_{12}} & -\frac{Eh^3}{2m^4 y_2}\alpha_{m_{22}} \end{bmatrix} \tag{9b}$$

Equations (9) give the exact solution for the influence coefficients in the present problem. The labor involved in their determination is simplified somewhat by the reciprocity relations which require that the matrix of influence coefficients, Equations (9b), must be symmetrical. Thus ten independent influence coefficients must be calculated.

An Approximate Solution

The computational difficulties involved in the exact solution given in the preceding section are severe principally because of the presence of Kelvin functions, ber, bei, ker, and kei. It is well known that these functions may be replaced by their asymptotic expansions when the argument is sufficiently large; for example, greater than about 6. The arguments of the Kelvin functions involved in the present problem are always ξ_1 or ξ_2. Of these, ξ_1 is always the smaller. However, for thin shells, i.e., for radius to wall-thickness ratios ranging from 10 to 20, ξ_1 is greater than 6

even for semiapex angles as large as 75 deg. Hence it would seem possible to get a reasonably good approximate solution by replacing the Kelvin functions by their asymptotic expansions in the exact solution previously given.

If only the lowest order terms are retained, the asymptotic expansions for the Kelvin functions of second order and their first derivatives are given by

$$\mathrm{ber}_2\,\xi = -\frac{e^{\xi/\sqrt{2}}}{(2\pi\xi)^{1/2}}\cos\left(\frac{\xi}{\sqrt{2}} - \frac{\pi}{8}\right) \tag{10a}$$

$$\mathrm{bei}_2\,\xi = -\frac{e^{\xi/\sqrt{2}}}{(2\pi\xi)^{1/2}}\sin\left(\frac{\xi}{\sqrt{2}} - \frac{\pi}{8}\right) \tag{10b}$$

$$\mathrm{ber}_2'\,\xi = -\frac{e^{\xi/\sqrt{2}}}{(2\pi\xi)^{1/2}}\cos\left(\frac{\xi}{\sqrt{2}} + \frac{\pi}{8}\right) \tag{10c}$$

$$\mathrm{bei}_2'\,\xi = -\frac{e^{\xi/\sqrt{2}}}{(2\pi\xi)^{1/2}}\sin\left(\frac{\xi}{\sqrt{2}} + \frac{\pi}{8}\right) \tag{10d}$$

$$\mathrm{ker}_2\,\xi = -\left(\frac{\pi}{2\xi}\right)^{1/2} e^{-\xi/\sqrt{2}}\cos\left(\frac{\xi}{\sqrt{2}} + \frac{\pi}{8}\right) \tag{10e}$$

$$\mathrm{kei}_2\,\xi = +\left(\frac{\pi}{2\xi}\right)^{1/2} e^{-\xi/\sqrt{2}}\sin\left(\frac{\xi}{\sqrt{2}} + \frac{\pi}{8}\right) \tag{10f}$$

$$\mathrm{ker}_2'\,\xi = +\left(\frac{\pi}{2\xi}\right)^{1/2} e^{-\xi/\sqrt{2}}\cos\left(\frac{\xi}{\sqrt{2}} - \frac{\pi}{8}\right) \tag{10g}$$

$$\mathrm{kei}_2'\,\xi = -\left(\frac{\pi}{2\xi}\right)^{1/2} e^{-\xi/\sqrt{2}}\sin\left(\frac{\xi}{\sqrt{2}} - \frac{\pi}{8}\right) \tag{10h}$$

By replacing the Kelvin functions in Equations (3*d*) and (6*b*) by the appropriate asymptotic expansion from among those in Equations (10), the nondimensional influence coefficients can be calculated by means of Equation (9*a*). The ten independent influence coefficients thus obtained are as follows:

$$2\beta\delta_{f_{11}}^* = -\frac{\xi_1}{\sqrt{2}}\left[\chi_1(2\mu) - \Phi_2(2\mu)\right] + 4\nu \tag{11a}$$

$$2\beta\delta_{f_{12}}^* = -2\beta\delta_{f_{21}}^* = (2\xi_1\xi_2)^{1/2}[\chi_2(\mu)\cos\mu - \Phi_2(\mu)\cosh\mu] \tag{11b}$$

$$2\beta\delta_{f_{13}}^* = 2\beta\delta_{f_{31}}^* = -[\chi_1(\mu)\sinh\mu + \Phi_2(\mu)\sin\mu] \tag{11c}$$

$$2\beta\delta_{f_{14}}^* = -2\beta\delta_{f_{41}}^* = \left(\frac{\xi_1}{\xi_2}\right)^{1/2}[\chi_2(\mu)\sin\mu + \Phi_1(\mu)\sinh\mu] \tag{11d}$$

$$2\beta\delta_{f_{22}}^* = \frac{\xi_2}{\sqrt{2}}\left[\chi_2(2\mu) - \Phi_1(2\mu)\right] + 4\nu \tag{11e}$$

$$2\beta\delta_{f_{23}}^* = -2\beta\delta_{f_{32}}^* = \left(\frac{\xi_2}{\xi_1}\right)^{1/2}[\chi_1(\mu)\sin\mu + \Phi_2(\mu)\sinh\mu] \tag{11f}$$

$$2\beta\delta_{f_{24}}^* = 2\beta\delta_{f_{42}}^* = -[\chi_2(\mu)\sinh\mu + \Phi_1(\mu)\sin\mu] \tag{11g}$$

$$2\beta\delta_{f_{33}}^* = -\frac{\sqrt{2}}{2\xi_1}\left[\chi_1(2\mu) + \Phi_2(2\mu)\right] \tag{11h}$$

$$2\beta\delta_{f_{34}}^* = -2\beta\delta_{f_{43}}^* = \frac{1}{2\sqrt{\nu}}\left(\frac{\xi_2}{\xi_1}\right)^{1/2}[\chi_1(\mu)\sin\mu - \phi_2(\mu)\sinh\mu] \tag{11i}$$

$$2\beta\delta_{f_{44}}^* = \frac{\sqrt{2}}{2\xi_2}\left[\chi_2(2\mu) + \Phi_1(2\mu)\right] \tag{11j}$$

where

$$\mu = (\xi_2 - \xi_1)/\sqrt{2} \tag{11k}$$

$$2\beta = \sinh^2\mu - \sin^2\mu \tag{11l}$$

and

$$\chi_1(\mu) = \sinh\mu + \frac{2\sqrt{2\nu}}{\xi_2}\cosh\mu \tag{12a}$$

$$\chi_2(\mu) = \sinh\mu - \frac{2\sqrt{2\nu}}{\xi_1}\cosh\mu \tag{12b}$$

$$\Phi_1(\mu) = \sin\mu + \frac{2\sqrt{2\nu}}{\xi_1}\cos\mu \tag{12c}$$

$$\Phi_2(\mu) = \sin\mu - \frac{2\sqrt{2\nu}}{\xi_2}\cos\mu \tag{12d}$$

Equations (11) and (12) were obtained by neglecting terms which were obviously negligible compared to those that were retained. In Equations (12) the second terms were retained since they are not, in general, negligible compared to the first terms. For example, when $\mu = 1.0$ and $\xi_1 = 10$, $2(2\nu)^{1/2}\cosh\mu/\xi_2 = 0.115$ which is not negligibly small compared to $\sinh\mu = 1.175$. By omitting these second terms we get exactly the solution obtained by Horvay, Linkous, and Born.[1] However, as we have just pointed out, this omission is subject to question.

Properties of the Approximate Solution

One of the first questions that arises with regard to the analysis of truncated conical shells is: "Under what conditions must interaction effects be considered?" In answer to this question, three of the dimensionless influence coefficients are plotted in Figs. 3, 4, and 5 as functions of μ and ξ_1 or ξ_2. These co-ordinates were used for simplicity since if, for example, the axial length of the shell and radius of its smaller edge were used as co-ordinates, a family of such plots would be required to reproduce these results. As μ increases for a given value of ξ_1 or ξ_2, the slant length of the shell must increase. Thus we expect that as μ increases, the values of the influence coefficients should level off at constant values. These values should agree with the long-shell theory presented by Taylor and Wenk.[2]

This, in fact, is the case in Figs. 3, 4, and 5. We see that, in

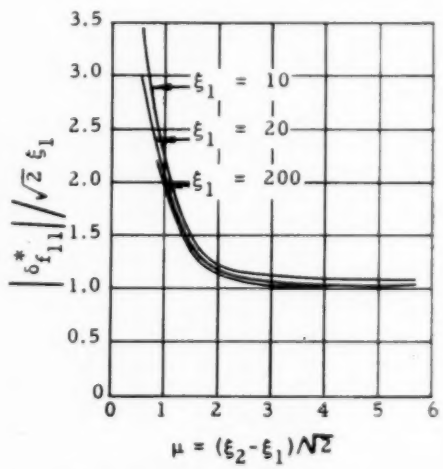

Fig. 3 Variation of $\delta_{f_{11}}^*$ with μ and ξ_1

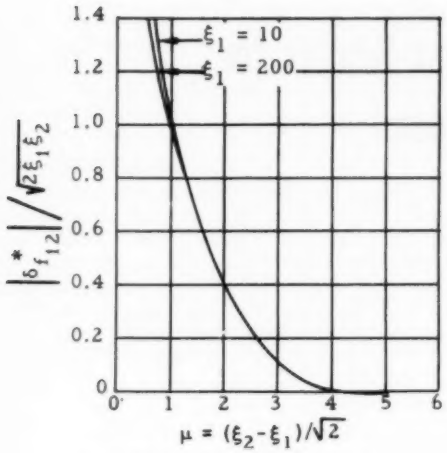

Fig. 4 Variation of $\delta_{f_{12}}{}^*$ with μ and ξ_1

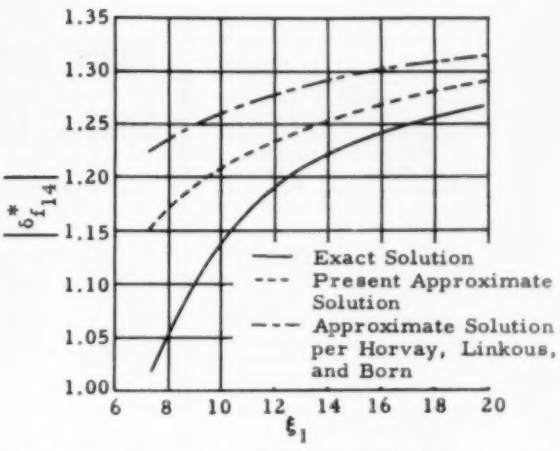

Fig. 6 Comparison of exact and approximate solutions: $\delta_{f_{14}}{}^*$. $\mu = \sqrt{2}$

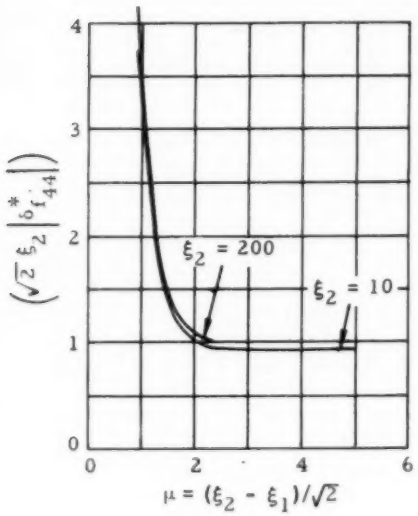

Fig. 5 Variation of $\delta_{f_{44}}{}^*$ with μ and ξ_2

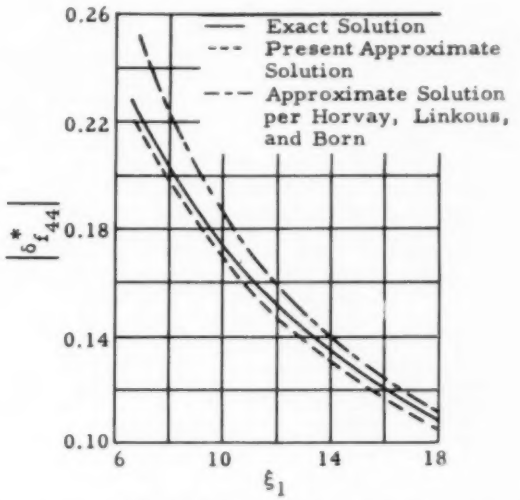

Fig. 7 Comparison of exact and approximate solutions: $\delta_{f_{44}}{}^*$. $\mu = \sqrt{2}$

each instance for $\mu > 4$, the value of the influence coefficient no longer increases with μ, regardless of the value of ξ_1 or ξ_2. The values at which the influence coefficients leveled off compared favorably with the long-shell theory of Taylor and Wenk.

As a result of these considerations, we conclude that for $\mu > 4$ long-shell theory may be used, while for $\mu < 4$ short-shell theory must be used for satisfactory results.

The next logical question that arises concerns the accuracy of the approximate solution. The influence coefficients under discussion are usually used to compute edge displacements and rotations so that a logical discussion of the approximate theory should concern the edge displacements and rotations. These latter quantities are given as sums of products of the influence coefficients and the edge loads and moments as shown by Equations (5). Thus the accuracy of edge displacements and rotations can only be discussed on specification of the edge loading or, what is equivalent, on definition of a specific problem. Here we shall restrict ourselves to a consideration of the accuracy of the influence coefficients only.

In Figs. 6 and 7, values of two of the dimensionless influence coefficients are plotted as calculated (*a*) by the exact solution, (*b*) by the present approximate solution, and (*c*) by Horvay, Linkous, and Born. We see that when ξ_1 has increased to a value of 16 the present approximate solution differs from the exact solution by about 2 per cent. The difference between the Horvay, Linkous, and Born solution and the exact solution is somewhat greater in each instance. For large values of $\xi_1 \sim 100$, the difference between the two approximate solutions is insignificant and the agreement with the exact solution will be excellent. Therefore, for smaller values of ξ_1, the present approximate solution may be used with greater accuracy than can the Horvay, Linkous, and Born solution.

F. C. APPL
Assistant Professor, Department of Mechanical Engineering, Carnegie Institute of Technology, Pittsburgh, Pa. Now, Research Engineer, Jersey Production Research Company, Tulsa, Okla. Assoc. Mem. ASME

C. F. ZOROWSKI
Assistant Professor, Department of Mechanical Engineering, Carnegie Institute of Technology, Pittsburgh, Pa. Assoc. Mem. ASME

Upper and Lower Bounds for Special Eigenvalues[1]

A method for finding upper and lower bounds for the fundamental eigenvalue in special eigenvalue problems is presented. The method is systematic and is shown to provide convergence from above and below to the exact eigenvalue under certain conditions. The method is based on the relatively well-known enclosure or comparison theorem of Collatz, and makes use of a power series to approximate the eigenfunction. The method is applied to two examples concerning the critical-elastic buckling load of variable-section columns with pinned ends. Results for the first example compare well with the exact solution, which is known; the second example is presented as an addition to the literature.

ONE of the simplest methods of finding upper and lower bounds for a class of boundary-value problems, known as special eigenvalue problems, is based on the relatively well-known comparison or enclosure theorem of Collatz.[2] Using a trial function which satisfies the boundary conditions, but not necessarily the differential equation, one performs a few simple operations and obtains upper and lower bounds for the eigenvalue. These bounds may not be very good, however, unless the trial function is close to the exact solution of the problem. The fact that the method is relatively simple to apply for any given function indicates that it might become much more useful if a systematic procedure were added for "choosing" these trial functions.

Proceeding in this direction, this paper develops a systematic method of generating upper and lower bounds for problems in which the enclosure theorem is valid, and shows that under certain conditions these bounds converge from above and below to the exact eigenvalue. The method is particularly attractive in that no integration is required as it is in so many of the current methods.

Special Eigenvalue Problems

In solving special eigenvalue problems[3] it is necessary to determine constants λ, and corresponding functions ϕ, such that a differential equation

$$L_{2m}[\phi] = \lambda g \phi \tag{1}$$

is satisfied throughout a domain D, and boundary conditions

$$B_i[\phi] = 0, \quad i = 1, 2, 3, \ldots m \tag{2}$$

are satisfied at each point on the boundary of D. The symbol L_{2m} denotes a linear homogeneous differential operator of order $2m$, and the function g is positive and continuous in the domain D.

Although the complete solution consists of both the eigenfunction and its corresponding eigenvalue, often only the eigenvalue

[1] Submitted in partial fulfillment of the requirements for the degree of Doctor of Philosophy at the Carnegie Institute of Technology by F. C. Appl.

[2] L. Collatz, "Eigenvertaufgaben mit technischen Anwendung," Akademische Verlagsgesellschaft M.G.H., Leipsig, 1949, p. 126.

For presentation at the Summer Conference of the Applied Mechanics Division, Troy, N. Y., June 18–20, 1959, of THE AMERICAN SOCIETY OF MECHANICAL ENGINEERS.

Discussion of this paper should be addressed to the Secretary, ASME, 29 West 39th Street, New York, N. Y., and will be accepted until July 20, 1959, for publication at a later date. Discussion received after the closing date will be returned.

NOTE: Statements and opinions advanced in papers are to be understood as individual expressions of their authors and not those of the Society. Manuscript received by ASME Applied Mechanics Division, April 24, 1958. Paper No. 59—APM-18.

[3] S. H. Crandall, "Engineering Analysis, A Survey of Numerical Procedures," McGraw-Hill Book Company, Inc., New York, N. Y., 1956, p. 285.

Nomenclature

- D = a finite, simply connected domain
- ϕ = eigenfunction in domain D
- λ = eigenvalue
- m = number of boundary conditions at each point on boundary of D
- g = a given function in domain D
- $L_{2m}[\ ]$ = linear, homogeneous, differential operator of order $2m$
- $B_i[\ ]$ = equation for ith boundary condition
- x = independent variable pertaining to domain D in one dimension; axial distance along column
- x_1, x_2 = boundary points of domain D in one dimension
- $\phi(x)$ = eigenfunction for one dimension; deflection of column
- $g(x)$ = a given function of x
- $\psi(x)$ = a function of x
- R = bounding function
- ϵ = error function
- β = parameter, with values in neighborhood of eigenvalue
- y = a function which satisfies necessary boundary conditions for special eigenvalue problem
- y_n = nth degree approximation for eigenfunction
- A_i = coefficient of ith degree term of y_n
- r, s = integers
- E = modulus of elasticity for column material
- I = moment of inertia of column cross section
- P = critical elastic buckling load of column
- L = length of column
- $f(x)$ = functional variation of moment of inertia of column cross section
- a, b = problem parameters associated with shape of column

Unusual Notation

- $\min_x, \max_x$ = subscripts indicating minimum and maximum values with respect to x
- $\min_\beta, \max_\beta$ = subscripts indicating minimum and maximum values with respect to β

is essential. This is true, for example, in such cases as the buckling or the vibration of elastic members, where the eigenvalue is associated with the critical buckling load or the frequency of vibration of the member. The method which follows is applicable to problems of this nature.

Determination of Bounds

Consider the solution of equation (1) in one dimension

$$L_{2m}[\phi(x)] = \lambda g(x)\phi(x), \quad \text{for} \quad x_1 \leq x \leq x_2 \tag{3}$$

where $\phi(x)$ has a convergent Maclaurin's series expansion in the closed interval $x_1 \leq x \leq x_2$, but does not vanish in the open interval $x_1 < x < x_2$; and where $g(x)$ is positive in the closed interval $x_1 \leq x \leq x_2$. The solution $\phi(x)$ must also satisfy the boundary conditions (2) which become

$$B_i[\phi(x_1)] = 0, \quad B_i[\phi(x_2)] = 0, \quad \text{for } i = 1, 2, 3, \ldots, m \tag{4}$$

A "bounding" function R and an "error" function ϵ are defined as follows:

$$R(\psi, x) = \frac{L_{2m}[\psi(x)]}{g(x)\psi(x)} \tag{5}$$

$$\epsilon(\beta, \psi, x) = L_{2m}[\psi(x)] - \beta g(x)\psi(x) \tag{6}$$

It is noted that

$$R(\phi, x) \equiv \lambda \tag{7}$$

$$\epsilon(\lambda, \phi, x) \equiv 0, \quad \text{for} \quad x_1 \leq x \leq x_2 \tag{8}$$

For development of upper and lower bounds it is convenient to define a function $y_n(x)$ in series form

$$y_n(x) = \sum_{i=0}^{n} A_i x^i, \quad i = 0, 1, 2, \ldots n \tag{9}$$

This function $y_n(x)$ is made to approximate closely the exact eigenfunction $\phi(x)$ by requiring that it satisfy the following conditions; these conditions consist of a set of linear simultaneous equations, which will be used to determine the unknown coefficients A_i:

$$\begin{aligned}
&B_1[y_n(x_1)] = 0 && \epsilon(\beta, y_n, x_1) = 0 \\
&B_2[y_n(x_1)] = 0 && \frac{d}{dx}\epsilon(\beta, y_n, x)\Big|_{x_1} = 0 \\
&\quad\cdots && \quad\cdots \\
&B_m[y_n(x_1)] = 0 && \frac{d^r}{dx^r}\epsilon(\beta, y_n, x)\Big|_{x_1} = 0 \\
&B_1[y_n(x_2)] = 0 && \epsilon(\beta, y_n, x_2) = 0 \\
&B_2[y_n(x_2)] = 0 && \frac{d}{dx}\epsilon(\beta, y_n, x)\Big|_{x_2} = 0 \\
&\quad\cdots && \quad\cdots \\
&B_m[y_n(x_2)] = 0 && \frac{d^s}{dx^s}\epsilon(\beta, y_n, x)\Big|_{x_2} = 0
\end{aligned} \tag{10}$$

where

$$r = s = \frac{n-2}{2} - m, \quad \text{for} \quad n \text{ even}$$

$$r = \frac{n-1}{2} - m \quad \text{for} \quad n \text{ odd}$$

$$s = \frac{n-3}{2} - m$$

The first $2m$ equations of this set insure that $y_n(x)$ will satisfy the boundary conditions (4), while the remaining $(n - 2m)$ equations cause the error and several of its derivatives to vanish at each end of the interval. The importance of these last equations will be considered later in the development.

There is now a total of n equations in the set (10) in terms of the $(n + 1)$ unknown coefficients A_i, plus the unknown β; making n equations in $(n + 2)$ unknowns. Since the solution of problems of this nature can be determined only to within an arbitrary constant,[4] there is no loss of generality in assigning an arbitrary value to one of the A_i. The unknown β is treated as a parameter, which if given a value leaves n equations in n unknowns, which then can be solved for a corresponding set of A_i. Thus the coefficients A_i become functions of β, which means the approximate solution y_n becomes a function of both x and β, which satisfies the necessary boundary conditions of the problem. Equation (9) becomes

$$y_n(\beta, x) = \sum_{i=0}^{n} A_i(\beta)x^i, \quad i = 0, 1, 2, \ldots n \tag{11}$$

Upper and lower bounds for λ are now obtained by substituting this function into equation (5) and looking for the maximum and minimum values[5] of R with respect to x, in the closed interval $x_1 \leq x \leq x_2$. This yields the relation

$$R(y_n, x)_{\min_x} \leq \lambda \leq R(y_n, x)_{\max_x}, \quad \text{for} \quad x_1 \leq x \leq x_2 \tag{12}$$

Since $y_n(\beta, x)$ now depends on the parameter β, the upper and lower bounds will also be functions of β. The nature of dependence will become clear if equation (5) is written in terms of the error defined by equation (6). This leads to

$$R(y_n, x) = \beta + \frac{\epsilon(\beta, y_n, x)}{g(x)y_n(x)} \tag{13}$$

Formal expansions of the error into Taylor's series about the points x_1 and x_2, respectively, are now substituted into equation (13). The following equations for $R(y_n, x)$ are the results:

$$\begin{aligned}
R(y_n, x) &= \beta \\
&\quad + \frac{\epsilon(\beta, y_n, x_1) + \frac{d}{dx}\epsilon(\beta, y_n, x)\Big|_{x_1}(x - x_1) + \cdots}{g(x)y_n(x)} \\
R(y_n, x) &= \beta \\
&\quad + \frac{\epsilon(\beta, y_n, x_2) + \frac{d}{dx}\epsilon(\beta, y_n, x)\Big|_{x_2}(x - x_2) + \cdots}{g(x)y_n(x)}
\end{aligned} \tag{14}$$

In view of the fact that the error and its derivative with respect to x have been made to vanish at x_1 and x_2, equations (10), it is seen from equation (13) that the bounding function $R(y_n, x)$ begins with the value β at x_1 and ends with the value β at x_2. Furthermore, the form of equations (14) suggests[6] that as more derivatives of the error are made to vanish at the end points, the bounding function $R(y_n, x)$ will deviate less from the value β, and consequently the bounds $R_{\min_x}$ and $R_{\max_x}$ will move closer[5]

[4] The amplitude of the mode is arbitrary.

[5] These are known to be bounds by virtue of the enclosure theorem of Collatz[2]; the essentials of this theoren. are discussed by Crandall,[3] p. 291.

[6] A more detailed argument for convergence is presented in the Appendix.

Table 1 Values for elastic buckling load for compressed column of example I

	$n = 11$		$I = I_0(1 + ax)^2$		Maximum
a	Lower bound	Upper bound	Mean value	Exact[a]	possible (%) error
0.00	9.86956	9.86967	9.86961	9.86960	0.021
0.25	12.40379	12.40400	12.40390	12.40391	0.021
0.50	15.06999	15.07167	15.07083	15.07084	0.026
0.75	17.86676	17.86904	17.86790	17.86792	0.026
1.00	20.78599	20.80142	20.79370	20.79229	0.057

[a] Exact values according to solution given by Bleich.[8]

together. It becomes clear then, that β should be assigned values in the neighborhood of λ, and that n should be sufficiently large to effect acceptable accuracy of the bounds. The bounds for a particular value of n can be improved by observing $\underset{x}{R_{\min}}$ and $\underset{x}{R_{\max}}$ for a few values of β to ascertain which value or values of β give the best bounds; i.e., determine the maximum of $\underset{x}{R(y_n, x)_{\min}}$ with respect to β and the minimum of $\underset{x}{R(y_n, x)_{\max}}$ with respect to β. This leads to the most accurate upper and lower bounds for the nth degree approximation $y_n(x)$. Hence the final bounding relation

$$\underset{x}{R(y_n, x)_{\min}}\ \underset{\beta}{\max} \leq \lambda \leq \underset{x}{R(y_n, x)_{\max}}\ \underset{\beta}{\min} \tag{15}$$

To calculate upper and lower bounds for the eigenvalue in a specific problem, the procedure is to set up the necessary equations (10) for a particular value of n, and solve for the corresponding set of bounds (15); if the accuracy of this set of bounds is not acceptable, the procedure is repeated using an increased value for n.

Examples

In the examples which follow, the problem is to determine the smallest elastic buckling load P of a pinned-pinned column with variable moment of inertia I, as shown in Fig. 1. Defining the co-ordinate system shown in Fig. 2, and making the assumptions of simple beam theory leads to the classical equation[7]

$$-EI(x)\frac{d^2\phi}{dx^2} = PL^2\phi(x), \quad \text{for} \quad 0 \leq x \leq 1 \tag{16}$$

where $\phi(x)$ is the deflection, E the modulus of elasticity, and L the length of the beam. Introduce the following notation:

$$I(x) = I_0 f(x)$$

$$\lambda = \frac{PL^2}{EI_0} \tag{17}$$

Substitution into equation (16) yields for the differential equation

[7] The equation is written in terms of the dimensionless variable x.

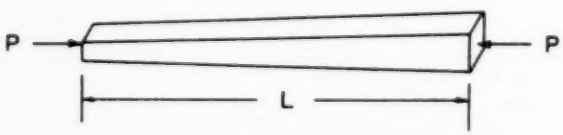

Fig. 1 Compressed column with variable moment of inertia

Fig. 2 Co-ordinate system for compressed column

$$-f(x)\frac{d^2\phi}{dx^2} = \lambda\phi(x) \quad \text{for} \quad 0 \leq x \leq 1 \tag{18}$$

The pinned ends require the boundary conditions

$$\phi(0) = 0$$
$$\phi(1) = 0 \tag{19}$$

The problem is reduced to finding the lowest nontrivial value for λ according to equations (18) and (19); hence the preceding method can be applied to determine upper and lower bounds for λ.

The first example treats the case of a column with moment of inertia given by

$$I(x) = I_0(1 + ax)^2$$

or

$$f(x) = (1 + ax)^2 \tag{20}$$

where I_0 and a are constants. In Table 1, the bounds for this problem are compared with the exact solution, as reported by Bleich,[8] to demonstrate the accuracy and validity of the method.

Table 2 Values for elastic buckling load for compressed column of example II

		$n = 11$		$I = I_0(1 + ax + bx^2)^2$	
b	a	Lower bound	Upper bound	Mean value	Maximum possible (%) error
−0.4	0.0	6.2137	6.4975	6.3556	2.30
	0.2	9.3100	9.3571	9.3335	0.27
	0.4	12.6449	12.6700	12.6575	0.12
	0.6	16.3190	16.3363	16.3277	0.073
	0.8	20.3290	20.4008	20.3649	0.20
	1.0	24.6595	24.8155	24.7375	0.34
−0.2	0.0	8.1643	8.1701	8.1672	0.055
	0.2	11.2070	11.2098	11.2084	0.032
	0.4	14.6000	14.6161	14.6080	0.075
	0.6	18.3500	18.3755	18.3627	0.089
	0.8	22.4405	22.5058	22.4731	0.17
	1.0	26.8224	27.0433	26.9329	0.43
0.0	0.0	9.8696	9.8697	9.8696	0.021
	0.1	11.3938	11.3954	11.3946	0.027
	0.2	13.0070	13.0100	13.0085	0.032
	0.3	14.7090	14.7160	14.7125	0.044
	0.4	16.4980	16.5023	16.5002	0.033
	0.6	20.3321	20.3381	20.3351	0.035
	0.8	24.4878	24.5520	24.5199	0.15
	1.0	28.9283	29.2101	29.0692	0.51
0.2	0.0	11.4999	11.5282	11.5141	0.14
	0.2	14.7534	14.7596	14.7565	0.041
	0.4	18.3003	18.3521	18.3262	0.16
	0.6	22.2002	22.2773	22.2387	0.19
	0.8	26.4986	26.5238	26.5112	0.067
	1.0	30.9833	31.3246	31.1540	0.57
0.4	0.0	13.1146	13.1552	13.1349	0.17
	0.2	16.4493	16.5013	16.4753	0.18
	0.4	20.0702	20.1627	20.1164	0.25
	0.6	24.0248	24.1761	24.1004	0.33
	0.8	28.4011	28.4750	28.4380	0.15
	1.0	32.9989	33.3821	33.1905	0.60

[8] Friedrich Bleich, "Buckling Strength of Metal Structures," McGraw-Hill Book Company, Inc., New York, N. Y., 1952, p. 189.

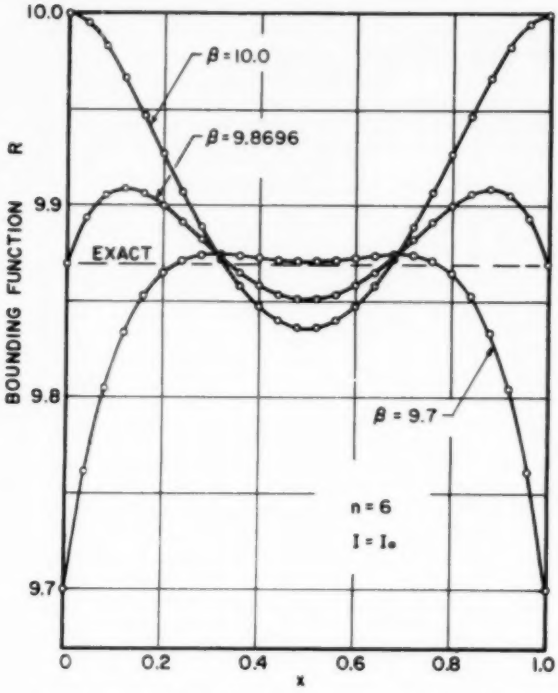

Fig. 3 Characteristics of bounding function for uniform column

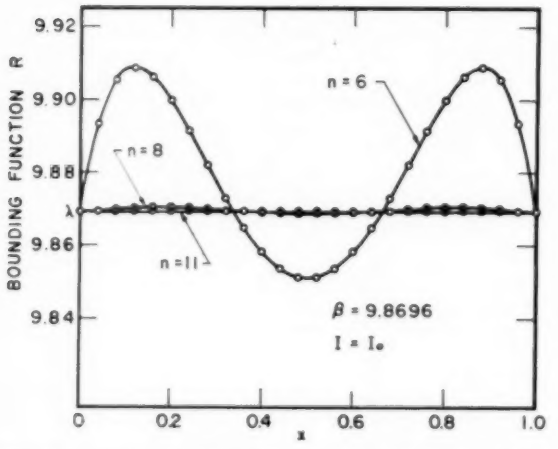

Fig. 4 Convergence properties of bounding function for uniform column

The second example deals with a case which does not appear in the literature; namely,

$$I(x) = I_0(1 + ax + bx^2)^4$$

or (21)

$$f(x) = (1 + ax + bx^2)^3$$

Results for this example are shown in Table 2.

The numerical work for these examples was done on an IBM 650 digital computer. Therefore, owing to the arithmetic operations involved, there is a small error inherent in the computed

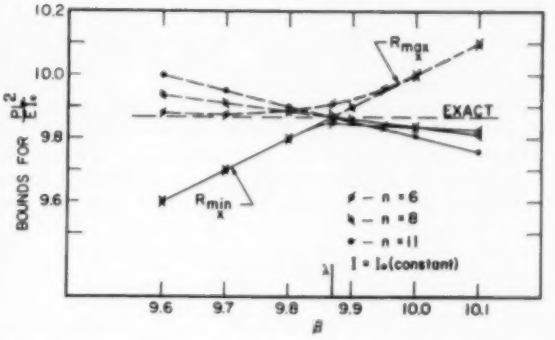

Fig. 5 Convergence characteristics of bounds for elastic buckling load for uniform column

values of the upper and lower bounds. This error was estimated to be of the order of 0.01 per cent, and is included in the values of the maximum possible error of the mean value of the bounds, given in Tables 1 and 2.

To clarify the effects of the degree n and the parameter β on the convergence of the bounds, a study was made for various values of β and values of $n = 6$, 8, and 11 for several specific examples. A graphical representation of the convergence properties of the bounds for the uniform column of Example I are presented in Figs. 3, 4, and 5.

Discussion

At first glance, the method seems somewhat lengthy in that a relatively large amount of arithmetic is involved. For this reason, a computer is very useful, for then the application is essentially reduced to algebraic manipulations for the necessary equations, and the formulation of a program to execute the arithmetic. In fact, it is possible to construct a program which is completely automatic; that is, the machine can be made to alter its own instructions in such a way that when specific values of the problem parameters are supplied, the machine automatically will compute the best values for the upper and lower bounds $R_{\max_x \min_\beta}$ and $R_{\min_x \max_\beta}$. Such a program represents, for all practical purposes, the solution of the problem.

It is also to be noted that the operations needed to establish the necessary equations require nothing more elegant than algebra and differentiation. This simplicity, together with the fact that results can be obtained to a high degree of accuracy, seem to constitute the major advantages of the method.

The method worked quite well for the two examples, giving values which check very well for the case with a known solution. The convergence becomes slightly worse as the column becomes more tapered, but this is thought to be no serious limitation, since the simple beam equations do not remain valid for large taper ratios.

The computer time necessary to obtain a set of bounds corresponding to a given value of β was found to be in the neighborhood of 7 min. And since the mean value of the bounds for a trial value of β was soon found to be a fairly reliable indication of how to change β, acceptable bounds were consistently obtained in a reasonable length of time.

Finally, it should be noted that the number of significant figures in the resulting bounds depends on the number of places carried in the arithmetic of the procedure. It was found for these examples that solutions of higher degree require that more places be carried.

Conclusions

The results obtained in the two examples indicate that the convergence properties of the method are well within the range of present-day computers, such as the IBM 650, and that the method will become even more practical as larger and more efficient computers are developed. Therefore, this method, when used with such machines, becomes a powerful tool for obtaining essentially exact results for many practical as well as theoretical problems, which have not yet been solved with such accuracy.

APPENDIX

A Note on Convergence

In the consideration of convergence it will be necessary to determine if there exists a limiting solution of equations (10) as n becomes large, for some value of β in the neighborhood of λ, such that the error approaches zero, throughout the closed interval $x_1 \leq x \leq x_2$, as n approaches infinity. Then, according to equation (13), the bounding function R would approach the constant value β; and hence the bounds would be convergent, in the limit as n becomes large, to that value of β. The following argument indicates that such a solution exists only for a unique value of β.

It is known, from the general theory of eigenvalue problems, that corresponding to the unique eigenfunction $\phi(x)$ there exists a unique eigenvalue λ. By definition the error corresponding to this solution is identically zero in the closed interval $x_1 \leq x \leq x_2$, equation (8). In thinking of the expansions of this error function $\epsilon(\lambda, \phi, x)$ into Taylor's series about the points x_1 and x_2, respectively, it is noted that if the error is to be identically zero, as required, then the following equations are satisfied:

$$\begin{aligned} &\epsilon(\lambda, \phi, x_1) = 0 && \epsilon(\lambda, \phi, x_2) = 0 \\ &\frac{d}{dx}\epsilon(\lambda, \phi, x)\Big|_{x_1} = 0 && \frac{d}{dx}\epsilon(\lambda, \phi, x)\Big|_{x_2} = 0 \\ &\frac{d^2}{dx^2}\epsilon(\lambda, \phi, x)\Big|_{x_1} = 0 && \frac{d^2}{dx^2}\epsilon(\lambda, \phi, x)\Big|_{x_2} = 0 \\ &\cdots\cdots && \cdots\cdots \end{aligned} \tag{22}$$

By definition, the solution $\phi(x)$ also satisfies the boundary conditions (4), so that equations (22) together with conditions (4) are identical with the limit of the set of equations (10) as n approaches infinity. Hence the limiting solution, which causes the error to vanish, is known to exist for the unique value of β equal to λ; it is concluded that the bounds are convergent to the exact eigenvalue λ, as n approaches infinity and β approaches λ.

C. W. THURSTON

Assistant Professor
of Civil Engineering,
Columbia University, New York, N. Y

H. DERESIEWICZ

Associate Professor
of Mechanical Engineering,
Columbia University, New York, N. Y.
Assoc. Mem. ASME.

Analysis of a Compression Test of a Model of a Granular Medium[1]

A granular medium is idealized here by a model composed of contiguous like spheres arranged in a face-centered cubic lattice. Total stress-strain relations for this model are derived by integrating incremental relations, given previously by Duffy and Mindlin, for a loading program which consists of a uniaxial compression applied concurrently with a related isotropic pressure. Further, the failure stress in uniaxial compression is determined as a function of initial pressure. Results of experimental work are reported which agree with predictions of the theory.

Introduction

In recent years, a number of investigations have been made with a view toward arriving at an analytical description of the mechanical behavior of granular aggregates. Relations between quantities descriptive of applied forces and quantities measuring deformation were sought by various authors who studied models of granular media in which the individual granules were assumed to be in direct, elastic contact. Initially, only the normal stiffness of contact was accounted for, as in the work of Hara [1],[2] Iida [2] ,Takahashi and Satô [3], and Gassmann [4], whose models consisted of like spheres in regular arrays, and of Brandt [5], who analyzed an irregular assemblage of spherical as well as nonspherical particles.

Consideration of tangential stiffness of contact in addition to normal stiffness complicates the problem by introducing load-displacement relations which, in general, are not only nonlinear but also inelastic.[3] That is, such relations at any instant of the loading cycle are affected by the history of loading. As a consequence, if a stress-strain law is sought, it must be written in incremental (or differential) form. For regular arrays of like spheres, this was done by Duffy and Mindlin [7] for the face-centered cubic, Deresiewicz [8] for the simple cubic, and Duffy [9] for the close-packed hexagonal lattices. Such incremental relations are useful in discussing behavior of the medium under variations of stress which are small compared with the initial state, as in problems of small vibrations or of elastic wave propagation. However, when the response of the medium is sought to stresses whose variation is of the order of the initial stresses, as in static loading tests, it is necessary to employ a total (or finite) stress-strain law. This may be obtained by integrating the incremental form of the law, but the operation can be effected only after the loading process is specified. An example of this procedure is afforded in [8] where the integration was carried out in closed form for homothetic loading from an arbitrary initial state.

The present paper is concerned with the prediction of the variation of strain with stress in an axial compression test of a granular bar. The model of the medium is chosen to be a face-centered cubic array of like spheres, and the appropriate incremental relations [7] are taken as the starting point of the computation. The coefficients in these relations are functions of the instantaneous stiffnesses of contact which, in turn, depend on the contact forces and the instantaneous relative rates of change of their tangential and normal components. But the expressions for the contact forces already contain the compliances, so that the integration involves, in general, solution of a system of simultaneous, nonlinear, integrodifferential equations. To cast the problem in tractable form, a simple variation of the instantaneous tangential, relative to the normal, component of contact force is chosen, and a loading history determined for which the incremental stress-strain relations are directly integrable. The loading corresponds to a uniaxial compressive force imposed simultaneously with an isotropic compression, but such that the two force systems are related in a prescribed manner.

The paper contains, further, a description of an experiment designed to check the theoretical work and carried out on a specially constructed granular bar. It is found that the stress-strain relations obtained in the laboratory correspond closely to those predicted by the theory.

In addition, the problem of failure of a granular bar under uniaxial compression is investigated and the least stress which causes gross relative displacement of the constituent granules determined as a function of the initial isotropic pressure. Again, results of experiments indicate agreement with theoretical predictions.

Incremental Relations

According to the Hertz theory, if two elastic spheres, each having radius R, shear modulus μ, and Poisson's ratio ν, are mutually compressed by normal forces N, the resulting surface of contact is a plane bounded by a circle of radius [10]

$$a = [3(1 - \nu)RN/8\mu]^{1/3}, \tag{1}$$

and the normal compliance of the contract, obtained from the relative approach α of the spheres, is

$$C = d\alpha/dN = (1 - \nu)/2\mu a \tag{2}$$

When, instead, the spheres are subjected to a system of compressive forces consisting of an initial normal force N_0 and a subsequent, monotonically increasing, inclined force, the relative

---

[1] This investigation was supported by the Office of Naval Research under Contract Nonr-266(09) with Columbia University.

[2] Numbers in brackets designate References at end of paper.

[3] A detailed discussion of the general problem may be found in a recent survey of the field [6].

Contributed by the Applied Mechanics Division and presented at the Annual Meeting, November 30–December 5, 1958, New York, N. Y., of The American Society of Mechanical Engineers.

Discussion of this paper should be addressed to the Secretary, ASME, 29 West 39th Street, New York, N. Y., and will be accepted until July 10, 1959, for publication at a later date. Discussion received after the closing date will be returned.

Note: Statements and opinions advanced in papers are to be understood as individual expressions of their authors and not those of the Society. Manuscript received by ASME Applied Mechanics Division, February 10, 1958. Paper No. 58—A-48.

displacement of the centers of spheres has a tangential component δ as well as a normal component α. For a loading sequence in which the rate of change of the tangential component T with respect to the normal component N of the additional force is constant, the compliance in the normal direction is still given by (2), and in the tangential direction by $S = d\delta/dT$, or [11]

$$S = \frac{2-\nu}{4\mu a}\left[\theta + (1-\theta)\left(1 - \frac{L}{1+\theta L}\right)^{-1/2}\right], \quad \theta \leq 1$$
$$= \frac{2-\nu}{4\mu a}, \quad \theta \geq 1 \tag{3}$$

where $L = T/fN_0$, f is the coefficient of friction of the contact, and $\theta = fdN/dT$ is constant. The constancy of θ implies a constant obliquity of the additional inclined force. The contact radius a appearing in (2) and (3) is determined from (1) by replacing N by $N_0 + N$. It should be noted that, although the first of (3) is valid only for a loading process, the second of (3) is applicable for loading and unloading.

Consider now a unit cube of like spheres in a face-centered cubic arrangement, loaded by external forces, as shown in Fig. 1. Each sphere in the array is in contact with twelve others; there are, then, in general, thirty-six independent rectangular components of contact forces per sphere. For a homogeneous state of stress, the forces on diametrically opposed contacts are equal and oppositely directed. As a result, the number of independent components is reduced to eighteen, and of these eighteen components six are normal and twelve are tangential (Fig. 2). All contacts occur at points on the sphere at which the normals lie in the coordinate planes. Accordingly, it is convenient to identify the various components of normal forces by N_{ij}, the subscripts corresponding to the planes in which the components lie. The two tangential force components at each contact are chosen to lie in and normal to the co-ordinate planes, and are identified by T_{ij} and T_{kk}, respectively. i, j, and k each assume the values x, y, and z (except that $i \neq j \neq k$), and the order in which they appear is immaterial. Moreover, at all contacts at which the normal has direction cosines of unlike sign, the force components are further distinguished by primes.

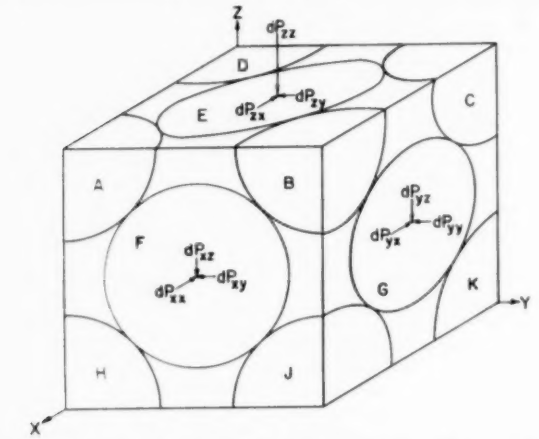

Fig. 1 Unit cube of a face-centered cubic array of equal spheres subjected to incremental forces

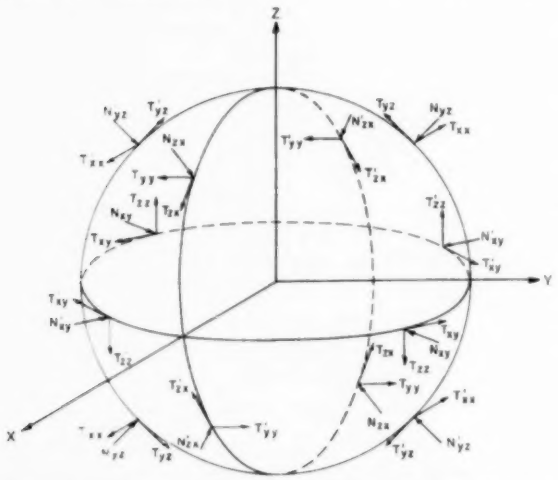

Fig. 2 Forces acting on a typical sphere of the array shown in Fig. 1

The product of each component of incremental contact force and the associated instantaneous compliance yields the corresponding component of the incremental relative displacement between centers of spheres:

$$d\alpha_{ij} = C_{ij}dN_{ij} \qquad d\alpha_{ij}' = C_{ij}'dN_{ij}'$$
$$d\delta_{ij} = S_{ij}dT_{ij} \qquad d\delta_{ij}' = S_{ij}'dT_{ij}' \tag{4}$$
$$d\delta_{kk} = S_{kk}dT_{kk} \qquad d\delta_{kk}' = S_{kk}'dT_{kk}'$$

These expressions[4] permit the transformation of all equations involving incremental displacements into equations involving increments of contact forces.

The incremental strains in the array, expressed in terms of the relative displacements of centers of spheres, are

$$d\epsilon_{ii} = (d\alpha_{ij} + d\delta_{ij} + d\alpha_{ij}' + d\delta_{ij}')/4R$$
$$d\gamma_{ij} = 2d\epsilon_{ij} = (d\alpha_{ij} - d\alpha_{ij}')/2R \tag{5}$$

Substitution of (4) into (5) yields the strains in terms of compliances and components of incremental contact forces. Hence the incremental stress-strain relations are determined when the incremental contact forces are found in terms of the stresses applied to the unit cube (provided that the compliances appearing in the equations can be evaluated).

The applied force increments, $dP_{ij} = 8R^2d\sigma_{ij}$, acting on the faces of the unit cube are assumed distributed among the spheres cut by each face in proportion to the intercepted sectional areas. They are related to the incremental contact forces between spheres by nine independent equations of equilibrium. The simultaneous solution of these nine equations together with nine additional independent equations expressing the compatibility of relative displacements of neighboring spheres yields the eighteen incremental components of contact forces between spheres.

Duffy and Mindlin [7] have solved these equations for two initial states of stress for which symmetry considerations reduce the number of unequal compliances. For an initial isotropic pressure, denoted by $\sigma_0^{(0)}$ and attained by loading homothetically, all initial contact forces between spheres are purely normal, their magnitude being $N_0 = \sqrt{2}\,R^2\sigma_0^{(0)}$. For additional general incremental loading which is small compared to the initial loading, the normal compliance at all contacts is given by (2) and the tangential compliance by the second of (3). In each of these, a is determined from (1) in which N is replaced by N_0. The expressions for the components of incremental contact forces and the general incremental stress-strain relations, appropriate to the case of initial isotropic compression, are given, respectively, by (14) and (18) of [7].

For an initial state of stress whose (compressive) components,

[4] They are given by (12) of [7]. It should be noted that the summation convention on repeated subscripts does not apply here.

referred to the co-ordinate axes of Fig. 1, are $\sigma_{xx} = \sigma_{yy} = \sigma_0^{(0)}$, $\sigma_{zz} = \sigma_0^{(0)} + \sigma_a^{(0)}$, and $\sigma_{yz} = \sigma_{zx} = \sigma_{xy} = 0$, and which was attained by variations in σ_0 and σ_a alone, symmetry arguments may be invoked to show some of the components of contact forces to be equal to each other and some to be equal to zero:

$$\begin{aligned} N_{xy} &= N_{xy}' = N_1 \qquad T_{xy} = T_{xy}' = T_1 = 0 \\ N_{yz} &= N_{yz}' = N_{zx} = N_{zx}' = N_2 \\ -T_{yz} &= -T_{yz}' = T_{zx} = T_{zx}' = T_2 \\ T_{xx} &= T_{xx}' = T_{yy} = T_{yy}' = T_{zz} = T_{zz}' = 0 \end{aligned} \tag{6}$$

Moreover, contacts with identical load histories have equal compliances:

$$\begin{aligned} C_{xy} &= C_{xy}' = C_1 \quad C_{yz} = C_{yz}' = C_{zx} = C_{zx}' = C_2 \\ S_{xy} &= S_{xy}' = S_1 \quad S_{yz} = S_{yz}' = S_{zx} = S_{zx}' = S_2 \\ S_{zz} &= S_{zz}' = S_1 \quad S_{yy} = S_{yy}' = S_{xx} = S_{xx}' = S_2 \end{aligned} \tag{7}$$

The expressions for the components of contact force and the ensuing incremental stress-strain relations appropriate to the initial state of stress specified above are given in [7] by (22) and (23), respectively. The general form of such stress-strain relations, valid for arbitrary initial loading, has been given elsewhere [12].

Total Relations

To arrive at total, or finite, stress-strain relations, it is necessary to integrate (5) after they have been put in suitable form. This form would appear to be obtainable by the substitution of (4) in (5) and the subsequent insertion of (22) of [7], resulting in expressions relating increments of strain and increments of external load. This procedure, however, leads to complications arising from the fact that the tangential compliances at the contacts depend on the loading history.

Attention herein will be confined to loading consisting of hydrostatic plus uniaxial compression specified by the components

$$\begin{aligned} dP_{xx} = dP_{yy} &= 8R^2 d\sigma_0 \qquad dP_{zz} = 8R^2(d\sigma_0 + d\sigma_a) \\ dP_{yz} &= dP_{zx} = dP_{xy} = 0 \end{aligned} \tag{8}$$

imposed on a similar initial state. For this case, (22) of [7], which furnish the expressions for the increments in components of contact force, become

$$\begin{aligned} dN_1 &= \zeta[(3C_2 + S_2)d\sigma_0 + (C_2 - S_2)d\sigma_a] \\ dN_2 &= \zeta[(3C_1 + S_2)d\sigma_0 + (C_1 + S_2)d\sigma_a] \\ dT_1 &= 0 \\ dT_2 &= \zeta[(C_2 - C_1)d\sigma_0 + (C_2 + C_1)d\sigma_a] \end{aligned} \tag{9}$$

where $\zeta = \sqrt{2}R^2/(2C_1 + C_2 + S_2)$ and the subscripts refer to forces and compliances identified, respectively, by (6) and (7). The remaining tangential components of the incremental contact forces are zero. The normal compliances C_1 and C_2 depend on the instantaneous values of N_1 and N_2, respectively, and are determined from (2). However, for arbitrary increases in σ_0 and σ_a, the tangential compliance S_2 depends not only on the instantaneous values of N_2 and T_2 but also on their relative rate of change [11]. Since each of the latter quantities depends, in turn, on S_2, the difficulties involved in the integration of (9) and the subsequent determination of the stress-strain relations for finite loading are, in general, considerable, involving the solution of simultaneous nonlinear integrodifferential equations.

The present discussion is limited, further, to loading for which the form of the contact compliances is known. Accordingly, it is assumed at the outset that the external forces give rise to contact forces of constant obliquity, i.e., at each contact, $dT/dN = \beta$ (constant). Moreover, the loading is assumed to result in positive increments dN, and, to facilitate the computation, the constant β is taken to be less than or at most equal to f, the coefficient of friction of the contact. The appropriate tangential compliance is, therefore, given by the second of (3).

Finally, the discussion is limited to an array subjected to initial isotropic pressure, $\sigma_0^{(0)}$ (due to which the forces at all contacts are purely normal and of magnitude $N_0 = \sqrt{2}R^2\sigma_0^{(0)}$). It is as a result of this and the preceding restrictions that the integrodifferential system is reducible to a set of quadratures. If, now, the additional hydrostatic plus uniaxial loading, given by (8), is such that

$$dT_2/dN_2 = \beta \leq f \tag{10}$$

then (9) may be written

$$\begin{aligned} dN_1 &= \eta[(3 + k)d\sigma_0 + (1 - k)d\sigma_a] \\ dN_2 &= \eta[(3\xi + k)d\sigma_0 + (\xi + k)d\sigma_a] \\ dT_1 &= 0 \\ dT_2 &= \eta[(1 - \xi)d\sigma_0 + (1 + \xi)d\sigma_a] \end{aligned} \tag{11}$$

where

$$\eta = \sqrt{2}R^2/(\xi + 1 + k), \quad k = S_2/C_2 = (2 - \nu)/2(1 - \nu),$$

and

$$\xi = C_1/C_2 = [(N_0 + N_2)/(N_0 + N_1)]^{1/3} \tag{12}$$

With the aid of (10), the increments $d\sigma_0$ and $d\sigma_a$ may be eliminated from (11) to yield

$$dN_2/dN_1 = \lambda\xi \tag{13}$$

where $\lambda = (1 - k\beta)^{-1}$. Insertion of (12) in (13) and subsequent integration results in a relation between the normal components of the finite additional contact forces:

$$(1 + N_1/N_0)^{2/3} = \beta k + (1 - \beta k)(1 + N_2/N_0)^{2/3} \tag{14}$$

Further, $T_1 = 0$ and $T_2 = \beta N_2$ so that all force components are expressible in terms of a single one.

Equations (11) may also be integrated to furnish a relation between the force components N_1 and N_2, and the additional uniaxial stress σ_a. This is done by eliminating $d\sigma_0$ from (11), inserting (10) and (14) in the result, and subsequently integrating. The resulting expression is

$$1 + N_1/N_0 = (2\sigma_a/\sigma_0^{(0)} + 3\beta)/[(1 + 3\beta)\xi^3 - 1] \tag{15}$$

An expression for σ_a may now be found, from (12), (14), and (15) in terms of the parameter ξ:

$$2\sigma_a/\sigma_0^{(0)} = [(\lambda - 1)/(\lambda - \xi^2)]^{3/2}[(1 + 3\beta)\xi^3 - 1] - 3\beta \tag{16}$$

A similar process of substitution, elimination, and integration yields a companion expression for the additional isotropic component σ_0:

$$2\sigma_0/\sigma_0^{(0)} = [(\lambda - 1)/(\lambda - \xi^2)]^{3/2}[(1 - \beta)\xi^3 + 1] - (2 - \beta) \tag{17}$$

The parametric equations (16) and (17) prescribe the required interdependence of the additional components of isotropic and uniaxial stress. The relation is shown in Fig. 3 for $\nu = 0.28$ and for two values of β. The range of values of ξ may be seen, from (16), to be $1 \leq \xi \leq (1 - k\beta)^{-1/3}$. It is of interest to note that, despite the complicated appearance of (16) and (17), the relation between σ_0 and σ_a is very nearly linear, because the influence of the ξ^3 term in each increases rapidly with increasing ξ.

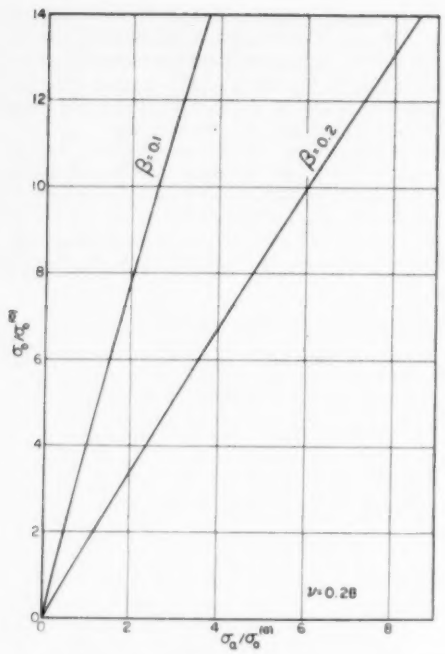

Fig. 3 Relation between additional isotropic compressive stress (σ_0) and additional uniaxial compressive stress (σ_a) governed by (16) and (17)

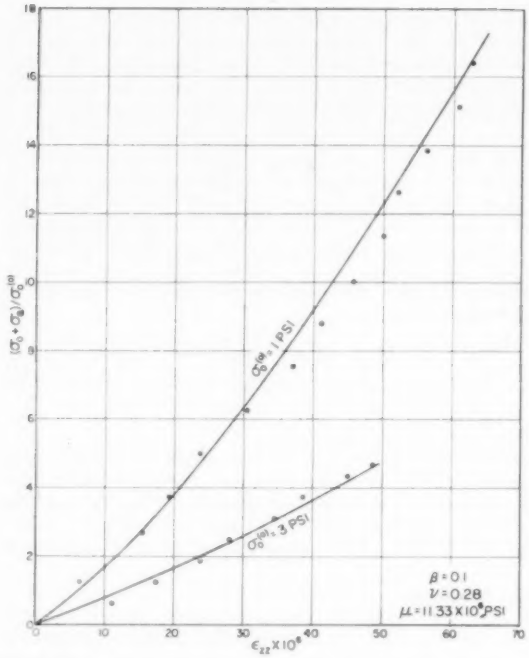

Fig. 4 Relation between components of additional stress and strain in the direction of the uniaxial compression; comparison of theory with experiment

The incremental strain components may be expressed as functions of only the contact force component N_1 by inserting (4), (10), (12), and (13) in (5), with the result

$$d\epsilon_{zz} = d\epsilon_{yy} = d\epsilon_{xx}/\lambda(1 + k\beta) = (C_1/2R)dN_1$$
$$d\epsilon_{yz} = d\epsilon_{xz} = d\epsilon_{xy} = 0 \tag{18}$$

The nonzero components in (18) may, in turn, be expressed, with the aid of (11), in terms of the increment $d\sigma_a$:

$$d\epsilon_{zz} = d\epsilon_{yy} = \frac{1 - k\beta}{1 + k\beta}\, d\epsilon_{zz}$$
$$= \frac{K[\sigma_0^{(0)}]^{-1/3}(\lambda - \xi^2)^{1/3}}{(\lambda - 1)^{1/3}[(1 + 3\beta)\lambda\xi - 1]}\, d\sigma_a \tag{19}$$

where

$$K = [2(1 - \nu)^2/3\mu^2]^{1/3}$$

Integration of (19), accomplished through the use of (16), results, finally, in

$$\epsilon_{zz} = \epsilon_{yy} = \frac{1 - k\beta}{1 + k\beta}\,\epsilon_{zz} = \frac{3K}{4}\,[\sigma_0^{(0)}]^{2/3}\left(\frac{\xi^2 - 1}{\lambda - \xi^2}\right) \tag{20}$$

Equations (20), in conjunction with (16) and (17), furnish a parametric form of the integrated stress-strain relations.[5] The variation of ϵ_{zz} with the corresponding additional (dimensionless) stress is shown in Fig. 4 for two values of the initial pressure.

The special case of additional purely isotropic compression may be extracted from the preceding result by letting $\sigma_a \to 0$. However, since $\xi, \lambda \to 1$, the latter by virtue of $\beta \to 0$, the expression for the strains, (20), becomes indeterminate. It may be evaluated by noting, from (12) and (14), that

$$(\xi^2 - 1)/(\lambda - \xi^2) = (1 + N_1/N_0)^{2/3} - 1$$

Moreover, in the limit, $N_1/N_0 = \sigma_0/\sigma_0^{(0)}$ [from (17)], so that the nonzero components of strain now read

$$\epsilon_{zz} = \epsilon_{yy} = \epsilon_{zz} = (3K/4)\,[\sigma_0^{(0)}]^{2/3}[(1 + \sigma_0/\sigma_0^{(0)})^{2/3} - 1] \tag{21}$$

Failure

Let the face-centered cubic array of spheres, initially under isotropic pressure, now be subjected to a monotonically increasing compressive force directed along a principal axis of the array. Depending on the value of the initial pressure, there is a limiting magnitude of the axial force beyond which rearrangement of the spheres within the structure occurs. The process of rearrangement consists of a series of shearing displacements of individual layers of spheres, and is initiated in layers containing planes in which the density of sphere centers is greatest, i.e., the $\{111\}$ planes. The spheres in such a layer undergo a homogeneous displacement (with respect to a parallel contiguous layer), in a $<1\bar{2}1>$ direction, of magnitude equal to one third of a lattice spacing. This displacement is followed by a similar relative displacement of an adjacent layer, the process being repeated indefinitely. In crystalline materials the analogous rearrangement is called "twinning" [13], and is seen to be such that the magnitude of the displacement of any given layer is proportional to its distance from the initial shearing (twinning) plane. Because the displacements of the spheres in this process are of magnitudes several orders greater than the elastic displacements accompanying static loading, the onset of twinning is herein considered equivalent to failure. It may be noted that the structure which results from twinning is again a face-centered cubic array differing from the original one only in spatial orientation.

One of several equally likely twinning motions may be described in terms of the displacement of sphere B, Fig. 1, this being a

[5] Because of the elastic nature of the special form of the tangential compliance [the second of (3)], these relations are equally valid for the corresponding unloading process.

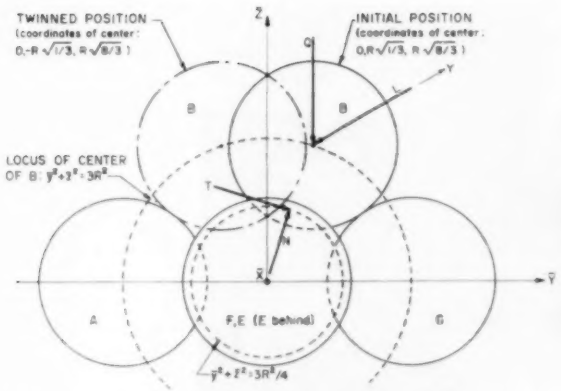

Fig. 5 Forces acting on a typical sphere, B, and path of B during twinning

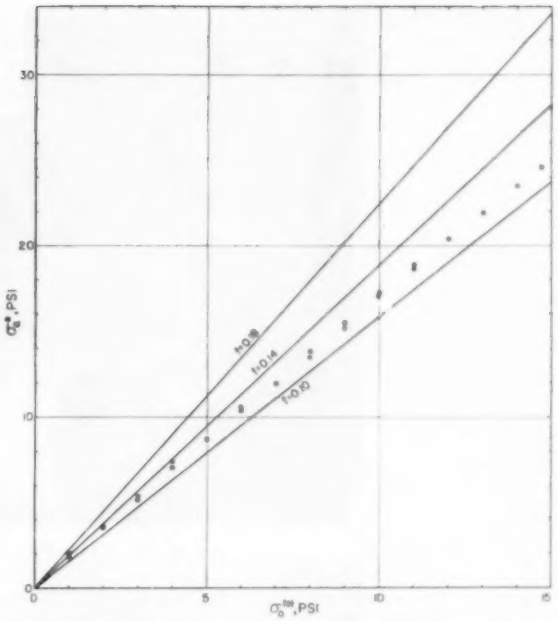

Fig. 6 Failure stress σ_a^* as a function of the initial pressure $\sigma_0^{(0)}$; comparison of theory (23) with experiment

typical sphere in a layer of spheres having centers in a (111) plane. A "deformation twin" is produced by a homogeneous (111) $[1\bar{2}1]$ shearing displacement of this layer through a distance $R\sqrt{4/3}$ relative to the layer containing spheres A, C, and J. (The movement of B takes place from the hollow between the mutually contiguous spheres E, F, and G to the hollow between spheres A, E, and F.) The distance between the planes containing the centers of the spheres in these layers varies during the twinning, its magnitude being $R\sqrt{8/3}$ at the start and the end of the process and reaching a maximum of $R\sqrt{3}$ as B rides over the valley between E and F.

The twinning then progresses by virtue of a shearing of the layer containing spheres A, C, and J relative to the layer containing spheres D, K, and H, followed by similar relative displacements of successive layers. The resulting spatial orientation of the unit cube is determined by a linear transformation (from the axes of Fig. 1) whose matrix is

$$\begin{pmatrix} -1/3 & 2/3 & 2/3 \\ 2/3 & -1/3 & 2/3 \\ 2/3 & 2/3 & -1/3 \end{pmatrix}$$

The path of sphere B in the course of twinning is depicted in Fig. 5 in which the $\bar{x}$, $\bar{y}$, and $\bar{z}$-axes are the $[10\bar{1}]$, $[\bar{1}2\bar{1}]$, and [111] directions, respectively, of Fig. 1. Referred to these axes, the locus of the center of B during motion is an arc of the circle $\bar{y}^2 + \bar{z}^2 = 3R^2$ in the plane $\bar{x} = 0$. In terms of the $\bar{y}$-co-ordinate of the center of B, the direction cosines of the normal force of E on B are

$$l_N = 1/2, \quad m_N = \bar{y}/2R, \quad n_N = [3/4 - (\bar{y}/2R)^2]^{1/2};$$

those of the normal force of F on B are the same except that $l_N' = -1/2$; and those of the (Coulomb) friction forces of each of E and F on B are

$$l_T = 0, \quad m_T = [1 - (\bar{y}/R\sqrt{3})^2]^{1/2}, \quad n_T = -\bar{y}/R\sqrt{3}$$

In its initial position $(0, R\sqrt{1/3}, R\sqrt{8/3})$, in addition to being in contact with spheres E, F, and G, sphere B is in contact with nine other spheres, six in its own (111) layer and three in the layer above. Each of these nine spheres exerts a normal force $N_0 = \sqrt{2}R^2\sigma_0^{(0)}$ on B due to the initial isotropic pressure, $\sigma_0^{(0)}$. Because neither $\sigma_0^{(0)}$ nor the relative position of the nine spheres with respect to B changes during the twinning, the resultant of the nine normal forces is a constant force of magnitude $Q = 2\sqrt{3}R^2\sigma_0^{(0)}$ acting in the negative $\bar{z}$-direction.

Under an axial compressive stress σ_a, parallel to the y-axis, there is a force of magnitude $8R^2\sigma_a$ exerted on the xz-face of each elementary cube. This force is distributed to all spheres on a given {111} plane that project on the loaded face, the distribution being in proportion to the magnitude of the projected area of each sphere. The force per sphere, given by $L = 2R^2\sigma_a$, has direction cosines $l_L = 0, m_L = -\sqrt{2/3}, n_L = -\sqrt{1/3}$, as shown in Fig. 5, and these do not vary during twinning.

When motion impends, and thereafter, sphere G breaks contact with, and hence exerts no force on B. The magnitude of the frictional forces of E and F on B is assumed equal, in each case, to the product of the corresponding normal force and the coefficient of friction f in accordance with Coulomb's law. These frictional forces are tangent to the surface of B and directed so as to oppose the twinning. The torque they exert on B is opposed by tangential forces exerted by each of the nine other spheres in contact with B. In the equations which follow the latter forces are assumed to be statically equivalent to a pure couple whose moment is sufficient to insure rotational equilibrium of B.

Consideration of the equilibrium of forces acting on sphere B at any point in its path (as specified by the $\bar{y}$-co-ordinate of its center) leads to the value of the force L which causes impending motion:

$$\frac{L}{2R^2\sigma_0^{(0)}} = \frac{3[2f(1-t^2)^{1/2} + t\sqrt{3}\,]}{(\sqrt{6} - 2f)(1-t^2)^{1/2} - t(\sqrt{3} + 2\sqrt{2}f)} \qquad (22)$$

where $t = \bar{y}/R\sqrt{3}$. This force attains its maximum value when sphere B is in its initial position (i.e., $\bar{y} = R/\sqrt{3}$); the failure stress, σ_a^*, is, accordingly, given by

$$\sigma_a^*/\sigma_0^{(0)} = (\sqrt{6} + 8f)/(\sqrt{6} - 4f), \qquad (23)$$

the relation between the failure and initial stresses being illustrated in Fig. 6. Since L assumes its maximum value when B is in its initial position, it is seen that, once initiated, the twinning will proceed to completion.

The foregoing computation may be generalized by considering the force L imposed such that it is inclined at angles α, β, γ with

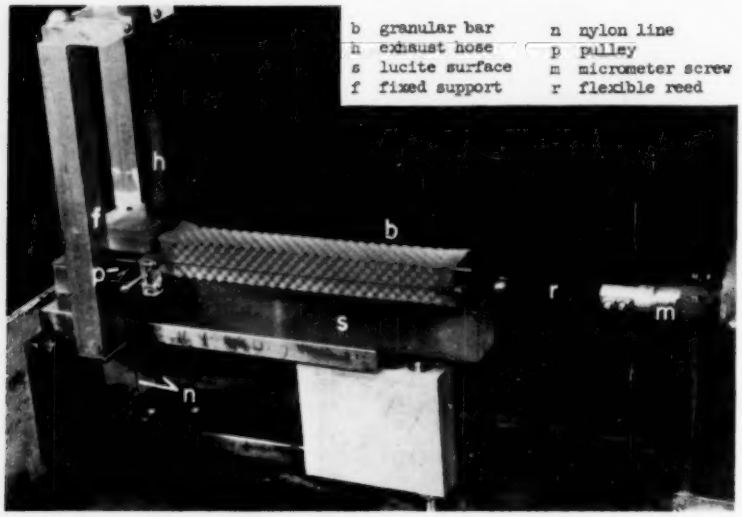

Fig. 7 Over-all view of experimental setup of compression test of granular bar

the $\bar{x}$, $\bar{y}$, $\bar{z}$-axes instead of being applied parallel to a principal (y)-axis of the cube. For twinning to occur in the [1$\bar{2}$1] direction of the (111) plane (as in the case discussed above), the force causing failure is given by

$$\frac{L^*}{2R^2\sigma_0^{(0)}} = -\frac{3 + 4\sqrt{6}f}{2(\sqrt{6} - f)\cos\beta - (\sqrt{3} + 4\sqrt{2}f)\cos\gamma} \tag{24}$$

and its line of action must be confined to the region of space bounded by the (100), (111), and (001) planes.

Since the face-centered cubic is a packing of maximum density, for all intermediate positions during the twinning process, the array will have a lower density than initially. The increase in bulk volume accompanying shearing distortion has been termed "dilatancy" by Reynolds [14]. It is evident that, if the boundaries of a volume of spheres in face-centered cubic array were unyielding, so that no decrease in density could be accommodated within their confines, the twinning described above would not be possible.

Experiments

To test the foregoing theoretical results, experiments were performed on bars made of steel bearing balls arranged in face-centered cubic array. The arrangement of the balls was maintained by confining them under pressure inside a thin rubber "skin." The stress-strain relations for hydrostatic plus uniaxial compressive loading were checked by load-deformation tests. Other tests were performed to determine, for a range of initial pressures, the axial compressive stress at which twinning occurs.

The balls used in the test bars were stainless-steel spheres (AISI No. 440C) having a diameter of $0.125 \pm 20 \times 10^{-6}$ in. They were cleaned by successive baths of carbon tetrachloride, toluol, and acetone immediately before use. The bars, a modification of the ones used by Duffy and Mindlin [7], were constructed by lining an open-top rectangular box with a loose rubber sheet 0.007 in. thick, placing hardened steel bearing plates at the ends of the box, and then carefully stacking the spheres in the space between the plates in such fashion that the [010] direction of Fig. 1 was parallel to the longitudinal axis of the box. Upon completion of this process, the rubber sheet was sealed, enclosing the array and the sides of the bearing plates, and the air inside evacuated through an aperture in one of the end plates. In this condition, the external atmospheric pressure locked the spheres in position so that the relatively rigid "bar of spheres" could be removed from the box. When supported on a flat surface, the bar preserved its shape under pressures as low as 0.25 psi.

Fig. 7 affords an over-all view of the testing arrangement. The granular bar (b) was supported on a polished lucite surface (s) lubricated by "Molycote." The end of the bar through which the air was evacuated via a hose (h) was clamped to a fixed support (f) and the other end was unrestrained but subjected to the horizontal pull of both ends of a slender nylon line (n). These ends were fastened to the sides of the free end-bearing plate at mid-height, and the line was led horizontally along both sides of the bar, over two pulleys (p) at the fixed end, thence vertically downward, and finally looped under a third pulley supporting a weight pan (not shown). All pulleys were grooved, miniature precision bearings with low torque characteristics. Before the test bars were constructed, the weight of the line and the third pulley and its housing was adjusted to balance the horizontal frictional force exerted by the lubricated lucite surface on the free end-bearing plate. During tests the axial component of stress on the bar was applied by adding measured amounts of size "DD" lead shot to the weight pan.

To correlate the test results with theory, it was necessary to consider a mathematical model of the actual bar. This model consisted of 216 of the unit cubes of Fig. 1, arranged 3 wide by 3 high by 24 long, containing (the equivalent of) 864 spheres. Each real bar differed from the model in that the portions of spheres on the boundary were replaced by full ones, making the outside dimensions of the bar (exclusive of end plates) 4.368 in. × 0.655 in. × 0.655 in. (compared with 4.243 in. × 0.530 in. × 0.530 in. for the model). Although this replacement increased the number of spheres in the bar to 1201, it did not alter the number of individual contacts (5796). When converting from axial loads to axial stresses, the cross-sectional area of the test bars was taken to be nine times the area of one face of a unit cube because the load applied by the end-bearing plates to the spheres at each end of the bar was transmitted only through contact points interior to the boundary of the mathematical model.

The axial component of strain in the loaded bar was calculated from the displacement of the outside face of the free end-bearing

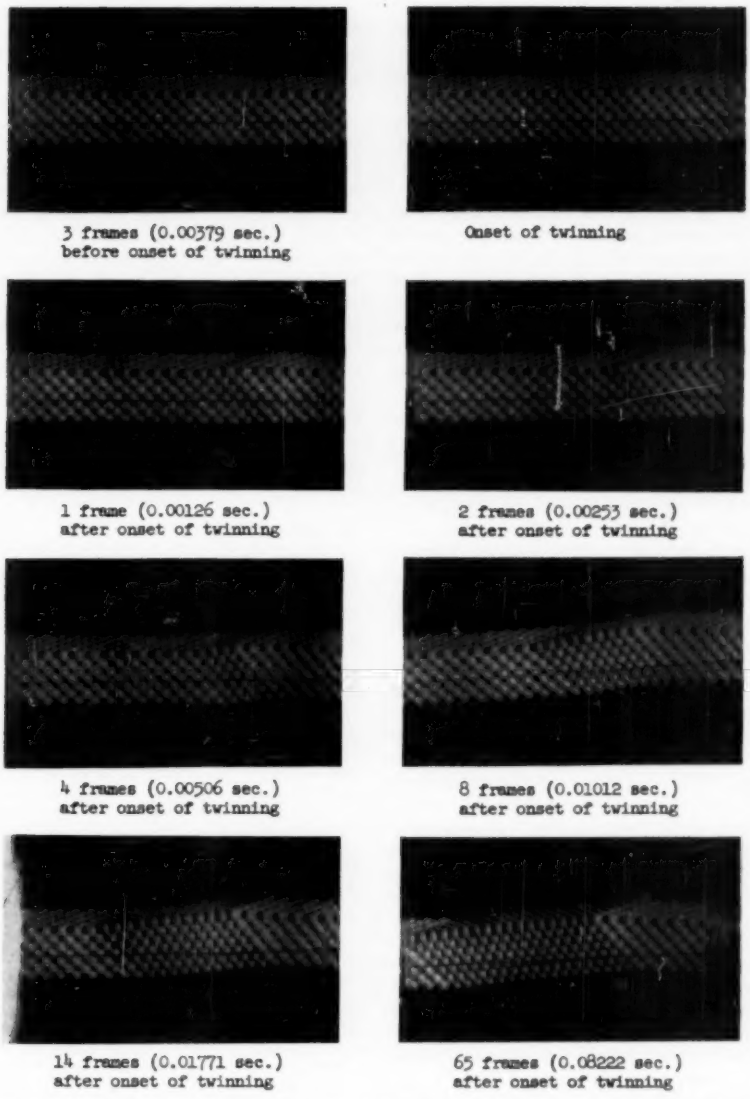

Fig. 8 Motion picture sequence of failure by twinning in a granular bar due to axial compression

plate as measured by a micrometer screw (m) (accurate to within $\pm 20 \times 10^{-6}$ in.) mounted in line with the test bar. One end of a flexible reed (r) was fastened to the anvil of the screw and the other end left free to vibrate. The screw was rotated manually by means of a pinion gear (100:1 reduction of angular motion) until a vertical ridge on the center line of the outside face of the bearing plate damped the vibrations, indicating the screw had made contact.

This method of determining the displacement of the plate was chosen because it added no measurable axial load to the test bar, and yet was sufficiently reliable to enable readings to be repeated to within the calibrated accuracy of the screw. But because of the difference of the boundaries of the test bar and those of the model for which the stress-strain relations were derived, it was necessary to adjust the measured displacements before they were used to calculate the components of strain. The micrometer screw measured the contraction not only of the model but also of the end-bearing plates, and, in addition, the relative approach of each plate and the centers of the contiguous spheres. The compression of each plate was negligibly small compared with that of the model, but the approach was not. For isotropic compression beyond an initial isotropic state of stress, the sum of both approaches, as calculated from Hertz theory, was 9.37 per cent of the total axial displacement between centers of the end spheres of the test bar [as computed from (21)]. For isotropic plus uniaxial compressive loading, this percentage was only slightly lower. Accordingly, measured displacements were reduced by an amount equal to the sum of the calculated approaches at each end, and only the balance was considered in computing the axial strain in the bar.

Isotropic pressure, initial as well as additional, was applied to the test bar by adjusting the vacuum within the rubber sheet. Although this arrangement limited the maximum total pressure available to 1 atm, it avoided using special equipment which

would both house the test bar under greater pressure and yet permit measuring displacements with reasonable facility and accuracy. The source of the vacuum was a continuously operating, two-stage, eccentric cam pump, connected to the bar via a surge chamber. The vacuum was regulated by a variable-setting control which was sufficiently sensitive to hold the pressure at the test bar (as measured by a mercury manometer) to within ± 0.1 psi.

At the start of all tests, the bar was preloaded with a full atmosphere of pressure to permit alignment of the bar when it was most rigid and to compensate partially for the frictional restraint of the support. Upon release of the preload the rubber skin on the bottom of the bar did not return to its initial position, but to a semicontracted, intermediate one. This partial contraction tended to eliminate an intermittent "stick-slip" type of motion of the rubber over the support which would have been present otherwise.

In the first group of tests, after an initial isotropic pressure had been imposed, hydrostatic and uniaxial loads were applied at a relative rate predetermined in accordance with (16) and (17). This was accomplished approximately as follows: Corresponding to the constant $\beta = 0.1$, companion increments of additional isotropic and axial stress were computed, the increments in isotropic pressure being taken at 1 psi. Then while the isotropic increment was building up to its full value, the amount of lead shot causing the corresponding axial increment was gradually added to the weight pan. After both load increments were fully applied the accompanying displacement was measured.

Test results are plotted in Fig. 4 for two values of initial stress together with the corresponding theoretical stress-strain relations. For both tests, measured strains are in good agreement with predicted results in the range examined. It is of interest to note that erratic results were obtained in similar tests for which the loading program was based on $\beta = 0.2$, a value known to be in excess of the coefficient of friction, f, between the spheres. Tests based on other permissible values of β were not conducted because preliminary investigations pointed to results having a maximum difference from those for $\beta = 0.1$ no greater than the minimum displacement which could be discerned by the micrometer screw.

A second group of tests was performed to determine, for a range of initial isotropic pressures, the axial failure stress. Axial load was applied to the bar by adding lead shot slowly to the weight pan until twinning occurred, and the failure stress was calculated from the weight of the shot which initiated twinning. In Fig. 6 this stress is shown as a function of the corresponding isotropic pressure on the bar.

Twinning occurred as predicted on one or more $\{111\}$ planes and then, in rapid succession, on several contiguous planes. Multiple twinning also occurred, more frequently for low initial pressures (3–5 psi) than for high ones (10–14 psi). Photographs of the twinning were taken with a 16-mm Fastax camera at a speed of approximately 790 frames per sec. A typical sequence is shown in Fig. 8.

According to (23), the failure stress is a function of both the initial isotropic pressure and the coefficient of friction between spheres. A comparison of theoretical curves with the test curve, Fig. 6, indicates that the coefficient of friction during tests was approximately 0.12. An independent evaluation of this coefficient was undertaken and a wide range of values obtained. While it was possible to prepare contacting surfaces with the same degree of surface finish and cleanliness as in the twinning experiments, the exact conditions of test were not duplicated. Thus tests in which a spherical surface tended to slide over a plane surface yielded values of 0.18–0.19, while tests in which a spherical surface tended to rotate in the hollow between three mutually contacting spheres furnished values of 0.06–0.09. Consequently, it is not possible to state with certainty what the actual value of the coefficient of friction was in the twinning experiments.

Some known sources of error were present in the latter experiments. Thus it was impossible to add lead shot to the weight pan without some jarring, and this jarring may have triggered the sliding before the maximum frictional force between spheres was mobilized. Such a reduced value of frictional force would be reflected in the results as an apparently lowered friction coefficient. Further, the presence of undersize or oversize spheres in the array may have been a source of error; in fact, since the normal approach between centers of contacting spheres was of the order of magnitude of their dimensional tolerance, some of the contacts may not have even "made" during tests. No significant difference in data was encountered, however, when the test was performed on a bar constructed of spheres having a dimensional tolerance two and one half times greater than that of the spheres in the original test bars.

Acknowledgment

The authors take pleasure in expressing their appreciation to Prof. R. D. Mindlin for many illuminating discussions and to Mr. W. Claypoole for his aid in determining the coefficient of friction.

References

1 G. Hara, "Theorie der akustischen Schwingungsausbreitung in gekörnten Substanzen und Experimentelle Untersuchungen an Kohlepulver," *Elektrische Nachrichten-Technik*, vol. 12, 1935, pp. 191–200.

2 K. Iida, "Velocity of Elastic Waves in a Granular Substance," *Bulletin Earthquake Research Institute*, Tokyo University, vol. 17, 1939, pp. 783–808.

3 T. Takahashi and Y. Satô, "On the Theory of Elastic Waves in Granular Substance," *Bulletin Earthquake Research Institute*, Tokyo University, vol. 27, 1949, pp. 11–16; vol. 28, 1950, pp. 37–43.

4 F. Gassmann, "Elastic Waves Through a Packing of Spheres," *Geophysics*, vol. 16, 1951, pp. 673–685; vol. 18, 1953, p. 268.

5 H. Brandt, "A Study of the Speed of Sound in Porous Granular Media," JOURNAL OF APPLIED MECHANICS, vol. 22, TRANS. ASME, vol. 77, 1955, pp. 479–486.

6 H. Deresiewicz, "Mechanics of Granular Matter," *Advances in Applied Mechanics*, vol. 5, Academic Press, New York, N. Y., 1958, pp. 233–306.

7 J. Duffy and R. D. Mindlin, "Stress-Strain Relations and Vibrations of a Granular Medium," JOURNAL OF APPLIED MECHANICS, vol. 24, TRANS. ASME, vol. 79, 1957, pp. 585–593.

8 H. Deresiewicz, "Stress-Strain Relations for a Simple Model of a Granular Medium," JOURNAL OF APPLIED MECHANICS, vol. 25, TRANS. ASME, vol. 80, 1958, pp. 402–406.

9 J. Duffy, "A Differential Stress-Strain Relation for the Hexagonal Close-Packed Array of Elastic Spheres," JOURNAL OF APPLIED MECHANICS, vol. 26, TRANS. ASME, vol. 81, 1959, pp. 88–94.

10 S. Timoshenko and J. N. Goodier, "Theory of Elasticity," McGraw-Hill Book Company, Inc., New York, N. Y., 1951, pp. 372–377.

11 R. D. Mindlin and H. Deresiewicz, "Elastic Spheres in Contact Under Varying Oblique Forces," JOURNAL OF APPLIED MECHANICS, vol. 20, TRANS. ASME, vol. 75, 1953, pp. 327–344.

12 C. W. Thurston, discussion of reference [7], JOURNAL OF APPLIED MECHANICS, vol. 25, TRANS. ASME, vol. 80, 1958, pp. 310–311.

13 C. S. Barrett, "Structure of Metals," McGraw-Hill Book Company, Inc., New York, N. Y., 1952, pp. 376–384.

14 O. Reynolds, "On the Dilatancy of Media Composed of Rigid Particles in Contact, With Experimental Illustrations," *Philosophical Magazine*, series 5, vol. 20, 1885, pp. 469–481.

A Reassessment of Deformation Theories of Plasticity

BERNARD BUDIANSKY

Associate Professor
of Structural Mechanics,
Division of Engineering and Applied Physics,
Harvard University,
Cambridge, Mass.

It is shown that deformation theories of plasticity may be used for a range of loading paths other than proportional loading without violation of general requirements for the physical soundness of a plasticity theory. The extent to which deviations from proportional loading are admissible on this basis is calculated quantitatively for the simple deformation theory of Nadai. It is shown that the lower the strain-hardening rate of the uniaxial stress-strain curve, the greater are the permissible deviations from proportional loading.

Introduction

THE state of strain in a plastically deformed element of strain-hardening material may depend on the entire history of stress to which the element has been subjected. However, for the particular type of stress history known as proportional loading, in which the components of the stress tensor increase in constant ratio to each other, the strains obviously can be expressed in terms of the final state of stress, for in this case specification of the final stress state also specifies the stress history. The so-called deformation, or finite, theories of plasticity, which relate total plastic strain to final stress, are therefore applicable to proportional loading. On the other hand, it has been shown repeatedly, by means of physical arguments, that a deformation theory cannot have general validity for all stress histories.

Unfortunately, these two characteristics of deformation theories—validity for proportional loading, and lack of general validity for all types of loading—seem to have led to the widespread but unjustified belief that the predictions of a deformation theory are physically unsound for any stress history except proportional loading. This belief ignores the possibility that the law governing plastic strain might exhibit independence of the stress history for a limited range of loading regimes that includes, but is not restricted to, proportional loading. Such limited path independence is a feature of the slip theory of plasticity [1, 2][1] and of the theory of Sanders [3, 4]. Furthermore, both of these theories are fully consistent with the basic postulates and assumptions used by Drucker to establish the general incremental theory of plasticity [5], which relates increments of plastic strain to stress increments and stress history.

In the present paper, satisfaction of Drucker's basic requirements is assumed to be the criterion for physical soundness of a plasticity theory. It is shown that deformation theories are consistent with these requirements for a range of loading paths in the vicinity of proportional loading. The well-known simple deformation theory of Nadai is particularly amenable to assessment on the basis of Drucker's requirements, and a quantitative study is made of the extent to which deviations from proportional loading are permissible for this theory. It is already known that the incremental theory of Sanders coincides rigorously with the Nadai theory for certain nonproportional loading paths; it will be seen from the present results that the use of Nadai's theory may be permissible with deviations from proportional loading considerably wider than those established by Sanders.

Review of Basic Concepts

The present discussion is restricted to initially isotropic materials with all time-dependent effects (e.g., creep) ignored. The strain tensor ϵ_{ij} is assumed to be the sum of an elastic part ϵ_{ij}^{E} and a plastic part ϵ_{ij}^{P}, with ϵ_{ij}^{E} related by Hooke's law to the stress tensor σ_{ij}. The fundamental problem of the theory of plasticity is the determination of ϵ_{ij}^{P} in terms of the history of σ_{ij}. Alternatively, one may seek to relate the plastic strain rate $\dot{\epsilon}_{ij}^{P}$ to the history of stress, and the stress rate $\dot{\sigma}_{ij}$. (This latter relation, of course, would be homogeneous in the stress and strain rates, since the time scale has been assumed irrelevant.)

A concept basic to all plasticity theories is that of the yield surface in stress space. It is convenient to deal with the six-dimensional space having co-ordinates σ_x, σ_y, σ_z, $\sqrt{2}\,\tau_{xy}$, $\sqrt{2}\,\tau_{yz}$ and $\sqrt{2}\,\tau_{zx}$; then every state of stress σ_{ij} is represented by a point in this space, and the distance from the origin to the point is simply $(\sigma_{ij}\sigma_{ij})^{1/2}$. It is sometimes useful to regard σ_{ij} as a six-dimensional vector $\vec{\sigma}$. A loading history $\sigma_{ij}(t)$ is represented by a (curved) line in the stress space. It is assumed that to each instant of a given stress history there corresponds a connected region E—the elastic region—in stress space having the following properties: (*a*) The current state of stress is contained in E; (*b*) continuation of the loading path into E produces no additional plastic strain and leaves E unchanged; but (*c*) penetration of the loading path into the exterior of E does produce a change in the plastic strain and, as a consequence of (*a*), changes the region E.

The yield surface S at each instant is defined as the boundary of E.

If the material is plastically incompressible, ϵ_{ii}^{P} always vanishes. Furthermore, if the plastic strain is supposed to be independent of hydrostatic stress, the yield surface is perpendicular to the hyperplane $\sigma_{ii} = 0$ (since if σ_{ij}^{*} is in E, so is the point $\sigma_{ij}^{*} + k\delta_{ij}$ for all k—and the line $k\delta_{ij}$ is normal to the plane $\sigma_{ii} = 0$). The projection of the point σ_{ij} on the plane $\sigma_{ii} = 0$ is the stress deviation

$$s_{ij} = \sigma_{ij} - \frac{1}{3}\,\sigma_{kk}\delta_{ij}$$

and so, when hydrostatic stress is irrelevant, the stress deviation path $s_{ij}(t)$ in the five-dimensional space $\sigma_{ii} = 0$ determines the plastic strain and the yield surface.

Incremental plasticity theory seeks to relate the strain rate

---

[1] Numbers in brackets designate References at end of paper.

Contributed by the Applied Mechanics Division and presented at the Annual Meeting, November 30–December 5, 1958, New York, N. Y., of THE AMERICAN SOCIETY OF MECHANICAL ENGINEERS.

Discussion of this paper should be addressed to the Secretary, ASME, 29 West 39th Street, New York, N. Y., and will be accepted until July 10, 1959, for publication at a later date. Discuss ionreceived after the closing date will be returned.

NOTE: Statements and opinions advanced in papers are to be understood as individual expressions of their authors and not those of the Society. Manuscript received by ASME Applied Mechanics Division, April 14, 1958. Paper No. 58—A-54.

$\dot{\epsilon}_{ij}{}^P$ to the history of stress and the stress rate $\dot{\sigma}_{ij}(=\vec{\sigma})$ imposed at a given point σ_{ij} of the history, Fig. 1. Clearly, $\dot{\epsilon}_{ij}{}^P$ vanishes whenever σ_{ij} is in the interior of E; $\dot{\epsilon}_{ij}{}^P$ also vanishes when σ_{ij} is on S, but the stress rate vector $\vec{\sigma}$ (with origin at σ_{ij}) points toward the interior of E. But for σ_{ij} on S, and $\dot{\sigma}_{ij}$ pointing to the exterior of S, "loading" is said to occur, and plastic flow—nonvanishing $\dot{\epsilon}_{ij}{}^P$—occurs. By continuity arguments, it also is reasonable to demand that $\dot{\epsilon}_{ij}{}^P$ vanish when $\dot{\sigma}_{ij}$ is tangential to S.

Drucker's Requirements

Drucker [5] has postulated a definition of work-hardening on the basis of some quasi-thermodynamic arguments. This definition led to the following two inequalities concerning the strain rate $\dot{\epsilon}_{ij}{}^P$ produced by a "loading" $\dot{\sigma}_{ij}$:

$$\dot{\sigma}_{ij}\dot{\epsilon}_{ij}{}^P > 0 \tag{1}$$

$$(\sigma_{ij} - \sigma_{ij}{}^*)\dot{\epsilon}_{ij}{}^P \geq 0 \tag{2}$$

where σ_{ij} is the current stress state (on S) and $\sigma_{ij}{}^*$ is any other stress state in E. (The second inequality is called the principle of maximum plastic work by Bishop and Hill [6], who prove it for single crystals that deform plastically by slip, and use arguments of a statistical character to extend its applicability for polycrystals composed of such single crystals.)

The following facts are shown by Drucker to be immediate consequences of inequality (2):

(*a*) The yield surface is convex.

(*b*) Suppose the current stress state σ_{ij} is on S, Fig. 1(*b*), and suppose S is smooth at σ_{ij}; i.e., there exists a unique hyperplane through σ_{ij} that does not enter E. Then, for any loading $\dot{\sigma}_{ij}$ the direction of the strain-rate vector $\vec{\epsilon}^P$ (having components $\dot{\epsilon}_x{}^P$, $\dot{\epsilon}_y{}^P$, $\dot{\epsilon}_z{}^P$, $\dot{\gamma}_{xy}{}^P/\sqrt{2}$, $\dot{\gamma}_{yz}{}^P/\sqrt{2}$, and $\dot{\gamma}_{zx}{}^P/\sqrt{2}$) must be that of the exterior normal to the yield surface at σ_{ij}.

(*c*) But suppose S is not smooth at σ_{ij}; that is, there is not a unique normal at σ_{ij} to surface elements of S. Then $\dot{\epsilon}_{ij}{}^P$ must merely point toward the (convex) region bounded by the cone of normals to S at σ_{ij}, Fig. 2. Statements (*a*), (*b*), and (*c*) are, in fact, equivalent to inequality (2).

The possibility of sharp corners in the yield surface, and the consequent relaxed restriction in the direction of $\dot{\epsilon}_{ij}{}^P$ described in (*c*), will be exploited in the discussions that follow.

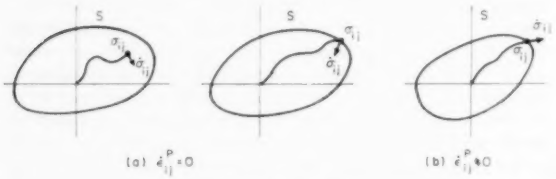

Fig. 1 Loading and unloading conditions

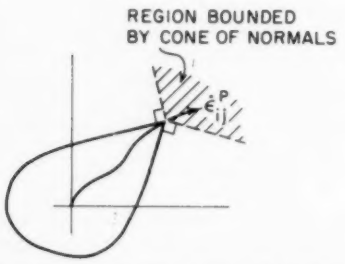

Fig. 2 Direction of $\dot{\epsilon}_{ij}{}^P$ for σ_{ij} at a corner of the yield surface

Deformation Theories of Plasticity

Prager [7] has formulated the following general relation between plastic strain and stress for the case of proportional loading:

$$\epsilon_{ij}{}^P = f(J_2, J_3)s_{ij} + g(J_2, J_3)t_{ij} \tag{3}$$

This equation applies to small strains of initially isotropic materials, the plastic deformation of which is without change of volume and is unaffected by hydrostatic stress. "Proportional loading" is now understood to mean that the components of the stress deviation tensor s_{ij} vary monotonically in constant ratio to each other; that is, $s_{ij} = \lambda(t)s_{ij}{}^0$, with $\lambda(0) = 0$, and $\dot{\lambda} > 0$. The only restriction that need be placed on the forms of f and g is that implied by the so-called condition of irreversibility [8]; that is, for proportional loading, the specific plastic power $s_{ij}\dot{\epsilon}_{ij}{}^P$ must be positive. Differentiation of (3) gives

$$\dot{\epsilon}_{ij}{}^P = \left(\frac{\partial f}{\partial J_2}\dot{J}_2 + \frac{\partial f}{\partial J_3}\dot{J}_3\right)s_{ij} + f\dot{s}_{ij} + \left(\frac{\partial g}{\partial J_2}\dot{J}_2 + \frac{\partial g}{\partial J_3}\dot{J}_3\right)t_{ij} + g\dot{t}_{ij} \tag{4}$$

During proportional loading, $\dot{s}_{ij} = \dot{\lambda}s_{ij}{}^0 = (\dot{\lambda}/\lambda)s_{ij}$, and also $\dot{t}_{ij} = (2\dot{\lambda}/\lambda)t_{ij}$, $\dot{J}_2 = (2\dot{\lambda}/\lambda)J_2$, $\dot{J}_3 = (3\dot{\lambda}/\lambda)J_3$; hence

$$s_{ij}\dot{\epsilon}_{ij}{}^P = \frac{\dot{\lambda}}{\lambda}\left[4J_2{}^2\frac{\partial f}{\partial J_2} + 6J_2J_3\left(\frac{\partial f}{\partial J_3} + \frac{\partial g}{\partial J_2}\right) + 9J_3{}^2\frac{\partial g}{\partial J_3} + 2J_2f + 6J_3g\right] \tag{5}$$

and so the bracketed quantity in (5) must be positive. [Equation (3) would be identical with a stress-strain relation of small strain nonlinear elasticity if, in addition, the condition

$$\frac{\partial f}{\partial J_3} = \frac{\partial g}{\partial J_2} \tag{6}$$

were fulfilled; for then there would exist a function $H(J_2, J_3)$ such that

$$\frac{\partial H}{\partial J_2} = f \quad \frac{\partial H}{\partial J_3} = g$$

and (3) could be written

$$\epsilon_{ij}{}^P = \frac{\partial H}{\partial J_2}s_{ij} + \frac{\partial H}{\partial J_3}t_{ij}$$

or

$$\epsilon_{ij}{}^P = \frac{\partial H}{\partial \sigma_{ij}}$$

In small-strain nonlinear elasticity, H would represent the complementary-energy-density of an incompressible material. But if (3) is only supposed to apply to plastic strains, there is no evident reason to insist upon the fulfillment of (6).]

It is important to note that the statement of the stress-strain law (3) for proportional loading does not automatically determine the yield surface associated with proportional loading up to the current stress state, nor does its use for proportional loading require any hypothesis concerning the yield surface. As will be seen, the freedom of choice available for the specification of the shape of the yield surface will permit a consistent extension of (3) to certain nonproportional loading paths.

Suppose that after proportional loading to s_{ij}, a stress rate $\dot{s}_{ij}$ not proportional to s_{ij} is imposed; does the strain rate $\dot{\epsilon}_{ij}{}^P$ calculated from (4) violate Drucker's requirements? Consider, first, condition (1), which, for incompressible materials, requires $\dot{s}_{ij}\dot{\epsilon}_{ij}{}^P > 0$. For proportional loading the condition of irreversi-

bility $s_{ij}\dot{\epsilon}_{ij}^{P} > 0$ is satisfied; but therefore $\dot{s}_{ij}\dot{\epsilon}_{ij}^{P} > 0$ when $\dot{s}_{ij}$ is proportional to s_{ij}. Consequently, by continuity, there must then be some set A of $\dot{s}_{ij}$ for which $\dot{s}_{ij}\dot{\epsilon}_{ij}^{P} > 0$.

Next, consider condition (2); whether or not this condition is fulfilled by the $\dot{\epsilon}_{ij}^{P}$ produced by some $\dot{s}_{ij}$ depends on the shape of the yield surface. We must certainly assume that the yield surface is convex, but its shape in the vicinity of s_{ij} is not known. Suppose the yield surface were smooth at s_{ij}; then, in accordance with (*b*), the unique normal to the surface would have the direction of the plastic strain rate associated with proportional loading. But the directions of $\dot{\epsilon}_{ij}^{P}$ given by (4) for $\dot{s}_{ij} \neq (\dot{\lambda}/\lambda)s_{ij}$ are different, and hence violate condition (*b*), which requires a unique direction of plastic strain rate for all $\dot{s}_{ij}$.

But now suppose that the yield surface S has a corner at s_{ij}; then, according to condition (*c*), the $\dot{\epsilon}_{ij}^{P}$ associated with proportional loading must lie within the cone of normals to S. Furthermore, again by continuity, there will exist a set B of $\dot{s}_{ij}$ for which the corresponding $\dot{\epsilon}_{ij}^{P}$ given by (4) would also fall within the cone of normals, thus satisfying condition (*c*) [and hence (2)].

Consequently, after proportional loading up to s_{ij}, the strain rate $\dot{\epsilon}_{ij}^{P}$ given by (4) is consistent with Drucker's requirements for each $\dot{s}_{ij}$ that is contained in set A as well as in set B. The hypothesis of a corner in the yield surface at s_{ij} insures the existence of such an admissible set of $\dot{s}_{ij}$.

Let us now consider the conditions under which the $\dot{\epsilon}_{ij}^{P}$ all along some curved loading path can be considered to be consistent with Drucker's requirements. Suppose we postulate (tentatively) that at each instant the yield surface in the vicinity of the current stress state is the same as it would have been after proportional loading to the current stress state. Then Drucker's conditions are satisfied if, at each s_{ij}, $\dot{s}_{ij}$ is a member of both of the sets A and B previously defined for the case of proportional loading up to s_{ij}. But now a new requirement must be satisfied before the postulated behavior of the yield surface can be considered acceptable. It is implausible to suppose that the elastic region would not continue to include the stress point s_{ij} when the stress is changed to $s_{ij} + \dot{s}_{ij}dt$. Consequently, the assumed dependence of the yield surface on s_{ij} is admissible only if $\dot{s}_{ij}$ always lies in the external (forward) cone of the tangents to the yield surface, Fig. 3. Denote the set of $\dot{s}_{ij}$ in this forward cone by C; then, finally, for every stress history $s_{ij}(t)$ such that $\dot{s}_{ij}$ is always in all three of the sets A, B, and C, the predictions (3) of deformation theory are physically sound, in the sense that neither Drucker's condition nor any other obvious plausibility consideration is violated.

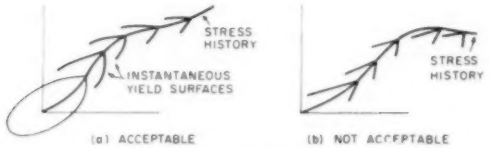

Fig. 3 Yield surfaces (locally) dependent on s_{ij} only

Such acceptable loading paths will be called "total loading" paths; the total loading paths for Nadai's deformation theory will be discussed in detail in the next section.

Total Loading Paths for Nadai's Theory

The stress-strain law of Nadai's deformation theory (also called simple deformation theory, J_2 deformation theory, octahedral shear deformation theory, Ilyushin's theory of small elastoplastic deformations) is given by the following very special case of the general relation (3):

$$\epsilon_{ij}^{P} = f(J_2)s_{ij} \tag{7}$$

This stress-strain relationship can be stated equivalently, but more explicitly, as follows:

$$\epsilon_{ij}^{P} = \frac{3}{2}\left(\frac{1}{E_s} - \frac{1}{E}\right)s_{ij} \tag{8}$$

where E_s depends on the effective stress

$$\sigma_e = \left[\frac{3}{2}\,s_{ij}s_{ij}\right]^{1/2} \tag{9}$$

in the same way that the secant modulus depends on the stress in a uniaxial tension test, Fig. 4.

Differentiation of (8) gives

$$\dot{\epsilon}_{ij}^{P} = \frac{3}{2}\left(\frac{1}{E_s} - \frac{1}{E}\right)\dot{s}_{ij} + \frac{3}{2}\,\frac{\dot{\sigma}_e}{\sigma_e}\left(\frac{1}{E_t} - \frac{1}{E_s}\right)s_{ij} \tag{10}$$

where E_t represents the tangent modulus (as a function of σ_e), and use has been made of the relationship

$$\frac{d}{dt}\left(\frac{1}{E_s}\right) = \frac{\dot{\sigma}_e}{\sigma_e}\left(\frac{1}{E_t} - \frac{1}{E_s}\right) \tag{11}$$

Consider first the conditions under which the inequality (1) is satisfied. From (10)

$$\dot{\sigma}_{ij}\dot{\epsilon}_{ij}^{P} = s_{ij}\dot{\epsilon}_{ij}^{P} = \frac{3}{2}\left(\frac{1}{E_s} - \frac{1}{E}\right)s_{ij}\dot{s}_{ij} + \frac{3}{2}\,\frac{\dot{\sigma}_e}{\sigma_e}\left(\frac{1}{E_t} - \frac{1}{E_s}\right)s_{ij}\dot{s}_{ij}$$

But, from (9)

$$\sigma_e\dot{\sigma}_e = \frac{3}{2}\,s_{ij}\dot{s}_{ij} \tag{12}$$

Hence

$$\dot{\sigma}_{ij}\dot{\epsilon}_{ij}^{P} = \frac{3}{2}\left(\frac{1}{E_s} - \frac{1}{E}\right)(s_{ij}\dot{s}_{ij}) + \left(\frac{1}{E_t} - \frac{1}{E_s}\right)(\dot{\sigma}_e)^2 \tag{13}$$

is certainly positive as long as $E > E_s > E_t$—which holds (in the plastic range) for all materials having the (usual) monotonically

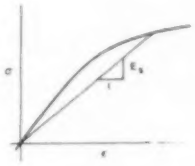

Fig. 4 Uniaxial stress-strain curve; secant modulus

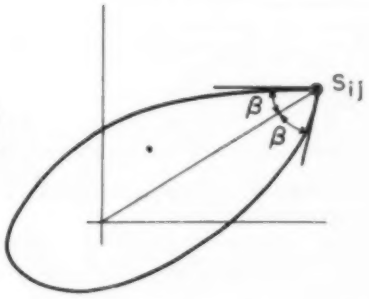

Fig. 5 Assumed yield surface (in $\sigma_{ii} = 0$) after proportional loading

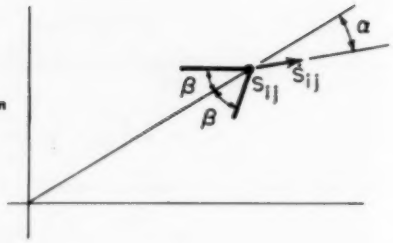

Fig. 6 Angle between $\dot{s}_{ij}$ and s_{ij}

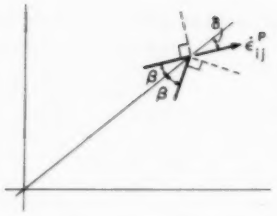

Fig. 7 Angle between $\dot{\epsilon}_{ij}^{P}$ and s_{ij}

increasing, concave downward, stress-strain curve. Thus every $\dot{s}_{ij}$ is a member of the set A.

The satisfaction of inequality (2) is a much more stringent requirement. It is to be emphasized at the outset that the loading criterion $\dot{\sigma}_e > 0$ often used in conjunction with (8) or (10) must be abandoned. The assumption will be made instead that (in the hyperplane $\sigma_{ii} = 0$) the tangents to the yield surface at s_{ij} after proportional loading generate a hypercone about the axis s_{ij} with semivertex angle $\beta < \pi/2$, Fig. 5. The precise shape of the yield surface away from the current stress state s_{ij} will not be specified, but, of course, it must be convex. The magnitude of β may depend on s_{ij}.

With β specified, one immediate restriction on $\dot{s}_{ij}$ is that it be contained in the set C; i.e., that the angle between $\dot{s}_{ij}$ and s_{ij} be not greater than β. Let α be the angle between $\dot{s}_{ij}$ and s_{ij}, Fig. 6; then

$$\cos\alpha = \frac{s_{ij}\dot{s}_{ij}}{[s_{kl}s_{kl}]^{1/2}[\dot{s}_{pq}\dot{s}_{pq}]^{1/2}} = \frac{\vec{s}\cdot\dot{\vec{s}}}{|s|\,|\dot{s}|} \tag{13}$$

If we define the unit vectors $\vec{z} = \vec{s}/|s|$ and $\dot{\vec{r}} = \dot{\vec{s}}/|\dot{s}|$ in the directions of s_{ij} and $\dot{s}_{ij}$, respectively, then

$$\cos\alpha = \dot{\vec{z}}\cdot\vec{r} \tag{14}$$

and we must have $\alpha \leq \beta$.

Now impose the final requirement that $\dot{s}_{ij}$ be in set B; i.e., that it produce an $\dot{\epsilon}_{ij}^{P}$ that lies in the cone of normals to the yield surface. Define the unit vector

$$e = \frac{\dot{\epsilon}_{ij}^{P}}{[\dot{\epsilon}_{pq}^{P}\dot{\epsilon}_{pq}^{P}]^{1/2}} = \frac{\dot{\vec{\epsilon}}^{P}}{|\dot{\epsilon}^{P}|}$$

in the direction of $\dot{\epsilon}_{ij}^{P}$, and let δ be the angle between $\dot{\epsilon}_{ij}^{P}$ and s_{ij}. Then

$$\cos\delta = \vec{z}\cdot\vec{e}$$

and (see Fig. 7) we must have

$$\delta + \beta \leq \frac{\pi}{2} \tag{15}$$

or

$$\cos\delta \geq \cos\left(\frac{\pi}{2} - \beta\right) = \sin\beta$$

$$(\cos^2\delta) \geq (1 - \cos^2\beta) \tag{16}$$

Since, from (9) and (12)

$$\frac{\dot{\sigma}_e}{\sigma_e} = \frac{s_{ij}\dot{s}_{ij}}{s_{pq}s_{pq}} = \frac{\vec{s}\cdot\dot{\vec{s}}}{|s|^2}$$

Equation (10) for the plastic strain rate can be rewritten in the convenient vector form

$$\dot{\vec{\epsilon}}^{P} = \frac{3}{2}\left(\frac{1}{E_s} - \frac{1}{E}\right)\dot{\vec{s}} + \frac{3}{2}\,\frac{\vec{s}\cdot\dot{\vec{s}}}{|s|^2}\left(\frac{1}{E_t} - \frac{1}{E_s}\right)\vec{s} \tag{17}$$

or

$$\dot{\vec{\epsilon}}^{P} = \frac{3}{2}\,|\dot{s}|\left\{\left(\frac{1}{E_s} - \frac{1}{E}\right)\vec{r} + (\vec{z}\cdot\vec{r})\left(\frac{1}{E_t} - \frac{1}{E_s}\right)\vec{z}\right\}$$

$$= \frac{3}{2}\,|\dot{s}|\left(\frac{1}{E_s} - \frac{1}{E}\right)\{\vec{r} + (N-1)(\vec{z}\cdot\vec{r})\vec{z}\} \tag{18}$$

where

$$N = \left(\frac{\dfrac{1}{E_t} - \dfrac{1}{E}}{\dfrac{1}{E_s} - \dfrac{1}{E}}\right) \tag{19}$$

Then

$$\vec{e} = \frac{\vec{r} + (N-1)(\vec{z}\cdot\vec{r})(\vec{z})}{[1 + 2(N-1)(\vec{z}\cdot\vec{r})^2 + (N-1)^2(\vec{z}\cdot\vec{r})^2]^{1/2}}$$

$$= \frac{\vec{r} + (N-1)(\cos\alpha)\vec{z}}{[1 + (N^2-1)\cos^2\alpha]^{1/2}} \tag{20}$$

so

$$\vec{z}\cdot\vec{e} = \cos\delta = \frac{N\cos\alpha}{[1 + (N^2-1)\cos^2\alpha]^{1/2}} \tag{21}$$

and, by (16), we must have

$$\frac{N^2\cos^2\alpha}{[1 + (N^2-1)\cos^2\alpha]} \geq 1 - \cos^2\beta \tag{22}$$

Then

$$\frac{N^2}{\tan^2\alpha + N^2} \geq 1 - \frac{1}{1 + \tan^2\beta} = \frac{\tan^2\beta}{1 + \tan^2\beta}$$

whence

$$\tan^2\alpha \leq \frac{N^2}{\tan^2\beta}$$

or

$$\tan\alpha \leq \frac{N}{\tan\beta} \tag{23}$$

To summarize, then, a total loading path must satisfy both

$$\alpha \leq \beta \tag{24a}$$

and

$$\alpha \leq \tan^{-1}\frac{N}{\tan\beta} \tag{24b}$$

For given N and β, the smaller of the right-hand sides of (24*a*) and (24*b*) determines the largest admissible α.

An alternative point of view is useful; suppose N is known (as it would be if s_{ij}—and hence σ_e—is specified); what value of β

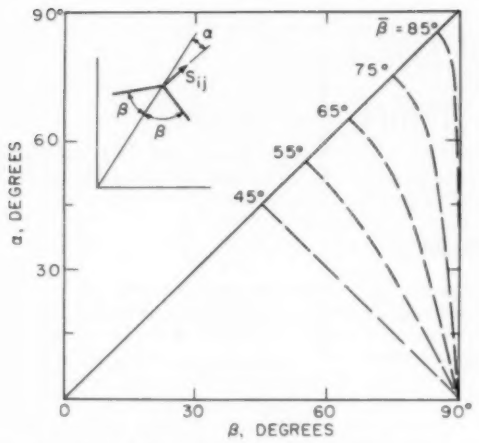

Fig. 8 Dependence of admissible directions of stress increment on semivertex angle of yield surface

would permit the largest α, i.e., the largest deviation from proportional loading? On the basis of (24*a*), we would like β to be as large as possible; but the limit on α prescribed by (24*b*) decreases with increasing β. The optimum $\beta = \bar{\beta}$ is therefore determined by the equation

$$\bar{\beta} = \tan^{-1}\left(\frac{N}{\tan\bar{\beta}}\right)$$

or

$$\tan^2\bar{\beta} = N \tag{25}$$

Consequently, as long as

$$\alpha \leq \bar{\beta} \tag{26}$$

a value of β exists for which α is admissible. The admissible α must satisfy the inequality

$$\tan^2\alpha \leq N$$

From Equation (25)

$$\cos\bar{\beta} = \left(\frac{1}{1+N}\right)^{1/2}$$

Hence the condition (26) can be written in terms of s_{ij} and $\dot{s}_{ij}$ as:

$$\frac{s_{ij}\dot{s}_{ij}}{[s_{kl}s_{kl}]^{1/2}[\dot{s}_{pq}\dot{s}_{pq}]^{1/2}} \geq \left[\frac{1}{1+\dfrac{\dfrac{1}{E_t}-\dfrac{1}{E}}{\dfrac{1}{E_s}-\dfrac{1}{E}}}\right]^{1/2} \tag{27}$$

To repeat: If we are willing to assume that β may attain its optimum value $\bar{\beta}$, a loading path is admissible if at each instant $\alpha \leq \bar{\beta}$, which will hold if inequality (27) is satisfied. Note that $\bar{\beta}$ depends only on σ_s and that since $N \geq 1$, $\bar{\beta}$ is always at least 45 deg.

On the other hand, if β is assumed (or known) to be different from $\bar{\beta}$, the limitations on α are given by (24*a*, *b*), which may be rewritten

$$\begin{cases} \alpha \leqq \beta \\ \alpha \leqq \tan^{-1}\left[\dfrac{\tan^2\bar{\beta}}{\tan\beta}\right] \end{cases} \tag{28}$$

Fig. 8 shows, for several values of $\bar{\beta}$, how the maximum admissible α varies with β. In each case, α must lie below the line $\alpha = \beta$, and the dotted curve, obtained from (28), for the appropriate value of $\bar{\beta}$. Also, for a given value of α, the interval between the solid line and the appropriate dotted curve (corresponding to a given $\bar{\beta}$) defines the range of β for which the α is admissible.

It is of interest to study the variation of $\bar{\beta}$ with the stress level and the shape of the uniaxial stress-strain curve. Suppose first that in pure tension the Ramberg-Osgood relationship

$$\epsilon = \frac{\sigma}{E} + K\sigma^n \tag{29}$$

applies. Then

$$\frac{1}{E_s} - \frac{1}{E} = K\sigma_s^{n-1}$$

$$\frac{1}{E_t} - \frac{1}{E} = nK\sigma_s^{n-1}$$

and so

$$\tan\bar{\beta} = (n)^{1/2} \tag{30}$$

independently of the stress level. Thus the more sharply the stress strain curve bends, i.e., the higher n is, the greater is the permissible deviation from proportional loading.

A modification of the stress-strain relation (29) that corresponds to a material with a definite elastic limit σ_y is given by

$$\begin{aligned} \epsilon &= \frac{\sigma}{E} \quad \text{for} \quad \sigma < \sigma_y \\ &= \frac{\sigma}{E} + K(\sigma - \sigma_y)^n \quad \text{for} \quad \sigma > \sigma_y \end{aligned} \tag{31}$$

For this case

$$\frac{1}{E_s} - \frac{1}{E} = \frac{K(\sigma_s - \sigma_y)^n}{\sigma_s}$$

$$\frac{1}{E_t} - \frac{1}{E} = nK(\sigma_s - \sigma_y)^{n-1}$$

and so

$$\tan\bar{\beta} = \left[n\frac{1}{\left(1-\dfrac{\sigma_y}{\sigma_s}\right)}\right]^{1/2} \tag{32}$$

In this case, therefore, $\bar{\beta}$ varies from 90 deg at the virgin yield surface $\sigma_s = \sigma_y$ down to $\bar{\beta} = \tan^{-1}(n)^{1/2}$ for σ_s very large. Thus the permissible deviations from proportional loading are even greater than for the material without a definite yield point.

A direct comparison, in this second case, is possible with the criterion for total loading obtained by Sanders for his incremental theory [4]. In this theory, the semivertex angle β_S at the corner of the yield surface produced by proportional loading is given by

$$\sin\beta_S = \frac{\sigma_y}{\sigma_s} \tag{33}$$

and for the simple deformation theory to remain valid, Sanders finds that α must be less than β_S.

From (32)

$$\sin\bar{\beta} = \left[\frac{n}{n+\left(1-\dfrac{\sigma_y}{\sigma_s}\right)}\right]^{1/2} \tag{34}$$

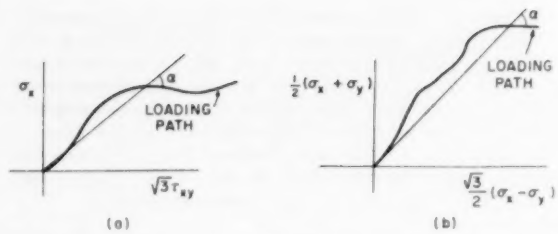

Fig. 9 Diagrams for the determination of the angle α between $\dot{s}_{ij}$ and s_{ij} for the cases (a) tension-shear and (b) biaxial tension

and it can be verified without difficulty that, for all values of $\sigma_x/\sigma_y \geq 1$ and $n \geq 1$, $\bar{\beta} > \beta_\beta$; hence the permissible deviations from proportional loading, according to the present study, are greater than those permitted in Sanders' theory.

The criterion (27) for total loading will now be exemplified in a concrete fashion for the case of combined tension σ_x and shear τ_{xy}. In this case:

$$s_{ij}s_{ij} = \frac{2}{3}(\sigma_x^2 + 3\tau_{xy}^2) = \frac{2}{3}\sigma_e^2$$

$$s_{ij}\dot{s}_{ij} = \frac{2}{3}(\sigma_x\dot{\sigma}_x + 3\tau_{xy}\dot{\tau}_{xy}) = \frac{2}{3}\sigma_e\dot{\sigma}_e$$

$$\dot{s}_{ij}\dot{s}_{ij} = \frac{2}{3}(\dot{\sigma}_x^2 + 3\dot{\tau}_{xy}^2)$$

So

$$\cos\alpha = \frac{\dot{\sigma}_e}{[(\dot{\sigma}_x)^2 + 3\dot{\tau}_{xy}^2]^{1/2}}$$

Hence if the loading path is plotted on a diagram of σ_x versus $\sqrt{3}\,\tau_{xy}$, Fig. 9(*a*), the radius vector to any point is σ_e, and α is the angle between this radius vector and the tangent to the loading path. If α is less than $\bar{\beta}$ at each point on the loading path, values of β exist for which the criterion for total loading can be satisfied.

A convenient diagram for the case of biaxial tension is also available for the purpose of checking the possibility of total loading. In this case, let

$$\xi = \frac{1}{2}(\sigma_x + \sigma_y)$$

$$\eta = \frac{1}{2}(\sigma_x - \sigma_y)$$

Then

$$\sigma_e^2 = \xi^2 + 3\eta^2$$

and, analogously to the case of tension and shear, the angle α is that between the radius vector and the tangent to the loading path in the $(\xi, \sqrt{3}\,\eta)$ plane, Fig. 9(*b*).

Conclusion

The present analysis does not pretend to demonstrate that the predictions of a deformation theory for total loading paths necessarily constitute a correct description of the plastic behavior of any given material; only experiment can determine the accuracy of the predictions. What has been shown is that, for a total loading path, a deformation theory is a respectable competitor to other theories (such as incremental theories with smooth yield surfaces) and should not be subjected to a priori rejection on physical grounds.

Acknowledgment

The financial support of the Office of Naval Research under Contract Nonr 1866(02) is gratefully acknowledged.

References

1 S. B. Batdorf and Bernard Budiansky, "A Mathematical Theory of Plasticity Based on the Concept of Slip," NACA TN 1871, April, 1949.

2 S. B. Batdorf and Bernard Budiansky, "Polyaxial Stress-Strain Relations of a Strain-Hardening Metal," JOURNAL OF APPLIED MECHANICS, vol. 21, TRANS. ASME, vol. 76, 1954, pp. 323–326.

3 J. L. Sanders, Jr., "Plastic Stress-Strain Relations Based on Linear Loading Functions," Proceedings of the Second U. S. National Congress of Applied Mechanics, ASME, 1954, pp. 445–460.

4 J. L. Sanders, Jr., "Plastic Stress-Strain Relations Based on Infinitely Many Plane Loading Surfaces," Brown University Report No. A11-106, 1952.

5 D. C. Drucker, "A More Fundamental Approach to Plastic Stress-Strain Relations," Proceedings of the First U. S. National Congress of Applied Mechanics, ASME, 1951, pp. 487–491.

6 J. F. W. Bishop and R. Hill, "A Theory of the Plastic Distortion of a Polycrystalline Aggregate Under Combined Stresses," *Philosophical Magazine*, series 7, vol. 42, April, 1951, pp. 414–427.

7 W. Prager, "Strain Hardening Under Combined Stress," *Journal of Applied Physics*, vol. 16, 1945, pp. 837–840.

8 W. Prager, "The Stress-Strain Laws of the Mathematical Theory of Plasticity—A Survey of Recent Progress," JOURNAL OF APPLIED MECHANICS, vol. 15, TRANS. ASME, vol. 70, 1948, pp. 226–233.

Collapse Loads of Rings and Flanges Under Uniform Twisting Moment and Radial Force[1]

BURTON PAUL

Assistant Professor of Engineering, Brown University, Providence, R. I. Assoc. Mem. ASME

Limit loads are found for rigid-plastic rings of arbitrary cross section subjected to uniform twisting moments and radial forces distributed over the circumference. It is shown that the interaction curves for limiting values of twisting moment and radial force have the same shape as interaction curves for limiting bending and stretching of straight beams. For rings of small uniform thickness the collapse loads are found to agree very well with those predicted by thin-plate theory. The theory is applied to find the collapse load of thin-walled corrugated tubes under axial thrust.

1 Introduction

In this paper the toroidal collapse (or inversion) of rigid-plastic circular rings due to the action of twisting moments and radial forces uniformly distributed over the circumference shall be considered from the limit-analysis point of view. Aside from the intrinsic interest of such an analysis, the collapse load of a ring is frequently required in the analysis of more complex structures. Typical situations where such information is required are illustrated in Figs. 1–3, where the rings in question are attached to symmetrically loaded cylindrical shells.

The elastic analysis of ring-reinforced structures has been understood for some time [1].[2] However, in the consideration of the rigid-plastic limit analysis of such systems, the appropriate boundary conditions are not as readily formulated as in the purely elastic case. If collapse of the supported shell occurs before collapse of the ring, then the shell may be considered to be built in at the ends and the limit loads can be found [2, 3, 4]. If, on the other hand, the rings tend to collapse first, the boundary conditions can only be determined from a limit analysis of the ring.

In what follows the stress resultants (hoop force and bending moment) acting on a cross section of the ring shall be considered the generalized stresses of the problem [5, 6]. These generalized stresses are in equilibrium with the applied surface loads; however, just as in the case of beam or plate theory, the use of generalized stresses prohibits a too detailed specification of the manner of distribution of the surface loads.

Thus the present analysis will be concerned with a set of internal hoop forces and bending moments in equilibrium with a given set of surface loads which are statically equivalent to a uniformly distributed radial force and twisting moment as illustrated in Fig. 4. The foregoing choice of generalized stresses will naturally eliminate the possibility of predicting failure in modes where generalized stresses of a type neglected herein are predominant. For example, collapse due to shearing forces or internal radial stresses (such as given by the solution of Lamé for an elastic disk) cannot be predicted by the present analysis. Nor can collapse due to radial bending moments, such as that illustrated in Fig. 3, be predicted. However, the neglect of shear stresses has proved to be very reasonable in the case of shallow beams [7] and is assumed to be of equal validity in the present case for rings having small ratios of depth to diameter. Although collapse due to formation of hinge circles cannot be predicted by the present analysis, the portion of the ring below the hinge circle shown in Fig. 3 can be analyzed by the methods of this paper. This will be illustrated by an example in Section 3.

In the next section the toroidal collapse load of a rigid-plastic ring, of arbitrary cross section, subjected to a uniform radial force of Q lb per in. and twisting moment M in-lb/in., as illustrated in

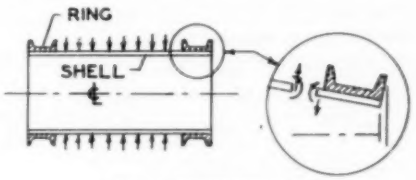

Fig. 1 Ring-reinforced shell

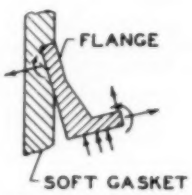

Fig. 2 Flanged shell

Fig. 3 Flange with yield hinge

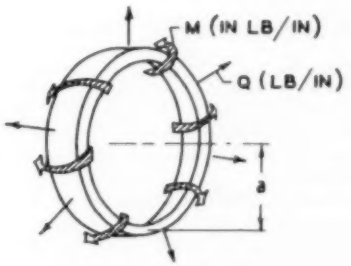

Fig. 4 Loads on ring

[1] This paper was written at the Polytechnic Institute of Brooklyn, Brooklyn, N. Y., under the sponsorship of the Naval Research Office.

[2] Numbers in brackets designate References at end of paper.

Contributed by the Applied Mechanics Division and presented at the Annual Meeting, November 30–December 5, 1958, New York, N. Y., of The American Society of Mechanical Engineers.

Discussion of this paper should be addressed to the Secretary, ASME, 29 West 39th Street, New York, N. Y., and will be accepted until July 10, 1959, for publication at a later date. Discussion received after the closing date will be returned.

Note: Statements and opinions advanced in papers are to be understood as individual expressions of their authors and not those of the Society. Manuscript received by ASME Applied Mechanics Division, April 21, 1958. Paper No. 58—A-55.

Fig. 4, will be determined. In Section 3 the special case of a ring of uniform thickness will be treated. It will be shown that for rings subjected to various surface loadings the present analysis agrees very well with thin-plate theory, wherein a much closer view is taken of the actual distribution of surface loading. In Section 4 the ring analysis will be used to find the collapse load of a corrugated tube subjected to a uniform axial force as shown in Fig. 12. The final section will contain conclusions.

2 Determination of Collapse Loads

A velocity field is said to be kinematically admissible if it satisfies all geometric boundary conditions and the condition that the work rate of the external forces be non-negative. A stress field is said to be statically admissible if it is in equilibrium with prescribed surface loads and nowhere violates the yield inequality.

According to the theorems of limit analysis [6, 8] the unique collapse load of a structure can be determined by finding a kinematically admissible velocity field associated, by means of the plastic potential flow law, with a statically admissible stress distribution.

A suitable velocity field is provided for the present problem by the assumption that all cross sections of the ring rotate without distortion, through a small angle ϑ in their respective planes, about an axis O located a distance d from the centroid c of the cross section, as shown in Fig. 5. A generic element of the cross section, located a distance ξ from the center of rotation, undergoes a pure circumferential strain ϵ. The strain rate is given by

$$\dot{\epsilon} = \xi\dot{\vartheta}/a. \tag{1}$$

The plastic potential-flow law requires that all circumferential fibers undergo a normal stress σ which is equal to the tensile yield stress in magnitude and whose sign is the same as that of $(\xi\dot{\vartheta})$. Retaining the spirit of beam and plate theory the radial normal stresses and all shearing forces are ignored.

Thus the state of stress is essentially uniaxial and given by

$$\begin{aligned} \sigma &= Y \quad (0 < \xi\dot{\vartheta}), \\ \sigma &= -Y \quad (\xi\dot{\vartheta} < 0), \end{aligned} \tag{2}$$

where Y is the yield stress in tension.

If the cross-sectional shape of the ring is known the resultant circumferential (hoop) force T acting on any cross section, as well as the resultant bending moment M_b with respect to the centroid may be obtained as functions of the parameter d. The relationships between these stress resultants and the external loads may be found easily from the free-body diagram in Fig. 6, which shows the force and moment vectors acting on an elementary sector of the ring. These relationships are

$$T(d) = Qa, \tag{3a}$$

$$M_b(d) = Ma. \tag{4a}$$

The external work rate $\dot{W}$ is given by

$$\dot{W} = 2\pi a(M\dot{\vartheta} + Q\dot{\vartheta}d) = 2\pi\dot{\vartheta}(M_b + Td). \tag{5}$$

The quantity $(M_b + Td)$ is simply the bending moment of the circumferential stresses σ with respect to the axis OO'. It follows from Equations (2) that this quantity is either positive or negative according as $\dot{\vartheta}$ is positive or negative. Thus the work rate $\dot{W}$ of the external forces is necessarily positive, as required for kinematic admissibility.

By eliminating the parameter d from Equations (3a) and (4a), a relationship between M and Q may be obtained which is associated with a kinematically admissible velocity field. If the functions $T(d)$ and $M_b(d)$ have been computed on the assumption

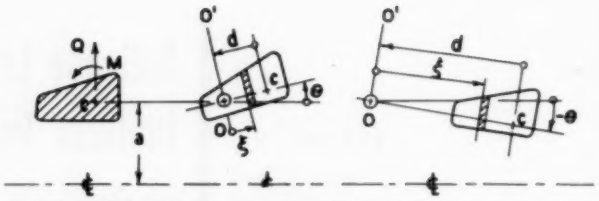

Fig. 5 (a) Undeflected cross section. (b) Deflected state ($\theta > 0$; $d > 0$). (c) Deflected state ($\theta < 0$; $d > 0$).

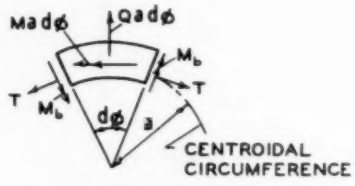

Fig. 6 Ring sector

that $M_b > 0$, a set of equations analogous to (3a), (4a) may be derived upon assuming $M_b < 0$. These will take the form

$$T(d) = -Qa, \tag{3b}$$

$$M_b(d) = -Ma, \tag{4b}$$

where the functional forms of $T(d)$ and $M_b(d)$ are identical with those in Equations (3a), (4a).

The stress (resultant) field given by Equations (2), (3), (4) is evidently statically admissible. Therefore any combination of Q and M satisfying Equations (2), (3), and (4) will produce collapse of the ring.

Equations (3) and (4) are the parametric representations of a closed curve in the (Q, M)-plane, known as the interaction curve. Any point within the interaction curve represents a safe loading condition and any point on the curve represents a collapse loading system. Onat and Prager [9] have discussed the interaction curve for a straight beam subjected to the simultaneous action of bending moment and axial force. The stress distribution at a fully plastic cross section of such a beam is the same as that in the circular ring under discussion, hence the interaction curves are identical. However, the point of view adopted here is to treat the radial force Q and twisting moment M as generalized stress variables (rather than axial force and bending moment) so that the associated generalized strain variables [5, 6] are the radial deflection ϑd and angle of twist ϑ (rather than extension and curvature). The interaction curves may be nondimensionalized by writing

$$q = Q/Q_0 = aQ/YA \tag{6}$$

$$m = M/M_0 = aM/2YS \tag{7}$$

where A is the cross-sectional area and S is the first static moment of the cross-sectional area on either side of the centroid (i.e., to the left or right of point c in Fig. 5a) about an axis through c. Using this notation, the interaction curves for a right triangular cross section, a rectangular cross section, and an ideal H cross section can be represented, respectively, by

$$\pm m = (27/8)(1 \mp q)\left\{1 - \left[\frac{1}{2}(1 \mp q)\right]^{1/2}\right\} \tag{8}$$

$$\pm m = 1 - q^2 \tag{9}$$

$$\pm m = 1 - |q| \tag{10}$$

where the upper signs are to be used for $m \geq 0$.

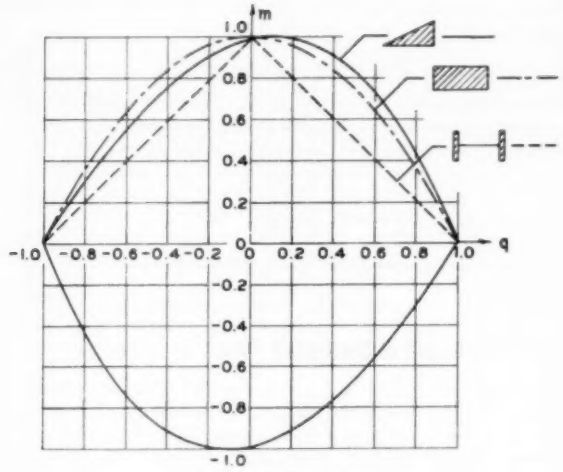

Fig. 7 Interaction curves

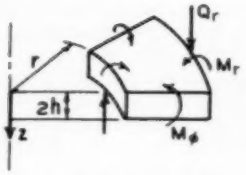

Fig. 8 Plate element

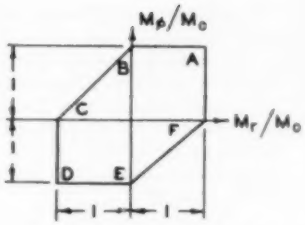

Fig. 9 Interaction curve for plate

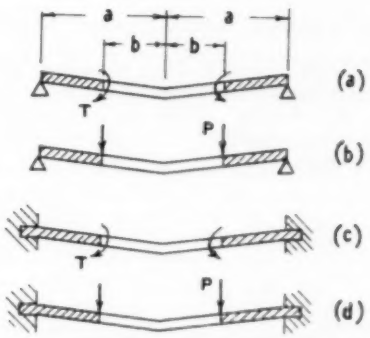

Fig. 10 Manner of loading and supporting plates

Equations (8)–(10) are illustrated in Fig. 7. The curves for rectangular and H cross sections are symmetrical with respect to both co-ordinate axes and are therefore shown in part only. This symmetry is typical of any cross section having a line of symmetry or skew symmetry. When bending of a beam takes place in a principal plane such symmetry usually will prevail and, as noted by Onat and Prager [9], the interaction curves for most structural sections will fall in between the parabola and the broken straight line shown in Fig. 7.

The triangular cross section is of interest as an approximation to a tapered flange, Fig. 2, or to a transition section of pipe. For such a cross section it is seen that the interaction curve is bounded by the parabola and the broken straight line in only two of the four quadrants.

3 Comparison With Theory of Plates

A ring of small uniform thickness may be thought of as an annular plate. Since the manner of surface loading may be specified with greater precision in the theory of plates than in the foregoing analysis of rings, it is desirable to compare the predictions of the two theories in a few representative cases.

The limit analysis of symmetrically loaded thin circular plates has been treated fully by Hopkins and Prager [10], and affords a very useful check on the theory presented in this paper. In view of the assumptions which underlie the present theory, exact agreement with the theory of plates cannot be expected for a purely arbitrary loading system. However, it will be demonstrated that the two theories concur exactly in a wide variety of cases and can, in any case, be expected to compare very favorably as the ratio of ring depth to diameter becomes smaller and smaller.

Let M_r, M_φ, Q_r represent the radial bending moment, circumferential bending moment, and lateral shear force per unit length, respectively, acting as shown in Fig. 8, on an element of a symmetrically loaded thin flat plate of width $2h$.

The equation of moment equilibrium [10] takes the form

$$\frac{d}{dr}(rM_r) - M_\varphi = rQ_r = -\int_0^r rp(r)dr \tag{11}$$

where $p(r)$ is a radially symmetric surface loading. It may be shown that the interaction curve for M_r, M_φ, based on the Tresca yield condition [10, 11] takes the form shown in Fig. 9, where $M_0 = Yh^2$. The flow law requires that the curvature rate vector $(\kappa_r, \kappa_\varphi)$ must necessarily have the direction of the exterior normal to the interaction curve for any plastic point in the plate. If w designates the rate of lateral deflection in the direction of positive z (see Fig. 8) the following relationships prevail:

$$\kappa_r = -d^2w/dr^2$$
$$\kappa_\varphi = -dw/rdr \tag{12}$$

In general, it may be shown that no finite region of the plate can be in the plastic regimes represented by line segments AF and CD of the interaction curve. If the entire plate lies in regime AB or DE the flow law requires that

$$\kappa_r = 0;\ w = c_1r + c_2 \tag{13}$$

where c_1, c_2 are constants of integration; that is, all radii of the plate remain straight in the deformed state. This corresponds to the same kinematically admissible deformation assumed for the ring, therefore the collapse loads predicted by both plate and ring theory will coincide exactly. A typical loading pattern corresponding to regime AB is shown in Fig. 10(a) where the inner boundary is loaded by a moment of intensity T in. lb per in. It may be verified by substitution into Equation (11) that for this case a statically admissible stress distribution is given by

$$M_r = M_0(1 - a/r);\ M_\varphi = M_0$$
$$T = -M_0(1 - a/b) \tag{14}$$

where T is the collapse load according to both plate and ring theory.

A typical case of loading such that the entire plate corresponds to corner B of the interaction curve is shown in Fig. 10(b). A statically admissible stress distribution is given in this case by

$$M_r = 0;\ M_\varphi = M_0;$$
$$P = M_0/b. \tag{15}$$

In this case, the form of the deflected plate is indeterminate, but it is to be noted that, once again, the plate and ring theories both predict the same collapse load.

As a final example of loading where the two theories agree perfectly, consider the case shown in Fig. 10(*c*). The plate theory predicts a plastic hinge circle at the built-in edge. This case can be treated by the ring theory developed in the foregoing if the fully plastic hinge moment M_0 at the outer boundary is treated as an external moment acting on the ring. This corresponds to the case shown in Fig. 3. It may be verified that a statically admissible stress distribution corresponding to the loading of Fig. 10(*c*) is given by

$$M_r = M_\varphi = -M_0$$
$$T = M_0 \tag{16}$$

where T is the same collapse moment predicted by both plate and ring theory.

All of the previous examples shared a common characteristic in that the same kinematically admissible velocity field served for both ring and plate theories. If, however, part of the plate happens to be in plastic regimes BC or EF, the vector $(\kappa_r, \kappa_\varphi)$ must satisfy the relationship

$$\kappa_r = -\kappa_\varphi. \tag{17}$$

Therefore

$$\frac{d^2w}{dr^2} + \frac{1}{r}\frac{dw}{dr} = 0 \tag{18}$$

or

$$w = C_1 + C_2 \log r. \tag{19}$$

Obviously, the deformations of ring and plate theory cannot agree in this case. Typical of such situations is the loading pattern shown in Fig. 10(*d*). It can be verified that a statically admissible stress-resultant field for the plate is given by:

$$M_r = (M_0 - bP) \log (r/b) \tag{20}$$

$$M_\varphi = M_0 + M_r, \tag{21}$$

$$P = M_0[1 + \log(a/b)]/b \log (a/b). \tag{22}$$

The associated velocity field is given by

$$W = c \log r/a \tag{23}$$

where c is a positive constant.

To treat this problem by means of ring theory the hinge moment must be considered as an external load acting on the ring. Consideration of Fig. 11 will show that the total moment M per unit of centroidal circumference is given by

$$M = [2Pb(a - b) - 2M_0a]/(a + b) \tag{24}$$

Thus the ring theory leads via Equations (7) and (9) to the collapse load

$$P = M_0(2a - b)/b(a - b). \tag{25}$$

Although Equations (22) and (25) are superficially different it can easily be shown that for rings having small ratio of depth to diameter, both theories lead to the same result; that is, if

$$a/b = 1 + \Delta,$$
$$\Delta \ll 1, \tag{26}$$

both Equations (22) and (25) lead to the collapse load

$$P = M_0/b\Delta. \tag{27}$$

4 Collapse Load of Corrugated Tube

The previous analysis may be used to derive the approximate collapse loads of corrugated tubes under axisymmetric loading. Fig. 12 shows a corrugated tube, consisting of any number of constant-width conical frustrum shell elements. The tube is closed by rigid caps supporting a total axial load of $2\pi aP$ pounds.

A kinematically admissible collapse mode is provided by the assumption that plastic hinge circles form at each crest and trough, and that between hinge circles each conical section undergoes a toroidal deformation with cone generators remaining straight lines. Thus each conical frustrum may be thought of as a ring loaded by the forces shown in Fig. 12, where M_A and M_B are the plastic hinge moments per unit length at crest and trough, respectively.

The total twisting moment M per unit of centroidal circumference acting on a ring is

$$M = [Pa(a - b) - M_Bb - M_Aa]\Big/\frac{1}{2}(a + b). \tag{28}$$

Since the radial force Q is zero, the collapse load may be found from Equations (9) and (7) to be given by

$$M = 2YS\Big/\frac{1}{2}(a + b), \tag{29}$$

where

$$S = h(a - b)^2 \cot^2 (\alpha/4) \cos \alpha. \tag{30}$$

In order to determine M_A and M_B it must be noted that the conical frustum is actually a shell of revolution, and as such is governed by the yield surface derived by Onat and Prager [12]. By consideration of the discontinuity of slope in the meridional direction at a hinge circle it may be concluded that the pertinent portion of the yield surface is given by the first line in Table II of reference [12]. Noting that the meridional stress resultant N_φ

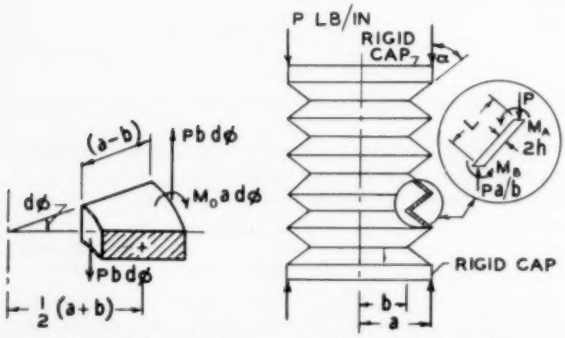

Fig. 11 Loading on ring

Fig. 12 Corrugated tube

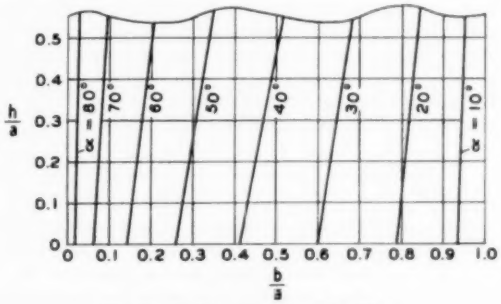

Fig. 13 Regions of static admissibility

at a cross section of radius r for the present problem is,

$$N = -P(a/r) \cos \alpha \tag{31}$$

it follows from [12] that, at a plastic hinge circle, the meridional bending moment M_φ is related to N_φ by

$$\pm M_\varphi/Yh^2 = 1 - (N_\varphi/2Yh)^2 \tag{32}$$

Upon appropriate interpretation of symbols, Equation (32) reduces identically to Equation (9).

Although no conceptual difficulties arise if Equation (32) is retained, the limitations of the analysis are somewhat easier to formulate if Equation (32) is linearized in the same manner that Equation (9) is linearized to form Equation (10). In the event that the corrugated tube consists of an ideal sandwich or H cross section, no approximation is involved.

With this simplification the hinge moments may be expressed by

$$M_A/Yh^2 = 1 - P \cos \alpha/2Yh, \tag{33}$$

$$M_B/Yh^2 = 1 - P(a/b) \cos \alpha/2Yh, \tag{34}$$

where

$$0 \leq P \leq 2Yhb/a \cos \alpha. \tag{35}$$

Equations (33) and (34) are analogous to Equation (10). The inequality (35) stipulates that the generalized stress point remains on the required interaction curve (or remains within the first quadrant of the analogous broken-line curve shown in Fig. 7).

Equations (28)–(30), (33), (34) may be combined to give the collapse load

$$\frac{P}{Yh} = \frac{(h/a)(1 + b/a) + (1 - b/a)^2 \cos \alpha/2 \sin^2 \alpha}{(1 - b/a) + (h/a) \cos \alpha} \tag{36}$$

In order to consider the limiting case of a perfect cylinder it should be noted from Fig. 12 that $L \sin \alpha = a - b$. If the slant height L is held fixed and the angle α decreased, Equation (36) leads to

$$P_{\alpha=0} = 2Yh(1 + L^2/4ah) \tag{37}$$

This result seems reasonable in view of the fact that a perfect cylinder may be thought of as the limiting case of a corrugated tube with any L whatsoever. Since the cylinder will actually collapse in the kinematically admissible mode associated with the lowest value of P, it will collapse in that mode for which $L = 0$; that is, failure is due to pure compression with no bending effect.

Equation (37) also indicates in a qualitative manner that small wave-length axisymmetric deviations of initially cylindrical shells will produce only second-order effects on the limit load (ignoring stability effects).

The collapse load given by Equation (36) is associated with a statically admissible stress-resultant field if Inequality (35) is valid. Equation (36) shows that the absolute maximum meridional stress resultant

$$N_{\varphi\max} = P(a/b) \cos \alpha$$

is a linear fractional form, in (h/a), which is monotonically increasing or decreasing accordingly as

$$2(1 + b/a) \gtrless (1 - b/a) \cot^2 \alpha. \tag{38}$$

Furthermore, $|N_\varphi|_{\max} = 2Yh$, when

$$(h/a) \cos^2 \alpha \sin^2 \alpha = (b/a)(1 + \sin^2 \alpha) - \cos^2 \alpha \tag{39}$$

Therefore in order to have a statically admissible stress field it is necessary that

$$\frac{1 - b/a}{1 + b/a} \geqslant 2 \tan^2 \alpha \tag{40}$$

and

$$\left(\frac{h}{a}\right) \geqslant \frac{(b/a)(1 + \sin^2 \alpha) - \cos^2 \alpha}{\cos^2 \alpha \sin^2 \alpha} \tag{41}$$

where the upper signs are used together, and the lower signs are used together. These inequalities limit the range of the three geometric parameters $(b/a, h/a, \alpha)$ over which the solution is correct. It may be verified that the satisfaction of the lower of Inequalities (41) guarantees the satisfaction of the lower of Inequalities (40).

In Fig. 13 those values of (h/a) and (b/a) for which the lower of inequalities (41) is valid for a given angle α lies to the right of an inclined line labeled with the given value of α. These labeled lines will be referred to as demarcation lines. Fig. 13 shows only the region of physical interest $0 < h/a < 1/2$; however, the following comments apply to the entire range $0 < h/a < 1$.

Obviously, a sufficient condition for the present solution to be statically admissible is that the point (b/a), (h/a) lie to the right of the appropriate demarcation line. It may be shown further by use of the upper of inequalities (40) that this is also a necessary condition for static admissibility if $\alpha > 34.2°$. For lower values of α the present solution is valid for all values of $b/a < (1 - 3 \sin^2 \alpha)/(1 + \sin^2 \alpha)$. These values of b/a, however, are (except for very small values of α) so small that they are of no interest for the problem under consideration.

In short, the collapse load predicted by Equation (35) is both statically and kinematically admissible for what should prove to be the greatest range of practical interest of the three governing geometrical parameters h/a, b/a, α.

5 Conclusion

The interaction curve for simultaneous extension and flexure of a straight bar may serve as the interaction curve for the toroidal deformations of a ring, provided that the associated generalized stresses and strains are interpreted accordingly. Although the choice of twisting moment and radial force as generalized stresses prohibits a distinction between any two statically equivalent surface loadings of the type under consideration, it has been shown that in the limiting case of thin rings of uniform thickness, the resulting inaccuracies approach the vanishing point as the ratio of depth to diameter decreases. What inaccuracies do arise seem well compensated for by the increased generality of the theory which, contrary to the limit analysis of plates outlined in [10], can treat rings of arbitrary cross section and include the effect of radial forces.

It is to be understood that the present theory is not applicable if the hoop stress is of sufficiently large negative value to introduce instability effects.

The foregoing application to an axially loaded corrugated tube is to be considered only a typical example. The present theory also can include the effect of internal or external fluid pressure.

The application of the results of this paper to the problem of reinforced pressure vessels will be considered elsewhere.

Acknowledgment. The author would like to thank Prof. P. G. Hodge, Jr., for valuable criticism.

References

1 S. Timoshenko, "Strength of Materials, Part II," D. Van Nostrand Co., Inc., New York, N. Y., 1941, pp. 177–183.

2 E. T. Onat, "The Plastic Collapse of Cylindrical Shells Under Axially Symmetric Loading," *Quarterly of Applied Mathematics*, vol. 13, 1955, pp. 63–72.

3 P. G. Hodge, Jr., "The Rigid-Plastic Analysis of Symmetrically Loaded Cylindrical Shells," JOURNAL OF APPLIED MECHANICS, vol. 21, TRANS. ASME, vol. 76, 1954, pp. 336–342.

4 D. C. Drucker, "Limit Analysis of Cylindrical Shells Under Axially-Symmetric Loading," Proceedings of First Midwest Conference on Solid Mechanics, Urbana, Ill., vol. 3, 1954.

5 W. Prager, "The General Theory of Limit Design," Proceedings of Eighth International Congress of Applied Mechanics, Istanbul, 1952, vol. 2, 1956, pp. 65–72.

6 J. N. Goodier and P. G. Hodge, Jr., "Elasticity and Plasticity," John Wiley and Sons, Inc., New York, N. Y., 1958. (Vol. 1 of Midwest Research Institute Series.)

7 P. G. Hodge, Jr., "Interaction Curves for Shear and Bending of Plastic Beams," JOURNAL OF APPLIED MECHANICS, vol. 24, TRANS. ASME, vol. 79, 1957, pp. 453–456.

8 D. C. Drucker, W. Prager, and H. J. Greenberg, "Extended Limit Design Theorems for Continuous Media," *Quarterly of Applied Mathematics*, vol. 9, 1952, pp. 381–389.

9 E. T. Onat and W. Prager, "The Influence of Axial Forces on the Collapse Loads of Frames," Proceedings of First Midwest Conference on Solid Mechanics, Urbana, Ill., 1954.

10 H. G. Hopkins and W. Prager, "The Load Carrying Capacities of Circular Plates," *Journal of the Mechanics and Physics of Solids*, vol. 2, 1953, pp. 1–13.

11 B. Paul and P. G. Hodge, Jr., "Bending Moment Interaction Curve for Thin Plates With Arbitrary Yield Condition," PIBAL Report No. 348, Polytechnic Institute of Brooklyn, Brooklyn, N. Y., 1956.

12 E. T. Onat and W. Prager, "Limit Analysis of Shells of Revolution, I, II," *Proceedings Koninkl. Nederl. Akadamie Van Wetenschappen-Amsterdam*, series B, vol. 57, no. 5, 1954.

Creep of Thick-Walled Tubes Under Internal Pressure Considering Large Strains

F. P. J. RIMROTT

Assistant Professor,
Department of Engineering Mechanics,
The Pennsylvania State University,
University Park, Pa.
Assoc. Mem. ASME

Using the generally accepted assumptions of constant density, zero axial strain, and the distortion-energy law, equations are derived for the creep rates, strains, and stresses of a thick-walled, closed-end, circular, hollow cylinder under internal pressure and made of an isotropic and homogeneous material. The strains are considered large, requiring the use of the finite-strain theory. A known creep rate versus stress relation is then used to solve a specific problem.

In problems concerned with the deformation in the elastic and primary creep ranges it is sufficiently accurate to assume that the strains are small and that the deformations can be referred to the original dimensions of the cylinder rather than the instantaneous deformed values. The magnitude of deformation during secondary and tertiary creep, however, may reach values where infinitesimal strains can no longer be assumed.

In order to obtain a pressure-versus-creep rate relation, the usual assumptions used in the theory of creep for combined stress will be made. It will be assumed that during creep:

1 The cylinder is made of an isotropic and homogeneous material and retains its circular shape.

2 The volume of the material remains constant, or

$$\epsilon_\varphi + \epsilon_r + \epsilon_z = 0 \tag{1}$$

3 The axial strain rate is zero

$$\dot{\epsilon}_z = 0 \tag{2}$$

It can be shown that this assumption yields the correct value for the axial force.

4 The ratios of the principal shear-strain rates to the principal shear stresses are equal; that is

$$\frac{\dot{\epsilon}_\varphi - \dot{\epsilon}_r}{\sigma_\varphi - \sigma_r} = \frac{\dot{\epsilon}_r - \dot{\epsilon}_z}{\sigma_r - \sigma_z} = \frac{\dot{\epsilon}_z - \dot{\epsilon}_\varphi}{\sigma_z - \sigma_\varphi} \tag{3}$$

5 There is a significant stress-versus-rate of true strain relationship, which coincides with the true stress-versus-creep rate relationship in simple tension; that is

$$\sigma = f(\dot{\epsilon}) \tag{4}$$

The foregoing assumptions also were made by Bailey [1, 2],[1] Soderberg [8], Marin [6], Nadai [3], Johnson [4], and Weir [5], with the exception that equations (3) and (4) are expressed in terms of true stress and true strain in the new theory in place of the nominal values.

As the magnitude of the creep deformation increases, a condition is soon reached where an analysis of the state of stress and creep rate demands the application of the finite-strain concept.

The present paper, making use of the foregoing assumptions, extends the finite-strain theory developed in a paper by MacGregor, Coffin, and Fisher [9], for application to the creep of thick-walled, closed-end cylinders under internal pressure.

The results of this study show that the creep rate of a cylinder subjected to a constant internal pressure increases with deformation, when the creep rate of the same material in simple tension under constant stress is constant. They are intended to warn the design engineer that the customary assumption of infinitesimal strains in the study of creep of thick-walled cylinders leads to results (e.g., in determinination of the wall thickness) on the unsafe side. They should aid the design engineer in predicting the correct creep rates, strains, and stresses in cases where large creep deformations of cylinders are permissible.

Derivation of Basic Equation

The radial equilibrium in a deformed cylinder, as shown in Fig. 1, requires that

$$r' \frac{d\sigma_r}{dr'} = \sigma_\varphi - \sigma_r \tag{5}$$

For presentation at the Summer Conference of the Applied Mechanics Division, Troy, N. Y., June 18–20, 1959, of THE AMERICAN SOCIETY OF MECHANICAL ENGINEERS.

Discussion of this paper should be addressed to the Secretary, ASME, 29 West 39th Street, New York, N. Y., and will be accepted until July 20, 1959, for publication at a later date. Discussion received after the closing date will be returned.

NOTE: Statements and opinions advanced in papers are to be understood as individual expressions of their authors and not those of the Society. Manuscript received by ASME Applied Mechanics Division, January 27, 1958. Paper No. 59—APM-6.

[1] Numbers in brackets designate References at end of paper.

Nomenclature

B = a material constant
T = a function of time
a = original internal radius
a' = actual internal radius
b = external radius
n = a material constant
p = internal pressure
t = time
u = radial displacement
ϵ = natural strain, also significant natural strain
$\dot{\epsilon}$ = rate of natural strain, also rate of significant natural strain
σ = true stress, also significant true stress
σ_0 = a constant

Subscripts

a = at internal radius
b = at external radius
r = radial
z = axial
φ = tangential

Constants Used in Example

$B = 5 \cdot 10^{-12}$ 1/day
$n = 6$
$p = 40{,}000$ psi
$b/a = 5$
$\sigma_0 = 1000$ psi

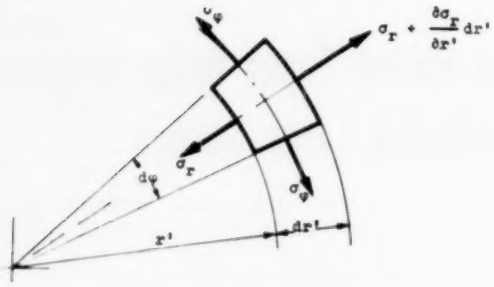

Fig. 1 Element of deformed cylinder

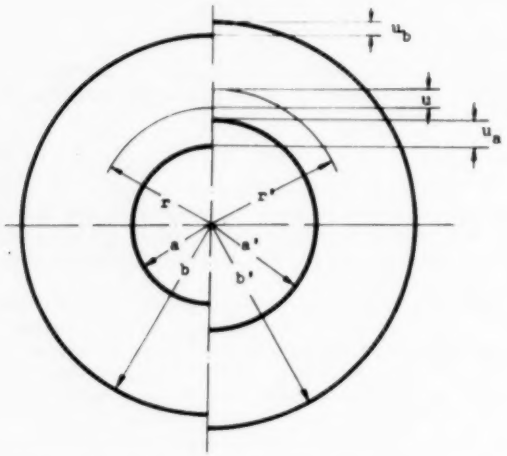

ORIGINAL STATE DEFORMED STATE

Fig. 2 Cross section of thick-walled cylinder

Fig. 2 shows the cylinder in its original shape and its deformed shape. The cross section of the cylinder with the inside radius a and the outside radius b expands to the inside radius $a' = a + u_a$ and the outside radius $b' = b + u_b$. An arbitrary element at the radius r has moved to the position $r' = r + u$. The natural tangential strain becomes

$$\epsilon_\varphi = \ln \frac{r'd\varphi}{rd\varphi} = \ln \frac{r'}{r} = \ln \left(1 + \frac{u}{r}\right) \tag{6}$$

and the radial strain

$$\epsilon_r = \ln \frac{\partial r'}{\partial r} = \ln \left(1 + \frac{\partial u}{\partial r}\right) \tag{7}$$

After elimination of u in equations (6) and (7), the equation of compatibility of the strains is arrived at,

$$r \frac{\partial \epsilon_\varphi}{\partial r} = e^{\epsilon_r - \epsilon_\varphi} - 1 \tag{8}$$

If use is made of the relationships given in equations (6), (7), and (8), the equilibrium equation (5) can be obtained as

$$r \frac{\partial \sigma_r}{\partial r} = (\sigma_\varphi - \sigma_r) e^{\epsilon_r - \epsilon_\varphi} \tag{9}$$

The closed-end cylinder under internal pressure is one of the cases where the use of significant strain leads to the same result as the use of the significant strain rate. The derivation of the basic equation therefore may be based on either quantity. The significant strain, which will be used here, is defined by

$$\epsilon = \frac{\sqrt{2}}{3} [(\epsilon_\varphi - \epsilon_r)^2 + (\epsilon_r - \epsilon_z)^2 + (\epsilon_z - \epsilon_\varphi)^2]^{1/2} \tag{10}$$

By using equations (1) and (2), the significant strain becomes for the cylinder

$$\epsilon = \frac{2}{\sqrt{3}} \epsilon_\varphi \tag{11}$$

or

$$\epsilon = -\frac{2}{\sqrt{3}} \epsilon_r \tag{12}$$

The significant stress is defined as

$$\sigma = \frac{1}{\sqrt{2}} [(\sigma_\varphi - \sigma_r)^2 + (\sigma_r - \sigma_z)^2 + (\sigma_z - \sigma_\varphi)^2]^{1/2} \tag{13}$$

Observing that $\sigma_z = {}^1/_2(\sigma_r + \sigma_\varphi)$ because of the conditions expressed by equations (2) and (3), equation (13) becomes

$$\sigma = \frac{\sqrt{3}}{2} (\sigma_\varphi - \sigma_r) \tag{14}$$

It is found that for the thick-walled cylinder $\sigma_\varphi > \sigma_r$, such that the significant stress σ is always a positive quantity.

Substitution of $\sigma_\varphi - \sigma_r$ in the equation of equilibrium (9) by the expression of equation (14), and of ϵ_r and ϵ_φ by the expressions given in equations (12) and (11), results in

$$r \frac{\partial \sigma_r}{\partial r} = \frac{2}{\sqrt{3}} \sigma e^{-\sqrt{(3)}\epsilon} \tag{15}$$

The compatibility equation (8) may be integrated. Replacing ϵ_r and ϵ_φ by ϵ as given in equations (12) and (11), the integral of equation (8) is found to be

$$\epsilon = \frac{1}{\sqrt{3}} \ln \left[1 + \frac{T(t)}{r^2}\right] \tag{16}$$

where $T(t)$, the integration constant for the integration with respect to r, is a function of time.

Equation (16), solved for r^2, is

$$r^2 = \frac{T(t)}{e^{\sqrt{(3)}\epsilon} - 1} \tag{17}$$

and solved for the square of the inside radius a,

$$a^2 = \frac{T(t)}{e^{\sqrt{(3)}\epsilon_a} - 1} \tag{18}$$

The strain at any radius r may be evaluated from equations (17) and (18) as

$$\epsilon = \frac{1}{\sqrt{3}} \ln \left[1 + \left(\frac{a}{r}\right)^2 (e^{\sqrt{(3)}\epsilon_a} - 1)\right] \tag{19}$$

By differentiating equation (19) with respect to time, the creep rate $\dot{\epsilon}$ at any radius r is obtained as function of a given creep rate $\dot{\epsilon}_a$ at the inside radius a,

$$\dot{\epsilon} = \frac{\left(\frac{a}{r}\right)^2 e^{\sqrt{(3)}\epsilon_a}}{1 + \left(\frac{a}{r}\right)^2 (e^{\sqrt{(3)}\epsilon_a} - 1)} \dot{\epsilon}_a \tag{20}$$

With the help of equations (17), (18), (19), and (20) a relation between creep rates and strains can be established. It is

$$\dot{\epsilon} = \frac{1 - e^{-\sqrt{(3)}\epsilon}}{1 - e^{-\sqrt{(3)}\epsilon_a}} \dot{\epsilon}_a \tag{21}$$

Determining the partial derivative of $\dot{\epsilon}$, as given by equation (20) with respect to r, and making use of the relation expressed by equation (19), leads to

$$\frac{\partial \dot{\epsilon}}{\partial r} = -\frac{2}{r} \dot{\epsilon}\, e^{-\sqrt{(3)}\epsilon} \tag{22}$$

The radial stress is $\sigma = f(\dot{\epsilon})$, and the creep rate is $\dot{\epsilon} = f(r, t)$, hence

$$\frac{d\sigma_r}{d\dot{\epsilon}} = \frac{\partial \sigma_r / \partial r}{\partial \dot{\epsilon} / \partial r} \tag{23}$$

With the help of the relations given in equations (15) and (22),

$$\frac{d\sigma_r}{d\dot{\epsilon}} = -\frac{\sigma}{\sqrt{(3)}\dot{\epsilon}} \tag{24}$$

By selecting appropriate limits, the internal pressure is eventually obtained from equation (24) as a function of the creep rate as

$$p = \frac{1}{\sqrt{3}} \int_{\dot{\epsilon}_b}^{\dot{\epsilon}_a} \frac{\sigma}{\dot{\epsilon}}\, d\dot{\epsilon} \tag{25}$$

where

$$\dot{\epsilon}_b = \frac{\left(\frac{a}{b}\right)^2 e^{\sqrt{(3)}\epsilon_a}}{1 + \left(\frac{a}{b}\right)^2 (e^{\sqrt{(3)}\epsilon_a} - 1)} \dot{\epsilon}_a \tag{26}$$

is obtained from relation (20).

Time Dependence of Strain

An inspection of equation (25) will show that the pressure p can be obtained as a function of the creep strain ϵ and the creep rate $\dot{\epsilon}$, provided the stress-versus-strain rate relation $\sigma = f(\dot{\epsilon})$ is given.

Placing $\sigma = f(\dot{\epsilon})$ in equation (25) and integrating gives

$$p = f_1(\dot{\epsilon}_a, \epsilon_a) \tag{27}$$

If $\dot{\epsilon}_a$ can be obtained explicitly and ϵ_a and p can be kept separate, equation (27) may be rewritten to give

$$\dot{\epsilon}_a f_2(\epsilon_a) = f_3(p) \tag{28}$$

Equation (28) can be integrated by separating the variables. Then

$$\int_0^{\epsilon_a} f_2(\epsilon_a) d\epsilon_a = \int_0^t f_3(p) dt \tag{29}$$

After carrying out the integration in equation (29), the strain at $r = a$ is available as a function of time,

$$\epsilon_a = f_4(t) \tag{30}$$

and the strain at any other radius may be obtained by employing equation (19).

Stress Distribution During Creep

For a given significant natural strain ϵ_a and creep rate $\dot{\epsilon}_a$, both at $r = a$, the significant true stress is obtained as a function of the radius r by equation (4),

$$\sigma = f(\dot{\epsilon}) \tag{4}$$

where, from equation (20),

$$\dot{\epsilon} = \frac{\left(\frac{a}{r}\right)^2 e^{\sqrt{(3)}\epsilon_a}}{1 + \left(\frac{a}{r}\right)^2 (e^{\sqrt{(3)}\epsilon_a} - 1)} \dot{\epsilon}_a \tag{20}$$

The radial stress is obtained from equation (24) by integration between appropriate limits as

$$\sigma_r = -p + \frac{1}{\sqrt{3}} \int_{\dot{\epsilon}}^{\dot{\epsilon}_a} \frac{\sigma}{\dot{\epsilon}}\, d\dot{\epsilon} \tag{31}$$

The tangential stress is given by rewriting equation (14),

$$\sigma_\varphi = -p + \frac{1}{\sqrt{3}} \int_{\dot{\epsilon}}^{\dot{\epsilon}_a} \frac{\sigma}{\dot{\epsilon}}\, d\dot{\epsilon} + \frac{2}{\sqrt{3}} f(\dot{\epsilon}) \tag{32}$$

The axial stress is the average of σ_r and σ_φ, or

$$\sigma_z = -p + \frac{1}{\sqrt{3}} \int_{\dot{\epsilon}}^{\dot{\epsilon}_a} \frac{\sigma}{\dot{\epsilon}}\, d\dot{\epsilon} + \frac{1}{\sqrt{3}} f(\dot{\epsilon}) \tag{33}$$

Application

Let us now make the assumption that the cylinder is made of a material which creeps according to a power function

$$\dot{\epsilon} = B \left(\frac{\sigma}{\sigma_0}\right)^n \tag{34}$$

in which B, σ_0, and n are constants, which are determined in a simple tension test. Assumption 5 will now have to be applied to relate the results in simple tension to the complex state of stress in the cylinder. A more detailed discussion of the use of significant stress and strain is given in [7]. Equation (34) rewritten states that

$$\sigma = \frac{\sigma_0}{B^{1/n}} \dot{\epsilon}^{1/n} \tag{35}$$

This expression for σ can now be inserted into equation (25), where, after integration, the following expression is obtained,

$$p = \frac{\sigma_0 n}{\sqrt{3} B^{1/n}} (\dot{\epsilon}_a^{1/n} - \dot{\epsilon}_b^{1/n}) \tag{36}$$

where $\dot{\epsilon}_b$ is given by equation (26).

During creep under a constant pressure, the internal cross sec-

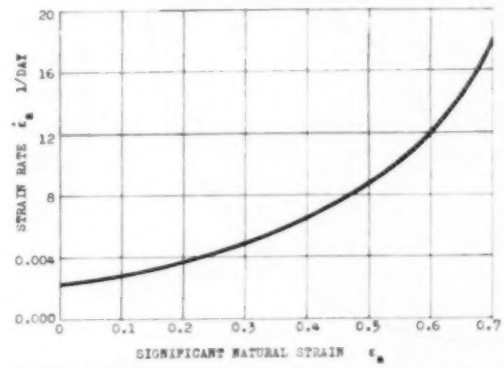

Fig. 3 Significant natural strain rate versus significant natural strain, both at the internal radius a

tion of the cylinder is increasing and the wall thickness decreasing, both causing a continuous increase of the creep rate. The creep rate $\dot{\epsilon}_a$ at $r = a$ is found as a function of the strain ϵ_a by rearranging equation (36),

$$\dot{\epsilon}_a = \frac{\sqrt{(3)^n B p^n}}{\sigma_0^n n^n} \left\{ 1 - \left[\frac{\left(\frac{a}{b}\right)^2 e^{\sqrt{(3)}\epsilon_a}}{1 + \left(\frac{a}{b}\right)^2 (e^{\sqrt{(3)}\epsilon_a} - 1)} \right]^{1/n} \right\}^{-n} \tag{37}$$

This dependence is shown in Fig. 3 for a typical case.

In order to establish the strain as a function of time at a constant internal pressure, one obtains after rearrangement and integration of equation (37),

$$\int_0^{\epsilon_a} \left\{ 1 - \left[\frac{\left(\frac{a}{b}\right)^2 e^{\sqrt{(3)}\epsilon_a}}{1 + \left(\frac{a}{b}\right)^2 (e^{\sqrt{(3)}\epsilon_a} - 1)} \right]^{1/n} \right\}^{n} = \frac{\sqrt{(3)^n B p^n}}{\sigma_0^n n^n} t \tag{38}$$

The integral on the left side of the equation may be solved either numerically or graphically. The latter involves the familiar construction of a time-position curve from a velocity-position curve, and has been used to obtain the diagram in Fig. 4 from the diagram in Fig. 3.

Figs. 5, 6, and 7 show successive stress distributions in the wall of the vessel. Fig. 5 is the elastic distribution of stress, which can be assumed to prevail immediately after the application of the in-

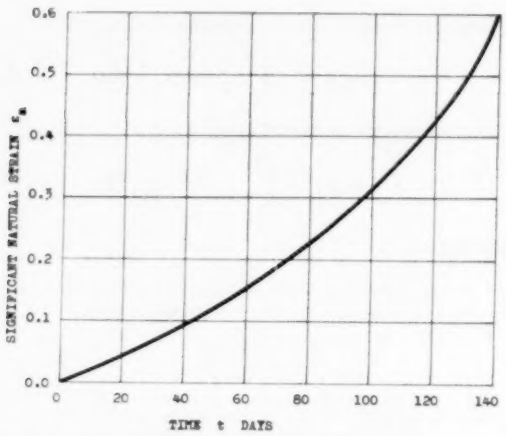

Fig. 4 Significant natural strain at internal radius versus time

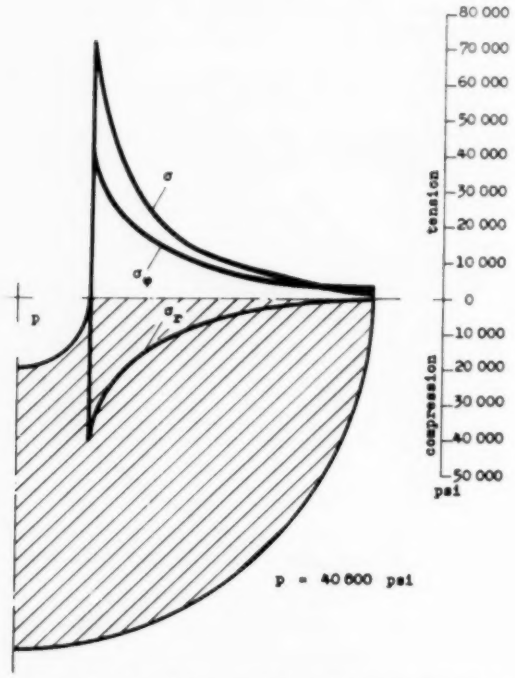

Fig. 5 Stress distribution before onset of creep (elastic-stress distribution)

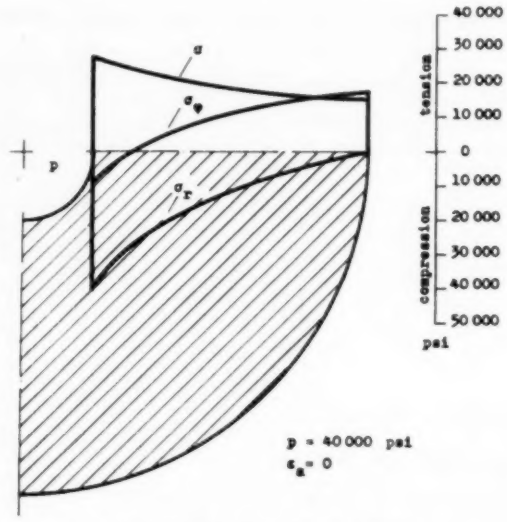

Fig. 6 Stress distribution after onset of creep

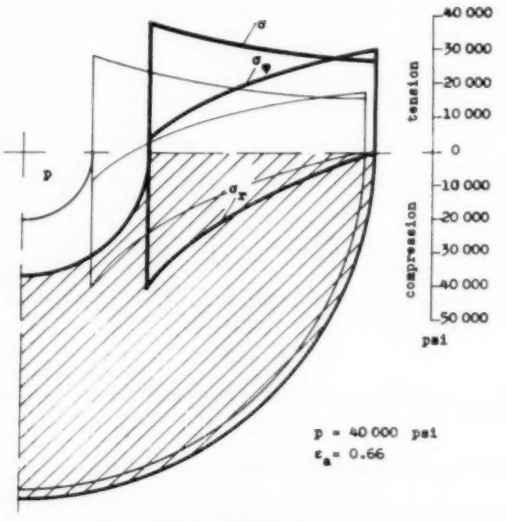

Fig. 7 Stress distribution during creep

ternal pressure, and is given by the well-known equations of the theory of elasticity. After creep has become effective the stresses will rearrange themselves to the pattern shown in Fig. 6, obtained from equations (4), (31), and (32), by assuming that the deformation can be approximated by $\epsilon_a = 0$. After considerable deformation (e.g., $\epsilon_a = 0.66$) the stresses obtained from the same equations have increased. They are plotted in Fig. 7 against the cross section of the deformed cylinder. The increase of stress is accompanied by an increase of creep rate, as plotted in Fig. 3.

Conclusion

Using the generally accepted assumptions of constant density and that the distortion energy relation is applicable, equations were derived for the creep rates, strains, and stresses in a thick-walled closed-end circular hollow cylinder under internal pressure. The strains were considered large and required the use of the finite strain theory. The equations derived were then applied to cylinders made of a material which is assumed to creep according to an n-power law.

The use of finite strains in the creep theory of thick-walled cylindrical vessels under internal pressure shows an important effect which is overlooked in the methods assuming the usual small or infinitesimal strains. By considering finite strains it is found that the creep rate of a thick-walled cylinder under internal pressure increases, even though the creep rate of the same material when subjected to constant true stress in simple tension is constant. The assumption of infinitesimal strain leads to a prediction of wall thickness which is on the unsafe side.

Acknowledgments

This paper represents part of a PhD thesis conducted under the supervision of Dr. J. Marin. The work was partially supported by the Pressure Vessel Research Committee of the Welding Research Council.

References

1 R. W. Bailey, "The Utilization of Creep Test Data in Engineering Design," The Institution of Mechanical Engineers, London, England, 1935, p. 246.

2 R. W. Bailey, "Creep Relationships and Their Application to Pipes, Tubes, and Cylindrical Parts Under Internal Pressure," *Proceedings of The Institution of Mechanical Engineers*, vol. 164, 1951, pp. 425–431.

3 A. Nadai, "On the Creep of Solids at Elevated Temperature," *Journal of Applied Physics*, vol. 8, 1937, pp. 418–446.

4 A. E. Johnson, "Creep Under Complex Stress Systems at Elevated Temperatures," *Proceedings of The Institution of Mechanical Engineers*, vol. 164, 1951, pp. 432–446.

5 C. D. Weir, "The Creep of Thick Tubes Under Internal Pressure," JOURNAL OF APPLIED MECHANICS, vol. 24, TRANS. ASME, vol. 79, 1957, pp. 464–466.

6 J. Marin, "Design of Members Subjected to Creep at High Temperatures," JOURNAL OF APPLIED MECHANICS, vol. 4, TRANS. ASME, vol. 59, 1937, p. A-21.

7 J. Marin "Engineering Materials," Prentice-Hall, Inc., Englewood Cliffs, N. J., 1952.

8 C. R. Soderberg, discussion on Bailey, "Design Aspects of Creep," JOURNAL OF APPLIED MECHANICS, vol. 3, TRANS. ASME, vol. 57, 1936, pp. A-150–A-154.

9 C. W. MacGregor, L. F. Coffin, and J. C. Fisher, "The Plastic Flow of Thick-Walled Tubes With Large Strains," *Journal of Applied Physics*, vol. 19, 1948, pp. 291–297.

NICHOLAS PERRONE

Assistant Professor of Engineering Science, Pratt Institute, Brooklyn, N. Y.

P. G. HODGE, JR.

Professor of Mechanics, Illinois Institute of Technology, Chicago, Ill. Mem. ASME

Strain-Hardening Solutions to Plate Problems[1]

Two sets of strain-hardening flow laws based on an analogy with a kinematic model are derived for circular plates made of an initially Tresca material. The two sets of flow laws, called complete and direct hardening, differ in the point at which the plane-stress assumption is introduced. The complete-hardening flow laws are more consistent since the plane-stress assumption is made at the latest possible stage in their derivation. Complete and direct-hardening solutions are obtained to each of three different plate problems. The results indicate that the direct-hardening solutions give a fair approximation to the complete-hardening ones.

WITHIN the past decade an extensive amount of work has been done on limit analysis of structures. More recently, with the development of mathematically tractable hardening theories, some attention has been turned to strain-hardened structures.

As yet, there is little experimental evidence as to the complete effect of strain-hardening on the subsequent plastic behavior of the material. The simplest assumption is that the material hardens isotropically; i.e., the yield curve expands uniformly about the origin. A quite different theory based on the phenomenon of slip has been proposed by Batdorf and Budiansky [1].[2] Neither of these theories accounts for the so-called Bauschinger effect which is observed in many real materials.

In 1955, Prager [2] proposed a quite different type of strain-hardening mechanism which is most simply described with reference to a kinematic model. The present paper is concerned with the applications of Prager's kinematic hardening to circular plate problems. Specifically, two possible methods of applying the theory to plate problems will be discussed and compared.

The first section contains a general discussion of the application of kinematic hardening to problems of plane stress. This may be done in two ways; namely, by adopting the kinematic model before or after the assumption of plane stress is made. The resulting theories are known, respectively, as complete and direct kinematic hardening.

The next section is concerned with the formulation of the complete and direct hardening flow laws for plates. In the third section an example is treated in considerable detail, and further examples are discussed in the fourth section. Finally, some comparisons and conclusions are made in the last two sections.

1 Complete and Direct Hardening

In the kinematic-hardening theory proposed by Prager the initial yield surface is represented by a rigid movable frame whose size and shape are fixed [2]. The translatory motion of the frame in the stress-strain space is a measure of the strain-hardening. The frame can experience motion only when the smooth stress pin, representative of the stress state of the material, is pushing against it.

When applied to special stress states, such as plane stress, the model at first glance appears to be immediately simplified. Consider, for example, the plane-stress state associated with a material whose initial yield surface corresponds to the Tresca yield condition, Fig. 1(*a*). Since the stress pin is restricted to the $\sigma_3 = 0$ plane, it would appear that a two-dimensional frame model might suffice. However, when the pin comes in contact with a portion of the yield surface, say AB, the kinematic-hardening law dictates that ϵ_3 strains also can arise since the $\sigma_3 = 0$ plane is a nonright section of the yield cylinder. [Mathematically speaking, $\partial f/\partial\sigma_3(\sigma_1, \sigma_2, \sigma_3) \neq 0$ for $\sigma_3 = 0$, where f is the yield function.] Hence a consistent kinematic-hardening theory must account for all stress directions, even those which are associated with zero stresses. This was illustrated by Perrone and Hodge in a particularly simple example involving bending of an idealized I-beam [3]. The consistent kinematic-hardening theory is called complete hardening; the inconsistent theory which evolves by neglecting the zero stress directions is termed direct hardening.

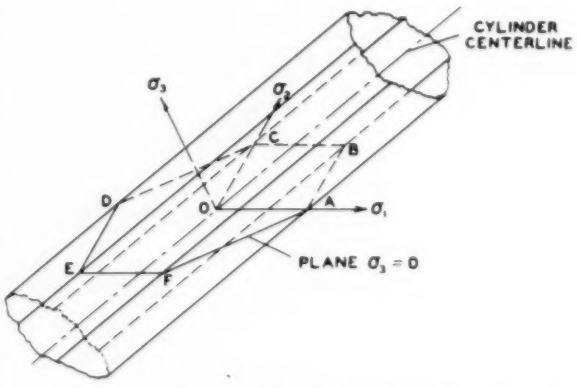

Fig. 1(a) Perspective of Tresca yield surface

[1] The results presented here represent a portion of a dissertation submitted by one of the authors (NP) in partial fulfillment of the requirements for the degree of Doctor of Philosophy in Applied Mechanics at the Polytechnic Institute of Brooklyn, Brooklyn, N. Y. The authors would like to express their thanks to the Office of Naval Research who sponsored the work reported herein.

[2] Numbers in brackets designate References at end of paper.

Presented at the West Coast Conference of the Applied Mechanics Division, Los Angeles, Calif., September 8–10, 1958, of THE AMERICAN SOCIETY OF MECHANICAL ENGINEERS. This paper was not preprinted.

Discussion of this paper should be addressed to the Secretary, ASME, 29 West 39th Street, New York, N. Y., and will be accepted until July 10, 1959, for publication at a later date. Discussion received after the closing date will be returned.

NOTE: Statements and opinions advanced in papers are to be understood as individual expressions of their authors and not those of the Society. Manuscript received by ASME Applied Mechanics Division, April 1, 1958.

Table 1 Integrated complete plane-stress-flow laws for regular progressions

Sides

AB	BC	CD	DE	EF	FA
$\sigma_1 - Y = c\epsilon_1$	$\sigma_2 - Y = c\epsilon_2$	$\sigma_2 - \sigma_1 - Y = c\epsilon_2$	$\sigma_1 + Y = c\epsilon_1$	$\sigma_2 + Y = c\epsilon_2$	$\sigma_1 - \sigma_2 - Y = c\epsilon_1$
$\epsilon_2 = 0$	$\epsilon_1 = 0$	$\epsilon_2 = 0$	$\epsilon_2 = 0$	$\epsilon_1 = 0$	$\epsilon_2 = 0$
$\epsilon_3 = -\epsilon_1$	$\epsilon_3 = -\epsilon_2$	$\epsilon_1 + \epsilon_2 = 0$	$\epsilon_3 = -\epsilon_1$	$\epsilon_3 = -\epsilon_2$	$\epsilon_1 + \epsilon_2 = 0$

Corners

A	B	C
$\sigma_1 - Y = c(\epsilon_1 + \epsilon_2/2)$	$\sigma_1 - Y = c(\epsilon_1 + \epsilon_2/2)$	$\sigma_1 = c(\epsilon_1 + \epsilon_2/2)$
$\sigma_2 = c(\epsilon_1/2 + \epsilon_2)$	$\sigma_2 - Y = c(\epsilon_2 + \epsilon_1/2)$	$\sigma_2 - Y = c(\epsilon_1/2 + \epsilon_2)$
$\epsilon_3 = -(\epsilon_1 + \epsilon_2)$	$\epsilon_3 = -(\epsilon_1 + \epsilon_2)$	$\epsilon_3 = -(\epsilon_1 + \epsilon_2)$

D	E	F
$\sigma_1 + Y = c(\epsilon_1 + \epsilon_2/2)$	$\sigma_1 + Y = c(\epsilon_1 + \epsilon_2/2)$	$\sigma_1 = c(\epsilon_1 + \epsilon_2/2)$
$\sigma_2 = c(\epsilon_1/2 + \epsilon_2)$	$\sigma_2 + Y = c(\epsilon_1/2 + \epsilon_2)$	$\sigma_2 + Y = c(\epsilon_1/2 + \epsilon_2)$
$\epsilon_3 = -(\epsilon_1 + \epsilon_2)$	$\epsilon_3 = -(\epsilon_1 + \epsilon_2)$	$\epsilon_3 = -(\epsilon_1 + \epsilon_2)$

Table 2 Integrated direct-hardening flow laws for regular progressions

Sides

AB	BC	CD	DE	EF	FA
$\sigma_1 - Y = c_d\epsilon_1$	$\sigma_2 - Y = c_d\epsilon_2$	$\sigma_2 - \sigma_1 - Y = 2c_d\epsilon_2$	$\sigma_1 + Y = c_d\epsilon_1$	$\sigma_2 + Y = c_d\epsilon_2$	$\sigma_2 - \sigma_1 + Y = 2c_d\epsilon_2$
$\epsilon_2 = 0$	$\epsilon_1 = 0$	$\epsilon_1 + \epsilon_2 = 0$	$\epsilon_2 = 0$	$\epsilon_1 = 0$	$\epsilon_1 + \epsilon_2 = 0$

Corners

A	B	C	D	E	F
$\sigma_1 - Y = c_d\epsilon_1$	$\sigma_1 - Y = c_d\epsilon_1$	$\sigma_2 - Y = c_d\epsilon_2$	$\sigma_1 + Y = c_d\epsilon_1$	$\sigma_1 + Y = c_d\epsilon_1$	$\sigma_1 = c_d\epsilon_1$
$\sigma_2 = c_d\epsilon_2$	$\sigma_2 - Y = c_d\epsilon_2$	$\sigma_1 = c_d\epsilon_1$	$\sigma_2 = c_d\epsilon_2$	$\sigma_2 + Y = c_d\epsilon_2$	$\sigma_2 + Y = c_d\epsilon_2$

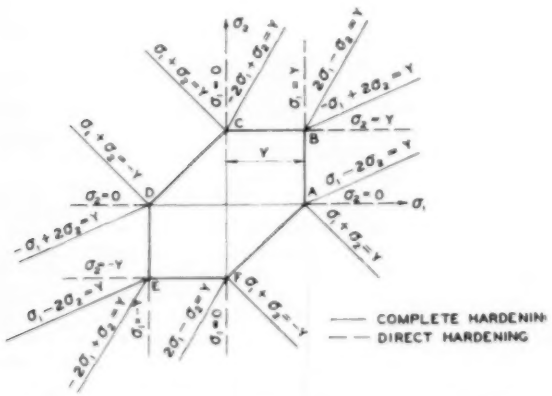

Fig. 1(b) Tresca yield condition—plane-stress dividing lines

Hodge [4, 5] and Budiansky [6] first pointed out the inconsistency of the direct-hardening approach. Shield and Ziegler [7] have discussed general conditions under which direct and complete hardening reduce to the same theory.

Even in cases where the direct hardening is not consistent, it may be of some value as a simplifying approximation. A primary purpose of the present paper is to compare solutions of the two theories in order to discuss the effect of such an approximation.

By using the kinematic model appropriate to each theory the complete and direct-hardening flow laws for plane stress may be determined [8]. These flow laws for a rigid plastic Tresca material are shown in Tables 1 and 2 in integrated form for regular progressions. Hodge has called those flow paths, wherein the flow laws can be integrated without explicitly considering transitional stresses and strains, regular progressions [4]. In particular, such integrations are possible when the stress point goes from the unstrained state to a side, and then to a corner.

The dividing lines which denote the boundary between different flow regimes also can be determined for each theory [8], and are shown in Fig. 1(*b*). The fact that the complete-hardening dividing lines are not normal to the sides is a reflection of three-dimensional hardening effects.

The hardening constants in each theory (c and c_d) can be associated with the tensile hardening rate c'. They resolve to

$$c = \frac{4}{3}c' \tag{1}$$

$$c_d = c' \tag{2}$$

2 Plate Flow Laws

Let r, φ, and z (positive downward) be cylindrical co-ordinates whose origin is at the center of a circular plate of constant thickness $2h$, and outer radius R. The median surface coincides with the plane $z = 0$. If the plate is loaded and supported in a rotationally symmetric manner, then the shear stresses $\tau_{\varphi z}$ and τ_{rz} must vanish. For thin plates it is reasonable to assume that each lamina is in a state of plane stress; hence

$$\sigma_z = 0$$

Therefore, the existing state of stress is two dimensional. Further, since r and φ are the principal directions, σ_r and σ_φ are the principal stress components. Hence the Tresca flow laws of Table 1 and dividing lines of Fig. 1(*b*) can be used if 1 and 2 are replaced by r and φ, respectively.

It can be shown readily that the yield curve in terms of the stress resultants M_r and M_φ has the same shape as the original one [9], Fig. 2. M_r and M_φ, the radial and tangential moments, respectively, are also the principal bending moments. A positive moment is taken as one for which the upper fiber ($-z$) is in compression. M_0 is the yield moment for a section of unit width. In the present case it has the value Yh^2.

Before actually deriving the flow laws, it is necessary to introduce the deflections and curvatures. Let w be the displacement (positive in z-direction). The principal curvatures are then given by

$$\kappa_r' = -w_{,rr}, \quad \kappa_\varphi' = -w_{,r}/r, \tag{3}$$

where comma subscripts denote differentiation. Generally, primed quantities will be used for dimensional terms, and unprimed ones for the corresponding dimensionless terms.

The flow laws are determined for a typical side and corner in

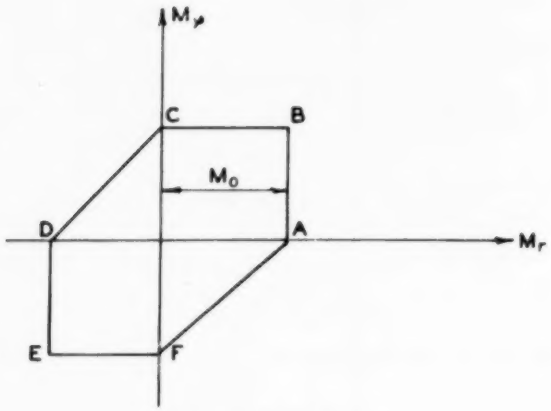

Fig. 2 Yield curve for plates

Fig. 2. First, flow from side AB in Fig. 2 is considered. Strain considerations clearly demonstrate that for this side the upper half of the plate should be on side DE and the lower one on AB, Fig. 1(b) (r and φ are, of course, 1 and 2). Therefore, since the strains are given by

$$\epsilon_r = z\kappa_r', \quad \epsilon_\varphi = z\kappa_\varphi' = 0, \tag{4}$$

it follows from Table 1 that

$$M_r = \int_{-h}^{h} \sigma_r z\, dz = \int_{-h}^{0} (-Y + c\epsilon_r)z\, dz + \int_{0}^{h} (Y + c\epsilon_r)z\, dz$$
$$= Yh^2 + (2/3)ch^3\kappa_r' \tag{5}$$

Similarly, if the moment point is in corner B, the stress point for the upper and lower halves of the plate must be in E and B, respectively, Fig. 1(b). Therefore, for the corner B,

$$M_r = Yh^2 + \frac{2ch^3}{3}(\kappa_r' + \kappa_\varphi'/2),$$
$$M_\varphi = Yh^2 + \frac{2ch^3}{3}(\kappa_\varphi' + \kappa_r'/2) \tag{6}$$

In a similar fashion the flow laws for all other sides and corners may be determined. The results can be expressed conveniently in terms of the dimensionless quantities

$$m_r = M_r/M_0, \qquad m_\varphi = M_\varphi/M_0,$$
$$\kappa_r = \frac{2}{3}\frac{c'}{Y}h\kappa_r', \qquad \kappa_\varphi = \frac{2}{3}\frac{c'}{Y}h\kappa_\varphi', \tag{7}$$
$$\xi = r/R, \qquad W = \frac{2}{3}\frac{c'}{Y}\frac{h}{R^2}w$$

where c' is the tensile hardening constant. The curvatures (3) may now be written in the dimensionless form

$$\kappa_r = -W_{,\xi\xi}, \quad \kappa_\varphi = -W_{,\xi}/\xi \tag{8}$$

In terms of the dimensionless quantities defined in (7) the flow laws for corner B, Equations (6), take the form

$$m_r = 1 + \left(\frac{c}{c'}\right)(\kappa_r + \kappa_\varphi/2) = 1 + \frac{4}{3}(\kappa_r + \kappa_\varphi/2),$$
$$m_\varphi = 1 + \left(\frac{c}{c'}\right)(\kappa_\varphi + \kappa_r/2) = 1 + \frac{4}{3}(\kappa_\varphi + \kappa_r/2) \tag{9}$$

The integrated flow laws and dividing lines in dimensionless form for all regions are portrayed in Fig. 3. In Fig. 3 each region contains two rows of letters. The top refers to the stress state for the upper plate half, and the bottom row to the bottom plate half, Fig. 1(b). For instance, $\frac{E}{B}$ signifies that for this flow region the top of the plate is at corner E and the bottom at B, Fig. 1(b), As previously, the integrations are valid only for regular progressions of the stress point.

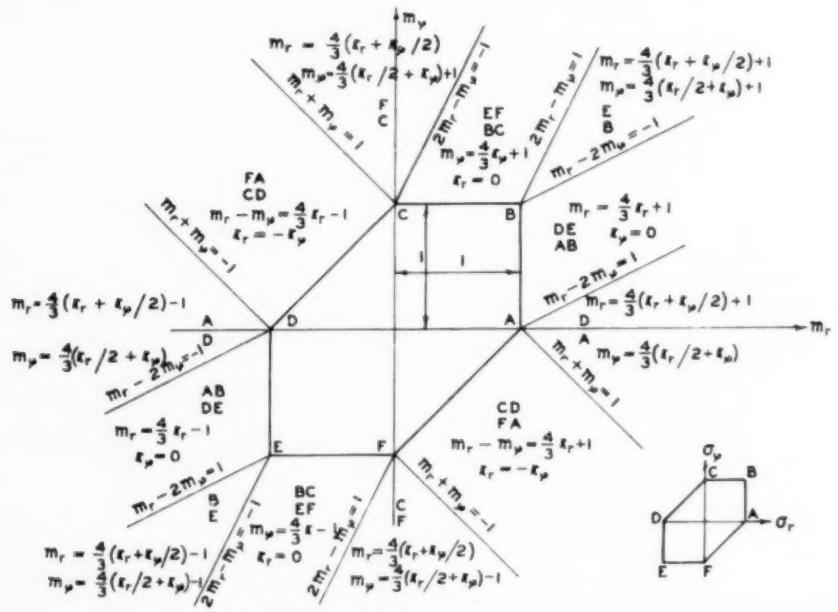

Fig. 3 Integrated plate flow laws—complete hardening

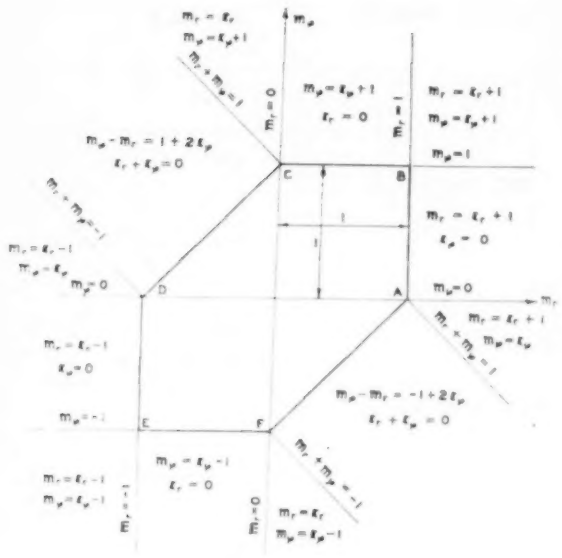

Fig. 4 Integrated plate flow laws—direct hardening

The direct-hardening plate-flow laws can be determined with greater ease. The M_r, M_φ yield curve is immediately treated as a rigid frame without any direct concern with plane-stress considerations. The flow laws and dividing lines are easily found, and the results shown in Fig. 4.

3 Example—Annular Plate

The solution to any physical problem always entails the use of the equilibrium condition. If flow is taking place, the appropriate flow law should be utilized simultaneously. If a portion of the structure is rigid, then the stresses therein can still be found by using an elastic compatibility condition.

For plates the equilibrium equation with the shear eliminated takes the form [10]

$$(rM_r)_{,r} - M_\varphi = -\int_0^r rp\,dr,$$

where p, the loading, is a function of r only. In terms of the dimensionless pressure

$$P = pR^2/6Yh^2,$$

the equilibrium condition becomes

$$(\xi m_r)_{,\xi} - m_\varphi = -\int_0^\xi 6\xi\, P d\,\xi \qquad (10a)$$

If the load is uniform, then (10a) reduces to

$$(\xi m_r)_{,\xi} - m_\varphi = -3P\,\xi^2 \qquad (10b)$$

An example will now be considered in complete detail, namely, an annular plate of outer radius unity and inner radius μ. A uniform moment m is applied at the simply supported outer edge. In view of the loading considered, the right-hand side of the equilibrium equations (10) vanishes.

Under small loads, of course, the entire plate is rigid. However, this does not preclude the existence of stresses throughout the plate. In order to determine these stresses the plate material is thought of as being elastic, but having an infinite Young's modulus. Hence the stress-compatibility equation is still valid. In dimensionless variables this takes the form [11]:

$$(\xi m_\varphi)_{,\xi} - m_r = 0$$

The solution to the compatibility and equilibrium equations with boundary conditions

$$m_r(\mu) = 0, \quad m_r(1) = m$$

is

$$m_r = [m/(1 - \mu^2)](1 - \mu^2/\xi^2),$$
$$m_\varphi = [m/(1 - \mu^2)](1 + \mu^2/\xi^2)$$

The stress profile which is determined by elimination of ξ is

$$m_r + m_\varphi = 2m/(1 - \mu^2)$$

This is valid up to $m = (1 - \mu^2)/2$, Fig. 5.

For moments in excess of $(1 - \mu^2)/2$ there are two regimes

$$\mu \le \xi \le \rho, \quad BC$$
$$\rho \le \xi \le 1, \quad \text{Rigid}$$

The solution for this stress state shows that for some range of load

$$(1 - \mu^2)/2 \le m \le 1 - \mu,$$

a portion of the plate is in regime BC with no plastic flow. The solution for the foregoing load range is

$$m_\varphi = 1 \qquad \mu \le \xi \le \rho,$$
$$m_r = 1 - \mu/\xi$$
$$m_\varphi = -C_1/\xi^2 + C_2 \qquad \rho \le \xi \le 1,$$
$$m_r = C_1/\xi^2 + C_2$$

where

$$C_1 = m - 1 + \mu/(2\rho),$$
$$C_2 = 1 - \mu/(2\rho),$$
$$\rho = (1 - m)/\mu - \{[(1 - m)/\mu]^2 - 1\}^{1/2}$$

The stress profiles for $m \le 1 - \mu$ are summarized in Fig. 6. For $m = 1 - \mu$ the entire stress profile lies along BC. This is, in fact, the perfectly plastic collapse load. When loads in excess of $1 - \mu$ are applied two solutions will exist, one for complete and the other for direct hardening.

For the complete-hardening problem a reasonable choice of stress profile, which is verified *a posteriori*, is

$$\mu \le \xi \le \gamma, \quad C$$
$$\gamma \le \xi \le 1, \quad BC$$

Regional solutions of the flow law and equilibrium condition are

$$C \quad W = 3/4[C_6 \ln \xi + C_8\,\xi^2/2 + C_9 + (\xi^2/4)(1/2 - \ln \xi)],$$
$$m_r = C_7/(2\xi^2) - 3/2\,C_8 + 1/2 + (3/4)\ln \xi,$$
$$m_\varphi = -C_7/(2\xi^2) - 3/2\,C_8 + 5/4 + 3/4 \ln \xi;$$
$$BC \quad W = 3/4[C_4\,\xi + C_5],$$
$$m_r = 1 - C_4 \ln \xi/\xi + C_5/\xi,$$
$$m_\varphi = 1 - C_4/\xi$$

Enforcement of the boundary and continuity conditions leads to the solution. The division point between C and BC is denoted by γ. It is convenient to define a second quantity in terms of it. Let

$$\lambda = \gamma/\mu$$

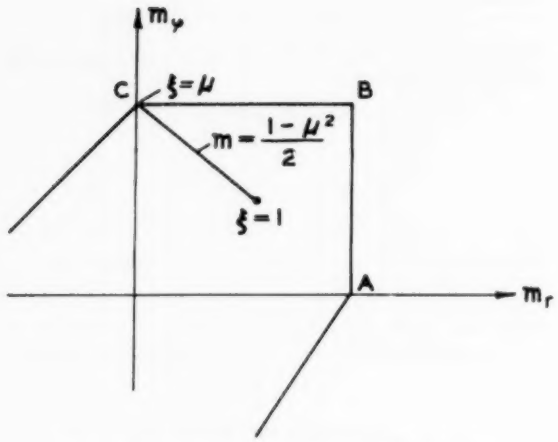

Fig. 5 Finite annular-plate maximum elastic-stress profile

The desired solution is then implicitly expressed by

$$C_7 = (\mu^2/2)\left(\frac{1 + 3\ln\lambda}{1 - 3/\lambda^2}\right),$$

$$C_8 = C_7/\lambda^2 + (1/2)(1 + \ln\gamma),$$

$$C_4 = \frac{\gamma}{2(\lambda^2 - 3)}(\lambda^2 + 6\ln\lambda - 1),$$

$$m = \gamma/2\left[-\frac{(\ln\lambda + \ln\mu)(\lambda^2 - 1 + 6\ln\lambda) + 3\ln\lambda - 6.5 + 2.5\lambda^2}{3 - \lambda^2}\right] + 1,$$

$$C_6 = m - 1,$$

$$C_9 = C_4(\gamma - 1) + (\gamma^2/4)(\ln\gamma - 1/2) - C_7\ln\gamma - C_8\gamma^2/2$$

The foregoing solution is valid for the loads

$$1 - \mu \leq m \leq m^*,$$

where m^* refers to the load for which the stress profile first touches the complete-hardening dividing line. It will be determined later.

When $m > m^*$ there will be three regions of flow

$$\mu \leq \xi \leq \gamma, \quad C,$$

$$\gamma \leq \xi \leq \beta, \quad BC,$$

$$\beta \leq \xi \leq 1, \quad B,$$

where β is the new dividing point between BC and B. The regional solution of B is

$$W = 3/4[C_1\ln\xi + C_2\xi^2/2 + C_3],$$

$$m_r = 1 + C_1/(2\xi^2) - 3/2C_2,$$

$$m_\varphi = 1 - C_1/(2\xi^2) - 3/2C_2,$$

and the other regional solutions are unchanged.

The complete solution for $m > m^*$ in implicit form is

$$C_7 = (\mu^2/2)\left(\frac{1 + 3\ln\lambda}{1 - 3/\lambda^2}\right), \quad C_8 = C_7/\gamma^2 + (1/2)(1 + \ln\gamma),$$

$$C_4 = \frac{\gamma}{2(\lambda^2 - 3)}(\lambda^2 + 6\ln\lambda - 1),$$

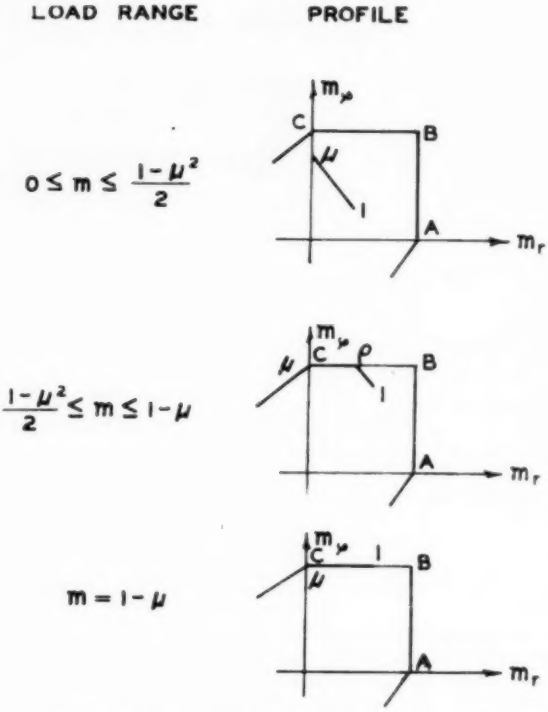

Fig. 6 Finite annular-plate solutions for $m \leq 1 - \mu$

$$C_6 = +C_4(\ln\beta - 1/2),$$

$$C_1 = C_4\beta/2,$$

$$C_2 = C_4/(2\beta),$$

$$C_3 = -C_4/(4\beta),$$

$$C_5 = C_1\ln\beta + C_2\beta^2/2 + C_3 - C_4\beta,$$

$$C_9 = C_4\gamma + C_5 - C_7\ln\gamma - C_8\gamma^2/2 + (\gamma^2/4)(\ln\gamma - 1/2),$$

$$m = 1 + (C_4/4)(\beta - 3/\beta),$$

$$\ln(\beta/\gamma) - 1/2 = -\frac{C_7/\gamma - 5/4\gamma}{2C_7/\gamma + \gamma/2}$$

From the last equation a β versus γ-curve may be made which facilitates the solution. A curve showing m as a function of γ is also quite useful. For $\mu = 1/3$ these curves are shown in Figs. 7 and 8, respectively. The value of m^* is found by determining the value of γ corresponding to $\beta = 1$ (from Fig. 7) and using this result in Fig. 8.

For the particular plate specified by $\mu = 1/3$, numerical results are found by using the general complete-hardening solution obtained here. Stress profiles and deflections are shown in Figs. 9 and 10, respectively, for various load values.

The direct-hardening solution to the same annular-plate problem is analytically simpler and can be obtained in a similar manner. For the load range

$$1 - \mu \leq m \leq 1$$

the entire plate experiences hardened flow from regime BC, whereas for $m > 1$ the outer portion of the plate begins to flow from corner B. All details of the solution can be found in ref-

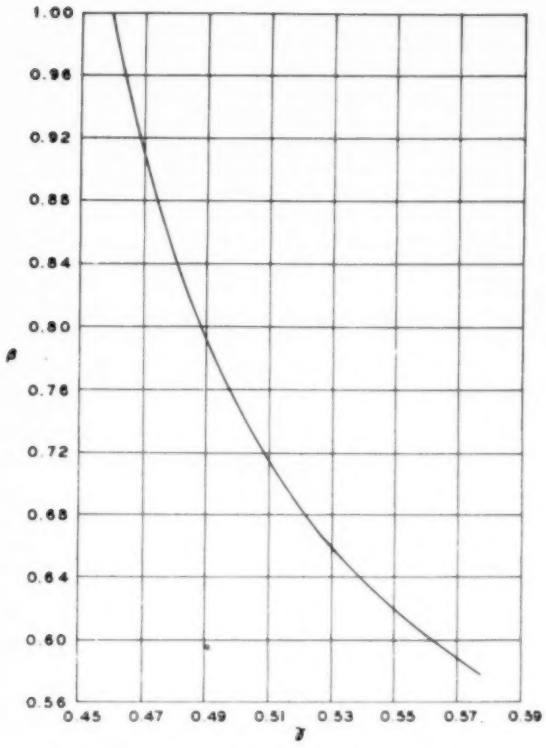

Fig. 7 Finite annular plate β versus γ for $\mu = 1/3$

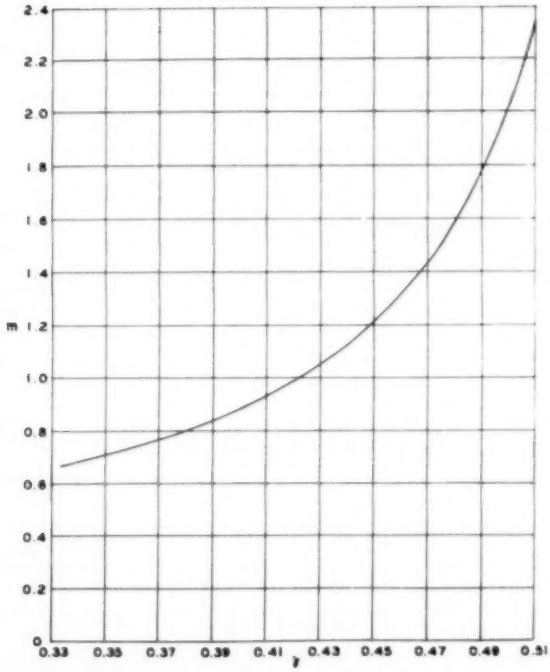

Fig. 8 Finite annular plate—complete hardening $\mu = 1/3$

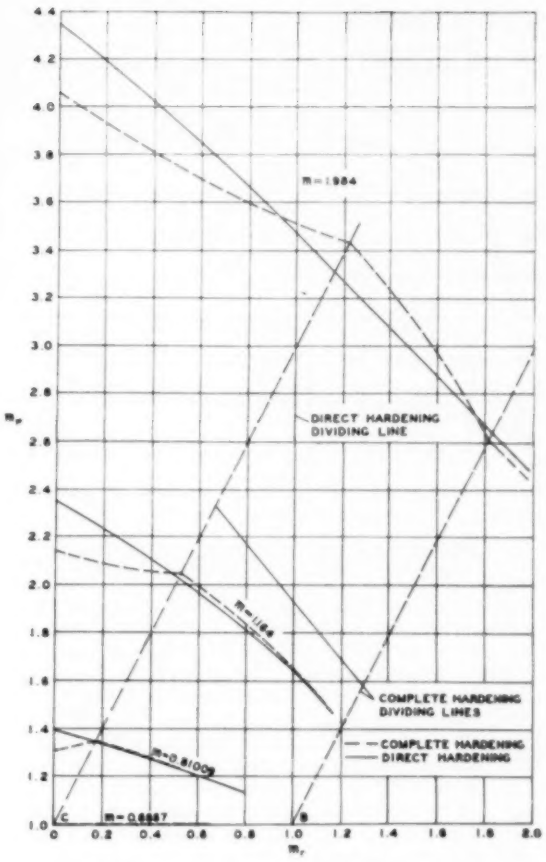

Fig. 9 Finite annular plate—stress profiles $\mu = 1/3$

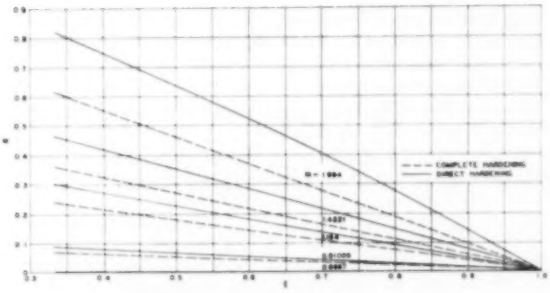

Fig. 10 Finite annular plate—deflections $\mu = 1/3$

erence [8]. Numerical solutions have been obtained for the plate $\mu = 1/3$. For the same load values as the complete-hardening problem, stress profiles and deflected shapes are shown in Figs. 9 and 10.

4 Additional Examples

Two other strain-hardening plate problems have received some attention in the literature; namely, the simply supported uniformly loaded circular plate [5, 12, 13], and the infinite annular plate with uniform moment along the inner simply supported edge [11].

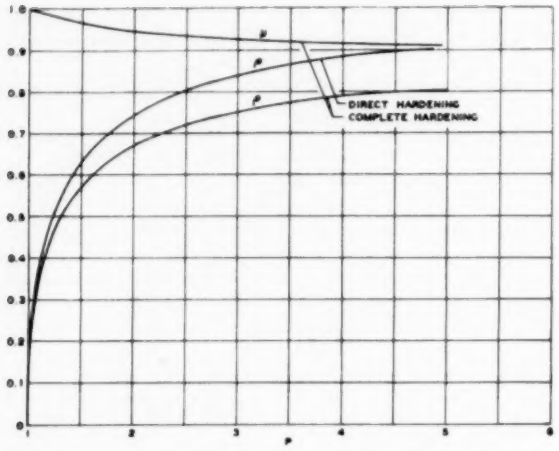

Fig. 11 Load versus interface location for uniformly loaded plate

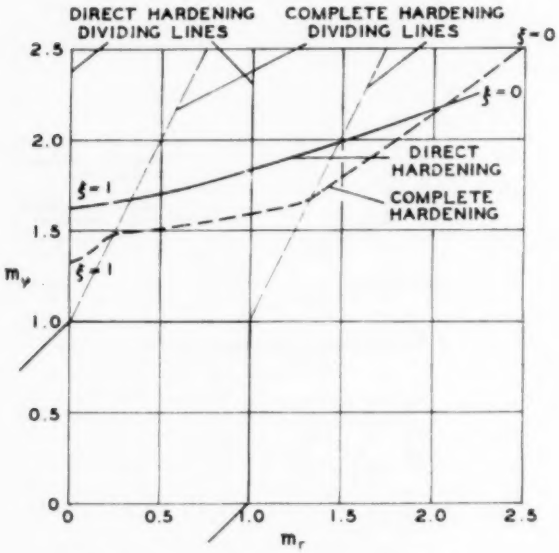

Fig. 12 Plate—uniform load; stress profiles $P = 2$

The complete and direct-hardening solution to both problems have been determined [8]. Some numerical results of that analysis are reproduced here in graphical form, Figs. 11–18. All analytical details for the general solutions are given in reference [8]. It will suffice here to give a general discussion on the nature of the solutions.

The complete-hardening solution to the simply supported, uniformly loaded circular plate problem reveals that hardened flow proceeds from three regimes, Fig. 3:

$$0 \leq \xi \leq \rho, \quad B$$

$$\rho \leq \xi \leq \mu, \quad BC$$

$$\mu \leq \xi \leq 1, \quad C$$

where the plate radius is taken to be unity. On the other hand in the direct-hardening solution flow occurs from two regimes, Fig. 4:

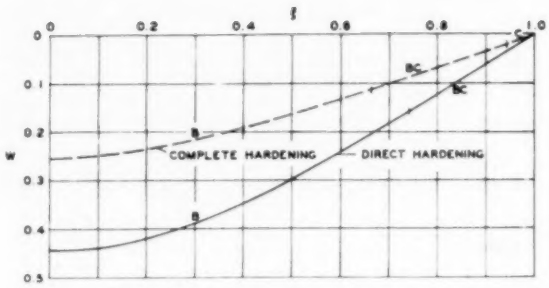

Fig. 13 Plate—uniform load; deflections for $P = 2$

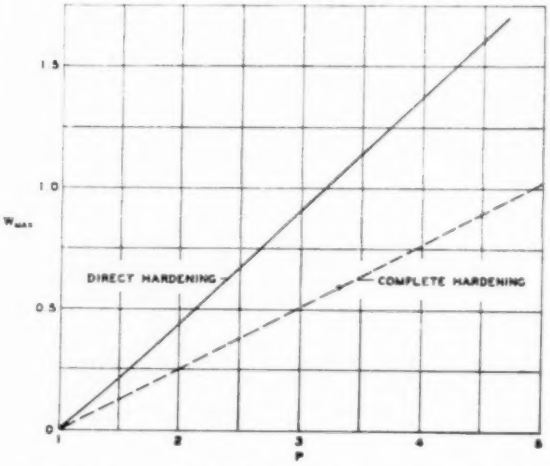

Fig. 14 Plate—uniform load; maximum deflection versus load

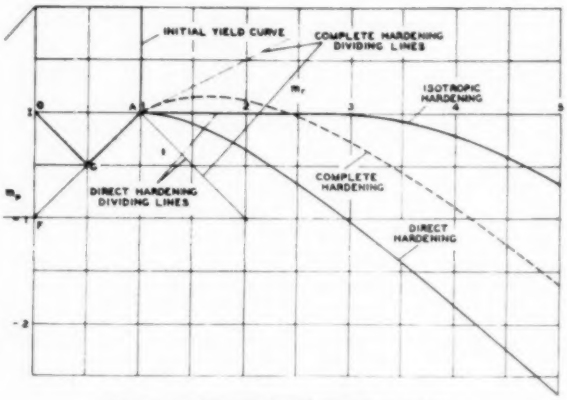

Fig. 15 Infinite annular plate—stress profile

$$0 \leq \xi \leq \rho, \quad B$$

$$\rho \leq \xi \leq 1, \quad BC$$

For both solutions curves of interface location as a function of load are given in Fig. 11, and stress profiles and deflections are shown in Figs. 12, 13, and 14. The direct-hardening solution was first obtained by Prager [12].

In the afore-mentioned infinite annular-plate problem, virtually no qualitative difference is evident between the complete and direct-hardening solutions. The radius of the inner simply sup-

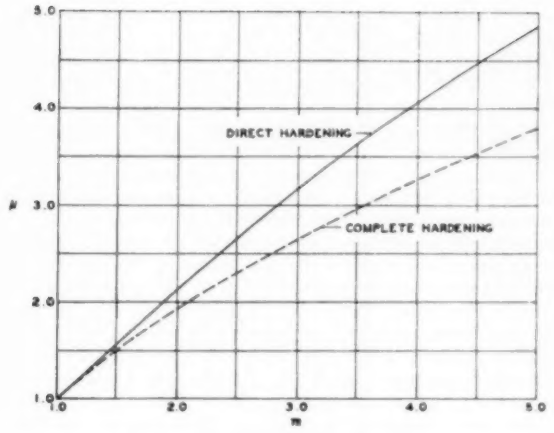

Fig. 16 Infinite annular plate m versus μ

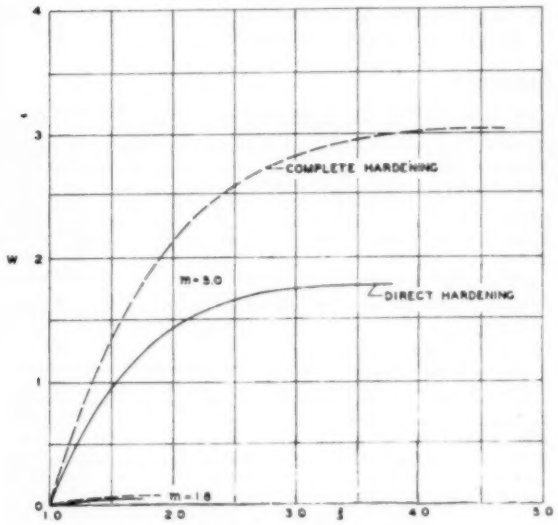

Fig. 17 Infinite annular-plate deflection curves

ported edge is taken as unity, and the dimensionless moment acting there is denoted by m. For both solutions, when $m > 1$ flow occurs in the following manner:

$$1 \leq \xi \leq \mu, \quad A$$

$$\mu \leq \xi \leq \rho, \quad FA$$

$$\rho \leq \xi \leq \infty, \quad \text{Rigid}$$

Actually, only the first region experiences plastic flow from corner A. For $m \leq 1$ no plastic flow occurs. Various pertinent curves are displayed in Figs. 15–18. It is worth noting that Hodge solved the same problem with an isotropic hardening law [11]. In his solution a fourth regime arose since the material in corner A eventually returned to side FA. For comparison his solution is included with the other stress profiles in Fig. 15.

5 Numerical and Theoretical Comparisons

It is of interest to compare the numerical results of the complete and direct-hardening solutions.

The solutions to the finite annular-plate problem give some interesting comparisons. Although the two solutions involve different plastic regimes, the resulting stresses and displacements are similar. For small loads, $2/3 \leq m \leq 1$, the direct-hardening solution is concerned with one regime BC, whereas the complete solution has two regimes, BC and C, Fig. 9. When m is slightly greater than 1, the complete solution is qualitatively unchanged, but the direct solution shows added flow at corner B. Finally, for m much greater than 1 the direct solution remains essentially unchanged, but the complete one also starts to flow from corner B. In spite of marked differences in flow patterns, the numerical comparison of stress profiles shows an average difference of only 5 per cent, and for deflection about 25 per cent.

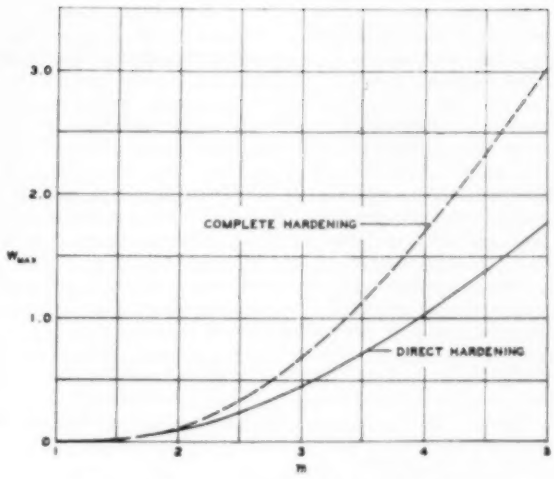

Fig. 18 Infinite annular-plate maximum deflections

In the uniformly loaded solid plate an important qualitative difference exists in the two solutions, as evidenced by the stress profile. The complete-hardening solution entails flow from three regimes; the direct-hardening solution shows flow from two regimes. Although the stress profile and deflection curves have the same general shape for each solution, the direct-hardening stresses and deflections are usually higher. The average difference is about 15 per cent in stresses and 50 per cent in deflections.

Both solutions to the infinite annular-plate problem are similar in that they involve the same three regimes of the yield curve. The only flow that takes place occurs in the third regime, corner A, Fig. 15. For this regime the stress profiles differ appreciably. Also, between loads of 1 and about 2.4 the m_φ component is positive for complete hardening and negative for direct hardening. In the load range considered, i.e., up to $m = 5$, the direct-hardening stresses are generally much higher, and the deflections much smaller, than the complete-hardening ones. It might be mentioned that both solutions differ qualitatively and quantitatively from a solution by Hodge for the same problem with an isotropic-hardening law [11], Fig. 15. He found that for loads greater than about 2.8 the material went from the corner A back to the side FA. This solution, unlike all the solutions obtained in the present work, entailed a nonregular progression of the stress point.

It would be well now to examine more carefully the similarities and differences between the complete-hardening theory and the direct-hardening approximation to it.

Direct and complete hardening are similar in that each is based on an analogy with a kinematic model, and each retains a Bauschinger effect. Also, roughly speaking, the general nature of the flows laws and dividing lines, for the problems considered, are similar.

The differences between the two methods are more pronounced, and greater in number. Complete hardening refers back to a basic flow mechanism, such as the Tresca yield condition; direct hardening does not. Consequently, the complete-hardening flow laws are more realistic. For example, they satisfy the incompressibility condition, whereas the direct-flow laws do not. From the kinematic viewpoint this difference can be attributed to a neglect of transverse-frame motion in the direct-hardening analysis. This ignored component of frame motion generally increases with increasing loads. Hence it is reasonable to expect the two solutions to diverge as the load increases. In all solutions to the plate problems this was found to be the case.

The neglect of the transverse-frame motion also has the effect of altering the hardening rate. This greatly complicates the task of effecting a sensible comparison between the two solutions. In the present work the comparison was made by adjusting the hardening rates of the complete and direct-hardening materials so that their tensile hardening properties were identical.

Finally, the complete and direct-hardening materials differ from one another in that the former is initially isotropic whereas the latter is not.

6 Conclusions

In the present paper, solutions have been obtained to a number of problems by using the complete three-dimensional Tresca yield surface as the kinematic model, and subsequently simplifying the results to the plane-stress condition. These are called complete-hardening solutions; a second set of solutions which neglect the third direction are called direct-hardening solutions.

It has been demonstrated that the complete-hardening problem as applied to plates is capable of consistent formulation and solution. However, at times the work entailed in reaching such a solution has proved to be quite lengthy. Usually, fair approximate solutions were obtained with noticeably less work by using the direct-hardening approach.

Direct-hardening solutions also might serve as aids in the search for complete-hardening solutions. For example, the direct-hardening solution to the uniformly loaded plate problem suggested what proved to be the correct stress profile for the complete-hardening problem.

The comparisons of kinematic and isotropic hardening solutions to the infinite annular-plate problem suggest an interesting conclusion. Isotropic hardening gave rise to nonregular stress progressions, but kinematic hardening did not. This is not surprising if we stop to consider that in isotropic hardening a much stronger restriction is placed on the stress point if it is to remain in a corner. (For example, to remain in corner A, m_φ must always be zero.) Hence, nonregular progressions, which are usually insurmountable analytical stumbling blocks, are probably more apt to occur with isotropic rather than kinematic hardening.

In the present work it has been assumed that strain-hardening materials behave in the manner predicted by the kinematic model. That is, the yield surface in a principal stress space can be treated as a movable frame which can translate freely in any of the fixed principal directions when loaded by way of a stress pin. Therefore, only those problems were, or can be, treated wherein the principal directions remained fixed. The problem would be considerably complicated by the introduction of variable principal directions.

There is not enough experimental work available to verify whether strain-hardening materials behave in the manner predicted by the kinematic model. However, in some recent work by Naghdi, Essenburg, and Koff [14] there is evidence of approximately such a behavior. In that work, combined torsion-tension-reversed torsion tests were conducted on a tubular aluminum alloy in the plastic range. The results in a shear stress-normal plane indicate a pronounced Bauschinger effect. However, these results cannot be correlated directly with the kinematic model since the principal directions are constantly changing. Tests are needed wherein the principal directions are fixed, and plastic-strain reversals are present. Overcoming stability effects probably constitutes the chief difficulty in performing such tests.

If subsequent experiments indicate that materials do not behave in the manner predicted by the kinematic model, then recourse might be had to a relatively general linear theory of strain-hardening developed by Hodge [4], in which complete hardening is included as a special case. If such were the situation and good experimental agreement resulted with a nonkinematic case, then the complete-hardening solutions probably could serve as useful guides in the quest for the appropriate solutions.

References

1 S. B. Batdorf and B. Budiansky, "A Mathematical Theory of Plasticity Based on the Concept of Slip," NACA TN 1871, 1949.

2 W. Prager, "The Theory of Plasticity: A Survey of Recent Achievements," *Proceedings of The Institution of Mechanical Engineers*, vol. 169, 1955, pp. 41–57.

3 Nicholas Perrone and P. G. Hodge, Jr., "Strain Hardening Solutions With Generalized Kinematic Models," Proceedings of the Third U. S. National Congress of Applied Mechanics, 1958, p. 641.

4 P. G. Hodge, Jr., "A General Theory of Piecewise Linear Plasticity Based on Maximum Shear," *Journal of the Mechanics and Physics of Solids*, vol. 5, 1957, pp. 242–260.

5 P. G. Hodge, Jr., "Piecewise Linear Plasticity," Proceedings of the Ninth International Congress of Applied Mechanics, vol. 8, University of Brussels, Belgium, 1957.

6 B. Budiansky, discussion of [12] in JOURNAL OF APPLIED MECHANICS, vol. 24, TRANS. ASME, vol. 79, 1957, p. 481.

7 R. T. Shield and H. Ziegler, "On Prager's Hardening Rule," *Journal of Applied Mathematics and Physics (ZAMP)*, vol. IXa, 1958, p. 260.

8 Nicholas Perrone and P. G. Hodge, Jr., "Applications of a Consistent Theory for Strain Hardening Plastic Solids," PIBAL Report No. 403, Polytechnic Institute of Brooklyn, N. Y., 1957.

9 B. Paul and P. G. Hodge, Jr., "Bending Moment Interaction Curve for Thin Plates with Arbitrary Yield Condition," PIBAL Report No. 348, Polytechnic Institute of Brooklyn, Brooklyn, N. Y., 1956.

10 H. G. Hopkins and W. Prager, "The Load Carrying Capacity of Circular Plates," *Journal of the Mechanics and Physics of Solids*, vol. 2, 1953, pp. 1–13.

11 P. G. Hodge, Jr., "Plastic Bending of an Annular Plate," *Journal of Mathematics and Physics*, vol. 36, 1957, pp. 130–137.

12 W. Prager, "A New Method of Analyzing Stresses and Strains in Work-Hardening Plastic Solids," JOURNAL OF APPLIED MECHANICS, vol. 23, TRANS. ASME, vol. 78, 1956, pp. 493–496.

13 W. E. Boyce, "The Bending of a Work Hardening Circular Plate by a Uniform Transverse Load," *Quarterly of Applied Mathematics*, vol. 14, 1956, p. 277.

14 P. M. Naghdi, F. Essenburg, and W. Koff, "An Experimental Study of Initial and Subsequent Yield Surfaces in Plasticity," JOURNAL OF APPLIED MECHANICS, vol. 25, TRANS. ASME, vol. 80, 1958, pp. 201–209.

Determination of the Creep Deflection of a Rivet in Double Shear

JOSEPH MARIN

Professor and Head,
Department of Engineering Mechanics,
The Pennsylvania State University,
University Park, Pa.
Mem. ASME

Structural components of modern aircraft are subjected to elevated temperatures by jet power plants and by skin friction resulting from supersonic speeds. Some of these high-temperature-aircraft structural components are riveted connections. Considerable experimental data are available on the creep of riveted connections used in aircraft [1].[1] However, a survey of the literature shows a lack of results on the theoretical prediction of creep in riveted connections from the usual creep and creep-rupture data for simple tension. The creep of a riveted joint is dependent on various factors including rivet diameter, rivet lengths, and plate thicknesses. This influence of size means that each particular riveted joint must be tested to obtain the necessary information. A basic approach to the problem is theoretically to predict the creep behavior of riveted joints from creep in simple tension. One of the important parts of the creep deformation of a riveted connection, Fig. 1(a), is the creep of the rivet. This paper deals with an approximate theoretical prediction of the creep deflection in a rivet based upon the creep constants of the material in simple tension.

In this paper, an analysis will be presented of the creep deflection of the rivet in the simple riveted joint shown in Fig. 1(*a*). It is realized that the theory developed herein is an approximate one. A more rigorous solution would consider the influence of combined stresses, and the effect of the normal stresses in the direction of the external loads. Such a solution should not require that a transverse plane before loading remain plane after loading, since it is known that this assumption does not hold for short beams in the elastic case. However, it is felt that the simplifications and assumptions made in this paper give sufficiently accurate results for engineering purposes.

In order to determine a theoretical creep deflection of a rivet, it will first be necessary to select a relation defining the creep-stress-time relation in simple tension. Many simple tension relations have been proposed. A relation which appears to give a good approximation is suggested in reference [2]; namely,

$$\boxed{\epsilon = k_1\sigma^n + k_2\sigma^n(1 - e^{-qt}) + B t\sigma^n} \tag{1}$$

where

ϵ = unit strain in simple tension
σ = unit stress
k_1, k_2, n, q, and B = experimental constants
e = base for natural logarithms
t = time

By Equation (1) the deformation is considered made up of three parts corresponding to the three terms on the right side of Equation (1): An instantaneous elastic-plastic deformation = $k_1\sigma^n$; a transient creep deformation = $k_2\sigma^n(1 - e^{-qt})$ (representing creep in the initial stages where the creep rate varies); and a "constant-rate" creep deformation = $B t\sigma^n$ (representing a steady state where the creep-time relation becomes approximately a straight line).

Equation (1) also can be expressed in a more compact form by the following equation:

$$\boxed{\epsilon = k\sigma^n} \tag{2}$$

where

$$\boxed{k = k_1 + k_2(1 - e^{-qt}) + Bt} \tag{3}$$

An examination of Equation (3) shows that k is a time function. The representation of the deformation by its three components, as given by Equation (1), is in agreement with physical concepts of creep as discussed by Orowan [3]. For long periods of time, the first and second terms on the right side in Equation (1) become small compared with the third term and the strain can be expressed by

$$\epsilon = B\sigma^n t \tag{4}$$

In the development of a mechanics of creep during the past 30 years, many investigators have used Equation (4). In recent years, Hoff [4] and others have used Equation (4) in the creep analysis of various aircraft-component parts. It should be noted that both Equations (2) and (4) lead to easier mathematical formulations than is possible by using most other creep-stress-time relations that have been proposed. Equation (2) is preferable to Equation (4) by giving a more accurate representation of the creep deformation. The increased accuracy results from the use of more constants in the relation and the consideration of the elastic, plastic, and initial creep deformations.

Creep Deflection of a Rivet in Double Shear

To determine the creep deflection of the rivet in Fig. 1(*a*) based upon Equation (1), the free-body diagram of the rivet as shown in Fig. 1(*b*) will be considered. It will be assumed that the rivet is supported at the center lines of the outer plates and that the ends of the rivet do not rotate,[2] Fig. 1(*b*). For a length

[1] Numbers in brackets designate References at end of paper.

Contributed by the Applied Mechanics Division and presented at the Annual Meeting, November 30–December 5, 1958, New York, N. Y., of The American Society of Mechanical Engineers.

Discussion on this paper should be addressed to the Secretary, ASME, 29 West 39th Street, New York, N. Y., and will be accepted until July 10, 1959, for publication at a later date. Discussion received after the closing date will be returned.

Note: Statements and opinions advanced in papers are to be understood as individual expressions of their authors and not those of the Society. Manuscript received by ASME Applied Mechanics Division, February 14, 1958. Paper No. 58—A-47.

[2] If desired, other assumptions can be made regarding the rigidity of restraint offered by the outer plates.

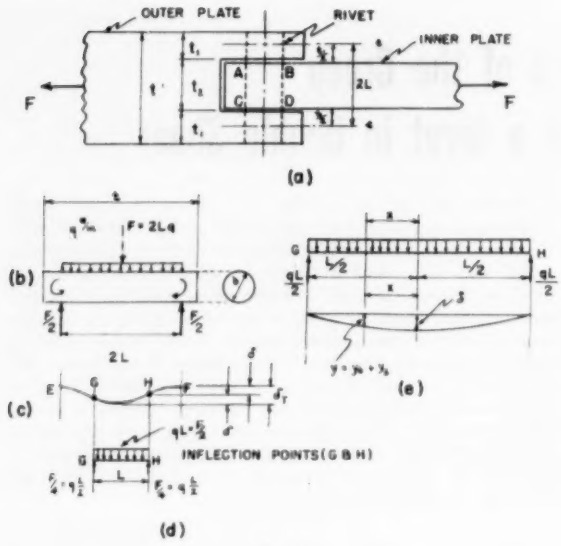

Fig. 1

of rivet between center lines equal to $2L$ the length between inflection points equals L. If the deflection of the rivet between inflection points is δ, as indicated in Fig. 1(d) and (e), then the resultant deflection of the rivet is

$$\delta_T = 2\delta \tag{a}$$

The problem now reduces to finding the creep deflection of the short, simply supported beam shown in Fig. 4(e). Since the beam is short, it will be necessary to find the creep deflection due to the transverse shear stresses in addition to the usual deflection due to bending stresses. These creep deflections would be derived based on the tension-creep relation in Equation (2). Using Equation (2) and assuming that plane sections remain plane, it can be shown that the creep deflection due to bending, y_b, is defined by the differential Equation (b)

$$D\frac{d^2y_b}{dx^2} = M^n \tag{b}$$

where

M = bending moment at a distance x
n = creep constant in tension as used in Equation (2)
D = a function of beam cross section (rivet diameter), time t and tension-creep constants. The value of D for a circular cross section is evaluated in Appendix 1.

To obtain the creep deflection y_s due to the transverse shear stresses, the geometric condition is used so that the slope of the deflection curve produced by shear is equal to the shear strain ρ at the centroid of the cross section as shown in Fig. 2. By definition, the shear strain at the centroidal axis is $\gamma_m = \tan\rho \approx \rho$ and since ρ = the slope of the deflection curve or dy_s/dx, then

$$\frac{dy_s}{dx} = \gamma_m \tag{c}$$

Since shear is a special case of combined stresses, it will be necessary to consider the combined creep stress-strain relations to determine the creep shear stress-strain relation. If σ_1, σ_2, and σ_3 are the principal stresses and ϵ_1, ϵ_2, and ϵ_3 the principal creep strains, then in a manner similar to that used in reference [6][1] it

[1] Reference [5], p. 246.

Fig. 2

can be shown that the principal creep strains in terms of the stresses are

$$\left.\begin{aligned}
\epsilon_1 &= \frac{k}{2^{\frac{n+1}{2}}}\left[(\sigma_1-\sigma_2)^2+(\sigma_2-\sigma_3)^2+(\sigma_3-\sigma_1)^2\right]^{\frac{n-1}{2}}(2\sigma_1-\sigma_2-\sigma_3)\\
\epsilon_2 &= \frac{k}{2^{\frac{n+1}{2}}}\left[(\sigma_1-\sigma_2)^2+(\sigma_2-\sigma_3)^2+(\sigma_3-\sigma_1)^2\right]^{\frac{n-1}{2}}(2\sigma_2-\sigma_3-\sigma_1)\\
\epsilon_3 &= \frac{k}{2^{\frac{n+1}{2}}}\left[(\sigma_1-\sigma_2)^2+(\sigma_2-\sigma_3)^2+(\sigma_3-\sigma_1)^2\right]^{\frac{n-1}{2}}(2\sigma_3-\sigma_1-\sigma_2)
\end{aligned}\right\} \tag{5}$$

For pure shear, $\sigma_1 = -\sigma_3 = \tau$ and $\gamma = 2\epsilon_1$. Then the first of Equations (5),

$$\gamma = 3^{\frac{n+1}{2}}k\tau^n \tag{d}$$

where k and n are the creep constants in simple tension. For the element at the centroidal axis $\gamma = \gamma_m = (\gamma)_{y=0}$ and $\tau = (\tau)_{y=0}$ and Equation (d) becomes

$$\gamma_m = 3^{\frac{n+1}{2}}k\tau_m^n \tag{e}$$

If V = the total shear force at any cross section and A = the cross-sectional area of the rivet, then the shear stress at the neutral and centroidal axis becomes

$$\tau_m = \alpha_1\frac{V}{A} \tag{f}$$

where α_1 is a constant which depends upon the creep constant n and the shape of the beam cross section. The value of α_1 for a circular cross section is determined in Appendix 2.

From Equations (e) and (f)

$$\gamma_m = 3^{\frac{n+1}{2}}k\left(\alpha_1\frac{V}{A}\right)^n \tag{g}$$

Equating the values of γ_m from Equations (c) and (g),

$$\frac{dy_s}{dx} = 3^{\frac{n+1}{2}}k\left(\alpha_1\frac{V}{A}\right)^n \tag{h}$$

The curvature produced by the transverse shear forces can now be found by Equation (h) by differentiating with respect to x. That is,

$$\frac{d}{dx}\left(\frac{dy_s}{dx}\right) = \frac{d^2y_s}{dx^2} = \left[\frac{3^{\frac{n+1}{2}}k\alpha_1^n}{A^n}\right]\left[nV^{n-1}\frac{dV}{dx}\right] \tag{i}$$

Referring to Fig. 1(*e*), the shear force V in terms of the load is

$$V = \frac{qL}{2} - q\left(\frac{L}{2} - x\right) = qx \qquad \text{(j)}$$

and

$$\frac{dV}{dx} = q \qquad \text{(k)}$$

where

$$q = F/(2L) \qquad \text{(l)}$$

In Equation (l), the total axial force F acting on the riveted connection is assumed uniformly distributed between the rivet reactions. Placing the values of V and dV/dx from Equations (j) and (k) in Equation (i),

$$\frac{d^2y_s}{dx^2} = \frac{\left(3^{\frac{n+1}{2}} nk\alpha_1{}^n q^n\right)}{A^n}(x)^{n-1} \qquad \text{(m)}$$

Equation (m) defines the beam curvature d^2y_s/dx^2 due to shear in terms of known quantities.

In order to determine the resultant curvature and deflection due to both transverse shear and bending moments, the curvatures as expressed by Equations (b) and (m) can be added. That is, the resultant curvature is

$$\frac{d^2y}{dx^2} = \frac{d^2}{dx^2}(y_b + y_s) = \frac{d^2y_b}{dx^2} + \frac{d^2y_s}{dx^2} \qquad \text{(n)}$$

or

$$\frac{d^2y}{dx^2} = \frac{M^n}{D} + \frac{\left(3^{\frac{n+1}{2}} kn\alpha_1{}^n q^n\right)}{A^n} x^{n-1} \qquad \text{(o)}$$

To integrate Equation (o) for the deflection y, it will be necessary to express the moment M in terms of the co-ordinate x. Referring to Fig. 1(*e*),

$$M = \frac{qL}{2}\left(\frac{L}{2} - x\right) - \frac{q}{2}\left(\frac{L}{2} - x\right)^2 = \frac{q}{2}\left(\frac{L^2}{4} - x^2\right) \qquad \text{(p)}$$

Substituting the value of M from Equation (p) in Equation (o)

$$\frac{d^2y}{dx^2} = k_2\left(1 - \frac{4x^2}{L^2}\right)^n + k_3 x^{n-1} \qquad \text{(q)}$$

where

$$k_2 = \frac{q^n L^{2n}}{2^{3n} D}, \quad k_3 = \frac{3^{\frac{n+1}{2}} kn\alpha_1{}^n q^n}{A^n} \qquad \text{(r)}$$

In order to integrate Equation (q), it will be necessary to expand the term $(1 - 4x^2/L^2)^n$ appearing in Equation (q) into a series. It can be shown that

$$\left(1 - \frac{4x^2}{L^2}\right)^n = 1 - n\left(\frac{4x^2}{L^2}\right) + n\frac{(n-1)}{2}\left(\frac{4x^2}{L^2}\right)^2 - \frac{n(n-1)(n-2)}{6}\left(\frac{4x^2}{L^2}\right)^3 \qquad \text{(s)}$$

Placing the value of $(1 - 4x^2/L^2)^n$ from Equation (s) in Equation (q),

$$\frac{d^2y}{dx^2} = k_2\left[1 - n\left(\frac{4x^2}{L^2}\right) + \frac{n(n-1)}{2}\left(\frac{4x^2}{L^2}\right)^2 - \frac{n(n-1)(n-2)}{6}\left(\frac{4x^2}{L^2}\right)^3 \cdots\right] + k_3 x^{n-1} \qquad \text{(t)}$$

Integrating Equation (t) and noting that $(dy/dx)_{x=0} = 0$,

$$\frac{dy}{dx} = k_2\left[x - \frac{4nx^3}{3L^2} + \frac{8n(n-1)}{5L^4}x^5 - \frac{32n(n-1)(n-2)}{21L^6}x^7 \cdots\right] + k_3\frac{x^n}{n} \qquad \text{(u)}$$

Integrating Equation (u),

$$y_2 = k_2\left[\frac{x^2}{2} - \frac{nx^4}{3L^2} + \frac{8n(n-1)}{30L^4}x^6 - \frac{4n(n-1)(n-2)}{21L^6}x^8 \cdots\right] + \frac{k_3 x^{n+1}}{n(n+1)} + c_2 \qquad \text{(v)}$$

Using the boundary condition $(y)_{x=L/2} = 0$, c_2 can be obtained by Equation (v). The maximum deflection $\delta = (y)_{x=0} = c_2$. Then by Equation (v),

$$\delta = k_2\frac{L^2}{2}\left[\frac{1}{2} - \frac{n}{2} + \frac{n(n-1)}{60} - \frac{n(n-1)(n-2)}{336} \cdots\right] + \frac{k_3\left(\frac{L}{2}\right)^{n+1}}{n(n+1)} \qquad \text{(w)}$$

Placing values of k_2 and k_3 from Equation (r), q from Equation (l), and D from Appendix 1 in Equation (w) and noting that the rivet deflection is $\delta_T = 2\delta$, Equation (w) can be written

$$\boxed{\delta_T = \left[\frac{kF^nL^{n+2}}{d^{3n+1}}\right](J)} \qquad (6)$$

where

$$J = \left(\frac{d}{2L}\right)^{n+1}\alpha_1{}^n\alpha_2 + \alpha_3/\alpha_4$$

$$\alpha_1 \approx \frac{\pi(2n+1)(4n+1)(6n+1)(97n^2+36n+3)}{4(136n^2+42n+3)(n+1)(3n+1)(5n+1}$$

$$\alpha_2 = \frac{3^{\frac{n+1}{2}} 2^{n+1}}{\pi^n(n+1)} \qquad (7)$$

$$\alpha_3 \approx \left[\frac{1}{2} - \frac{n}{2} + \frac{n(n-1)}{60} - \frac{n(n-1)(n-2)}{336} \cdots\right]\frac{1}{2^{n-1}}$$

$$\alpha_4 \approx \left[\frac{n(136n^2+42n+3)}{2(2n+1)(4n+1)(6n+1)}\right]^n$$

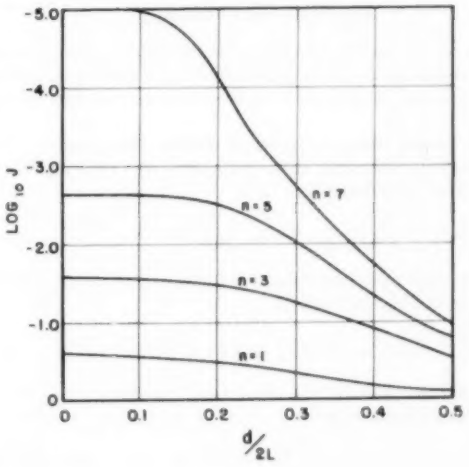

Fig. 3

The value of α_1 given in Equation (7) is derived in Appendix 2 and the value of α_4 is determined in Appendix 1. Equation (6) expresses the creep deflection of a rivet considering both shear and bending. In order to simplify the use of Equation (6), Fig. 3 gives values of $\log_{10} J$ in terms of values of n and $d/2L$.

Conclusion

An approximate theory is developed in this paper for the determination of the creep deflection of a rivet in double shear in terms of creep constants of the material in simple tension. The analysis considers the deflection due to both shear and bending. The creep of a rivet may represent an important part of the creep in a riveted connection. Creep of riveted connections is a significant consideration in the design of aircraft components subjected to high temperatures by jet engines or skin friction.

Acknowledgment

The study presented in this paper was made possible through the sponsorship of the Wright Air Development Center. The encouragement and technical assistance provided by Messrs. W. J. Trapp and E. L. Horne in this investigation are greatly appreciated by the author.

References

1 L. Mordfin and A. C. Legate, "Creep Behavior of Structural Joints of Aircraft Materials Under Constant Loads and Temperatures," NACA Technical Note 3842, January, 1957. (This paper gives a number of publications relating to creep of riveted joints.)

2 J. E. Griffith and J. Marin, "Creep Relaxation for Combined Stresses," *Journal of the Mechanics and Physics of Solids*, vol. 4, 1956, pp. 283–293.

3 E. Orowan, "Creep in Metallic and Non-Metallic Materials," Proceedings of the First U. S. National Congress on Applied Mechanics, ASME, 1953, pp. 453–472.

4 N. J. Hoff, "Stress Distribution in the Presence of Steady Creep," Proceedings of the Conference on High-Speed Aeronautics, pp. 272–310; see also *Applied Mechanics Reviews*, No. 1168, 1957.

5 J. Marin, "Mechanical Properties of Materials and Design," McGraw-Hill Book Co., Inc., New York, N. Y., 1942.

6 S. Timoshenko, "Strength of Materials," Part I, D. Van Nostrand Book Company, New York, N. Y., 1955.

APPENDIX 1

Creep Deflection Factor D for a Circular Bar Subjected to Bending

Fig. 4 represents a bar of circular section subjected to bending. To determine the creep deflection factor D as given in Equation (b), it will first be necessary to determine an equation for the stress.

Creep Bending Stress in a Bar of Circular Cross Section. For pure bending, creep tests show that plane cross sections remain plane. Then referring to Fig. 4 (*b*),

$$\epsilon_y/\epsilon = y/r \quad \text{or} \quad \epsilon_y = (y/r)\epsilon \tag{a'}$$

Assuming that the creep deformation-stress relation for tension applies to all fibers in bending,

$$\epsilon_y = k\sigma_y^n \quad \text{and} \quad \epsilon = k\sigma^n \tag{b'}$$

By placing the values of the strain from Equations (b′) in Equation (a′), the stress σ_y is

$$\sigma_y = (y/r)^{1/n}\sigma \tag{c'}$$

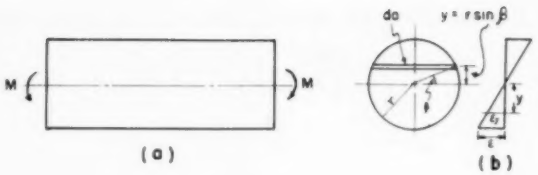

Fig. 4

For equilibrium of the stresses over the cross section,

$$M = 2\int_0^r (\sigma_y da)y = 2\sigma \int_0^r (y/r)^{1/n}(2r\cos\beta)y\,dy \tag{d'}$$

Noting that $\cos\beta = \dfrac{(r^2 - y^2)^{1/2}}{r}$, Equation (d′) becomes

$$M = (4\sigma r^{1-1/n})\int_0^r (y^{1/n+1})\left[1 - \left(\frac{y}{r}\right)^2\right]^{1/2} dy \tag{e'}$$

In order to integrate Equation (e′) the term $[1 - (y/r)^2]^{1/2}$ will be expanded into a series. Then

$$M = (4\sigma r^{1-1/n})\int_0^r y^{1/n+1}\left[1 - \frac{1}{2}\left(\frac{y}{r}\right)^2 - \frac{1}{8}\left(\frac{y}{r}\right)^4 - \frac{1}{16}\left(\frac{y}{r}\right)^6 \cdots\right] dy \tag{f'}$$

Integrating Equation (f′) and solving for maximum bending stress σ

$$\boxed{\sigma = \frac{Mr}{I}\,Q_m = \sigma_e Q_m} \tag{8}$$

where

$$Q_m = \frac{\pi}{16\left[\dfrac{1}{2 + 1/n} - \dfrac{1}{2(4 + 1/n)} - \dfrac{1}{8(6 + 1/n)} - \dfrac{1}{16(8 + 1/n)} \cdots\right]} \tag{9}$$

Equation (8) defines the maximum bending creep stress σ in terms of the elastic stress $\sigma_e = Mr/I$ and a material factor Q_m given in Equation (9). With the stress σ known, the creep curvature in bending can be determined.

Creep Curvature in Bending. Fig. 5 shows the radius of curvature f in creep bending due to bending moments M. Considering the similar triangles AOB and BCD,

$$\overline{AB}/\overline{AO} = \overline{CD}/\overline{BC} \quad \text{or} \quad dx/f = \epsilon dx/r \tag{g'}$$

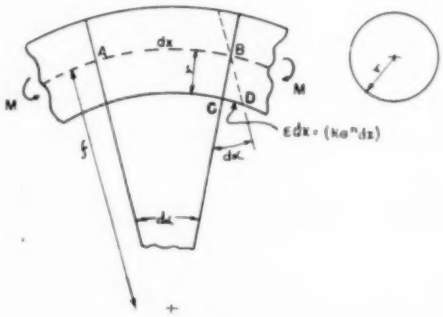

Fig. 5

or

$$1/f = \epsilon/r = k\sigma^n/r \tag{h'}$$

For small creep deflections, the deflection is related to the radius of curvature f by the equation

$$1/f = d^2y/dx^2 \tag{i'}$$

Equating the values of $1/f$ from Equations (h') and (i') and using the value of σ from Equation (8)

$$\boxed{D\frac{d^2y}{dx^2} = M^n} \tag{10}$$

where

$$D = \frac{rI^n}{kQ_m{}^n r^n} \tag{j'}$$

Placing the value of Q_m from Equation (9) in Equation (j')

$$D = \frac{4^n r^{3n+1}}{k}\left[\frac{1}{2+1/n} - \frac{1}{2(4+1/n)} - \frac{1}{8(6+1/n)} - \frac{1}{16(8+1/n)}\right]^n \tag{11}$$

It can be shown that it is sufficiently accurate to use three terms of the converging series in Equation (11). Then by Equation (11),

$$D = \left(\frac{r^{3n+1}}{k}\right)\left[\frac{n(136n^2+42n+3)}{2(2n+1)(4n+1)(6n+1)}\right]^n \tag{12}$$

or

$$\boxed{D = (d/2)^{3n+1}(\alpha_4/k)} \tag{13a}$$

where

$$\alpha_4 = \left[\frac{n(136n^2+42n+3)}{2(2n+1)(4n+1)(6n+1)}\right]^n \tag{13b}$$

That is, the differential equation for creep deflection produced by bending moments is expressed by Equation (10) where the value of D in Equation (10) is given by Equations (13).

APPENDIX 2

Maximum Transverse Creep Shear Stress in a Beam of Circular Cross Section

If V is the total transverse shear force for the circular beam cross section in Fig. 6(b), then the maximum shear stress is at the neutral axis and can be expressed by the equation

$$\tau = \alpha_1 \frac{V}{A} \tag{k'}$$

In Equation (k'), A is the cross-sectional area so that V/A is the average shear stress and α_1 is a factor which depends upon the shape of the cross section. To determine α_1 the following analysis was developed. Fig. 6(a) shows a length dx of a beam with circular cross section. The moment on section m_1n_1 is M and the moment on section mn is $(M + dM)$. The normal force on the area dA of the cross section shown in Fig. 6(b) is

$$\sigma_x dA = \sigma(y/r)^{1/n}dA \tag{l'}$$

Placing the value of the stress σ from Equation (8) in Equation (l'),

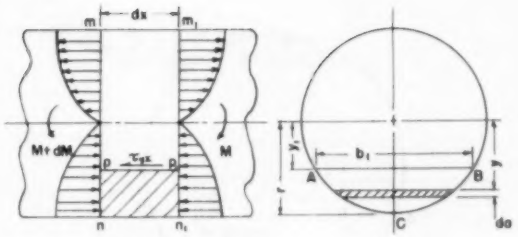

Fig. 6

$$\sigma_x dA = \left(\frac{Mr}{I}\right)(Q_m)(y/r)^{1/n}dA \tag{m'}$$

The summation of the forces $\sigma_x dA$ for the area ABC of the cross section m_1n_1 becomes,

$$\int_{y_1}^{r}\sigma_x dA = \int_{y_1}^{r}\left(\frac{Mr}{I}\right)(Q_m)\left(\frac{y}{r}\right)^{1/n}dA \tag{n'}$$

In the same way for section mn the total normal force for the area ABC is

$$\int_{y_1}^{r}\sigma_x dA = \int_{y_1}^{r}\left(\frac{M+dM}{I}\right)(rQ_m)\left(\frac{y}{r}\right)^{1/n}dA \tag{o'}$$

The total shear force for the plane pp_1, Fig. 6(a), is

$$F_x = \tau_x b_1 dx \tag{p'}$$

For the forces expressed by Equations (n'), (o'), and (p') to be in equilibrium,

$$\tau_{xy}b_1 dx = \int_{y_1}^{r}\left(\frac{M+dM}{I}\right)(rQ_m)\left(\frac{y}{r}\right)^{1/n}dA - \int_{y_1}^{r}\left(\frac{Mr}{I}\right)(Q_m)\left(\frac{y}{r}\right)^{1/n}dA$$

or

$$\tau_{xy} = \left(\frac{V}{Ib_1}\right)(Q_m r^{3-1/n})\int_{y_1}^{r} y^{1/n}dA \tag{q'}$$

Noting that $dA = [2(r^2 - y^2)^{1/2}]\,dy$ and $b_1 = 2(r^2 - y_1^2)^{1/2}$ Equation (q') becomes,

$$\tau_{xy} = \frac{VQ_m}{Ir^{1/n-2}(r^2-y_1^2)^{1/2}}\int_{y_1}^{r} y^{1/n}\left[1-\left(\frac{y}{r}\right)^2\right]^{1/2}dy$$

or

$$\tau_{xy} = \frac{VQ_m}{r^{1/n-2}I(r^2-y_1^2)^{1/2}}\left[\int_{y_1}^{r} y^{1/n}\left[1 - \frac{1}{2}\left(\frac{y}{r}\right)^2 - \frac{1}{8}\left(\frac{y}{r}\right)^4 - \frac{1}{16}\left(\frac{y}{r}\right)^6 \cdots\right]dy\right] \tag{r'}$$

Integrating Equation (r')

$$\tau_{xy} = \left[\frac{VQ_m r^2}{I(r^2-y_1^2)^{1/2}}\right]\left[\left\{\frac{1}{1+1/n} - \frac{1}{2(3+1/n)}\cdots\right\} - \left(\frac{y_1}{r}\right)^{1+\frac{1}{n}}\left\{\frac{1}{1+1/n} - \frac{y_1^2}{2r^2(3+1/n)}\cdots\right\}\right] \tag{s'}$$

As indicated in Fig. 7, the shear-stress component τ_{xy} will be

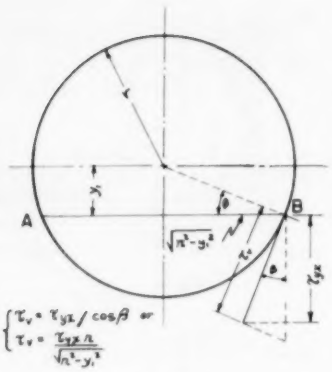

Fig. 7

taken as the vertical shear-stress component. To obtain the shear stress τ_v, the procedure used in reference [7][4] will be used. Referring to Fig. 7,

$$\tau_v = \tau_{xy}/\cos\beta = \frac{\tau_{xy} r}{(r^2 - y_1^2)^{1/2}} \qquad (t')$$

From Equations (s') and (t')

$$\tau_v = \left[\frac{VQ_m r^4}{I(r^2 - y_1^2)}\right]\left[\left\{\frac{1}{1 + 1/n} - \frac{1}{2(3 + 1/n)} \cdots\right\} - \left(\frac{y_1}{r}\right)^{1+\frac{1}{n}} \left\{\frac{1}{1 + 1/n} - \frac{y_1^2}{2r^2(3 + 1/n)} \cdots\right\}\right] \qquad (u')$$

The maximum value of the shear stress τ_v occurs for $y_1 = 0$ or by Equation (u'),

$$\tau = (\tau_v)_{max} = \alpha_1 \frac{V}{A} \qquad (14)$$

where

$$\frac{1}{\alpha_1} = \frac{\frac{4}{\pi}\left[\frac{1}{2 + 1/n} - \frac{1}{2(4 + 1/n)} - \frac{1}{8(6 + 1/n)} \cdots\right]}{\left[\frac{1}{1 + 1/n} - \frac{1}{2(3 + 1/n)} - \frac{1}{8(5 + 1/n)}\right]} \qquad (15)$$

It can be shown that it is sufficiently accurate to use three terms in the series of Equation (15). Then the value of α_1 becomes

$$\alpha_1 = \frac{\pi}{4}\left[\frac{(2n + 1)(4n + 1)(6n + 1)(97n^2 + 36n + 3)}{(n + 1)(3n + 1)(5n + 1)(136n^2 + 42n + 3)}\right] \qquad (16)$$

The maximum transverse shear stress in a beam of circular cross section subjected to bending is defined in Equation (14) where α_1 is given with sufficient accuracy by Equation (16).

[4] Reference [6], p. 121.

Journal of APPLIED MECHANICS — **Design Data and Methods**

It is important that the data contained in technical papers be made readily available to design engineers. In order to satisfy these needs of industry, this section of the Journal includes a concise presentation of data and information drawn chiefly from papers previously published by the Applied Mechanics Division of The American Society of Mechanical Engineers.

The Frequency of Vibration of Rectangular Isotropic Plates[1]

HARVEY J. FLETCHER[2]

R. F. S. HEARMON[3] has given the characteristic frequencies of a rectangular plate with various boundary conditions. He treated three cases with opposite edges supported. The remaining three cases have been studied and the characteristic frequencies are given in Table 1 with $a = b$ and $\nu = 0.3$.

Table 1 Values of k for a square plate

Edge Conditions	Mode numbers 1	2	3	4	5	6
F / S□S / F	9.631	16.13	36.72	38.94	46.74	70.75
F / S□S / S	11.68	27.76	41.20	59.07	61.86	90.29
F / S□S / C	12.69	33.06	41.70	63.01	72.40	90.61

NOTE: This paper is an addendum to "The Frequency of Vibration of Rectangular Plates," by R. F. S. Hearmon, in "Design Data and Methods," ASME, 1953, p. 192.

[1] Condensed from Technical Report No. 6 of Army Ordnance Contract DA-04-495-ORD-560, September 12, 1956, "Natural Frequencies of Plates With Opposite Edges Supported," by H. J. Fletcher, N. Woodfield, and K. Larsen.

[2] Associate Professor in Mathematics, Brigham Young University, Provo, Utah.

[3] R. F. S. Hearmon, "The Frequency of Vibration of Rectangular Isotropic Plates," JOURNAL OF APPLIED MECHANICS, vol. 19, TRANS. ASME, vol. 74, 1952, p. 402.

Manuscript received by ASME Applied Mechanics Division, February, 9, 1957; second draft received, July 28, 1958.

Journal of APPLIED MECHANICS

Brief Notes

On the recommendation of the Executive Committee of the ASME Applied Mechanics Division, it was decided to initiate a section devoted to brief notes on technical matters in mechanics. These notes must not be longer than 750 words (about 2½ double-spaced typewritten pages, including figures) and will be subject to the usual review procedure prior to publication. After approval such notes will be published as soon as possible, normally in the next issue of the Journal. The notes should be submitted to the Technical Editors of the Journal of Applied Mechanics.

Large Deflections of a Clamped Elliptical Plate Subjected to Uniform Pressure[1]

W. A. NASH[2] **and I. D. COOLEY**[3]

The problem of the nonlinear large deflections of a clamped edge thin elliptical plate subject to a uniform normal load is treated by the method of successive approximations based upon the smallness of central deflection. Results of the analysis are shown to be in excellent agreement with experimental data obtained from test of an aluminum plate.

ONLY TWO treatments of the large deflections of elliptical plates are to be found in the literature. The first, due to Perry,[4] employs expansions into Mathieu functions which unfortunately are available in tabular form for only very limited ranges of arguments. The second, due to Weil and Newmark,[5] is based upon the Ritz method and involves quite laborious computations.

Consider a thin, initially flat elliptical plate having semimajor and semiminor axes designated as a and b, respectively. The thickness of the plate is denoted by h and the uniform normal pressure by q. The x and y-axes are oriented along the major and minor axes as shown in Fig. 1, and the z-axis is normal to the middle surface of the plate. We shall let u, v, and w denote the x, y, and z components of displacement of a point in the middle surface of the plate.

The nonlinear large deflections of thin plates are governed by the von Karman equations. If $D = Eh^3/12(1-\nu^2)$, E represents Young's modulus, and ν denotes Poisson's ratio which is taken to be 0.3, then these equations may be expressed entirely in terms of the displacements u, v, and w as follows:

$$\frac{\partial^2 u}{\partial x^2} + \left(\frac{1-\nu}{2}\right)\frac{\partial^2 u}{\partial y^2} + \left(\frac{1+\nu}{2}\right)\frac{\partial^2 v}{\partial x \partial y} + \frac{\partial w}{\partial x}\cdot\frac{\partial^2 w}{\partial x^2} + \left(\frac{1-\nu}{2}\right)\frac{\partial w}{\partial x}\cdot\frac{\partial^2 w}{\partial y^2} + \left(\frac{1+\nu}{2}\right)\frac{\partial w}{\partial y}\cdot\frac{\partial^2 w}{\partial x \partial y} = 0 \quad (1)$$

$$\left(\frac{1+\nu}{2}\right)\frac{\partial^2 u}{\partial x \partial y} + \left(\frac{1-\nu}{2}\right)\frac{\partial^2 v}{\partial x^2} + \frac{\partial^2 v}{\partial y^2} + \frac{\partial w}{\partial y}\cdot\frac{\partial^2 w}{\partial y^2} + \left(\frac{1+\nu}{2}\right)\frac{\partial w}{\partial x}\cdot\frac{\partial^2 w}{\partial x \partial y} + \left(\frac{1-\nu}{2}\right)\frac{\partial^2 w}{\partial x^2}\cdot\frac{\partial w}{\partial y} = 0 \quad (2)$$

$$D\nabla^4\nabla^2 w = q + \frac{\partial^2 w}{\partial x^2}\left\{\frac{Eh}{(1-\nu^2)}\left[\frac{\partial u}{\partial x} + \frac{1}{2}\left(\frac{\partial w}{\partial x}\right)^2 + \nu\frac{\partial v}{\partial y} + \frac{\nu}{2}\left(\frac{\partial w}{\partial y}\right)^2\right]\right\} + \frac{\partial^2 w}{\partial y^2}\left\{\frac{Eh}{(1-\nu^2)}\left[\frac{\partial v}{\partial y} + \frac{1}{2}\left(\frac{\partial w}{\partial y}\right)^2 + \nu\frac{\partial u}{\partial x} + \frac{\nu}{2}\left(\frac{\partial w}{\partial x}\right)^2\right]\right\} + \frac{\partial^2 w}{\partial x \partial y}\left\{\frac{Eh}{(1+\nu)}\left[\frac{\partial u}{\partial y} + \frac{\partial v}{\partial x} + \frac{\partial w}{\partial x}\cdot\frac{\partial w}{\partial y}\right]\right\} \quad (3)$$

To investigate the large deflections of a clamped-edge elliptical plate oriented as shown in Fig. 1, Equations (1), (2), and (3) must be solved with regard to the boundary conditions:

$$\left.\begin{aligned} u = v = w = 0 \\ \frac{\partial w}{\partial x} = \frac{\partial w}{\partial y} = 0 \end{aligned}\right\} \text{ along } \frac{x^2}{a^2} + \frac{y^2}{b^2} = 1 \quad (4)$$

We shall now employ the perturbation method based upon the

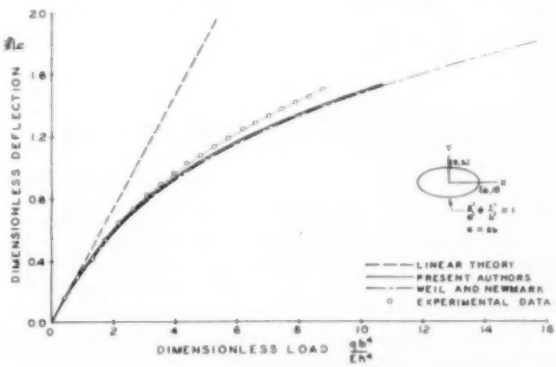

Fig. 1

[1] These results were obtained in the course of research conducted under Grant G-1652 from the National Science Foundation.

[2] Professor of Engineering Mechanics, the University of Florida, Gainesville, Fla.

[3] Instructor of Engineering Mechanics, the University of Florida, Gainesville, Fla.

[4] C. L. Perry, "The Bending of Thin Elliptical Plates," Proceedings of Symposia in Applied Mathematics, vol. III, "Elasticity," McGraw-Hill Book Co., Inc., New York, N. Y., 1950, pp. 131–139.

[5] N. A. Weil and N. M. Newmark, "Large Deflections of Elliptical Plates," JOURNAL OF APPLIED MECHANICS, vol. 23, TRANS. ASME, vol. 78, 1956, pp. 21–26.

Discussion of papers in Brief Notes should be addressed to the Secretary, ASME, 29 West 39th Street, New York, N. Y., and will be accepted until July 10, 1959, for publication at a later date. Discussion received after the closing date will be returned.

NOTE: Statements and opinions advanced in papers are to be understood as individual expressions of their authors and not those of the Society. Manuscript received by Applied Mechanics Division, October 1, 1958.

smallness of the central deflection of the elliptical plate. This technique has been used successfully by Chien[6] in the treatment of large deflections of a circular plate. We begin by denoting the central deflection by W_0 and then expanding in ascending powers of W_0 each of the quantities q, w, u, and v, viz:

$$q = \alpha_1 W_0 + \alpha_3 W_0^3 + \dots \tag{5}$$

$$w = w_1(x, y)W_0 + w_3(x, y)W_0^3 + \dots \tag{6}$$

$$u = s_2(x, y)W_0^2 + s_4(x, y)W_0^4 + \dots \tag{7}$$

$$v = t_2(x, y)W_0^2 + t_4(x, y)W_0^4 + \dots \tag{8}$$

where α_1 and α_3 are constants and w_1, w_3, s_2, s_4, t_2, and t_4 are functions of x, y to be determined. It is also necessary that

$$\left.\begin{aligned} w_1(0, 0) &= 1 \\ w_3(0, 0) &= w_5(0, 0) \dots = 0 \end{aligned}\right\} \tag{9}$$

in order that $w = W_0$ at $x = 0$, $y = 0$.

Substituting the expressions (5) through (8) into Equation (3) and equating terms involving W_0 leads to the usual linear small deflection solution

$$w = \frac{q}{D\left(\frac{24}{a^4} + \frac{16}{a^2b^2} + \frac{24}{b^4}\right)}\left(1 - \frac{x^2}{a^2} - \frac{y^2}{b^2}\right)^2 \tag{10}$$

Next, substitution of expressions (5) through (8) into Equations (1) and (2) and the equating of terms involving W_0^2 yields the linear equations

$$\frac{\partial^2 s_2}{\partial x^2} + \left(\frac{1-\nu}{2}\right)\frac{\partial^2 s_2}{\partial y^2} + \left(\frac{1+\nu}{2}\right)\frac{\partial^2 t_2}{\partial x \partial y} + \frac{\partial w_1}{\partial x}\cdot\frac{\partial^2 w_1}{\partial x^2} + \left(\frac{1-\nu}{2}\right)\frac{\partial w_1}{\partial x}\cdot\frac{\partial^2 w_1}{\partial y^2} + \left(\frac{1+\nu}{2}\right)\frac{\partial w_1}{\partial y}\cdot\frac{\partial^2 w_1}{\partial x \partial y} = 0 \tag{11}$$

$$\left(\frac{1+\nu}{2}\right)\frac{\partial^2 s_2}{\partial x \partial y} + \left(\frac{1-\nu}{2}\right)\frac{\partial^2 t_2}{\partial x^2} + \frac{\partial^2 t_2}{\partial y^2} + \frac{\partial w_1}{\partial y}\cdot\frac{\partial^2 w_1}{\partial y^2} + \left(\frac{1+\nu}{2}\right)\frac{\partial w_1}{\partial x}\cdot\frac{\partial^2 w_1}{\partial x \partial y} + \left(\frac{1-\nu}{2}\right)\frac{\partial^2 w_1}{\partial x^2}\cdot\frac{\partial w_1}{\partial y} = 0 \tag{12}$$

The associated boundary conditions are

$$s_2 = t_2 = 0 \text{ along } \frac{x^2}{a^2} + \frac{y^2}{b^2} = 1 \tag{13}$$

Polynomial solutions satisfying Equations (11) and (12) as well as the boundary conditions (13), and possessing the obvious requirements regarding even and odd characteristics that the u and v displacement components must exhibit, are:

$$s_2 = \left(1 - \frac{x^2}{a^2} - \frac{y^2}{b^2}\right)x(A_2 + B_2x^2 + C_2y^2 + D_2x^4 + E_2y^4 + F_2x^2y^2) \tag{14}$$

$$t_2 = \left(1 - \frac{x^2}{a^2} - \frac{y^2}{b^2}\right)y(A_2 + B_2x^2 + C_2y^2 + D_2x^4 + E_2y^4 + F_2x^2y^2) \tag{15}$$

Substitution of these expressions (14) and (15) into Equations (11) and (12) and the equating of terms involving corresponding powers of x and y yields twelve linear algebraic equations for the coefficients A_2, $B_2 \dots A_3$, $B_3 \dots$. At this point in the solution it is desirable to introduce the ratio of major to minor axes, which was selected as 2:1. All succeeding computations were made on this basis.

Lastly, substitution of expressions (5) through (8) into Equation (3) and the equating of terms involving W_0^3 yields the linear equation

$$D\left(\frac{\partial^4 w_3}{\partial x^4} + 2\frac{\partial^4 w_3}{\partial x^2 \partial y^2} + \frac{\partial^4 w_3}{\partial y^4}\right) = \alpha_3 + \frac{\partial^2 w_1}{\partial x^2}\left\{\frac{Eh}{(1-\nu^2)}\left[\frac{\partial s_2}{\partial x} + \frac{1}{2}\left(\frac{\partial w_1}{\partial x}\right)^2 + \nu\frac{\partial t_2}{\partial y} + \frac{\nu}{2}\left(\frac{\partial w_1}{\partial y}\right)^2\right]\right\} + \frac{\partial^2 w_1}{\partial y^2}\left\{\frac{Eh}{(1-\nu^2)}\left[\frac{\partial t_2}{\partial y} + \frac{1}{2}\left(\frac{\partial w_1}{\partial y}\right)^2 + \nu\frac{\partial s_2}{\partial x} + \frac{\nu}{2}\left(\frac{\partial w_1}{\partial x}\right)^2\right]\right\} + 2\frac{\partial^2 w_1}{\partial x \partial y}\left\{\frac{Eh}{2(1+\nu)}\left[\frac{\partial s_2}{\partial y} + \frac{\partial t_2}{\partial x} + \frac{\partial w_1}{\partial x}\cdot\frac{\partial w_1}{\partial y}\right]\right\} \tag{16}$$

The associated boundary conditions are

$$w_3 = \frac{\partial w_3}{\partial x} = \frac{\partial w_3}{\partial y} = 0 \text{ along } \frac{x^2}{a^2} + \frac{y^2}{b^2} = 1 \tag{17}$$

A polynomial solution satisfying Equations (16), (17), and possessing the requirement that the deflection be an even function of both x and y is

$$w_3 = \left(1 - \frac{x^2}{a^2} - \frac{y^2}{b^2}\right)^2(B_4x^2 + C_4y^2 + D_4x^4 + E_4y^4 + F_4x^2y^2) \tag{18}$$

This solution also satisfies the condition (9). If this expression together with the previously found values of w_1, s_2, and t_2 be substituted in Equation (16) and terms involving like powers of x and y are equated, a system of six linear algebraic equations in the six unknowns α_3, B_4, C_4, D_4, E_4, and F_4 is obtained.

The two-term load-deflection relation is thus (for $a = 2b$)

$$q = D\left(\frac{24}{a^4} + \frac{16}{a^2b^2} + \frac{24}{b^4}\right)W_0 + \frac{19.2419D}{h^2b^4}W_0^3 \tag{19}$$

Obviously the approximation could be extended by successively considering equations arising from equating higher powers of the central deflection. However, it will be shown next that the relation (19) is in satisfactory agreement with experimental evidence and hence in general it should not be necessary to consider additional terms involving powers of the central deflection greater than the third.

No experimental investigations of the load-deflection charac-

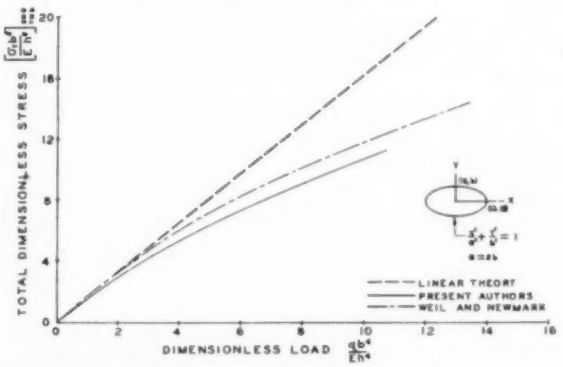

Fig. 2

[6] W. Z. Chien, "Large Deflection of a Circular Clamped Plate Under Uniform Pressure," *Chinese Journal of Physics*, vol. 7, 1947, pp. 102–113.

teristics of elliptical plates are to be found in the literature. Consequently, for the purpose of investigating the validity of the above solution, a 24S-T aluminum plate, dimensions $h = 0.13$ in., $a = 10$ in., $b = 5$ in., was tested under normal pressure with clamped-edge conditions. The Young modulus of the material was $10 \cdot 10^6$ lb/in^2. The plate was loaded only in the elastic range of action of the material, and the experimentally determined variation of central deflection with load is shown in dimensionless form in Fig. 1.

The variation of central deflection with pressure for an elliptical plate having a ratio of major to minor axis of 2:1 as indicated by the theory advanced by the present authors is shown in dimensionless form in Fig. 1. Also shown are the results of Weil and Newmark as well as the predictions of the linear small deflection theory.

The membrane stresses at any point in the plate are readily obtained once the expressions for u, v, and w have been determined. Likewise, the bending stresses are found from the usual moment-deflection relations of plate theory. The peak stress occurs in the outer fibers at the ends of the minor axis of the ellipse in the direction of that axis, and the sum of the dimensionless membrane and bending stresses at that point as indicated by the theory of the present writers is shown in Fig. 2. Also shown are the corresponding quantities as indicated by the work of Weil and Newmark as well as by the linear small deflection theory. The work of Weil and Newmark is at variance with that of the present writers because the former treatment does not specifically take account of compatibility.

The computational difficulties encountered in the solution advanced by the present writers are not serious and represent considerably less labor than either of two alternate approaches to this problem that are to be found in the literature.

Thermal Stress at Spherical Cavities and Circular Holes in Uniform Heat Flow[1]

A. L. FLORENCE[2] and J. N. GOODIER[3]

Localized thermal stress occurs when a uniform heat flow is disturbed by a cavity, and dimensional analysis shows that the maximum stress developed, under the simplest conditions of linear thermoelasticity, is $k \cdot E\alpha\tau a$, where E is Young's modulus, α the coefficient of expansion, τ the undisturbed uniform temperature gradient, a a representative linear dimension of the cavity, and k depends only on the shape and orientation of the cavity and on Poisson's ratio ν. The problem is of interest in connection with fatigue failure in thermal cycling. It is solvable for a variety of cavity shapes. In this note, results are given for the spherical cavity and the circular hole.

The Spherical Cavity

The harmonic function representing the temperature in a steady heat flow (gradient τ) disturbed by a spherical cavity (insulated) is, Fig. 1

$$T(r, \theta) = \tau\left(r + \frac{a^3}{2r^2}\right)\cos\theta \tag{1}$$

the cavity being $r = a$, and $\theta = 0, \pi$ being the axis of symmetry. The thermal stress is due to the term $(\tau a^3/2r^2)\cos\theta$. The associated displacement potential[4] χ, satisfying the Poisson equation

$$\nabla^2\chi = \frac{1+\nu}{1-\nu}\alpha\tau\,\frac{a^3}{2r^2}\cos\theta \tag{2}$$

is taken as the particular solution

$$\chi = -\frac{1+\nu}{1-\nu}\cdot\frac{1}{2}\,\alpha\tau a^3\cos\theta \tag{3}$$

The corresponding displacement is grad χ, and the stress components are (referred to spherical co-ordinates r, θ, γ)

$$[\sigma_r, \sigma_\theta, \sigma_\gamma, \tau_{r\theta}] = -s\left[2\,\frac{a^3}{r^3}\cos\theta,\ \frac{a^3}{r^3}\cos\theta,\ \frac{a^3}{r^3}\cos\theta,\ \frac{a^3}{r^3}\sin\theta\right] \tag{4}$$

where

$$s = G\cdot\frac{1+\nu}{1-\nu}\cdot\frac{1}{2}\,\alpha\tau a \tag{5}$$

and G is the shear modulus.

To solve the cavity problem, the implied cavity surface tractions

$$\sigma_{r_{r=a}} = -G\,\frac{1+\nu}{1-\nu}\,\alpha\tau a\cos\theta,$$

$$\tau_{r\theta_{r=a}} = -G\,\frac{1+\nu}{1-\nu}\cdot\frac{1}{2}\,\alpha\tau a\sin\theta \tag{6}$$

must be annulled. For this we use the Boussinesq-Papcovitch form of linear elastic displacement due to surface forces, in the axially symmetric form[5]

$$\text{grad}\,\phi + \text{grad}(\psi\cdot r\cos\theta) - 4(1-\nu)[\psi\cos\theta, -\psi\sin\theta, 0] \tag{7}$$

with $\nabla^2\phi = 0$, $\nabla^2\psi = 0$, each function being a zonal harmonic

[1] From research carried out under a contract between the Office of Naval Research and Stanford University [Nonr 225(29), Project NR-064-241].

[2] Research Assistant, Division of Engineering Mechanics, Stanford University, Stanford, Calif.

[3] Professor of Engineering Mechanics, Stanford University, Mem. ASME.

Manuscript received by ASME Applied Mechanics Division, November 12, 1958.

[4] S. Timoshenko and J. N. Goodier, "Theory of Elasticity," McGraw-Hill Book Co., Inc., New York, N. Y., 1951, p. 443.

[5] The corresponding stress components are given by E. L. McDowell and E. Sternberg, "Axisymmetric Thermal Stresses in a Spherical Shell of Arbitrary Thickness," Journal of Applied Mechanics, vol. 24, Trans. ASME, vol. 79, 1957, pp. 376–380.

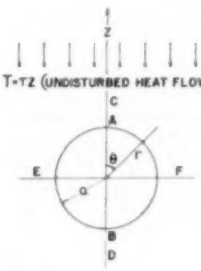

TABLE OF MAXIMUM STRESSES

	A	B	C	D	E	F
$\frac{r}{a}$	1	1	$\sqrt{2}$	$\sqrt{2}$	$\sqrt{2}$	$\sqrt{2}$
$\frac{\sigma_r}{2s}$			$-\frac{1}{4}$	$\frac{1}{4}$		
$\frac{\sigma_\theta}{2s}$	-1	1				
$\frac{\sigma_\gamma}{2s}$	-1	1				
$\frac{\tau_{r\theta}}{2s}$					$\frac{1}{8}$	$-\frac{1}{8}$

$2s = 6\left[\frac{1+\nu}{1-\nu}\right]\alpha\tau a$

Fig. 1 Stress values for a spherical cavity in steady flow

The present problem requires local effects, and ϕ and ψ must therefore consist of series of the zonal harmonics $r^{-n-1}P_n(\cos\theta)$. It turns out that ψ is not required, and ϕ consists of one term only,

$$\phi = \frac{1}{3}\, s\, \frac{a^4}{r^2}\cos\theta \tag{8}$$

The stress components derived from this are added to (4) to give the final stress components in the form

$$\sigma_r = -2s\left(\frac{a^2}{r^2} - \frac{a^4}{r^4}\right)\cos\theta;$$

$$\sigma_\theta = \sigma_\gamma = -s\left(\frac{a^2}{r^2} + \frac{a^4}{r^4}\right)\cos\theta \tag{9}$$

$$\tau_{r\theta} = -s\left(\frac{a^2}{r^2} - \frac{a^4}{r^4}\right)\sin\theta \tag{10}$$

The greatest value is $2s$, that is, $E\alpha\tau a/2(1-\nu)$, attained by σ_θ and σ_γ at the poles $\theta = 0, \pi$ on the cavity, compressive at the hot pole ($\theta = 0$), tensile at the cool pole ($\theta = \pi$). The temperature drop in a diameter of the cavity $2a$ is $2\tau a$ in the undisturbed flow. If this is 100 F in steel, $2s$ is about 3200 psi. Further stress values are shown in Fig. 1.

The Circular Hole in Plane Stress

The undisturbed heat flow in the plane of the plate (the x-y-plane) has the temperature $T = \tau y$. With the hole ($r = a$) we have

$$T = \tau\left(r + \frac{a^2}{r}\right)\sin\theta$$

and this is the real part of

$$Z = T + iQ = -i\tau\left(z - \frac{a^2}{z}\right), \quad z = x + iy$$

In accordance with the formula[6]

$$u_2 - u_1 + i(v_2 - v_1) = \int_1^2 Z dz$$

this temperature gives rise to a stress free state with a discontinuity in radial displacement along a cut $\theta = 0 (r > a)$ given by

$$(u_r)_{\theta=0+} - (u_r)_{\theta=2\pi-} = \delta \quad \text{where} \quad \delta = 2\pi a^2\alpha\tau$$

This discontinuity is annulled by superposing a dislocation represented by the complex potentials[7]

$$\psi(z) = -\frac{E\delta}{8\pi}\, i\log z, \quad \chi(z) = -\frac{E\delta}{8\pi}\, i\left(\frac{a^2}{z} - z\log z\right)$$

with

$$2G(u_r - iu_\theta) = e^{i\theta}\left[\frac{3-\nu}{1+\nu}\bar{\psi}(z) - z\psi'(z) - \chi'(z)\right]$$

$$\sigma_r + \sigma_\theta = 4\mathrm{Re}\cdot\psi'(z), \quad \sigma_\theta - \sigma_r + 2i\tau_{r\theta} = 2e^{2i\theta}[\bar{z}\psi''(z) + \chi''(z)]$$

The resulting thermal stress due to the hole is given by

$$\sigma_r, \sigma_\theta, \tau_{r\theta} = -\frac{1}{2}\, E\alpha\tau a\left[\left(\frac{a}{r} - \frac{a^3}{r^3}\right)\sin\theta,\right.$$

$$\left.\left(\frac{a}{r} + \frac{a^3}{r^3}\right)\sin\theta, -\left(\frac{a}{r} - \frac{a^3}{r^3}\right)\cos\theta\right]$$

The greatest value, $E\alpha\tau a$, is attained by σ_θ at the poles $\theta = \pi/2$, $\theta = 3\pi/2$, compressive at the hot pole, tensile at the cool pole. For $2\tau a = 100°$ F, it is about 4480 psi in steel. Further stress values are given in Fig. 2.

The plane strain problem of the circular cylindrical cavity can be solved by simple adaptation of these results, in the manner detailed in Chapter 14 of the reference in footnote 4.

Solutions of the corresponding problems for inclusions of different linear materials are evidently feasible.

[6] See p. 430 of the reference in footnote 4.

[7] Compare p. 197, problem 2(d), of the reference in footnote 4.

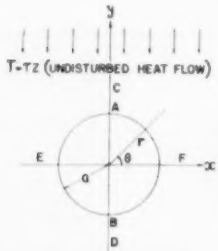

TABLE OF MAXIMUM STRESSES

	A	B	C	D	E	F
$\frac{r}{a}$	1	1	$\sqrt{3}$	$\sqrt{3}$	$\sqrt{3}$	$\sqrt{3}$
$\frac{\sigma_r}{E\alpha\tau a}$			$-\frac{1}{3\sqrt{3}}$	$\frac{1}{3\sqrt{3}}$		
$\frac{\sigma_\theta}{E\alpha\tau a}$	-1	1				
$\frac{\tau_{r\theta}}{E\alpha\tau a}$					$-\frac{1}{3\sqrt{3}}$	$\frac{1}{3\sqrt{3}}$

Fig. 2 Stress values for a circular hole in steady heat flow

Deflection of a Thick Ring in Diametral Compression by Test and by Strength-of-Materials Theory

ALEXANDER BLAKE[1]

Experimental and theoretical deflection studies are briefly described for several steel rings, of uniform rectangular cross section, compressed by two forces along a diameter and having D/d ratios ranging from 1.3 to 1.9.[2] *The calculations are based on the principle of Castigliano and expressions for strain energy due to bending, normal, and shear stresses. Discrepancies between the theoretical estimate and the tests are shown.*

Nomenclature

- b = width of ring cross section, in.
- D = outer diameter of ring, in.
- d = inner ring diameter, in.
- E = modulus of elasticity, psi
- P = compressive load, lb
- X = horizontal deflection, in.
- Y = vertical deflection, in.
- λ = ratio of mean radius to depth of ring cross section

In making the analysis of the deflection of a continuous plane ring compressed by two forces along a diameter, it is customary to assume that normal and shear stresses can be neglected provided the cross-sectional dimensions are small compared with the mean radius of the ring. However, when the elastic ring has an appreciable radial thickness in relation to the mean radius, the more exact engineering procedure is to employ the curved-beam

[1] Section Head, Theoretical and Applied Mechanics, Research Center, Associated Spring Corporation, Bristol, Conn.

[2] A. Blake, "The Calculation of the Deflection of Circular Arches and a Study of the Deflection of Thick Rings," MSc thesis, University of London, London, England, 1955.

Manuscript received by ASME Applied Mechanics Division, December 1, 1958.

theory which takes into account the effects of shear and direct stresses.

Knowledge of the load-deflection characteristics of a relatively thick ring of rectangular cross section may be of importance in design of machine parts such as, for instance, proving rings, hollow rollers, and similar components.

Experimental studies pertaining to deflection appear to have been rather few. Some fifty years ago Goodenough and Moore[2] computed the deflection for a steel ring in compression, having the ratio of D/d equal to 1.3. Their calculations based on bending and direct stresses were in agreement with experimental results. A few years later similar tests were made at Kiev Polytechnicum in Russia in which the ratios of outer to inner ring diameter only went about as high as 1.2, but the results were not published. Pippard and Miller[4] made calculations and tests for a circular ring having ratio of 1.22. The strain energy due to bending, shear, and normal stresses was taken into account, although no allowance was made for shear distribution and displacement of neutral axis. The tests agreed with the computations.

The basic concepts of the theoretical analysis of deflection for a thick curved bar has been outlined in detail by Timoshenko[5] and others. Using the well-known method of analysis of the plain and continuous ring, which represents a statically indeterminate structure, the following equations have been derived with the aid of the principle of Castigliano.

$$Y = \frac{P\lambda}{bE}\,[1.788\lambda^2 + 3.091 - 0.637/(1 + 12\lambda^2)] \qquad (1)$$

$$X = \frac{P\lambda}{bE}\,[1.644\lambda^2 + 0.926 + 0.637/(1 + 12\lambda^2)] \qquad (2)$$

The tests were conducted on seven steel rings machined from a plate 0.923 in. thick, varying the ratio of outer to inner diameter while maintaining a constant mean diameter of 8.970 in. The compressive load acting along the vertical diameter was applied gradually by equal increments producing stresses below the elastic limit of the material. The vertical decrease in diameter was measured at the inner ring surface using a dial gage mounted to the ring under test and reading directly to 0.0001 or by interpolation to 0.00005 in. Two independent sets of readings of vertical deflection were taken for each ring, and their plots represented accurate straight lines. The value of the modulus of elasticity for use in the calculation was found experimentally to be 30×10^6 psi.

The ratios of the experimental to the computed vertical deflections from equation (1) and those evaluated on the basis of the thin ring theory are plotted in Fig. 1 as a function of ratio D/d. The results appear to indicate that, while the thin-ring theory underestimates, the curved-beam theory overestimates the deflection values to a marked degree as ratio D/d increases. The discrepancy between the calculated curved-beam deflection along the vertical axis and the test data may be due to the change in the radial depth of the ring as a result of the diametral compression which is not accounted for in the curved-beam theory. It is possible therefore that better agreement between theory and test would be obtained for larger values of D/d if a more exact method based on the theory of elasticity were used.

Additional experiments made on a ring, having the highest ratio of D/d under test, have shown that the agreement between the theory [equation (2)] and measurements, in a horizontal sense, was considerably better; see Fig. 2. This provided further evidence that the effect of radial strain in line of action of the compressive load may be of importance. It seems therefore that under such conditions the curved-beam theory loses much of its advantage over the simple thin-ring theory.

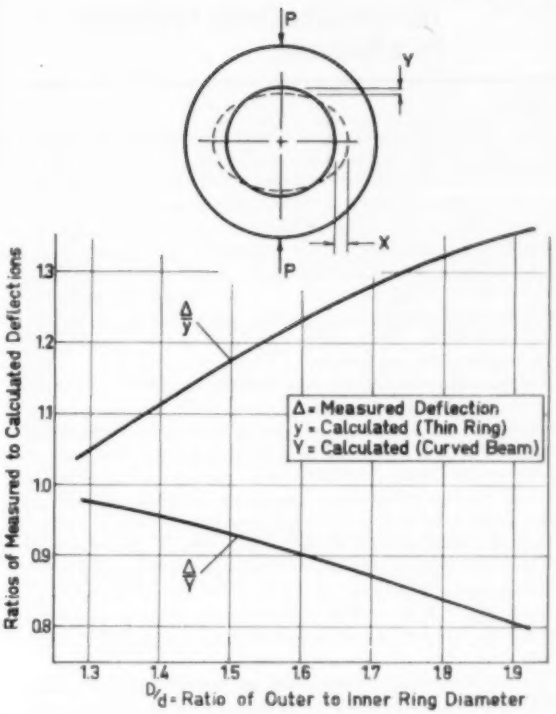

Fig. 1 Comparison of experimental and theoretical results evaluated according to thin-ring and curved-beam theories

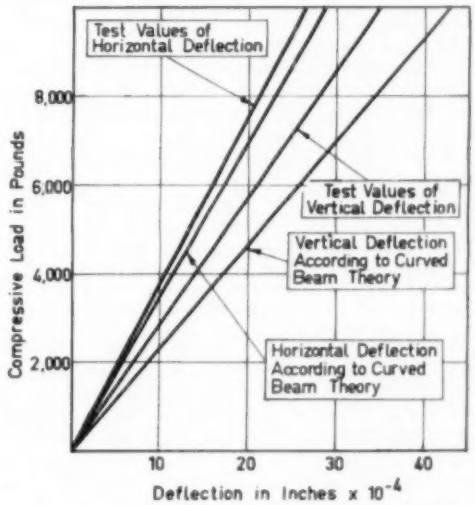

Fig. 2 Comparison of theory and experiment for vertical and horizontal deflections in a ring subjected to diametral compression (D = 11.815 in.; d = 6.125 in.; b = 0.923 in.; E = 30 × 10^6 psi)

[2] G. A. Goodenough and H. F. Moore, "The Strength of Chain Links," University of Illinois Bulletin no. 18, 1906.

[4] A. J. S. Pippard and C. V. Miller, "Stresses in Links and Their Alteration in Length Under Load," Proceedings of The Institution of Mechanical Engineers, London, 1923.

[5] S. Timoshenko, "Strength of Materials," D. Van Nostrand Co., Inc., New York, N. Y., 1956.

The Biot-Willis Elastic Coefficients for a Sandstone

I. FATT[1]

THE writer has recently presented in the geological literature[2] data which can be used to calculate, for the first time, the Biot-Willis elastic coefficients for sandstone from both bulk-volume and pore-volume measurements at various external and internal hydrostatic pressures. Biot and Willis[3] have shown that five coefficients are required to fix the properties of a porous, elastic solid containing a compressible fluid. If the porous solid is a perfect elastic body, then only four coefficients are required. Geertsma[4] has presented a theoretical treatment similar to that of Biot and Willis. These authors, however, did not give numerical examples of the coefficients.

The standstone for which the Biot-Willis coefficients will be calculated is a feldspathic graywacke quarried in Boise, Idaho. This sandstone has fairly well-sorted angular to subangular grains. Grains total 70 per cent of the solid volume and are mostly quartz (35 per cent) with lesser quantities of feldspar (29 per cent) and rock fragments (6 per cent). The 30 per cent intergranular material is mostly chert and clayey material (23 per cent) and a small amount of biotite (7 per cent). Porosity is 26 per cent and permeability is about 800 millidarcies. This sandstone appears to be uniform and isotropic in the size sample used (1 in. × 1 in. × 2 in.). Although not a petroleum reservoir sandstone, it has the texture and composition typical of oil-field sandstones.

The experimental procedure for measuring the elastic coefficients has been described previously[2] and will not be presented here.

The numerical values for the Biot-Willis coefficients of Boise standstone saturated with kerosene are summarized in Table 1. Column 1 gives the symbol used by Biot and Willis; column 2 gives the physical meaning of each coefficient; and column 3 gives its numerical value for the Boise sandstone.

Biot and Willis showed that a correction term must be added to their coefficients when applying them to nonlinear elastic porous materials. The corrections are functions of pressure. The coefficients therefore become functions of pressure. The threefold variation of the κ coefficient for Boise sandstone in the range zero to 14,000 psi indicates the nonlinear nature of this material.

Biot and Willis state that ". . . . the significance of α may be seen to be the ratio of change in pore volume to dilatation in a jacketed test." This means that for a linear elastic porous solid α can be calculated from bulk volume changes by means of the equation $\alpha = \left(1 - \frac{\delta}{\kappa}\right)$ and also from the ratio of change in pore volume to dilatation in a jacketed test. This ratio is given by the slope of the line in Fig. 4 of Fatt.[2] If the Boise sandstone were a linear elastic porous solid and if the experimental data were sufficiently precise, this slope would be in the range 0.72 to 0.92. Experimental difficulties caused the data of Fig. 4 to be scattered, but a slope in the range 0.72 to 0.92 is within the scatter of the data. There may be, however, a real difference between α calculated from the dilatation and from pore-volume data because Boise sandstone is not a linear elastic solid.

Geertsma[4] has given in his equation (6) a relation between the change in bulk volume and the change in external stress and internal pore pressure. The relation is

$$\frac{dV_B}{V_B} = C_r dp_i + C_B(dP_e - dP_i) \tag{1}$$

where C_B is defined by

$$C_B = -\frac{1}{V_B}\left(\frac{\partial V_B}{\partial P_e}\right)_{P_i}$$

C_r is the compressibility of the rock material, and the other terms are as defined in Table 1.

Table 1

1 Biot-Willis coefficient	2 Physical meaning	3 Numerical value for Boise sandstone
κ	$-\frac{1}{V_B}\left(\frac{\partial V_B}{\partial P_e}\right)_{P_i=0}$	2.7×10^{-6} psi^{-1} (1000 psi) 1.5×10^{-6} psi^{-1} (5000 psi) 1.2×10^{-6} psi^{-1} (10000 psi) 0.8×10^{-6} psi^{-1} (14000 psi) (Average of two samples)
δ	$-\frac{1}{V_B}\left(\frac{dV_B}{dP_{e,i}}\right)$	0.22×10^{-6} psi^{-1} (2000 to 7000 psi)
γ	$f(c - \delta)$	1.2×10^{-6} psi^{-1} (2000 to 7000 psi)
μ	Shear modulus	Not measured
α	$\left(1 - \frac{\delta}{\kappa}\right)$	0.92 (1000 psi) 0.85 (5000 psi) 0.82 (10000 psi) 0.72 (14000 psi)

c = fluid compressibility $= -\frac{1}{V}\frac{dV}{dP} = 5 \times 10^{-6}$ psi^{-1} for kerosene; f = porosity = pore volume/bulk volume; P_e = external pressure on jacketed sample; P_i = internal pressure on jacketed sample; $P_{e,i}$ = pressure on unjacketed sample; V_B = bulk volume.

For $dP_e = 0$ equation (1) becomes,

$$\frac{1}{V_B}\left(\frac{\partial V_B}{\partial P_i}\right)_{P_e} = C_r - C_B \tag{2}$$

For $dP_i = 0$ equation (1) yields the definition of C_B. Dividing equation (2) by the equation that defines C_B gives,

$$\frac{\frac{1}{V_B}\left(\frac{\partial V_B}{\partial P_i}\right)_{P_e}}{\frac{1}{V_B}\left(\frac{\partial V_B}{\partial P_e}\right)_{P_i}} = \frac{C_B - C_r}{C_B} \tag{3}$$

Geertsma has shown that $(C_B - C_r)/C_B$ is equal to α of the Biot and Willis theory. A test of the Biot-Willis and Geertsma theories can be made by showing experimentally the equivalence stated by equation (3).

Column 2 of Table 2 gives numerical values of the left-hand side of equation (3) obtained by direct measurement of the quantities in the numerator and denominator as described by Fatt.[2] Column 3 gives numerical values for the right-hand term in equation (3) obtained by direct measurement of C_B and using $C_r = 0.20 \times 10^{-6}$ psi^{-1}. This value of C_r is about that of quartz or feldspar. C_r need not be known to be a high degree of accuracy because a 10 per cent variation in C_r for a given C_B results in only a one per cent change in $(C_B - C_r)/C_B$.

A comparison of columns 2 and 3 in Table 2 indicates at least a

---

[1] Associate Professor of Petroleum Engineering, University of California, Berkeley, Calif.

[2] I. Fatt, "The Compressibility of Sandstones at Low to Moderate Pressures," Bulletin of the American Association of Petroleum Geologists, vol. 42, 1958, pp. 1924–1957.

[3] M. A. Biot and D. G. Willis, "The Elastic Coefficients of the Theory of Consolidation," JOURNAL OF APPLIED MECHANICS, vol. 24, TRANS. ASME, vol. 79, 1957, pp. 594–601.

Manuscript received by ASME Applied Mechanics Division, September 9, 1958.

[4] J. Geertsma, "The Effect of Fluid Pressure Decline on Volume Changes of Porous Rocks," Transactions of the American Institute of Mining and Metallurgical Engineers, vol. 210, 1957, pp. 331–340.

Table 2 Ratio of $\frac{1}{V_B}\left(\frac{\partial V_B}{\partial P_i}\right)_{P_e}$ to $\frac{1}{V_B}\left(\frac{\partial V_B}{\partial P_e}\right)_{P_i}$ for Boise sandstone as a function of pressure

External pressure—Internal pressure $P_e - P_i$, psi	$\frac{1}{V_B}\left(\frac{\partial V_B}{\partial P_i}\right)_{P_e = 12000\text{ psi}} \Big/ \frac{1}{V_B}\left(\frac{\partial V_B}{\partial P_e}\right)_{P_i = 0}$	$\frac{C_B - C_r}{C_B}$
0	1.00	0.98
500	0.97	0.98
1000	0.95	0.93
2000	0.87	0.92
4000	0.77	0.88
6000	0.77	0.83
8000	0.77	0.81
10000	0.77	0.81
	$\frac{1}{V_B}\left(\frac{\partial V_B}{\partial P_i}\right)_{P_e = 6{,}000} \Big/ \frac{1}{V_B}\left(\frac{\partial V_B}{\partial P_e}\right)_{P_i = 0}$	
0	1.00	0.98
500	0.97	0.98
1000	0.95	0.93
2000	0.90	0.92
4000	0.84	0.88
6000	0.78	0.83

[a] $C_B = -\frac{1}{V_B}\left(\frac{\partial V_B}{\partial P_e}\right)_{P_i = 0}$

$C_r = 0.20 \times 10^{-6}\ \text{psi}^{-1}$

semiquantitative agreement. There is also semiquantitative agreement between the values given for α of Boise sandstone in Table 1 with those given for the same material in columns 2 and 3 of Table 2. All of the data show that α decreases from 1.00 at zero pressure to about 0.70 at 14,000 psi.

Acknowledgment

The author wishes to thank the California Research Corporation for a research grant in support of this work.

Circular Plates on a Generalized Elastic Foundation

G. D. GALLETLY[1]

It was recently pointed out by Yu[2] that solutions of the equation

$$D\nabla^4 w - K\nabla^2 w + kw = 0 \tag{1}$$

which are suitable for the problem of a symmetrically loaded complete circular plate may be written in the form

$$w = AI_0(\alpha r), + BI_0(\beta r), \tag{2}$$

where

D = flexural rigidity of the plate
K = rotation modulus of the foundation and/or the in-plane force
k = deflection modulus of the foundation
r = radial co-ordinate
w = lateral deflection of the plate
A, B = real constants

$$\alpha, \beta = \left[\frac{K \pm i(4kD - K^2)^{1/2}}{2D}\right]^{1/2}$$

$$\nabla^2 = (d^2/dr^2) + r^{-1}(d/dr)$$

$$i = \sqrt{-1}$$

and the functions I_0 are modified Bessel functions of zero order and the first kind. The subscripts r and i refer to the real and imaginary parts of the functions and they apply when the quantity K^2-$4kD$ is negative.

The purpose of this note is to call attention to a paper written by Yakovlev[3] in 1954 in which he solved equation (1) using so-called Dinnik functions. He has tabulated these and related functions for the range of interest normally occurring in heat-exchanger problems.

Yakovlev first gives the solution of equation (1) in the form

$$w = \bar{A}J_0\left(\frac{r}{\beta}e^{i\phi}\right) + \bar{B}J_0\left(\frac{r}{\beta}e^{-i\phi}\right) \tag{3}$$

where

$\beta^4 = D/k$
$\cos 2\phi = -\beta^2 K/2D$
$\bar{A}, \bar{B}$ = complex constants

and J_0 are Bessel functions of zero order and the first kind.

Introducing next the Dinnik functions, which are the real and imaginary parts of the relation

$$J_0\left(\frac{r}{\beta}e^{\pm i\phi}\right) = U_0\left(\frac{r}{\beta}e^{i\phi}\right) \pm iV_0\left(\frac{r}{\beta}e^{i\phi}\right) \tag{4}$$

he expresses the solution (3) in the form

$$w = AU_0\left(\frac{r}{\beta}e^{i\phi}\right) + BV_0\left(\frac{r}{\beta}e^{i\phi}\right) \tag{5}$$

where A and B are real constants.

Using the definition of $\cos 2\phi$ given above, it may be verified that

$$e^{i\phi} = i\beta\left[\frac{K \pm i(4kD - K^2)^{1/2}}{2D}\right]^{1/2} \tag{6}$$

Since $I_0(x) \equiv J_0(ix)$, it follows that solutions (2) and (5) are the same.

For $K = 0$, $e^{i\phi}$ reduces to $i^{3/4}$ or $i^{5/4}$. Thus the Dinnik functions reduce to Kelvin functions as K tends toward zero ($U_0 \to$ ber, $V_0 \to -$bei).

Yakovlev has tabulated U_0, V_0, U_0', V_0' and combinations of these expressions used in calculating the moments, shears, displacements, etc., for $\phi = 46$ deg, 47 deg . . . 50 deg and for values of r/β up to 8.0. He states that the range of ϕ given should cover most practical cases. However, since he did not consider in-plane forces in his work, this remains to be seen. Yu did consider this and he showed that the effects of rotational stiffness of the foundation and in-plane forces were equivalent to each other. Thus, while the differential equations of equilibrium are not altered by considering in-plane forces, the range of parameters of practical interest may be.

It should be noted that tabulations of U_0, V_0, etc., other than that of Yakovlev's, also exist. See, in connection with this, the book by Fletcher, et al.[4]

[1] Mechanical and Electrical Engineering Department, Shell Development Company, Emeryville, Calif.

[2] Yi-Yuan Yu, "Axisymmetrical Bending of Circular Plates Under Simultaneous Action of Lateral Load, Force in the Middle Plane, and Elastic Foundation," JOURNAL OF APPLIED MECHANICS, vol. 24, TRANS. ASME, vol. 79, 1957, p. 141.

Manuscript received by ASME Applied Mechanics Division, September 15, 1958.

[3] Yu. V. Yakovlev, "On the Calculation of Heat-Exchange Apparatus" (in Russian), *Trudi Kharkovsk. Aviats. Inst.*, no. 15, 1954, pp. 133–158. See also *Applied Mechanics Reviews* No. 1380, May 1957, p. 193.

[4] A. Fletcher, J. C. P. Miller, and L. Rosenhead, "Index of Mathematical Tables," McGraw-Hill Book Company, Inc., New York, N. Y., 1946, p. 289, section 19.6.

Effect of Rotatory Inertia on the Frequencies of Vibration of Stiffened Plates

R. L. THORKILDSEN[1] AND W. H. HOPPMANN, II[2]

In recent years, the effect of rotatory inertia on strain wave velocities and vibration characteristics of beams, plates, and shells has been studied extensively. The purpose of this note is to demonstrate its practical importance to the behavior of orthogonally stiffened plates.

In this analysis, the stiffened plate is treated as an equivalent uniformly thick plate with orthotropic elastic properties. The usual assumptions of the small deflection theory of thin plates are used throughout.

Rotatory inertia is accounted for by including, in the equations of motion, the calculated mass moments of inertia about principal centroidal axes of a small characteristic element of stiffened plate.[3] The elastic constants S_{ij}, defining the anisotropy of the plate, have been determined experimentally[4] for the particular example studied.

Frequencies obtained from the analysis are compared with experimental values for a stiffened aluminum plate which is simply supported on all four edges.[5]

Nomenclature

$A_x,\ A_{xy},\ A_y$ = $\dfrac{h^2}{12}\left[\dfrac{s_{22}}{s^*},\ 2\left(\dfrac{2}{s_{66}}-\dfrac{s_{12}}{s^*}\right),\ \dfrac{s_{11}}{s^*}\right]$

I_x, I_y = mass moments of inertia, per unit area, of a small characteristic element of stiffened plate, about lines which pass through the mass centroid of the element and which are parallel to the y and x-axes, respectively

(Q_x, Q_y) = $\displaystyle\int_{-\frac{h}{2}}^{\frac{h}{2}} (\tau_{xz}, \tau_{yz})dz$ = shear forces

$(M_x, M_y, M_{yx} = -M_{xy})$ = $\displaystyle\int_{-\frac{h}{2}}^{\frac{h}{2}} (\sigma_x, \sigma_y, \tau_{xy})z dz$ = bending and twisting couples

S_{ij} = elastic constants

S^* = $\begin{vmatrix} S_{11} & S_{13} \\ S_{23} & S_{22} \end{vmatrix}$

a = width of the plate in the x-direction

b = length of the plate in the y-direction

d = distance from the bottom (flat) surface, of the stiffened plate, to the mass centroid of the characteristic element

f_x, f_y, f_z = accelerations of a point in an elastic solid

h = thickness of the equivalent plate

m, n = mode numbers corresponding to the x and y-directions, respectively

$p(x, y, t)$ = transverse load per unit area, acting in the $+z$-direction

p_{mn} = circular frequency of m, n mode of vibration

t = time

$u, v = -z\left(\dfrac{\partial w}{\partial x}, \dfrac{\partial w}{\partial y}\right)$ = bending displacements in the x and y-directions, respectively

w = deflection, in the $+z$-direction, of the middle surface of the equivalent plate

x, y = co-ordinates perpendicular and parallel to the stiffeners

z = co-ordinate perpendicular to the plane of the equivalent plate

γ = shear strain

ϵ_i = extensional strains

ρ = mass density

σ_i = extensional stress

τ = shear stress

$\dfrac{\partial^2 w}{\partial t^2}$ = transverse acceleration

$\dfrac{\partial^2}{\partial t^2}\left(\dfrac{\partial w}{\partial x}, \dfrac{\partial w}{\partial y}\right)$ = angular accelerations about lines parallel to the y and x-axes, respectively

(ρh^*) = mass per unit area of the equivalent plate (measured quantity)

Units are in., lb, and sec.

Analysis

The three-dimensional stress equations of motion, for an element of plate, neglecting body forces, are:

$$\frac{\partial \sigma_x}{\partial x} + \frac{\partial \tau_{yx}}{\partial y} + \frac{\partial \tau_{zx}}{\partial z} = \rho f_x$$

$$\frac{\partial \tau_{xy}}{\partial x} + \frac{\partial \sigma_y}{\partial y} + \frac{\partial \tau_{zy}}{\partial z} = \rho f_y \qquad (1\text{–}3)$$

$$\frac{\partial \tau_{xz}}{\partial x} + \frac{\partial \tau_{yz}}{\partial y} + \frac{\partial \sigma_z}{\partial z} = \rho f_z$$

Using the usual conditions $[\tau_{xz}, \tau_{yz}]_{\pm\frac{h}{2}} = 0$; $[\sigma_z]_{\pm\frac{h}{2}} = 0, -p$ (4–5)

and neglecting stretch of the middle surface, Equations (1–3) can be integrated over the thickness h of a uniformly thick plate to obtain

$$\frac{\partial M_x}{\partial x} + \frac{\partial M_{yx}}{\partial y} - Q_x = -I_x \frac{\partial^2 w}{\partial x \partial t^2}$$

$$-\frac{\partial M_{xy}}{\partial x} + \frac{\partial M_y}{\partial y} - Q_y = -I_y \frac{\partial^2 w}{\partial y \partial t^2} \qquad (6\text{–}8)$$

$$\frac{\partial Q_x}{\partial x} + \frac{\partial Q_y}{\partial y} + p = \rho h^* \frac{\partial^2 w}{\partial t^2}$$

The stress-strain relations for an orthotropic plate may be written

[1] General Electric Company. Assoc. Mem. ASME.

[2] Professor of Mechanics, Rensselaer Polytechnic Institute, Troy, N. Y. Mem. ASME.

[3] W. H. Hoppmann, II, "Mechanics of Stiffened Plates and Shells," ONR Final Report, Contract NONR 248(12), The Johns Hopkins University, Baltimore, Md., March, 1958, p. 6.

[4] W. H. Hoppmann, II, "Elastic Compliances of Orthogonally Stiffened Plates," Proceedings of the Society of Experimental Stress Analysis, vol. 14, 1956, pp. 137–144.

[5] W. H. Hoppmann, II, and L. S. Magness, "Nodal Patterns of the Free Flexural Vibrations of Stiffened Plates," Journal of Applied Mechanics, vol. 24, Trans. ASME, vol. 79, 1957, pp. 526–530.

Manuscript received by ASME Applied Mechanics Division, November 17, 1958.

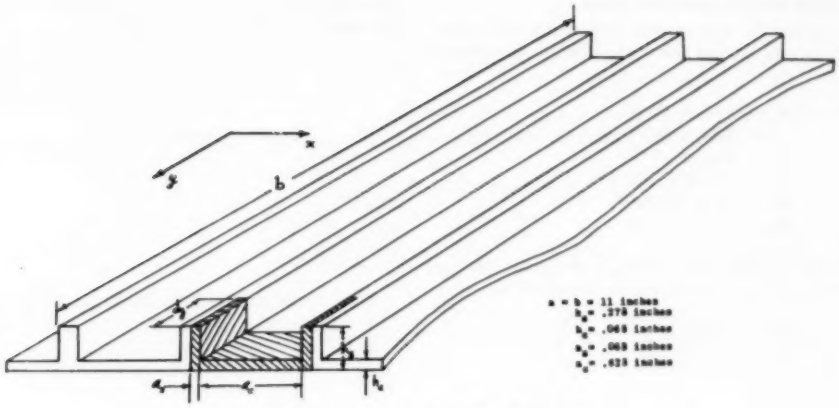

Fig. 1 Dimensions of the stiffened plate

MODE NUMBER n		MODE NUMBER m				
		1	2	3	4	5
1	EXPERIMENTAL	244	340	538	800	1152
	ROTATORY INERTIA NEGLECTED	238	336	536	831	1220
	ROTATORY INERTIA INCLUDED	237	332	520	793	1135
2	EXPERIMENTAL	794	940	1020	1268	1580
	ROTATORY INERTIA NEGLECTED	880	954	1100	1344	1689
	ROTATORY INERTIA INCLUDED	877	941	1070	1282	1570
3	EXPERIMENTAL	1700	1800	1840	2110	2340
	ROTATORY INERTIA NEGLECTED	1950	2020	2150	2349	2638
	ROTATORY INERTIA INCLUDED	1940	1983	2090	2238	2451

Fig. 2 Comparison of theoretical and experimental frequencies of flexural vibrations

$$\epsilon_i = S_{ij}\sigma$$
$$\gamma = S_{66}\tau$$

where

$$S_{ij} = S_{ji},\ i \neq j \tag{9–11}$$

The strains have the usual expressions

$$(\epsilon_x, \epsilon_y, \gamma) \equiv \left(\frac{\partial u}{\partial x}, \frac{\partial v}{\partial y}, \frac{\partial v}{\partial x} + \frac{\partial u}{\partial y}\right) \tag{12}$$

where

$$u = -z\frac{\partial w}{\partial x}$$

$$v = -z\frac{\partial w}{\partial y}$$

so that substituting (12) into (9–10) solved for stresses, and integrating through the thickness the resulting couples are

$$M_x = -\frac{h^3}{12S^*}\left(S_{22}\frac{\partial^2 w}{\partial x^2} - S_{21}\frac{\partial^2 w}{\partial y^2}\right)$$

$$M_y = -\frac{h^3}{12S^*}\left(-S_{12}\frac{\partial^2 w}{\partial x^2} + S_{11}\frac{\partial^2 w}{\partial y^2}\right) \tag{13–15}$$

$$M_{xy} = -\frac{h^3}{6S_{66}}\frac{\partial^2 w}{\partial x \partial y}$$

Substituting (13–15) into (6–8)

$$A_x\frac{\partial^4 w}{\partial x^4} + A_{xy}\frac{\partial^4 w}{\partial x^2 \partial y^2} + A_y\frac{\partial^4 w}{\partial y^4} + \frac{\partial^2}{\partial t^2}\left(\rho h^* w - I_x\frac{\partial^2 w}{\partial x^2} - I_y\frac{\partial^2 w}{\partial y^2}\right) = p(x, y, t) \tag{16}$$

A solution of (16) which satisfies simply supported boundary conditions is

$$w(x, y, t) = \sum\sum \sin\frac{m\pi x}{a}\sin\frac{n\pi y}{b}\,T(t) \tag{17}$$

where $T(t)$ is harmonic. Substituting (17) into the homogeneous part of (16), the resulting natural circular frequencies are

$$p_{mn} = \pi^2\left[\frac{A_x\left(\frac{m}{a}\right)^4 + A_{xy}\left(\frac{mn}{ab}\right)^2 + A_y\left(\frac{n}{b}\right)^4}{\rho h^* + \pi^2\left[I_x\left(\frac{m}{a}\right)^2 + I_y\left(\frac{n}{b}\right)^2\right]}\right]^{1/2} \tag{18}$$

The frequency equation for a uniformly thick orthotropic plate, neglecting rotary inertia terms is[5]

$$p_{mn} = \pi^2\left[\frac{A_x\left(\frac{m}{a}\right)^4 + A_{xy}\left(\frac{mn}{ab}\right)^2 + A_y\left(\frac{n}{b}\right)^4}{\rho h^*}\right]^{1/2} \tag{19}$$

Equations (18) and (19) are compared below for a stiffened aluminum plate.

Numerical Example and Experimental Data

Experimental values for the natural frequencies and elastic constants S_{ij} of the plate shown below are given in Hoppmann-Magness.[5]

$$\left.\begin{aligned} \rho h^* &= 2.37 \times 10^{-5} \\ \rho &= 2.32 \times 10^{-4} \\ S_{11} &= 306 \times 10^{-6}/h^3 \\ S_{12} &= -8.35 \times 10^{-6}/h^3 \\ S_{22} &= 13 \times 10^{-6}/h^3 \\ S_{66} &= 370 \times 10^{-6}/h^3 \end{aligned}\right\} \qquad (20)$$

(Units are in. and lb.) The mass moments of inertia, per unit area, for the small characteristic elements (crosshatched) are

$$I_x = \frac{\rho}{a_c + 2a_s}\left\{a_c h_c\left[\frac{h_c^2 + a_c^2}{12} + \left(d - \frac{h_c}{2}\right)^2\right] + 2a_s h_s\left[\frac{h_s^2 + a_s^2}{12} + \left(d - \frac{h_s}{2}\right)^2 + \left(\frac{a_s + a_c}{2}\right)^2\right]\right\} = 1800 \times 10^{-9} \qquad (21)$$

$$I_y = \frac{\rho}{a_c + 2a_s}\left\{a_c h_c\left[\frac{h_c^2}{12} + \left(d - \frac{h_c}{2}\right)^2\right] + 2a_s h_s\left[\frac{h_s^2}{12} + \left(d - \frac{h_s}{2}\right)^2\right]\right\} = 1.35 \times 10^{-3} \qquad (22)$$

$$\text{where } d = \frac{a_c h_c^2 + 2a_s h_s^2}{2(a_c h_c + 2a_s h_s)} = 8.1 \times 10^{-2} \text{ in.} \qquad (23)$$

Experimental and theoretical frequencies (cps) for several mode shapes are summarized in Fig. 2.

Conclusions

The effect of rotatory inertia, shown in Fig. 2, accounts for a large part of the difference between theoretical frequencies, neglecting rotatory inertia, and measured frequencies. The effect becomes increasingly important as the frequency of vibration is increased. In fact, for the highest frequency in Fig. 2, the discrepancy is reduced from 12.7% to 4.7%.

The effect of rotatory inertia appears to be of practical concern for the type of stiffened plates investigated and may be of greater importance if the stiffeners are deeper.

Design of a π Network for a Heat-Flow Analog

D. G. STEPHENSON[1] **and G. O. STARKE**[1]

THE TRANSIENT thermal behavior of a slab with one-dimensional heat flow can be simulated by a resistance-capacitance network. The accuracy of such a network analog can, in general, be improved by using more resistance and capacitance elements. This note shows that the accuracy of even a two lump network can be very good when the condensers are attached at the 21 per cent and 79 per cent points on the resistor instead of at the usual 25 and 75 per cent points.

If an electric circuit is to have the same characteristics as a homogeneous slab, the corresponding terms in their transmission matrixes[2] must be equal. For sinusoidal temperature variation the matrix of a homogeneous slab is

$$\begin{vmatrix} \cosh(1+i)\varphi, & R\cdot\dfrac{\sinh(1+i)\varphi}{(1+i)\varphi} \\ \dfrac{(1+i)\varphi\cdot\sinh(1+i)\varphi}{R}, & \cosh(1+i)\varphi \end{vmatrix}$$

where

$\varphi = \left[\dfrac{wL^2}{2\alpha}\right]^{1/2}$
$R = L/k$
α = thermal diffusivity of slab material
k = thermal conductivity
L = thickness of slab
$w = 2\pi \times$ frequency of the temperature oscillation

Fig. 1 shows a symmetrical π network. The transmission matrix for this network is

$$\begin{vmatrix} A' & B' \\ D' & A' \end{vmatrix}$$

where

$$A' = 1 - w^2 a\,bR^2C^2 + iwRC$$

[1] Building Services Section, Division of Building Research, National Research Council, Ottawa, Canada.

Manuscript received by ASME Applied Mechanics Division, January 5, 1959.

[2] L. A. Pipes, "Matrix Analysis of Heat Transfer Problems," *Journal of the Franklin Institute*, vol. 263, 1957, pp. 195–206.

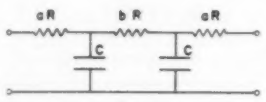

Fig. 1 A symmetrical π network

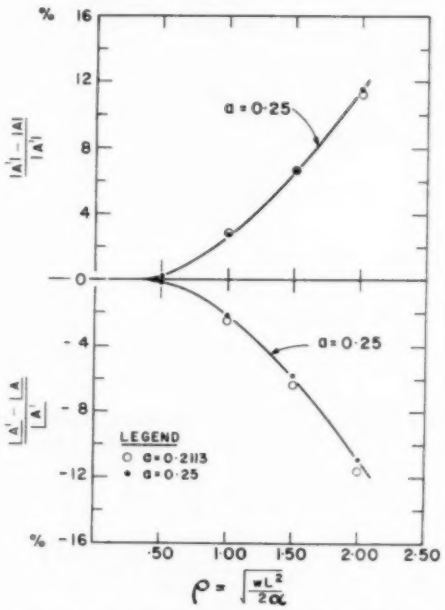

Fig. 2(a) Comparison of first matrix coefficient for network and homogeneous slab

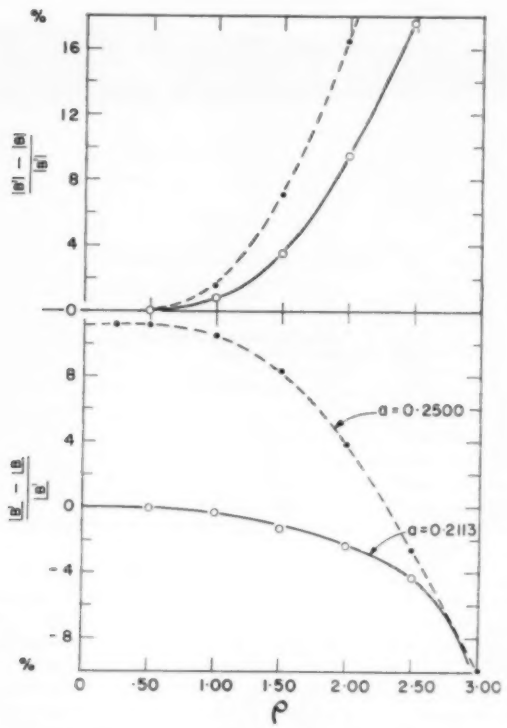

Fig. 2(b) Comparison of second matrix coefficient for network and homogeneous slab

$$B' = R\{1 - w^2a^2bR^2C^2 + iw(2a^2 + 2ab)RC\}$$

$$D' = \frac{(A')^2 - 1}{B'}$$

The coefficients of the matrix for the homogeneous slab can be expressed in the following power series

$$\text{Cosh } (1 + i)\varphi = A = 1 - \frac{\varphi^4}{6} + \frac{\varphi^8}{2520} - \cdots\cdots\cdots + i\left\{\varphi^2 - \frac{\varphi^6}{90} + \cdots\cdots\cdots\right\}$$

$$R\frac{\sinh (1 + i)\varphi}{(1 + i)\varphi} = B = R\left[1 - \frac{\varphi^4}{30} + \frac{\varphi^8}{22680} - \cdots\cdots + i\left\{\frac{\varphi^2}{3} - \frac{\varphi}{630} + \cdots\cdots\right\}\right]$$

If $\varphi^2 = wRC$, the difference between A and A' will depend on φ^4 and higher powers and will be small for low values of φ. Similarly, the difference between B and B' will depend on φ^4 and higher powers if $2a^2 + 2ab = 1/3$.

Since $b = 1 - 2a$, this requirement becomes

$$a^2 - a + 1/6 = 0$$

so

$$a = 0.2113$$

The differences between A and A' and B/R and B'/R are shown as functions of φ for $a = 0.25$ and $a = 0.2113$ in Figs. 2(a) and 2(b). These show that the network simulation of a slab is much improved when $a = 0.2113$ rather than 0.25.

Stress Distribution in a Square Tube With Rounded Corners Loaded by Internal Pressure

M. A. SADOWSKY[1] **and E. E. ZWICKY, JR.**[2]

THE stresses in a square-shaped thick-walled tube under internal pressure p are determined by methods of the theory of elasticity. Comparing the results with approximations obtainable by strength of materials methods (beam approach), it is found that the inaccuracy of the beam theory is less than 20 per cent at places of maximum stress (inner corners and mid-points of outer sides). The elasticity solution also reveals significant qualitative features such as appearance of regions of compressive hoop stress at outer corners and at mid-points of inner sides and appearance of extensive regions of tensile radial stress at outer corners.

Doing some curve fitting with the use of analytic and differential geometry, we find as an acceptable profile for the tube the parametric curves $\alpha = \pm 0.2$ in the curvilinear α, β system defined by

$$\frac{x + iy}{c} = 8e^{\alpha+i\beta} - \frac{1}{3}e^{-3(\alpha+i\beta)} - \frac{1}{5}e^{5(\alpha+i\beta)}$$

An infinite system of potential and bipotential functions is available in the form of $e^{n(\alpha+i\beta)}$ and $(x - iy)e^{n(\alpha+i\beta)}$. The problem is amenable to a straightforward stress function treatment in orthogonal curvilinear co-ordinates and leads through a Fourier series expansion to an infinite linear system in the unknown coef-

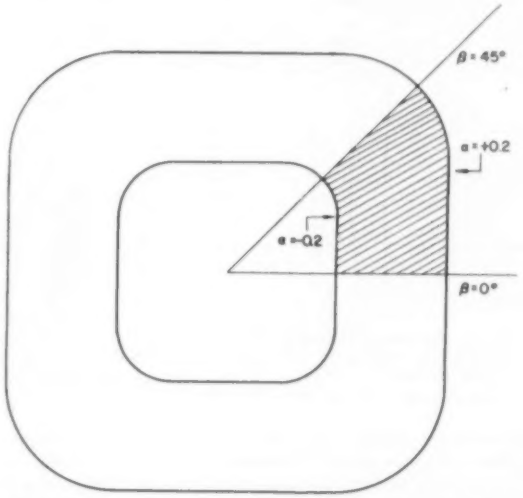

Fig. 1 Square-shaped tube of uniform wall thickness with rounded-off corners

[1] Professor of Mechanics, Rensselaer Polytechnic Institute, Troy, N. Y.

[2] Large Steam Turbine Generator Department, General Electric Company, Schenectady, N. Y.

Manuscript received by ASME Applied Mechanics Division, June 11, 1958.

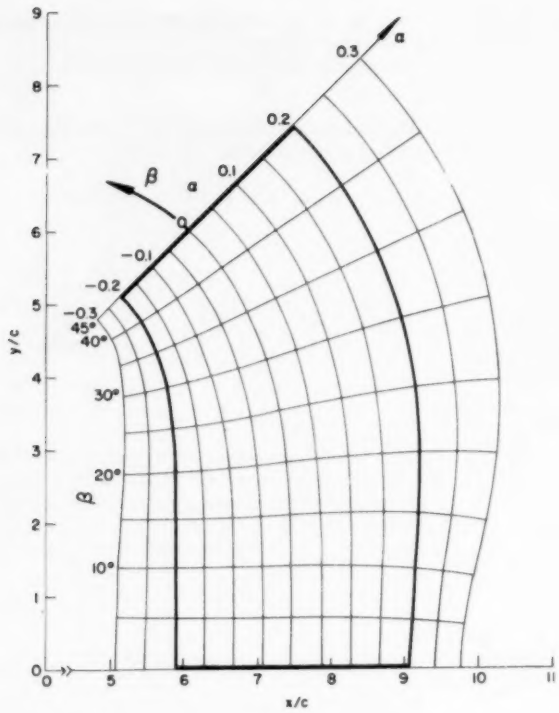

Fig. 2 Conformal map pattern of the parametric α, β curves

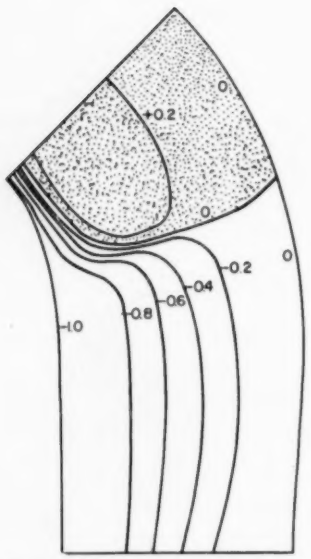

Fig. 3 Contours of the dimensionless stress σ_α/p. Region in which σ_α is tensile is shaded.

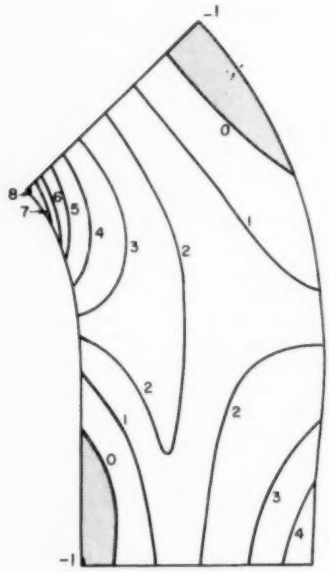

Fig. 4 Contours of the dimensionless hoop stress σ_β/p. Regions in which σ_β is compressive are shaded.

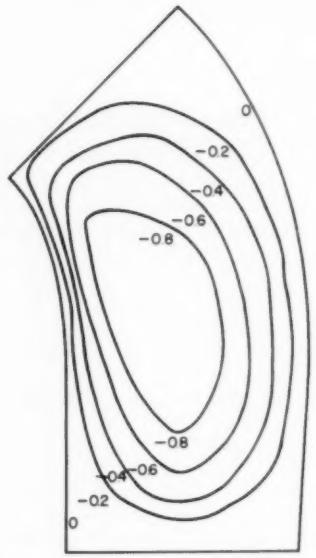

Fig. 5 Contours of the dimensionless shearing stress $T\alpha\beta/p$

ficients of superposition of the biharmonics. Except at the beginning, the equations involve 24 unknowns each. The single-valuedness of the displacements in the multiply connected region is secured a priori as there is no resultant force acting on the tube.

Further details of the theoretical analysis are described in Technical Information Series report No. TR-56-TG-100 of the General Electric Company in Schenectady, N. Y.

The extensive numerical work was performed by Mrs. P. Lamb, formerly of the General Electric Company, on an IBM-701 computer.

Kinematic Drift of Single-Axis Gyroscopes[1]

C. L. EMMERICH.[2] The effect described in this paper should be evaluated with particular care in applications which do not require complete stabilization of the gyro platform about all three axes. For example, in star-tracking applications it is frequently only necessary to stabilize to the line of sight while rotations of the platform *about* the line of sight are permitted. This means that Φ_y may reach large values because no effort is made to reduce rotations about the line of sight as would be the case in a platform stabilized fully about all three axes.

B. T. PLYMALE.[3] The phenomenon described in the paper has been observed in the laboratories of the Boeing Airplane Company. An analysis of this effect has been reported.[4] This analysis is in complete agreement with the results reported in the subject paper.

The kinematic drift of the stable platform arises from torques applied to the stable platform by various means. Among these are platform gimbal inertial reaction torques resulting from nonorthogonal gimbals subjected to angular vibration and reaction torques resulting from platform unbalance and platform gimbal unbalance subjected to linear vibration. Either of the above causes of kinematic drift can be materially reduced by proper shock mounting of the platform assembly. Also, by incorporating high damping into the platform stabilization servos, the displacement of the gyro and platform due to vibration is reduced which results in a significant reduction in kinematic drift.

Kinematic drift caused by angular vibration can be essentially eliminated by adding a fourth gimbal to the platform assembly. This redundant gimbal is servo-controlled from the inner Y-gimbal axis so that the gimbal axes shown in the paper remain orthogonal at all times. When the gimbal axes are orthogonal, angular vibration will not result in an inertial reaction torque on the platform and thus no kinematic drift will be induced. The reduction in kinematic drift realized by this technique depends on the degree to which the redundant gimbal servo can maintain the orthogonality of the remaining gimbal axes.

The addition of the redundant gimbal also makes possible a significant reduction in the moments of inertia of the other two platform gimbals since limited freedom is then required about the inner Y-axis. Since the inertial reaction torque is proportional to the gimbal inertia, an additional reduction in kinematic drift can be realized.

When the kinematic drift is caused by linear vibration acting on the mass unbalance of the platform or gimbals, a reduction in drift can be realized by balancing the platform and gimbals accurately.

It is believed that addition of the redundant gimbal, special care in balancing the platform and gimbals, proper shock mounting of the platform assembly, and a high degree of stabilization servo damping are all necessary in order to meet accuracy requirements of inertial navigation systems in the presence of this potential source of error.

J. M. SLATER.[5] The rectification drift phenomena in gyro-stabilized platforms, which are analyzed and described in the paper, were, especially at first, very obscure and difficult to disentangle from each other and from other effects. They are also rather difficult to expound in a form readily comprehensible by nonspecialists. The author is to be complimented for the lucidity of his analysis and exposition.

The paper also serves a useful purpose in pointing up the fact that performance of inertial components can only be specified in terms of their associated servo systems and dynamical environment in general. We have here a striking case of an instrument (gyro) which may be blameless in itself, behaving like an imperfect instrument because of dynamical conditions such that it is "fooled."

N. F. TODA.[6] The author's conclusions are based on his linear differential equation (3) which approximately represents the motion of the gyro:

$$I_z\ddot{\theta} + H\dot{\phi}_y\theta = -H\dot{\phi}_x \tag{3}$$

The author discusses the solution of (3) for the case:

$$\frac{H\dot{\phi}_y}{I_z} = \frac{H}{I_z}(\dot{\phi}_y)_{\text{peak}} \cos wt = d_y \cos wt$$

$$\frac{H\dot{\phi}_x}{I_z} = \frac{H}{I_z}(\dot{\phi}_x)_{\text{peak}} \cos wt = d_x \cos wt$$

Thus (3) becomes

$$\ddot{\theta} + (d_y \cos wt)\theta = -d_x \cos wt \tag{1}$$

It should be noted that equation (1) of this discussion is a special form of the Mathieu equation with the addition of a sinusoidal forcing function.

The author obtains a second approximation by using Picard's method of successive approximations.

The change of variable

$$\theta(t) = -\frac{d_x}{d_y} + \varphi(t) \tag{2}$$

transforms equation (1) to the special case of the Mathieu equation

$$\ddot{\varphi} + (d_y \cos wt)\varphi = 0 \tag{3}$$

[1] By R. H. Cannon, Jr., published in the September, 1958, issue of the JOURNAL OF APPLIED MECHANICS, vol. 25, TRANS. ASME, vol. 80, pp. 357–360.

[2] United Aircraft Corporation, Norden Laboratories Department, White Plains, N. Y.

[3] Physical Research Staff, Boeing Airplane Company, Seattle, Wash.

[4] "An Analysis of Vibration Induced Drift of a Gyro-Stabilized Platform," Boeing Airplane Company Document D2-1784, May 27, 1957.

[5] Staff Specialist, Preliminary Engineering, Autonetics, a Division of North American Aviation, Inc., Downey, Calif.

[6] Senior Engineer, Sperry Gyroscope Company, Great Neck, N. Y.

It is well known that the solution of equation (3) of this discussion is bounded[7] if (d_y) is sufficiently small (d_y approximately less than $0.44w^2$) and is unbounded for most values of $|d_x| > 0.44w^2$.[8]

Thus for sufficiently small angular velocities $\dot{\phi}_y$ and $\dot{\phi}_x$ and the addition of viscous damping the solution $\varphi(t) \to 0$ and $\theta(t) \to -(d_x/d_y)$ as times increases. Thus the theory reported by the author ($\theta \cong$ const + sinusoidal terms) approximately represents only the initial portion of the transient response; furthermore, the solution of the author's linearized equation (3) is not unbounded for sufficiently small $\dot{\phi}_y$ and $\dot{\phi}_x$.

Author's Closure

The author is grateful to Messrs. Emmerich, Plymale, and Slater for their corroborative comments on the paper and to Mr. Toda for pointing out some more mathematical aspects.

The author was, of course, familiar with Mr. Plymale's work, having studied his earlier paper (footnote 4 in the paper under discussion) and having discussed the problem with members of the Boeing staff just prior to submitting the paper. Mr. Plymale's additional comments on inertial reaction torques due to nonorthogonal gimbals are particularly welcome because the author had personally worked only with redundant-gimbal systems in which this effect was not important.

The two-axis problem described by Mr. Emmerich is important and may require a more careful treatment because of the large angles that may be involved (particularly in the light of Mr. Toda's remarks). In this connection, the paper by Goodman and Robinson[9] presented at the same time as the author's paper should be quite helpful.

Ducted Fan Design Theory[1]

C. KELLER[2] and K. HOLLIGER.[3] The evolution of the axial-flow fan design method as summarized in this paper is based on the applications of airfoil theory, as in earlier studies in this field. We think that no new theory as claimed in the introductory paragraph has been added to the art, but some refinement and better approximations to real flow conditions in ducted fans for special purposes may result from the paper. Nevertheless, also with this method calculation assumptions for loss coefficients in stator and rotor bladings and for kinetic losses are necessary. It is therefore questionable if a more refined and complex theory can furnish more reliable values of fan dimensions for optimum conditions.

We have found that the design theory by Keller[4] leads to practically the same results. If we compare the author's formulas with those of the earlier study,[4] we find that all the basic equations up to equation (20) are the same. It is somewhat disturbing that the author has departed from the more or less internationally adopted nomenclatures and symbols, e.g., for pressure coefficients, flow coefficients, and so on, which makes comparison difficult (see Fig. 1 for comparison).

Similar to the earlier work, the author arrives at optimum values for flow coefficient $\psi_m = \varphi_m$ (Keller) and best radius R_m for given design-data volume, head, and rotating speed of the fan.

He also uses the characteristic number σ as design base. These optimum values differ only slightly in both studies and lead to fan dimensions (diameters) which are only a few per cent apart. For instance, in the example (page 328 of the paper) the author arrives in the design procedure at $R_m = 1.025$ ft. With Keller, one gets $R_m = 1.08$ ft. It is difficult to say which value is closer to real optimum condition as both design theories use approximations and make neglections in basic formulas in order to get a simple end formula.

If one follows the evolution step by step in both cases, one finds that the author's approximations are better, especially for characteristic fan numbers $\sigma < 1$; this means for high-pressure fans. But one should keep in mind that for this region the underlying airfoil and grid theory is somewhat doubtful anyway because blade distances are small. If $\sigma > 1$, then the differences in optimum value from both sources are becoming negligible for practical needs. It may be due to the fact that Keller's study has been out of print for such a long time that the details of his theory are overlooked.

It is valuable that the author has undertaken the work to evaluate a somewhat different approach for design procedure. His results show the influence of a different approximation in the design theory formula for the best diameter. But by this method one does not obtain, as with Keller, a closed analytic expression for the best flow coefficient which gives the influence and weight

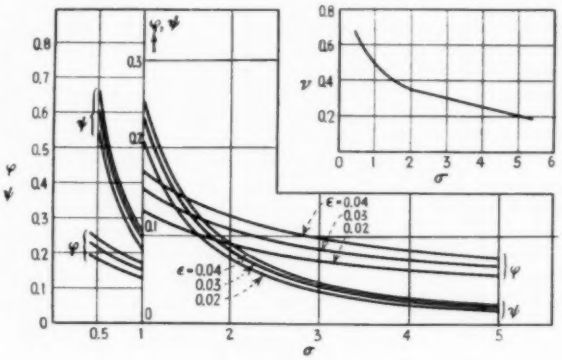

Fig. 1 Optimum φ and ψ for $\eta_s = 0.8$

Nomenclature

Keller	Van Niekerk
φ	ψ
ψ	ξ
ϵ	tan γ
σ	σ
ν	λ
η_s	η_a

(diffuser and/or annulus eff.)

o, x = φ and ψ calculated from Van Niekerk's curves.

[7] R. Bellman, "Stability Theory of Differential Equations," McGraw-Hill Book Company, Inc., New York, N. Y., 1953, p. 123.

[8] C. Hayashi, "Forced Oscillations in Non-Linear Systems," Nippon Printing and Publishing Company, Ltd., 1953, chapter 1.
J. J. Stoker, "Non-Linear Vibrations in Mechanical and Electrical Systems," Interscience Publishers, Inc., New York, N. Y., 1950, chapter 6.
N. Minorsky, "Introduction to Non-Linear Mechanics," J. W. Edwards, Inc., Ann Arbor, Mich., 1947, chapter 19.

[9] L. E. Goodman and A. R. Robinson, "Effect of Finite Rotations on Gyroscope Sensing Devices," JOURNAL OF APPLIED MECHANICS, vol. 25, TRANS. ASME, vol. 80, 1958, pp. 210–213.

[1] By C. G. Van Niekerk, published in the September, 1958, issue of the JOURNAL OF APPLIED MECHANICS, vol. 25, TRANS. ASME, vol. 80, pp. 325–331.

[2] Director of Research and Development, Escher Wyss Laboratories, Zurich, Switzerland. Mem. ASME.

[3] Research Engineer, Escher Wyss Laboratories, Zurich, Switzerland.

[4] C. Keller, "Theory and Performance of Axial Flow Fans," McGraw-Hill Book Company, Inc., New York, N. Y., 1937.

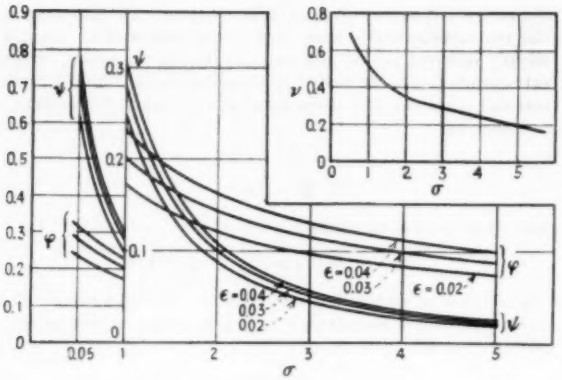

Fig. 2 Optimum φ and ψ for $\eta_s = 0.5$

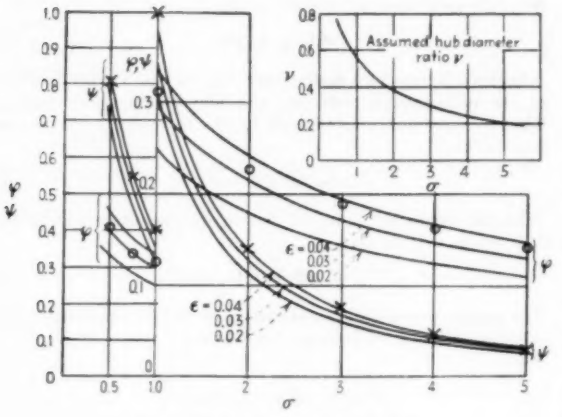

Fig. 3 Optimum φ and ψ for $\eta_s = 0$

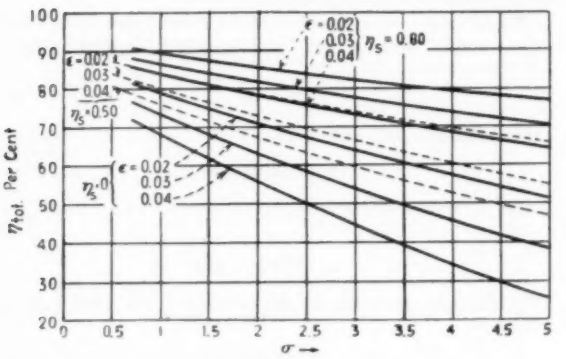

Fig. 4 Maximum obtainable efficiency as a function of the characteristic number

of changes by the fan design data and the influence of different drag coefficients. To get best values, auxiliary curves must be used. The author's published curves are valid for $\epsilon = 0.022$ only.

The reason why different grade theories do not lead to very different optimum figures lies in the fact that the total loss as a function of the flow coefficient shows always a relatively flat curve even when using different analytic expressions for blade friction losses.

Design procedure, according to Keller's study, is simplified by not widely known charts, Figs. 1, 2, 3, which give the optimum flow and pressure coefficients as function of the specific speed σ for different drag figures and valid for fans of the inlet guide vane type. In Fig. 1, crosses and circles indicate values calculated with the author's new method and show the close accordance with Keller's value. Fig. 4 gives the fan's maximum efficiency.

An analogous design theory for axial-flow turbines has been published by Keller and Bleuler.[5]

Contact Stresses Under Combined Pressure and Twist[1]

H. DERESIEWICZ.[2] The paper treats the important question of the effect of torsional loading on the stresses and displacements which occur in two spheres in Hertz contact, and it is particularly valuable in that it offers results both of theoretical treatment and of careful experimental investigation.

In the course of their analysis, the authors encounter three infinite integrals, involving Bessel functions of the first kind, which are functions of the cylindrical co-ordinates r and z (Equations [1], [2], [3]). On the surface of contact ($z = 0$) they evaluate, by means of a formula due to Sonine, the integral which expresses the component of surface traction $\tau_{z\theta}$, and compute numerically the integrals appearing in the expressions for the stress component $\tau_{r\theta}$ and the circumferential displacement v.

The purpose of this note is to call attention to the fact that these integrals can be evaluated in terms of functions which have been studied in the mathematical literature; specifically, in terms of the hypergeometric function ${}_2F_1$ and its generalizations. It appears highly unlikely, however, that the direct numerical evaluation carried out by the authors will thereby be superseded.

We may look upon the integrals on the contact surface $z = 0$ as Hankel transforms of certain combinations of Bessel functions and avail ourselves of the tables[3] compiled by the staff of the Bateman Manuscript Project. Thus, employing No. 30 in the tables,[4] which is a special case of Sonine's formula cited by the

$$\int_0^\infty J_1\left(\frac{r}{a}\,t\right) J_1^2\left(\frac{1}{2}\,t\right) dt = \begin{cases} (2/\pi)(1 - r^2/a^2)^{1/4}, & r/a < 1, \\ 0, & r/a > 1, \end{cases} \quad (1)$$

authors, we find in agreement with the authors' result leading to their Equation [5f].

Further, by means of No. 33 in the same tables (vol. 2, p. 52), we obtain

$$\int_0^\infty J_2\left(\frac{r}{a}\,t\right) J_1^2\left(\frac{1}{2}\,t\right) dt = \frac{3}{16}\left(\frac{a}{r}\right)^2 \left[{}_2F_1\left\{\frac{1}{2}, \frac{5}{2}; 2; \frac{1}{2} - \frac{1}{2}\left(1 - \frac{a^2}{r^2}\right)^{1/2}\right\}\right]^2, \quad r/a > 1, \quad (2a)$$

[5] C. Keller and Bleuler, "Theoretical Determination of the Most Favorable Diameter for Axial Flow Turbines," Escher Wyss News, No. 4, 1937.

[1] By M. Hetényi and P. H. McDonald, Jr., published in the September, 1958, issue of the JOURNAL OF APPLIED MECHANICS, vol. 25, TRANS. ASME, vol. 80, pp. 396–401.

[2] Associate Professor of Mechanical Engineering, Columbia University, New York, N. Y. Assoc. Mem. ASME.

[3] A. Erdélyi, W. Magnus, F. Oberhettinger, and F. Tricomi, "Tables of Integral Transforms," McGraw-Hill Book Company, Inc., New York, N. Y., 1954.

[4] Ibid., vol. 2, p. 51.

where the hypergeometric function is further reducible to an associated Legendre function of the first kind[5]; hence,

$$\int_0^\infty J_2\left(\frac{r}{a}\,t\right) J_1{}^2\left(\frac{1}{2}\,t\right) dt = \frac{4a}{3r}\left[P_{1/2}{}^1\left\{\left(1-\frac{a^2}{r^2}\right)^{1/2}\right\}\right]^2, \quad r/a > 1 \quad (2b)$$

A more general formula due to Bailey[6] enables us to write the integral appearing in the expression for v_i thus,

$$\int_0^\infty J_1\left(\frac{r}{a}\,t\right) J_1{}^2\left(\frac{1}{2}\,t\right)\frac{dt}{t} = \frac{a^2}{8r^2}\,F_4\left(\frac{1}{2},\ \frac{3}{2};\ 2, 2;\ \frac{a^2}{4r^2},\ \frac{a^2}{4r^2}\right), \quad r/a > 1, \quad (3)$$

where $F_4(\alpha, \beta;\ \gamma, \gamma';\ x, y)$ is Appell's fourth hypergeometric series of two variables.[7(a)]

The evaluation of the integrals in the authors' Equations [1], [2], and [3] is considerably more complicated. These may be viewed as the Laplace transforms of combinations of Bessel functions. The appropriate generic formula is given by No. 24 in the tables[8] (vol. 1, p. 184) by virtue of which each of the present integrals is expressible in terms of a Lauricella series[7(b)] in three variables. On account of their length, these results will not be reproduced here.

In conclusion, a comment appears in order on what the authors term "a singularity, a 'hole' " in the value of the components $\tau_{z\theta}$ and $\tau_{r\theta}$ at the center of the contact surface. The phenomenon is perhaps more aptly characterized by the statement that $\tau_{z\theta}$ and $\tau_{r\theta}$, as functions of the two variables r and z, are not continuous at the origin of co-ordinates.

Co-ordinates Which Uncouple the Equations of Motion of Damped Linear Dynamic Systems[1]

R. B. McCALLEY, Jr.[2] The author is commended for his work on damped linear systems which continue to be one of the more annoying problems in analysis. It is hoped that his contributions will stimulate a renewed interest in the work. This discussion presents an alternate expansion for the forces in terms of the modes of the reduced system as well as two complex mode relationships of the original system which do not appear to be well known.

Equation (18) in the paper gives an expansion for the force vector in terms of the modes weighted by the matrix $[R]$ rather than in terms of the modes directly. This is a perfectly valid procedure but it is also possible to make an expansion directly in terms of the modes without resorting to this stratagem. The difference in the two approaches is more readily demonstrated by using a slightly different format and notation than in the paper. Some extra symbolism is eliminated by using lower-case letters for vectors and upper case letters for matrices. In terms of the author's notation, let

$$f = \{F(t)\} \quad (1)$$

$$R = [R] \quad (2)$$

and construct a modal matrix

$$\Phi = [\{\Phi^{(1)}\}\{\Phi^{(2)}\} \ldots \{\Phi^{(2N)}\}] \quad (3)$$

whose columns are the eigenvectors of the reduced system. The author's approach is equivalent to constructing a column vector c for the equation:

$$f = R\Phi c \quad (4)$$

Upon multiplying both sides of this equation by the transpose Φ^T of the modal matrix,

$$\Phi^T f = \Phi^T R \Phi c \quad (5)$$

However, the resultant matrix operating on c is diagonal because of the orthogonality relations and may be inverted readily. Thus by premultiplying through by the inverse, the vector c is found to be:

$$c = (\Phi^T R\Phi)^{-1}\Phi^T f \quad (6)$$

With this resubstituted into Equation (4), the author's Equation (18) can be written as

$$f = R\Phi(\Phi^T R\Phi)^{-1}\Phi^T f \quad (7)$$

The elements in the diagonal matrix $(\Phi^T R\Phi)^{-1}$ are $1/R_n$ in the author's notation while each element of the vector $\Phi^T f$ is $F_n(t)$. Thus

$$(\Phi^T R\Phi)^{-1}\Phi^T f = \{F_n(t)/R_n\} \quad (8)$$

and the use of the modal matrix Φ eliminates the summation sign in the author's Equation (18).

The alternate expansion of the force vector f directly in terms of the normal modes is done by constructing a column vector d for the equation:

$$f = \Phi d \quad (9)$$

After premultiplying with $\Phi^T R$,

$$\Phi^T R f = \Phi^T R \Phi d \quad (10)$$

which is readily solved owing to the orthogonality relation to yield

$$d = (\Phi^T R\Phi)^{-1}\Phi^T R f \quad (11)$$

The alternate expansion directly in terms of the normal modes therefore is

$$f = \Phi(\Phi^T R\Phi)^{-1}\Phi^T R f \quad (12)$$

The fundamental difference between the two expansions is that the weighting matrix R is applied to the modes in the author's expansion but applied to the forces in the alternate expansion.

Two relationships for the complex modes of the original system can be derived by starting with the author's Equation (1). By taking a solution in the customary form:

$$q_i = e^{\lambda t}\phi_i \quad (13)$$

the equation for the rth eigenvalue λ_r with the associated mode coefficient $\phi_j{}^{(r)}$ is

[5] A. Erdélyi, W. Magnus, F. Oberhettinger, and F. Tricomi, "Higher Transcendental Functions," McGraw-Hill Book Company, Inc., New York, N. Y., vol. 1, 1953, p. 148.

[6] W. N. Bailey, "Some Infinite Integrals Involving Bessel Functions," *Proceedings of the London Mathematical Society*, vol. 40, 1936, p. 45, No. 7.1.

[7] P. Appell and J. Kampé de Fériet, "Fonctions Hypergéométriques et Hypersphériques; Polynomes d'Hermite," Gauthier-Villars, Paris, 1926; (*a*) chapter 2, (*b*) chapter 7.

[1] By K. A. Foss, published in the September, 1958, issue of the JOURNAL OF APPLIED MECHANICS, vol. 25, TRANS. ASME, vol. 80, pp. 361–364.

[2] Knolls Atomic Power Laboratory, General Electric Company, Schenectady, N. Y. Mem. ASME.

$$\lambda_r^2 \sum_j m_{ij}\phi_j^{(r)} + \lambda_r \sum_j r_{ij}\phi_j^{(r)} + \sum_j k_{ij}\phi_j^{(r)} = 0 \quad (14)$$

After multiplying through by $\phi_i^{(s)}$ and summing on i,

$$\lambda_r^2 \sum_i \sum_j m_{ij}\phi_i^{(s)}\phi_j^{(r)} + \lambda_r \sum_i \sum_j r_{ij}\phi_i^{(s)}\phi_j^{(r)} + \sum_i \sum_j k_{ij}\phi_i^{(s)}\phi_j^{(r)} = 0 \quad (15)$$

On the other hand, by starting with the equation for the sth eigenvalue, multiplying by $\phi_i^{(r)}$ and summing on i,

$$\lambda_s^2 \sum_i \sum_j m_{ij}\phi_i^{(r)}\phi_j^{(s)} + \lambda_s \sum_i \sum_j r_{ij}\phi_i^{(r)}\phi_j^{(s)} + \sum_i \sum_j k_{ij}\phi_i^{(r)}\phi_j^{(s)} = 0 \quad (16)$$

The corresponding double summation terms in these last two equations are equal, as can be seen by interchanging i and j and noting that the mass, damping, and stiffness matrices are symmetric.

By subtracting Equation (16) from Equation (15) and dividing through by $(\lambda_r - \lambda_s)$,

$$(\lambda_r + \lambda_s) \sum_i \sum_j m_{ij}\phi_i^{(r)}\phi_j^{(s)} + \sum_i \sum_j r_{ij}\phi_i^{(r)}\phi_j^{(s)} = 0 \quad (17)$$

Another relation is obtained by adding Equation (15) and (16):

$$(\lambda_r^2 + \lambda_s^2) \sum_i \sum_j m_{ij}\phi_i^{(r)}\phi_j^{(s)} + (\lambda_r + \lambda_s) \sum_i \sum_j r_{ij}\phi_i^{(r)}\phi_j^{(s)} + 2 \sum_i \sum_j k_{ij}\phi_i^{(r)}\phi_j^{(s)} = 0 \quad (18)$$

Next, let λ_r and λ_s be two complex conjugate roots, that is,

$$\lambda_s = \overline{\lambda_r} \quad (19)$$

$$\phi_j^{(s)} = \overline{\phi_j^{(r)}} \quad (20)$$

where the bars above the symbols indicate the complex conjugate. Using the customary notations of ω_r for the undamped natural frequency and ζ_r for the damping ratio of the rth mode,

$$\lambda_r = -\zeta_r\omega_r + i\omega_r(1 - \zeta_r^2)^{1/2} \quad (21)$$

and thus

$$\lambda_s = \overline{\lambda_r} = -\zeta_r\omega_r - i\omega_r(1 - \zeta_r^2)^{1/2} \quad (22)$$

From these two expressions, it will be found that

$$\lambda_r + \lambda_s = -2\zeta_r\omega_r \quad (23)$$

and

$$\lambda_r^2 + \lambda_s^2 = -2\omega_r^2(1 - 2\zeta_r^2) \quad (24)$$

After substituting Equation (23) into Equation (17), the first relation for the damped modes is found:

$$2\zeta_r\omega_r = \frac{\sum_i \sum_j r_{ij}\phi_i^{(r)}\overline{\phi_j^{(r)}}}{\sum_i \sum_j m_{ij}\phi_i^{(r)}\overline{\phi_j^{(r)}}} \quad (25)$$

By substituting Equations (23) and 24 into Equation (18), dividing through by 2, and using Equation (25) to eliminate the damping summation, the second relation for the damped modes is:

$$\omega_r^2 = \frac{\sum_i \sum_j k_{ij}\phi_i^{(r)}\overline{\phi_j^{(r)}}}{\sum_i \sum_j m_{ij}\phi_i^{(r)}\overline{\phi_j^{(r)}}} \quad (26)$$

The usefulness of these last two expressions lies in their analogy to the one-degree damped system. The numerator of Equation (25) is the generalized damping while the denominator is the generalized mass, and the numerator of Equation (26) is the generalized stiffness. These two relations have not been seen in print in this particular form although they are readily derived from relations given by other authors.

R. W. TRAILL-NASH.[2] The writer would like to draw attention to a report[4] in which a good deal of the content of the author's paper has been previously put forward. Only one of the orthogonality conditions noted by the author was presented, but separation of co-ordinates and derivation of response in terms of "static" and "transient" components are essentially the same as those of the present paper. The work of Williams[5] on the undamped system is also relevant.

Author's Closure

The author wishes to thank Mr. McCalley for his comments and his additional derivations.

The author regrets having had no prior knowledge of the work of Mr. Traill-Nash, and wishes to acknowledge his previous derivation[4] of the basic ideas of orthogonality and uncoupled co-ordinates for damped systems. As to the paper by D. Williams,[5] this work has been acknowledged in reference 4 of the present paper.

On the Transverse Vibrations of Rectangular Orthotropic Plates[1]

R. F. S. HEARMON.[2] The very complete treatment in the paper is valuable in enabling accurate frequencies to be calculated. It is, however, possible to derive simpler though approximate expressions for the frequencies by the Rayleigh method. Professor Huffington kindly showed the writer in advance the results of his calculations, and with their aid an estimate of the accuracy of the Rayleigh method may be obtained.

The Rayleigh method has been applied by Warburton[3] to isotropic plates, and the extension of his method to orthotropic plates was suggested in the discussion to his paper. It is intended to publish a description of the extension later, but its application leads to the general formula for the frequency of an orthotropic plate:

$$\frac{p_{mn}a^2}{(D_y/\rho h)^{1/2}} = n = \left\{ I\frac{D_x}{D_y} + J\frac{a^4}{b^4} + \frac{2a^2}{b^2}\left[K\frac{D_1}{D_y} + \frac{2LD_{xy}}{D_y}\right]\right\}^{1/2}, \quad (1)$$

where I, J, K, L are quantities which depend on the mode number

[2] Australian Defence Scientific Service, Structures Division, Aeronautical Research Laboratories, Department of Supply, Melbourne, Australia.

[4] R. W. Traill-Nash, "An Analysis of the Response of a Damped Dynamical System Subjected to Impressed Forces," Aeronautical Research Laboratories Report SM151, May, 1950.

[5] D. Williams, "Displacements of a Linear Elastic System Under Given Transient Load," *Aeronautical Quarterly*, vol. 1, part II, August, 1949, p. 123.

[1] By N. J. Huffington, Jr., and W. H. Hoppmann, II, published in the September, 1958, issue of the JOURNAL OF APPLIED MECHANICS, vol. 25, TRANS. ASME, vol. 80, pp. 389–395.

[2] Forest Products Research Laboratory, Princes Risborough, Bucks, England.

[3] G. B. Warburton, "The Vibration of Rectangular Plates," *Proceedings of the Institution of Mechanical Engineers*, vol. 168, 1954, pp. 371–384.

and on the boundary conditions of the plate; the remaining symbols in Equation (1) are as defined in the authors' nomenclature. For purposes of the Rayleigh treatment, it is assumed that the deflection of the plate is represented by the characteristic beam functions given by Warburton.[3]

In the fundamental mode of a plate with opposite edges supported, $I = \pi^4$ irrespective of the boundary conditions at the two other edges, and values of J, K, and L for all possible combinations of free, supported, and clamped conditions at the latter edges are given in Table 1.

Table 1 Fundamental frequency of vibration of an orthotropic plate with two opposite edges supported

Case no.	J	K	L	n [Equation (1)]
1	97.41	97.41	97.41	48.65
2	0	0	29.61	20.70
3	237.81	113.4	113.4	68.53
4	500.56	121.5	121.5	94.57
5	0	0	0	17.42
6	12.37	−8.5	45.9	26.22

The last column in Table 1 contains the values of n calculated from Equation (1) using Huffington's data for maple plywood. Comparison with his values shows that the Rayleigh estimates are only slightly higher than the exact results, and also that, at least in the fundamental mode, the Rayleigh treatment is adequate.

The advantages of this treatment are: (*a*) The frequencies are given by closed formulas; (*b*) the general Equation (1) applies to any combination of free, clamped, or supported edges, provided the appropriate values of I, J, K, and L are inserted and its use is not limited to plates with opposite edges supported; (*c*) the equation is applicable to the overtones, although caution would be needed in such application because the accuracy of the formula might well be reduced, and because at higher frequencies the effects of shear and rotatory inertia, which are not allowed for in the Rayleigh treatment, would become increasingly important.

J. S. THOMSEN.[4] The authors indicate that they carried out frequency calculations for special cases, but did not attempt any general tabulation program; hence they have not included any frequency data. However, it might be helpful if they could include frequency numbers for a few typical examples.

Authors' Closure

The authors wish to thank both discussers for their comments and questions regarding this problem.

Professor Thomsen's request for numerical examples is easily satisfied by presenting the results of calculations which were communicated privately to Mr. Hearmon. These calculations were based on the properties of an orthotropic material (5-ply maple plywood) for which the elastic constants had been determined experimentally:[5]

$$E_x = 1.87 \times 10^6 \text{ psi}$$
$$E_y = 0.60 \times 10^6 \text{ psi}$$
$$G_{xy} = 0.159 \times 10^6 \text{ psi}$$
$$\nu_{xy} = 0.12$$

A rectangular plate of this material with side ratio $b/a = 0.5$ (having symmetry axes of orthotropy parallel to the boundaries) will, for the boundary value cases of this paper, have the fundamental frequencies shown in Table 2. The agreement of Hearmon's values with these "exact" frequencies is indeed remarkably good. The corresponding fundamental mode shapes consist of the product of a half sine wave in the x-direction with the y-variation shown in Fig. 1. For Case V with these parameters the eigenvalue ψ_{11} is imaginary, resulting in the eigenfunction Y_{11} being composed of only hyperbolic terms.

Table 2 Fundamental frequencies for rectangular orthotropic plates (5-ply maple plywood)

CASE NO.	BOUNDARY CONDITIONS	$p_{11}a^2/\sqrt{D_y/\rho h}$	CODE
V	S F S F	17.39	C CLAMPED F FREE S SIMPLY SUPPORTED
II	S S S S	20.65	PARAMETERS
VI	S F S C	26.06	$r = \frac{b}{a} = 0.5$
I	S S S S	48.65	$\frac{D_x}{D_y} = 3.117$
III	S S S C	68.52	$\frac{D_1}{D_y} = 0.120$
IV	S C S C	94.56	$\frac{H}{D_y} = 0.648$

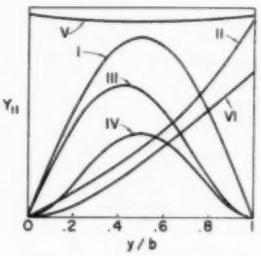

Fig. 1 y-variation of mode shapes

By extending Warburton's procedure as suggested by Hearmon, it is possible to evaluate the accuracy of the Rayleigh method for calculating overtone frequencies of orthotropic plates. Certain roots of the frequency equation for Case VI have been previously determined[6] for the same plywood material. Frequencies corresponding to these roots are compared with those determined by the Warburton-Hearmon procedure in Table 3.

Table 3 Comparison of exact and approximate frequencies of plywood plate for Case VI with $r = 0.5$

m	n	$p_{mn}a^2/(Dy/\rho h)^{1/2}$ Exact	$p_{mn}a^2/(Dy/\rho h)^{1/2}$ Warburton-Hearmon method
1	1	26.06	26.22
1	2	97.68	97.70
1	3	254.68	254.65
1	4	490.98	491.00
3	1	161.72	162.67
3	2	212.04	213.67
5	1	439.74	441.14

In an effort to evaluate the ability of Hearmon's Equation (1) to represent the frequency variation with side ratio properly, the fundamental frequency of a rectangular plate of the same orthotropic material was calculated for Case III with $a = 10b$. The frequency parameter n was determined to be 1546.68, as contrasted with the value 1546.96 obtained by use of Hearmon's Equation (1).

The agreement of the frequencies obtained by the Rayleigh

[4] Assistant Professor of Mechanical Engineering, The Johns Hopkins University, Baltimore, Md.

[5] R. F. S. Hearmon and E. H. Adams, "The Bending and Twisting of Anisotropic Plates," *British Journal of Applied Physics*, vol. 3, 1952, pp. 150–156.

[6] N. J. Huffington, Jr., and W. H. Hoppmann, II, "Blast Loading of Orthotropic Plates," Technical Memorandum ORO-T-239, Operations Research Office, The Johns Hopkins University, January, 1954.

method with those obtained from the frequency equations of this paper is impressive; however, I am sure that Mr. Hearmon will agree that no such excellent correspondence of strains calculated by the Rayleigh method using beam eigenfunctions with those of the exact solution is to be expected.

Natural Forcing Functions in Nonlinear Systems[1]

H. R. LANG.[2] The author has presented a very interesting procedure for determining the frequency response of nonlinear, one-dimensional, second-order systems. The property of periodicity, which is a more fundamental characteristic of vibrations than linearity and superposition, reduces the forced oscillations to free oscillations in those circumstances where the two have a common period and similar wave forms. These requirements lead naturally, as the author shows in his first example, to harmonic oscillations when the restoring function is linear.

The use of free nonlinear oscillation as an initial point for determining the behavior of forced nonlinear oscillations is also a feature of the iteration procedure used by Rauscher.[3,4] The usual textbook examples continue to emphasize sinusoidal forcing functions with period 2π.

A slightly more general development of author's Equations (2), (5), (6) is possible. Consider

$$\frac{d^2y}{d\theta^2} + f(y) = 0 \tag{1}$$

When $\theta = w_N t$ this is a free nonlinear oscillation of frequency w_N. When $\theta = (w_N^2 - K)^{1/2}t$, it is the author's Equation (5). Defining $s = dy/d\theta$ and

$$a^2 = s_0^2 - 2\int_0^{y_0} f(y)dy \tag{2}$$

$$\theta = \int_{y_0}^{y} \frac{dy_1}{\left[a^2 - 2\int_0^{y_1} f(y_1)dy_1\right]^{1/2}} \tag{3}$$

Equation (1) emphasizes more readily common features of the phase plane (s, y) description of the free and forced oscillations connected, respectively, with the two definitions of θ where, of course, periodic solutions are represented by closed cycles. Equation (2) is slightly more general since the definition of a^2 now incorporates both initial conditions y_0 and s_0.

The example of a hard system, specifically Fig. 1 of the paper, shows points where p exceeds m or equally where $|\delta| > 1.0$. This corresponds to K exceeding w_N^2. The square root $(w_N^2 - K)^{1/2}$ is imaginary and a question of interpretation arises in some of the equations. This is probably not serious because the branch of a square root can be regarded as determined by the requirement that the integral, as in author's Equation (7), represents a real period T. Nonetheless, it would be desirable to expand the discussion in the paper to clarify the interpretation of some of the equations.

In principle, the generalization of Equation (18) to include expressions of higher degree than $1 + m^2$ can be made as follows:

For various values of T_0/T and p, we construct curves of

$$\frac{(T_0/T)^2}{1 - (p/m)} = \frac{(T_0/T)^2}{1 - \delta} = g(m)$$

In the author's example $g(m) = 1 + m^2$. For any $g(m)$, we graphically compare $g(m)$ with those curves that closely fit it and construct the equivalent of the author's Fig. 1.

While it has little bearing on the author's paper, the writer cannot refrain from reflecting upon the fact that the distinction mathematically fundamental to obtaining useful solutions of any second-order, nonlinear differential equation depends on the absence of movable essential singularities. Those interested in nonlinear phenomena either have not noticed or have not been able to extract much engineering utility from the theory as presented, for example, by Ince.[5]

As a final comment, the concept of similar wave forms of like period can perhaps be extended to much wider circumstances; for example, ultra or subharmonic oscillations or combination tones whose frequency ratio is rational. To state this is an alternative form. We ask does there exist some useful similarity between the wave form of a restoring function of least period T and the wave form of a forcing function of least period $(p/q)T$-[(p/q) a rational fraction] so that Equation (5) of the paper can be generalized.

A possible line of argument proceeds as follows: Let $g(y) = h(y) + w_N^2 f(y)$ be a forcing function. Then

$$t = \int_0^{y_2} \frac{dy_2}{\left[V_0^2 + 2\int_0^{y_2} h(y)dy\right]^{1/2}} \quad [y_0 = 0) \tag{4}$$

Let $h(y)$, $f(y)$ be periodic with $h(y)$ of least period T_1; $f(y)$ of least period $T_0 \neq T_1$. Select for $h(y)$ a form which reduces the integrand in Equation (4) to a quartic in y so that the properties of elliptic functions could be used to fix a real period T_1. Frankly the writer does not know if this line of argument leads to any result of engineering usefulness.

S. TRAVERS.[6] The author has presented an interesting paper on nonlinear systems, always difficult to study even in the chosen symmetric case of a single degree of freedom and no damping.

To get rid of some nomenclature complications, the writer would suggest to take as time unit the period for free, very small oscillations divided by 2π. That would reduce ω_n^2 to unity and the equation for $y \to 0$, to $\ddot{y} + y = 0$.

If the restoring function is further developed in powers of y, unit of elongation should be chosen so as to equal absolute values of the first two terms for $y = 1$. In the symmetrical case, that would reduce the restoring function to $y \pm y^3$.

For coherence, the restoring function could be called $r(y)$ and the forcing function $f(y)$.

Such reductions and names do not introduce any new idea—but make things clearer. For instance, restoring functions $y + y^3$ and $y + 0$, $1y^3$ do not require separate Figs. 3 and 4.

For soft systems, amplitude is not well defined by maximum m of the restoring function, since that function can grow less after some elongation (pendulum). The writer suggests defining amplitude by the square root of the potential, or by the modulus of v_0 for free oscillations. For soft systems, that definition would work to the limit of stability, and it would remain operative even for grossly unsymmetrical systems.

The author's definitions of m and p suppose significance of maximum force, but physically the significant factor would be

[1] By T. J. Harvey, published in the September, 1958, issue of the JOURNAL OF APPLIED MECHANICS, vol. 25, TRANS. ASME, vol. 80, pp. 352–356.

[2] The Rand Corporation, Santa Monica, Calif.

[3] J. P. den Hartog, "Mechanical Vibrations," McGraw-Hill Book Company, Inc., New York, N. Y., 1940, p. 406.

[4] J. J. Stoker, "Non-Linear Vibrations," Interscience Publishers, Ltd., London, 1950, p. 110.

[5] E. L. Ince, "Ordinary Differential Equations," Dover Publications, New York, N. Y., 1944, pp. 317–355.

[6] Ingenieur en chef d'Artillerie Novale (R), Docteur ès-sciences physiques, Viroflay (S. et O.), France.

rather impulsion—a sharp blow not being more efficient on a swing than a push of seconds instead of milliseconds duration. Local "hardness" modifies maximum of $r(y)$ but is not significant for amplitude elongation or period of free oscillation.

Altering some nomenclature and definition would bring into clearer light all family relations between hard and soft systems proceeding from spring and pendulum.

Saving troublesome writing of ω_n^2, C_2, T . . . would also clear the way for interesting developments.

Quite undamped mechanical systems are exceptional if not equipped with some auxiliary energy source (pendulum). And the absence of damping would hinder realization of periodic movement, after dying out of free oscillations, as supposed by the author. For some given p and T, the choice between three m (Figs. 1, 3, 5 for moderate p and high frequency) should result from starting and damping conditions.

Let us write the equation of simple damping (one power term in $\dot{y}$):

$$\ddot{y} + d\dot{y}^n + r(y) = f(y)$$

If we write also:

$$f(y) = kr(y) + d\dot{y}^n$$

we can operate further on the author's lines for the undamped equation. Analogy would vary with damping d and period T of forced oscillations.

Such a generalization would bring out the fact that any perturbation must work to impress its own period and control a system where damping suppresses rival oscillations.

Author's Closure

The author would like to thank Dr. Lang for his comments which lead to a more concise presentation of the differential equation (1) and a more general statement of the initial conditions (2). The point regarding possible negative values of the quantity $(w_N^2 - K)$ for $T_0/T > 1.0$ needs clarification.

It is of interest here to consider only those cases where w_N^2 is positive. This is clear by analogy to the case of a linear system. The quantity of interest is then:

$$w_N^2\left(1 - \frac{K}{w_N^2}\right) = w_N^2(1 - \delta)$$

It is found δ is always negative for $T_0/T > 1.0$ and positive for $T_0/T < 1.0$. This result is completely analogous to the result for a linear system. With this established (which is easy to verify by obtaining roots of equation (17)), it is seen that $(w_N^2 - K)$ is always positive. This result would have been more obvious if the figures had shown the phase relationship between response and forcing function.

The discussion regarding use of graphical comparison between the function $g(m)$ (experimentally obtained, or obtained using phase plane techniques) and convenient polynomials is a major point which emphasizes the usefulness of the general results presented in equation (15). Extension of the solution to include higher harmonies or combination tones would appear to be possible using the approach suggested by Lang.

Certain errors appear in the paper which require correction. The function $f(t)$ should be designated $g(t)$ to distinguish it from $f(y)$. Equation (17) lacks p as a multiplier on m^2, and the equation under the heading "Duffing's Equation" should read

$$f(y) = y + C_2y^3$$

The author wishes to thank Dr. Travers for his suggestions. His ideas for simplifying nomenclature would make the presentation more clear. More important is the proposed use of the potential rather than maximum value of response as the ordinate of response curves. It appears that certain problems could indeed be overcome in this way.

The use of a forcing function of the form $f(y) = kr(y) + d\dot{y}^n$ yields a solution identical to that for the undamped system. It is not clear to the author how this solution can be used, since use of a forcing function identical to the damping function prohibits the existence of a limiting amplitude. The extension of the results to the case including damping would appear to require the use of forcing functions which admit the existence of "limit cycle" oscillations.

Physical Properties of Plastics for Photothermoelastic Investigations[1]

M. M. FROCHT[2] AND L. S. SRINATH.[3] The possible application of photoelasticity to the solution of thermal stresses has received rather limited attention in the past [1, 2, 3].[4] The paper by Tramposch and Gerard represents a significant extension of the optical method to thermal stress problems. Of particular interest are their results in Fig. 1, which show that the three materials considered, and especially Hysol, have an essentially constant fringe value over a large range of temperature. In view of this, the scope of thermophotoelasticity can be extended to three-dimensional problems with the aid of the newly developed nondestructive method, which employs scattered light [4, 5]. It should of course be noted that in these problems, as in others, the transition from model to prototype will depend on the mechanical properties of the material. If the material fringe value varied sharply over the range of temperature, the extension to three-dimensional problem would of course be more difficult, since this would require a knowledge of internal temperatures.

Since, in the nondestructive method the birefringence and isoclinic parameters are determined by means of a photometer, the search for a material with a great optical sensitivity is of secondary importance. Of greater importance would be to use a model material with a fringe value which remains essentially constant over a relatively large range of temperature. From this point of view Hysol would seem to be a suitable material. It is optically more sensitive than Castolite or Paraplex and its fringe value does not change appreciably. Some three-dimensional problems which may perhaps be attacked by the scattered light method are: (*a*) Temperature stresses in a cylinder, not necessarily circular, one end of which is cooled—say, by dry ice; (*b*) temperature stresses produced in a body containing an inclusion, such as a metal inclusion in a plastic sphere.

References

1 E. G. Coker and L. N. G. Filon, "A Treatise on Photoelasticity," Cambridge University Press, 1931, pp. 243–245.

2 Z. Levington, "Photoelastic Determination of Temperature Stresses in Arch Bridge Model," *The English Journal*, Dec. 1934.

3 E. D. Weibel, "Thermal Stresses in Cylinders by the Photoelastic Method," Proceedings of the Fifth International Congress of Applied Mechanics, 1938.

4 M. M. Frocht and L. S. Srinath, "A Non-Destructive Method for Three-Dimensional Photoelasticity," Proceedings of the Third National Congress of Applied Mechanics, ASME, 1958, pp. 329–337.

[1] By H. Tramposch and G. Gerard, published in the December, 1958, issue of the JOURNAL OF APPLIED MECHANICS, vol. 25, TRANS. ASME, vol. 80, pp. 525–528.

[2] Research Professor of Mechanics, Director of Experimental Stress Analysis, Illinois Institute of Technology, Chicago, Ill.

[3] Assistant Professor of Mechanics, Illinois Institute of Technology, Chicago, Ill.

[4] Numbers in brackets indicate References at end of discussion.

5 "A Non-Destructive Method for Three-Dimensional Photoelasticity," doctoral thesis by L. S. Srinath, Illinois Institute of Technology, Chicago, Ill.

Authors' Closure

We greatly appreciate the remarks of Drs. Frocht and Srinath and their interest in commenting on our work. As noted by the discussers, there is considerable current interest in three-dimensional thermal stress problems, and we would note that for the past year we have been exploring various three-dimensional photothermoelastic techniques. In addition to several other techniques, we have planned to use the scattered light approach in studying transient and steady-state thermal stresses in axisymmetric bodies.

In closing, we would like to discuss a small matter of semantics. We have chosen to call this interdisciplinary technique *photothermoelasticity* since it is concerned with the experimental analysis of thermoelasticity. We note that the discussers refer to it as *thermophotoelasticity* which implies the thermal aspects of photoelasticity. In view of Dr. Frocht's long association with photoelasticity we can appreciate his suggestion.

We have given considerable thought to naming this technique and believe that the term photothermoelasticity is more nearly correct.

In the interests of avoiding possible confusion, we hope that this technique will be referred to as photothermoelasticity in the future.

The Effect of Product-of-Inertia Coupling on the Natural Frequencies of a Rigid Body on Resilient Supports[1]

T. R. KANE.[2] The author's method for determining the frequency ratios ω/Ω_v complicates, rather than simplifies, the solution of the problem under consideration. Specifically, the problem is that of solving the author's Equation (15),

$$\left(\frac{\omega}{\Omega_v}\right)^6 - D\left(\frac{\omega}{\Omega_v}\right)^4 + E\left(\frac{\omega}{\Omega_v}\right)^2 - F = 0 \tag{1}$$

and the author describes a procedure for the computation of D, E, and F, this procedure involving, in part, either the use of graphs or the solution of a quadratic equation, both of which require prior evaluation of a number of quantities defined in the paper. But D, E, and F can be found directly by using the expressions

$$D = \left\{1 + \frac{m[a^2I_z + (b^2 + c^2)I_y]}{I_yI_z - I_{yz}^2}\right\}\eta + \frac{mb^2I_z}{I_yI_z - I_{yz}^2}$$

$$E = \frac{m(b^2 + c^2)(I_y + ma^2)}{I_yI_z - I_{yz}^2}\eta^2 + \frac{mb^2[I_z + m(b^2 + c^2)]}{I_yI_z - I_{yz}^2}\eta$$

$$F = \frac{m^2b^2(b^2 + c^2)}{I_yI_z - I_{yz}^2}\eta^2$$

where

$$\eta = \frac{k_x}{k_z} = \frac{k_y}{k_z} \tag{2}$$

and these are not so complicated as to require development of, in the author's words, "a procedure of sufficient simplicity to be useful for engineering purposes."

While the abstract preceding the body of the paper contains the statement ". . . a procedure suitable for engineering use is presented for evaluating the effect of product of inertia coupling," no such procedure is mentioned in the paper. On the contrary, after stating near the end of the paper, "It is not possible to draw general conclusions from a single numerical example," the author simply reopens the question by saying ". . . it is possible that the coupling effect of the product of inertia need be considered only for special problems." Now the relative effect of I_{yz} on the natural frequencies of the system clearly depends on many parameters, and it is therefore unlikely that one can resolve the entire question in any simple way. However, one of these parameters is the quantity η defined in Equation (2) of this discussion. As the effect of product-of-inertia coupling becomes more pronounced as η increases and η takes on rather large values in many practical situations, it may be worth while to point out that, when η is sufficiently large, the three natural frequencies in question are given, approximately, by

$$\frac{\omega}{\Omega_v} = \left(\frac{mb^2}{I_y + ma^2}\right)^{1/2}, \quad \left[\frac{d \pm (d^2 - 4e)^{1/2}}{2}\eta\right]^{1/2} \tag{3}$$

where

$$d = 1 + \frac{m[a^2I_z + (b^2 + c^2)I_y]}{I_yI_z - I_{yz}^2} \tag{4}$$

and

$$e = \frac{m(b^2 + c^2)(I_y + ma^2)}{I_yI_z - I_{yz}^2} \tag{5}$$

The use of these expressions obviates the necessity for solving a cubic equation and may thus be of some practical value. Furthermore, they may be used as a simple test to determine the relative importance of product-of-inertia coupling (when η is large): When I_{yz} is set equal to zero, Equation (1) reduces to [an alternative form of the author's Equation (20)]

$$\left[\left(\frac{\omega^2}{\Omega_v^2}\right)^2 - G\frac{\omega^2}{\Omega_v^2} + H\right]\left[\frac{\omega^2}{\Omega_v^2} - \frac{m(b^2 + c^2)}{I_z}\eta\right] = 0 \tag{6}$$

where

$$G = \frac{ma^2 + I_y}{I_y}\eta + \frac{mb^2}{I_y}, \quad H = \frac{mb^2}{I_y}\eta$$

and the three roots of Equation (6) can be compared readily with the corresponding values from Equation (3). As a matter of fact, it is not even necessary to solve a quadratic equation. For, when η is sufficiently large, Equation (6) [or, alternatively, Equations (3), (4) and (5), with $I_{yz} = 0$] leads to

$$\frac{\omega}{\Omega_v} = \left(\frac{mb^2}{I_y + ma^2}\right)^{1/2}, \left(\frac{I_y + ma^2}{I_y}\eta\right)^{1/2}, \left(\frac{b^2 + c^2}{I_z}m\eta\right)^{1/2} \tag{7}$$

For example, with $a = 4$ in., $b = c = 3$ in., $m = 0.1$ lb in.$^{-1}$ sec^2, $I_y = I_z = 0.2$ lb in. sec^2, $I_{yz} = 0.1$ lb in. sec^2, and $\eta = 10$, the frequency ratios have the values shown in Table 1.

It can be seen that, in this case: (*a*) the approximate values of the frequency ratios obtained by neglecting product-of-inertia coupling (line 3) are in error by, respectively, 0.1, 16.4, and 38.1 per cent of these values; (*b*) Equation (3) leads to results differing from the correct values by, respectively, 2.1, 0.97, and 1.23

[1] By C. E. Crede, published in the December, 1958, issue of the JOURNAL OF APPLIED MECHANICS, vol. 25, TRANS. ASME, vol. 80, pp. 541–545.

[2] Associate Professor of Applied Mechanics, University of Pennsylvania, Philadelphia, Pa.

Table 1 Values of frequency ratios

1	I_{yz} taken into account as per Equation (1)	0.692	7.935	13.388
2	I_{yz} taken into account as per Equation (3)	0.707	7.859	13.225
3	I_{yz} set equal to zero as per Equation (6)	0.693	9.487	9.696
4	I_{yz} set equal to zero as per Equation (7)	0.707	9.487	9.487

per cent; (*c*) when lines 2 and 3 (or 4) are compared, as a test to determine the relative importance of product-of-inertia coupling, it appears immediately that the frequencies of two of the principal modes are affected significantly.

Author's Closure

As pointed out by Professor Kane, the frequency equation of the paper is subject to simplification when the stiffness ratio η is large. An increase in the value of η tends to decrease the strength of the coupling between modes and to increase the spread of natural frequencies. For effective vibration isolation, it is preferable that $0.5 < \eta < 1.0$ to attain a small spread of natural frequencies together with adequate stability. Strong coupling then exists among the several modes, and the procedure described in the paper is useful for engineering purposes.

Pitch and Curvature Corrections for Helical Springs[1]

A. M. WAHL.[2] The authors are to be complimented on a very interesting theoretical analysis of the effects of pitch and curvature on the stresses and deflections in helical springs. The more accurate formulas given should prove of value in many cases where more precise calculations of spring characteristics are necessary.

In applying the results of the theoretical analysis to practical cases, it should be kept in mind that these results are based on the assumption that the coil radius R, pitch angle γ, and number of turns n remain essentially constant as the spring deflects. In actual springs, however, particularly for those having large ratios of coil-to-wire diameter, and also large pitch angles, the values of R, γ, and n may change appreciably during loading. Thus for best accuracy in design such changes should be considered.

The authors give an expression, Equation (6), for expansion of the coil diameter of the spring in being compressed from free to solid height. This is compared with a formula which the writer published in 1953 (reference [8] of the paper). This latter formula was based on a consideration of the spring as a thin helical rod under bending and torsion due to an axial load, the total length of the rod being assumed to remain constant. Using geometrical considerations, changes in R, γ, and n were taken into account by this method.

To evaluate results obtained using these two formulas, some test data on the diametral expansions of two steel helical springs when compressed from free to solid height are given in Table 1 herewith. These data were supplied by Messrs. B. Sterne and T. R. Weber of the SAE Spring Committee. Data also are given on spring dimensions. In this case the coils were free to unwind during loading. Diametral expansions ΔD calculated by the authors' Equation (6) and by the writer's formula (reference [8]) are also listed.

It appears from Table 1 that somewhat closer results, compared with the test values, are obtained using the formula of reference [8].

It is also of interest to compare the results obtained by using Equation (8) of the paper with actual test results. This equation gives the angle of "unwinding" of a compression spring when loaded by a load P. Comparison also may be made with the results obtained using an equation given in the writer's text.[3] Applied to a compression spring this latter equation may be written as:

$$\phi = \frac{2\pi n R_0}{\cos \gamma}\left[\frac{\cos \gamma_0}{R_0} - \frac{\cos \gamma}{R}\right] \qquad (1)$$

In this, ϕ = angle of unwinding, radians, R_0 and R are coil radii at free and solid height, γ_0 and γ are the corresponding pitch angles, and n = number of active coils at free height. The radius R may be calculated from the writer's formula, reference [8].

The results of tests on compression springs in which angular rotation (unwinding) of the spring ends was measured as the

[1] By C. J. Aneker, Jr., and J. N. Goodier, published in the December, 1958, issue of the JOURNAL OF APPLIED MECHANICS, vol. 25, TRANS. ASME, vol. 80, pp. 466–470.

[2] Advisory Engineer, Westinghouse Research Laboratories, Pittsburgh, Pa.

[3] Reference [5] of the paper, p. 61.

Table 1 Expansion of spring diameter

Spring No.	D	d	D/d	tan γ_0[a]	Test	ΔD, in. Authors' Eq. (6)	ΔD, in. Writer's formula Ref. [8]
1	2.95	0.188	15.7	0.237	0.15	0.187	0.155
2	12.6	1.03	12.2	0.19	0.40	0.48	0.397

[a] Pitch angle at free height.

Table 2 Angle of unwinding ϕ

Spring No.	D	d	D/d	tan γ_0	n	Angle ϕ, deg. Test	Calc.[a] Eq.(8)	Calc.[a] Eq. (1) of disc.
1	2.95	0.188	15.7	0.237	4.5	40	18	38
2	12.6	1.03	12.2	0.19	5.7	24	14	28
3	1.15	0.125	9.2	0.144	21	47	26	49
4	1.21	0.192	6.3	0.132	30	37	26	44
5	1.40	0.394	3.6	0.122	47	15.6	15	19

[a] Calculated results rounded off to nearest degree.

spring was compressed from free to solid height are shown in Table 2 of this discussion, together with pertinent data on spring dimensions. These test data include results obtained by Messrs. K. Maier, B. Sterne, and T. R. Weber of the SAE Spring Committee. For comparison, results calculated using Equation (1), herewith, and those from the authors' Equation (8) are also shown.

It appears from Table 2 that, for the larger indexes and pitch angles, the results calculated using Equation (1) came considerably closer to the test values than those calculated from Equation (8) of the paper. However, for the smallest index tested (spring No. 5) the latter equation appears to give somewhat more accurate results. Probably this is because the effects of curvature are more important for small-index springs.

It would be of interest if the authors could indicate how their formulas could be utilized for design use while taking into account effects of changing coil radius, number of turns, and pitch angle during deflection of the spring.

Authors' Closure

This discussion involves three papers which we shall refer to as A,[4] B,[5] and C.[6] The results of this study are expressions for stresses and deflections. These expressions are truncated series in the parameters, spring pitch (p), and curvature (a/R). In some deflection expressions, the number of coils (n) appears as a factor. As Dr. Wahl points out, p, R, and n are all functions of the load P. Thus for small loads the given equations are sufficient. However, for large loads they are not.

The incremental change in R with incremental load increase for the tension spring may be determined from K, in equation (19), paper B, and is

$$\Delta R = -\frac{2}{\pi a^4 G}\left(\frac{1+2\nu}{1+\nu}\right) R^3 p \Delta P. \quad (1)$$

Similarly, the incremental change in pitch is obtained from using equation (4), paper A,

$$\Delta p = \frac{2R^3}{\pi a^4 G R_0}\left[1 - \frac{3}{16}\left(\frac{a}{R}\right)^2 + \frac{(3+\nu)}{2(1+\nu)}p^2 + \frac{(1+2\nu)}{(1+\nu)}p_0 p\right]\Delta P, \quad (2)$$

where R_0 and p_0 are initial values. The incremental change in number of coils is obtained from equation (8), paper A,

$$\Delta n = \frac{\Phi}{2\pi} = \frac{2\nu}{(1+\nu)\pi a^4 G} npR^2 \Delta P. \quad (3)$$

In any particular design calculation a method of successive corrections can be employed. The load is divided into any convenient number of increments (say 10). The first load increment is applied and the first increment of the desired stress (deflection) is computed along with the first incremental change in R, p, n from equations (1), (2), (3) in this Closure. Using the new R, p, and n, the second increment of stress (deflection) and the new incremental changes in R, p, and n are computed, and so on. The total stress (deflection) is then the sum of the increments.

The same method can be applied to the deflection and uncoiling of a compression spring from free to solid height.

[4] C. J. Ancker, Jr., and J. N. Goodier, "Pitch and Curvature Corrections for Helical Springs," JOURNAL OF APPLIED MECHANICS, vol. 25, TRANS. ASME, vol. 80, 1958, pp. 466–470.

[5] C. J. Ancker, Jr., and J. N. Goodier, "Theory of Pitch and Curvature Corrections for the Helical Spring—I (Tension)," ibid., pp. 471–483.

[6] C. J. Ancker, Jr., and J. N. Goodier, "Theory of Pitch and Curvature Corrections for the Helical Spring—II (Torsion,)" ibid., pp. 484–495.

Equations similar to (1), (2), and (3) can be derived from paper C for the torsion spring.

A possible analytical approach would be the solution of equations (1), (2), and (3) as simultaneous differential equations to determine the functional relationships of p, R, and n with P.

We regret that in the time available we were unable to use the iterative procedure suggested above to compute some values for comparison with Dr. Wahl's experimental results.

Relief of Thermal Stresses Through Creep[1]

K. R. MERCKX.[2] The authors have presented a method of plastic analysis which extends the region of evaluation of mechanical behavior. Plastic relaxation of strain incompatibilities is an important factor in thermal-stress analysis which is needed in evaluating the failure criterion for strain cycling. Each new method of dealing with the equations of plasticity builds up the backlog of techniques necessary for general methods of solution for material models which will realistically represent material behavior. Some caution should be made in directly applying this solution to the cases where plastic strains may be several factors greater than the elastic strains. The initial relaxation is usually so rapid that it becomes difficult to calculate the change in stresses during the first time increments. In fact, the extrapolation of creep data to very small times is difficult, and interpretation of the initial relaxation in terms of experimentally evaluated material models is difficult. Thus in most practical applications the initial stress-and-strain distribution can be calculated with the theory of plastic deformations, and then further relaxation can be obtained with an analysis such as the one presented in this paper.

A. MENDELSON[3] **and S. S. MANSON.**[4] The authors are to be commended for a stimulating paper on stress relaxation due to creep. Although a considerable body of literature is being built up on the subject of steady-state creep, very little has as yet been done with regard to the transient state.

The authors rightfully point out that the method presented is rather approximate and that the accuracy of the final results is probably not better than 50 per cent. In the last paragraph they mention, however, the possibility of improving the accuracy by an iterative procedure.

A generalized method using iterative procedures or successive approximations has recently been published in a paper[5] and applied to several problems of practical interest using deformation theories of plasticity, and also extended[6] to the flow or incremental theories of plasticity. A detailed description of this technique has recently been presented[7] for the solution of general creep

[1] By H. Poritsky and F. A. Fend, published in the December, 1958, issue of the JOURNAL OF APPLIED MECHANICS, vol. 25, TRANS. ASME, vol. 80, 1958, pp. 589–597.

[2] Fuel Element Design Operation, Hanford Laboratories, General Electric Company, Richland, Wash.

[3,4] NASA Lewis Research Center, Cleveland, Ohio.

[5] A. Mendelson and S. S. Manson, "Practical Solution of Plastic Deformation Problems in the Elastic-Plastic Range," ASME paper no. 56—A-202, Nov., 1956 (also published as NACA TN 4088, Sept., 1957).

[6] R. S. Hanson, "Practical Solution of Plasticity Problems by the Incremental Theory of Plasticity," PhD thesis, Iowa State College, 1958.

[7] A. Mendelson, M. H. Hirschberg, and S. S. Manson, "A General Approach to the Practical Solution of Creep Problems," ASME Paper no. 58—A-98.

problems. It is shown in this paper[7] that the general method of successive approximations can be applied to different creep laws such as the time-hardening and life-fraction laws as well as the strain-hardening law used by the authors. It is also indicated that other hypotheses besides the Mises-Hencky hypothesis can be used with equal ease.

The authors point out that the amount of labor involved in obtaining a solution by their method is very great, thus indicating the need for high-speed computing machinery. If such machinery is to be used, then it may be advantageous to use the iterative procedures described which involve relatively little additional machine time but yield considerably increased accuracy.

The authors show for the example presented how the stresses are relieved through creep. The writers would be interested in knowing if the authors had considered the residual stresses resulting when the load is removed. This might be very important for cyclic operation. Perhaps the authors would care to comment on this.

Incidentally, it is to be noted that the solution of equation (39) can be found in various standard textbooks on mathematics and elasticity such as, for example, the one by Timoshenko and Goodier [8]

Authors' Closure

The authors are grateful to the discussers for their comments which form a valuable addition to the subject matter discussed, and for their references to other papers. To the references cited by Mendelson and Manson should be added a paper by Dr. Merckx.[9]

It is quite true, as Dr. Merckx points out, that in general the plastic extension during the initial stages of creep takes place so rapidly that it is practically impossible to calculate it near $r = 0$ during the first time increment, unless the duration of the latter is made fantastically small. The authors must confess that they threw away several creep laws on account of the fact that these led to the amounts of creep extension near $r = 0$ during the first time interval which exceeded by far the total initial strain due to the thermal stress, even for $(\Delta t)_1 = 10^{-6}$ sec, and would, therefore, have wiped out the thermal stresses completely before the calculation could even be launched. Under these conditions, as suggested by Dr. Merckx, it is best to give up the rate of creep calculation and use straight plastic deformation, at least for the inner, high-temperature portion of the cylinder where this difficulty occurs initially, before adopting the procedure of the paper.

It may be added, however, that the other assumptions which have been used in the paper, namely, that the temperature is brought up *instantaneously* to its steady-state value, and furthermore, that the material is initially completely free from stress, is in its virgin state ($\epsilon_p = 0$) so far as the creep is concerned, and these are far from valid in any practical case. Actually, it takes a finite length of time to bring up the temperature to its steady-state value, and during this time the plastic flow corresponding to the lower temperatures and thermal stresses takes place. Moreover, in the process of casting, swaging, forming, and machining, "internal" or "trapped" stresses are always set up, which may not be completely relieved by annealing. In any practical example, these trapped stresses and the total creep associated with them must form the starting point in the further thermal creep calculation.

The paper by Merckx treats essentially the same problem as the present paper. The paper by Mendelson, Hirschberg, and Manson[7] is particularly closely related to the present paper from which it differs in the nature of the examples, as well as in carrying out in greater detail some of the successive improvement schemes which are only described in general form in our paper. Our own calculations were actually carried out in 1955, and we regret the delay in publishing them.

While throughout the paper it has been assumed that the temperature locally does not vary with time, it is evident that the method can be applied equally well to cases where the temperature *does vary* with time; for instance, the specimen is allowed to cool down to room temperature as when a pile is shut off. It is, of course, necessary again to know how the rate of creep behaves under changes of both temperature and stress. If the specimen is allowed to cool to room temperature, any stresses left will be trapped stresses.

A similar method applies to the calculation of stresses resulting from casting and forging operations.

By way of conclusion, it is evident that creep calculation in certain somewhat simplified cases can now be set up on computing machines and evaluated on the basis of various "laws" of creep. On the other hand, the general three-dimensional cases with complex boundaries, while they can be reduced to the solution of certain nonlinear partial differential equations, lead to computational processes which are probably too complex for present high-speed computing machines. Even the solution of the linear equations of elasticity for general three-dimensional shapes is too complex for present-day computing machines, in spite of many available analytical techniques; the further complications due to the nonlinear rates of creep render the problem even more difficult.

Yet, by restricting oneself to cases where creep calculations *can* be carried out, using various hypotheses regarding creep, and comparing the predictions of the theory with the experimental measurements, tests of the theories may be obtained. There is great need for work of this kind so that definite criteria of strength and durability may be worked out for engineering structures in which temperature variations and plastic deformations and creep take place.

[8] S. Timoshenko and J. N. Goodier, "Theory of Elasticity," McGraw-Hill Book Co., Inc., New York, N. Y., 1951, p. 407.

[9] K. R. Merckx, "The Dependence of Thermal Stresses in Cylindrical Reactor Fuel Elements Upon the Method of Cooling," TRANS. ASME, vol. 80, July, 1958, pp. 985–990.

The Effect of Spin Upon the Rolling Motion of an Elastic Sphere on a Plane[1]

A. D. DE PATER.[2] The author's papers[3] give a most valuable contribution to the problem of the tangential contact between two elastic bodies, for in the literature published until now, the rolling motion has only been studied in the two-dimensional case. On the other hand, tangential-contact studies for the three-dimensional case have been restricted to the static contact.

It is an essential feature in such contact problems that the governing equations and conditions can be split up into two sets, one relating to the normal (Hertzian) problem, and one to the tangential problem. However, this can only be done in

[1] By K. L. Johnson, published in the September, 1958, issue of the JOURNAL OF APPLIED MECHANICS, vol. 25, TRANS. ASME, vol. 80, pp. 332–338.

[2] Professor of Applied Mechanics, Technische Hogeschool, Delft, Holland.

[3] This discussion applies also to "The Effect of a Tangential Contact Force Upon the Rolling Motion of an Elastic Sphere on a Plate," by K. L. Johnson, JOURNAL OF APPLIED MECHANICS, vol. 25, TRANS. ASME, vol. 80, pp. 339–346.

cases where the elastic constants of the two bodies are equal, so that a (probably small) coupling effect between the normal and the tangential-pressure distribution can be expected in the case of unequal elastic constants. The slight warping of the contact surface which occurs, for instance, when a sphere is in contact with a plane, is ignored in the Hertzian theory for the normal case and thus it can be ignored with equal reason in the tangential case.

The fact that in the two-dimensional case "the locked region must have one boundary coincident with the leading edge of the area contact, and that slip occurs after contacting points have rolled through the locked region, if the direction of slip is to be consistent with the laws of friction and to oppose the tangential force acting between the surface" was implied in Carter's solution, published 24 years before Poritsky's solution.

As the author himself rightly remarks, the solution in which the locked region and the slip region are separated by a circle tangential to the circle limiting the total contact area should be regarded as an approximative one. It can be shown that for vanishing small values of the creep ratios ξ_x, ξ_y, both in the case of a longitudinal force as in that of a transverse force, the slip region reduces itself to a narrow strip contiguous to the half circle forming the trailing edge of the contact area. The values of the creep ratio obtained in that case correspond excellently with the author's experimental results. On the other hand, it seems to be out of the question that an exact solution can be found when the creep ratios are not vanishing small.

The Strain-Energy Expression for Thin Elastic Shells[1]

H. L. LANGHAAR.[2] Any two-dimensional theory of shells must violate some of the equations of elasticity theory; in the present case, the equilibrium equations are not satisfied fully. Except for errors incurred by truncation of power series, all six of the compatibility equations of the linear theory of strain are satisfied, since the arbitrary functions ξ, η, ζ in Equation (4) of the paper provide a general solution of the compatibility equations for the shell co-ordinates. It appears that unwarranted complications arise from rigid enforcement of the compatibility conditions, while equilibrium conditions are replaced by the assumptions $\sigma_{xz} = \sigma_{yz} = \sigma_{zz} = 0$. For example, if a flat plate that is loaded by boundary forces in its plane is referred to rectangular co-ordinates (x, y), $\alpha = x, \beta = y, A = B = 1, 1/R_1 = 1/R_2 = 0$, and $w = 0$. Then Equation (14) retains several third derivatives of u and v with respect to x and y. The principle of stationary potential energy leads to two fourth-order partial differential equations for u and v and a number of unusual boundary conditions. The resulting problem is far more complicated than the biharmonic boundary-value problem of the classical theory of generalized plane stress, although the assumptions in the latter theory are less restrictive.[3]

The alternative strain-energy expression, Equation (15), obtained with the Kirchhoff-Love assumptions, is more compatible with accepted theories of flat plates, since it conforms to the condition that the strain energy of bending of a flat plate vanishes if $w = 0$. However, the use of power series has led to an undesirable proliferation of terms in Equation (15). When the Kirchhoff-Love assumptions are used, only simple rational functions of z arise, and they need not be expanded in power series. The general strain-energy expression for isotropic elastic shells that results from the Kirchhoff-Love assumptions without supplementary polynomial approximations is derived by Langhaar and Boresi.[4] The individual terms in the strain-energy expression of that reference are similar to those in Equation (15). However, after the coefficients a_i, b_i, c_i in Equation (15) are replaced by their expressions in the Appendix, there are more than three times as many terms in the integrand as in the corresponding formula of the reference.[4]

G. B. WARBURTON.[5] In their interesting paper on the strain-energy expression for thin elastic shells the authors suggest that investigations on the vibrations of thin shells might differentiate between the terms appearing in the various energy expressions. In a contribution to the discussion of an earlier paper [1],[6] the writer showed that for some modes of practical circular cylindrical shells the effect on frequency of using different strain-energy expressions was small. In this note the writer compares frequencies obtained from some of the expressions given by the authors.

For a thin cylindrical shell with freely supported ends a suitable nondimensional frequency factor is $\Delta^{1/2}$, where $\Delta = \rho a^2(1 - \mu^2) \times \omega^2/E$ (where ρ = density, a = mean radius of shell, μ = Poisson's ratio, ω = circular natural frequency, and E = Young's modulus). The factor $\Delta^{1/2}$ depends on the four parameters [2]: $\lambda = m\pi a/l$ = mean circumference/axial wave length (where m = number of axial half waves, l = length of shell); n = number of circumferential waves; h/a = thickness/mean radius; and μ. For any set of values of the four parameters the lowest root of the frequency equation corresponds to flexural vibrations of the walls of the cylindrical shell; in Table 1 of this discussion frequency factors $\Delta^{1/2}$ for this type of vibration are given for various values of the parameters. These factors are derived with the aid of:

A Basset's strain-energy expression, Equation (16) plus (16a).
B Flügge's strain-energy expression, Equation (16).
C Kennard's equations of motion [3].
D Love's strain-energy expression.
E Mirsky and Herrmann's theory [4], including the effects of transverse shear deformation and rotatory inertia.

Methods A, B, C, and D use expressions given in the authors' paper.

Comparing the frequencies obtained with different strain-energy expressions (methods A, B, C, and D), the percentage difference between the maximum and minimum values of $\Delta^{1/2}$ for the modes chosen is less than 0.6. It is seen that this difference increases with h/a, and the value $h/a = 1/10$ is often regarded as the limit of thin-shell theory.

Some results from method E, where the effects of transverse-shear deformation and rotatory inertia are included, are given in Table 1, herewith, for comparison. As each of the parameters h/a, n, and λ increases, the percentage difference between frequencies given by any conventional thin-shell theory, e.g., methods A to D, and by a corresponding Timoshenko-type theory, e.g., method E, increases. This can be seen by considering: (a) Table 2, where values of the frequency factor $\Delta^{1/2}$ are given for $\lambda = 3.770$ and various values of h/a and n by methods D and E, and (b) Yu's results [5], where frequencies are obtained from Donnell type equations, including and excluding the effects of transverse shear deformation and rotatory inertia. It is found that

[1] By J. H. Haywood and L. B. Wilson, published in the December, 1958, issue of the JOURNAL OF APPLIED MECHANICS, vol. 25, TRANS. ASME, vol. 80, pp. 546–552.

[2] Department of Theoretical and Applied Mechanics, University of Illinois, Urbana, Ill.

[3] N. I. Muskhelishvili, "Some Basic Problems in the Mathematical Theory of Elasticity," P. Noordhoff, Ltd., Groningen, Holland, 1953.

[4] H. L. Langhaar and A. P. Boresi, "Strain Energy and Equilibrium of a Shell Subjected to Arbitrary Temperature Distribution," Proceedings of The Third U. S. National Congress of Applied Mechanics, ASME, New York, N. Y., 1958, pp. 393–399.

[5] Head, Postgraduate School of Applied Dynamics, Department of Engineering, University of Edinburgh, Edinburgh, Scotland.

[6] Numbers in brackets designate References at end of this discussion.

Table 1 Values of frequency factor, $\Delta^{1/2}$. ($\mu = 0.3$)

h/a	n	λ	Method A	B	C	D	E
1/30	2	0.3142	0.03327	0.03343	0.03342	0.03339	
1/30	2	3.142	0.6627	0.6629	0.6627	0.6628	
1/30	6	0.3142	0.3331	0.3331	0.3331	0.3331	0.3312
1/30	6	3.142	0.4691	0.4701	0.4707	0.4695	
1/10	2	0.3142	0.08148	0.08187	0.08173	0.08166	
1/10	2	3.142	0.7420	0.7454	0.7421	0.7438	
1/10	6	0.3142	0.9992	0.9984	1.0025	0.9977	0.9424
1/10	6	3.142	1.284	1.287	1.291	1.283	1.198

Table 2 Values of frequency factor $\Delta^{1/2}$ for $\lambda = 3.770$. ($\mu = 0.3$)

h/a	Method	n = 2	3	4	5	6
1/30	D	0.7438	0.6048	0.5163	0.4940	0.5357
1/30	E	0.7433	0.6046	0.5158	0.4929	0.5326
1/10	D	0.8752	0.8409	0.9260	1.1256	1.4154
1/10	E	0.8645	0.8254	0.8948	1.0665	1.3139

neglecting these effects increases the frequency factor for $\lambda \leq 3.77$ by less than 0.6 per cent for $h/a = 1/30$, but by larger amounts, from 1.2 to 7.7 per cent depending on n, for $h/a = 1/10$.

Thus, as Yu has stated [5], frequencies obtained without allowance for transverse-shear deformation and rotatory inertia are satisfactory for λ less than 4, approximately. This range of λ is similar to that considered in Table 1. Hence, when conventional shell theory can be used to predict natural frequencies, the effect on frequency of using different expressions for strain energy is very small (Table 1); thus it seems unlikely that investigations of the vibrations of thin cylindrical shells will help to differentiate between the terms in the various strain-energy expressions.

Authors' Closure

The authors are grateful to Professor Langhaar and Dr. Warburton for their comments on the paper.

Professor Langhaar suggests that the complicated form of the energy expression and the associated equilibrium equations arises from the enforcement of the compatibility conditions. This cannot be avoided unless a particularly simple structure is treated or additional assumptions, such as the Kirkhoff-Love hypothesis, can be made. The former situation is exemplified by Professor Langhaar's discussion of the flat plate, where a biharmonic solution may be derived. A comparison is possible between the differential equations of equilibrium arising in the biharmonic method and the equations for a flat plate derived from the strain energy expression (14) of the paper by variational methods. In the former case, the differential equations take a simple form in which the deflections are defined as average deflections over the thickness of the cylinder (see footnote 3 in Professor Langhaar's discussion). In the latter case the deflections are explicit middle surface deflections. The two types of deflection are related by the compatibility equations. The use of the middle surface deflections in the paper seemingly leads to a more complicated set of differential equations because integration over the thickness of the plate is carried out beforehand, thus giving rise to terms of order h and h^3.

The authors are interested to learn that Professor Langhaar has obtained a strain expression for elastic shells, subject to the Kirkhoff-Love hypothesis, without the use of power-series expansions. As pointed out in the introduction, several authors have already done this for the circular cylinder. The use of power-series expansions was adopted throughout the paper in order to facilitate the analysis and to emphasise the differences between the various strain-energy expressions. In the application of energy methods the larger number of terms arising from the use of power-series expansions makes little difference to the numerical work involved, particularly if electronic computing is used.

The authors are pleased to see that Dr. Warburton has compared the effect of the different strain energy expressions on the frequency of vibration of thin circular cylindrical shells. The results confirm the authors' opinion that the energy expression derived using the Kirkhoff-Love hypothesis is adequate for circular cylindrical shells. However, the circular cylindrical shell is rather a special case and it should not be assumed that the same conclusions hold for noncircular shells.

References

1 Contribution by G. B. Warburton to discussion of "Tables for Frequencies and Modes of Free Vibration of Infinitely Long Thin Cylindrical Shells," JOURNAL OF APPLIED MECHANICS, vol. 22, TRANS. ASME, vol. 77, 1955, pp. 135–136.

2 R. N. Arnold and G. B. Warburton, "Flexural Vibrations of the Walls of Thin Cylindrical Shells Having Freely Supported Ends," *Proceedings of The Royal Society*, London, England, series A, vol. 197, 1949, pp. 238–256.

3 E. H. Kennard, "The New Approach to Shell Theory: Circular Cylinders," JOURNAL OF APPLIED MECHANICS, vol. 20, TRANS. ASME, vol. 75, 1953, pp. 33–40, Equation (14).

4 I. Mirsky and G. Herrmann, "Nonaxially-Symmetric Motions of Cylindrical Shells," *Journal of the Acoustical Society of America*, vol. 29, 1957, pp. 1116–1123. (Also as: AFOSR Contract AF 18(600)-1247, Technical Note No. 3, Columbia University, 1956.) Frequencies were calculated from tabulated data in the technical note and from data supplied by Professor Herrmann (private communication).

5 Y.-Y. Yu, "Vibrations of Thin Cylindrical Shells Analyzed by Means of Donnell-Type Equations," *Journal of the Aero/Space Sciences*, vol. 25, 1958, pp. 699–715. (Also as: AFOSR TN 57-390, AD 132465, Syracuse University Research Institute, 1957.)

Elasticity and Plasticity

Elasticity and Plasticity. Volume 1 of Surveys in Applied Mathematics. By J. N. Goodier and P. G. Hodge, Jr. John Wiley & Sons, Inc., New York, N. Y., 1958. Cloth, 9¼ × 6 in., ix and 152 pp., illus. $6.25.

REVIEWED BY D. C. DRUCKER[1]

IN THE words of Dr. F. J. Weyl in his preface to the book, "The present articles are therefore aimed not so much at research specialists, actively contributing to the subjects discussed, as they are aimed at a broader, mathematically literate audience, looking for contemporary information on the important problems and results in these disciplines, whether it be for use in classroom and seminar, or for the sake of possible application to problems in other fields of science and engineering, or simply for reasons of personal interest."

As Professor Goodier states in his introduction, his section on the Mathematical Theory of Elasticity "is not intended to be an exhaustive and proportional survey of all branches of the subject... Its principal aim is to draw attention to those significant recent developments believed least known to those readers whose first language is English."

Professor Hodge in his section on the Mathematical Theory of Plasticity also devotes much time to work abroad and includes a section on Russian contributions taken from a report by Professor W. Prager.

The topics covered by the authors are:

Elasticity: Plane stress and plane strain in the isotropic medium; Holes and fillets of assignable shapes. Approximate conformal mapping; Reinforcement of holes; Mixed boundary-value problems. The third fundamental problem in two dimensions; Eigensolutions for plane and axisymmetric states; Anisotropic elasticity; Thermal stress. Elastic waves induced by thermal shock; Three-dimensional contact problems; Wave propagation. Traveling loads and sources of disturbance; Diffraction. Pulse propagation; Seismic and vibrational problems.

Plasticity: Theory of perfectly plastic solids; Theory of strain-hardening plastic solids; Piecewise linear plasticity; Minimum principles of plasticity; Bending of a circular plate; Circular cylindrical shell; Plane strain and plane stress; Beams, bars, and rods.

An extensive bibliography accompanies each survey.

Thermal Turbomachines

Thermische Turbomaschinen. Vol. 1. By W. Traupel. Springer-Verlag, Berlin, Göttingen, Heidelberg, 1958. Cloth, 10⅞ in. × 7⅞ in., xii and 407 pp., 402 illus. DM 58.50.

REVIEWED BY MAX J. SCHILHANSL[2]

"THERMAL turbomachines" is a collective term for steam turbines, gas turbines, and turbocompressors, as the subtitle says. The first volume deals with calculation methods based on the principles of thermodynamics and fluid dynamics, while the second volume will be devoted to regulation, stress analysis, vibrations, and some special problems.

The first four chapters give a review of thermodynamics and fluid dynamics as far as both disciplines are needed for the understanding and the design of turbines. After explaining these fundamentals, the author proceeds to an elementary or one-dimensional theory of a stage. His statement, that "the equations of the one-dimensional theory should be understood as relations between integral values and are accurate even if they are not perfectly rigorous," is very significant.

The cascade theory represents a refinement of the one-dimensional theory and is treated by singularity methods as well as by conformal mapping. Radial equilibrium in vortex and wheel-type rotors is discussed in the following chapter.

Based on these theoretical considerations, methods for the layout of turbomachines are worked out in which experimental results are also taken into account.

While Chaps. 5 to 8 deal essentially with the flow through a single stage, the problems related to multistage turbines and compressors are treated in Chap. 9. Finally, some sections on labyrinth seals and on "off design" operation are added.

These subjects are essentially the contents of the first volume. At the end of each chapter is a list of references—total number of references exceeds 200—so that an engineer who likes to study any problem in more detail than it is described in the book can easily find where he can obtain more information.

The book is very well written. The first four chapters are the best ones. The remaining ones dealing with the long and arduous way from the differential equations to hardware are certainly of great interest for the engineer practicing in the United States who might compare his own methods with the ones recommended by Traupel.

Vibration

Random Vibration. Edited by Stephen H. Crandall. The Technology Press of the Massachusetts Institute of Technology, Cambridge, Mass., 1958. Paper bound, 8¹⁹/₁₆ × 6 in., viii and 406 pp., illus. $10.

REVIEWED BY CHARLES E. CREDE[3]

THIS paper-bound volume comprises the published lecture notes for a summer course on Random Vibration at M.I.T. Contributors to the volume are: S. H. Crandall, I. Dyer, R. M. Mains, F. A. McClintock, K. J. Metzger, T. H. Pian, H. Poritsky, A. Powell, D. E. Priest, T. P. Rona, and W. M. Siebert.

Each contributor evidently prepared his chapter independently of the other, but on an assigned topic which was co-ordinated with the other topics. These topics fall into the following subject groups: Mathematics of vibrating systems and random vibration; Mathematics of probability; Description of random mechanical processes; Damping and fatigue characteristics of materials and fabricated structures; Instrumentation, particularly for random vibration; Response of plates and missile-like structures to random excitation, including a description of the noise field near a missile; Vibration testing equipment; and Mechanical design for random loading.

[1] Professor and Chairman, Division of Engineering, Brown University, Providence, R. I.

[2] Professor of Engineering, Brown University, Providence, R. I.

[3] Associate Professor of Mechanical Engineering, California Institute of Technology, Pasadena, Calif.

Chaps. 1, 2, and 4 consist of a concise mathematical discussion of random vibration theory, probably the most lucid and coherent treatment available from the viewpoint of the mechanical engineer. Chaps. 8 and 9 discuss the response of plates to random excitation, using the normal mode concept, and the vibration of missile structures under random excitation. The average mechanical engineer will find the discussion of random vibration theory very useful, although he may wish that some of the concepts had been explained in somewhat more detail. The chapters on the vibration of plates and missile structures involve more advanced analysis which will be useful primarily to specialists in structural mechanics.

The chapters on materials discuss damping and fatigue effects, the latter from both metallurgical and engineering viewpoints. These chapters are essentially a concise review of the literature, and make little reference to random vibration. The content of these chapters, while of general engineering interest, is not explicitly relevant to the title of the book.

The design and operation of vibration testing equipment to meet current testing specifications are discussed in two chapters, a review of material readily available elsewhere in the technical literature. The last chapter, a reprint of four papers previously published, discusses methods for calculating the response of structures to random vibration and estimating the fatigue life of such structures. Although the title of this chapter suggests a design guide, the average designer will be overwhelmed by his unfamiliarity with the concepts and discouraged by the difficulty of applying them to ordinary design problems.

Random vibration has become a confused subject, not only because of concepts that are new to mechanical engineers but also because there has been no unified treatment of the basic subject which appears lucid to those versed in the mechanical disciplines. The present book, particularly the first four chapters, goes a long way toward filling this void. Every engineer who may be faced with design, measurement, or test work involving random vibration should have this volume on his bookshelf.

Kinematical Analysis of Mechanisms

Kinematisch-Getriebeanalytisches Praktikum. By R. Beyer Springer-Verlag, Berlin, Göttingen, Heidelberg, 1958. Cloth $9^{15}/_{16} \times 6^{13}/_{16}$ in., vii and 172 pp., illus. DM 28.53.

REVIEWED BY F. FREUDENSTEIN[4]

AN APPROXIMATE translation of the complete title of this book is: "Practical guide to the kinematical analysis of mechanisms—for the designer, for the lecturer, and for self-study."

The table of contents illustrates best the subject matter involved:

Part I. Velocities and curvature: Determination of mechanism configuration for a given output position—substitute mechanisms; Two infinitesimally near positions of a link; The pole curves; Curvature relationships of point-path trajectories; Technical applications of curvature relationship of point paths; Generating curves and envelopes; Determination of velocities in plane mechanisms.

Part II. Acceleration relationships in plane mechanisms: Elements; State of acceleration of a link in plane motion; State of acceleration in linkages; Coriolis' theorem; Further methods of acceleration analysis; Acceleration analysis of combinations of mechanisms—examples; Kinematic diagrams; Cam diagram laws relating input to output motion.

Part III. Exercises.

Part IV. Appendix. Material on cams, matrix algebra, and bibliography.

The purpose of this concise text is to provide the mechanisms designer with tools for analyzing the kinematical properties (velocities, accelerations, etc.) of a mechanism after the particular form of the mechanism is determined. Two approaches are stressed; the first is a systematic, recipe-like, exposition of the theory in a clear understandable fashion; the second is the analysis of examples which are sufficiently unidealized to be realistic. In this sense the book goes beyond other texts on this subject. For this reason also part III (Exercises) is particularly valuable in that it draws upon the author's rich industrial experience.

The material forms a good companion volume to the author's "Kinematische Getriebesynthese." Among the topics not yet covered by English texts on kinematics (except for Rosenauer and Willis' "Kinematics of Mechanisms") is the theory of curvature of a point path trajectory. This theory is useful and elementary and its introduction into English-language texts is believed to be largely a matter of time. The wealth of information clearly presented in this volume makes it commendable to those engaged in applied kinematics and machine design, in which field it is a noteworthy contribution.

A minor criticism discovered in many German texts is the use of the Gothic alphabet which would cause difficulty when used in an American classroom. This points out again the desirability of an international standard of nomenclature and symbols in this field. This is a minor objection, however, in an otherwise fine text graced by the author's known gifts of exposition.

Applied Mechanics

Höhere Technische Mechanik. By István Szabó. Second, revised, and enlarged edition. Springer-Verlag, Berlin, Göttingen, Heidelberg, 1958. Cloth, $9^{3}/_{8}$ in. $\times$ $6^{3}/_{8}$ in., 498 pp. DM 31.50.

REVIEWED BY J. R. M. RADOK[5]

APPLIED MECHANICS comprises here: (i) analytical mechanics; (ii) selected topics in static and dynamic elasticity, including variational methods and thermal effects; (iii) plasticity; (iv) hydrodynamics and high-speed gas dynamics. In spite of this universality and the restricted space, the author succeeds in penetrating deeply into each of these subjects with a presentation which is concise, but lucid and original. The more practical aspects of applied mechanics are emphasized throughout and illustrated by a large number of examples which occupy approximately one third of the book. These are worked out in complete detail and their advanced nature often places them in the class of contemporary research problems.

Among these worked examples, special reference should be made to the treatment of impact loads on plates, taking into account the mass of the plate, the stress analysis of tubes, reinforced by discrete rings, the plastic theory of rolling of metals, surface waves in channels, the theory of lubrication by viscous fluids, Laval nozzles, supersonic flow around cones. Other problems cover certain aspects of elastic stability of shells, thermoelastic analysis of tubes with temperature-dependent elastic properties, condensation shocks, and stress analysis of pressure vessels.

[4] Associate Professor and Chairman, Department of Mechanical Engineering, Columbia University, New York, N. Y.

[5] Associate Professor of Applied Mechanics, Polytechnic Institute of Brooklyn, Brooklyn, N. Y.

Journal of APPLIED MECHANICS

Information for Authors

• Manuscripts should be submitted in final form to the Technical Editors. Each manuscript must be accompanied by a statement that it has not been published elsewhere nor has it been submitted for publication elsewhere. A paper which would occupy more than five pages of the Journal may be returned to the author for abridgment.

• The author should state his business connection, the title of his position, and his mailing address. A short abstract (50 to 100 words) should be included on the first page immediately preceding the introductory paragraph of the paper.

• Three copies of the manuscript are required. One of these must be a carefully prepared printer's copy, typed in double spacing, on one side of the page only, with wide margins, on $8^1/_2$ by 11-in. opaque white paper. Mimeographed manuscripts, if prepared with exceptional care, can be accepted provided they are completely edited.

• As far as possible, all mathematical expressions should be typewritten. Greek letters and other symbols not available on the typewriter should be carefully inserted in ink. Care should be taken to distinguish between capital and lowercase letters, between zero (0) and the letter (*O*), between the numeral (1) and the letter (*l*), etc. A letter representing a vector cannot be printed with an arrow above or below it. The letter should be underscored with a single wavy line, wherever it appears in the text, to designate boldface type. A list of symbols carefully marked for the use of the editor (thus: κ, Greek l.c. kappa), if it has not been included in the body of the paper, should accompany the manuscript on a separate page.

• Before preparing a manuscript the author should study printed articles in the Journal, with special attention to the form and style of mathematical expressions, tables, footnotes, references, and abstract. Numbers that identify mathematical expressions should be enclosed in parentheses. Numbers that identify references at the end of the paper should be enclosed in brackets. Care should be taken to arrange all tables and mathematical expressions in such a way that they will fit into a single column when set in type. Equations that might extend beyond the width of one column (fractions that should not be broken or long expressions enclosed in parentheses) should be rephrased to go on two or more lines within column width. Fractional powers are preferred to root signs and should always be used in more elaborate formulas. The solidus should be used instead of the horizontal line for fractions wherever possible.

• A normal paper should not exceed five pages in the Journal. It is about 6000 words or twenty to twenty-five double-spaced typewritten pages inclusive of drawings. A Brief Note should not exceed 750 words or about one column in the Journal inclusive of drawings.

• Originals and two copies of figures must accompany the manuscript. Line drawings should not be larger than $8^1/_2 \times 11$ inches and should be planned for reduction to column width. Lettering should be large enough to be clearly legible when the illustration is reduced. The originals of line drawings must be in India ink on white or pale blue tracing paper or tracing cloth. Photographs of equipment or test specimens must be glossy prints and should be used sparingly. Captions for figures should be typed double-spaced and included as the last page of the manuscript. The figure number and author's name should be written in the margin or on the back of each illustration.

• Titles of papers should be brief.

• Authors can obtain copies of the ASME Manual MS-4, "An ASME Paper," from the Technical Editors and are urged to do so before drafting their papers in final form.

• Papers published in the Journal of Applied Mechanics must be presented at a Meeting, either in person or by title. Scheduling of papers is in the hands of the Secretary of the Applied Mechanics Division. Authors should indicate their preference in this respect to the Technical Editors when submitting a paper.

• An author is entitled to 25 preprints free of charge (in the case of two authors, 15 each; three or more authors, 10 each). Larger quantities of preprints or reprints can be ordered from Editorial Department, The American Society of Mechanical Engineers, 29 West 39th Street, New York 18, N. Y. Quotations will be sent on request.

ASME Publications Committee

Please address all communications to:

Technical Editors

Journal of Applied Mechanics, ASME

Division of Engineering

Brown University

Providence 12, R. I.

Dr. Durand was professor of mechanical engineering at Stanford University from 1904 until 1924. After his retirement he edited the six-volume work, "Aerodynamic Theory," which is still one of

DURAND

the important source works of information on aerodynamics. During World War II, when he was in his middle eighties, he was active in Washington in organizing research and development in jet propulsion.

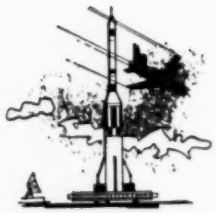

Centennial Conference

on the Problems of Hypersonic and Space Flight

The Conference will be held at Stanford University, Stanford, Calif., August 5–7, 1959. The meeting will be in honor of the 100th anniversary of the birth of WILLIAM FREDERICK DURAND, pioneer aeronautical engineer, who died last summer at the age of 99. The meeting will be sponsored by the Air Force Office of Scientific Research, The Office of Ordnance Research, and the National Science Foundation. Attendance at the Conference is not restricted. Room and board will be available on the Stanford campus for those who make arrangements in advance. The papers presented at the Conference will be published in a volume of Proceedings. Further information may be obtained from Dr. N. J. Hoff, Head of the Division of Aeronautical Engineering, Stanford University, Stanford, Calif.

THE SPEAKERS WILL INCLUDE

H. JULIAN ALLEN, Ames Research Center, NASA. **LUIGI BROGLIO,** University of Rome, Italy. **JOHANNES M. BURGERS,** University of Maryland. **FRANCIS CLAUSER,** The Johns Hopkins University. **HUGH L. DRYDEN,** National Aeronautics and Space Administration. **WILFRED H. DUKES,** Bell Aircraft Corporation. **ANTONIO FERRI,** Polytechnic Institute of Brooklyn. **RICHARD R. HELDENFELS,** Langley Research Center NASA. **WOLFGANG B. KLEMPERER,** Douglas Aircraft Company, Inc. **LESLIE S. G. KOVASZNAY,** The Johns Hopkins University. **HANS W. LIEPMANN,** California Institute of Technology. **GORDON N. PATTERSON,** University of Toronto. **SIR GEOFFREY TAYLOR,** Cambridge University. **R. H. THIELEMANN,** Deutsche Versuchsanstalt für Luftfahrt E. V.